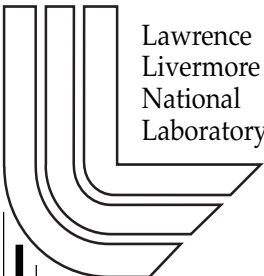


The $^{235}\text{U}(\text{n},2\text{n}\gamma)$ Yrast Partial Gamma-Ray Cross Sections: A Report on the 1998 – 1999 GEANIE Data and Analysis Techniques

W. Younes, J. A. Becker, L. A. Bernstein, P. E. Garrett, C. A. Mc Grath, D. P. McNabb, R. O. Nelson, M. Devlin, N. Fotiades, and G. D. Johns

September 1, 2000

U.S. Department of Energy



DISCLAIMER

This document was prepared as an account of work sponsored by an agency of the United States Government. Neither the United States Government nor the University of California nor any of their employees, makes any warranty, express or implied, or assumes any legal liability or responsibility for the accuracy, completeness, or usefulness of any information, apparatus, product, or process disclosed, or represents that its use would not infringe privately owned rights. Reference herein to any specific commercial product, process, or service by trade name, trademark, manufacturer, or otherwise, does not necessarily constitute or imply its endorsement, recommendation, or favoring by the United States Government or the University of California. The views and opinions of authors expressed herein do not necessarily state or reflect those of the United States Government or the University of California, and shall not be used for advertising or product endorsement purposes.

This work was performed under the auspices of the U. S. Department of Energy by the University of California, Lawrence Livermore National Laboratory under Contract No. W-7405-Eng-48.

This report has been reproduced directly from the best available copy.

Available electronically at <http://www.doc.gov/bridge>

Available for a processing fee to U.S. Department of Energy
And its contractors in paper from
U.S. Department of Energy
Office of Scientific and Technical Information
P.O. Box 62
Oak Ridge, TN 37831-0062
Telephone: (865) 576-8401
Facsimile: (865) 576-5728
E-mail: reports@adonis.osti.gov

Available for the sale to the public from
U.S. Department of Commerce
National Technical Information Service
5285 Port Royal Road
Springfield, VA 22161
Telephone: (800) 553-6847
Facsimile: (703) 605-6900
E-mail: orders@ntis.fedworld.gov
Online ordering: <http://www.ntis.gov/ordering.htm>

OR

Lawrence Livermore National Laboratory
Technical Information Department's Digital Library
<http://www.llnl.gov/tid/Library.html>

The $^{235}\text{U}(\text{n},2\text{n}\gamma)$ Yrast Partial Gamma-Ray Cross Sections:

A Report on the 1998 – 1999 GEANIE Data
and Analysis Techniques

W. Younes, J.A. Becker, L.A. Bernstein, P.E. Garrett, C.A. McGrath*, D.P. McNabb
Lawrence Livermore National Laboratory, Livermore, CA 94551-0808

**Present address: Idaho National Engineering and Environmental Lab, Idaho Falls, ID 83415*

R.O. Nelson, M. Devlin, N. Fotiades, G.D. Johns
Los Alamos National Laboratory, Los Alamos, NM 87545-1663

**The $^{235}\text{U}(\text{n},2\text{n}\gamma)$ Yrast Partial Gamma-Ray Cross Sections:
A Report on the 1998 and 1999 GEANIE Data and Analysis Techniques**

W. Younes, J.A. Becker, L.A. Bernstein, P.E. Garrett, C.A. McGrath*, D.P. McNabb

Lawrence Livermore National Laboratory, Livermore, CA 94551-0808

**present address: Idaho National Engineering and Environmental Lab, Idaho Falls, ID 83415*

R.O. Nelson, M. Devlin, N. Fotiades, G.D. Johns

Los Alamos National Laboratory, Los Alamos, NM 87545-1663

(Dated: September 1, 2000)

Measurements of partial $^{235}\text{U}(\text{n},2\text{n}\gamma)$ γ -ray cross sections have been carried out as a function of incident neutron energy using the GEANIE spectrometer at LANSCE/WNR. The yields of γ rays resulting from the population of discrete levels in the residual nucleus ^{234}U have been measured at incident neutron energies in the 1–20-MeV range. These data provide, with the aid of nuclear reaction modeling, a measurement of the $^{235}\text{U}(\text{n},2\text{n})$ reaction cross section and serve as a proof of principle of the γ -ray technique for the parallel $^{239}\text{Pu}(\text{n},2\text{n})$ measurement [1]. This paper presents the analysis of the γ -ray data and the extraction of partial γ -ray cross sections as a function of incident neutron energy. Uncertainties associated with the spectroscopic analysis of the data and validation of the results are discussed in detail.

CONTENTS

I	Introduction	2
A	Background	2
B	Organization of the Report	5
II	GEANIE 1998 Thin-Sample Data Analysis	6
A	Analysis of Raw Data	7
1	Gamma-Ray Energy Calibration	8
2	Fission Chamber Data Analysis	11
3	Partial Cross-Section Evaluation	18
B	Analysis of Background-Subtracted Data	26
III	Estimation of Energy-Dependent Systematic Uncertainties	35
IV	Validation of the 1998 Results with Respect to Energy-Dependent Uncertainties	36
V	GEANIE 1998 Thick-Sample Data Analysis	38
VI	Validation of the 1998 Results with Respect to Total Uncertainties	46
VII	GEANIE 1999 Data Analysis	48
A	$^{235}\text{U}(\text{n},2\text{n})$ Analysis	48
1	Partial Cross Section Evaluation	48
2	The Case of the $10_1^+ \rightarrow 8_1^+$ Transition	58
B	$^{56}\text{Fe}(\text{n},\text{n}')$ Analysis	61
1	Partial Cross Section Evaluation	61
VIII	Estimation of Energy-Dependent Systematic Uncertainties	66
IX	Validation of the 1999 Results with Respect to Energy-Dependent Uncertainties	66
X	Validation of the 1999 Results with Respect to Total Uncertainties	68

XI	Angular Distribution Effects	70
A	Formalism	70
B	Geometry of the GEANIE spectrometer	71
C	Estimate of the Angular-Distribution Correction	71
XII	Adopted Partial γ-Ray Cross Sections	83
A	Weighted Average	83
B	Optimized Average (Adopted Partial Cross Sections)	92
XIII	Summary of Observed Lines	103
A	Angular-Distribution Correction Factors	103
1	Angular-Distribution Correction Factor for Transitions in ^{234}U	103
2	Angular-Distribution Correction Factor for Transitions in ^{233}U	131
B	Observed Lines in ^{234}U	139
C	Observed Lines in ^{235}U	190
D	Observed Lines in ^{233}U	220
XIV	Conclusion	237
References		237
A	Lines Used for γ-ray Energy Calibration in 1998 Data	238
B	Values of (n,f) Cross Sections Used in Calculating the Neutron Flux	240
C	Energy-Independent Systematic Uncertainties	246
D	Partition of Relative Uncertainties	246
1	Notation and Formalism	246
a	The case of a single data set	246
b	The case of combined data sets	247
2	Specific Applications	248
a	Ratio of distinct γ -ray cross sections evaluated at the same neutron energy	248
b	Ratio of a γ -ray cross section evaluated at distinct neutron energies	248
c	Sum of individual γ -ray cross sections evaluated at the same neutron energy	249
3	Tabulated Results for the $^{235}\text{U}(\text{n},2\text{n})$ Channel	249
E	Detailed Check of Calculations	272
1	Analysis of the 98Thin Data Set	272
a	Kinematics	272
b	Analysis of the Fission-Chamber Data	273
c	Analysis of the γ -ray Data	275
2	Analysis of the 99Thin Data Set	276
a	Kinematics	276
b	Analysis of the Fission-Chamber Data	276
c	Analysis of the γ -ray Data	277
F	Check of XGAM Background Fits	278

I. INTRODUCTION

A. Background

A series of experiments has been carried out to measure accurately partial gamma-ray cross sections in the $^{235}\text{U}(\text{n},2\text{n}\gamma)$ and $^{239}\text{Pu}(\text{n},2\text{n}\gamma)$ channels as a function of incident neutron energy. The goal is to deduce the corresponding $(\text{n},2\text{n})$ channel cross sections, using robust model predictions of the partial-to-channel cross section ratio. This work was motivated primarily by the wide disagreement between previous measurements of the $^{239}\text{Pu}(\text{n},2\text{n})$

cross section [2] and the resulting large uncertainties in model predictions and evaluations of this cross section. The lack of reliability of prior measurements can be traced to the inherent difficulties of the neutron-counting methods used. In previous experiments, the $(n,2n)$ cross section was typically obtained as the difference between the observed neutron count and background neutron counts from scattered beam and fission events. The low value of the $(n,2n)$ cross section and the high values of the neutron-induced fission cross section ($\sigma_{(n,f)}$) and neutron multiplicity (\bar{v}) conspire to reduce the reliability of the neutron-counting methods for the $^{239}\text{Pu}(n,2n)$ case. The $^{235}\text{U}(n,2n)$ cross section measurement is, in many respects, an easier experiment. Both $\sigma_{(n,f)}$ and \bar{v} have lower values in the $^{235}\text{U}(n,2n)$ experiment compared to the $^{239}\text{Pu}(n,2n)$ case, and ^{235}U samples are less radioactive and easier to obtain in enriched form than ^{239}Pu samples.

In order to avoid many of the complications encountered in the neutron-counting techniques, the current set of experiments rely on the measurement of characteristic γ rays, produced in the de-excitation of the $(n,2n)$ product nucleus (see figure 1). This technique has clear advantages over neutron-counting because the characteristic gamma rays have well-defined energies and these energies can be measured with sufficient efficiency and resolutions of better than one part in ten thousand by current-generation germanium detectors. However, the channel cross section is obtained indirectly by this method and must rely on model predictions to deduce the $(n,2n)$ cross section from measured partial γ -ray yields. Therefore, measurements of γ -ray yields from the $^{235}\text{U}(n,2n\gamma)$ reaction, for which the channel $(n,2n)$ cross section has previously been measured [3], have been performed in parallel with the $^{239}\text{Pu}(n,2n)$ experiment. The ^{235}U measurements, and the deduced $^{235}\text{U}(n,2n)$ reaction cross section can be used to develop the necessary analysis techniques and to validate the method as a whole.

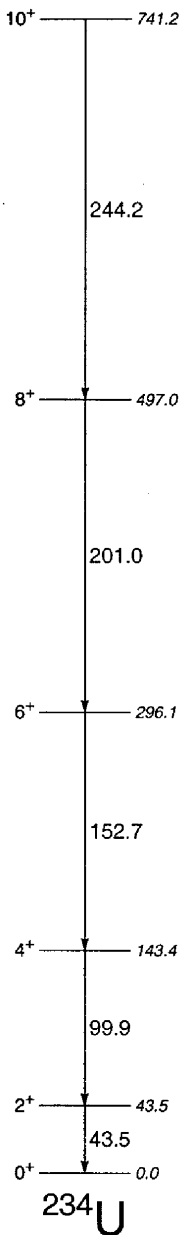


FIG. 1: Levels in the ground-state band of ^{234}U up to spin 10. Each level is labeled by its spin and parity on the left and by its excitation energy in keV on the right. Transitions between levels are shown as arrows and labeled by the transition energy in keV.

The $^{239}\text{Pu}(n,2n)$ and $^{235}\text{U}(n,2n)$ experiments were performed from 1997 to 1999, using the GEANIE (GERmanium Array for Neutron-Induced Excitations) spectrometer situated at the LANSCE/WNR facility. Detailed descriptions of the spectrometer and the LANSCE/WNR facility can be found in reference [4], and in the report on the analysis of the 1997 $^{235}\text{U}(n,2n)$ data [5]. The GEANIE spectrometer, in its current configuration, consists of 11 Compton-suppressed planar germanium detectors, 9 Compton-suppressed and 6 unsuppressed coaxial detectors situated at a distance of ≈ 14 cm from the focal point where the scattering sample is located. The planar detectors are grouped at mostly forward and backward angles, while the coaxial detectors are distributed about 90° . The efficiency of the array has been calibrated through a series of measurements with a calibrated radioactive source, supplemented by detailed modeling [9] using the transport code MCNP [12].

A “white” neutron source is produced at the LANSCE/WNR facility by spallation reactions from an 800 MeV proton beam incident on a natural tungsten target. The proton beam is typically bunched into $625\ \mu\text{s}$ macropulse trains of micropulses $1.8\ \mu\text{s}$ apart. The macropulses are typically generated at a frequency of 100 Hz, giving a 6% duty cycle. The spallation neutrons travel along shielded neutron flight paths of different lengths, and at various angles, to the different experimental areas. The GEANIE spectrometer is located at the end of the flight path 60 degrees to the right (60R) of the proton beam direction, 20.34 m downstream from the spallation target. A fission chamber [13], placed in the beam 1.86 m upstream from the GEANIE spectrometer, and containing both ^{235}U and ^{238}U fission foils, serves as a neutron flux monitor. Neutron energies are determined by the time-of-flight (TOF) technique, using the detection time of the flash of γ rays caused by the spallation reaction as a reference time. In general, the γ -ray data were sorted into separate E_γ -TOF matrices for summed planar and summed coaxial data. Equal-time TOF cuts were made on the planar-data E_γ -TOF matrix corresponding to neutron energies in the 5-20-MeV range. The resulting γ -ray spectra were fitted using the code XGAM[6] over the full γ -ray energy range. A background γ -ray spectrum was also constructed from a TOF gate on arrival times shorter than the γ flash reference time (i.e. a cut containing decays from long-lived states and events caused by slow neutrons “wrapped” from the previous beam pulse).

The $^{235}\text{U}(n,2n\gamma)$ data acquired using GEANIE can be grouped into four sets. The first data set was acquired between April and July 1997 and was analyzed to extract the shape of the $^{235}\text{U}(n,2n)$ cross section as a function of incident neutron energy. A discussion of the analysis and results can be found in [5]. Because the emphasis of this report is on the extraction of absolute partial γ -ray cross sections, and because the 1997 data were acquired without a precise measurement of array efficiency and sample thickness, these data are not discussed any further here. The remaining three data sets, which were acquired with the express purpose of extracting the $^{235}\text{U}(n,2n)$ cross section both in shape and in magnitude, are presented in this paper. Experiments were performed in October and December 1998, using both thin (12-mil) and thick (24-mil) highly-enriched ^{235}U samples. These two data sets have been analyzed separately and will be referred to as “**98Thin**” and “**98Thick**” throughout this paper. The final data set discussed here was acquired in November and December 1999. This data set will be referred to as “**99Thin**”. The array was kept in the same configuration as in the 1998 runs, with some improvements in the electronics. From the point of view of the analysis, the only relevant change in the electronics is the upgrade from 8k to 16k ADC (Analog-to-Digital Conversion) modules used to digitize the processed energy signals. This doubling in the number of digital channels available can be helpful in fitting complex spectra. There were also differences in the samples used in 1998 and 1999. The **99Thin** sample was 12-mil thick and encased in the same holder used for the ^{239}Pu measurements. In addition, thin (2-mil each) ^{nat}Fe foils were placed on either side of the ^{235}U sample to provide in-beam calibration to a known partial cross section in the $^{56}\text{Fe}(n,n'\gamma)$ channel.

B Organization of the Report

This report summarizes the analysis of both 1998 and 1999 GEANIE data sets to extract $^{235}\text{U}(n,2n)$ partial γ -ray cross sections. The work presented in this report is based on experimental information available as of 2/24/00 and GNASH calculations obtained on 5/13/99. The bulk of the discussion concerns the yrast (i.e. in this case, ground-state band members) $4_1^+ \rightarrow 2_1^+$, $6_1^+ \rightarrow 4_1^+$, $8_1^+ \rightarrow 6_1^+$, and $10_1^+ \rightarrow 8_1^+$ transitions. The 1998 thin-sample data (**98Thin**) is presented first, and in greatest detail, in section II, with specific discussions of the neutron flux deduced from the fission chamber and γ -ray energy calibration. Absolute partial γ -ray cross sections are extracted for the lowest observed members of the yrast band in ^{234}U from the raw data (i.e. with no γ -ray background subtraction). In section III, a neutron-energy-dependent systematic uncertainty, in addition to random statistical variations in the data, is inferred from a comparison i) between raw and background-subtracted data and ii) between the neutron flux extracted from the ^{235}U and ^{238}U fission-foil data. The partial cross sections obtained by using either fission chamber foils and the raw and subtracted data, are compared in section IV as a check of the deduced neutron-energy-dependent systematic uncertainty.

The analysis of the 1998 thick-sample data (**98Thick**) is discussed next in section V. Partial cross sections are

deduced and compared in section VI to the thin-sample data to validate the total uncertainty, consisting of random, neutron-energy-dependent systematic, and energy-independent systematic uncertainties. With this validation, the absolute partial cross sections extracted from the thin-sample raw data, normalized to the neutron flux measured with the ^{235}U fission foil, are taken as the optimal values for the 1998 GEANIE experiment, along with the deduced random and systematic errors.

The next section (VII) discusses the analysis of the 1999 GEANIE data (**99Thin**) for which an assembly of ^{235}U and ^{nat}Fe foils was used as a target. The same set of yrast partial cross sections is extracted from the raw data. The fits for the $10_1^+ \rightarrow 8_1^+$ transition in particular are revisited and the assertion that the peak consists of a doublet of lines is carefully examined. As in the 1998 data, neutron-energy-dependent systematic uncertainties are calculated. Partial cross sections for the $2_1^+ \rightarrow 0_1^+$ 846.8-keV transition in ^{56}Fe are inferred in section VII B, along with systematic uncertainties, from ^{nat}Fe foils placed on either side of the ^{235}U sample. In section IX the measured $^{235}\text{U}(n,2n)$ partial cross sections are checked against raw and subtracted data, normalized with either ^{235}U or ^{238}U fission foil. In section X, the total uncertainties are validated against the known ^{56}Fe partial γ -ray cross section standard at $E_n = 14.5$ MeV. The optimal partial cross sections extracted from the 1999 GEANIE experiment are taken from the raw, ^{235}U -fission-foil-normalized data.

Angular-distribution effects on the observed γ -ray yields are discussed in section XI. A statistical-model code is used to estimate the angular distribution of individual transitions. The model predictions are adjusted based on comparison with angular distributions observed in the GEANIE data, and angular-distribution correction factors are deduced for all $(n,2n)$ and $(n,3n)$ lines of interest.

In section XII A the best 1998 and 1999 data are compared and combined by two different methods. First the data are averaged by weighted mean to produce a recommended absolute partial cross section for the lowest observed yrast transitions in the $^{235}\text{U}(n,2n)$ channel. In a second approach, linear corrections are applied to both 1998 and 1999 data to account for systematic discrepancies between the data sets, and the resulting yields are then combined by weighted mean. Throughout the report, the partial cross sections obtained are compared to predictions from GNASH[7], a Hauser-Feshbach reaction code. The calculations shown here represent the best currently available predictions by the code, but are subject to revision as the reaction model is improved, especially in light of the present GEANIE results.

Finally, in the summary section XIII, all observed $(n,2n)$, (n,n') and $(n,3n)$ transitions are presented. The reader interested primarily in the results of the analysis, may consult this section directly, and refer to the remainder of the report for further details.

A natural division can be drawn between the experimental and theoretical steps involved in obtaining the $^{235}\text{U}(n,2n)$ channel cross section from measured γ -ray yields. The intent of this report is to present the experimental aspects of this process. The marriage of the partial γ -ray cross sections discussed here with theoretical predictions of the partial-to-channel cross-section ratios to deduce the $^{235}\text{U}(n,2n)$ channel cross-section will be treated in a separate report.

II. GEANIE 1998 THIN-SAMPLE DATA ANALYSIS

In October and December 1998 the GEANIE spectrometer was used to measure γ rays following neutron-induced reactions on ^{235}U . In order to account for target-thickness effects more accurately, the data were acquired with samples of two different thicknesses for approximately equal run durations. The experimental details for the thin-target (12-mil) data are summarized in the box below. The values quoted in the box were obtained from the experiment log book, data counted by scaler modules during the experiment, and reference [9]. For the purposes of this paper, the data from the 11 planar detectors have been summed and analyzed. In the $E_n = 1\text{-}20$ MeV range for the planar-detector sum, 1.02×10^8 single and higher-fold full-energy-peak counts were acquired. These raw counts in the measured spectrum break down into 45.4% from x rays (mostly from target activity), 43.1% from γ rays due to target activity, and 3.7% from an assortment of common contaminants (e.g. neutron bumps, 511 keV peak). The remaining 7.8% of photo-peak counts are likely due to γ rays from neutron-induced reactions on the ^{235}U sample (e.g. $(n,f\gamma)$, $(n,xn\gamma)$, etc.). Only 0.22% of the full-energy-peak counts in this neutron energy range could be assigned to the $^{235}\text{U}(n,2n)$ channel, and are distributed among 16 distinct peaks.

The relative weakness of the $(n,2n\gamma)$ component of the spectrum has two practical effects on the data analysis: i) the analysis is exacting and time-consuming and ii) specialized analysis tools had to be developed and used.

run label: 98Thin

log book pages: #3 pp. 220-229,277-278

run dates: 10/16/98-10/23/98 and 12/12/98-12/14/98

total run time recorded to tape: 701385 s (from 55 Hz pulser)

beam structure:

rep rate: 100 Hz (10/16/98-10/20/98 and 12/12/98-12/14/98),
116 Hz (10/20/98-10/23/98)

micropulse spacing: 1.8 μ s

beam gate length: 625 μ s

typical proton current: 2.5 μ A

beam absorbers:

10/16/98-10/19/98: 3" Pb + 1" polyethylene + 1" borated polyethylene

10/19/98-10/20/98: 1" Pb + 2" polyethylene

10/20/98-10/23/98: 1/2" Pb + 1" borated polyethylene

12/12/98-12/14/98: 1/2" Pb + 1" borated polyethylene

sample areal density corrected for ^{235}U enrichment: $0.524 \pm 0.037 \text{ g/cm}^2$

sample thickness: \approx 12 mil (2 laminated packages of two 3-mil foils each)

sample atomic assay: 93.2324% ^{235}U + 5.3729% ^{238}U + 1.1339% ^{234}U + 0.2581% ^{236}U

sample orientation: 251° on dial (19° with respect to beam)

sample mask: 0.030"-thick Ta foil (one on each side) 2.25" \times 2.25" with 1"-diameter hole

planar-detector absorbers: none

deadtimes:

planar-data sum: $45.32 \pm 1.36 \%$

coaxial-data sum: $45.57 \pm 1.37 \%$

^{235}U fission foil: $39.99 \pm 1.20 \%$

^{238}U fission foil: $40.84 \pm 1.22 \%$

average in-beam array rate: 1178 Hz (beam-gated γ -or rate)

average array rate: 1778 Hz (total γ -or rate)

A Analysis of Raw Data

The **98Thin** data set was first analyzed for the sum of the planars and in the energy range $E_n = 5\text{-}20 \text{ MeV}$ without any background subtraction. These data were sorted into a two-dimensional matrix with γ -ray energy along one axis, and time-of-flight (TOF) along the other. A gate placed on the TOF axis then produces a γ -ray spectrum corresponding to neutron energies included in the TOF gate. Thus a single TOF gate corresponding to the 5-20-MeV neutron energy range was used to generate a "total projection" γ -ray spectrum. The basic procedure used to extract excitation functions for each γ -ray line of interest can be broken down into the following steps:

1. obtain the best fit to the total $E_n = 5\text{-}20 \text{ MeV}$ total projection spectrum (i.e. a γ -ray spectrum)
2. fix all parameters in the best fit, except for:

- continuum-background polynomial coefficients
- peak heights

3. fit individual TOF cuts in the range $E_n = 5\text{-}20 \text{ MeV}$ using the fit settings obtained in step 2

The fits were carried out using the XGAM peak-fitting program [6] with the settings listed in table I. Step 3 in this procedure is fully automated, so that the fit parameters are essentially determined in step 2 with the better statistics of the total neutron-energy projection, and only individual peak heights and rough background shape were expected to vary as a function of neutron energy. Two precautions were adopted to avoid erroneous fits due to the low statistics in individual TOF cuts. First, the background parameters and peak heights were scaled down from their values in the fit to the total projection by the ratio of the number of TOF channels in the individual cut to that number in the total projection. In this way, the initial settings of the fit parameters are close to what might be expected for each individual fit in step 3. Second, the peak height was parameterized and varied as a squared value, in order to avoid the unphysical situation of a negative-height peak, compensating for a poor background fit, a problem which often arises in fitting programs.

TABLE I: Fit parameters used in XGAM for the 1998 GEANIE data [6]. The variable x refers to the γ -ray spectrum channel number, where each channel corresponds to 0.125 keV.

parameter	value
fitted range	690-7950 (ch), 86-994 (keV)
background polynomial order	21
peak width (ch)	$w = \sqrt{45.18 + 6.543 \frac{x}{1000} + 3.448 \left(\frac{x}{1000}\right)^2}$
x-ray width parameter (ch)	$\Gamma = -6.951 \times 10^{-1} + 1.354 \times 10^{-3}x$
low-energy tail (ch)	$R = 5.761 \times 10^{-3}x, \beta = 2.032$
high-energy tail (ch)	$R_h = 3.343 \times 10^{-3}x, \beta_h = 9.711$
Gaussian asymmetry (ch)	$p_3 = -3.017 \times 10^{-3} + 5.635 \times 10^{-6}x$ $p_4 = 5.024 \times 10^{-7} + 2.317 \times 10^{-10}x$
Compton step (ch)	$S = 2.228 \times 10^{-2}$
x-ray peaks	19
γ -ray peaks	395
neutron bumps	2
χ^2/ν for $E_n=5\text{-}20 \text{ MeV}$	2.66

1 Gamma-Ray Energy Calibration

A precise in-beam γ -ray energy calibration was obtained by identifying lines in the $E_n = 5\text{-}20 \text{ MeV}$ total-projection spectrum with precisely known [10] energies. In all, 76 lines were used and are listed in the table in appendix A. The calibration was obtained by first fitting the true energies $E_\gamma^{(true)}$ as a function of the channel centroid of the corresponding peak in the spectrum with a line, producing a first-order approximation $E_\gamma^{(lin)}$. The residuals $E_\gamma^{(true)} - E_\gamma^{(lin)}$ were then fitted with a fourth-order polynomial to correct for non-linearities in the electronics. This calibration process was performed using the program XGAMCAL [6] and is depicted in figure 2. The differences d_i between true and calibrated energies (i.e. linear + residual non-linearity) are distributed about a mean value of $\bar{d} = -3.5 \text{ eV}$ and with a standard deviation $\sigma_d = 111 \text{ eV}$. More specifically, the linear calibration and residual non-linearity are given by:

$$E_\gamma^{(lin)} = -2.8826 \times 10^{-1} + 1.2514 \times 10^{-1}x \quad (1)$$

$$\begin{aligned} E_\gamma^{(res)} &\equiv E_\gamma^{(true)} - E_\gamma^{(lin)} \\ &= -5.8128 \times 10^{-1} + 1.0030 \times 10^{-3}x - 5.3032 \times 10^{-7}x^2 + 1.0159 \times 10^{-10}x^3 - 6.6916 \times 10^{-15}x^4 \end{aligned} \quad (2)$$

where x is the digitization channel (at $\approx 0.125 \text{ keV}$ per channel) corresponding to the fitted centroid of the detected γ -ray energy signal. The uncertainties on the calibrated energies listed in the table in appendix A are obtained by a careful propagation of errors which takes into account: i) uncertainties in the channel centroid of the peak, ii)

uncertainties in the true energies, iii) uncertainties in the calibration polynomial terms and iv) covariance between the terms of the calibration polynomial.

Because γ -ray energy uncertainties obtained in this manner are typically under-predicted, it is customary to augment them by the standard deviation obtained in the non-linearity fitting process. This quantity then serves as an additional, systematic, uncertainty. Therefore, the γ -ray energies quoted in this paper carry an additional 111-eV uncertainty.

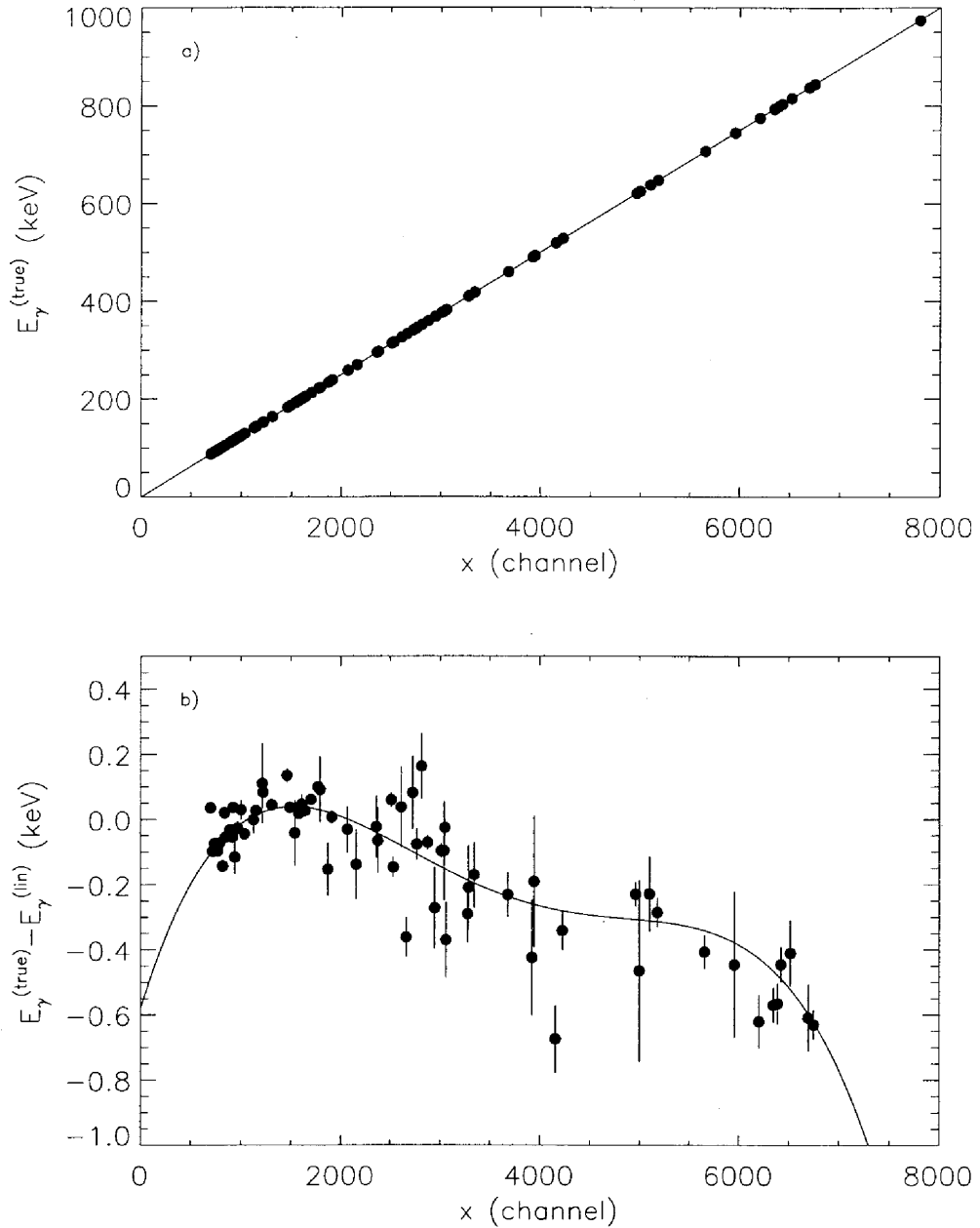


FIG. 2: Gamma-ray energy calibration: a) linear calibration and b) fourth-order polynomial non-linearity correction.

2 Fission Chamber Data Analysis

The fission chamber contains two thin ($\approx 400 \mu\text{g}/\text{cm}^2$) foils of isotopically enriched ^{235}U and ^{238}U material respectively. Fission fragments produced by neutron-induced reactions on either foil can be counted. Using the known[11] neutron-induced fission cross section, the incident neutron flux can be deduced. For each fission foil separately, the fission chamber data were sorted into a two-dimensional matrix of counts, with pulse height (i.e. energy) along the x-axis and TOF along the y-axis. The steps required to generate the fission counts $N_{fc}(\tau)$ for each 0.5-ns-wide TOF channel are summarized in figure 3. In each panel, the inset shows the projection of the matrix onto the pulse-height axis for all TOF. The range of the spectrum corresponding to fission counts is shaded in red. The projection onto the TOF axis of the matrix counts from a gate on the fission pulse-height range is displayed in the main panel. The γ flash (from the spallation reaction used to generate the neutrons) and a flat baseline background are labeled in each panel. The baseline represents counts primarily due to beam wrap-around. These TOF spectra are histogrammed in steps of 0.5 ns, corresponding to the digitization-channel size of the TDC modules used. In each TOF channel, $N_{fc}(\tau)$ is then the difference between the total and baseline counts in that channel.

The number of neutrons-per-energy (N_{nc}) can then be calculated for each 0.5-ns TOF channel according to:

$$N_{nc}(\tau) = \frac{1}{\epsilon_d(1 - f_{fc})} \times \frac{N_{fc}(\tau)}{\delta E \sum_i \sigma_{(n,f)}^{(i)} a_{foil}^{(i)}} \quad (3)$$

where ϵ_d is the fission chamber intrinsic detection efficiency, f_{fc} is the deadtime fraction for the fission chamber, δE is the energy width of the one-channel TOF bin, $\sigma_{(n,f)}^{(i)}$ is the known value of the neutron-induced total fission cross section for the i^{th} constituent in the foil, and $a_{foil}^{(i)}$ the areal density of the i^{th} constituent. Numerical values have been assigned to ϵ_d and $a_{foil}^{(i)}$ in the manuscript by McNabb [9]. The deadtime fraction for the fission chamber was measured at $f_{fc} = 0.3999 \pm 0.0120$ for the ^{235}U foil and 0.4084 ± 0.0122 for the ^{238}U foil, where we have adopted the 3% uncertainty recommended by McNabb [9]. The fission cross sections $\sigma_{(n,f)}^{(i)}$ were obtained from the ENDF/B-VI evaluation [11].

Finally, a flux normalization parameter N_ϕ is calculated from the neutron count in each TOF channel using the formula:

$$N_\phi(\tau) = N_{nc}(\tau) \times a_{sample} \times \delta E \quad (4)$$

where a_{sample} is the ^{235}U sample areal density (i.e. corrected for isotopic enrichment listed in the experimental details box in section II). For a TOF bin $[\tau_a, \tau_b]$ spanning several 0.5-ns channels, the appropriate[5] normalization parameter is given by:

$$N_\phi([\tau_a, \tau_b]) = \sum_{\tau=0}^{\infty} N_\phi(\tau) \int_{\tau_a}^{\tau_b} d\tau' \frac{1}{\sqrt{2\pi\sigma_\tau^2}} e^{-\frac{(\tau-\tau')^2}{2\sigma_\tau^2}} \quad (5)$$

where σ_τ is the detection timing uncertainty, deduced in our experiment to be 15 ns FWHM ($\Rightarrow \sigma_\tau = 6.37 \text{ ns}$). Equation 5 provides a correction to the neutron flux which takes into account the expected distribution of neutrons at all energies that might be detected in a given TOF bin. Within the same formalism, a mean and variance may be calculated for that distribution of incident neutrons [5]:

$$\overline{E_n}([\tau_a, \tau_b]) \equiv \frac{\sum_{\tau=0}^{\infty} E_n(\tau) N_\phi(\tau) \int_{\tau_a}^{\tau_b} d\tau' \frac{1}{\sqrt{2\pi\sigma_\tau^2}} e^{-\frac{(\tau-\tau')^2}{2\sigma_\tau^2}}}{\sum_{\tau=0}^{\infty} N_\phi(\tau) \int_{\tau_a}^{\tau_b} d\tau' \frac{1}{\sqrt{2\pi\sigma_\tau^2}} e^{-\frac{(\tau-\tau')^2}{2\sigma_\tau^2}}} \quad (6)$$

$$\sigma_{E_n}^2([\tau_a, \tau_b]) \equiv \frac{\sum_{\tau=0}^{\infty} [E_n(\tau) - \overline{E_n}([\tau_a, \tau_b])]^2 N_\phi(\tau) \int_{\tau_a}^{\tau_b} d\tau' \frac{1}{\sqrt{2\pi\sigma_\tau^2}} e^{-\frac{(\tau-\tau')^2}{2\sigma_\tau^2}}}{\sum_{\tau=0}^{\infty} N_\phi(\tau) \int_{\tau_a}^{\tau_b} d\tau' \frac{1}{\sqrt{2\pi\sigma_\tau^2}} e^{-\frac{(\tau-\tau')^2}{2\sigma_\tau^2}}} \quad (7)$$

The partial cross sections calculated in this paper have been corrected in this way, and are furthermore quoted with uncertainties in both neutron energy and yield. The uncertainties in neutron energy about a centroid position are meant to represent the underlying neutron distribution associated with the deduced yield. Some care in interpreting these uncertainties is warranted however, because that distribution is not Gaussian and, in fact, not symmetrical. For those data points where the TOF bin size is small compared to the timing uncertainty, the neutron distribution will approach a Gaussian form. Wherever the bin size is comparable to or larger than the timing uncertainty, the neutron distribution will assume a more complex shape. The proper interpretation and manipulation of GEANIE data with regard to the underlying neutron distribution will be discussed in greater detail in an upcoming report [8], with special emphasis on the formalism for converting partial into reaction cross sections.

Calculated values of N_{fc} , N_{nc} and N_ϕ for the 1998 thin-target data are listed in tables II for the ^{235}U fission foil and III for the ^{238}U fission foil. The flux normalization factors N_ϕ deduced from either fission foil are compared in figure 4. The agreement in the normalization parameter N_ϕ between the two fission chambers is generally better than 5% and always better than 10%, although the normalization factors extracted using the ^{235}U foil are systematically higher than those obtained from the ^{238}U foil. One possible explanation for the observed discrepancies might be the effect of “wrap-around” neutrons from a prior beam pulse, which cause a background in the ^{235}U fission foil data but, due to higher fission threshold, have little or no effect on the ^{238}U fission foil. An approximate correction for this effect is achieved by the constant-baseline subtraction discussed above. Uncertainty in the true shape of the “wrap-around” background would favor using the ^{238}U fission foil data for flux normalization. However, the lower (n,f) cross section for ^{238}U , compared to ^{235}U , translates into $\approx 87\%$ more counts (after baseline subtraction) in the ^{235}U fission foil data for $E_n = 5\text{-}20 \text{ MeV}$. Furthermore, the evaluated $^{238}\text{U}(n,f)$ cross sections are quoted without uncertainties in the ENDF/B-VI database [11]. Finally, the ^{235}U fission foil thickness is known[9] with considerably higher accuracy than the ^{238}U foil thickness (0.66% relative uncertainty for the ^{235}U foil thickness compared to 4.76% for the ^{238}U foil thickness). Because of these limitations, in the final evaluation of recommended cross sections in this paper, we prefer the ^{235}U fission foil data for flux normalization.

We also compare in figure 5 the shape of the neutron count (N_{nc}) deduced from the ^{235}U fission foil, to a calculation of the expected 60R WNR flux with $1/2''$ of lead and $1''$ of polyethylene absorbers, by fitting with an overall scale factor. The absorbers were placed in the beam to reduce the flux of low-energy ($E_n \lesssim 5 \text{ MeV}$) neutrons, which do not contribute to the $(n,2n)$ cross section but cause additional background from the (n,γ) and $(n,n'\gamma)$ channels, as well as from the γ flash. The agreement between theory and data is excellent, with the possible exception of the last three points near 20 MeV. However, since this comparison is only intended as a rough verification of the overall shape, this minor discrepancy is not a cause for concern.

TABLE II: Energy and neutron flux statistics calculated using equations 3-7 for 15-ns-wide TOF bins from $E_n = 4$ to 20 MeV, and applied to the ^{235}U fission-foil data with a baseline subtraction.

Bin	E_{min} (MeV)	E_{max} (MeV)	\bar{E}_n (MeV)	σ_E (MeV)	N_{fc}	N_{nc} (n/MeV)	N_ϕ (γ/b)
1	4.000	4.169	4.090	0.093	3267 ± 63	$(7.905 \pm 0.157) \times 10^{11}$	$(6.738 \pm 0.097) \times 10^6$
2	4.169	4.349	4.264	0.099	3441 ± 64	$(7.891 \pm 0.152) \times 10^{11}$	$(6.924 \pm 0.099) \times 10^6$
3	4.349	4.541	4.453	0.105	3464 ± 64	$(7.511 \pm 0.144) \times 10^{11}$	$(7.257 \pm 0.101) \times 10^6$
4	4.541	4.746	4.647	0.113	3485 ± 64	$(7.143 \pm 0.137) \times 10^{11}$	$(7.421 \pm 0.103) \times 10^6$
5	4.746	4.965	4.861	0.122	3365 ± 64	$(6.563 \pm 0.128) \times 10^{11}$	$(7.383 \pm 0.103) \times 10^6$
6	4.965	5.200	5.090	0.129	3595 ± 66	$(6.655 \pm 0.126) \times 10^{11}$	$(7.579 \pm 0.106) \times 10^6$
7	5.200	5.452	5.333	0.140	3444 ± 64	$(5.996 \pm 0.116) \times 10^{11}$	$(7.701 \pm 0.107) \times 10^6$
8	5.452	5.723	5.597	0.149	3570 ± 65	$(5.832 \pm 0.110) \times 10^{11}$	$(7.957 \pm 0.109) \times 10^6$
9	5.723	6.014	5.875	0.160	3844 ± 67	$(5.718 \pm 0.104) \times 10^{11}$	$(8.103 \pm 0.109) \times 10^6$
10	6.014	6.328	6.181	0.175	4068 ± 69	$(5.062 \pm 0.089) \times 10^{11}$	$(8.070 \pm 0.102) \times 10^6$
11	6.328	6.668	6.517	0.187	4976 ± 75	$(4.994 \pm 0.079) \times 10^{11}$	$(8.597 \pm 0.099) \times 10^6$
12	6.668	7.036	6.862	0.201	5796 ± 80	$(4.870 \pm 0.071) \times 10^{11}$	$(9.051 \pm 0.096) \times 10^6$
13	7.036	7.436	7.237	0.218	6310 ± 84	$(4.493 \pm 0.063) \times 10^{11}$	$(8.704 \pm 0.091) \times 10^6$
14	7.436	7.870	7.661	0.242	5998 ± 82	$(3.688 \pm 0.053) \times 10^{11}$	$(8.129 \pm 0.085) \times 10^6$
15	7.870	8.344	8.126	0.263	6127 ± 82	$(3.364 \pm 0.048) \times 10^{11}$	$(8.164 \pm 0.084) \times 10^6$
16	8.344	8.863	8.618	0.284	6468 ± 84	$(3.231 \pm 0.045) \times 10^{11}$	$(8.373 \pm 0.085) \times 10^6$
17	8.863	9.431	9.160	0.313	6463 ± 85	$(2.959 \pm 0.041) \times 10^{11}$	$(8.229 \pm 0.084) \times 10^6$
18	9.431	10.057	9.757	0.346	5937 ± 81	$(2.495 \pm 0.036) \times 10^{11}$	$(7.939 \pm 0.083) \times 10^6$
19	10.057	10.747	10.414	0.377	5790 ± 80	$(2.227 \pm 0.032) \times 10^{11}$	$(7.667 \pm 0.081) \times 10^6$
20	10.747	11.511	11.143	0.425	5316 ± 77	$(1.863 \pm 0.028) \times 10^{11}$	$(7.209 \pm 0.079) \times 10^6$
21	11.511	12.360	11.960	0.467	5498 ± 79	$(1.709 \pm 0.025) \times 10^{11}$	$(6.993 \pm 0.077) \times 10^6$
22	12.360	13.307	12.860	0.525	5436 ± 78	$(1.410 \pm 0.021) \times 10^{11}$	$(6.789 \pm 0.072) \times 10^6$
23	13.307	14.369	13.876	0.589	5729 ± 80	$(1.228 \pm 0.018) \times 10^{11}$	$(6.659 \pm 0.069) \times 10^6$
24	14.369	15.564	15.016	0.660	6017 ± 82	$(1.113 \pm 0.016) \times 10^{11}$	$(6.666 \pm 0.069) \times 10^6$
25	15.564	16.916	16.297	0.750	6115 ± 83	$(1.004 \pm 0.014) \times 10^{11}$	$(6.676 \pm 0.071) \times 10^6$
26	16.916	18.453	17.759	0.857	5768 ± 80	$(8.629 \pm 0.131) \times 10^{10}$	$(6.718 \pm 0.074) \times 10^6$
27	18.453	20.213	19.416	0.971	5765 ± 80	$(7.845 \pm 0.162) \times 10^{10}$	$(6.847 \pm 0.101) \times 10^6$

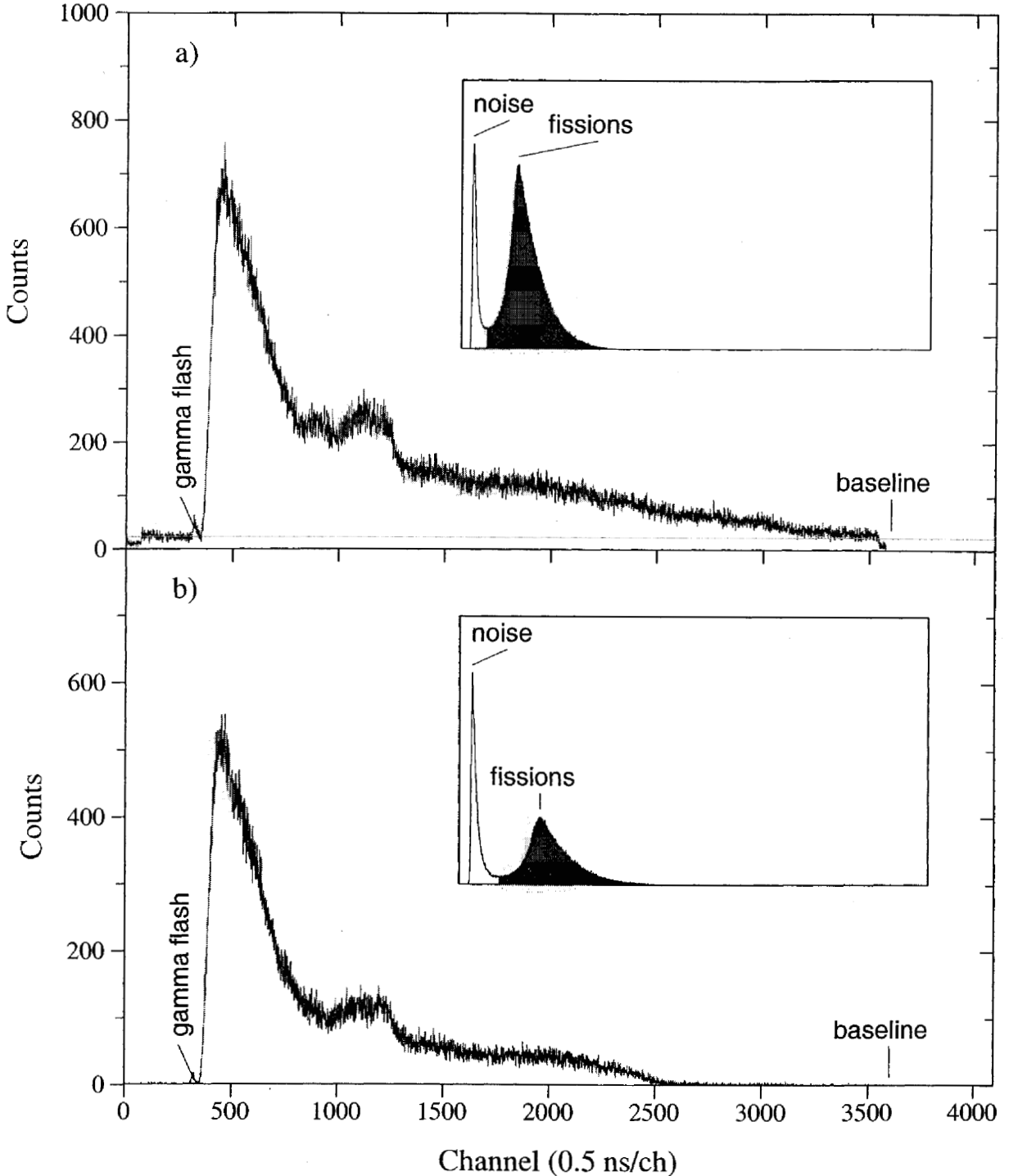


FIG. 3: TOF spectra for a) ^{235}U and b) ^{238}U fission foils from 1998 thin-target data. The baseline background, deduced from the “random” TOF region (before the gamma flash) is drawn and labeled in each case. The baseline is negligible in the case of the ^{238}U foil. The inset shows the pulse-height spectra for the fission foils and the range used to generate the corresponding TOF spectrum is shaded in red.

TABLE III: Energy and neutron flux statistics calculated using equations 3-7 for 15-ns-wide TOF bins from $E_n = 4$ to 20 MeV, and applied to the ^{238}U fission-foil data without baseline subtraction.

Bin	E_{min} (MeV)	E_{max} (MeV)	\bar{E}_n (MeV)	σ_E (MeV)	N_{fc}	N_{nc} (n/MeV)	N_ϕ (γ/b)
1	4.000	4.169	4.088	0.094	1550 \pm 39	(7.786 \pm 0.212) $\times 10^{11}$	(6.637 \pm 0.131) $\times 10^6$
2	4.169	4.349	4.263	0.098	1643 \pm 41	(7.727 \pm 0.206) $\times 10^{11}$	(6.733 \pm 0.133) $\times 10^6$
3	4.349	4.541	4.453	0.107	1559 \pm 39	(6.876 \pm 0.187) $\times 10^{11}$	(6.856 \pm 0.133) $\times 10^6$
4	4.541	4.746	4.650	0.113	1710 \pm 41	(7.110 \pm 0.186) $\times 10^{11}$	(7.258 \pm 0.139) $\times 10^6$
5	4.746	4.965	4.863	0.120	1796 \pm 42	(7.031 \pm 0.180) $\times 10^{11}$	(7.537 \pm 0.142) $\times 10^6$
6	4.965	5.200	5.086	0.129	1727 \pm 42	(6.350 \pm 0.166) $\times 10^{11}$	(7.536 \pm 0.142) $\times 10^6$
7	5.200	5.452	5.335	0.139	1734 \pm 42	(5.905 \pm 0.154) $\times 10^{11}$	(7.553 \pm 0.142) $\times 10^6$
8	5.452	5.723	5.596	0.149	1895 \pm 44	(5.889 \pm 0.147) $\times 10^{11}$	(7.816 \pm 0.143) $\times 10^6$
9	5.723	6.014	5.875	0.161	1971 \pm 44	(5.375 \pm 0.133) $\times 10^{11}$	(7.903 \pm 0.141) $\times 10^6$
10	6.014	6.328	6.180	0.174	2264 \pm 48	(4.976 \pm 0.116) $\times 10^{11}$	(7.922 \pm 0.133) $\times 10^6$
11	6.328	6.668	6.512	0.187	2847 \pm 53	(4.776 \pm 0.102) $\times 10^{11}$	(8.191 \pm 0.126) $\times 10^6$
12	6.668	7.036	6.863	0.202	3343 \pm 58	(4.634 \pm 0.092) $\times 10^{11}$	(8.404 \pm 0.123) $\times 10^6$
13	7.036	7.436	7.239	0.216	3422 \pm 58	(4.158 \pm 0.082) $\times 10^{11}$	(8.250 \pm 0.120) $\times 10^6$
14	7.436	7.870	7.657	0.244	3091 \pm 56	(3.371 \pm 0.069) $\times 10^{11}$	(7.557 \pm 0.111) $\times 10^6$
15	7.870	8.344	8.127	0.263	3157 \pm 56	(3.129 \pm 0.064) $\times 10^{11}$	(7.497 \pm 0.110) $\times 10^6$
16	8.344	8.863	8.621	0.284	3421 \pm 58	(3.085 \pm 0.061) $\times 10^{11}$	(7.771 \pm 0.113) $\times 10^6$
17	8.863	9.431	9.161	0.315	3235 \pm 57	(2.668 \pm 0.054) $\times 10^{11}$	(7.690 \pm 0.112) $\times 10^6$
18	9.431	10.057	9.760	0.342	3218 \pm 57	(2.432 \pm 0.049) $\times 10^{11}$	(7.599 \pm 0.112) $\times 10^6$
19	10.057	10.747	10.415	0.382	3189 \pm 56	(2.193 \pm 0.044) $\times 10^{11}$	(7.298 \pm 0.108) $\times 10^6$
20	10.747	11.511	11.141	0.418	2880 \pm 54	(1.791 \pm 0.038) $\times 10^{11}$	(6.993 \pm 0.106) $\times 10^6$
21	11.511	12.360	11.951	0.472	2728 \pm 52	(1.526 \pm 0.033) $\times 10^{11}$	(6.552 \pm 0.101) $\times 10^6$
22	12.360	13.307	12.867	0.525	2689 \pm 52	(1.320 \pm 0.028) $\times 10^{11}$	(6.356 \pm 0.098) $\times 10^6$
23	13.307	14.369	13.869	0.589	3026 \pm 55	(1.206 \pm 0.025) $\times 10^{11}$	(6.245 \pm 0.093) $\times 10^6$
24	14.369	15.564	15.012	0.660	3101 \pm 56	(1.017 \pm 0.021) $\times 10^{11}$	(6.157 \pm 0.091) $\times 10^6$
25	15.564	16.916	16.303	0.755	3254 \pm 57	(8.930 \pm 0.181) $\times 10^{10}$	(6.157 \pm 0.090) $\times 10^6$
26	16.916	18.453	17.794	0.873	3525 \pm 59	(8.518 \pm 0.172) $\times 10^{10}$	(6.438 \pm 0.103) $\times 10^6$
27	18.453	20.213	19.433	0.921	3618 \pm 60	(8.494 \pm 0.520) $\times 10^{10}$	(7.226 \pm 0.332) $\times 10^6$

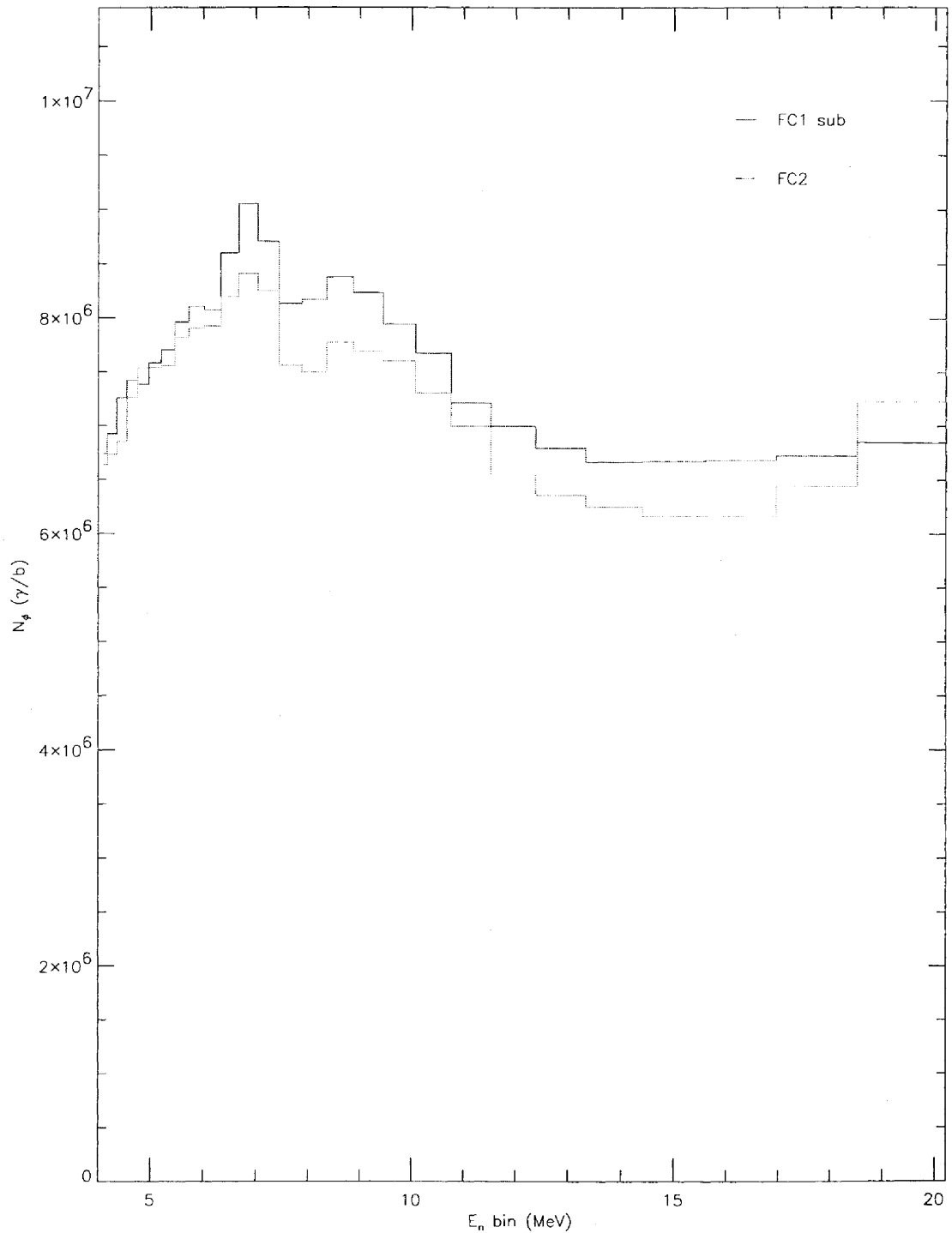


FIG. 4: Comparison between the flux normalizations N_ϕ deduced from the ^{235}U foil with baseline subtraction (denoted by “FC1 sub”) and from the ^{238}U without baseline subtraction (denoted by “FC2”).

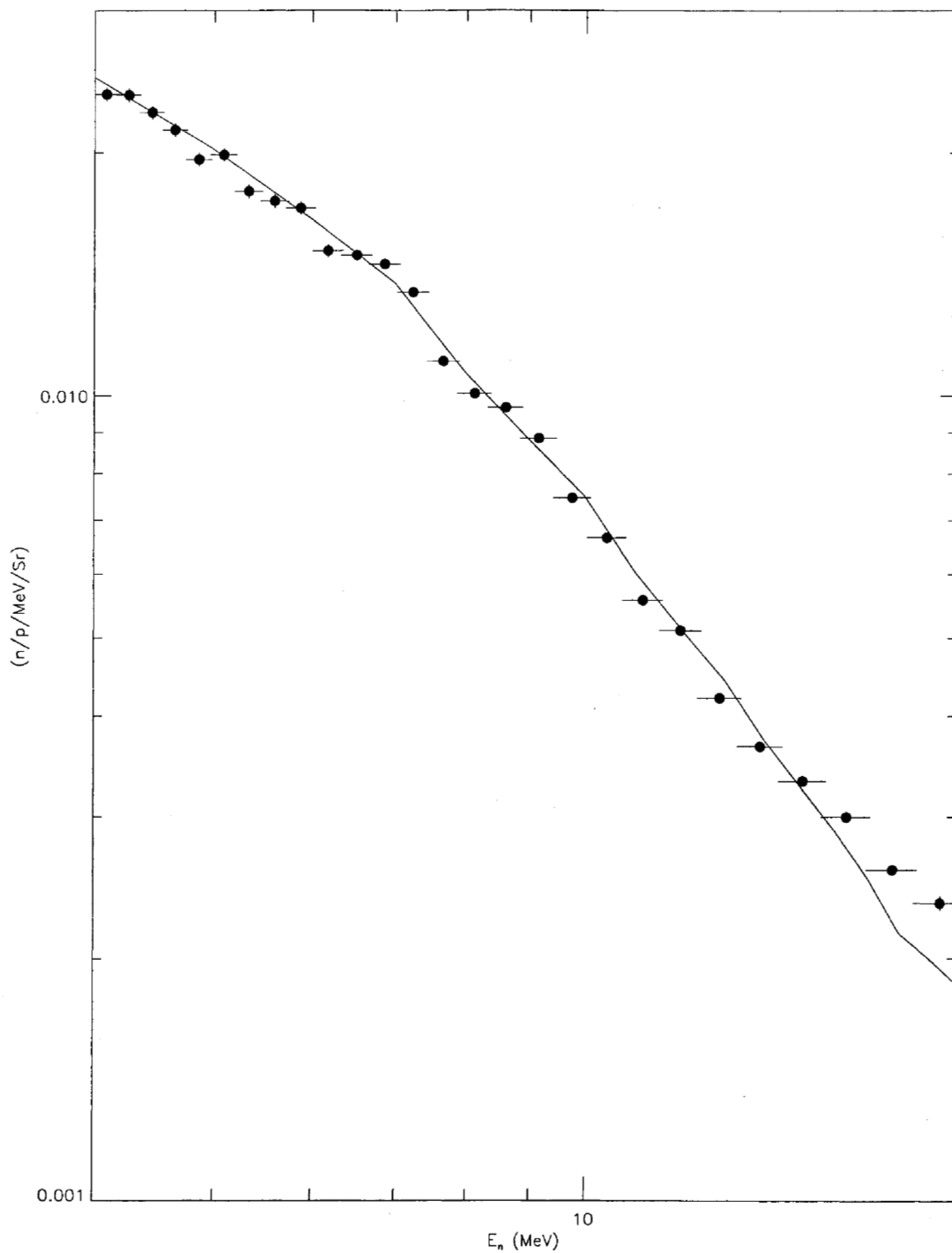


FIG. 5: Comparison between the shapes of the experimentally-deduced neutron flux and its theoretical prediction.

3 Partial Cross-Section Evaluation

Partial γ -ray cross sections were deduced from fitted full-energy peak areas A in a given neutron-energy bin according to the formula:

$$\sigma_{(n,2n\gamma)}(E_n) = \frac{1 + \alpha}{\epsilon_\gamma(1 - f_{ge})} \times \frac{A}{N_\phi} \quad (8)$$

with α the total internal conversion coefficient for the γ ray of interest, ϵ_γ the detection efficiency for that γ ray, f_{ge} ($= 0.4532 \pm 0.0136$) the deadtime fraction for the germanium detectors (in this case the sum of planar detectors), and N_ϕ the flux normalization parameter for the same-energy bin. Values for α and ϵ_γ can be found in reference [9] and are reproduced in table IV. The internal conversion coefficients carry an uncertainty of 6% but the uncertainty on the conversion correction factor $1 + \alpha$ is smaller and becomes negligible for $\alpha \ll 1$. The efficiency correction, which includes the intrinsic detector efficiency and γ -ray attenuation, carries an uncertainty of 5-7%, depending on γ -ray energy. Areas and deduced partial cross sections for the observed yrast lines over a sequence of neutron energy bins from $E_n = 4$ MeV to $E_n = 20$ MeV are listed in table V.

A sample of γ -ray fits at selected neutron energies is shown in figures 6-9 for each line of interest. Note the change in peak area for the γ ray of interest as a function of neutron energy. Though the γ -ray spectrum for each neutron-energy bin is fitted as a whole, the energy range around each γ -ray line presents its own difficulties in the fit and deserves special scrutiny. A brief discussion of the fit for each of the yrast lines follows.

The $4 \rightarrow 2$ transition: an energy of $E_\gamma = 99.993 \pm 2.418$ keV was extracted from the fit, which despite a large uncertainty is in good agreement with the accepted value [10] of 99.853 ± 0.003 keV. The fit for this line in particular presents the greatest challenge. Due to γ -ray absorption in the ^{235}U sample and internal conversion, this is the weakest of the four fitted yrast lines. The fit is also complicated by the proximity ($\Delta E_\gamma = 1.5$ keV) of the $4 \rightarrow 2$ line to the U K_{α_1} x-ray, the second strongest line in the entire spectrum. In addition, this transition is flanked on either side by satellite peaks, within detector resolution. The lower- E_γ contaminant at $E_\gamma = 99.3$ keV is a known transition in the decay daughter nucleus ^{231}Pa . The higher- E_γ contaminant at $E_\gamma = 100.6$ keV is unidentified, but likely due to a fission-fragment de-excitation, based on the shape of its excitation function.

The $6 \rightarrow 4$ transition: the extracted energy of $E_\gamma = 152.660 \pm 0.111$ keV agrees well with the accepted value [10] of 152.720 ± 0.002 keV. The fit for this peak is undoubtedly the most reliable of the four discussed here. Strong well-known peaks from ^{231}Th $\Delta E_\gamma = 8.9$ keV below and 10.7 keV above the $6 \rightarrow 4$ transition energy provide an excellent calibration of the peak-shape parameters. The background in this region is linear and well-behaved. The only possible contaminant is an $E_\gamma = 151.7$ keV transition in ^{102}Zr which is easily resolved from the line of interest.

The $8 \rightarrow 6$ transition: here also, the measured energy of $E_\gamma = 200.961 \pm 0.111$ keV is well within error of the accepted value [10] of 200.97 ± 0.03 . While in general quite good, this fit is complicated by two independent factors. First, the $8 \rightarrow 6$ transition is located $\Delta E_\gamma = 15.3$ keV higher in γ -ray energy than the strongest peak in the entire spectrum, an $E_\gamma = 185.7$ keV transition in ^{231}Th . Though these two peaks are sufficiently far apart to be resolved, the 185.7-keV line possesses a long high-energy tail which affects the background fit in the vicinity of the $8 \rightarrow 6$ peak. If that tail is not properly modeled, the fitted $8 \rightarrow 6$ peak area could be slightly affected. A second difficulty in fitting this line comes from its close proximity ($\Delta E_\gamma = 1.1$ keV) to an $E_\gamma = 202.1$ keV transition in ^{231}Th .

The $10 \rightarrow 8$ transition: the measured energy $E_\gamma = 244.405 \pm 2.626$ keV and accepted value [10] of 244.2 ± 0.5 keV both carry large uncertainties, but agree nonetheless. The principal difficulty encountered in this fit is due to the fact that it is most consistent with two closely-spaced peaks ($\Delta E_\gamma = 0.5$ keV) at the location of the $10 \rightarrow 8$ transition. The reliability of this assignment will be revisited in the discussion of the analysis of the 1999 GEANIE data (section VII A 2), which was acquired with superior channel dispersion in the ADC modules.

These qualitative descriptions suggest a hierarchy in the reliability of the individual fits, with the $6 \rightarrow 4$ peak modeled best, followed by the $8 \rightarrow 6$ peak fit, and with the $4 \rightarrow 2$ and $10 \rightarrow 8$ peak fits being the most problematic.

TABLE IV: Internal conversion coefficients (α) and efficiencies (ϵ_γ) used in the analysis of the **98**Thin data.

Transition	α	ϵ_γ
$4 \rightarrow 2$	13.7(8)	0.0237(13)
$6 \rightarrow 4$	2.192(132)	0.0154(10)
$8 \rightarrow 6$	0.7508(450)	0.0151(8)
$10 \rightarrow 8$	0.3754(225)	0.0132(6)

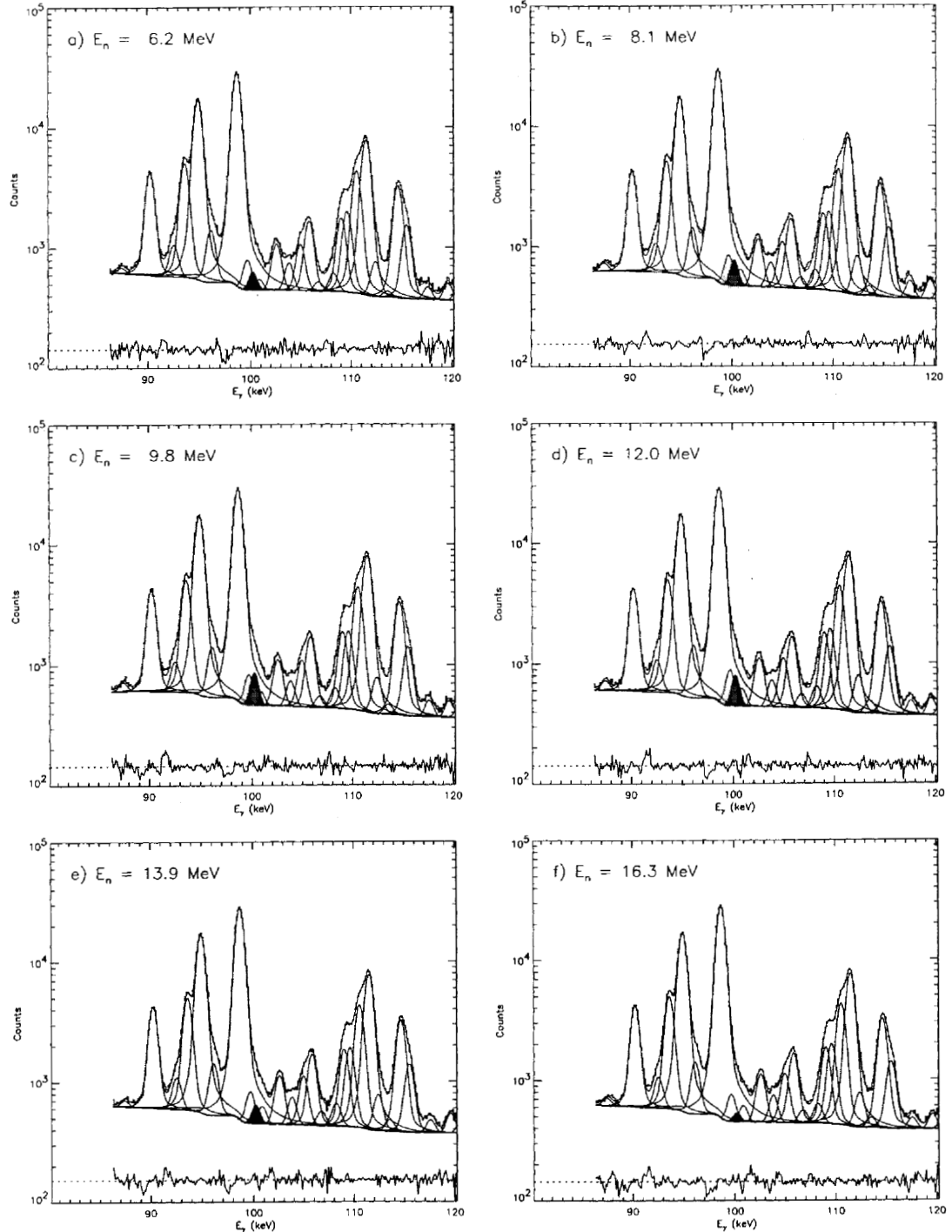


FIG. 6: Fits for the ^{234}U $4_1^+ \rightarrow 2_1^+$ transition in selected neutron-energy cuts of the GEANIE 1998 thin-target data. The $4_1^+ \rightarrow 2_1^+$ peak is shaded in red. The relative fit residual is plotted on an arbitrary scale.

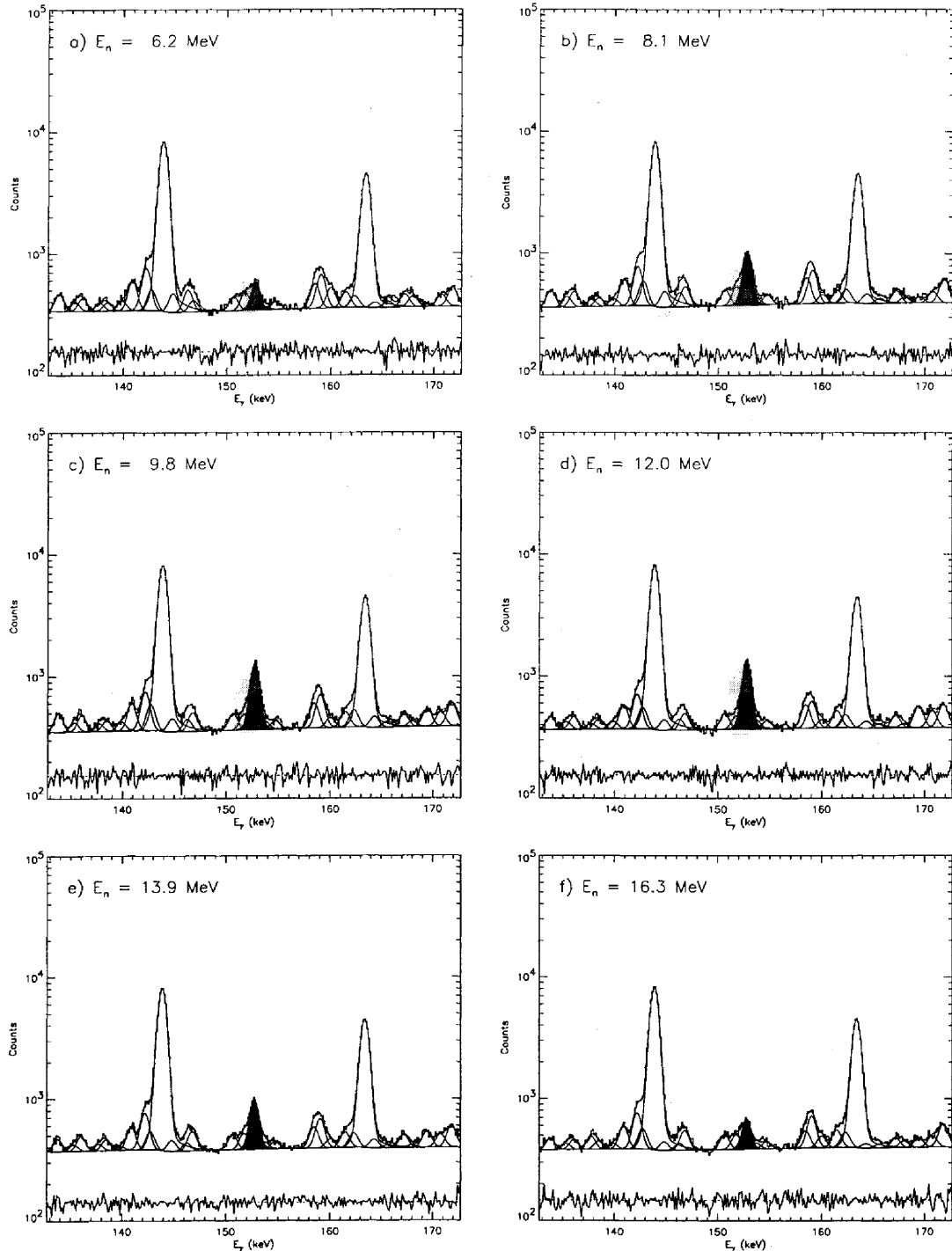


FIG. 7: Fits for the ^{234}U $6_1^+ \rightarrow 4_1^+$ transition in selected neutron-energy cuts of the GEANIE 1998 thin-target data. The $6_1^+ \rightarrow 4_1^+$ peak is shaded in red. The relative fit residual is plotted on an arbitrary scale.

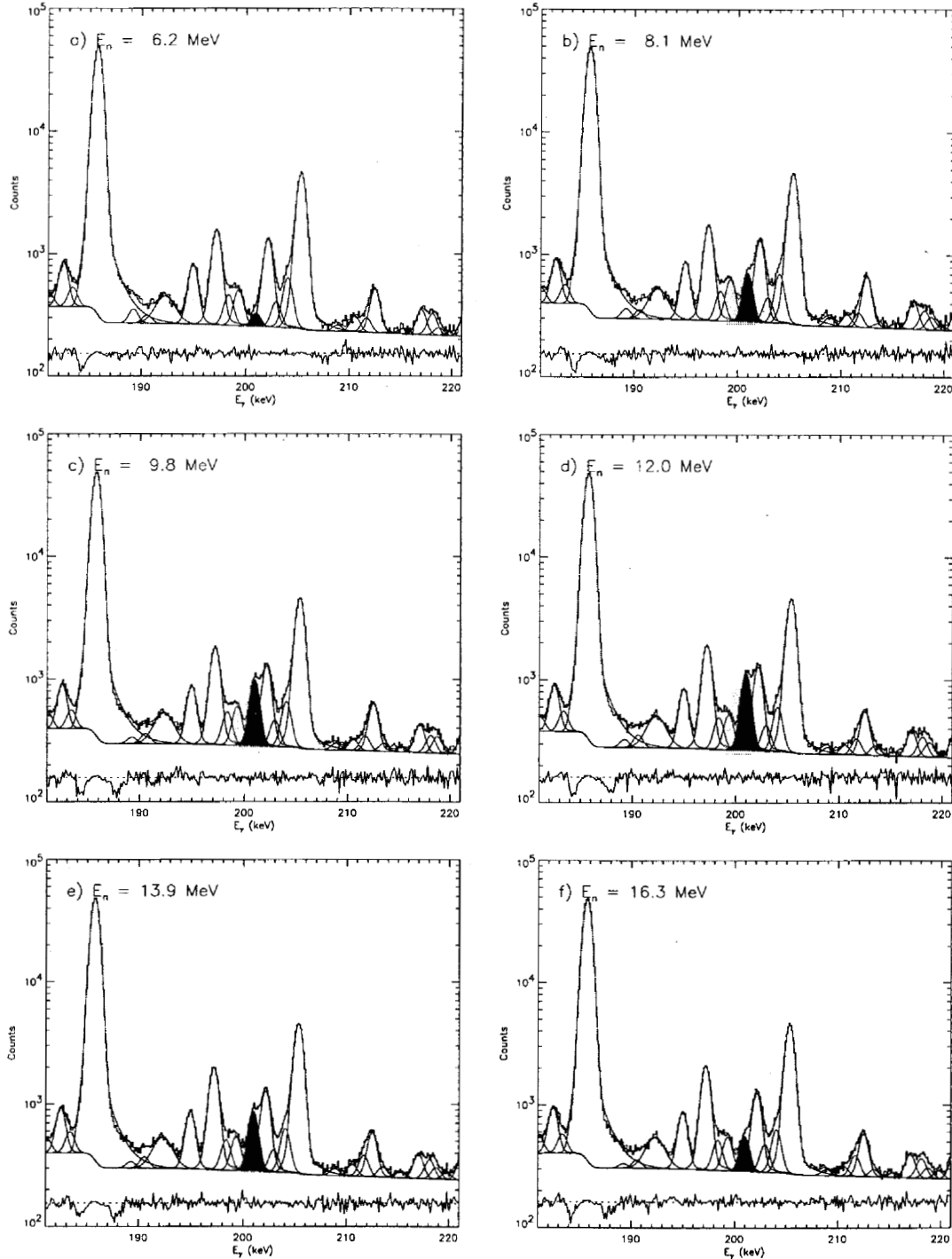


FIG. 8: Fits for the ^{234}U $8_1^+ \rightarrow 6_1^+$ transition in selected neutron-energy cuts of the GEANIE 1998 thin-target data. The $8_1^+ \rightarrow 6_1^+$ peak is shaded in red. The relative fit residual is plotted on an arbitrary scale.

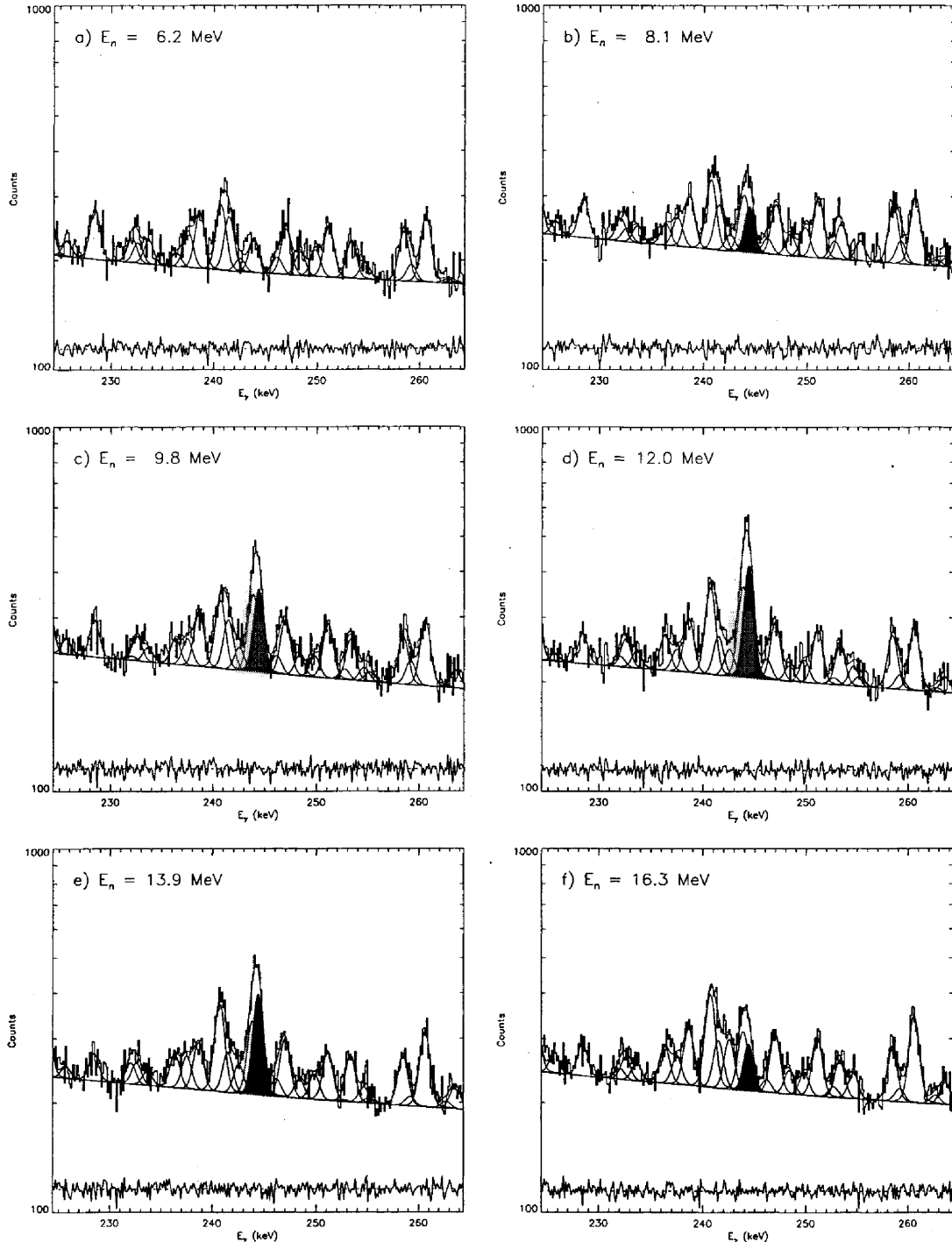


FIG. 9: Fits for the ^{234}U $10_1^+ \rightarrow 8_1^+$ transition in selected neutron-energy cuts of the GEANIE 1998 thin-target data. The $10_1^+ \rightarrow 8_1^+$ peak is shaded in red. The relative fit residual is plotted on an arbitrary scale.

The partial cross sections listed in table V are plotted and compared to GNASH predictions in figure 10. The agreement with GNASH seems best for the $6 \rightarrow 4$ transition, followed in order by the $8 \rightarrow 6$, $4 \rightarrow 2$, and $10 \rightarrow 8$ excitation functions. Though there is clear disagreement in magnitude, the shape of the $6 \rightarrow 4$ and $8 \rightarrow 6$ measured and predicted excitation functions agree from threshold to peak cross section. For the $4 \rightarrow 2$ transition, the experimental cross section shows a rapid rise immediately after threshold, in agreement with the GNASH calculation, but appears flatter near peak cross section than predicted. The $10 \rightarrow 8$ excitation function displays the most striking deviation from GNASH calculations, in both shape and overall magnitude. The measured overall magnitude is roughly 3 times lower than GNASH predictions and the peak cross section occurs ≈ 2 MeV lower in neutron energy. It is not clear from these data alone whether the discrepancies are due to difficulties in the data analysis, such as the ones discussed above, or to a failing of the model. However it should be pointed out that the $10 \rightarrow 8$ transition is weakly populated in both the GNASH calculation and in the GEANIE data. For example, at $E_n = 14$ MeV, GNASH predicts that the $10 \rightarrow 8$ partial cross section represents 33.7% of the $(n,2n)$ reaction cross section, compared to 72.3% for the $6 \rightarrow 4$ transition. For weak transitions such as the $10 \rightarrow 8$ γ -ray, small effects in the cross-section calculation become important, and it is therefore not surprising that the agreement between theory and experiment is not as good as in the case of the stronger lines.

The fits presented in this section, normalized using a flux deduced from the baseline-subtracted ^{235}U fission-foil counts are taken as the best estimate of the partial cross sections from the 1998 GEANIE data. The remainder of this paper is concerned with quantifying the best values and degree of reliability of the partial cross sections measured using this technique.

TABLE V: Fitted raw (i.e. without random-TOF subtraction) areas and deduced partial γ -ray cross sections for the $4 \rightarrow 2$, $6 \rightarrow 4$, $8 \rightarrow 6$, and $10 \rightarrow 8$ transitions. Quoted uncertainties represent random fluctuations only. The counts were normalized using ^{235}U fission foil data with baseline subtraction.

Bin	$A(4_1^+ \rightarrow 2_1^+)$	$\sigma_{4_1^+ \rightarrow 2_1^+}(b)$	$A(6_1^+ \rightarrow 4_1^+)$	$\sigma_{6_1^+ \rightarrow 4_1^+}(b)$	$A(8_1^+ \rightarrow 6_1^+)$	$\sigma_{8_1^+ \rightarrow 6_1^+}(b)$	$A(10_1^+ \rightarrow 8_1^+)$	$\sigma_{10_1^+ \rightarrow 8_1^+}(b)$
1	0 ± 0	0.000 ± 0.000	223 ± 73	0.013 ± 0.004	177 ± 71	0.006 ± 0.002	121 ± 78	0.003 ± 0.002
2	56 ± 198	0.009 ± 0.032	212 ± 73	0.012 ± 0.004	58 ± 70	0.002 ± 0.002	43 ± 77	0.001 ± 0.002
3	3 ± 70	0.000 ± 0.011	237 ± 74	0.012 ± 0.004	266 ± 73	0.008 ± 0.002	200 ± 79	0.005 ± 0.002
4	4 ± 75	0.001 ± 0.011	146 ± 73	0.007 ± 0.004	1 ± 20	0.000 ± 0.001	0 ± 0	0.000 ± 0.000
5	0 ± 22	0.000 ± 0.003	214 ± 74	0.011 ± 0.004	207 ± 73	0.006 ± 0.002	0 ± 0	0.000 ± 0.000
6	469 ± 210	0.070 ± 0.031	318 ± 76	0.016 ± 0.004	40 ± 74	0.001 ± 0.002	26 ± 80	0.001 ± 0.002
7	590 ± 212	0.087 ± 0.031	231 ± 75	0.011 ± 0.004	144 ± 74	0.004 ± 0.002	135 ± 82	0.003 ± 0.002
8	572 ± 211	0.082 ± 0.030	343 ± 78	0.016 ± 0.004	27 ± 69	0.001 ± 0.002	0 ± 1	0.000 ± 0.000
9	377 ± 213	0.053 ± 0.030	820 ± 83	0.038 ± 0.004	117 ± 75	0.003 ± 0.002	0 ± 0	0.000 ± 0.000
10	1495 ± 219	0.210 ± 0.031	2015 ± 93	0.095 ± 0.005	677 ± 80	0.018 ± 0.002	0 ± 0	0.000 ± 0.000
11	2035 ± 226	0.269 ± 0.030	3350 ± 104	0.148 ± 0.005	1775 ± 90	0.044 ± 0.002	106 ± 87	0.002 ± 0.002
12	1838 ± 227	0.231 ± 0.029	4162 ± 110	0.174 ± 0.005	2342 ± 96	0.055 ± 0.002	213 ± 91	0.004 ± 0.002
13	2327 ± 230	0.304 ± 0.030	4970 ± 114	0.216 ± 0.005	3043 ± 100	0.074 ± 0.003	456 ± 94	0.010 ± 0.002
14	2233 ± 227	0.312 ± 0.032	5076 ± 115	0.237 ± 0.006	3292 ± 101	0.086 ± 0.003	504 ± 95	0.012 ± 0.002
15	2502 ± 231	0.348 ± 0.032	5653 ± 118	0.263 ± 0.006	3949 ± 106	0.102 ± 0.003	700 ± 100	0.016 ± 0.002
16	2619 ± 234	0.355 ± 0.032	6751 ± 124	0.306 ± 0.006	5316 ± 114	0.134 ± 0.003	929 ± 102	0.021 ± 0.002
17	2686 ± 233	0.371 ± 0.032	7114 ± 126	0.328 ± 0.007	5765 ± 116	0.148 ± 0.003	1380 ± 108	0.032 ± 0.003
18	3211 ± 233	0.460 ± 0.034	7726 ± 129	0.369 ± 0.007	6491 ± 120	0.173 ± 0.004	1434 ± 109	0.035 ± 0.003
19	2835 ± 233	0.420 ± 0.035	7833 ± 129	0.387 ± 0.008	7088 ± 122	0.196 ± 0.004	1788 ± 112	0.045 ± 0.003
20	2557 ± 230	0.403 ± 0.037	8267 ± 131	0.435 ± 0.008	7661 ± 124	0.225 ± 0.004	2011 ± 114	0.053 ± 0.003
21	2836 ± 231	0.461 ± 0.038	8238 ± 131	0.447 ± 0.009	7940 ± 125	0.240 ± 0.005	2065 ± 114	0.056 ± 0.003
22	2625 ± 226	0.439 ± 0.038	7022 ± 125	0.392 ± 0.008	7136 ± 122	0.222 ± 0.004	2054 ± 114	0.058 ± 0.003
23	1589 ± 222	0.271 ± 0.038	4929 ± 115	0.281 ± 0.007	5404 ± 113	0.172 ± 0.004	1833 ± 112	0.053 ± 0.003
24	1161 ± 217	0.198 ± 0.037	3414 ± 106	0.194 ± 0.006	3626 ± 104	0.115 ± 0.004	1185 ± 105	0.034 ± 0.003
25	693 ± 216	0.118 ± 0.037	2361 ± 99	0.134 ± 0.006	2467 ± 97	0.078 ± 0.003	732 ± 101	0.021 ± 0.003
26	373 ± 215	0.063 ± 0.036	1905 ± 96	0.107 ± 0.006	2076 ± 94	0.065 ± 0.003	472 ± 98	0.013 ± 0.003
27	8 ± 210	0.001 ± 0.035	1708 ± 95	0.095 ± 0.005	1694 ± 92	0.052 ± 0.003	429 ± 99	0.012 ± 0.003

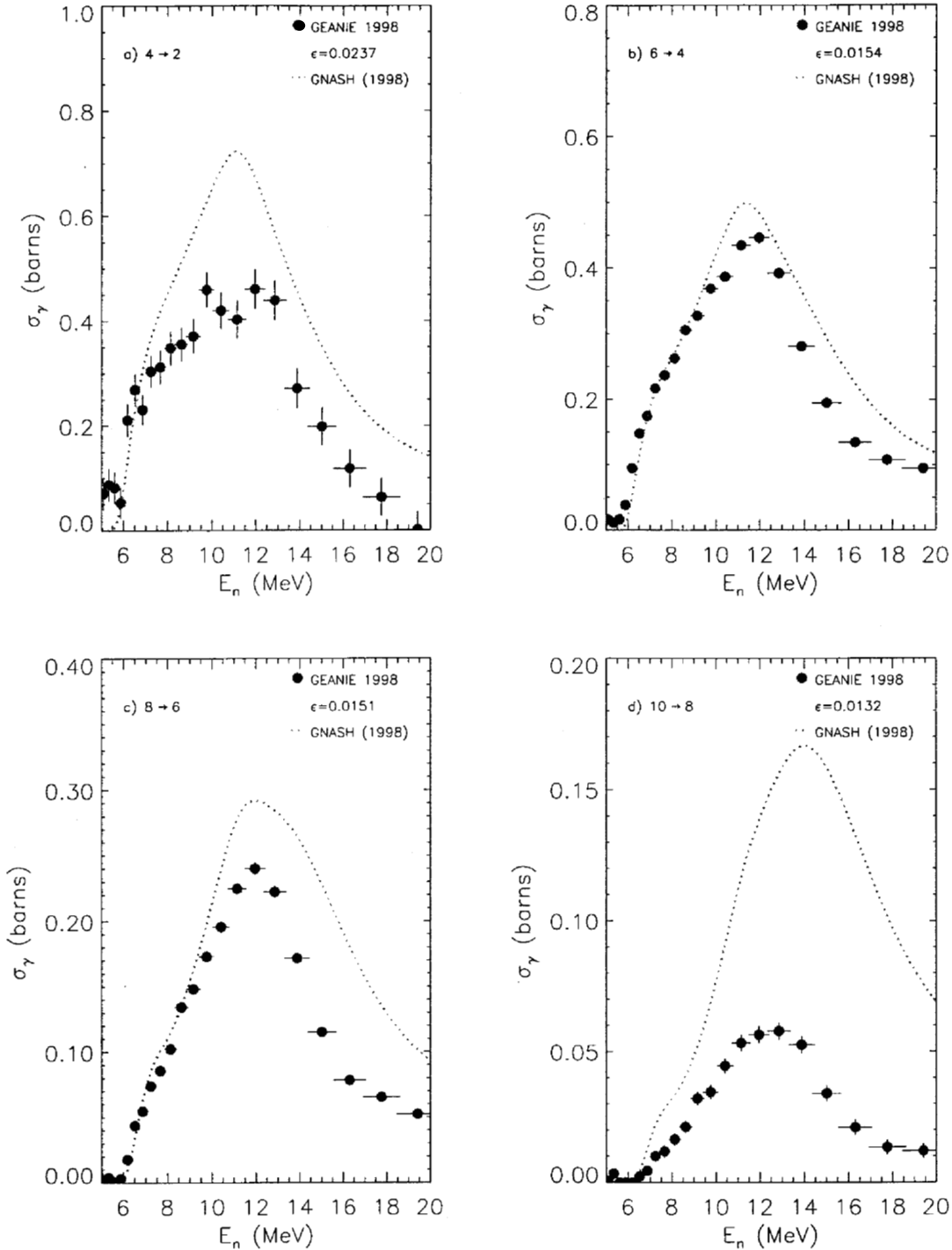


FIG. 10: Excitation functions for the ^{234}U a) $4_1^+ \rightarrow 2_1^+$, b) $6_1^+ \rightarrow 4_1^+$, c) $8_1^+ \rightarrow 6_1^+$ and d) $10_1^+ \rightarrow 8_1^+$ transitions, constructed from the GEANIE 1998 thin-target data. Only statistical errors are included. Fission-chamber data from the ^{235}U foil with a flat baseline subtraction were used to generate these yields. The detector efficiency used is quoted in each case.

B Analysis of Background-Subtracted Data

A background for the fitted γ -ray spectra can be generated from a gate on the random-TOF region of the TOF axis (i.e. before the arrival time of the γ flash). Contaminant peaks are greatly reduced in the resulting background-subtracted γ -ray spectra, and the lines of interest are more easily extracted. However this procedure necessarily lowers the overall statistics in the spectrum and increases statistical fluctuations in peak counts. As a result, fitted peak areas from a background-subtracted spectrum are not always more reliable than those extracted from an unsubtracted spectrum. Nonetheless, comparison of fits to subtracted and unsubtracted spectra can accentuate the effect of contaminant peaks and inadequate modeling of the continuum background. A comparison between fits to raw and random-TOF-subtracted spectra in the region of the $6 \rightarrow 4$ peak is shown in figure 11. The background subtraction virtually eliminates the strong contaminant peaks at $E_\gamma = 143.8$ and 163.4 keV produced by the decay daughter ^{231}Th . With the elimination of the contaminant peaks, the $6 \rightarrow 4$ peak is more prominent in the background-subtracted spectrum, however individual channels in this spectrum show a good deal of statistical fluctuation.

The individual background-subtracted TOF cuts were fitted using XGAM with the same parameters used for unsubtracted spectra (see table I). Fitted background-subtracted areas for the yrast transitions of interest and their corresponding partial cross sections are listed in table VI and plotted in figure 16, with their GNASH predictions. The ^{235}U -foil flux normalization quoted in table II was used. The corresponding fits are shown in figures 12-15. Background-subtracted and unsubtracted excitation functions are compared in figure 17. Only the $4 \rightarrow 2$ and $8 \rightarrow 6$ transitions appear to be affected by the background subtraction. For the $4 \rightarrow 2$ transition, the partial yields are systematically increased by the background subtraction, which might indicate a reduction in contamination, while the partial yields for the $8 \rightarrow 6$ are reduced by the procedure, indicating perhaps that the overall background is underestimated in the unsubtracted fits. In either case, the error bars from subtracted and unsubtracted data overlap and the effect of the background subtraction is small.

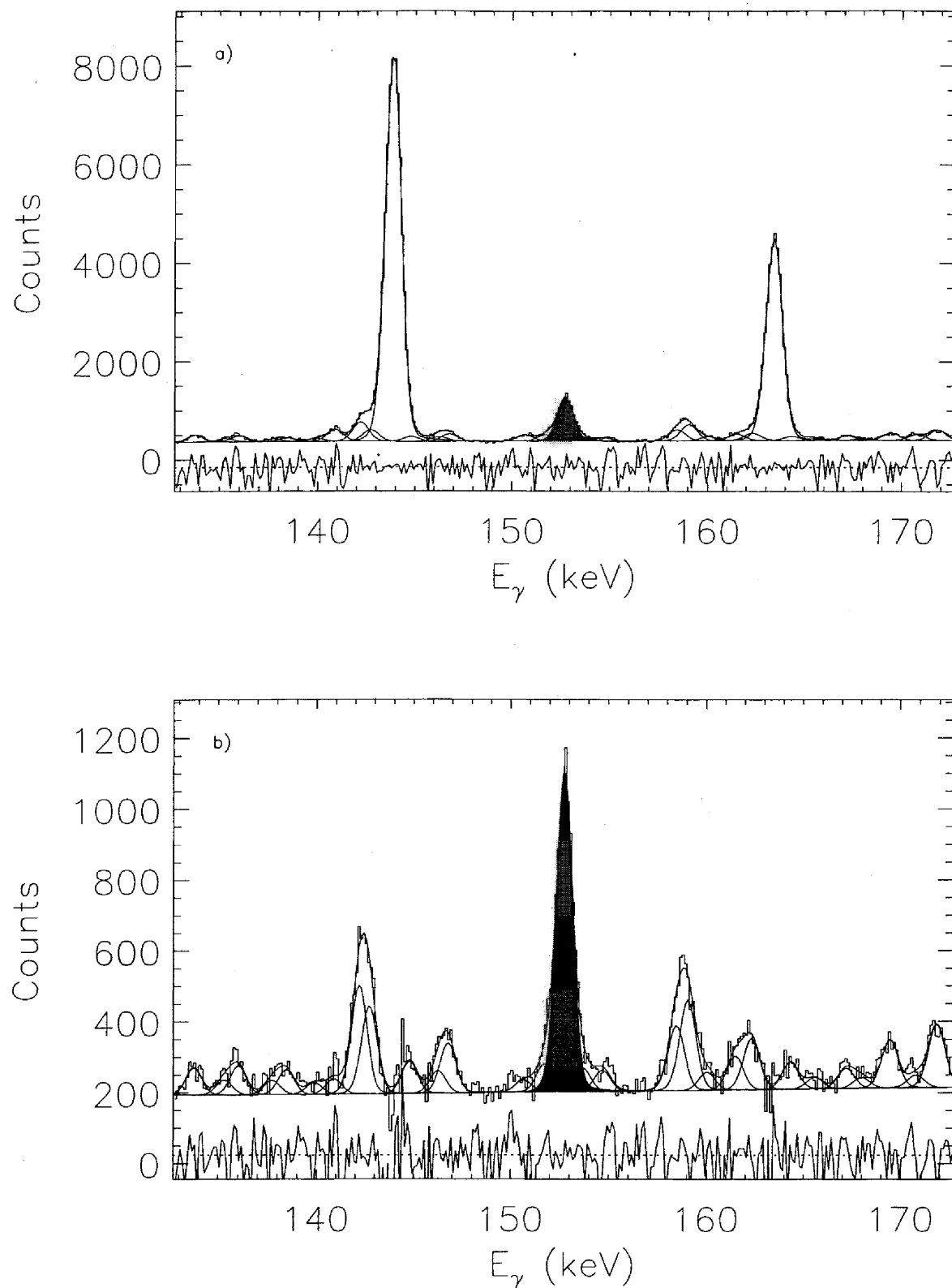


FIG. 11: Comparison of fits to a) the raw (unsubtracted) spectrum and b) the random-TOF-subtracted spectrum corresponding to $E_n = 12.0$ MeV in the region of the $6 \rightarrow 4$ peak (shaded in red).

TABLE VI: Fitted random-TOF-subtracted areas and deduced partial γ -ray cross sections for the $4 \rightarrow 2$, $6 \rightarrow 4$, $8 \rightarrow 6$, and $10 \rightarrow 8$ transitions. Quoted uncertainties represent random fluctuations only. The counts were normalized using ^{235}U fission foil data with baseline subtraction.

Bin	$A(4_1^+ \rightarrow 2_1^+)$	$\sigma_{4_1^+ \rightarrow 2_1^+}(b)$	$A(6_1^+ \rightarrow 4_1^+)$	$\sigma_{6_1^+ \rightarrow 4_1^+}(b)$	$A(8_1^+ \rightarrow 6_1^+)$	$\sigma_{8_1^+ \rightarrow 6_1^+}(b)$	$A(10_1^+ \rightarrow 8_1^+)$	$\sigma_{10_1^+ \rightarrow 8_1^+}(b)$
1	57 \pm 206	0.010 \pm 0.035	197 \pm 74	0.011 \pm 0.004	63 \pm 72	0.002 \pm 0.002	142 \pm 78	0.004 \pm 0.002
2	394 \pm 209	0.065 \pm 0.034	168 \pm 74	0.009 \pm 0.004	0 \pm 0	0.000 \pm 0.000	59 \pm 78	0.002 \pm 0.002
3	293 \pm 211	0.046 \pm 0.033	182 \pm 75	0.010 \pm 0.004	113 \pm 73	0.003 \pm 0.002	217 \pm 71	0.006 \pm 0.002
4	286 \pm 211	0.044 \pm 0.032	91 \pm 73	0.005 \pm 0.004	0 \pm 0	0.000 \pm 0.000	0 \pm 0	0.000 \pm 0.000
5	301 \pm 213	0.046 \pm 0.033	162 \pm 76	0.008 \pm 0.004	69 \pm 74	0.002 \pm 0.002	0 \pm 1	0.000 \pm 0.000
6	779 \pm 215	0.117 \pm 0.032	257 \pm 78	0.013 \pm 0.004	0 \pm 0	0.000 \pm 0.000	43 \pm 81	0.001 \pm 0.002
7	928 \pm 217	0.137 \pm 0.032	174 \pm 76	0.009 \pm 0.004	15 \pm 68	0.000 \pm 0.002	152 \pm 83	0.004 \pm 0.002
8	907 \pm 216	0.130 \pm 0.031	296 \pm 79	0.014 \pm 0.004	0 \pm 0	0.000 \pm 0.000	0 \pm 0	0.000 \pm 0.000
9	694 \pm 218	0.097 \pm 0.031	763 \pm 85	0.036 \pm 0.004	0 \pm 0	0.000 \pm 0.000	0 \pm 0	0.000 \pm 0.000
10	1836 \pm 224	0.259 \pm 0.032	1958 \pm 94	0.092 \pm 0.005	505 \pm 81	0.013 \pm 0.002	0 \pm 1	0.000 \pm 0.000
11	2400 \pm 231	0.317 \pm 0.031	3298 \pm 105	0.145 \pm 0.005	1615 \pm 91	0.040 \pm 0.002	133 \pm 87	0.003 \pm 0.002
12	2189 \pm 232	0.275 \pm 0.029	4105 \pm 110	0.172 \pm 0.005	2169 \pm 96	0.051 \pm 0.002	240 \pm 92	0.005 \pm 0.002
13	2671 \pm 235	0.349 \pm 0.031	4920 \pm 115	0.214 \pm 0.005	2831 \pm 100	0.069 \pm 0.003	480 \pm 95	0.011 \pm 0.002
14	2569 \pm 232	0.359 \pm 0.033	5026 \pm 116	0.234 \pm 0.006	3069 \pm 101	0.080 \pm 0.003	511 \pm 95	0.012 \pm 0.002
15	2863 \pm 236	0.398 \pm 0.033	5601 \pm 119	0.260 \pm 0.006	3719 \pm 106	0.096 \pm 0.003	712 \pm 100	0.017 \pm 0.002
16	2980 \pm 239	0.404 \pm 0.033	6703 \pm 125	0.303 \pm 0.006	5046 \pm 114	0.128 \pm 0.003	940 \pm 103	0.021 \pm 0.002
17	3063 \pm 238	0.423 \pm 0.033	7068 \pm 127	0.326 \pm 0.007	5526 \pm 116	0.142 \pm 0.003	1395 \pm 108	0.032 \pm 0.003
18	3559 \pm 238	0.509 \pm 0.034	7683 \pm 130	0.367 \pm 0.007	6261 \pm 120	0.167 \pm 0.004	1448 \pm 109	0.035 \pm 0.003
19	3214 \pm 237	0.476 \pm 0.035	7785 \pm 129	0.385 \pm 0.008	6850 \pm 122	0.189 \pm 0.004	1810 \pm 113	0.045 \pm 0.003
20	2898 \pm 235	0.457 \pm 0.037	8227 \pm 132	0.433 \pm 0.008	7400 \pm 124	0.217 \pm 0.004	2017 \pm 114	0.053 \pm 0.003
21	3196 \pm 236	0.519 \pm 0.039	8199 \pm 132	0.445 \pm 0.009	7711 \pm 126	0.233 \pm 0.005	2084 \pm 115	0.057 \pm 0.003
22	2973 \pm 231	0.497 \pm 0.039	6980 \pm 126	0.390 \pm 0.008	6860 \pm 123	0.214 \pm 0.004	2066 \pm 114	0.058 \pm 0.003
23	1968 \pm 227	0.336 \pm 0.039	4887 \pm 116	0.278 \pm 0.007	5152 \pm 114	0.164 \pm 0.004	1852 \pm 113	0.053 \pm 0.003
24	1518 \pm 223	0.259 \pm 0.038	3366 \pm 107	0.192 \pm 0.006	3389 \pm 104	0.107 \pm 0.003	1202 \pm 106	0.034 \pm 0.003
25	1054 \pm 221	0.179 \pm 0.038	2323 \pm 100	0.132 \pm 0.006	2233 \pm 97	0.071 \pm 0.003	754 \pm 102	0.022 \pm 0.003
26	748 \pm 220	0.127 \pm 0.037	1856 \pm 97	0.105 \pm 0.006	1816 \pm 94	0.057 \pm 0.003	488 \pm 98	0.014 \pm 0.003
27	364 \pm 220	0.060 \pm 0.037	1673 \pm 96	0.093 \pm 0.005	1460 \pm 92	0.045 \pm 0.003	435 \pm 99	0.012 \pm 0.003

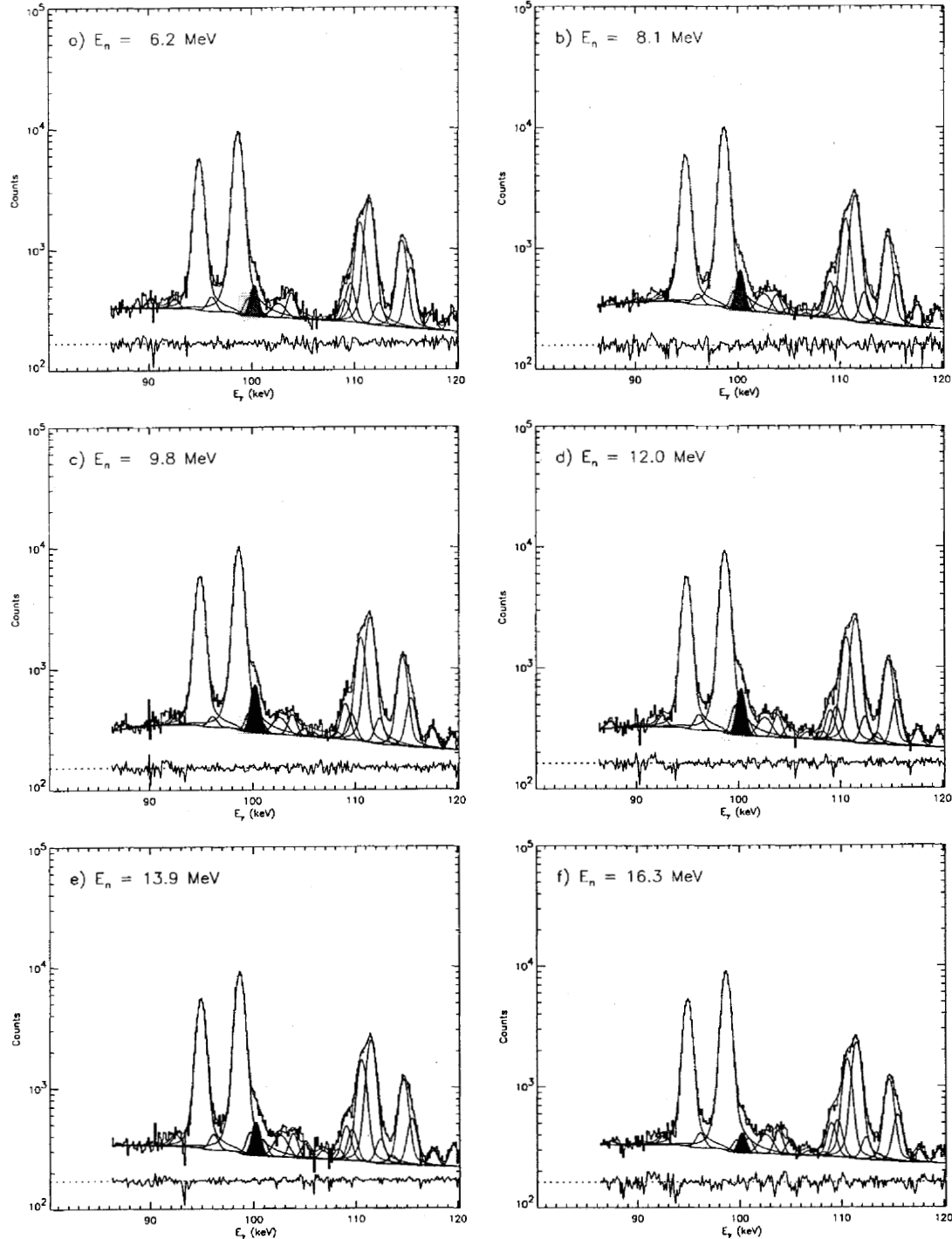


FIG. 12: Fits for the ^{234}U $4_1^+ \rightarrow 2_1^+$ transition in selected neutron-energy cuts of the GEANIE 1998 background-subtracted thin-target data. The $4_1^+ \rightarrow 2_1^+$ peak is shaded in red. The relative fit residual is plotted on an arbitrary scale.

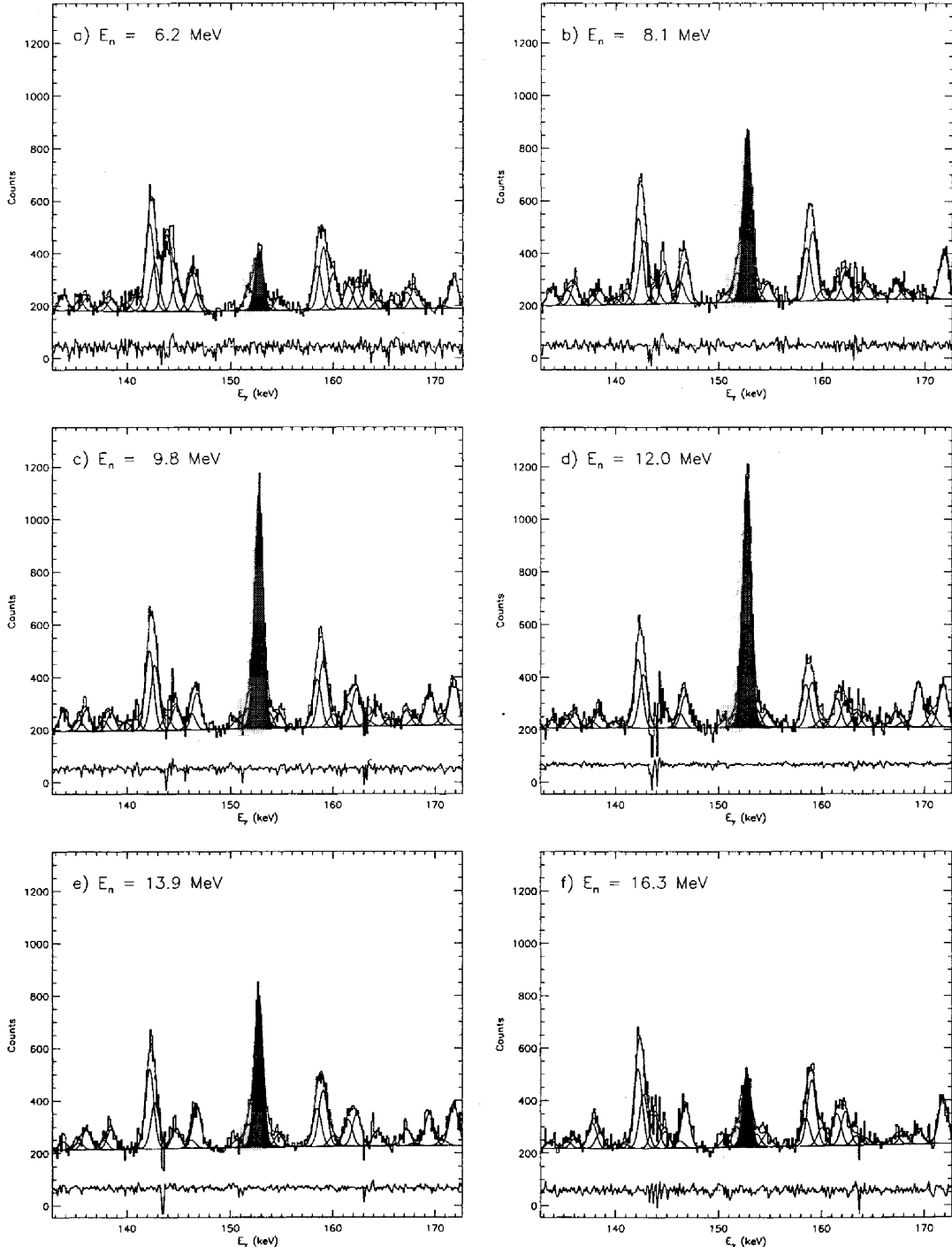


FIG. 13: Fits for the ^{234}U $6_1^+ \rightarrow 4_1^+$ transition in selected neutron-energy cuts of the GEANIE 1998 background-subtracted thin-target data. The $6_1^+ \rightarrow 4_1^+$ peak is shaded in red. The relative fit residual is plotted on an arbitrary scale.

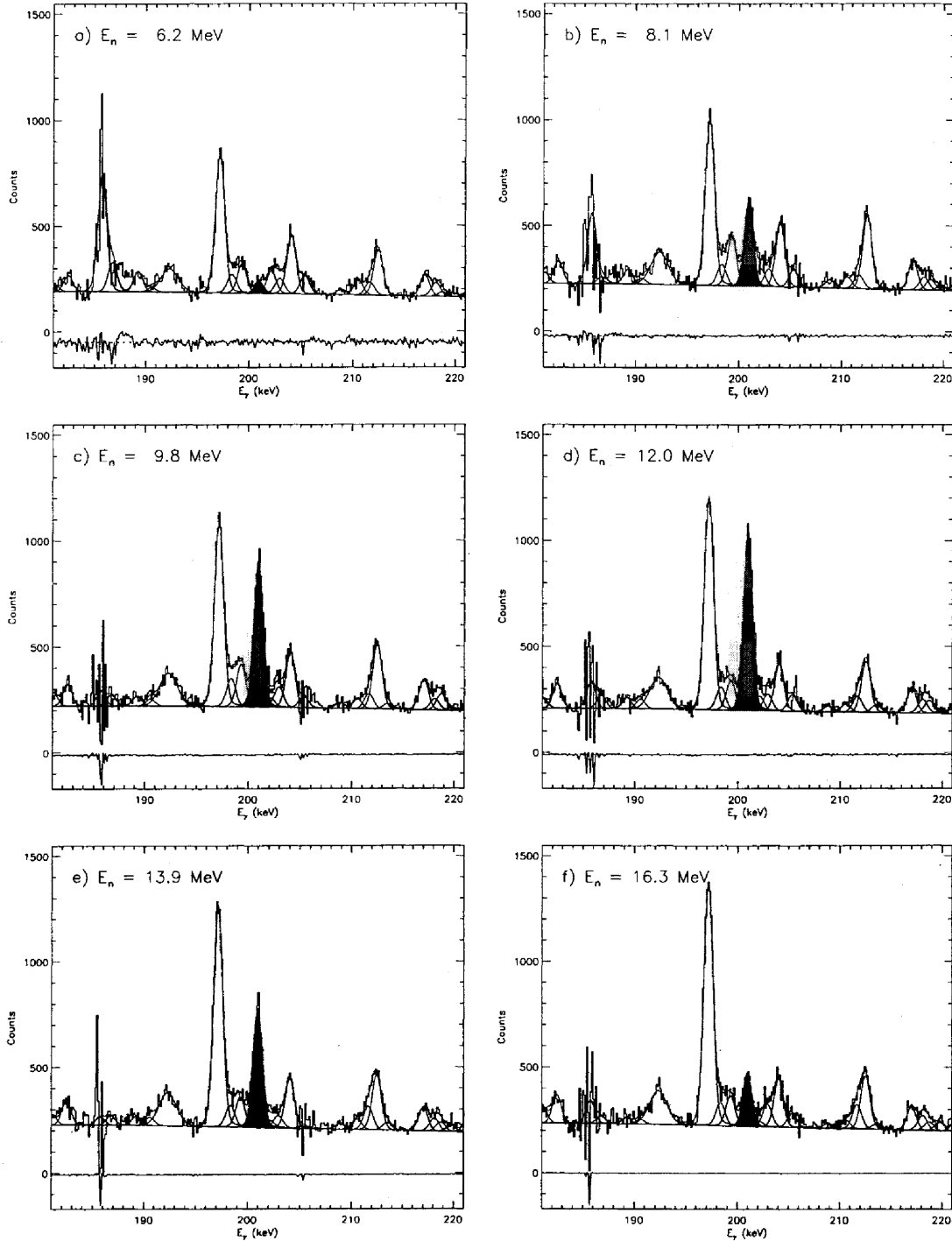


FIG. 14: Fits for the ^{234}U $8_1^+ \rightarrow 6_1^+$ transition in selected neutron-energy cuts of the GEANIE 1998 background-subtracted thin-target data. The $8_1^+ \rightarrow 6_1^+$ peak is shaded in red. The relative fit residual is plotted on an arbitrary scale.

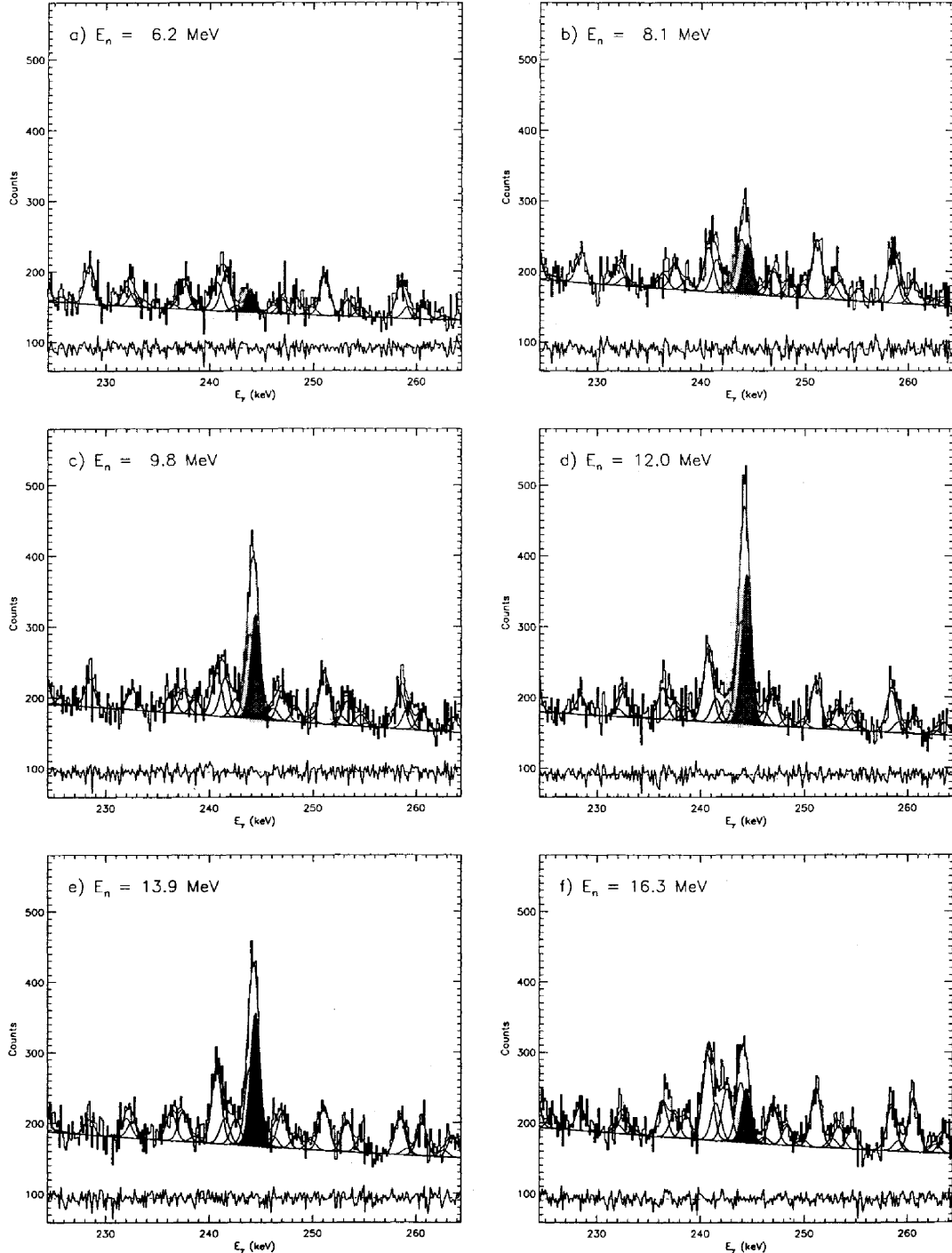


FIG. 15: Fits for the $^{234}\text{U } 10_1^+ \rightarrow 8_1^+$ transition in selected neutron-energy cuts of the GEANIE 1998 background-subtracted thin-target data. The $10_1^+ \rightarrow 8_1^+$ peak is shaded in red. The relative fit residual is plotted on an arbitrary scale.

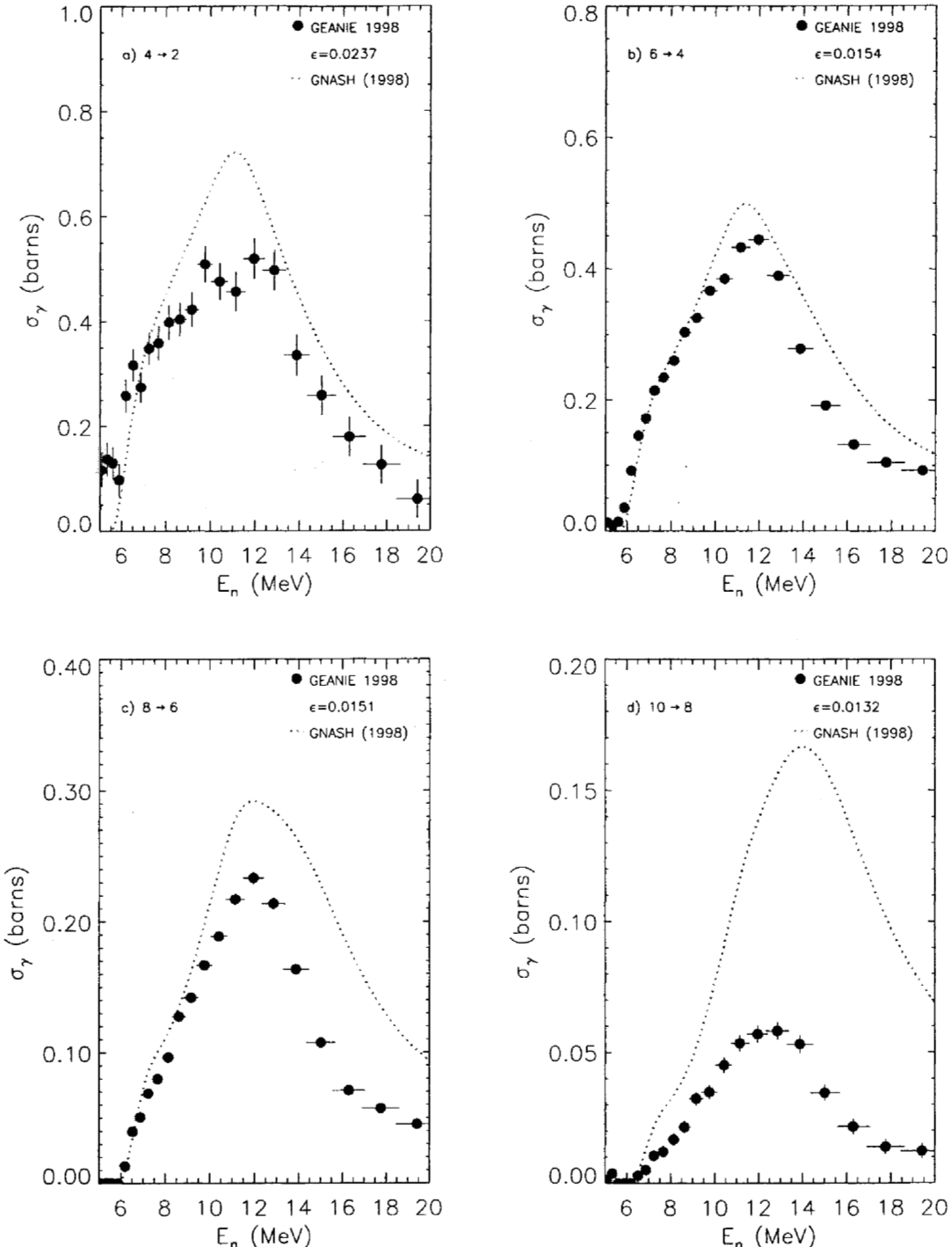


FIG. 16: Excitation functions for the ^{234}U a) $4_1^+ \rightarrow 2_1^+$, b) $6_1^+ \rightarrow 4_1^+$, c) $8_1^+ \rightarrow 6_1^+$ and d) $10_1^+ \rightarrow 8_1^+$ transitions, constructed from the GEANIE 1998 background-subtracted thin-target data. Only statistical errors are included. Fission-chamber data from the ^{235}U foil with a flat baseline subtraction were used to generate these yields. The detector efficiency used is quoted in each case.

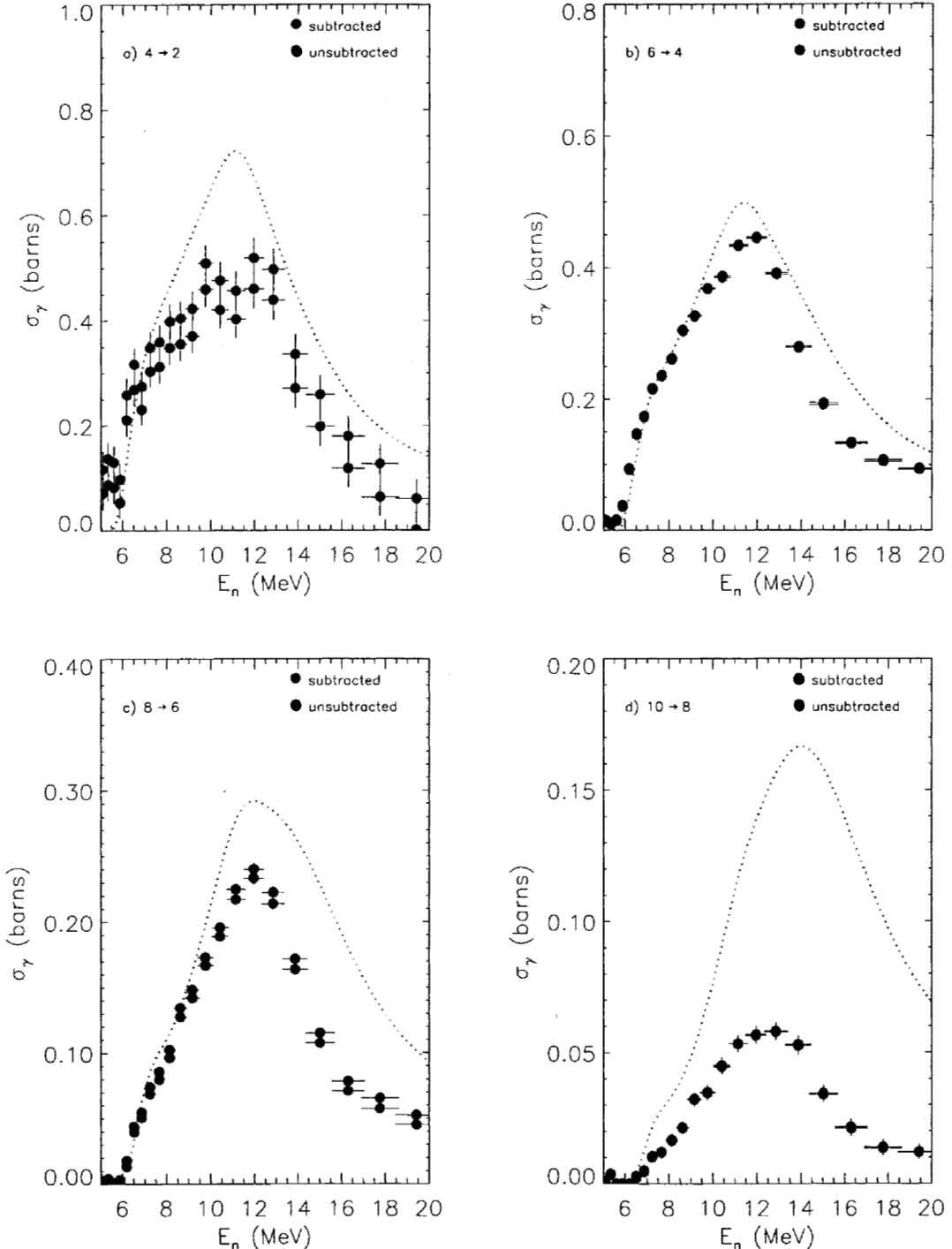


FIG. 17: Comparison of excitation functions for the ^{234}U a) $4_1^+ \rightarrow 2_1^+$, b) $6_1^+ \rightarrow 4_1^+$, c) $8_1^+ \rightarrow 6_1^+$ and d) $10_1^+ \rightarrow 8_1^+$ transitions, with and without random-TOF background subtraction for the GEANIE 1998 thin-target data. The GNASH prediction is shown as a dotted green curve. Only statistical errors are included. Fission-chamber data from the ^{235}U foil with a flat baseline subtraction were used to generate these yields.

III. ESTIMATION OF ENERGY-DEPENDENT SYSTEMATIC UNCERTAINTIES

In addition to random errors due to statistical fluctuations in the data, two sources of systematic errors have been identified in the ^{235}U analysis. One of these, designated as (neutron-) energy-independent uncertainty throughout this report, can be attributed to imprecise knowledge of quantities which only affect the overall magnitude of the partial cross sections (e.g. sample thickness, deadtimes, conversion coefficients, etc.). This class of systematic uncertainty has been carefully quantified by McNabb in reference [9]. The other source of systematic errors, designated as (neutron-) energy-dependent, is more difficult to define and quantify. It can be attributed in part to such factors as beam wrap-around background in the fission chamber counts, and inadequacy of the fitting model used to extract γ -ray peak areas and will in general be different from one neutron-energy bin to the next (hence the name). Because the wrap-around background spectrum could not be measured in this experiment, and because the choice of a fitting model (involving details such as the number of peaks and the continuum-background shape) is ultimately subjective, there is no direct way of assigning a value to the corresponding uncertainties.

We extract an approximate uncertainty for the neutron flux normalization due to unaccounted for wrap-around background by comparing the results from the ^{235}U (with baseline subtraction) and ^{238}U foil data listed in tables II and III. A standard deviation σ_d between the two sets of values for N_ϕ can be calculated using the formulas:

$$d_i \equiv N_\phi^{(i)}(^{238}\text{U}) - N_\phi^{(i)}(^{235}\text{U}) \quad (9)$$

$$\bar{d} \equiv \frac{1}{n} \sum_{i=1}^n d_i \quad (10)$$

$$\sigma_d \equiv \frac{1}{n-1} \sum_{i=1}^n [d_i - \bar{d}]^2 \quad (11)$$

If both fission foils were in perfect agreement, σ_d would be zero. In this case it represents an average residual difference between flux normalizations obtained from either the ^{235}U or ^{238}U fission foil data, which we attribute to improperly subtracted beam-wrap-around background.

The same formulas can be used to extract a systematic uncertainty for the reliability of the fit by comparing peak areas obtained with and without random-TOF-background subtraction, as listed in tables V and VI, respectively. The additional systematic uncertainties calculated with this procedure are summarized in table VII.

TABLE VII: Residual systematic uncertainties for the flux normalization and fitted areas calculated using equation 11. These uncertainties are added in quadrature to the uncertainties in the flux in and individual peak areas at each neutron energy.

Quantity	σ_d
$N_\phi (\gamma/\text{b})$	240366.1
$A(4_1^+ \rightarrow 2_1^+)$	59.8
$A(6_1^+ \rightarrow 4_1^+)$	7.8
$A(8_1^+ \rightarrow 6_1^+)$	78.3
$A(10_1^+ \rightarrow 8_1^+)$	8.3

Several remarks are in order before proceeding further. The first concerns the terminology used. We refer in this section to energy-dependent systematic uncertainties but quote constant (with respect to neutron-energy bins) values in table VII for these. It is important to remember that in this case, the designation “energy-dependent systematic uncertainty” does not refer to an underlying functional energy dependence. Rather it is meant to encompass variations from one neutron-energy bin to the next which cannot be precisely accounted for using the available data. The values listed in table VII approximate these variations with a single number in each case, determined from the fluctuations in all the bins. The second remark concerns some imperfections in the procedure summarized by equations 9-11. Namely, the procedure does not differentiate between discrepancies in the residuals d_i due to the effect we are attempting to quantify (e.g. wrap-around background for the flux normalization and inadequate fit model for the peak areas), from simple random fluctuations due to counting statistics. As a result, the deduced systematic uncertainties are likely slightly over-estimated. This weakness in the procedure could be only be avoided if, in the case of the flux normalization for example, the true N_ϕ values were known and used in equation 9. Then random and systematic deviations from the true exact values could be separated. Finally, we clarify the necessity of dividing uncertainties into random, systematic energy-independent and energy-dependent contributions. This decomposition is of practical

importance, depending on how the GEANIE data are used. Whenever these data are used to extract a shape of the partial cross sections, all neutron-energy-independent factors can be ignored, and only the energy-dependent uncertainties need be considered, along with random fluctuations in the data. Conversely, if both magnitude and shape of the partial γ -ray cross sections are of interest, all three contributions to the uncertainty must be included.

IV. VALIDATION OF THE 1998 RESULTS WITH RESPECT TO ENERGY-DEPENDENT UNCERTAINTIES

At this point in the report the **98Thin** data set has been analyzed by four slightly different means: either raw or random-TOF-subtracted γ -ray data, normalized to a neutron flux extracted from either ^{235}U or ^{238}U fission foil. Because it carries the smallest statistical uncertainties, the raw (unsubtracted) γ -ray data normalized using the ^{235}U foil data with baseline subtraction has been chosen as the optimal combination to extract partial γ -ray cross sections from the **98Thin** measurement. In section III we extracted a systematic uncertainty for these optimal partial cross sections, based on fluctuations in their shapes. However, as discussed in section III, these energy-dependent systematic uncertainties can only be determined approximately. Therefore, in order to check their validity, we compare the optimal partial cross sections to those generated from the remaining three variations on the analysis method, namely using: i) the raw (i.e. unsubtracted) γ -ray data normalized to the ^{238}U fission foil counts and the background-subtracted data normalized to ii) the ^{235}U fission-foil counts with baseline subtraction and iii) the ^{238}U fission foil counts. The differences between these four different treatments of the data are precisely those which led us to extract an additional energy-dependent systematic uncertainty (see section III). The comparison between the optimal results and the other three variations in the analysis is plotted in figure 18 for each γ ray of interest. Each panel in this figure shows the optimal cross section for a single transition of interest, obtained from the raw γ -ray data normalized to ^{235}U fission-foil counts with baseline subtraction and with both random and energy-dependent uncertainties summed in quadrature, as a one-sigma confidence band (dotted line). Overlayed on the same panel are the partial cross sections for that same transition obtained from the other three analysis variants (solid points). Despite fluctuations due to statistics, changes in the spectrum due to background-subtraction, and differences in the normalization obtained from the two fission foils, the plotted one-sigma band gives a good guideline for the variability in the data and its analysis.

In section VI, we consider the total uncertainty for the 1998 data, which must be quoted when both shape and magnitude of the partial cross sections are of interest.

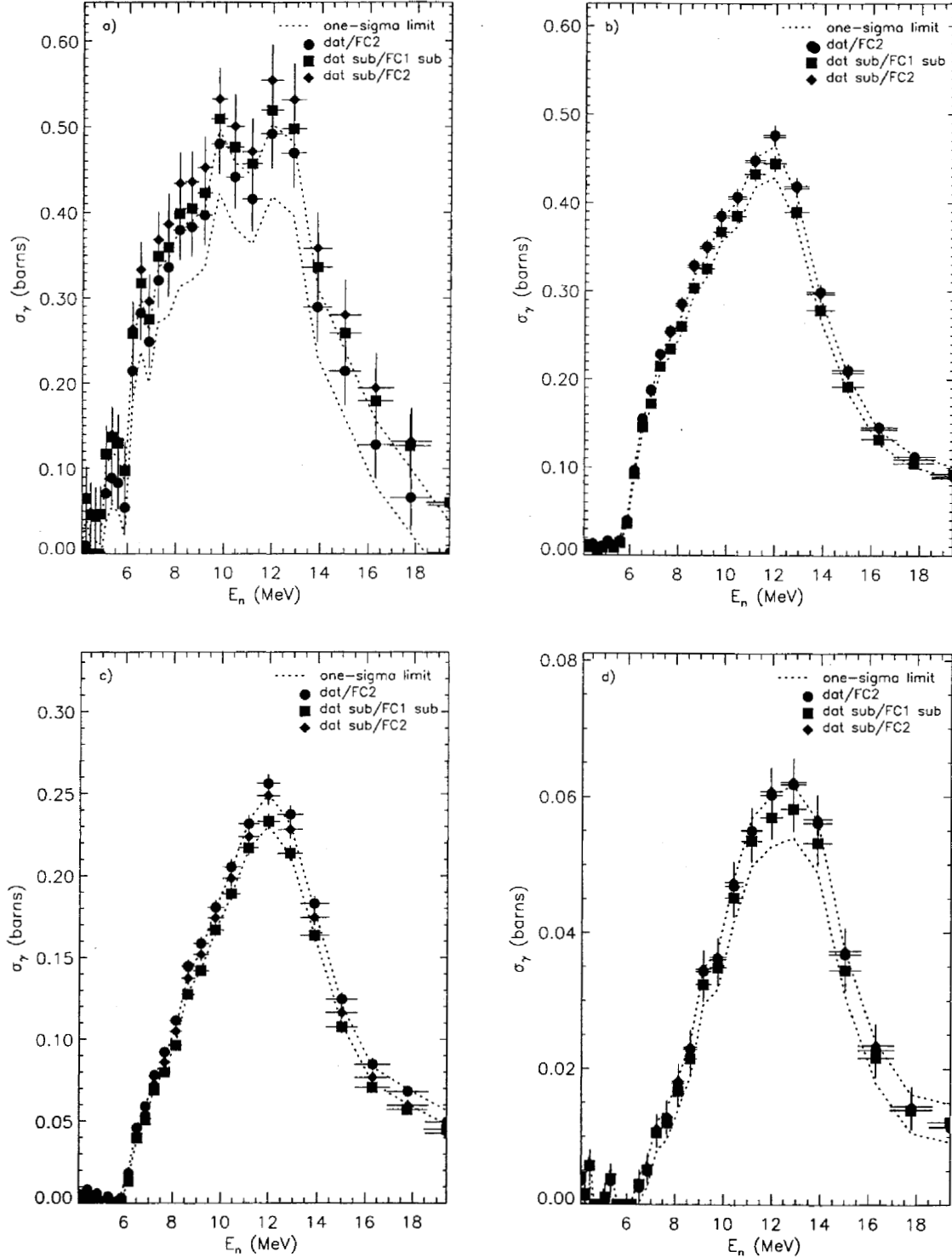


FIG. 18: Validation of the one-sigma confidence band (dotted lines) for the combined random and energy-dependent systematic uncertainties deduced from the unsubtracted 1998 data normalized to ^{235}U fission-foil counts with baseline subtraction. In the legend, raw data are labeled by the symbol “dat”, subtracted data by “dat sub”, ^{235}U -foil normalization with baseline subtraction is denoted by “FC1 sub” and ^{238}U -foil normalization is denoted by “FC2”.

V. GEANIE 1998 THICK-SAMPLE DATA ANALYSIS

Additional data were acquired in 1998 using a thick (24-mil) ^{235}U sample. The experimental details are summarized in the box below.

run label: 98thick

log book pages: #3 pp. 229-232,275-277

run dates: 10/23/98-10/26/98 and 12/6/98-12/12/98

total run time recorded to tape: 718378 s (from 55 Hz pulser)

beam structure:

- rep rate:** 116 Hz (10/23/98-10/26/98), 100 Hz (12/6/98-12/12/98)
- micropulse spacing:** 1.8 μs
- beam gate length:** 625 μs

typical proton current: 2.5 μA

beam absorbers: 1/2" Pb + 1" borated polyethylene

sample areal density corrected for ^{235}U enrichment: $1.002 \pm 0.050 \text{ g/cm}^2$

sample thickness: ≈ 24 mil (4 laminated packages of two 3-mil foils each)

sample atomic assay: 93.2324% ^{235}U + 5.3729% ^{238}U + 1.1339% ^{234}U + 0.2581% ^{236}U

sample orientation: 251° on dial (19° with respect to beam)

sample mask: 0.030"-thick Ta foil (one on each side) 2.25" \times 2.25" with 1"-diameter hole

planar-detector absorbers: none

deadtimes:

- planar-data sum:** $64.62 \pm 1.94 \%$
- coaxial-data sum:** $63.43 \pm 1.90 \%$
- ^{235}U fission foil:** $57.95 \pm 1.74 \%$
- ^{238}U fission foil:** $59.73 \pm 1.79 \%$

average in-beam array rate: 1300 Hz (beam-gated γ -or rate)

average array rate: 1845 Hz (total γ -or rate)

The same fitting model (see table I) was used for these data as for the thin-sample data analysis and was found to produce equally good fits (see e.g. figures 19-22). Only peak heights and background polynomial coefficients were allowed to vary. The thick-sample data have lower statistics in the ($n,2n$) channel for comparable thin-sample run time for two primary reasons: i) the increased amount of material results in greater array deadtime ii) the attenuation for those low-energy γ -rays produced throughout the sample is greater. As a result, the partial cross sections deduced from these data are less reliable than those obtained from the thin-sample data. The $4 \rightarrow 2$ transition is especially difficult to fit in these data and the peak becomes too weak to observe above $E_n = 14$ MeV. However, a comparison of the thin- and thick-sample data sets serves as a validation of the total experimental uncertainty, which includes a sizeable contribution from target-related variability. Therefore, we present the analysis of unsubtracted thick-sample GEANIE data acquired in 1998 (figures 19-22). Next, we extract partial cross sections for the observed yrast transitions using the ^{235}U fission foil normalizations listed in VIII. Note that the normalization parameters N_ϕ listed here are approximately twice those of the same-run-time thin-sample data (table II). This is due to the definition of N_ϕ in equation 4, which includes the sample thickness. The partial cross sections themselves can be found in table IX and are plotted in figure 23.

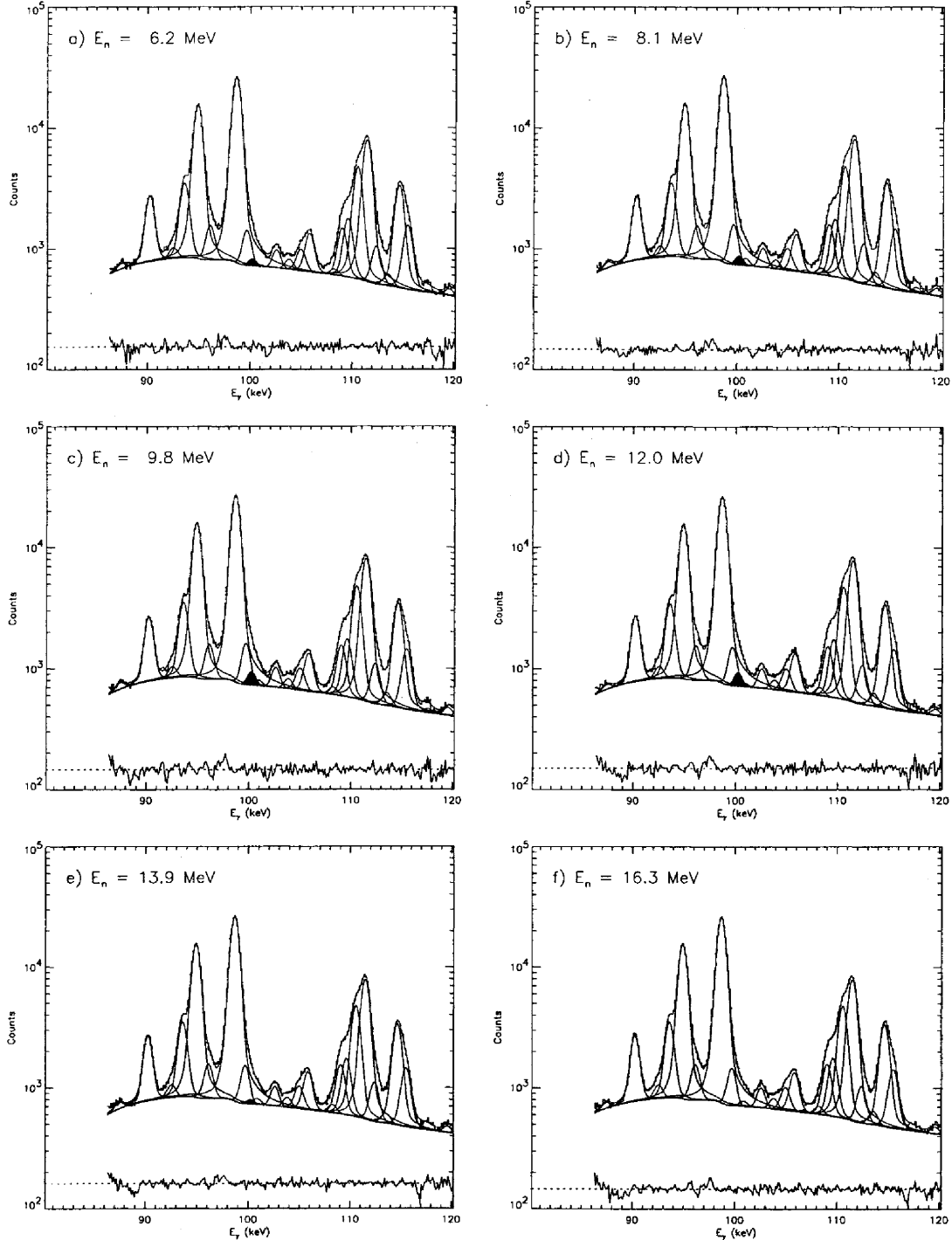


FIG. 19: Fits for the ^{234}U $4_1^+ \rightarrow 2_1^+$ transition in selected neutron-energy cuts of the GEANIE 1998 thick-target data. The $4_1^+ \rightarrow 2_1^+$ peak is shaded in red. The relative fit residual is plotted on an arbitrary scale.

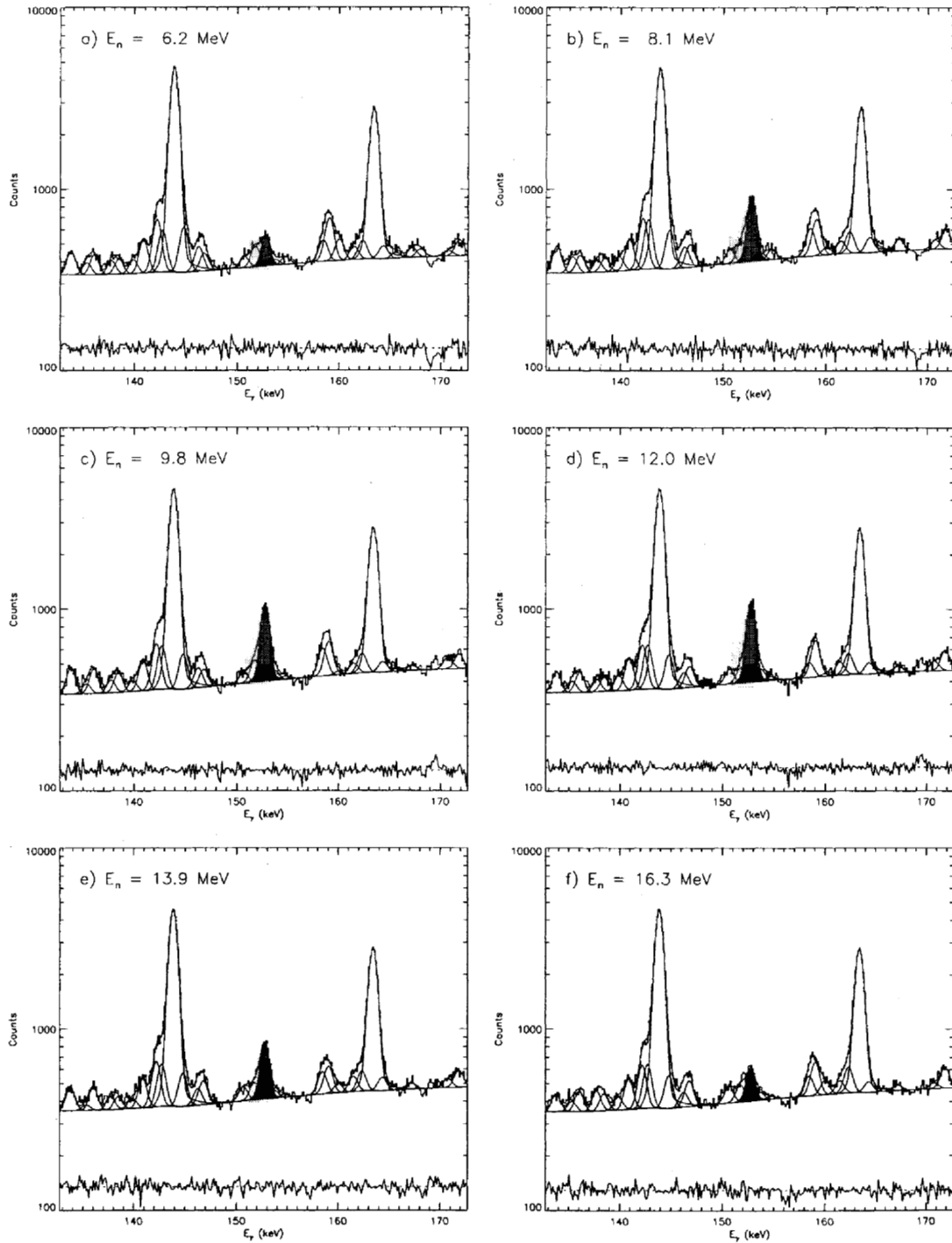


FIG. 20: Fits for the ^{234}U $6_1^+ \rightarrow 4_1^+$ transition in selected neutron-energy cuts of the GEANIE 1998 thick-target data. The $6_1^+ \rightarrow 4_1^+$ peak is shaded in red. The relative fit residual is plotted on an arbitrary scale.

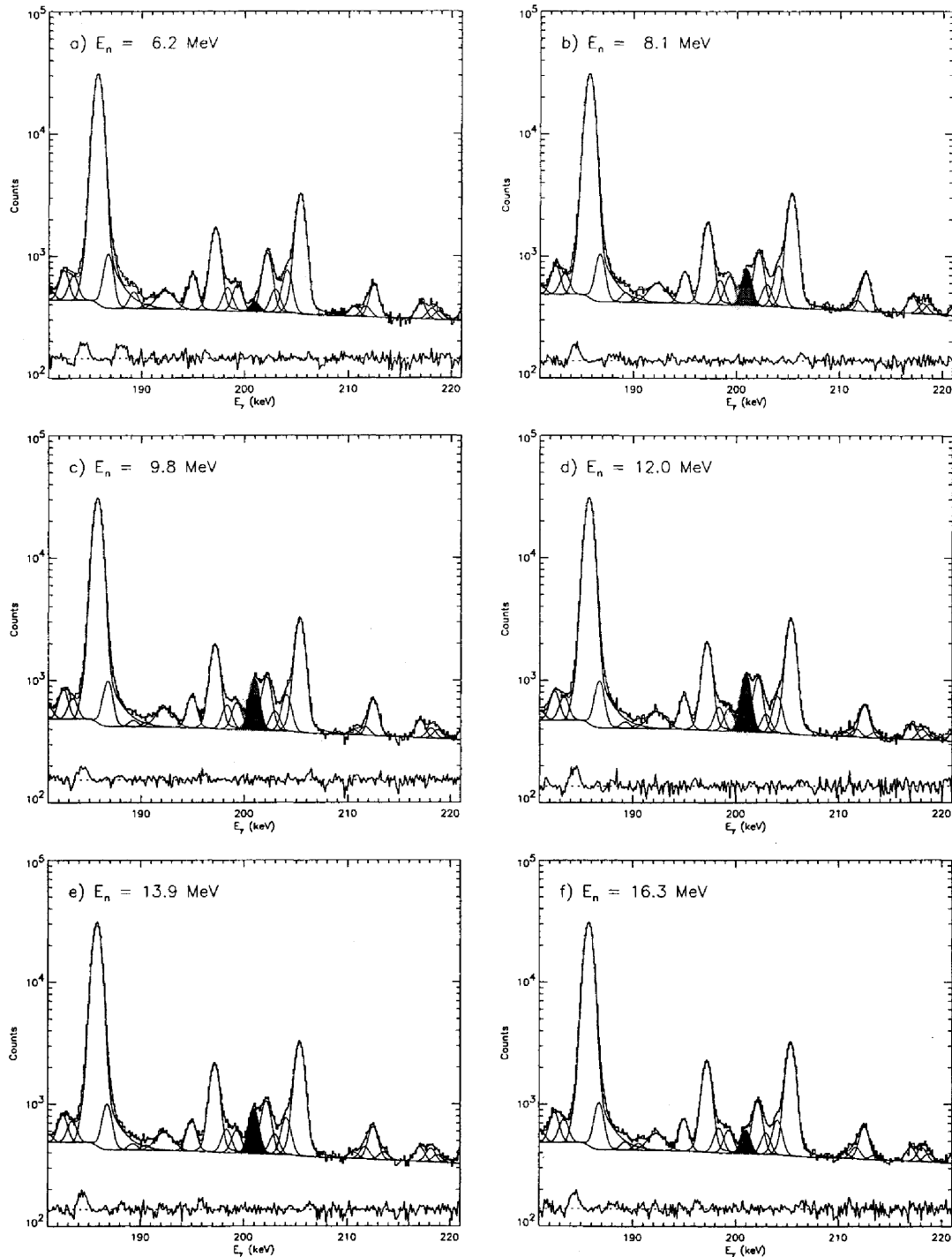


FIG. 21: Fits for the ^{234}U $8_1^+ \rightarrow 6_1^+$ transition in selected neutron-energy cuts of the GEANIE 1998 thick-target data. The $8_1^+ \rightarrow 6_1^+$ peak is shaded in red. The relative fit residual is plotted on an arbitrary scale.

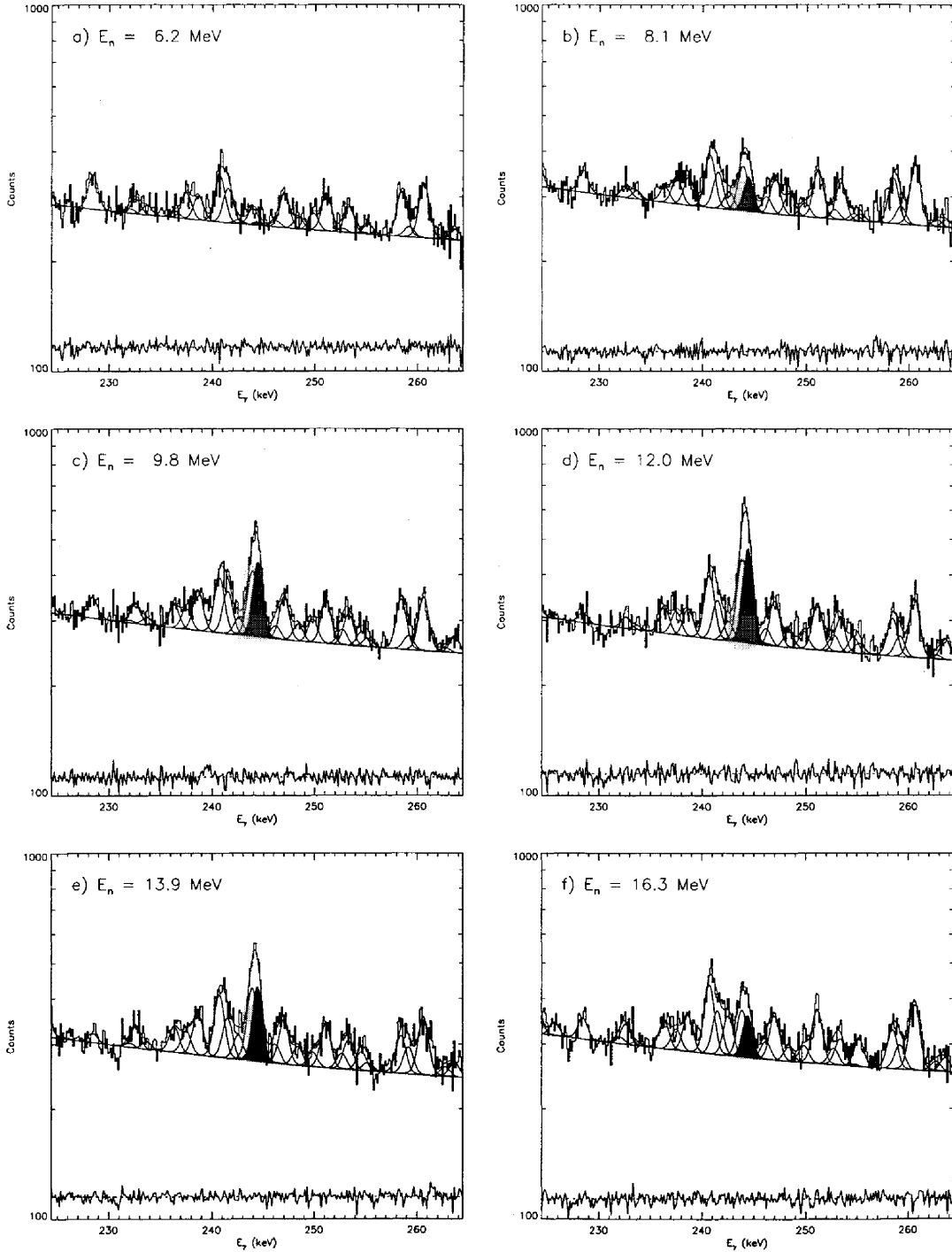


FIG. 22: Fits for the ^{234}U $10_1^+ \rightarrow 8_1^+$ transition in selected neutron-energy cuts of the GEANIE 1998 thick-target data. The $10_1^+ \rightarrow 8_1^+$ peak is shaded in red. The relative fit residual is plotted on an arbitrary scale.

TABLE VIII: Energy and neutron flux statistics calculated using equations 3-7 for 15-ns-wide TOF bins from $E_n = 4$ to 20 MeV, applied to the ^{235}U fission-foil data with a baseline subtraction.

Bin	E_{min} (MeV)	E_{max} (MeV)	\bar{E}_n (MeV)	σ_E (MeV)	N_{fc}	N_{nc} (n/MeV)	N_ϕ (γ/b)
1	4.000	4.169	4.088	0.092	2644 \pm 57	(9.132 \pm 0.201) \times 10 ¹¹	(1.465 \pm 0.024) \times 10 ⁷
2	4.169	4.349	4.263	0.100	2593 \pm 56	(8.490 \pm 0.189) \times 10 ¹¹	(1.450 \pm 0.024) \times 10 ⁷
3	4.349	4.541	4.454	0.106	2664 \pm 57	(8.247 \pm 0.180) \times 10 ¹¹	(1.517 \pm 0.024) \times 10 ⁷
4	4.541	4.746	4.651	0.113	2763 \pm 58	(8.079 \pm 0.173) \times 10 ¹¹	(1.608 \pm 0.025) \times 10 ⁷
5	4.746	4.965	4.860	0.120	2805 \pm 58	(7.809 \pm 0.166) \times 10 ¹¹	(1.650 \pm 0.025) \times 10 ⁷
6	4.965	5.200	5.090	0.129	2874 \pm 59	(7.594 \pm 0.160) \times 10 ¹¹	(1.665 \pm 0.026) \times 10 ⁷
7	5.200	5.452	5.334	0.141	2749 \pm 58	(6.831 \pm 0.147) \times 10 ¹¹	(1.687 \pm 0.026) \times 10 ⁷
8	5.452	5.723	5.596	0.146	2962 \pm 59	(6.903 \pm 0.142) \times 10 ¹¹	(1.767 \pm 0.027) \times 10 ⁷
9	5.723	6.014	5.871	0.161	2961 \pm 60	(6.280 \pm 0.130) \times 10 ¹¹	(1.726 \pm 0.026) \times 10 ⁷
10	6.014	6.328	6.179	0.174	3088 \pm 60	(5.485 \pm 0.111) \times 10 ¹¹	(1.681 \pm 0.024) \times 10 ⁷
11	6.328	6.668	6.515	0.189	3608 \pm 65	(5.176 \pm 0.096) \times 10 ¹¹	(1.732 \pm 0.023) \times 10 ⁷
12	6.668	7.036	6.864	0.199	4378 \pm 70	(5.252 \pm 0.088) \times 10 ¹¹	(1.853 \pm 0.023) \times 10 ⁷
13	7.036	7.436	7.241	0.219	4831 \pm 74	(4.902 \pm 0.078) \times 10 ¹¹	(1.822 \pm 0.021) \times 10 ⁷
14	7.436	7.870	7.656	0.240	4632 \pm 72	(4.070 \pm 0.066) \times 10 ¹¹	(1.721 \pm 0.020) \times 10 ⁷
15	7.870	8.344	8.123	0.265	4555 \pm 72	(3.573 \pm 0.059) \times 10 ¹¹	(1.662 \pm 0.020) \times 10 ⁷
16	8.344	8.863	8.623	0.284	4857 \pm 74	(3.460 \pm 0.055) \times 10 ¹¹	(1.716 \pm 0.020) \times 10 ⁷
17	8.863	9.431	9.158	0.312	4950 \pm 74	(3.236 \pm 0.051) \times 10 ¹¹	(1.711 \pm 0.020) \times 10 ⁷
18	9.431	10.057	9.756	0.343	4567 \pm 72	(2.737 \pm 0.045) \times 10 ¹¹	(1.648 \pm 0.020) \times 10 ⁷
19	10.057	10.747	10.410	0.381	4240 \pm 69	(2.327 \pm 0.039) \times 10 ¹¹	(1.557 \pm 0.019) \times 10 ⁷
20	10.747	11.511	11.144	0.423	3941 \pm 67	(1.970 \pm 0.034) \times 10 ¹¹	(1.465 \pm 0.018) \times 10 ⁷
21	11.511	12.360	11.959	0.470	4001 \pm 68	(1.776 \pm 0.031) \times 10 ¹¹	(1.411 \pm 0.018) \times 10 ⁷
22	12.360	13.307	12.859	0.523	4022 \pm 68	(1.489 \pm 0.026) \times 10 ¹¹	(1.372 \pm 0.017) \times 10 ⁷
23	13.307	14.369	13.871	0.591	4193 \pm 69	(1.282 \pm 0.021) \times 10 ¹¹	(1.328 \pm 0.016) \times 10 ⁷
24	14.369	15.564	15.020	0.662	4340 \pm 70	(1.145 \pm 0.019) \times 10 ¹¹	(1.328 \pm 0.016) \times 10 ⁷
25	15.564	16.916	16.302	0.748	4595 \pm 72	(1.076 \pm 0.018) \times 10 ¹¹	(1.352 \pm 0.016) \times 10 ⁷
26	16.916	18.453	17.764	0.860	4283 \pm 70	(9.141 \pm 0.158) \times 10 ¹⁰	(1.371 \pm 0.017) \times 10 ⁷
27	18.453	20.213	19.422	0.967	4381 \pm 70	(8.507 \pm 0.193) \times 10 ¹⁰	(1.418 \pm 0.023) \times 10 ⁷

TABLE IX: Fitted raw areas and deduced partial γ -ray cross sections for the $4 \rightarrow 2$, $6 \rightarrow 4$, $8 \rightarrow 6$, and $10 \rightarrow 8$ transitions. Quoted uncertainties represent random fluctuations only. The counts were normalized using ^{235}U fission foil data with baseline subtraction.

Bin	$A(4_1^+ \rightarrow 2_1^+)$	$\sigma_{4_1^+ \rightarrow 2_1^+}(b)$	$A(6_1^+ \rightarrow 4_1^+)$	$\sigma_{6_1^+ \rightarrow 4_1^+}(b)$	$A(8_1^+ \rightarrow 6_1^+)$	$\sigma_{8_1^+ \rightarrow 6_1^+}(b)$	$A(10_1^+ \rightarrow 8_1^+)$	$\sigma_{10_1^+ \rightarrow 8_1^+}(b)$
1	0 ± 0	0.000 ± 0.000	85 ± 73	0.005 ± 0.005	65 ± 77	0.002 ± 0.002	0 ± 0	0.000 ± 0.000
2	0 ± 0	0.000 ± 0.000	274 ± 75	0.018 ± 0.005	92 ± 77	0.003 ± 0.002	38 ± 89	0.001 ± 0.002
3	0 ± 2	0.000 ± 0.000	125 ± 74	0.008 ± 0.005	17 ± 71	0.000 ± 0.002	53 ± 90	0.001 ± 0.002
4	0 ± 0	0.000 ± 0.000	39 ± 74	0.002 ± 0.004	111 ± 78	0.003 ± 0.002	46 ± 90	0.001 ± 0.002
5	24 ± 191	0.004 ± 0.030	137 ± 76	0.008 ± 0.004	78 ± 79	0.002 ± 0.002	0 ± 0	0.000 ± 0.000
6	0 ± 0	0.000 ± 0.000	164 ± 77	0.009 ± 0.004	191 ± 80	0.005 ± 0.002	0 ± 0	0.000 ± 0.000
7	182 ± 228	0.028 ± 0.035	76 ± 76	0.004 ± 0.004	94 ± 80	0.002 ± 0.002	15 ± 92	0.000 ± 0.002
8	0 ± 1	0.000 ± 0.000	263 ± 79	0.014 ± 0.004	85 ± 80	0.002 ± 0.002	85 ± 95	0.002 ± 0.002
9	0 ± 0	0.000 ± 0.000	661 ± 84	0.036 ± 0.005	94 ± 81	0.002 ± 0.002	0 ± 0	0.000 ± 0.000
10	870 ± 236	0.133 ± 0.036	1508 ± 92	0.083 ± 0.005	664 ± 86	0.017 ± 0.002	62 ± 94	0.001 ± 0.002
11	1011 ± 242	0.150 ± 0.036	2750 ± 101	0.148 ± 0.006	1695 ± 95	0.043 ± 0.002	248 ± 100	0.005 ± 0.002
12	1252 ± 245	0.174 ± 0.034	3354 ± 106	0.168 ± 0.006	2416 ± 101	0.057 ± 0.002	348 ± 102	0.007 ± 0.002
13	852 ± 244	0.120 ± 0.034	3714 ± 109	0.190 ± 0.006	2771 ± 103	0.067 ± 0.003	447 ± 106	0.009 ± 0.002
14	1072 ± 242	0.160 ± 0.036	3954 ± 110	0.214 ± 0.006	3205 ± 105	0.082 ± 0.003	694 ± 107	0.015 ± 0.002
15	1148 ± 245	0.177 ± 0.038	4425 ± 113	0.248 ± 0.007	3678 ± 109	0.097 ± 0.003	655 ± 109	0.014 ± 0.002
16	1711 ± 249	0.256 ± 0.037	5228 ± 117	0.283 ± 0.007	4693 ± 115	0.120 ± 0.003	1127 ± 115	0.024 ± 0.002
17	1132 ± 246	0.170 ± 0.037	5620 ± 119	0.305 ± 0.007	5113 ± 117	0.131 ± 0.003	1059 ± 115	0.022 ± 0.002
18	1730 ± 247	0.270 ± 0.039	5672 ± 120	0.320 ± 0.008	5878 ± 120	0.157 ± 0.004	1582 ± 120	0.035 ± 0.003
19	1765 ± 244	0.291 ± 0.040	6103 ± 121	0.365 ± 0.008	6283 ± 122	0.178 ± 0.004	1773 ± 122	0.041 ± 0.003
20	1999 ± 246	0.351 ± 0.043	6071 ± 121	0.386 ± 0.009	6498 ± 123	0.195 ± 0.004	2136 ± 124	0.053 ± 0.003
21	1725 ± 243	0.314 ± 0.044	6078 ± 121	0.401 ± 0.009	6845 ± 124	0.213 ± 0.005	2068 ± 123	0.053 ± 0.003
22	1552 ± 241	0.291 ± 0.045	5278 ± 117	0.358 ± 0.009	6245 ± 121	0.200 ± 0.005	2288 ± 125	0.060 ± 0.003
23	515 ± 238	0.100 ± 0.046	3721 ± 108	0.261 ± 0.008	4805 ± 115	0.159 ± 0.004	1584 ± 120	0.043 ± 0.003
24	10 ± 223	0.002 ± 0.043	2652 ± 101	0.186 ± 0.007	3238 ± 107	0.107 ± 0.004	1213 ± 115	0.033 ± 0.003
25	1 ± 19	0.000 ± 0.004	1769 ± 96	0.122 ± 0.007	2048 ± 100	0.067 ± 0.003	823 ± 112	0.022 ± 0.003
26	0 ± 2	0.000 ± 0.000	1526 ± 94	0.103 ± 0.007	1587 ± 96	0.051 ± 0.003	462 ± 109	0.012 ± 0.003
27	0 ± 0	0.000 ± 0.000	1234 ± 92	0.081 ± 0.006	1450 ± 96	0.045 ± 0.003	368 ± 109	0.009 ± 0.003

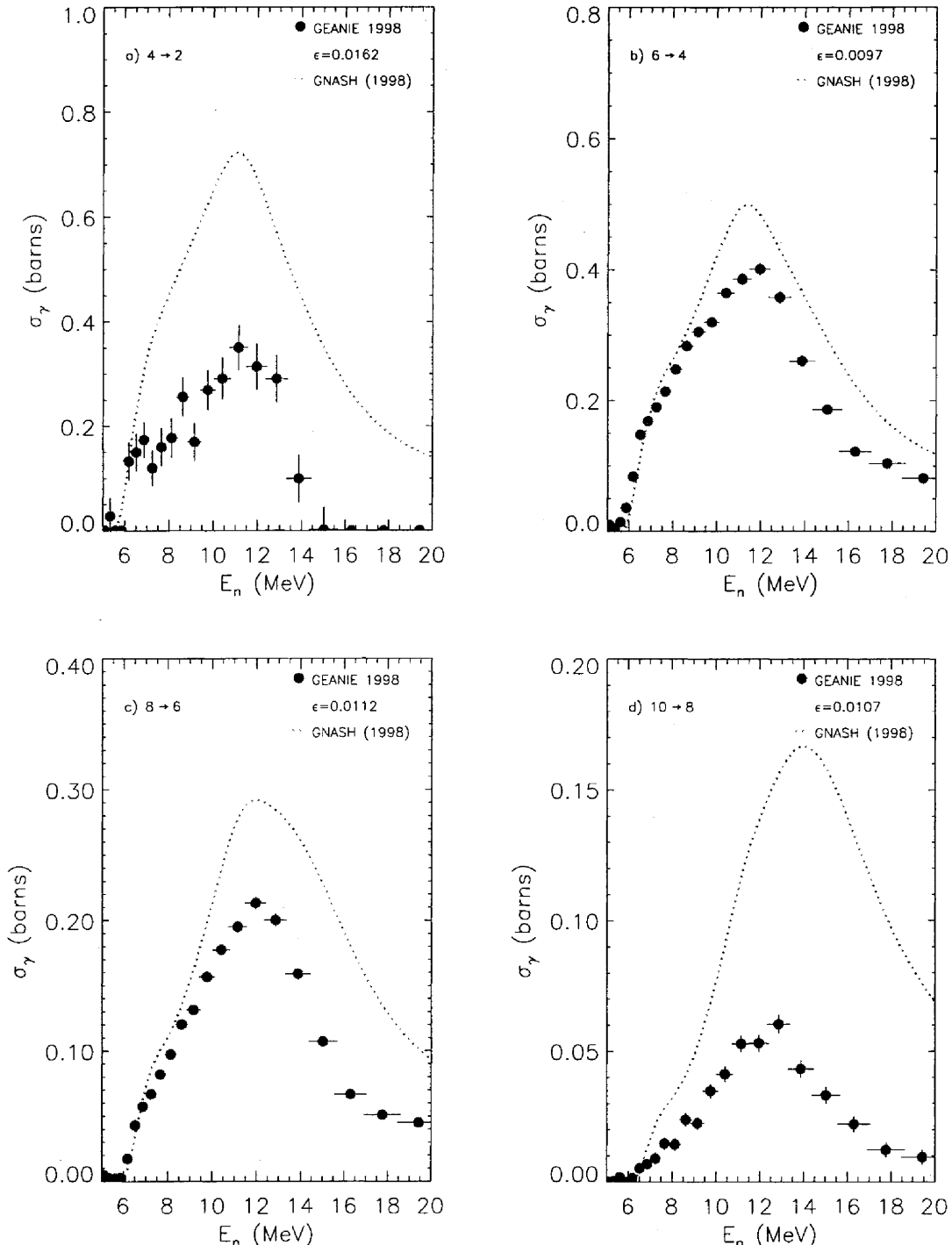


FIG. 23: Excitation functions for the ^{234}U a) $4_1^+ \rightarrow 2_1^+$, b) $6_1^+ \rightarrow 4_1^+$, c) $8_1^+ \rightarrow 6_1^+$ and d) $10_1^+ \rightarrow 8_1^+$ transitions, constructed from the GEANIE 1998 thick-target data. Only statistical errors are included. Fission-chamber data from the ^{235}U foil with a flat baseline subtraction were used to generate these yields. The detector efficiency used is quoted in each case.

VI. VALIDATION OF THE 1998 RESULTS WITH RESPECT TO TOTAL UNCERTAINTIES

Deviations between thin- and thick-sample-deduced partial cross sections can be used as a check of the total experimental uncertainty (i.e. arising from random, energy-dependent systematic and energy-independent systematic variability). The random uncertainties are obtained in the usual manner [15] from the error matrix in the fits, the energy-dependent systematic uncertainties discussed in section III of this report, and the energy-independent systematic uncertainties quantified in reference [9]. We plot in figure 24 the thick-sample-deduced partial cross sections (solid points) against the total-uncertainty one-sigma confidence band (dotted lines) constructed from the unsubtracted thin-sample data normalized to the ^{235}U fission-foil counts, with the mentioned uncertainty contributions summed in quadrature. In general, the data points fall within the band, with the exception of the $4 \rightarrow 2$ yields. As was noted above, the $4 \rightarrow 2$ peak in the thick-sample data is below the threshold of what can be reliably extracted by spectroscopic analysis. This can be clearly seen in the lack of smooth behavior in the excitation function, compared to the other three plots in figure 23. It should also be noted that the thick-sample data in figure 24 are consistently low within the one-sigma band. This systematic effect can be attributed to several causes. First there is sizeable uncertainty in the ^{235}U samples used in the 1998 experiments (about 7.1% for the thin sample and 5.0% for the thick sample). An under-estimation of the thin-sample thickness or over-estimation of the thick-sample thickness can account for some of the discrepancy. Second, a comparison of the fitted regions between the thin-sample data (figures 6-9) and thick-sample data (figures 19-22) suggests that the background height in the **98Thick** data analysis may be slightly over-estimated. However, only the **98Thin** and **99Thin** data sets are used in the final determination of partial cross sections. The backgrounds used for the XGAM fits of the **98Thin** and **99Thin** data are discussed in greater detail in appendix F, and are believed to be more accurate than those used in the **98Thick** data fits.

The inclusion of uncertainty from neutron-energy-independent factors increases the total uncertainty of partial cross sections extracted from the 1998 data by $\approx 10\%$ in quadrature (see [9]). However, this additional contribution is necessary when both magnitude and shape of the excitation functions are of concern.

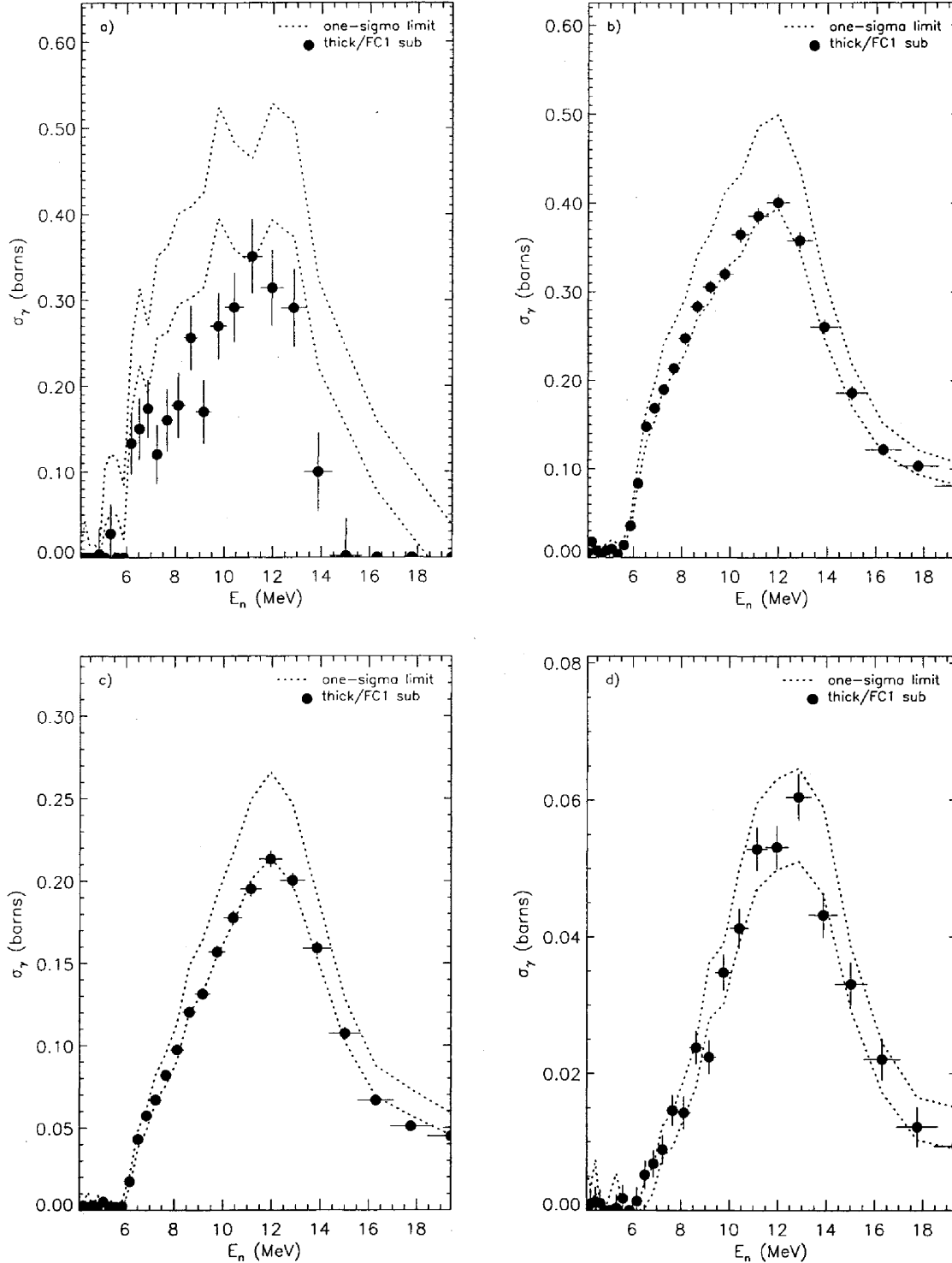


FIG. 24: Validation of the one-sigma confidence band (dotted lines) for the combined random, energy-dependent systematic and energy-independent systematic uncertainties deduced from the unsubtracted 1998 thin-sample data normalized to ^{235}U fission-foil counts with baseline subtraction. In the legend, the raw data is labeled as “thick” and the symbol “FC1 sub” refers to normalization using the ^{235}U fission foil with baseline subtraction.

VII. GEANIE 1999 DATA ANALYSIS

run label: 99thin

log book pages: #4 pp. 112-121, 128-130

run dates: 11/15/99-11/22/99 and 12/4/99-12/5/99

total run time recorded to tape: 641737 s (from 455 Hz pulser)

beam structure:

rep rate: 115-119 Hz

micropulse spacing: 1.8 μ s

beam gate length: 725 μ s

typical proton current: 5.4 μ A

beam absorbers: 1/2" Pb + 1" borated polyethylene

sample areal density corrected for ^{235}U enrichment: $0.4494 \pm 0.0025 \text{ g/cm}^2$

sample thickness: \approx 12 mil (2 laminated packages of two 3-mil foils each)

sample atomic assay: 93.2324% ^{235}U + 5.3729% ^{238}U + 1.1339% ^{234}U + 0.2581% ^{236}U

sample orientation: 251° on dial (19° with respect to beam)

sample mask: none

planar-detector absorbers: 20-mil Mo

deadtimes:

planar-data sum: $71.18 \pm 2.13 \%$

coaxial-data sum: $73.75 \pm 2.21 \%$

^{235}U fission foil: $65.68 \pm 1.97 \%$

^{238}U fission foil: $63.31 \pm 1.90 \%$

A $^{235}\text{U}(n,2n)$ Analysis

1 Partial Cross Section Evaluation

The analysis of 1999 n+ ^{235}U GEANIE data is discussed in this section. Due to a combination of factors including higher deadtime and shorter run time, statistics in the (n,2n) yrast γ rays are lower in this case than in the 1998 thin-sample data. The $6 \rightarrow 4$ transition in the $E_n = 5\text{-}20$ MeV range, for example, only has $\approx 75\%$ of the statistics of the 1998 data. The 1999 data were acquired using 16k ADC modules. In order to take full advantage of the improved dispersion, the γ -ray fits have been carried out using XGAM with the uncompressed 16k spectra. As with the 1998 analysis, data from all the planar detectors has been summed to obtain adequate statistics, and analyzed using the algorithm described in section II A. The pertinent fitting parameters are listed in table X. The corresponding γ -ray fits at select neutron energies are shown in figures 25-28. Neutron fluxes extracted using the ^{235}U (with baseline subtraction) and ^{238}U (without baseline subtraction) fission foils, are listed in tables XI and XII respectively, and the deduced partial γ -ray cross sections obtained using the ^{235}U fission foil for normalization are quoted in table XIII and plotted in figure 29. Note that the neutron flux (N_ϕ) listed in table XI is approximately twice that listed in table II for the "98thin" data. The higher value is due primarily to the roughly twofold increase in beam current. That advantage is canceled out however by increased deadtime. The increased dispersion in fitting 16k rather than 8k spectra is helpful in resolving closely-spaced peaks. This improvement however comes at the price of reduced statistics

in individual spectrum channels for the same total counts in a peak. As a result, weak peaks, such as the $4 \rightarrow 2$ line, will suffer from greater fluctuations, and residual counts may be observed for a line, even below its cross-section threshold. These effects can be seen in the $4 \rightarrow 2$ excitation function over its entire range and in the $8 \rightarrow 6$ excitation function below threshold.

TABLE X: Fit Parameters used in XGAM for the 1999 GEANIE data [6]. The variable x refers to the γ -ray spectrum channel number, where each channel corresponds to 0.125 keV.

parameter	value
fitted range	1380-15900 (ch), 86-994 (keV)
background polynomial order	18
peak width (ch)	$w = \sqrt{92.33 + 34.92 \frac{x}{1000} + 2.258 \left(\frac{x}{1000}\right)^2}$
x-ray width parameter (ch)	$\Gamma = -3.707 + 2.777 \times 10^{-3}x$
high-energy tail (ch)	$R_h = 5.964, \beta_h = 24.459$
Gaussian asymmetry (ch)	$p_3 = 6.145 \times 10^{-3} + 2.131 \times 10^{-6}x$ $p_4 = 4.749 \times 10^{-7} + 4.921 \times 10^{-10}x$
Compton step (ch)	$S = 1.068 \times 10^{-2} - 7.276 \times 10^{-7}x$
x-ray peaks	18
γ -ray peaks	410
neutron bumps	3
χ^2/ν for $E_n=5-20$ MeV	1.29

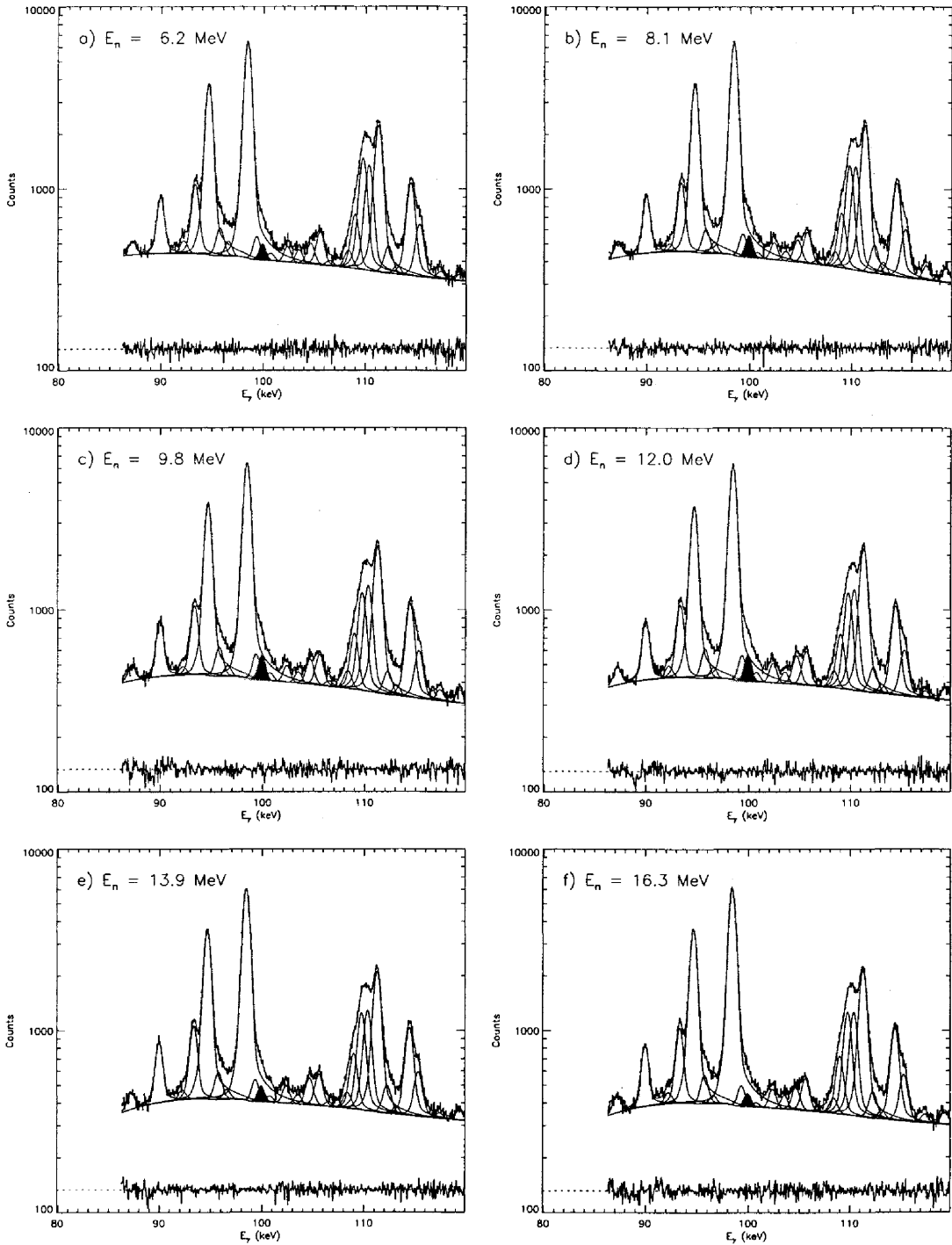


FIG. 25: Fits for the ^{234}U $4_1^+ \rightarrow 2_1^+$ transition in selected neutron-energy cuts of the GEANIE 1999 data. The $4_1^+ \rightarrow 2_1^+$ peak is shaded in red. The relative residual is plotted on an arbitrary scale.

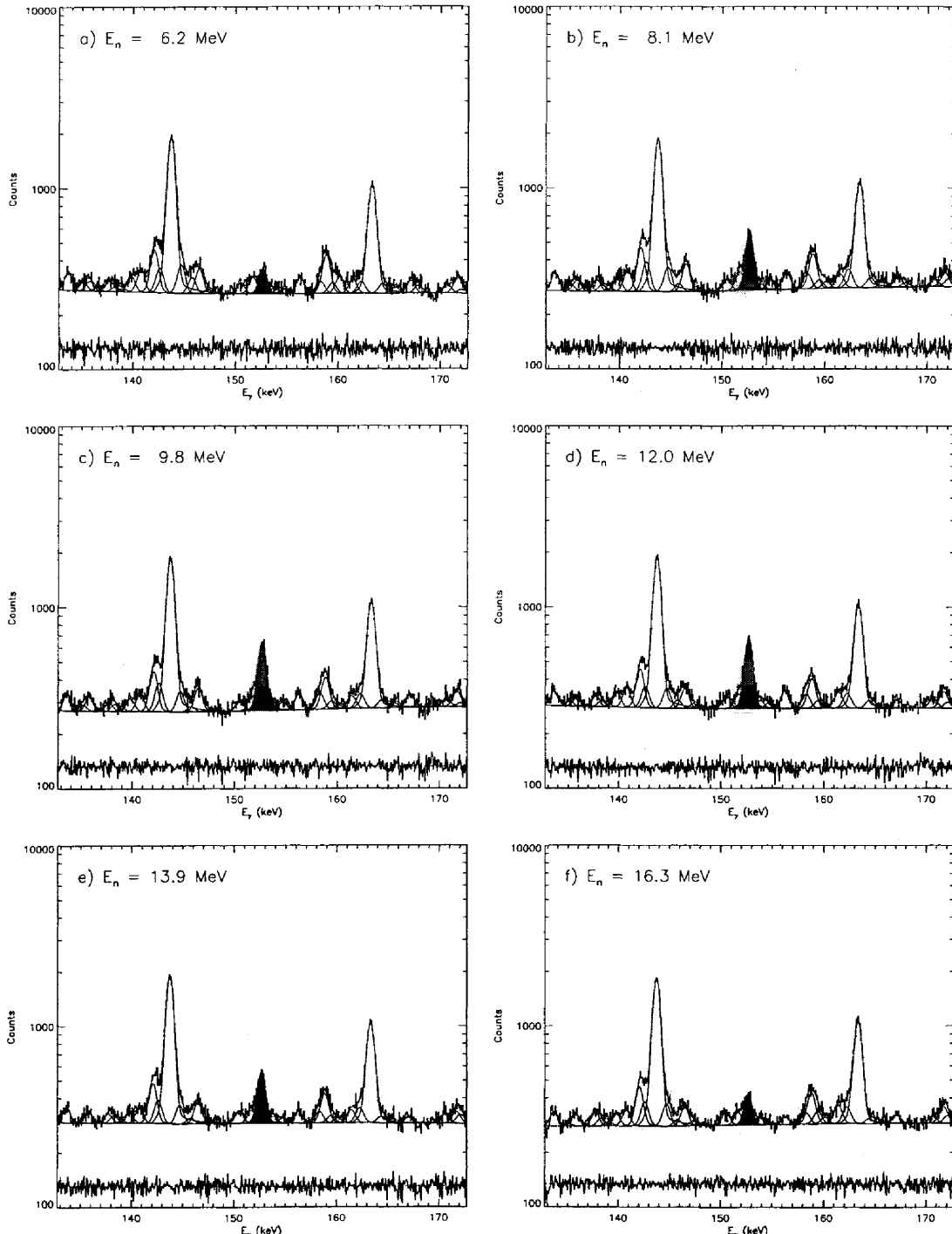


FIG. 26: Fits for the ^{234}U $6_1^+ \rightarrow 4_1^+$ transition in selected neutron-energy cuts of the GEANIE 1999 data. The $6_1^+ \rightarrow 4_1^+$ peak is shaded in red. The relative residual is plotted on an arbitrary scale.

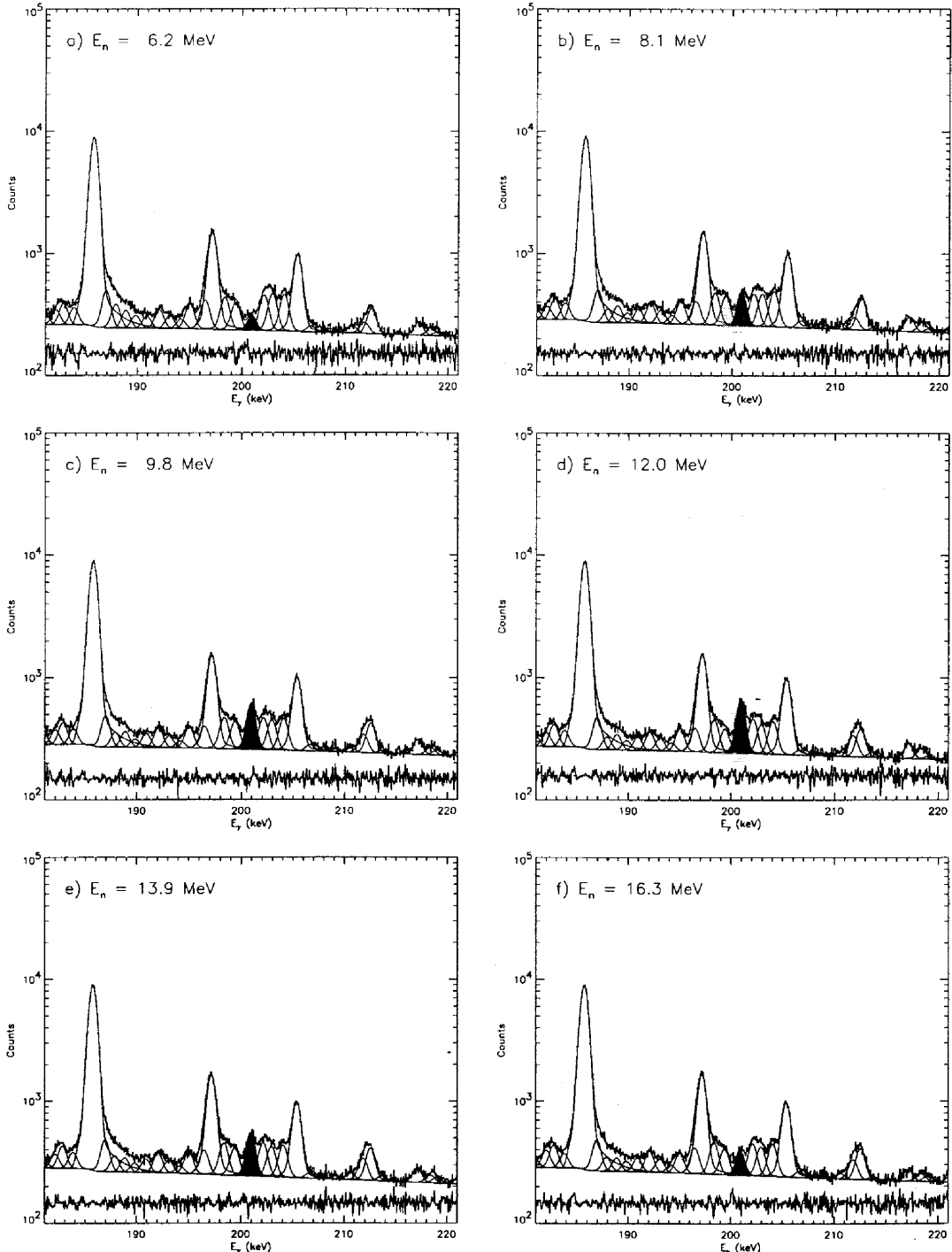


FIG. 27: Fits for the ^{234}U $8_1^+ \rightarrow 6_1^+$ transition in selected neutron-energy cuts of the GEANIE 1999 data. The $8_1^+ \rightarrow 6_1^+$ peak is shaded in red. The relative residual is plotted on an arbitrary scale.

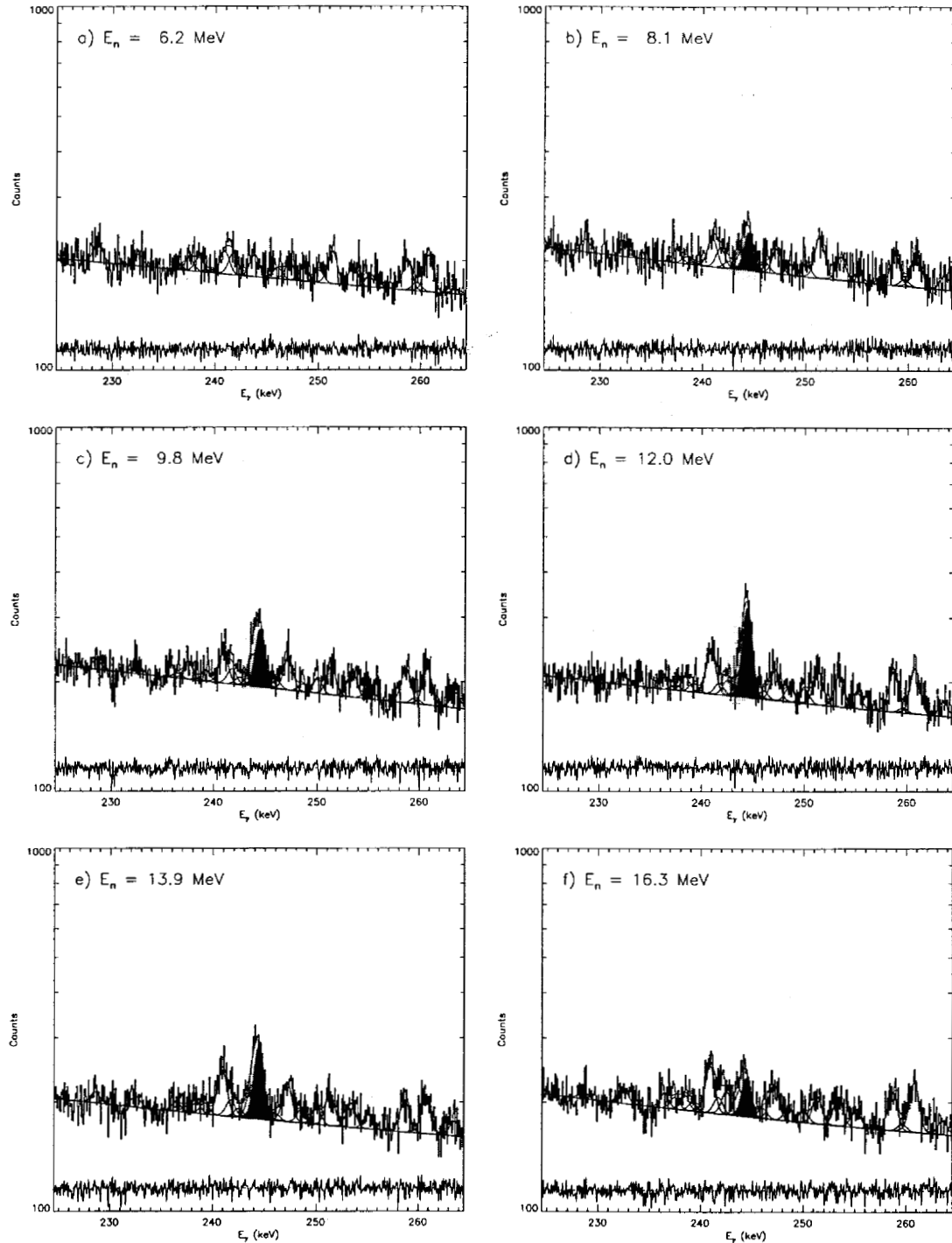


FIG. 28: Fits for the ^{234}U $10_1^+ \rightarrow 8_1^+$ transition in selected neutron-energy cuts of the GEANIE 1999 data. The $10_1^+ \rightarrow 8_1^+$ peak is shaded in red. The relative residual is plotted on an arbitrary scale.

TABLE XI: Energy and neutron flux statistics calculated using equations 3-7 for 15-ns-wide TOF bins from $E_n = 4$ to 20 MeV, applied to the ^{235}U fission-foil data with a baseline subtraction.

Bin	E_{min} (MeV)	E_{max} (MeV)	\bar{E}_n (MeV)	σ_E (MeV)	N_{fc}	N_{nc} (n/MeV)	N_ϕ (γ/b)
1	4.000	4.169	4.089	0.092	4271 \pm 71	(1.807 \pm 0.031) \times 10 ¹²	(1.312 \pm 0.017) \times 10 ⁷
2	4.169	4.349	4.264	0.100	4342 \pm 72	(1.741 \pm 0.030) \times 10 ¹²	(1.328 \pm 0.017) \times 10 ⁷
3	4.349	4.541	4.452	0.105	4424 \pm 72	(1.678 \pm 0.029) \times 10 ¹²	(1.397 \pm 0.017) \times 10 ⁷
4	4.541	4.746	4.648	0.113	4537 \pm 73	(1.626 \pm 0.027) \times 10 ¹²	(1.432 \pm 0.018) \times 10 ⁷
5	4.746	4.965	4.862	0.121	4471 \pm 72	(1.524 \pm 0.026) \times 10 ¹²	(1.459 \pm 0.018) \times 10 ⁷
6	4.965	5.200	5.089	0.129	4723 \pm 74	(1.529 \pm 0.025) \times 10 ¹²	(1.491 \pm 0.018) \times 10 ⁷
7	5.200	5.452	5.332	0.140	4411 \pm 72	(1.343 \pm 0.023) \times 10 ¹²	(1.493 \pm 0.018) \times 10 ⁷
8	5.452	5.723	5.594	0.149	4486 \pm 73	(1.283 \pm 0.022) \times 10 ¹²	(1.507 \pm 0.018) \times 10 ⁷
9	5.723	6.014	5.879	0.160	4894 \pm 76	(1.270 \pm 0.021) \times 10 ¹²	(1.542 \pm 0.018) \times 10 ⁷
10	6.014	6.328	6.181	0.175	5235 \pm 78	(1.139 \pm 0.018) \times 10 ¹²	(1.570 \pm 0.018) \times 10 ⁷
11	6.328	6.668	6.513	0.186	6380 \pm 85	(1.122 \pm 0.016) \times 10 ¹²	(1.646 \pm 0.017) \times 10 ⁷
12	6.668	7.036	6.859	0.200	7184 \pm 89	(1.057 \pm 0.014) \times 10 ¹²	(1.684 \pm 0.016) \times 10 ⁷
13	7.036	7.436	7.236	0.220	7654 \pm 92	(9.530 \pm 0.123) \times 10 ¹¹	(1.586 \pm 0.015) \times 10 ⁷
14	7.436	7.870	7.662	0.243	7208 \pm 89	(7.752 \pm 0.103) \times 10 ¹¹	(1.485 \pm 0.014) \times 10 ⁷
15	7.870	8.344	8.126	0.262	7635 \pm 92	(7.334 \pm 0.095) \times 10 ¹¹	(1.500 \pm 0.014) \times 10 ⁷
16	8.344	8.863	8.619	0.284	7837 \pm 93	(6.841 \pm 0.087) \times 10 ¹¹	(1.534 \pm 0.014) \times 10 ⁷
17	8.863	9.431	9.159	0.312	7929 \pm 93	(6.348 \pm 0.080) \times 10 ¹¹	(1.507 \pm 0.014) \times 10 ⁷
18	9.431	10.057	9.756	0.346	7208 \pm 89	(5.295 \pm 0.070) \times 10 ¹¹	(1.445 \pm 0.014) \times 10 ⁷
19	10.057	10.747	10.414	0.379	6929 \pm 88	(4.657 \pm 0.062) \times 10 ¹¹	(1.388 \pm 0.013) \times 10 ⁷
20	10.747	11.511	11.143	0.424	6421 \pm 85	(3.931 \pm 0.054) \times 10 ¹¹	(1.312 \pm 0.013) \times 10 ⁷
21	11.511	12.360	11.959	0.471	6497 \pm 85	(3.536 \pm 0.048) \times 10 ¹¹	(1.263 \pm 0.013) \times 10 ⁷
22	12.360	13.307	12.862	0.522	6678 \pm 86	(3.028 \pm 0.040) \times 10 ¹¹	(1.239 \pm 0.012) \times 10 ⁷
23	13.307	14.369	13.874	0.589	6993 \pm 88	(2.620 \pm 0.034) \times 10 ¹¹	(1.209 \pm 0.011) \times 10 ⁷
24	14.369	15.564	15.017	0.664	7101 \pm 89	(2.298 \pm 0.030) \times 10 ¹¹	(1.205 \pm 0.011) \times 10 ⁷
25	15.564	16.916	16.298	0.749	7556 \pm 91	(2.170 \pm 0.028) \times 10 ¹¹	(1.217 \pm 0.012) \times 10 ⁷
26	16.916	18.453	17.766	0.857	7066 \pm 89	(1.847 \pm 0.026) \times 10 ¹¹	(1.234 \pm 0.012) \times 10 ⁷
27	18.453	20.213	19.413	0.967	7062 \pm 89	(1.684 \pm 0.034) \times 10 ¹¹	(1.266 \pm 0.018) \times 10 ⁷

TABLE XII: Energy and neutron flux statistics calculated using equations 3-7 for 15-ns-wide TOF bins from $E_n = 4$ to 20 MeV, applied to the ^{238}U fission-foil data.

Bin	E_{min} (MeV)	E_{max} (MeV)	\bar{E}_n (MeV)	σ_E (MeV)	N_{fc}	N_{nc} (n/MeV)	N_ϕ (γ/b)
1	4.000	4.169	4.088	0.092	2360 \pm 49	(1.910 \pm 0.044) \times 10 ¹²	(1.331 \pm 0.023) \times 10 ⁷
2	4.169	4.349	4.263	0.100	2213 \pm 47	(1.678 \pm 0.039) \times 10 ¹²	(1.323 \pm 0.022) \times 10 ⁷
3	4.349	4.541	4.451	0.106	2276 \pm 48	(1.621 \pm 0.038) \times 10 ¹²	(1.356 \pm 0.023) \times 10 ⁷
4	4.541	4.746	4.649	0.112	2346 \pm 48	(1.572 \pm 0.036) \times 10 ¹²	(1.392 \pm 0.023) \times 10 ⁷
5	4.746	4.965	4.861	0.122	2410 \pm 49	(1.522 \pm 0.034) \times 10 ¹²	(1.410 \pm 0.023) \times 10 ⁷
6	4.965	5.200	5.091	0.128	2427 \pm 49	(1.438 \pm 0.033) \times 10 ¹²	(1.464 \pm 0.024) \times 10 ⁷
7	5.200	5.452	5.330	0.139	2478 \pm 50	(1.361 \pm 0.031) \times 10 ¹²	(1.474 \pm 0.024) \times 10 ⁷
8	5.452	5.723	5.596	0.150	2524 \pm 50	(1.264 \pm 0.028) \times 10 ¹²	(1.469 \pm 0.024) \times 10 ⁷
9	5.723	6.014	5.875	0.160	2688 \pm 52	(1.183 \pm 0.026) \times 10 ¹²	(1.493 \pm 0.024) \times 10 ⁷
10	6.014	6.328	6.181	0.175	3085 \pm 56	(1.093 \pm 0.023) \times 10 ¹²	(1.495 \pm 0.022) \times 10 ⁷
11	6.328	6.668	6.509	0.187	3862 \pm 62	(1.048 \pm 0.020) \times 10 ¹²	(1.538 \pm 0.021) \times 10 ⁷
12	6.668	7.036	6.861	0.201	4590 \pm 68	(1.026 \pm 0.018) \times 10 ¹²	(1.561 \pm 0.021) \times 10 ⁷
13	7.036	7.436	7.239	0.220	4419 \pm 66	(8.658 \pm 0.156) \times 10 ¹¹	(1.504 \pm 0.020) \times 10 ⁷
14	7.436	7.870	7.661	0.242	4272 \pm 65	(7.504 \pm 0.137) \times 10 ¹¹	(1.424 \pm 0.019) \times 10 ⁷
15	7.870	8.344	8.125	0.262	4322 \pm 66	(6.904 \pm 0.125) \times 10 ¹¹	(1.423 \pm 0.019) \times 10 ⁷
16	8.344	8.863	8.618	0.284	4587 \pm 68	(6.670 \pm 0.118) \times 10 ¹¹	(1.443 \pm 0.019) \times 10 ⁷
17	8.863	9.431	9.155	0.312	4296 \pm 66	(5.715 \pm 0.104) \times 10 ¹¹	(1.397 \pm 0.018) \times 10 ⁷
18	9.431	10.057	9.759	0.347	3993 \pm 63	(4.862 \pm 0.090) \times 10 ¹¹	(1.334 \pm 0.018) \times 10 ⁷
19	10.057	10.747	10.418	0.379	4012 \pm 63	(4.450 \pm 0.082) \times 10 ¹¹	(1.304 \pm 0.018) \times 10 ⁷
20	10.747	11.511	11.141	0.421	3787 \pm 62	(3.801 \pm 0.072) \times 10 ¹¹	(1.249 \pm 0.017) \times 10 ⁷
21	11.511	12.360	11.961	0.470	3614 \pm 60	(3.256 \pm 0.062) \times 10 ¹¹	(1.196 \pm 0.017) \times 10 ⁷
22	12.360	13.307	12.863	0.524	3628 \pm 60	(2.874 \pm 0.055) \times 10 ¹¹	(1.175 \pm 0.016) \times 10 ⁷
23	13.307	14.369	13.882	0.590	4052 \pm 64	(2.598 \pm 0.047) \times 10 ¹¹	(1.165 \pm 0.015) \times 10 ⁷
24	14.369	15.564	15.012	0.657	4297 \pm 66	(2.272 \pm 0.041) \times 10 ¹¹	(1.175 \pm 0.015) \times 10 ⁷
25	15.564	16.916	16.291	0.756	4423 \pm 67	(1.959 \pm 0.036) \times 10 ¹¹	(1.154 \pm 0.015) \times 10 ⁷
26	16.916	18.453	17.797	0.877	4652 \pm 68	(1.815 \pm 0.033) \times 10 ¹¹	(1.188 \pm 0.018) \times 10 ⁷
27	18.453	20.213	19.424	0.913	4840 \pm 70	(1.848 \pm 0.115) \times 10 ¹¹	(1.340 \pm 0.063) \times 10 ⁷

TABLE XIII: Fitted raw areas and deduced partial γ -ray cross sections for the $4 \rightarrow 2$, $6 \rightarrow 4$, $8 \rightarrow 6$, and $10 \rightarrow 8$ transitions. Quoted uncertainties represent random fluctuations only. The counts were normalized using ^{235}U fission foil data with baseline subtraction.

Bin	$A(4_1^+ \rightarrow 2_1^+)$	$\sigma_{4_1^+ \rightarrow 2_1^+}(b)$	$A(6_1^+ \rightarrow 4_1^+)$	$\sigma_{6_1^+ \rightarrow 4_1^+}(b)$	$A(8_1^+ \rightarrow 6_1^+)$	$\sigma_{8_1^+ \rightarrow 6_1^+}(b)$	$A(10_1^+ \rightarrow 8_1^+)$	$\sigma_{10_1^+ \rightarrow 8_1^+}(b)$
1	583 \pm 143	0.157 \pm 0.039	166 \pm 78	0.011 \pm 0.005	639 \pm 87	0.021 \pm 0.003	0 \pm 0	0.000 \pm 0.000
2	540 \pm 147	0.144 \pm 0.039	62 \pm 78	0.004 \pm 0.005	813 \pm 89	0.027 \pm 0.003	29 \pm 87	0.001 \pm 0.003
3	632 \pm 151	0.160 \pm 0.038	172 \pm 79	0.010 \pm 0.005	712 \pm 89	0.022 \pm 0.003	21 \pm 86	0.001 \pm 0.002
4	557 \pm 152	0.138 \pm 0.038	213 \pm 81	0.012 \pm 0.005	787 \pm 90	0.024 \pm 0.003	156 \pm 90	0.004 \pm 0.002
5	469 \pm 152	0.114 \pm 0.037	36 \pm 74	0.002 \pm 0.004	913 \pm 92	0.027 \pm 0.003	172 \pm 90	0.005 \pm 0.002
6	394 \pm 152	0.093 \pm 0.036	0 \pm 9	0.000 \pm 0.001	856 \pm 92	0.025 \pm 0.003	192 \pm 93	0.005 \pm 0.002
7	645 \pm 151	0.153 \pm 0.036	0 \pm 1	0.000 \pm 0.000	708 \pm 92	0.021 \pm 0.003	138 \pm 93	0.004 \pm 0.002
8	492 \pm 150	0.115 \pm 0.035	23 \pm 83	0.001 \pm 0.005	654 \pm 92	0.019 \pm 0.003	13 \pm 92	0.000 \pm 0.002
9	832 \pm 153	0.191 \pm 0.035	439 \pm 89	0.024 \pm 0.005	804 \pm 94	0.023 \pm 0.003	27 \pm 93	0.001 \pm 0.002
10	1319 \pm 154	0.297 \pm 0.035	1467 \pm 98	0.078 \pm 0.005	1308 \pm 97	0.036 \pm 0.003	3 \pm 53	0.000 \pm 0.001
11	1841 \pm 158	0.395 \pm 0.034	2572 \pm 106	0.130 \pm 0.006	1941 \pm 103	0.052 \pm 0.003	155 \pm 97	0.004 \pm 0.002
12	1892 \pm 160	0.397 \pm 0.034	3414 \pm 112	0.169 \pm 0.006	2711 \pm 109	0.070 \pm 0.003	331 \pm 100	0.008 \pm 0.002
13	1552 \pm 158	0.346 \pm 0.035	3735 \pm 113	0.196 \pm 0.006	3023 \pm 111	0.083 \pm 0.003	298 \pm 99	0.007 \pm 0.002
14	1741 \pm 157	0.414 \pm 0.038	3779 \pm 112	0.212 \pm 0.007	3367 \pm 112	0.099 \pm 0.003	704 \pm 102	0.018 \pm 0.003
15	1890 \pm 159	0.445 \pm 0.038	4633 \pm 118	0.257 \pm 0.007	3906 \pm 116	0.114 \pm 0.004	971 \pm 105	0.025 \pm 0.003
16	2067 \pm 160	0.476 \pm 0.037	5057 \pm 121	0.274 \pm 0.007	4735 \pm 121	0.135 \pm 0.004	1198 \pm 108	0.030 \pm 0.003
17	2314 \pm 161	0.543 \pm 0.038	5597 \pm 122	0.309 \pm 0.007	5336 \pm 124	0.155 \pm 0.004	1597 \pm 111	0.041 \pm 0.003
18	2175 \pm 159	0.532 \pm 0.039	5845 \pm 123	0.336 \pm 0.008	5784 \pm 126	0.175 \pm 0.004	1594 \pm 112	0.043 \pm 0.003
19	2163 \pm 159	0.551 \pm 0.041	6227 \pm 124	0.373 \pm 0.008	6337 \pm 127	0.200 \pm 0.004	2160 \pm 114	0.060 \pm 0.003
20	2097 \pm 157	0.565 \pm 0.043	6353 \pm 125	0.403 \pm 0.009	6645 \pm 128	0.221 \pm 0.005	2621 \pm 117	0.077 \pm 0.004
21	2278 \pm 159	0.638 \pm 0.045	6191 \pm 125	0.408 \pm 0.009	7059 \pm 129	0.244 \pm 0.005	2575 \pm 117	0.079 \pm 0.004
22	2133 \pm 158	0.609 \pm 0.045	5350 \pm 122	0.359 \pm 0.009	6566 \pm 127	0.232 \pm 0.005	2421 \pm 115	0.076 \pm 0.004
23	1285 \pm 152	0.376 \pm 0.045	4080 \pm 116	0.281 \pm 0.008	5073 \pm 120	0.183 \pm 0.005	1943 \pm 111	0.062 \pm 0.004
24	940 \pm 149	0.276 \pm 0.044	2824 \pm 109	0.195 \pm 0.008	3560 \pm 113	0.129 \pm 0.004	1395 \pm 107	0.045 \pm 0.003
25	992 \pm 148	0.288 \pm 0.043	2087 \pm 104	0.143 \pm 0.007	2471 \pm 107	0.089 \pm 0.004	943 \pm 104	0.030 \pm 0.003
26	529 \pm 144	0.151 \pm 0.041	1431 \pm 100	0.096 \pm 0.007	2153 \pm 105	0.076 \pm 0.004	695 \pm 102	0.022 \pm 0.003
27	812 \pm 147	0.227 \pm 0.041	1150 \pm 99	0.076 \pm 0.007	1834 \pm 104	0.063 \pm 0.004	610 \pm 103	0.019 \pm 0.003

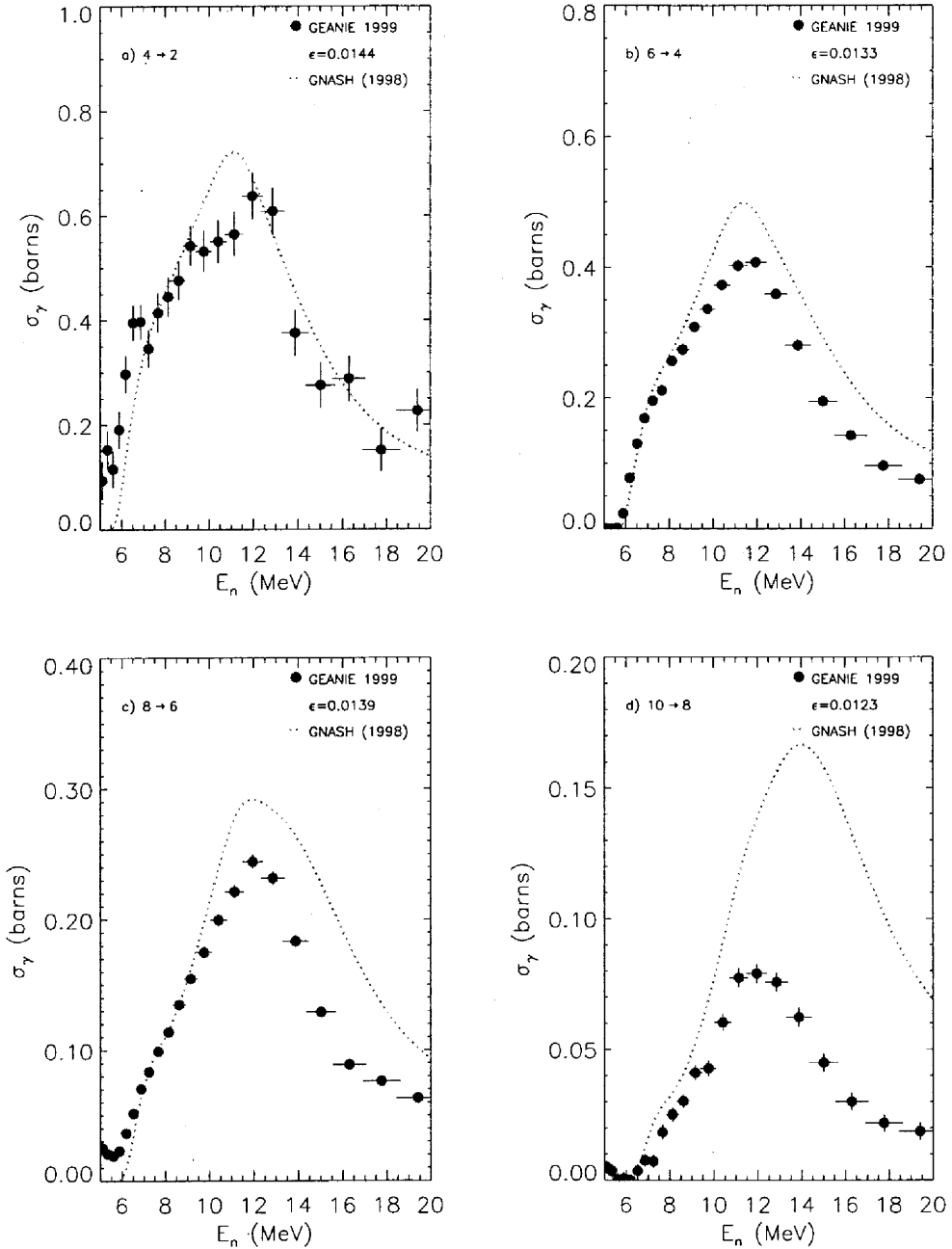


FIG. 29: a)-d): Excitation functions for the ^{234}U $4_1^+ \rightarrow 2_1^+$, $6_1^+ \rightarrow 4_1^+$, $8_1^+ \rightarrow 6_1^+$ and $10_1^+ \rightarrow 8_1^+$ transitions, constructed from the GEANIE 1999 data. Only statistical errors are included. Fission-chamber data from the ^{235}U foil with a flat baseline subtraction was used to generate these yields. The detector efficiency used is quoted in each case.

2 The Case of the $10_1^+ \rightarrow 8_1^+$ Transition

A special concern arises for the $10 \rightarrow 8$ transition. In both 1998 and 1999 GEANIE data sets, the $10 \rightarrow 8$ line has been fitted as a member of a pair of lines separated by less than the detector resolution FWHM. Centroid γ -ray energies of 243.9 and 244.4 keV were obtained in the 1998 fits for the two members of the doublet, with large uncertainties of 2.8 and 2.6 keV, respectively. Both these energies agree with the accepted [10] energy of 244.2 ± 0.5 keV for this transition. We have identified the higher-energy member of the doublet as the $10 \rightarrow 8$ transition, in part because its centroid energy is slightly closer to the accepted energy, but mostly because its excitation function shows the expected behavior near threshold (the excitation function for the 243.9-keV line remains well above zero below threshold, whereas the 244.4 keV line's yield vanishes below threshold). However it must be pointed out that the excitation functions for both lines in the doublet have generally similar shapes, which might indicate cross-contamination between the two peaks in the fitting.

In this section, we present the evidence in support of a two-peak fit for the feature near 244 keV, and extract an upper bound for the $10 \rightarrow 8$ partial cross section. In order to investigate the nature of this peak, we show in figure 30 the fits in the region of the peak in the 1999 GEANIE data assuming i) that the peak is a doublet (panel a), ii) that the peak is a single line with its width calculated from the fit to the entire spectrum as listed in table X (panel b), and iii) that the peak is a singlet whose width must be fit separately and independently of the remainder of the spectrum (panel c). A comparison of residuals in figure 30 a) and b) shows that if the peak width obtained from fitting peaks across the entire range of the spectrum with a well-known γ -ray energy dependence is accurate, then the two-peak model is the correct one. However, the proximity of these two peaks means that some contamination of the partial cross section plotted for the 244.4-keV line is to be expected. An upper bound for this cross section is obtained by allowing the peak width in the one-peak fit to vary freely (figure 30c), and extracting yields at individual neutron energies using this new fitting model as a template. It was necessary to allow the peak width to increase from 16.2 channels (or 1.014 keV) to 20.3 channels (1.269 keV) in order to fit the 244-keV peak as a single line, an increase of $\approx 25\%$. Furthermore, the strongest γ ray in the spectrum, a transition in the α -decay daughter ^{231}Th , can be found nearby at $E_\gamma = 185.7$ keV, and is expected to be a single line with no significant contamination. Therefore, the width extracted from that line should be very accurate. The $10 \rightarrow 8$ transition energy is only ≈ 58 keV higher and, according to the width function in table X, an increase of only 10.4% in peak width is expected from $E_\gamma = 185.7$ keV to $E_\gamma = 244.2$ keV. Instead, a 38.1% increase was needed for a one-peak fit. In light of this excessive requirement, we favor the two-peak model fit for the $10 \rightarrow 8$ transition.

The excitation functions corresponding to the fits in figure 30 a) and c) are compared in figure 31. The upper limit cross section given by the one-peak-fit is only modestly higher ($\approx 25\%$ at peak cross section) than the two-peak-fit cross section. Yet even this upper limit is over-estimated by GNASH by a factor of ≈ 1.7 . We quote in this report the cross section obtained from the two-peak fit as the best estimate of the $10 \rightarrow 8$ partial cross section, with the caveats discussed here.

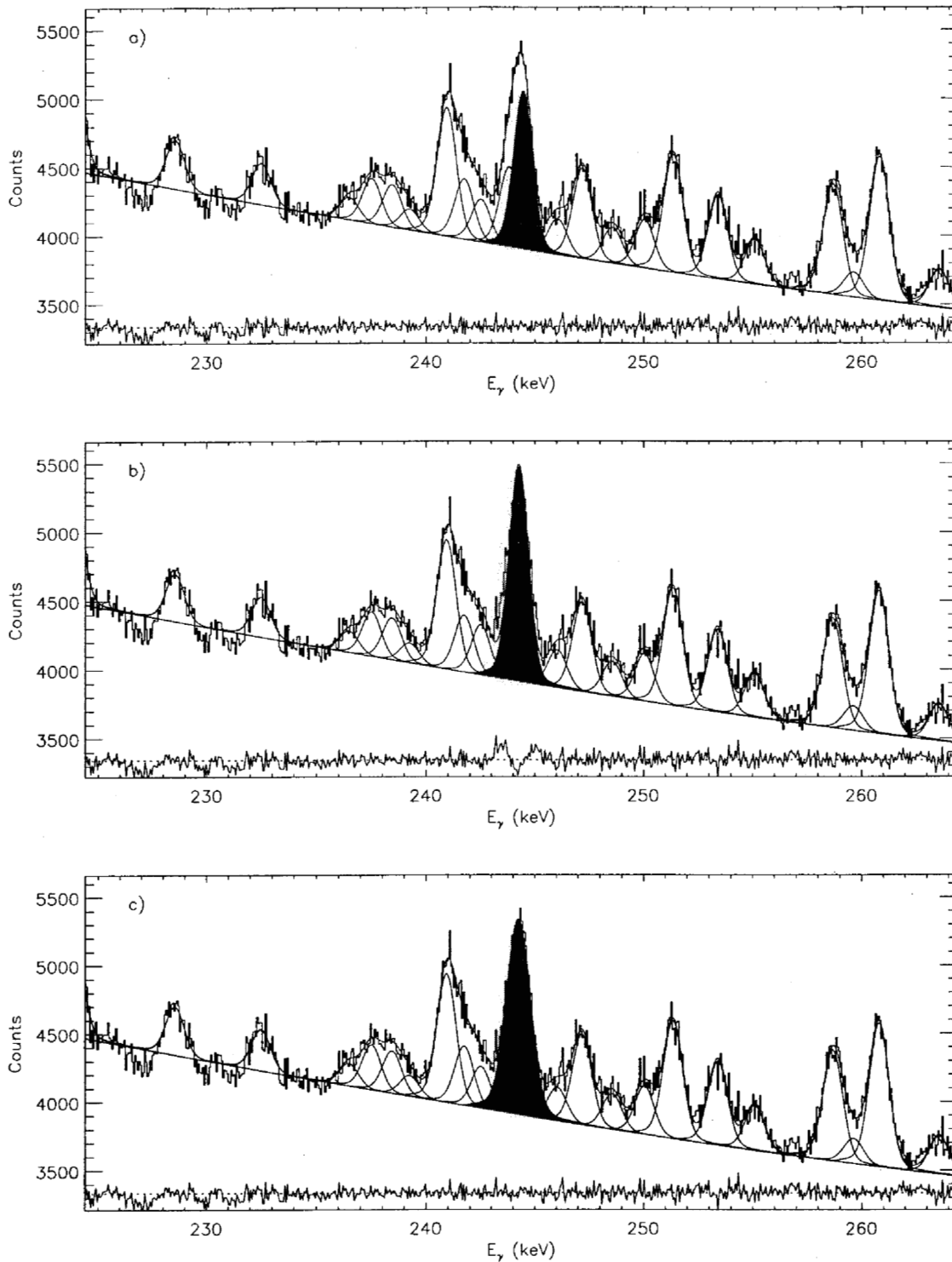


FIG. 30: Fits of the 244-keV peak assuming: a) a pair of lines, b) a single line with peak width determined from the global spectrum fit, and c) a single line with locally-fit peak width. The relative residual spectrum is plotted on an arbitrary scale.

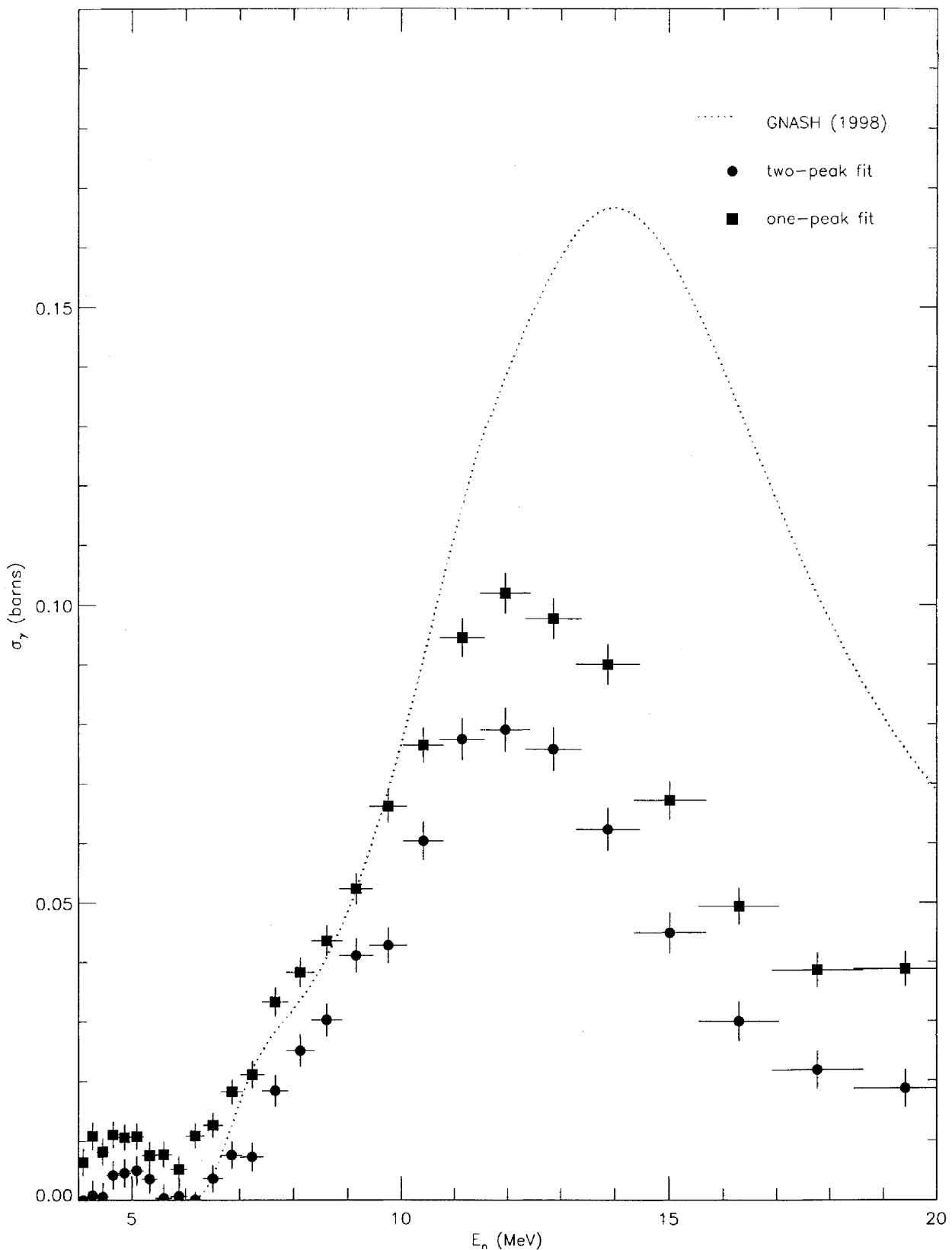


FIG. 31: Partial cross sections constructed from the one-peak and two-peak fits, compared with the GNASH prediction.

B $^{56}\text{Fe}(n,n')$ Analysis

1 Partial Cross Section Evaluation

The 1999 GEANIE data provide an independent verification of the procedure used to extract partial cross sections from the γ -ray data. The experiment was carried out with four 2-mil ^{nat}Fe foils, two on either side of the ^{235}U sample, with a total areal density of 0.164 g/cm², and with an enrichment in the ^{56}Fe isotope of 91.8%. Therefore a partial cross section could be extracted for the 846.8-keV $2 \rightarrow 0$ transition in ^{56}Fe , and compared to an accepted experimental standard [18] of 785 ± 48 mb at $E_n = 14.5$ MeV.

The 846.8-keV line is located on top of the 847-keV neutron bump, caused by the de-excitation of recoiling ^{76}Ge nuclei inside the detectors. The functional form provided in XGAM [6] to model neutron bumps was used to obtain an accurate fit to the $^{56}\text{Fe} 2 \rightarrow 0$ peak, otherwise the fit parameters are those listed in table X. A sample of fits at select neutron energies is displayed in figure 32. The residual spectrum for each fit attests to the quality of that fit. In fact, the fit of the 846.8-keV line shows a smaller residual than the surrounding region; this is due to the large peak-to-background-height ratio for this peak: at $E_n = 6.2$ MeV, this ratio is ≈ 21.4 and is still as high as ≈ 6.5 at $E_n = 16.3$ MeV.

Angular-distribution effects were examined for the 846.8-keV transition using the code AVALANCHE (see section XI) and found to produce a less than 1% correction to the observed excitation function. Therefore, no correction for angular-distribution effects was necessary for this line in the $E_n = 4\text{--}20$ MeV range.

The deduced partial cross section can be found in table XIV which lists results using both fission-foil normalizations. The corresponding cross-section plots are displayed in figures 33 and 34 for ^{235}U and ^{238}U fission-foil normalizations respectively. The standard cross section for the $^{56}\text{Fe} 2 \rightarrow 0$ transition at $E_n = 14.5$ MeV is also shown, and the agreement between the GEANIE data and the standard value is clearly excellent.

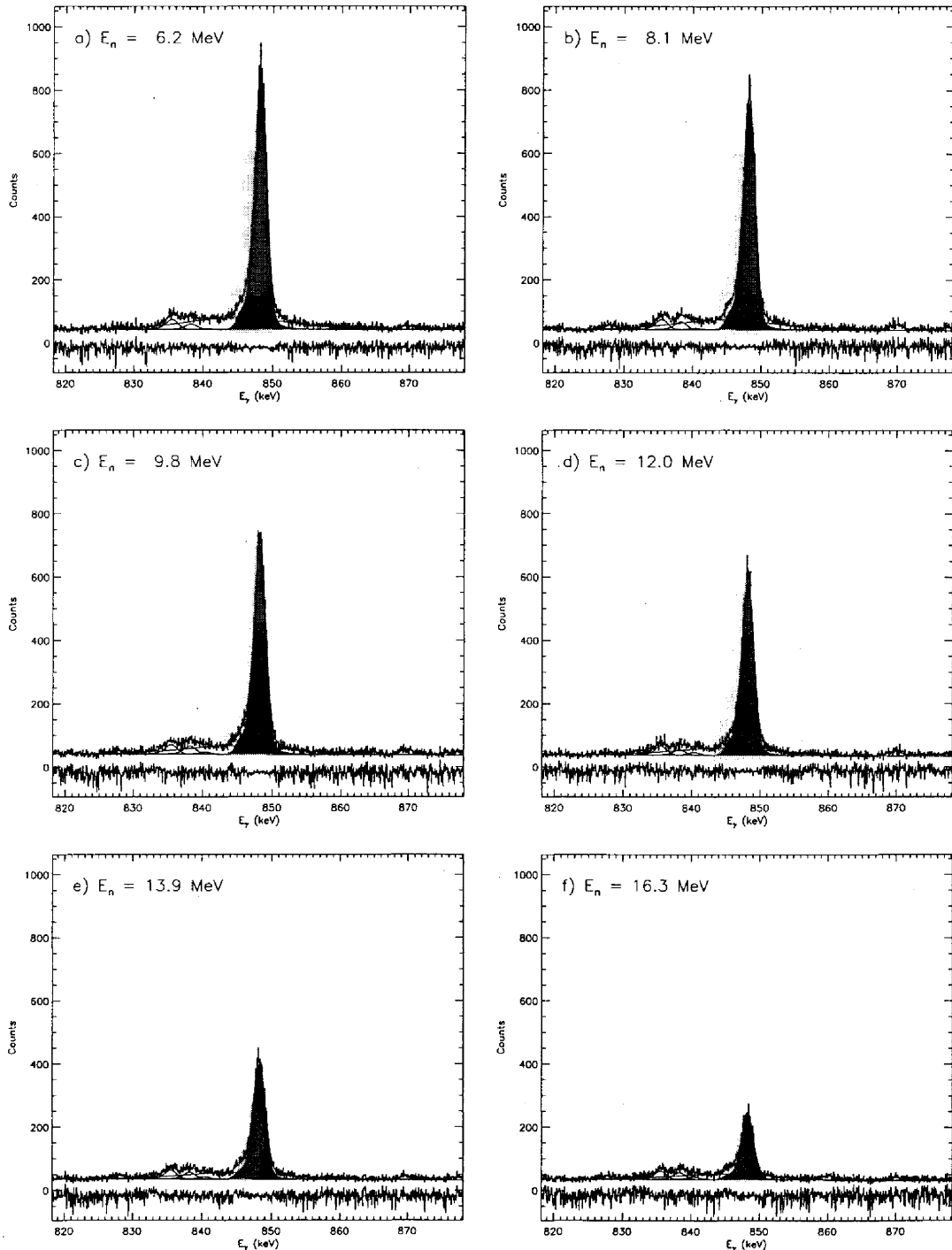


FIG. 32: Fits for the ^{56}Fe $2_1^+ \rightarrow 0_1^+$ transition in selected neutron-energy cuts of the GEANIE 1999 data. The $2_1^+ \rightarrow 0_1^+$ peak is shaded in red. The relative fit residual is plotted on an arbitrary scale.

TABLE XIV: Fitted raw areas and deduced partial γ -ray cross sections for the $2 \rightarrow 0$ transition in ^{56}Fe using both ^{235}U (denoted by “FC1 sub”) and ^{238}U (denoted by “FC2”) fission-foil normalizations. Quoted uncertainties represent random fluctuations only.

Bin A($2_1^+ \rightarrow 0_1^+$)	$\sigma_{2_1^+ \rightarrow 0_1^+}(b)$ (from FC1 sub)	$\sigma_{2_1^+ \rightarrow 0_1^+}(b)$ (from FC2)
1	24840 \pm 190	1.526 \pm 0.023
2	24310 \pm 185	1.475 \pm 0.022
3	24500 \pm 189	1.412 \pm 0.021
4	27040 \pm 197	1.521 \pm 0.022
5	28180 \pm 200	1.556 \pm 0.022
6	29580 \pm 201	1.598 \pm 0.022
7	29540 \pm 201	1.594 \pm 0.022
8	30140 \pm 203	1.611 \pm 0.023
9	30790 \pm 205	1.609 \pm 0.022
10	29820 \pm 206	1.531 \pm 0.020
11	30900 \pm 208	1.512 \pm 0.019
12	31050 \pm 209	1.486 \pm 0.017
13	29840 \pm 205	1.516 \pm 0.018
14	26970 \pm 196	1.464 \pm 0.018
15	27070 \pm 196	1.454 \pm 0.017
16	27350 \pm 197	1.436 \pm 0.017
17	25870 \pm 192	1.383 \pm 0.017
18	25030 \pm 189	1.395 \pm 0.017
19	24150 \pm 185	1.402 \pm 0.017
20	22860 \pm 181	1.403 \pm 0.018
21	20700 \pm 173	1.321 \pm 0.017
22	17770 \pm 163	1.156 \pm 0.015
23	13740 \pm 146	0.915 \pm 0.013
24	9985 \pm 131	0.668 \pm 0.011
25	7475 \pm 117	0.495 \pm 0.009
26	5963 \pm 110	0.389 \pm 0.008
27	5107 \pm 105	0.325 \pm 0.008
		0.307 \pm 0.016

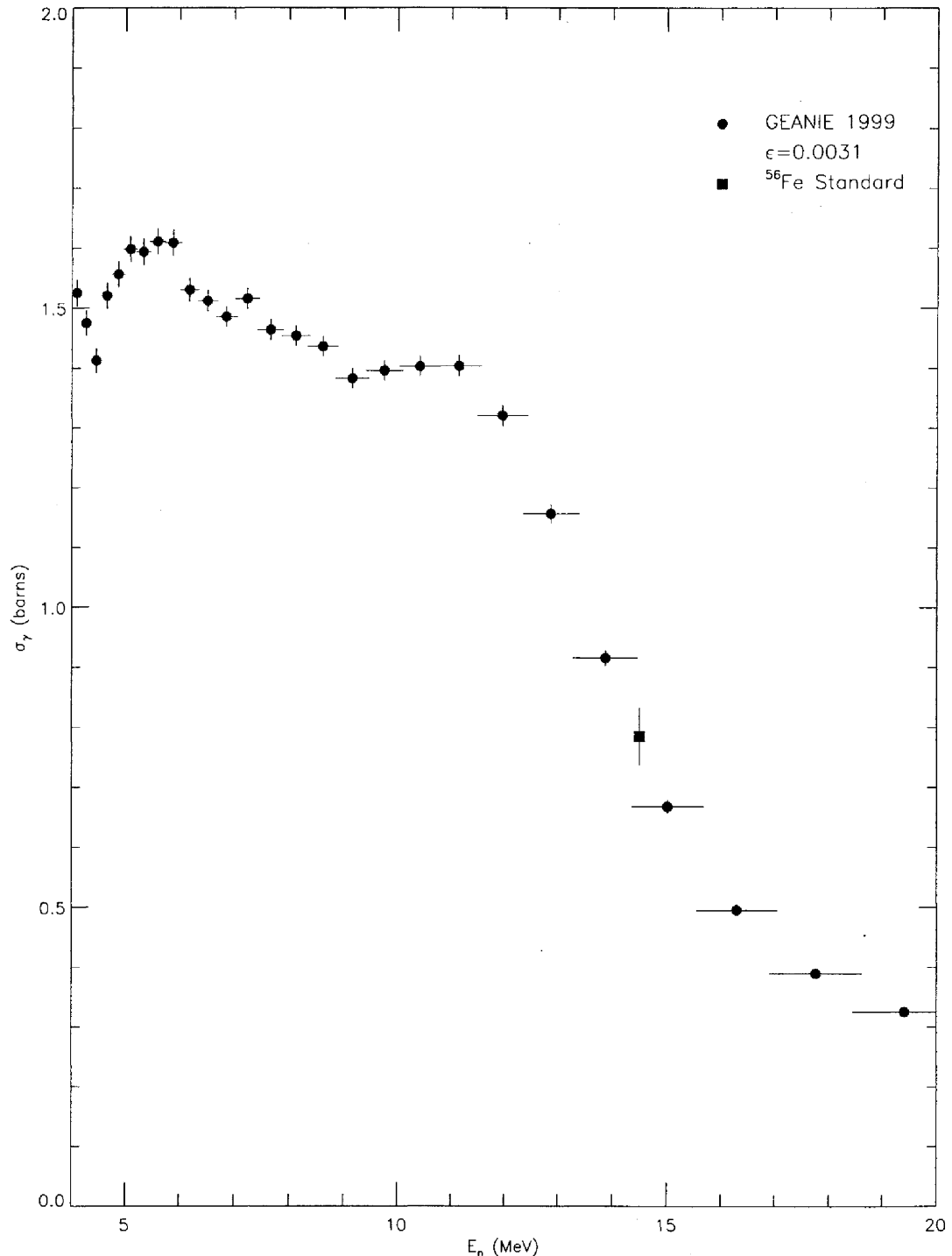


FIG. 33: Comparison of the $^{56}\text{Fe}(n,n')$ $2_1^+ \rightarrow 0_1^+$ partial cross section extracted from the GEANIE 1999 data without background subtraction to the evaluated standard at $E_n = 14.5$ MeV. Data are flux-normalized using the ^{235}U fission foil with full baseline subtraction. The detector efficiency used is quoted in the legend.

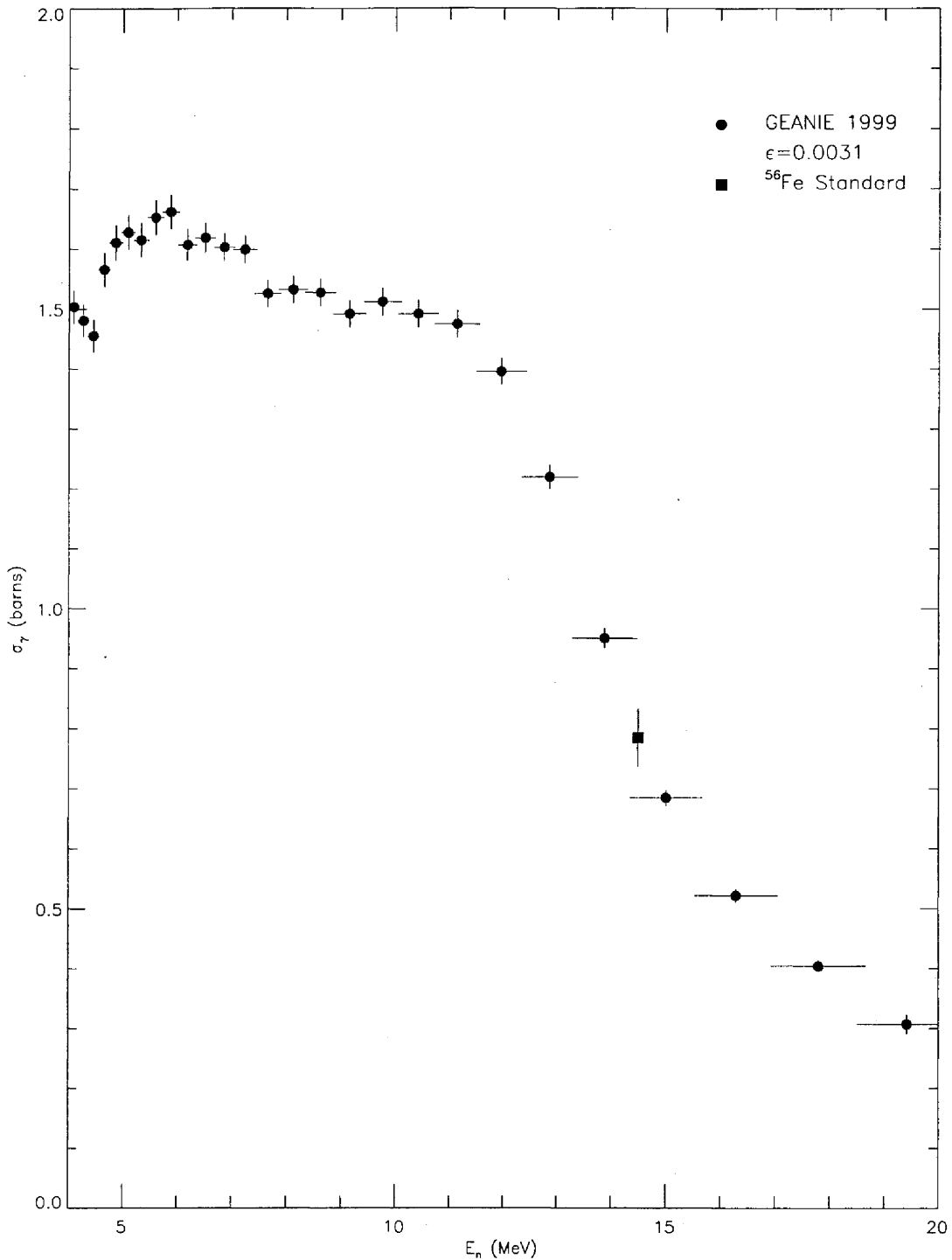


FIG. 34: Comparison of the $^{56}\text{Fe}(n,n')$ $2_1^+ \rightarrow 0_1^+$ partial cross section extracted from the GEANIE 1999 data without background subtraction to the evaluated standard at $E_n = 14.5$ MeV. Data are flux-normalized using the ^{238}U fission foil without baseline subtraction. The detector efficiency used is quoted in the legend.

VIII. ESTIMATION OF ENERGY-DEPENDENT SYSTEMATIC UNCERTAINTIES

The procedure described in section III to calculate energy-dependent systematic uncertainties is applied to the 1999 GEANIE data. As in the **98Thin** analysis, these systematic uncertainties are attributed to unaccounted-for beam-wrap-around background in the flux normalization data, and inadequacies in the γ -ray fitting model used to extract peak areas (e.g. incorrect treatment of the continuum background around the peak, missing or spurious peaks, etc ...). Here as well, these uncertainties are approximated by comparing ^{235}U - and ^{238}U -fission-foil data, and by comparing random-TOF-background subtracted and unsubtracted γ -ray data. A residual standard deviation σ_d is calculated for each quantity using equations 9-11. The results are shown in table XV which shows σ_d for the flux normalization N_ϕ , for the measured peak areas in the $^{235}\text{U}(\text{n},2\text{n})^{234}\text{U}$ channel, and for the measured $2_1^+ \rightarrow 0_1^+$ peak area for the ^{56}Fe foil.

TABLE XV: Residual systematic uncertainties for the flux normalization and fitted areas calculated using equation 11. These uncertainties are added in quadrature to the uncertainties in the flux in and individual peak areas at each neutron energy.

Quantity	σ_d
$N_\phi (\gamma/\text{b})$	412914.3
$^{234}\text{U} A(4_1^+ \rightarrow 2_1^+)$	25.7
$^{234}\text{U} A(6_1^+ \rightarrow 4_1^+)$	11.8
$^{234}\text{U} A(8_1^+ \rightarrow 6_1^+)$	9.9
$^{234}\text{U} A(10_1^+ \rightarrow 8_1^+)$	3.0
$^{56}\text{Fe} A(2_1^+ \rightarrow 0_1^+)$	11.1

As with the **98Thin** data, we take the raw (i.e. not random-TOF subtracted) data, normalized to the ^{235}U -fission-foil flux with baseline subtraction as the best 1999 data, and the sum in quadrature of random and energy-dependent systematic uncertainties determined here as the corresponding uncertainties on the excitation function shape. These “shape” uncertainties are tested in section IX and the corresponding total uncertainties, which include additional systematic uncertainties on neutron-energy-independent factors (e.g. target thickness, etc ...) are discussed in section X.

IX. VALIDATION OF THE 1999 RESULTS WITH RESPECT TO ENERGY-DEPENDENT UNCERTAINTIES

We verify the deduced energy-dependent uncertainties in the same way as for the 1998 data. Though they are not discussed in detail here, random-TOF-subtracted spectra were created for the “99thin” data and fitted using the parameters in table X. The raw and subtracted data, normalized with either fission foil are plotted in figure 35 against the one-sigma band about the raw data normalized with the ^{235}U foil, which we take as the best values for the partial cross sections. The data, analyzed by various means are seen to lie generally within the uncertainty band. From this, we gain greater confidence in the assigned uncertainties.

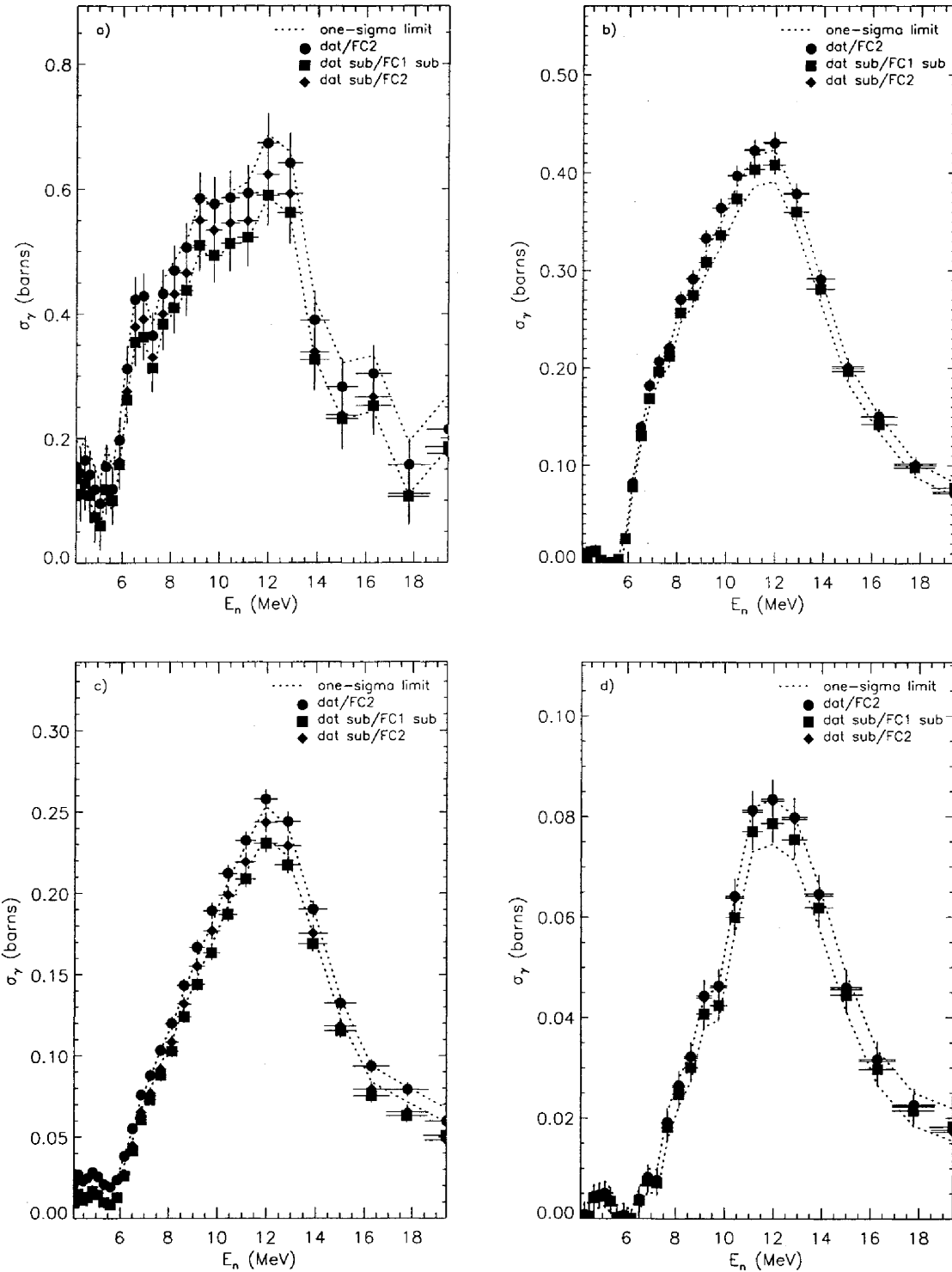


FIG. 35: Validation of the one-sigma confidence band for the combined random and energy-dependent systematic uncertainties deduced from the unsubtracted 1999 data normalized to ^{235}U fission-foil counts with baseline subtraction. In the legend, raw data are labeled by the symbol “dat”, subtracted data by “dat sub”, ^{235}U -foil normalization with baseline subtraction is denoted by “FC1 sub” and ^{238}U -foil normalization is denoted by “FC2”.

X. VALIDATION OF THE 1999 RESULTS WITH RESPECT TO TOTAL UNCERTAINTIES

As a verification of the total uncertainty (see section VI for a definition), the standard ^{56}Fe $2 \rightarrow 0$ partial yield at E_n 14.5 MeV is plotted in figure 36 against the total-uncertainty one-sigma band about the partial cross section deduced from raw 1999 data, normalized using counts from the ^{235}U fission foil. The agreement is clearly excellent.

Unlike the validation of the "98thin" total uncertainties in section VI, the agreement in figure 36 provides more than an internal consistency check. Because the ^{56}Fe standard has been measured by independent means, this agreement builds confidence in the entire procedure used to extract a partial cross section from measured γ -ray counts.

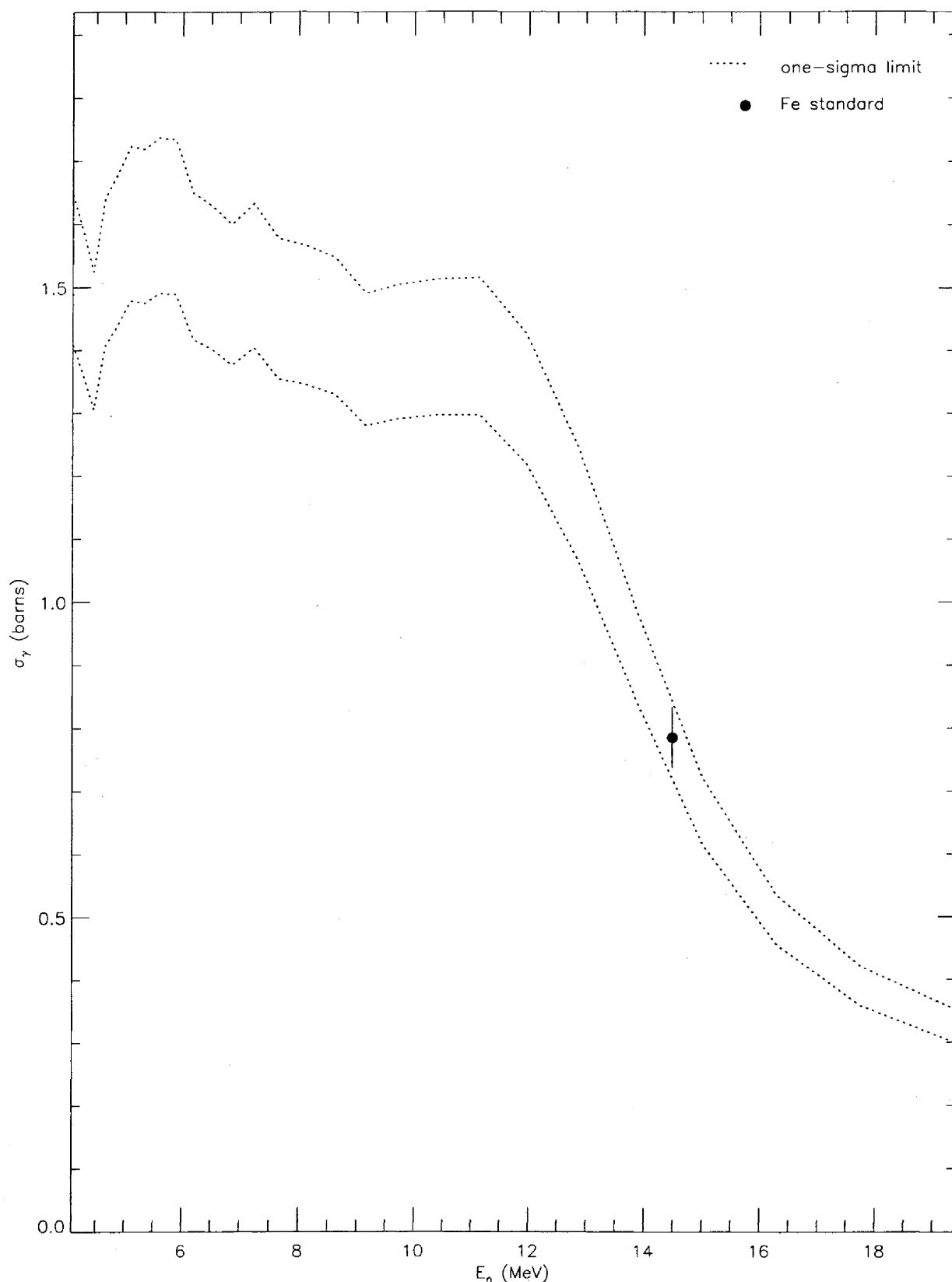


FIG. 36: Comparison of the standard partial ^{56}Fe $2 \rightarrow 0$ cross section to the one-sigma total-uncertainty band for the 1999 GEANIE data.

XI. ANGULAR DISTRIBUTION EFFECTS

A Formalism

The partial γ -ray cross sections discussed so far have assumed that photons are emitted by the decaying nucleus isotropically. This is not an accurate assumption as the incident neutron beam will partially align the nuclear spins in a plane orthogonal to the beam direction. In mathematical terms, this means that for a given state with spin J , and if we take the z-axis along the direction of the incident beam, the corresponding magnetic substates (with quantum number $m = -J \dots J$) will not be occupied with a uniform probability distribution. A formulation often used in such cases is to assume a Gaussian distribution among magnetic substates given by [19]:

$$P(m) = \frac{e^{-\frac{m^2}{2\sigma^2}}}{\sum_{m'=-J}^J e^{-\frac{(m')^2}{2\sigma^2}}} \quad (12)$$

where the standard deviation σ is a measure of the degree of alignment of the nuclear spin (i.e. $\sigma \rightarrow 0$ for a fully aligned state and $\sigma \rightarrow \infty$ for no alignment). The angular distribution of emitted photons can be described as a function of the angle of observation with respect to the beam direction as an expansion in Legendre polynomials P_k :

$$W(\theta) = \sum_k A_k P_k(\cos\theta) \quad (13)$$

where k is even, and for most practical applications, does not exceed 4 (i.e. $k = 0, 2, 4$). The transition between two nuclear states can be characterized by four quantum numbers which determine the A_k coefficients: the spins J_i and J_f of the initial and final states respectively and the multipoles L_1 and L_2 of the two most important competing decay modes (e.g. dipole versus quadrupole, etc.). Then:

$$A_k(J_i, L_1, L_2, J_f) = \rho_k(J_i) \frac{1}{1 + \delta^2} [F_k(J_f, L_1, L_1, J_i) + 2\delta F_k(J_f, L_1, L_2, J_i) + \delta^2 F_k(J_f, L_2, L_2, J_i)] \quad (14)$$

where δ is the mixing ratio between the competing L_1 -pole and L_2 -pole decay modes, given by the ratio of the reduced transition matrix elements:

$$\delta \equiv \frac{\langle J_f || L_2 || J_i \rangle}{\langle J_f || L_1 || J_i \rangle} \quad (15)$$

The F_k coefficients in equation 14 have explicit forms which involve only the quantum numbers on which they depend. These forms are complicated and do not add to the present discussion, the interested reader can find explicit expressions for the F_k coefficients in reference [19], along with tabulated values for all relevant instances of the quantum numbers.

The statistical tensor ρ_k incorporates the magnetic-substate distribution from equation 12:

$$\rho_k(J) = \sqrt{2J+1} \sum_m (-1)^{J-m} \langle J \ m \ J - m | k \ 0 \rangle P(m) \quad (16)$$

In addition, it is possible to correct for the variation of the γ -ray intensity across the face of a detector, when its angular distribution is not isotropic. This typically results in a “damping” of the observed angular distribution and can be modeled by introducing the factors Q_2 and Q_4 which multiply the theoretical A_2 and A_4 coefficients in equation 13. These coefficients have been both calculated and measured in the literature [20] for a variety of detector types and geometries. For the GEANIE spectrometer in particular, those coefficients have been calculated [21] to be:

$$Q_2 = 0.978 \quad (17)$$

$$Q_4 = 0.928 \quad (18)$$

and are applicable in the $E_\gamma = 150\text{--}200\text{-keV}$ energy range.

TABLE XVI: GEANIE detector angles with respect to the beam direction.

Detector Type	Angle
1	planar 141.07°
2	planar 141.82°
3	planar 143.62°
4	planar 144.13°
5	coaxial 129.50°
6	coaxial 100.48°
7	coaxial 100.91°
8	coaxial 78.50°
9	planar 58.24°
10	planar 58.65°
11	planar 26.50°
12	planar 29.02°
13	planar 29.02°
14	planar 25.20°
15	coaxial 56.69°
16	coaxial 56.60°
17	coaxial 76.90°
18	coaxial 100.22°
19	coaxial 100.48°
20	planar 128.00°

B Geometry of the GEANIE spectrometer

Most planar detectors in the GEANIE spectrometers are located near forward and backward angles with respect to the beam direction, while most coaxial detectors are distributed about 90° with respect to the beam direction. More specifically the precise angle with respect to beam for each detector can be found in table XVI.

The biased distribution of detectors in the array means, for example, that stretched (i.e. $|J_f - J_i| = L$ where L is the multipole of the $J_i \rightarrow J_f$ transition) quadrupole transitions which produce photons at mostly forward and backward angles with respect to beam, will be over-counted in most planar detectors if an isotropic angular distribution is assumed for the γ rays. Conversely, stretched dipole transitions, which peak near 90°, will be under-counted in most planar detectors. These trends will be reversed in the coaxial detectors.

C Estimate of the Angular-Distribution Correction

In general, a fully aligned transition can show intensity variations as a function of angle of up to $\approx 30\%$. However, the decay of the nucleus through "unstretched" transitions—transitions for which the multipole order exceeds the difference in spins between initial and final states—destroys the alignment of the nucleus [19]. At higher incident neutron energies above the reaction threshold, the number of decay paths through "unstretched" transitions increases and we expect the angular distribution effects to become less important.

If the true angular distribution $W(\theta)$ of a particular γ ray is known, then the correction to the assumption that it is emitted isotropically (i.e. that $W(\theta) \equiv 1$) is given by the multiplicative factor:

$$C_\gamma = \frac{\sum_i \epsilon_i (1 - f_{ge}^{(i)})}{\sum_i \epsilon_i (1 - f_{ge}^{(i)}) W(\theta_i)} \quad (19)$$

where the index i extends over the detectors of a particular type (i.e. $i = 1, 2, 3, 4, 9, 10, 11, 12, 13, 14, 20$ for the planar-sum data and $i = 5, 6, 7, 8, 15, 16, 17, 18, 19$ for the coaxial-sum data), ϵ_i is the efficiency for the γ ray of interest in the i^{th} detector, θ_i is the angle of the i^{th} detector with respect to beam (given in table XVI, and $f_{ge}^{(i)}$ is the deadtime for the i^{th} detector. Thus for example, for a quadrupole transition observed in the planar-detector-sum data, $W(\theta_i) > 1$ for most planar detectors and the correction factor $C_\gamma < 1$, compensating for the over-counting of the isotropic assumption. It can be shown using equation 19 for the GEANIE spectrometer that even a fully aligned, stretched transition will produce a correction of less than $\approx 15\%$.

Ideally, the angular distribution for each γ ray of interest should be measured as a function of incident neutron energy, so that an experimentally-determined correction can be applied to the data. This cannot be done systematically and accurately for the present data for four main reasons: i) the geometry of the GEANIE spectrometer provides only six independent angles with respect to beam ($\approx 27^\circ, 57^\circ, 77^\circ, 100^\circ, 129^\circ$, and 143°), as a close inspection of table XVI will reveal, whereas precise angular-distribution measurements often involve 10 or more angles, ii) two of those six angles, namely near 77° and 100° are only realized in the coaxial detectors, for which no reliable efficiency correction could be extracted below $E_\gamma \approx 300$ keV [9], iii) the detectors were positioned only ≈ 14 cm on average from the focal point of the spectrometer and therefore subtend large angles than is normally desirable for an angular distribution measurement, and iv) the statistics are largely inadequate for all but a few lines to observe angular-distribution effects. Only the $6_1^+ \rightarrow 4_1^+$ and $8_1^+ \rightarrow 6_1^+$ transitions have sufficient statistics in the $(n,2n\gamma)$ channel so that a four-angle distribution may be extracted from the data as a function of incident neutron energy. Even then, some allowances must be made to maximize the counts at each angle. First, planar detectors at approximately the same angle with respect to beam are grouped, and their counts combined. Thus detectors 1 through 4 in table XVI are combined as a single detector with averaged angle 142.66° , detectors 1 and 9 are grouped at an averaged angle of 58.44° , detectors 11 through 14 are grouped at 27.44° , and detector 20 is alone among the planar detectors at 128.00° . Second, wide neutron-energy bins are used to obtain sufficient counts in individual detector groups. Specifically we divide the neutron-energy range of interest into three regions: $E_n = 6\text{--}8, 8\text{--}12$, and $12\text{--}20$ MeV.

It is also possible to model the expected angular distribution of observed γ rays in the $(n,2n)$ reaction channel by a careful accounting of incoming and outgoing partial waves in the reaction process as well as de-alignment effects from the subsequent statistical decay of the nucleus to the levels of interest. This calculation has been made using the code AVALANCHE [22][23]. In this program, the Gaussian hypothesis of equation 12 is relaxed so that separate standard deviations σ_2 and σ_4 can be obtained for the A_2 and A_4 coefficients in equation 13, respectively.

In order to compare the AVALANCHE predictions to the measured angular distributions of the $6_1^+ \rightarrow 4_1^+$ and $8_1^+ \rightarrow 6_1^+$ transitions, we must compensate for the wide neutron-energy bins used in the angular-distribution data analysis. For this, the $\sigma_2(E_n)/J$ and σ_4/J values listed in tables XX and XXI must be weighted by the partial γ -ray cross section and the neutron flux before being integrated over the neutron-energy bin of interest (overall scale factors are not important in the extraction of angular distributions). In order to mimic the experimental situation, we generate a neutron-energy-bin dependent angular distribution from the predicted $\sigma_2(E_n)/J$ and $\sigma_4(E_n)/J$ values in the AVALANCHE program:

$$W'(\theta, [E_{min}, E_{max}]) \equiv \frac{\int_{E_{min}}^{E_{max}} dE_n \sigma_\gamma(E_n) N_\phi(E_n) W(\theta, E_n)}{\int_{E_{min}}^{E_{max}} dE_n \sigma_\gamma(E_n) N_\phi(E_n)} \quad (20)$$

where $[E_{min}, E_{max}]$ specifies the neutron-energy bin range, $\sigma_\gamma(E_n)$ is the partial cross section, $N_\phi(E_n)$ the neutron flux and the neutron-energy dependence in the angular distribution $W(\theta, E_n)$ is completely determined by $\sigma_2(E_n)/J$ and $\sigma_4(E_n)/J$. The lowest neutron-energy bin extends from $E_n = 6$ to 8 MeV. This range includes the $E_n = 6$ MeV point for which the AVALANCHE code cannot calculate an angular distribution for either the $6_1^+ \rightarrow 4_1^+$ or $8_1^+ \rightarrow 6_1^+$ transition. Though we have stated that, in general, the behavior of $\sigma_2(E_n)/J$ and $\sigma_4(E_n)/J$ is difficult to extrapolate, we must do so in this case in order to compare prediction and experiment. We note that for the $6_1^+ \rightarrow 4_1^+$ and $8_1^+ \rightarrow 6_1^+$ transitions in particular, the trends of $\sigma_2(E_n)/J$ and $\sigma_4(E_n)/J$ are well reproduced by low-order polynomial fits, as can be seen in figure 37. For the remainder of the terms in equation 20, we use the partial cross sections predicted by GNASH and the experimentally-deduced neutron flux from the **98Thin** ^{235}U -fission-foil data. The comparison between experimental and predicted angular distributions is shown in figure 38 for the $6_1^+ \rightarrow 4_1^+$ transition and figure 39 for the $8_1^+ \rightarrow 6_1^+$ transition. We plot the experimental angular distributions extracted both with the Gaussian assumption for the m-substate distribution (labeled as “constrained” in the figures) and without that assumption, but taking $A_4 = 0$ (labeled as “free” in the figures). The corresponding observed and predicted A_2 and A_4 coefficients are listed in tables XVII and XVIII. In general, the experimental angular distributions and AVALANCHE calculations are in good agreement. The agreement with the “free” fit (i.e. without Gaussian assumption) can be significantly improved if the A_2 and A_4 coefficients are multiplied by a uniform factor of 0.8351 for the $6_1^+ \rightarrow 4_1^+$ distribution and 0.7938 for the $8_1^+ \rightarrow 6_1^+$ distribution. We can combine these two factors by weighted average to obtain a single factor of 0.8068 which we apply systematically to all the AVALANCHE calculations for the $(n,2n)$ channel. In other words, based on the observed angular distributions for the $6_1^+ \rightarrow 4_1^+$ and $8_1^+ \rightarrow 6_1^+$ transitions, we conclude that AVALANCHE systematically over-predicts the alignment of all transitions by $\approx 23.9\%$ (which we compensate for with the 0.8068 “damping” factor). In addition, we use the size of this damping factor as an estimate of uncertainty in the AVALANCHE prediction. Thus, if we vary this factor by ± 0.1932 (this amount is chosen such that at one extreme, $0.8068 + 0.1932 = 1$, and the calculations are not damped), the deduced planar-detector correction factor (using equation 19) at $E_n = 6$ MeV, where the angular-distribution effect is largest, is less than 2.0% for the $6_1^+ \rightarrow 4_1^+$

transition and less than 2.5% for the $8_1^+ \rightarrow 6_1^+$ transition. Based on this, we adopt a systematic uncertainty of 2.5% on all angular-distribution correction factor predicted using the AVALANCHE code.

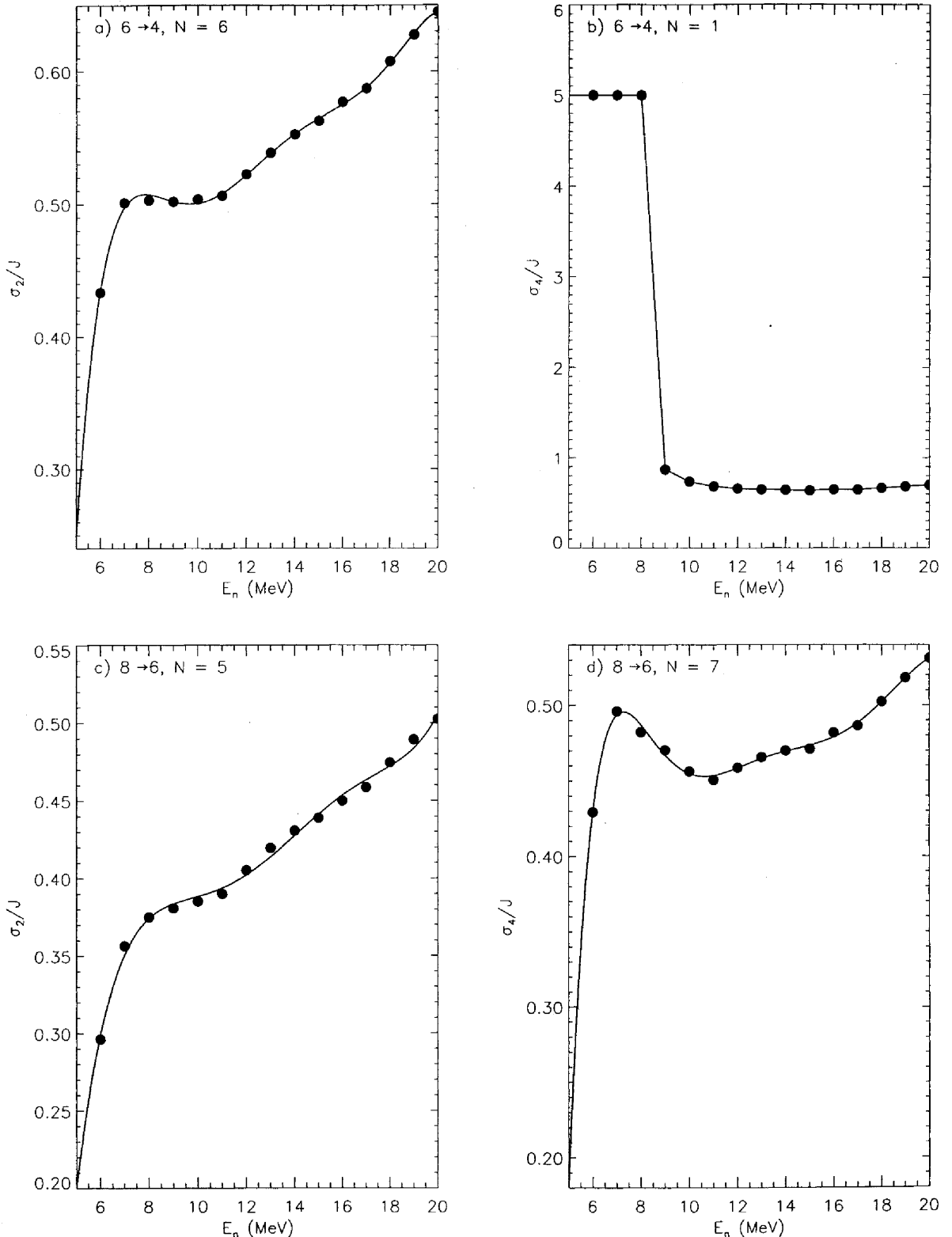


FIG. 37: Values of a) $\sigma_2(E_n)/J$ and b) $\sigma_4(E_n)/J$ for the $6_1^+ \rightarrow 4_1^+$ transition and c) $\sigma_2(E_n)/J$ and b) $\sigma_4(E_n)/J$ for the $8_1^+ \rightarrow 6_1^+$ transition predicted by the AVALANCHE program. The solid line represents a polynomial fit to the points, the order N of the polynomial is quoted in each panel.

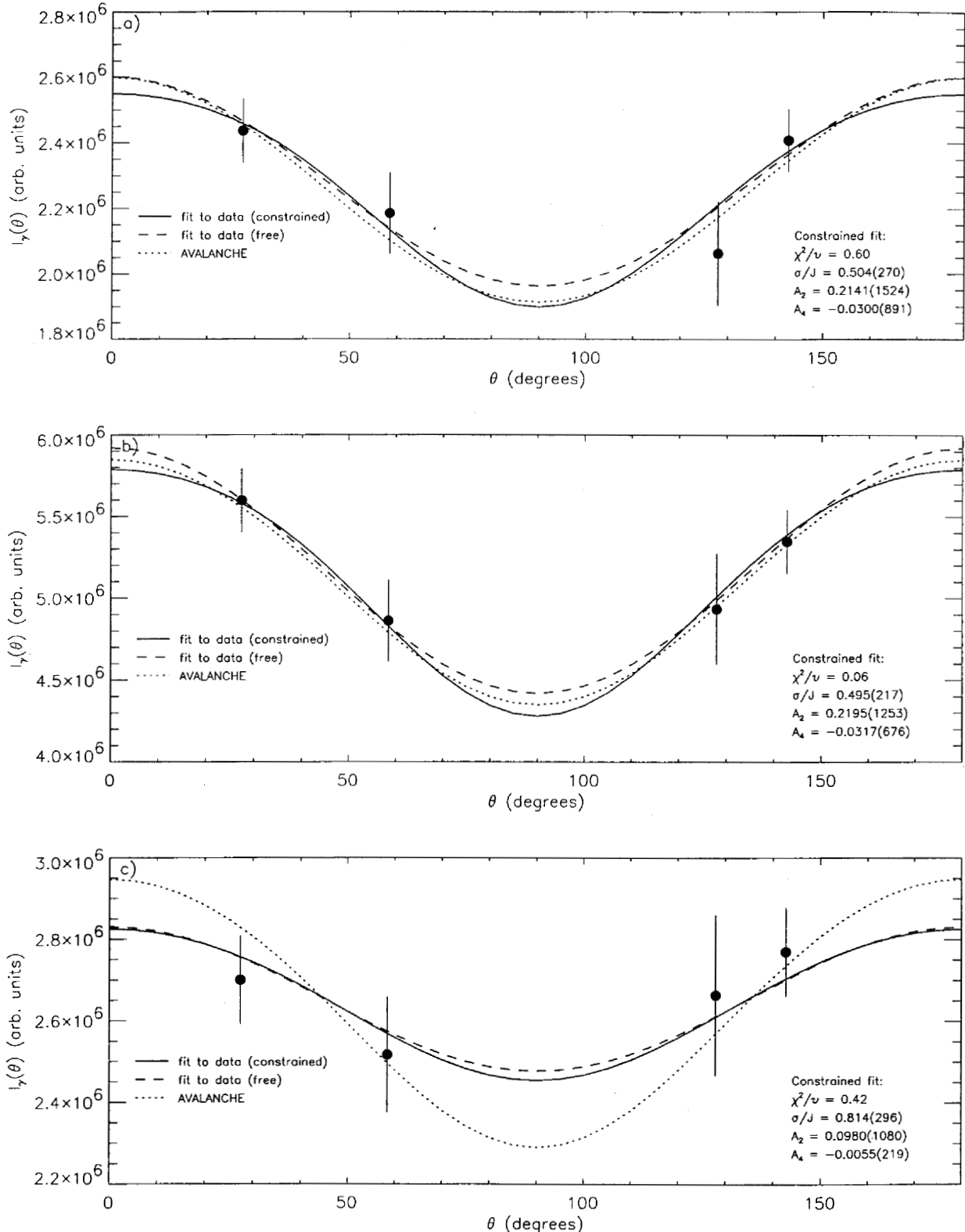


FIG. 38: Angular distributions extracted from the **98Thin** data set for the $6_1^+ \rightarrow 4_1^+$ transition and compared to AVALANCHE calculations in the a) $E_n = 6\text{--}8 \text{ MeV}$, b) $E_n = 8\text{--}12 \text{ MeV}$, and c) $E_n = 12\text{--}20 \text{ MeV}$ energy ranges. In each panel, the parameters resulting from the constrained fit to the GEANIE data are quoted.

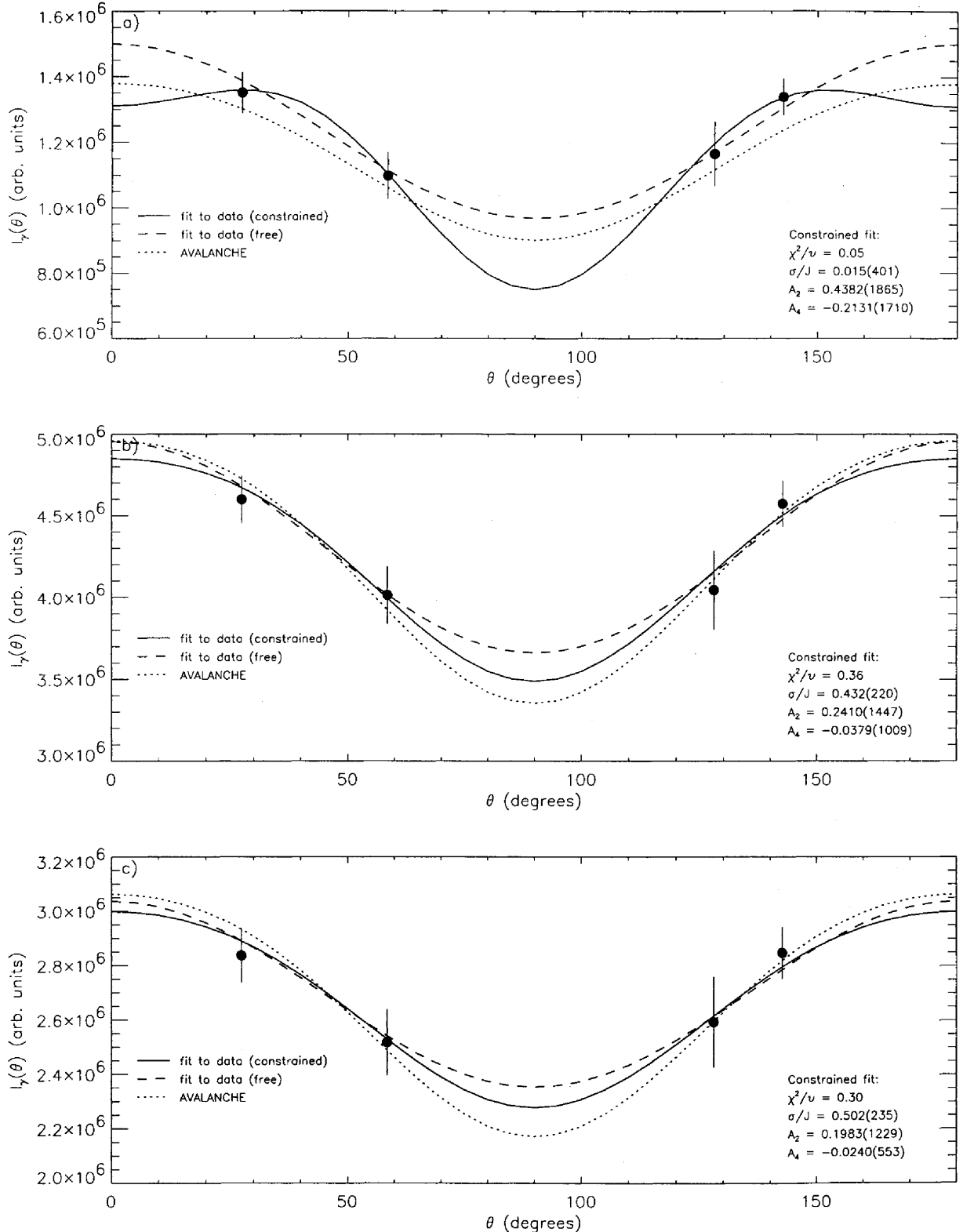


FIG. 39: Angular distributions extracted from the **98Thin** data set for the $8_1^+ \rightarrow 6_1^+$ transition and compared to AVALANCHE calculations in the a) $E_n = 6\text{--}8$ MeV, b) $E_n = 8\text{--}12$ MeV, and c) $E_n = 12\text{--}20$ MeV energy ranges. In each panel, the parameters resulting from the constrained fit to the GEANIE data are quoted.

TABLE XVII: Comparison of predicted and fitted angular-distribution parameters for the $6_1^+ \rightarrow 4_1^+$ transition. The AVALANCHE prediction has been weighted according to equation 20 to account for the finite neutron-energy bin size.

$E_n^{(\min)} - E_n^{(\max)}$ (MeV)	Quantity	Predicted	Constrained fit	Unconstrained fit
6.0–8.0	A ₂	0.2136	0.2141 \pm 0.1524	0.1956 \pm 0.0895
	A ₄	-0.0000	-0.0300 \pm 0.0891	0.0000 \pm 0.0000
8.0–12.0	A ₂	0.2081	0.2195 \pm 0.1253	0.2034 \pm 0.0795
	A ₄	-0.0068	-0.0317 \pm 0.0676	0.0000 \pm 0.0000
12.0–20.0	A ₂	0.1783	0.0980 \pm 0.1080	0.0909 \pm 0.0849
	A ₄	-0.0116	-0.0055 \pm 0.0219	0.0000 \pm 0.0000

TABLE XVIII: Comparison of predicted and fitted angular-distribution parameters for the $8_1^+ \rightarrow 6_1^+$ transition. The AVALANCHE prediction has been weighted according to equation 20 to account for the finite neutron-energy bin size.

$E_n^{(\min)} - E_n^{(\max)}$ (MeV)	Quantity	Predicted	Constrained fit	Unconstrained fit
6.0–8.0	A ₂	0.3086	0.4382 \pm 0.1865	0.3102 \pm 0.1031
	A ₄	-0.0304	-0.2131 \pm 0.1710	0.0000 \pm 0.0000
8.0–12.0	A ₂	0.2848	0.2410 \pm 0.1447	0.2106 \pm 0.0689
	A ₄	-0.0370	-0.0379 \pm 0.1009	0.0000 \pm 0.0000
12.0–20.0	A ₂	0.2498	0.1983 \pm 0.1229	0.1765 \pm 0.0751
	A ₄	-0.0329	-0.0240 \pm 0.0553	0.0000 \pm 0.0000

The angular-distribution correction factors, calculated using AVALANCHE and equation 19 and assuming a 0.8068 damping factor can be found in tables XIX-XXII for the four yrast transitions of interest. For the first few neutron-energy points, the AVALANCHE code could not predict a significant population of the parent levels for the transitions of interest. In these cases, the correction factors were obtained by quadratic-polynomial extrapolation from the higher-neutron-energy points, which were found to follow the quadratic form rather closely in general. We choose to extrapolate the correction factors themselves, rather than the σ/J values because, in general, the former vary more slowly and predictably (see for example figure 37).

We also show in figure 40 the angular distribution for extracted from GEANIE data for the $E_\gamma = 131.3\text{-keV}$ in the $E_n = 5\text{--}20\text{-MeV}$ range. In this case, the observed angular distribution is consistent with that of a dipole, which agrees with the E1 multipolarity assignment made for this line in the literature [10].

TABLE XIX: Angular distribution correction factors calculated for the $4_1^+ \rightarrow 2_1^+$ transition using the code AVALANCHE for the sum of planar and coaxial data, and for both **98Thin** and **99Thin** data sets. Corrections marked by a “*” symbol were obtained by quadratic extrapolation from higher- E_n values in the table.

E_n (MeV)	σ_2/J	σ_2/J	98Thin planar	98Thin coaxial	99Thin planar	99Thin coaxial
5.3	0.0000	0.0000	0.9628*	N/A	0.9605*	N/A
6.0	0.7847	7.4997	0.9620	N/A	0.9596	N/A
7.0	0.7915	7.4997	0.9626	N/A	0.9602	N/A
8.0	0.7710	7.4997	0.9609	N/A	0.9584	N/A
9.0	0.7575	7.4997	0.9597	N/A	0.9572	N/A
10.0	0.7468	7.4997	0.9587	N/A	0.9561	N/A
11.0	0.7438	1.5922	0.9584	N/A	0.9558	N/A
12.0	0.7625	1.1340	0.9599	N/A	0.9575	N/A
13.0	0.7825	1.0530	0.9615	N/A	0.9592	N/A
14.0	0.8007	1.0130	0.9630	N/A	0.9608	N/A
15.0	0.8150	0.9842	0.9640	N/A	0.9619	N/A
16.0	0.8353	0.9915	0.9655	N/A	0.9635	N/A
17.0	0.8492	0.9752	0.9665	N/A	0.9645	N/A
18.0	0.8790	0.9925	0.9685	N/A	0.9666	N/A
19.0	0.9093	1.0172	0.9703	N/A	0.9685	N/A
20.0	0.9357	1.0393	0.9718	N/A	0.9701	N/A

TABLE XX: Angular distribution correction factors calculated for the $6_1^+ \rightarrow 4_1^+$ transition using the code AVALANCHE for the sum of planar and coaxial data, and for both **98Thin** and **99Thin** data sets. Corrections marked by a “*” symbol were obtained by quadratic extrapolation from higher- E_n values in the table.

E_n (MeV)	σ_2/J	σ_2/J	98Thin planar	98Thin coaxial	99Thin planar	99Thin coaxial
5.3	0.0000	0.0000	0.9282*	N/A	0.9236*	N/A
6.0	0.4333	4.9998	0.9231	N/A	0.9184	N/A
7.0	0.5010	4.9998	0.9353	N/A	0.9312	N/A
8.0	0.5028	4.9998	0.9356	N/A	0.9316	N/A
9.0	0.5020	0.8683	0.9351	N/A	0.9311	N/A
10.0	0.5037	0.7338	0.9351	N/A	0.9312	N/A
11.0	0.5065	0.6817	0.9353	N/A	0.9315	N/A
12.0	0.5225	0.6567	0.9378	N/A	0.9341	N/A
13.0	0.5387	0.6490	0.9402	N/A	0.9368	N/A
14.0	0.5523	0.6442	0.9422	N/A	0.9389	N/A
15.0	0.5625	0.6382	0.9436	N/A	0.9404	N/A
16.0	0.5767	0.6485	0.9457	N/A	0.9425	N/A
17.0	0.5870	0.6477	0.9470	N/A	0.9440	N/A
18.0	0.6073	0.6645	0.9497	N/A	0.9468	N/A
19.0	0.6275	0.6832	0.9522	N/A	0.9494	N/A
20.0	0.6448	0.6990	0.9542	N/A	0.9515	N/A

TABLE XXI: Angular distribution correction factors calculated for the $8_1^+ \rightarrow 6_1^+$ transition using the code AVALANCHE for the sum of planar and coaxial data, and for both **98Thin** and **99Thin** data sets. Corrections marked by a “*” symbol were obtained by quadratic extrapolation from higher- E_n values in the table.

E_n (MeV)	σ_2/J	σ_2/J	98Thin planar	98Thin coaxial	99Thin planar	99Thin coaxial
5.3	0.0000	0.0000	0.9046*	N/A	0.8998*	N/A
6.0	0.2961	0.4293	0.9004	N/A	0.8956	N/A
7.0	0.3563	0.4961	0.9126	N/A	0.9081	N/A
8.0	0.3749	0.4823	0.9159	N/A	0.9117	N/A
9.0	0.3807	0.4703	0.9169	N/A	0.9127	N/A
10.0	0.3851	0.4562	0.9175	N/A	0.9134	N/A
11.0	0.3900	0.4506	0.9183	N/A	0.9143	N/A
12.0	0.4051	0.4586	0.9213	N/A	0.9174	N/A
13.0	0.4195	0.4657	0.9241	N/A	0.9203	N/A
14.0	0.4306	0.4699	0.9262	N/A	0.9225	N/A
15.0	0.4389	0.4711	0.9277	N/A	0.9241	N/A
16.0	0.4499	0.4818	0.9298	N/A	0.9262	N/A
17.0	0.4586	0.4866	0.9314	N/A	0.9279	N/A
18.0	0.4745	0.5024	0.9342	N/A	0.9309	N/A
19.0	0.4894	0.5184	0.9369	N/A	0.9336	N/A
20.0	0.5025	0.5314	0.9391	N/A	0.9359	N/A

TABLE XXII: Angular distribution correction factors calculated for the $10_1^+ \rightarrow 8_1^+$ transition using the code AVALANCHE for the sum of planar and coaxial data, and for both **98Thin** and **99Thin** data sets. Corrections marked by a “*” symbol were obtained by quadratic extrapolation from higher- E_n values in the table.

E_n (MeV)	σ_2/J	σ_2/J	98Thin planar	98Thin coaxial	99Thin planar	99Thin coaxial
5.3	0.0000	0.0000	0.8931*	N/A	0.8891*	N/A
6.0	0.2509	0.2441	0.8912	N/A	0.8872	N/A
7.0	0.2864	0.3040	0.8991	N/A	0.8949	N/A
8.0	0.3105	0.3328	0.9042	N/A	0.9001	N/A
9.0	0.3200	0.3398	0.9061	N/A	0.9020	N/A
10.0	0.3254	0.3397	0.9071	N/A	0.9030	N/A
11.0	0.3308	0.3434	0.9082	N/A	0.9042	N/A
12.0	0.3437	0.3579	0.9110	N/A	0.9070	N/A
13.0	0.3563	0.3690	0.9136	N/A	0.9097	N/A
14.0	0.3653	0.3754	0.9155	N/A	0.9116	N/A
15.0	0.3720	0.3791	0.9168	N/A	0.9130	N/A
16.0	0.3810	0.3892	0.9188	N/A	0.9150	N/A
17.0	0.3887	0.3962	0.9203	N/A	0.9166	N/A
18.0	0.4017	0.4106	0.9231	N/A	0.9194	N/A
19.0	0.4137	0.4247	0.9255	N/A	0.9219	N/A
20.0	0.4242	0.4359	0.9276	N/A	0.9241	N/A

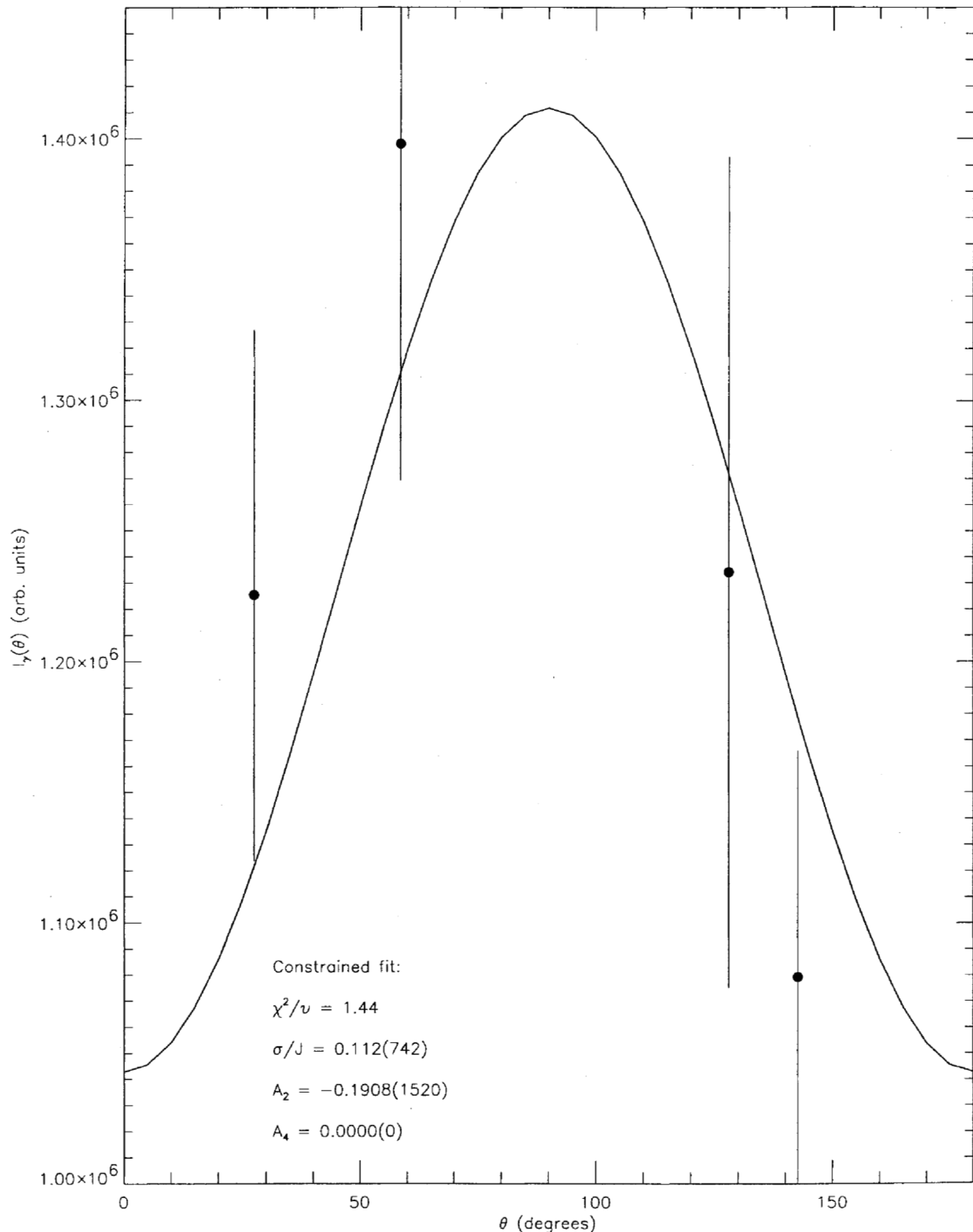


FIG. 40: Angular distributions extracted from the **98Thin** data set for the $5^- \rightarrow 6^+$ $E_\gamma = 131.6$ -keV transition in the $E_n = 5\text{--}20$ MeV range. The parameters resulting from the constrained fit to the GEANIE data are quoted.

XII. ADOPTED PARTIAL γ -RAY CROSS SECTIONS

In this section we pool the **98Thin** and **99Thin** data sets and arrive at a recommended set of partial γ -ray cross sections for the yrast transitions in the $^{235}\text{U}(n,n)$ channel. We present two procedures for combining the data sets. In the first method, a weighted average is used, relying on the uncertainties established for each yield as weights. In the second approach, we use a priori knowledge about the relative qualities of the 1998 and 1999 data sets and derive linear corrections to these data which account for systematic differences between the partial cross sections. After applying these corrections, the data are combined by weighted average. In statistical terms, the first method can be qualified as a “classical” approach, while the second is “Bayesian” in nature.

A Weighted Average

The partial cross sections deduced from 1998 and 1999 unsubtracted data, and normalized using counts from the ^{235}U fission foil with baseline subtraction, are combined to produce recommended values for the $4_1^+ \rightarrow 2_1^+$, $6_1^+ \rightarrow 4_1^+$, $8_1^+ \rightarrow 6_1^+$ and $10_1^+ \rightarrow 8_1^+$ yields. The cross sections are combined point-by-point using a weighted average[16]:

$$\sigma_\gamma(E_n) = \frac{\sigma_\gamma^{(1998)}(E_n) / [u_\gamma^{(1998)}(E_n)]^2 + \sigma_\gamma^{(1999)}(E_n) / [u_\gamma^{(1999)}(E_n)]^2}{1/[u_\gamma^{(1998)}(E_n)]^2 + 1/[u_\gamma^{(1999)}(E_n)]^2} \quad (21)$$

$$u_\gamma^2(E_n) = \frac{1}{1/[u_\gamma^{(1998)}(E_n)]^2 + 1/[u_\gamma^{(1999)}(E_n)]^2} \quad (22)$$

where the symbol $u_\gamma(E_n)$ has been used to designate the total uncertainty for a partial cross section at neutron energy E_n , in order to avoid confusion with the usual cross-section symbol. The total uncertainty discussed in sections IX and IX must be used in the averaging process, since even neutron-energy-independent factors, which do not affect the shape of the partial cross section in an individual data set, will affect the shape of the weighted mean value in equation 21.

The best partial cross sections calculated in this manner, and their associated uncertainties (from equation 22), are listed in tables XXIII-XXVI and plotted in figures 41-44. In each figure, the top panel shows the 1998 and 1999 partial cross sections plotted individually along with their weighted average and uncertainty, drawn as solid and dotted curves respectively. As expected, the averaged partial cross sections show greater stability against fluctuations and carry smaller uncertainties than either 1998 or 1999 excitation functions taken individually. For the $10_1^+ \rightarrow 8_1^+$ partial cross section, we have used the two-peak fits discussed in section VII A 2 from both 1998 and 1999 data sets. The reader is referred to that section for the pertinent caveats. The bottom panel in each figure shows the recommended cross section, plotted as individual points with both x- and y-error bars, and compared to the best current GNASH partial cross-section predictions. While the agreement is good overall, GNASH over-predicts the experimental cross sections by $\approx 15\%$ for the $6_1^+ \rightarrow 4_1^+$ and $8_1^+ \rightarrow 6_1^+$ transitions and $\approx 40\%$ for the $4_1^+ \rightarrow 2_1^+$ transition (near peak cross section). The disagreement in both shape and overall magnitude for the $10_1^+ \rightarrow 8_1^+$ is such that quantitative comparisons between experiment and current GNASH calculations are not recommended.

TABLE XXIII: Best partial cross sections deduced from the weighted mean of 1998 and 1999 GEANIE measurements for the $4_1^+ \rightarrow 2_1^+$ transition.

E_n (MeV)	$A^{(1998)}$	$\sigma^{(1998)}$	$A^{(1999)}$	$\sigma^{(1999)}$	$\sigma^{(wei)}$	$\sigma^{(wei,corr)}$
4.090 ± 0.093	0 ± 0	0.0002 ± 0.0101	583 ± 143	0.1568 ± 0.0438	0.0080 ± 0.0098	0.0080 ± 0.0098
4.264 ± 0.099	56 ± 198	0.0092 ± 0.0340	540 ± 147	0.1435 ± 0.0436	0.0599 ± 0.0268	0.0599 ± 0.0268
4.453 ± 0.105	3 ± 70	0.0005 ± 0.0144	632 ± 151	0.1597 ± 0.0436	0.0161 ± 0.0137	0.0161 ± 0.0137
4.647 ± 0.113	4 ± 75	0.0006 ± 0.0147	557 ± 152	0.1372 ± 0.0417	0.0157 ± 0.0139	0.0157 ± 0.0139
4.861 ± 0.122	0 ± 22	0.0002 ± 0.0098	469 ± 152	0.1135 ± 0.0399	0.0066 ± 0.0095	0.0066 ± 0.0095
5.090 ± 0.129	469 ± 210	0.0703 ± 0.0338	394 ± 152	0.0932 ± 0.0383	0.0803 ± 0.0253	0.0803 ± 0.0253
5.333 ± 0.140	590 ± 212	0.0870 ± 0.0341	645 ± 151	0.1525 ± 0.0410	0.1139 ± 0.0262	0.1095 ± 0.0253
5.597 ± 0.149	572 ± 211	0.0817 ± 0.0328	492 ± 150	0.1152 ± 0.0385	0.0958 ± 0.0250	0.0921 ± 0.0241
5.875 ± 0.160	377 ± 213	0.0529 ± 0.0317	832 ± 153	0.1905 ± 0.0428	0.1015 ± 0.0255	0.0973 ± 0.0245
6.181 ± 0.175	1495 ± 219	0.2105 ± 0.0407	1319 ± 154	0.2966 ± 0.0511	0.2439 ± 0.0318	0.2343 ± 0.0309
6.517 ± 0.187	2035 ± 226	0.2689 ± 0.0445	1841 ± 158	0.3947 ± 0.0601	0.3134 ± 0.0357	0.3013 ± 0.0348
6.862 ± 0.201	1838 ± 227	0.2307 ± 0.0402	1892 ± 160	0.3965 ± 0.0600	0.2820 ± 0.0334	0.2711 ± 0.0325
7.237 ± 0.218	2327 ± 230	0.3037 ± 0.0476	1552 ± 158	0.3453 ± 0.0560	0.3211 ± 0.0363	0.3088 ± 0.0353
7.661 ± 0.242	2233 ± 227	0.3121 ± 0.0496	1741 ± 157	0.4138 ± 0.0642	0.3501 ± 0.0393	0.3364 ± 0.0382
8.126 ± 0.263	2502 ± 231	0.3482 ± 0.0531	1890 ± 159	0.4446 ± 0.0674	0.3851 ± 0.0417	0.3697 ± 0.0406
8.618 ± 0.284	2619 ± 234	0.3554 ± 0.0535	2067 ± 160	0.4754 ± 0.0703	0.3994 ± 0.0426	0.3832 ± 0.0414
9.160 ± 0.313	2686 ± 233	0.3708 ± 0.0553	2314 ± 161	0.5418 ± 0.0779	0.4280 ± 0.0451	0.4103 ± 0.0438
9.757 ± 0.346	3211 ± 233	0.4595 ± 0.0648	2175 ± 159	0.5312 ± 0.0775	0.4890 ± 0.0497	0.4685 ± 0.0483
10.414 ± 0.377	2835 ± 233	0.4201 ± 0.0616	2163 ± 159	0.5501 ± 0.0805	0.4681 ± 0.0489	0.4483 ± 0.0475
11.143 ± 0.425	2557 ± 230	0.4029 ± 0.0612	2097 ± 157	0.5640 ± 0.0832	0.4595 ± 0.0493	0.4401 ± 0.0479
11.960 ± 0.467	2836 ± 231	0.4607 ± 0.0677	2278 ± 159	0.6365 ± 0.0924	0.5222 ± 0.0546	0.5008 ± 0.0531
12.860 ± 0.525	2625 ± 226	0.4393 ± 0.0659	2133 ± 158	0.6077 ± 0.0896	0.4985 ± 0.0531	0.4788 ± 0.0517
13.876 ± 0.589	1589 ± 222	0.2711 ± 0.0511	1285 ± 152	0.3751 ± 0.0655	0.3104 ± 0.0403	0.2986 ± 0.0391
15.016 ± 0.660	1161 ± 217	0.1979 ± 0.0452	940 ± 149	0.2754 ± 0.0565	0.2282 ± 0.0353	0.2198 ± 0.0342
16.297 ± 0.750	693 ± 216	0.1179 ± 0.0407	992 ± 148	0.2877 ± 0.0569	0.1755 ± 0.0331	0.1690 ± 0.0321
17.759 ± 0.857	373 ± 215	0.0631 ± 0.0385	529 ± 144	0.1513 ± 0.0460	0.0994 ± 0.0295	0.0961 ± 0.0286
19.416 ± 0.971	8 ± 210	0.0013 ± 0.0362	812 ± 147	0.2264 ± 0.0506	0.0776 ± 0.0295	0.0748 ± 0.0286

TABLE XXIV: Best partial cross sections deduced from the weighted mean of 1998 and 1999 GEANIE measurements for the $6_1^+ \rightarrow 4_1^+$ transition.

E_n (MeV)	$A^{(1998)}$	$\sigma^{(1998)}$	$A^{(1999)}$	$\sigma^{(1999)}$	$\sigma^{(wei)}$	$\sigma^{(wei,corr)}$
4.090 ± 0.093	223 ± 73	0.0126 ± 0.0044	166 ± 78	0.0105 ± 0.0051	0.0117 ± 0.0033	0.0117 ± 0.0033
4.264 ± 0.099	212 ± 73	0.0116 ± 0.0042	62 ± 78	0.0039 ± 0.0050	0.0083 ± 0.0032	0.0083 ± 0.0032
4.453 ± 0.105	237 ± 74	0.0124 ± 0.0042	172 ± 79	0.0102 ± 0.0049	0.0115 ± 0.0032	0.0115 ± 0.0032
4.647 ± 0.113	146 ± 73	0.0075 ± 0.0039	213 ± 81	0.0123 ± 0.0050	0.0093 ± 0.0030	0.0093 ± 0.0030
4.861 ± 0.122	214 ± 74	0.0110 ± 0.0040	36 ± 74	0.0020 ± 0.0043	0.0068 ± 0.0029	0.0068 ± 0.0029
5.090 ± 0.129	318 ± 76	0.0159 ± 0.0043	0 ± 9	0.0001 ± 0.0008	0.0006 ± 0.0008	0.0006 ± 0.0008
5.333 ± 0.140	231 ± 75	0.0114 ± 0.0039	0 ± 1	0.0001 ± 0.0007	0.0004 ± 0.0006	0.0003 ± 0.0006
5.597 ± 0.149	343 ± 78	0.0163 ± 0.0042	23 ± 83	0.0013 ± 0.0046	0.0095 ± 0.0031	0.0088 ± 0.0029
5.875 ± 0.160	820 ± 83	0.0384 ± 0.0059	439 ± 89	0.0236 ± 0.0056	0.0305 ± 0.0041	0.0281 ± 0.0038
6.181 ± 0.175	2015 ± 93	0.0947 ± 0.0119	1467 ± 98	0.0776 ± 0.0105	0.0851 ± 0.0079	0.0783 ± 0.0074
6.517 ± 0.187	3350 ± 104	0.1477 ± 0.0177	2572 ± 106	0.1297 ± 0.0161	0.1378 ± 0.0119	0.1275 ± 0.0113
6.862 ± 0.201	4162 ± 110	0.1743 ± 0.0207	3414 ± 112	0.1683 ± 0.0205	0.1713 ± 0.0145	0.1595 ± 0.0138
7.237 ± 0.218	4970 ± 114	0.2165 ± 0.0256	3735 ± 113	0.1955 ± 0.0237	0.2052 ± 0.0174	0.1918 ± 0.0166
7.661 ± 0.242	5076 ± 115	0.2368 ± 0.0281	3779 ± 112	0.2113 ± 0.0257	0.2229 ± 0.0189	0.2083 ± 0.0181
8.126 ± 0.263	5653 ± 118	0.2625 ± 0.0310	4633 ± 118	0.2564 ± 0.0309	0.2594 ± 0.0219	0.2421 ± 0.0209
8.618 ± 0.284	6751 ± 124	0.3057 ± 0.0359	5057 ± 121	0.2736 ± 0.0328	0.2882 ± 0.0242	0.2688 ± 0.0231
9.160 ± 0.313	7114 ± 126	0.3278 ± 0.0385	5597 ± 122	0.3083 ± 0.0369	0.3176 ± 0.0266	0.2963 ± 0.0254
9.757 ± 0.346	7726 ± 129	0.3690 ± 0.0434	5845 ± 123	0.3358 ± 0.0402	0.3511 ± 0.0295	0.3276 ± 0.0281
10.414 ± 0.377	7833 ± 129	0.3874 ± 0.0457	6227 ± 124	0.3726 ± 0.0447	0.3798 ± 0.0319	0.3544 ± 0.0305
11.143 ± 0.425	8267 ± 131	0.4348 ± 0.0515	6353 ± 125	0.4020 ± 0.0484	0.4174 ± 0.0353	0.3896 ± 0.0336
11.960 ± 0.467	8238 ± 131	0.4466 ± 0.0530	6191 ± 125	0.4070 ± 0.0491	0.4253 ± 0.0360	0.3979 ± 0.0345
12.860 ± 0.525	7022 ± 125	0.3921 ± 0.0468	5350 ± 122	0.3586 ± 0.0435	0.3741 ± 0.0319	0.3509 ± 0.0305
13.876 ± 0.589	4929 ± 115	0.2806 ± 0.0338	4080 ± 116	0.2802 ± 0.0344	0.2804 ± 0.0241	0.2637 ± 0.0231
15.016 ± 0.660	3414 ± 106	0.1942 ± 0.0237	2824 ± 109	0.1946 ± 0.0244	0.1944 ± 0.0170	0.1831 ± 0.0164
16.297 ± 0.750	2361 ± 99	0.1341 ± 0.0168	2087 ± 104	0.1424 ± 0.0184	0.1379 ± 0.0124	0.1302 ± 0.0120
17.759 ± 0.857	1905 ± 96	0.1075 ± 0.0138	1431 ± 100	0.0963 ± 0.0133	0.1017 ± 0.0096	0.0963 ± 0.0092
19.416 ± 0.971	1708 ± 95	0.0946 ± 0.0124	1150 ± 99	0.0754 ± 0.0111	0.0840 ± 0.0083	0.0799 ± 0.0080

TABLE XXV: Best partial cross sections deduced from the weighted mean of 1998 and 1999 GEANIE measurements for the $8_1^+ \rightarrow 6_1^+$ transition.

E_n (MeV)	$A^{(1998)}$	$\sigma^{(1998)}$	$A^{(1999)}$	$\sigma^{(1999)}$	$\sigma^{(wei)}$	$\sigma^{(wei,corr)}$
4.090 ± 0.093	177 ± 71	0.0056 ± 0.0034	639 ± 87	0.0213 ± 0.0038	0.0125 ± 0.0025	0.0125 ± 0.0025
4.264 ± 0.099	58 ± 70	0.0018 ± 0.0032	813 ± 89	0.0267 ± 0.0042	0.0109 ± 0.0026	0.0109 ± 0.0026
4.453 ± 0.105	266 ± 73	0.0078 ± 0.0032	712 ± 89	0.0222 ± 0.0038	0.0139 ± 0.0024	0.0139 ± 0.0024
4.647 ± 0.113	1 ± 20	0.0000 ± 0.0023	787 ± 90	0.0240 ± 0.0039	0.0063 ± 0.0020	0.0063 ± 0.0020
4.861 ± 0.122	207 ± 73	0.0059 ± 0.0031	913 ± 92	0.0273 ± 0.0041	0.0137 ± 0.0025	0.0137 ± 0.0025
5.090 ± 0.129	40 ± 74	0.0011 ± 0.0030	856 ± 92	0.0250 ± 0.0039	0.0100 ± 0.0024	0.0100 ± 0.0024
5.333 ± 0.140	144 ± 74	0.0040 ± 0.0030	708 ± 92	0.0207 ± 0.0036	0.0109 ± 0.0023	0.0098 ± 0.0021
5.597 ± 0.149	27 ± 69	0.0007 ± 0.0028	654 ± 92	0.0189 ± 0.0034	0.0080 ± 0.0022	0.0071 ± 0.0019
5.875 ± 0.160	117 ± 75	0.0031 ± 0.0028	804 ± 94	0.0227 ± 0.0037	0.0104 ± 0.0023	0.0093 ± 0.0020
6.181 ± 0.175	677 ± 80	0.0177 ± 0.0035	1308 ± 97	0.0364 ± 0.0049	0.0240 ± 0.0028	0.0216 ± 0.0026
6.517 ± 0.187	1775 ± 90	0.0437 ± 0.0055	1941 ± 103	0.0515 ± 0.0064	0.0470 ± 0.0041	0.0424 ± 0.0038
6.862 ± 0.201	2342 ± 96	0.0547 ± 0.0064	2711 ± 109	0.0702 ± 0.0083	0.0605 ± 0.0051	0.0550 ± 0.0047
7.237 ± 0.218	3043 ± 100	0.0740 ± 0.0084	3023 ± 111	0.0832 ± 0.0098	0.0779 ± 0.0064	0.0711 ± 0.0059
7.661 ± 0.242	3292 ± 101	0.0857 ± 0.0096	3367 ± 112	0.0989 ± 0.0116	0.0911 ± 0.0074	0.0833 ± 0.0069
8.126 ± 0.263	3949 ± 106	0.1023 ± 0.0113	3906 ± 116	0.1136 ± 0.0132	0.1071 ± 0.0086	0.0979 ± 0.0080
8.618 ± 0.284	5316 ± 114	0.1343 ± 0.0146	4735 ± 121	0.1346 ± 0.0154	0.1344 ± 0.0106	0.1229 ± 0.0099
9.160 ± 0.313	5765 ± 116	0.1482 ± 0.0161	5336 ± 124	0.1545 ± 0.0176	0.1511 ± 0.0119	0.1383 ± 0.0111
9.757 ± 0.346	6491 ± 120	0.1729 ± 0.0187	5784 ± 126	0.1746 ± 0.0199	0.1737 ± 0.0136	0.1590 ± 0.0128
10.414 ± 0.377	7088 ± 122	0.1955 ± 0.0212	6337 ± 127	0.1992 ± 0.0228	0.1972 ± 0.0155	0.1806 ± 0.0145
11.143 ± 0.425	7661 ± 124	0.2248 ± 0.0244	6645 ± 128	0.2209 ± 0.0253	0.2229 ± 0.0176	0.2043 ± 0.0165
11.960 ± 0.467	7940 ± 125	0.2401 ± 0.0261	7059 ± 129	0.2438 ± 0.0280	0.2418 ± 0.0191	0.2223 ± 0.0180
12.860 ± 0.525	7136 ± 122	0.2223 ± 0.0243	6566 ± 127	0.2313 ± 0.0266	0.2264 ± 0.0180	0.2088 ± 0.0170
13.876 ± 0.589	5404 ± 113	0.1716 ± 0.0190	5073 ± 120	0.1831 ± 0.0213	0.1767 ± 0.0142	0.1634 ± 0.0134
15.016 ± 0.660	3626 ± 104	0.1151 ± 0.0131	3560 ± 113	0.1289 ± 0.0152	0.1210 ± 0.0099	0.1121 ± 0.0094
16.297 ± 0.750	2467 ± 97	0.0782 ± 0.0093	2471 ± 107	0.0886 ± 0.0108	0.0826 ± 0.0070	0.0767 ± 0.0067
17.759 ± 0.857	2076 ± 94	0.0654 ± 0.0080	2153 ± 105	0.0761 ± 0.0094	0.0699 ± 0.0061	0.0652 ± 0.0058
19.416 ± 0.971	1694 ± 92	0.0523 ± 0.0068	1834 ± 104	0.0632 ± 0.0080	0.0568 ± 0.0052	0.0533 ± 0.0049

TABLE XXVI: Best partial cross sections deduced from the weighted mean of 1998 and 1999 GEANIE measurements for the $10_1^+ \rightarrow 8_1^+$ transition.

E_n (MeV)	$A^{(1998)}$	$\sigma^{(1998)}$	$A^{(1999)}$	$\sigma^{(1999)}$	$\sigma^{(wei)}$	$\sigma^{(wei,corr)}$
4.090 \pm 0.093	121 \pm 78	0.0034 \pm 0.0023	0 \pm 0	0.0000 \pm 0.0001	0.0000 \pm 0.0001	0.0000 \pm 0.0001
4.264 \pm 0.099	43 \pm 77	0.0012 \pm 0.0021	29 \pm 87	0.0008 \pm 0.0025	0.0010 \pm 0.0016	0.0010 \pm 0.0016
4.453 \pm 0.105	200 \pm 79	0.0053 \pm 0.0022	21 \pm 86	0.0006 \pm 0.0024	0.0032 \pm 0.0016	0.0032 \pm 0.0016
4.647 \pm 0.113	0 \pm 0	0.0000 \pm 0.0002	156 \pm 90	0.0042 \pm 0.0025	0.0001 \pm 0.0002	0.0001 \pm 0.0002
4.861 \pm 0.122	0 \pm 0	0.0000 \pm 0.0002	172 \pm 90	0.0046 \pm 0.0024	0.0001 \pm 0.0002	0.0001 \pm 0.0002
5.090 \pm 0.129	26 \pm 80	0.0007 \pm 0.0020	192 \pm 93	0.0050 \pm 0.0025	0.0024 \pm 0.0016	0.0024 \pm 0.0016
5.333 \pm 0.140	135 \pm 82	0.0034 \pm 0.0021	138 \pm 93	0.0036 \pm 0.0024	0.0034 \pm 0.0016	0.0031 \pm 0.0014
5.597 \pm 0.149	0 \pm 1	0.0000 \pm 0.0002	13 \pm 92	0.0003 \pm 0.0024	0.0000 \pm 0.0002	0.0000 \pm 0.0002
5.875 \pm 0.160	0 \pm 0	0.0000 \pm 0.0002	27 \pm 93	0.0007 \pm 0.0023	0.0000 \pm 0.0002	0.0000 \pm 0.0002
6.181 \pm 0.175	0 \pm 0	0.0000 \pm 0.0002	3 \pm 53	0.0001 \pm 0.0013	0.0000 \pm 0.0002	0.0000 \pm 0.0002
6.517 \pm 0.187	106 \pm 87	0.0024 \pm 0.0020	155 \pm 97	0.0036 \pm 0.0023	0.0029 \pm 0.0015	0.0026 \pm 0.0013
6.862 \pm 0.201	213 \pm 91	0.0045 \pm 0.0020	331 \pm 100	0.0076 \pm 0.0024	0.0057 \pm 0.0015	0.0051 \pm 0.0014
7.237 \pm 0.218	456 \pm 94	0.0100 \pm 0.0023	298 \pm 99	0.0073 \pm 0.0025	0.0088 \pm 0.0017	0.0079 \pm 0.0015
7.661 \pm 0.242	504 \pm 95	0.0118 \pm 0.0025	704 \pm 102	0.0184 \pm 0.0033	0.0142 \pm 0.0020	0.0128 \pm 0.0018
8.126 \pm 0.263	700 \pm 100	0.0164 \pm 0.0029	971 \pm 105	0.0250 \pm 0.0039	0.0195 \pm 0.0023	0.0176 \pm 0.0021
8.618 \pm 0.284	929 \pm 102	0.0212 \pm 0.0032	1198 \pm 108	0.0302 \pm 0.0043	0.0244 \pm 0.0026	0.0221 \pm 0.0023
9.160 \pm 0.313	1380 \pm 108	0.0321 \pm 0.0041	1597 \pm 111	0.0410 \pm 0.0053	0.0354 \pm 0.0033	0.0320 \pm 0.0030
9.757 \pm 0.346	1434 \pm 109	0.0345 \pm 0.0044	1594 \pm 112	0.0427 \pm 0.0056	0.0377 \pm 0.0035	0.0341 \pm 0.0032
10.414 \pm 0.377	1788 \pm 112	0.0446 \pm 0.0054	2160 \pm 114	0.0602 \pm 0.0074	0.0500 \pm 0.0043	0.0453 \pm 0.0040
11.143 \pm 0.425	2011 \pm 114	0.0533 \pm 0.0063	2621 \pm 117	0.0773 \pm 0.0093	0.0609 \pm 0.0052	0.0553 \pm 0.0048
11.960 \pm 0.467	2065 \pm 114	0.0565 \pm 0.0066	2575 \pm 117	0.0789 \pm 0.0095	0.0638 \pm 0.0054	0.0581 \pm 0.0051
12.860 \pm 0.525	2054 \pm 114	0.0578 \pm 0.0068	2421 \pm 115	0.0756 \pm 0.0092	0.0642 \pm 0.0055	0.0585 \pm 0.0051
13.876 \pm 0.589	1833 \pm 112	0.0526 \pm 0.0064	1943 \pm 111	0.0622 \pm 0.0078	0.0564 \pm 0.0049	0.0516 \pm 0.0046
15.016 \pm 0.660	1185 \pm 105	0.0340 \pm 0.0047	1395 \pm 107	0.0448 \pm 0.0061	0.0380 \pm 0.0037	0.0348 \pm 0.0034
16.297 \pm 0.750	732 \pm 101	0.0210 \pm 0.0036	943 \pm 104	0.0300 \pm 0.0047	0.0243 \pm 0.0029	0.0223 \pm 0.0027
17.759 \pm 0.857	472 \pm 98	0.0134 \pm 0.0031	695 \pm 102	0.0218 \pm 0.0040	0.0166 \pm 0.0025	0.0153 \pm 0.0023
19.416 \pm 0.971	429 \pm 99	0.0120 \pm 0.0030	610 \pm 103	0.0186 \pm 0.0038	0.0146 \pm 0.0024	0.0135 \pm 0.0022

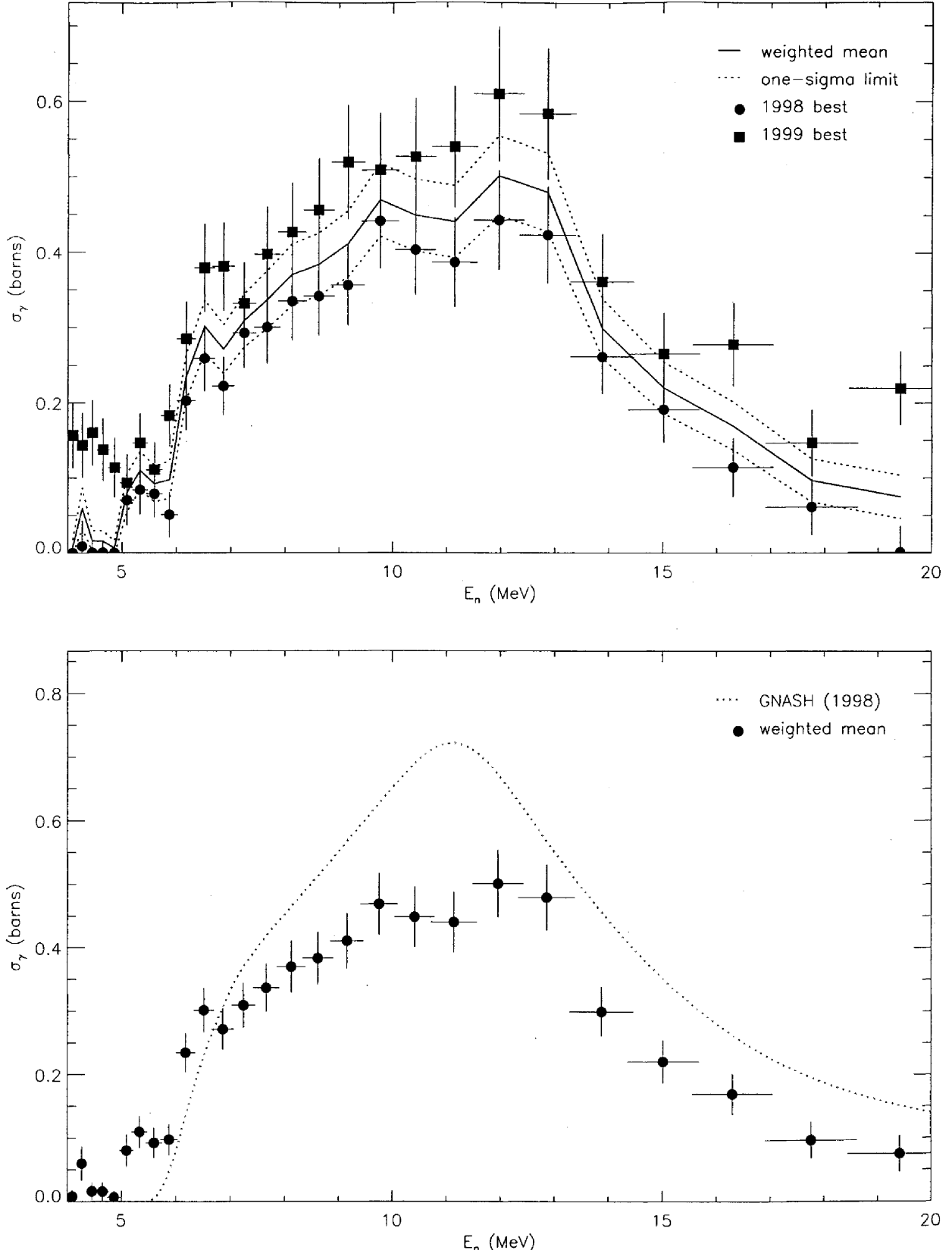


FIG. 41: Best $4_1^+ \rightarrow 2_1^+$ partial cross section obtained by weighted mean of the best 1998 and 1999 results. The top panel shows the 1998 and 1999 partial cross sections and the weighted mean, plotted as a solid line with a one-sigma confidence band. The bottom panel shows the same weighted-mean partial cross section compared to GNASH.

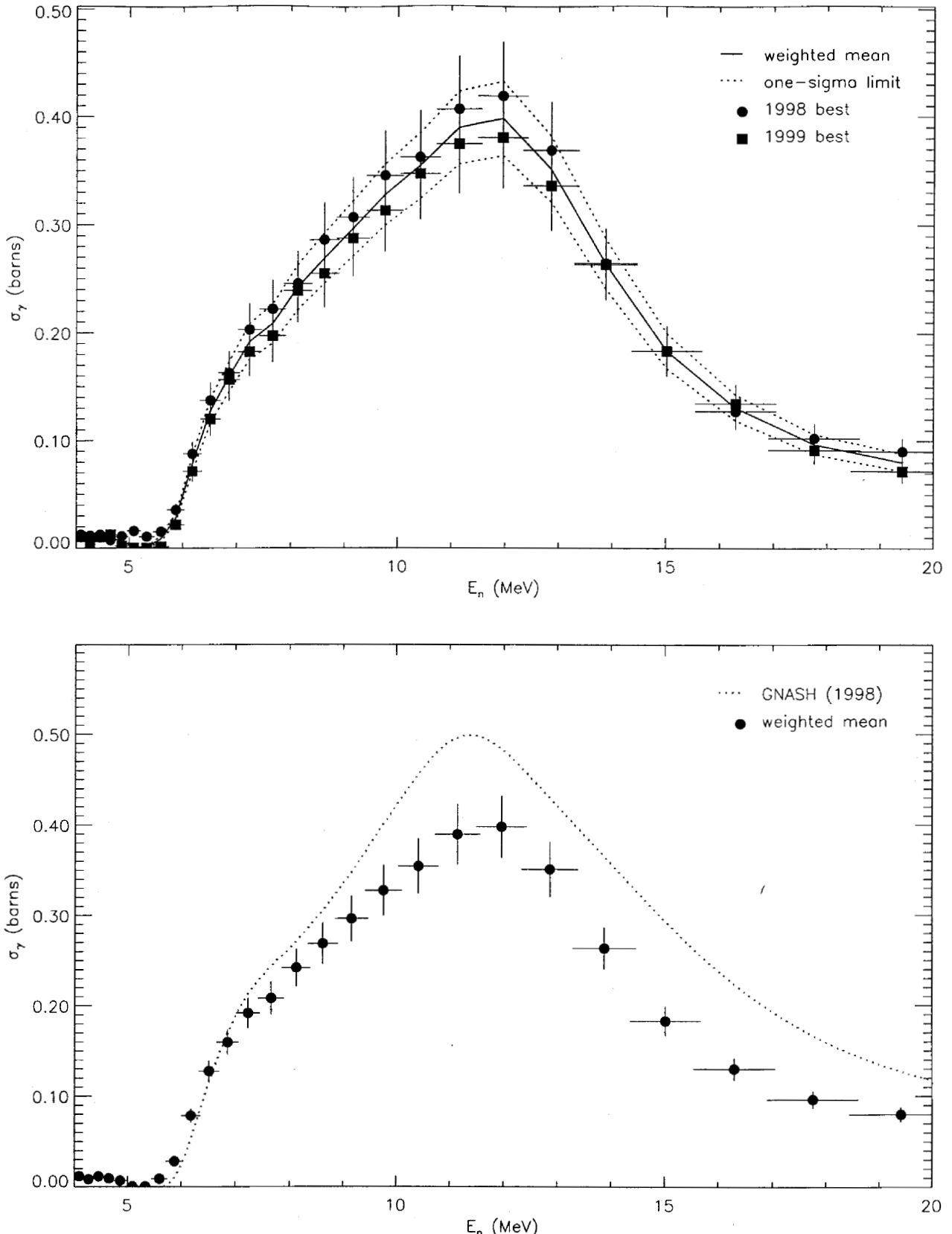


FIG. 42: Best $6_1^+ \rightarrow 4_1^+$ partial cross section obtained by weighted mean of the best 1998 and 1999 results. The top panel shows the 1998 and 1999 partial cross sections and the weighted mean, plotted as a solid line with a one-sigma confidence band. The bottom panel shows the same weighted-mean partial cross section compared to GNASH.

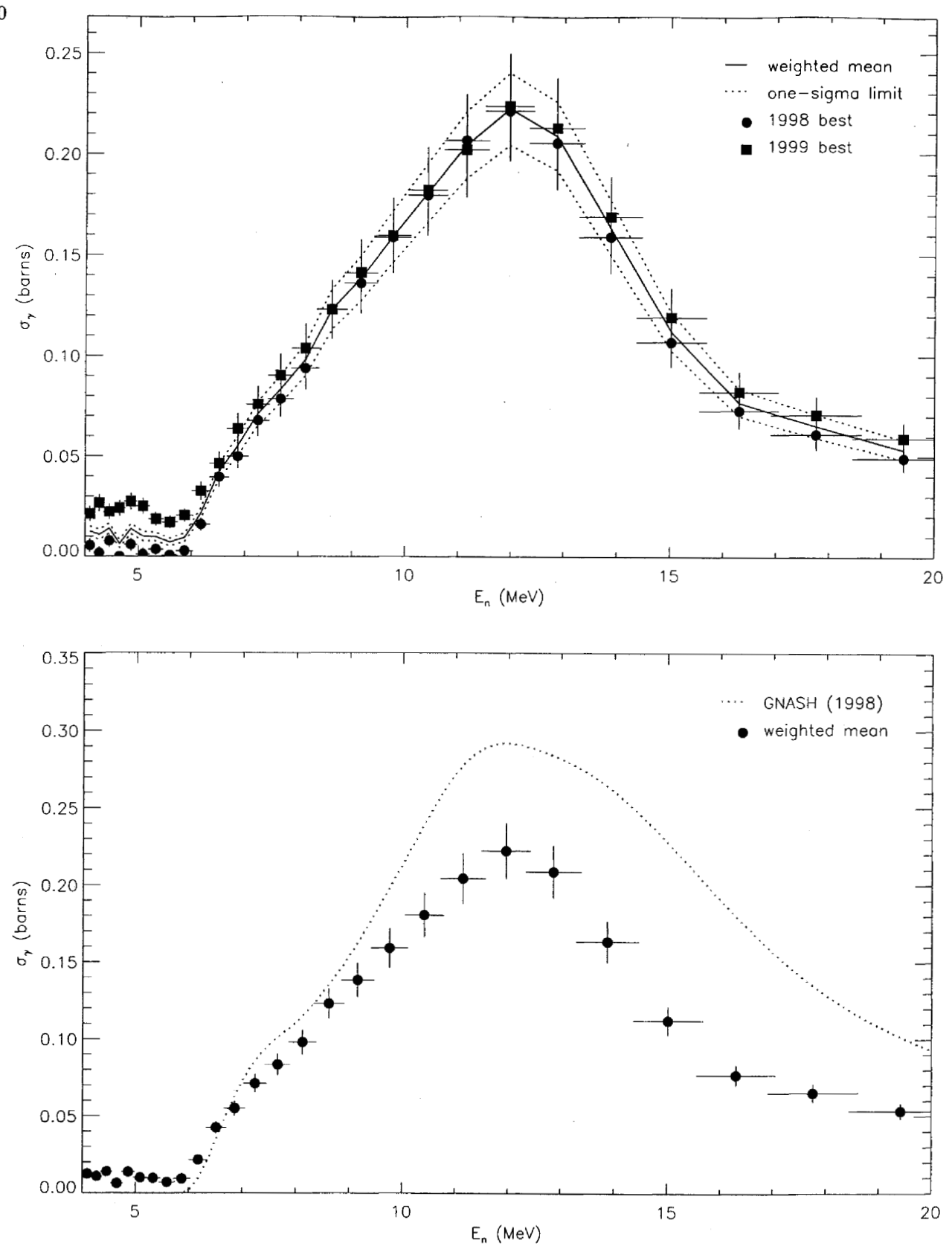


FIG. 43: Best $8_1^+ \rightarrow 6_1^+$ partial cross section obtained by weighted mean of the best 1998 and 1999 results. The top panel shows the 1998 and 1999 partial cross sections and the weighted mean, plotted as a solid line with a one-sigma confidence band. The bottom panel shows the same weighted-mean partial cross section compared to GNASH.

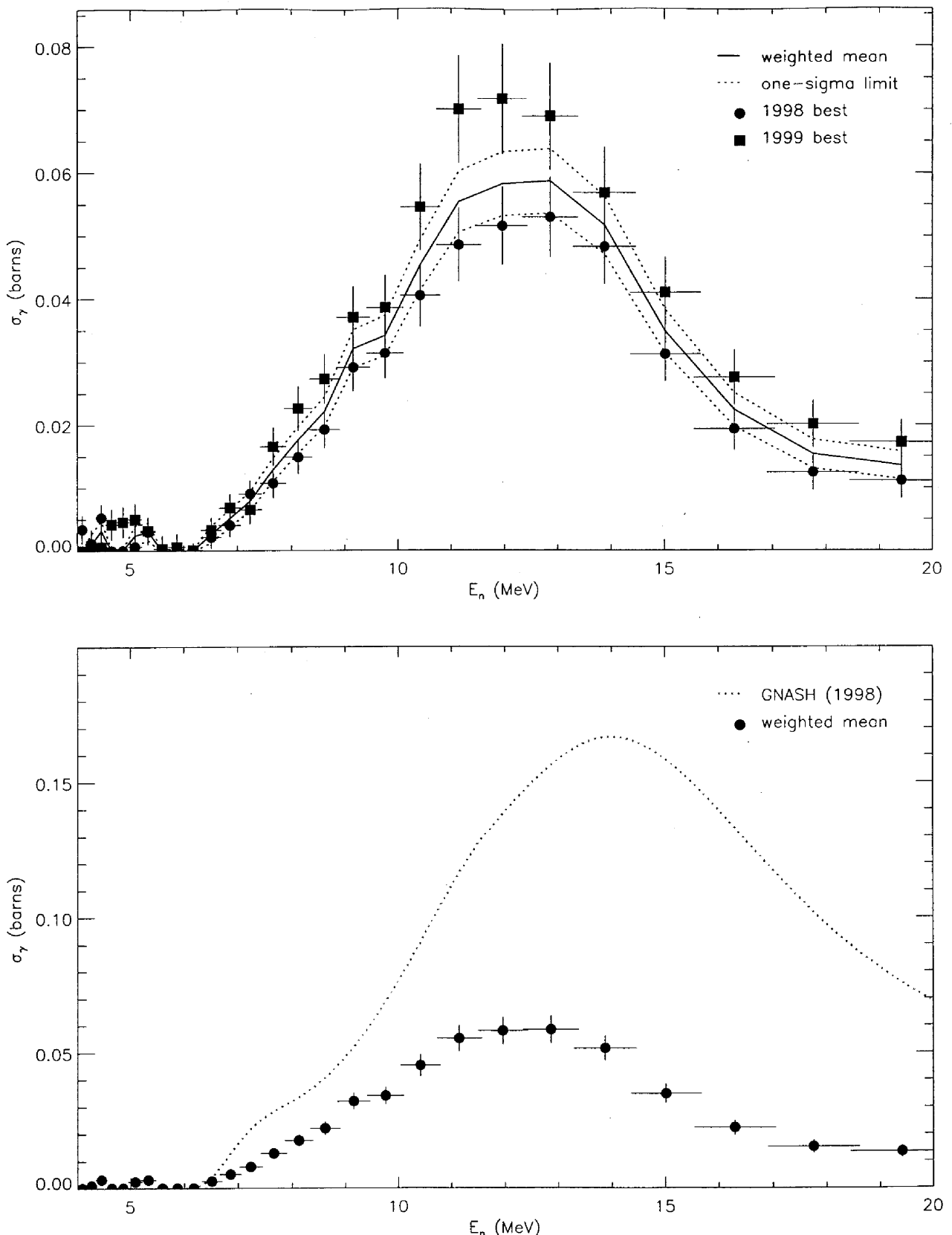


FIG. 44: Best $10_1^+ \rightarrow 8_1^+$ partial cross section obtained by weighted mean of the best 1998 and 1999 results. The top panel shows the 1998 and 1999 partial cross sections and the weighted mean, plotted as a solid line with a one-sigma confidence band. The bottom panel shows the same weighted-mean partial cross section compared to GNASH.

B Optimized Average (Adopted Partial Cross Sections)

Figures 41-44 show systematic discrepancies between the 1998 and 1999 data. For the $4 \rightarrow 2$ and $10 \rightarrow 8$ transitions, the **99Thin** data are systematically higher than the **98Thin** data, whereas for the $6 \rightarrow 4$ and $8 \rightarrow 6$ transitions that trend is reversed. The differences between data sets are due in part to neutron-energy-independent factors, such as the poorly known sample thickness for the **98Thin** data. However, because the same trend is not observed for each of the four yrast transitions, target thickness alone cannot account for the observed systematic deviations. This point can be made clearer if we plot ratios of measured yields, as in figures 45-47. These ratios of $\sigma_{6 \rightarrow 4}/\sigma_{4 \rightarrow 2}$, $\sigma_{8 \rightarrow 6}/\sigma_{6 \rightarrow 4}$, and $\sigma_{10 \rightarrow 8}/\sigma_{8 \rightarrow 6}$ respectively depend only on fitted areas, conversion coefficients, and relative γ -ray efficiencies. All other factors in equation 8 are cancelled out. Furthermore, the internal conversion coefficients used are the same for the 1998 and 1999 data. Therefore, any observed discrepancies between the same ratio extracted from 1998 and 1999 data is likely due to either inadequacies in the fitting model or in the relative γ -ray efficiencies. Since the ratios involve transition that are close in γ -ray energy, it is most likely that, in spite of the fastidiousness applied to the fitting procedure, some systematic deviations remain. These effects can be observed in figures 45-47.

Because of these systematic differences between the **98Thin** and **99Thin** data sets, it may not be appropriate to combine them by a simple weighted average. Instead, we attempt to remove the systematic discrepancy before combining the data sets by making the following subjective assumptions:

1. The **98Thin** data probably give the correct shape for the partial γ -ray cross sections, but with the wrong overall magnitude.
2. The **99Thin** data are likely to have the correct overall magnitude (because such quantities as sample thickness were measured more precisely), but, because of poor statistics, the excitation function shapes are not as reliable.

These assumptions are based on observations regarding the quality of the 1998 and 1999 data fits in general and for the four ^{234}U yrast transitions in particular. In particular, the 1999 data show residual counts for the $4 \rightarrow 2$ and $8 \rightarrow 6$ excitation functions below the $(n,2n)$ reaction threshold, while the $10 \rightarrow 8$ peak is fitted as a nearly unresolvable pair of lines. Only the $6 \rightarrow 4$ transition is sufficiently strong and in a sufficiently sparse region of the γ -ray spectrum to be fitted reliably in both **98Thin** and **99Thin** data sets. Therefore we expect that the observed discrepancy in the $6 \rightarrow 4$ partial cross sections between 1998 and 1999 is primarily due to an incorrect value for the 1998 sample thickness. In this case, the data indicate that the 1998 sample thickness may have been under-estimated by $\approx 10\%$.

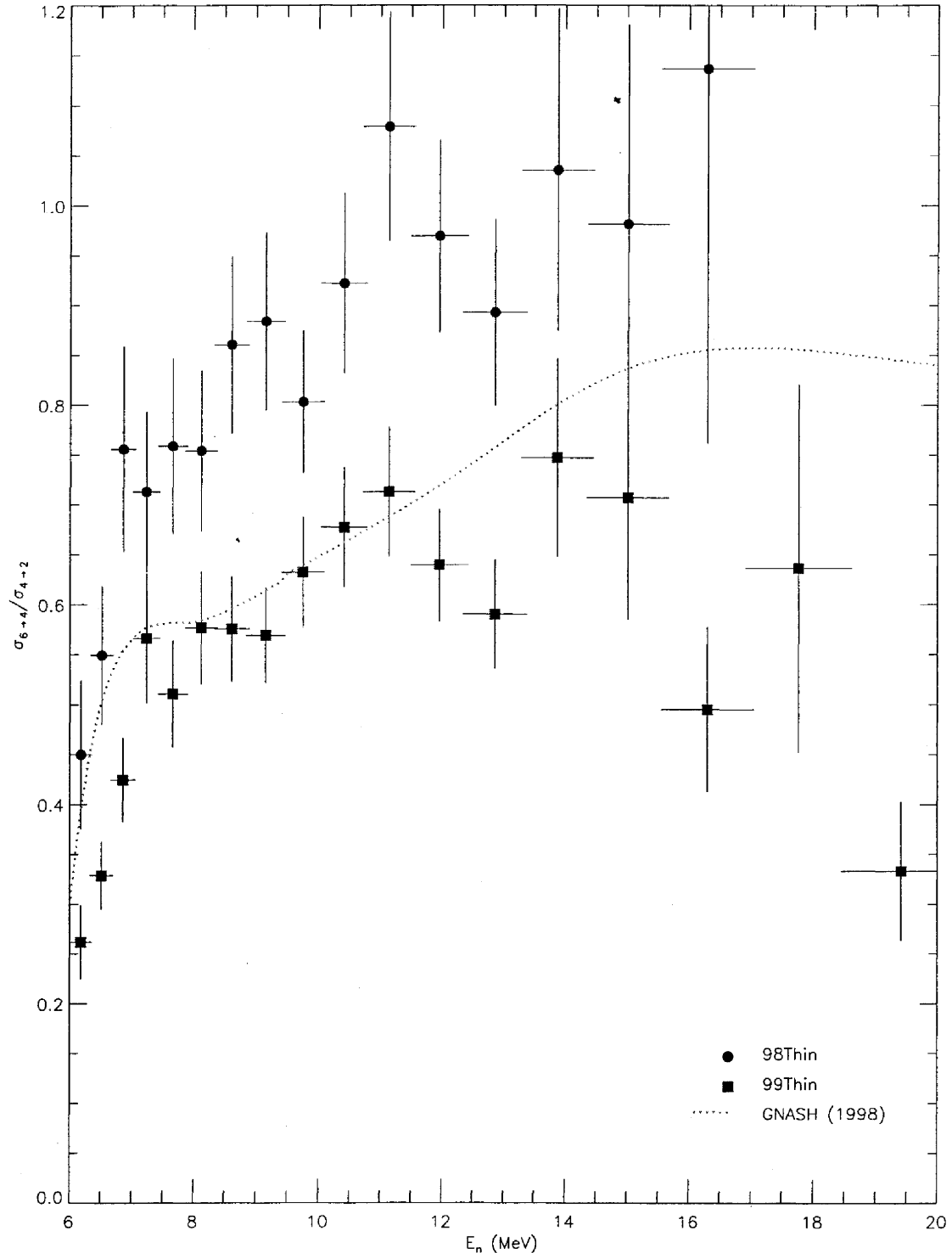


FIG. 45: Ratio of partial γ -ray cross sections $\sigma_{6 \rightarrow 4} / \sigma_{4 \rightarrow 2}$ plotted for the **98Thin** and **99Thin** GEANIE data sets and compared to the GNASH prediction. Angular-distribution corrections are not included.

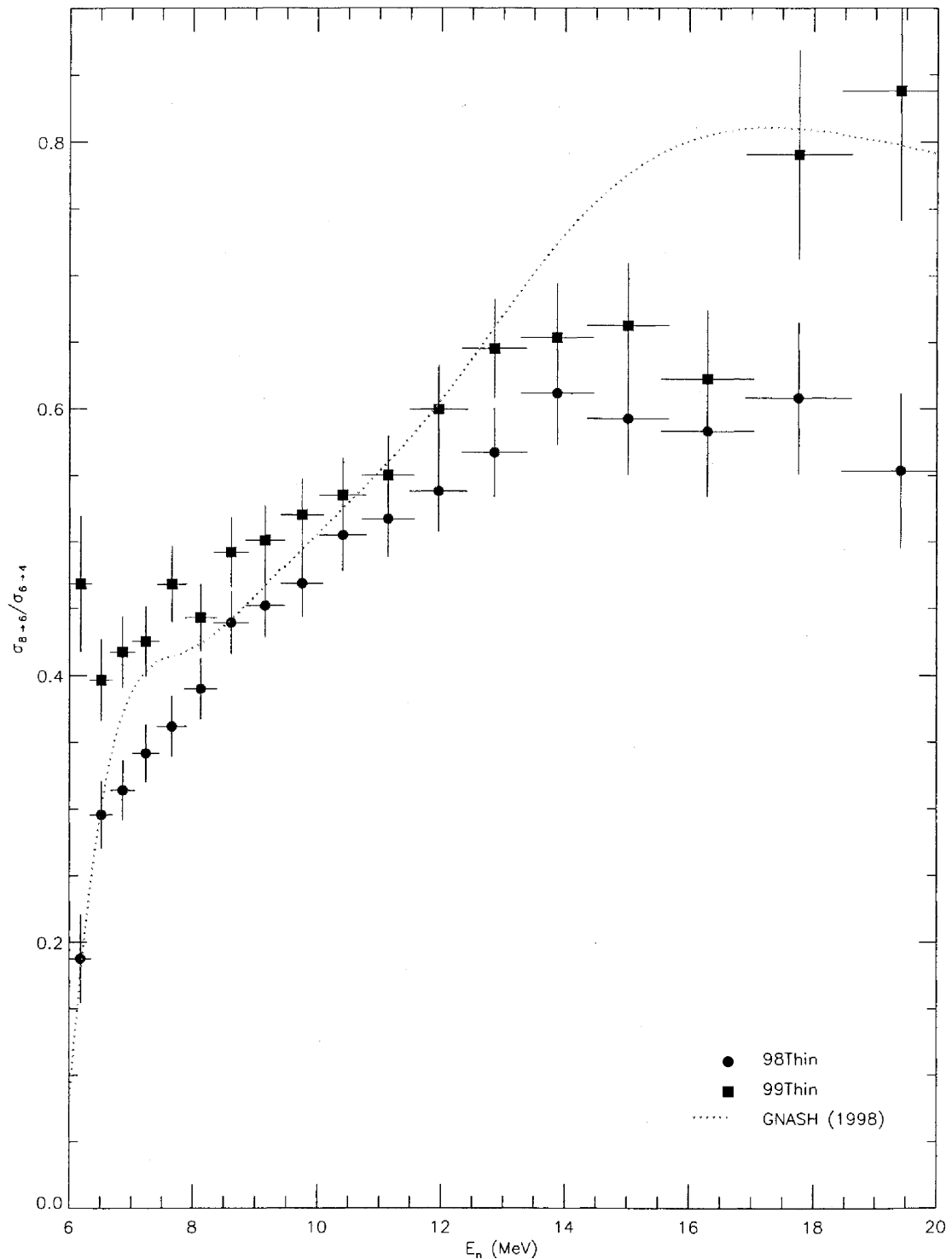


FIG. 46: Ratio of partial γ -ray cross sections $\sigma_{8 \rightarrow 6} / \sigma_{6 \rightarrow 4}$ plotted for the **98Thin** and **99Thin** GEANIE data sets and compared to the GNASH prediction. Angular-distribution corrections are not included.

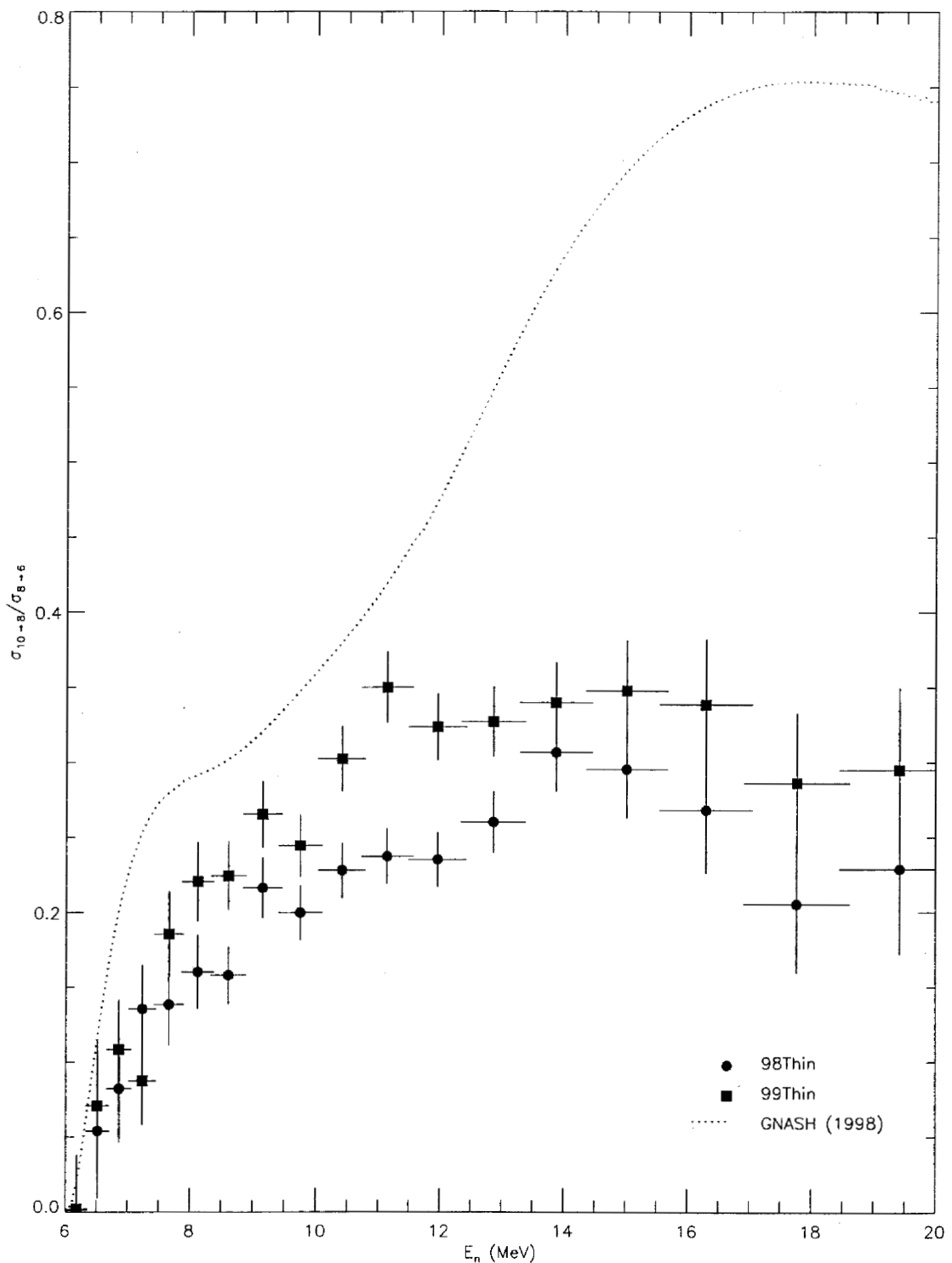


FIG. 47: Ratio of partial γ -ray cross sections $\sigma_{10-8}/\sigma_{8-6}$ plotted for the **98Thin** and **99Thin** GEANIE data sets and compared to the GNASH prediction. Angular-distribution corrections are not included.

Based on these observations and the assumptions made above, we can correct the 1998 data by applying an overall scale factor, to adjust target thickness and other global factors, and we adjust the 1999 data by subtracting a systematic background, which we approximate as a constant baseline at all neutron energies. Mathematically, this is summarized by the equation:

$$\sigma_{\gamma}^{(1999)}(E_n) - a_0 \Leftrightarrow a_1 \times \sigma_{\gamma}^{(1998)}(E_n) \quad (23)$$

In practice, we obtain the correction coefficients a_0 and a_1 by minimizing the expression:

$$\chi^2 = \sum_{i=1}^n \frac{1}{\sigma_i^2} \left[\sigma_{\gamma}^{(1999)}(E_n) - a_0 - a_1 \times \sigma_{\gamma}^{(1998)}(E_n) \right]^2 \quad (24)$$

with respect to a_0 and a_1 . In this expression, the summation extends over all the points in the excitation functions, and σ_i is taken as the uncertainty $u_{\gamma}^{(1998)}(E_n)$ in the 1998 yields. After these coefficients are extracted, they are applied to the original data according to equation 23 and their uncertainties σ_{a_0} and σ_{a_1} are propagated according to the expressions:

$$\left[u_{\gamma}^{(1998)}(E_n) \right]^2 \rightarrow a_1^2 \times \left[\sigma_{\gamma}^{(1998)}(E_n) \right]^2 \times \left\{ \frac{\left[u_{\gamma}^{(1998)}(E_n) \right]^2}{\left[\sigma_{\gamma}^{(1998)}(E_n) \right]^2} + \frac{\sigma_{a_1}^2}{a_1^2} \right\} \quad (25)$$

$$\left[u_{\gamma}^{(1999)}(E_n) \right]^2 \rightarrow \left[u_{\gamma}^{(1999)}(E_n) \right]^2 + \sigma_{a_0}^2 \quad (26)$$

These “optimized” partial γ -ray cross sections can then be combined by weighted average, in the same manner as in section XII A. This optimization, followed by the weighted mean procedure is summarized for each transition in figures 48-51. In each figure the correction parameters a_0 and a_1 are listed in the top panel, along with their uncertainties and the χ^2/ν of the linear fit. It is interesting to note that for the $4 \rightarrow 2$, $6 \rightarrow 4$, and $8 \rightarrow 6$ transitions, the scaling corrections a_1 extracted from the fits all lie close to each other and are consistent with a 10-15% under-estimation of the 1998 sample thickness. The $10 \rightarrow 8$ transition must be treated separately. The scaling factor obtained in that case is larger than 1 and could be interpreted as arising from contamination by the nearby peak. Because the contaminant peak is so close in γ -ray energy, the effect will be seen in the scaling factor rather than as an overall baseline, and in keeping with the assumptions made above, contributes a background proportional to $\sigma_{\gamma}^{(1998)}(E_n)$ to the 1998 data which does not therefore affect its shape.

These optimized-and-averaged partial γ -ray cross sections are also listed in table XXVII. In figure 52 we compare the recommended results obtained by either averaging approach. Both methods produce nearly identical excitation functions for the $6 \rightarrow 4$ transition, which reinforces the observation that, apart from an overall scale factor, the 1998 and 1999 measurements of this partial γ -ray cross section are highly consistent. For the $4 \rightarrow 2$ and $8 \rightarrow 6$ transitions, the simple weighting approach yields systematically higher excitation functions, but in both cases, the yield does not vanish below the $(n,2n)$ reaction threshold. For the $10 \rightarrow 8$ transition, the simple weighting methods produces a overall lower yields than the more involved treatment described in this section.

In the end, a single set of partial cross sections must be selected as the recommended set. Because we have taken full advantage of all information in both **98Thin** and **99Thin** with the correction method described in this section, we feel that this set of four excitation functions represents our most reliable estimate partial γ -ray cross sections. More specifically, we place the greatest confidence in the results for the $6 \rightarrow 4$ transition, which seem robust regardless of how the 1998 and 1999 data are analyzed and combined.

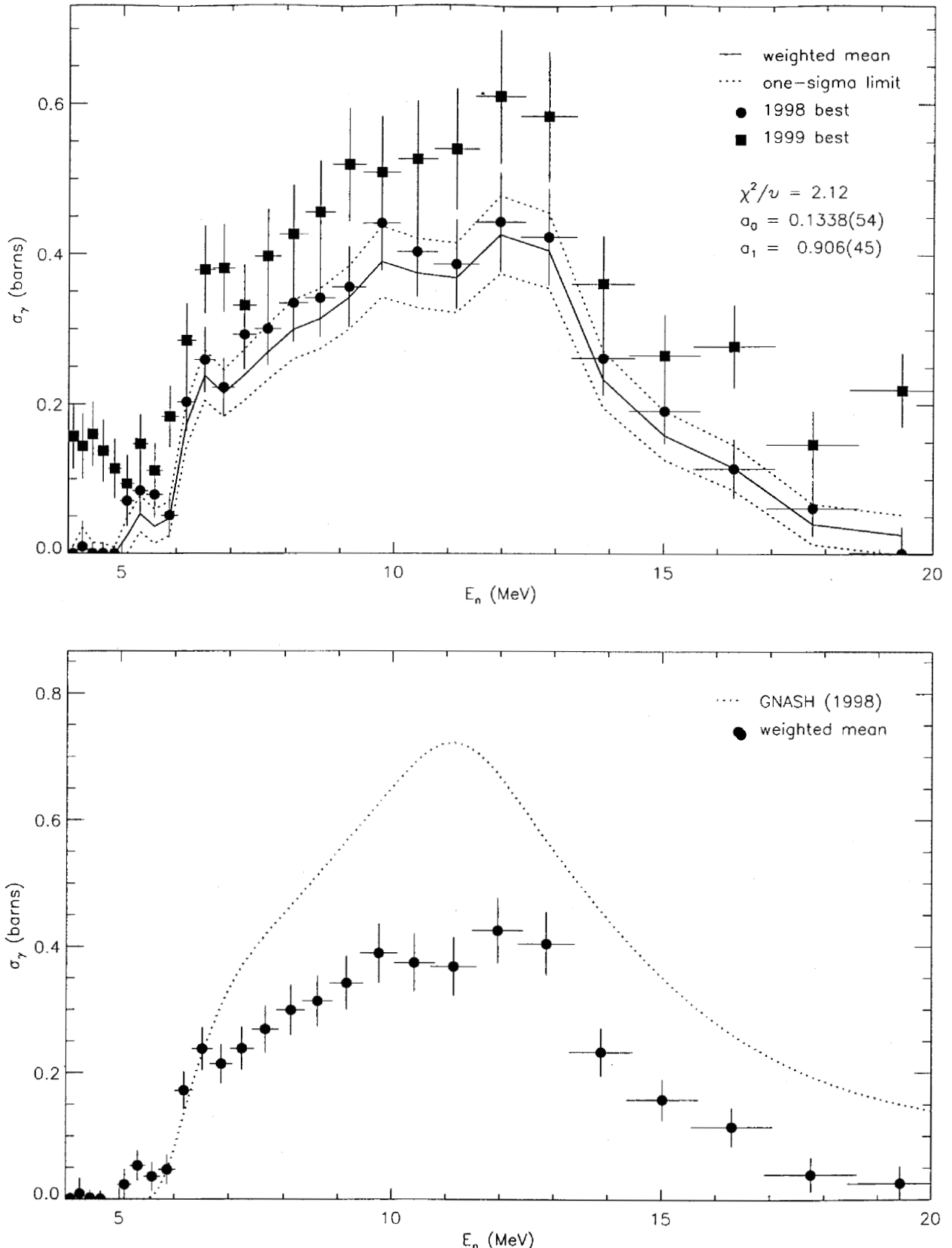


FIG. 48: Best $4_1^+ \rightarrow 2_1^+$ partial cross section obtained by weighted mean of the best 1998 and 1999 results optimized according to equation 23. The top panel shows the adjusted 1998 and 1999 partial cross sections and the weighted mean, plotted as a solid line with a one-sigma confidence band. The bottom panel shows the same weighted-mean partial cross section compared to GNASH.

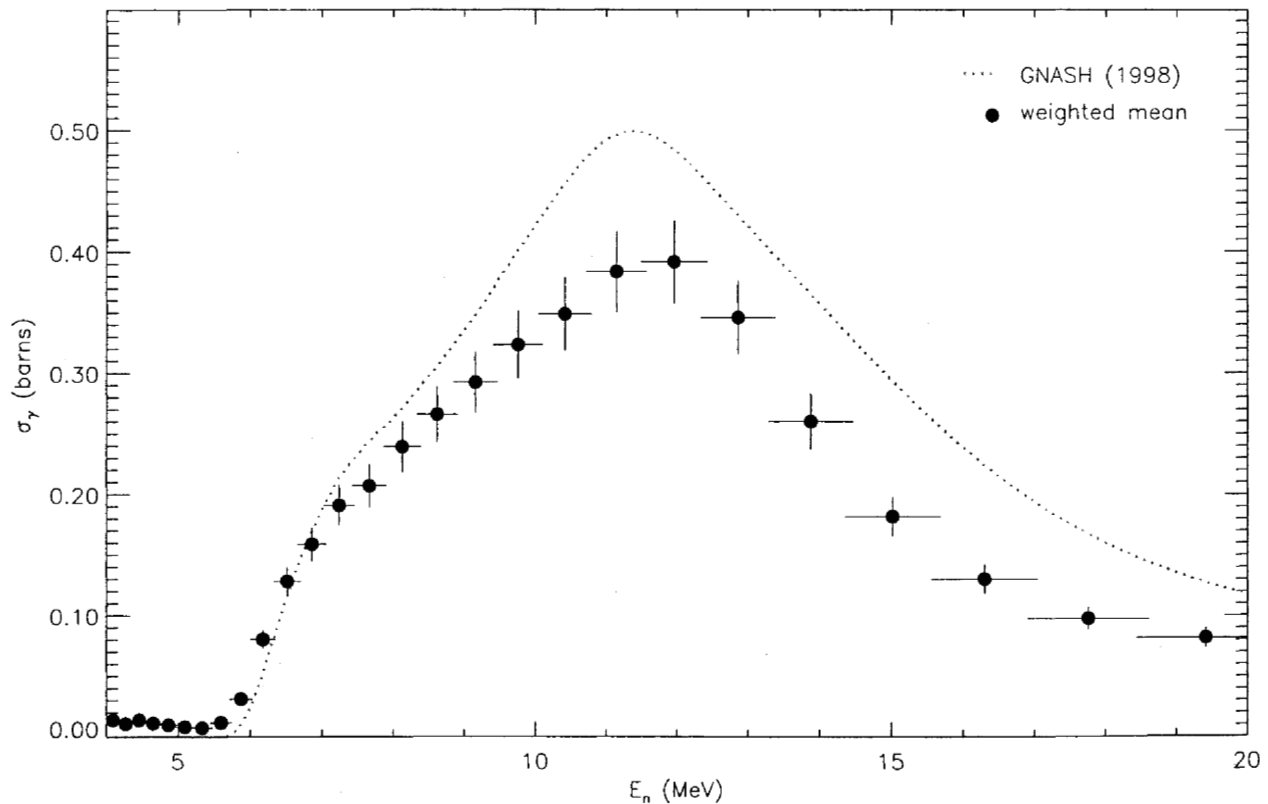
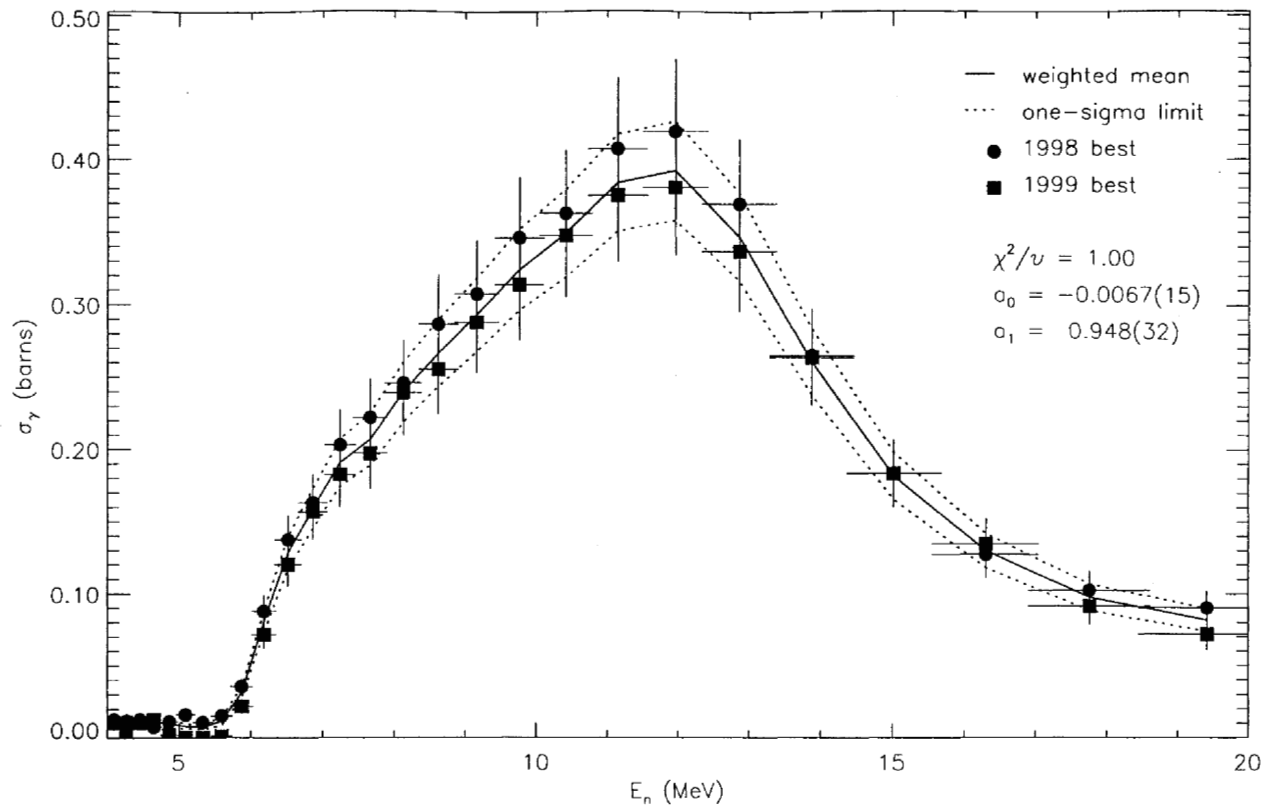


FIG. 49: Best $6_1^+ \rightarrow 4_1^+$ partial cross section obtained by weighted mean of the best 1998 and 1999 results optimized according to equation 23. The top panel shows the adjusted 1998 and 1999 partial cross sections and the weighted mean, plotted as a solid line with a one-sigma confidence band. The bottom panel shows the same weighted-mean partial cross section compared to GNASH.

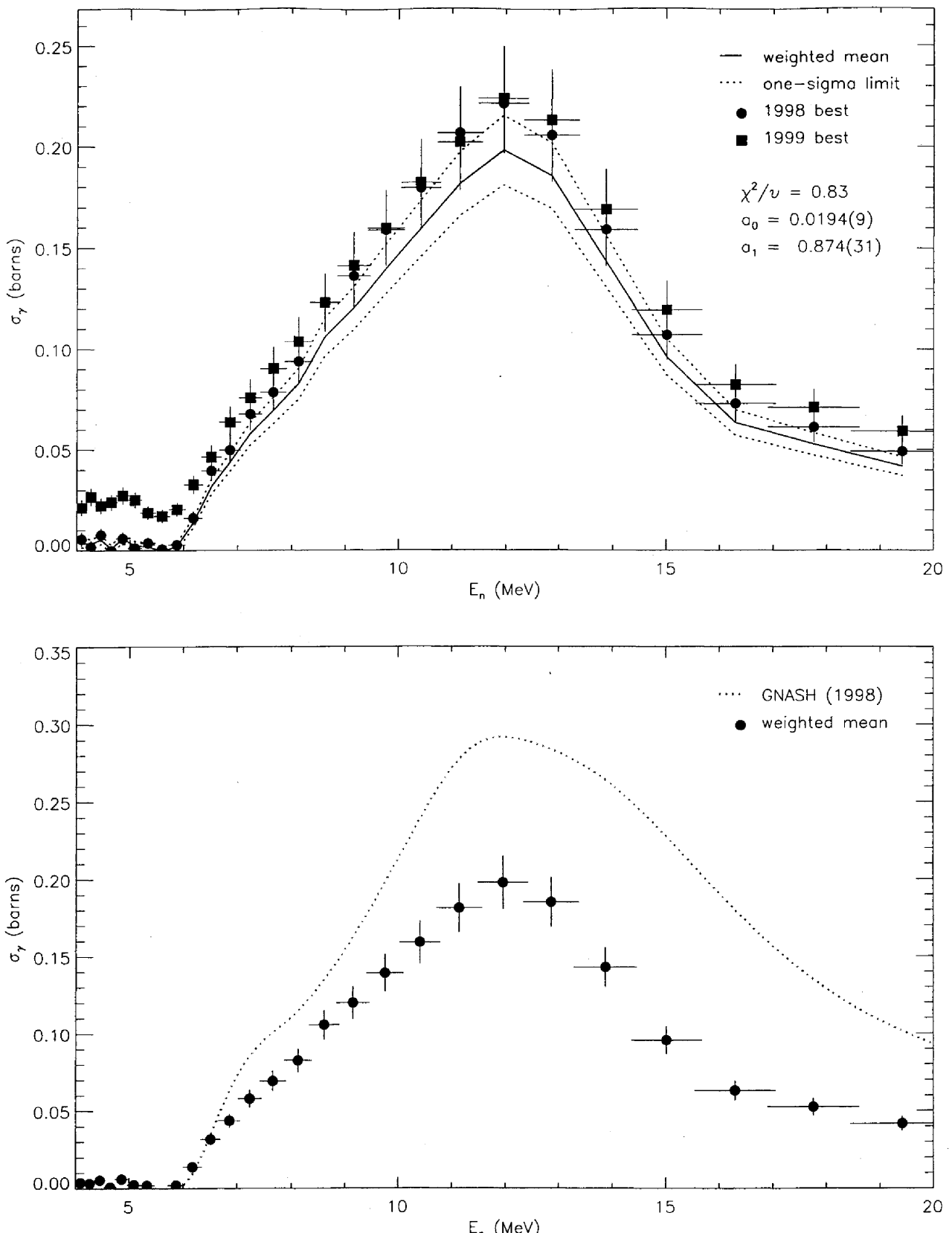


FIG. 50: Best $8_1^+ \rightarrow 6_1^+$ partial cross section obtained by weighted mean of the best 1998 and 1999 results optimized according to equation 23. The top panel shows the adjusted 1998 and 1999 partial cross sections and the weighted mean, plotted as a solid line with a one-sigma confidence band. The bottom panel shows the same weighted-mean partial cross section compared to GNASH.

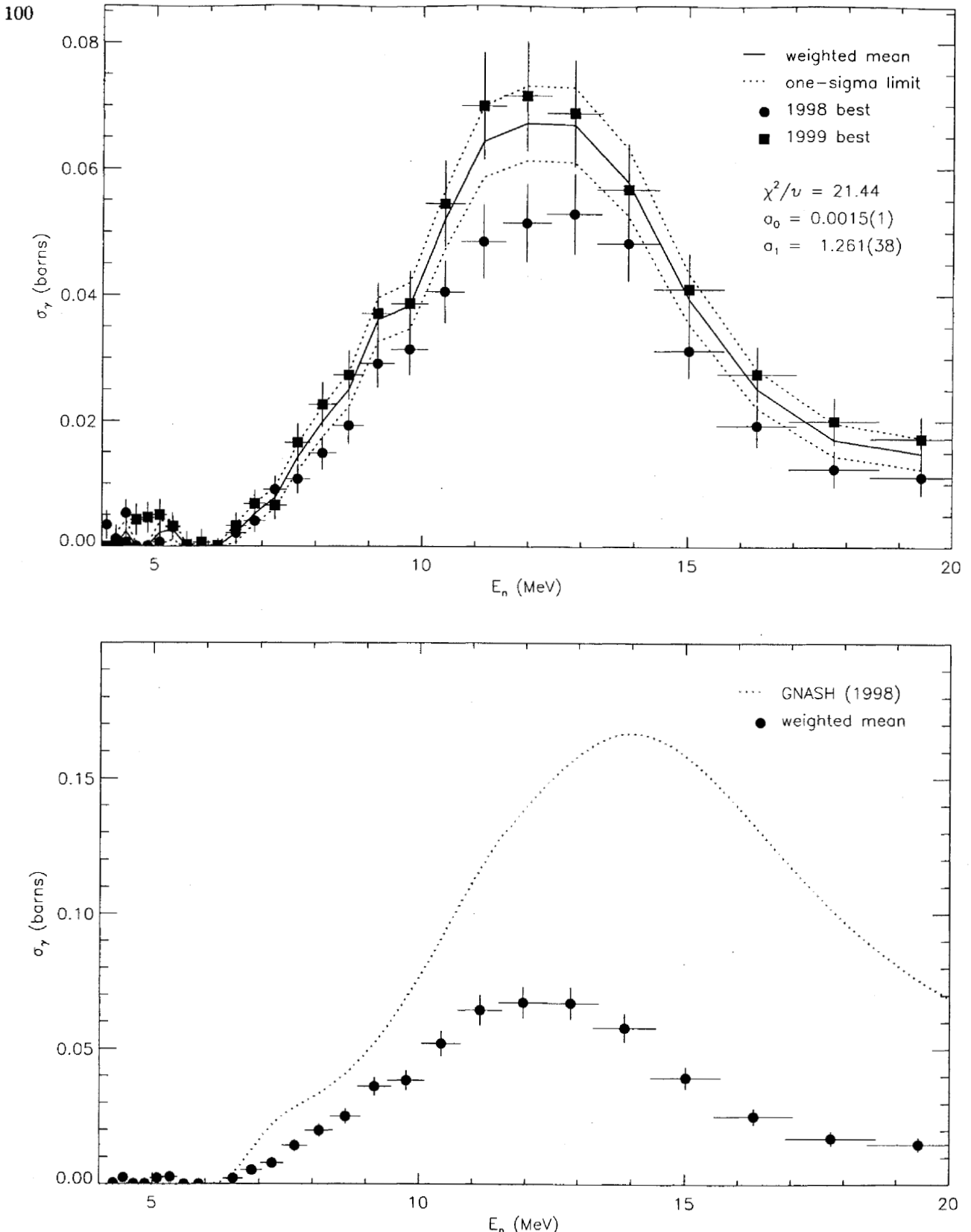


FIG. 51: Best $10_1^+ \rightarrow 8_1^+$ partial cross section obtained by weighted mean of the best 1998 and 1999 results optimized according to equation 23. The top panel shows the adjusted 1998 and 1999 partial cross sections and the weighted mean, plotted as a solid line with a one-sigma confidence band. The bottom panel shows the same weighted-mean partial cross section compared to GNASH.

TABLE XXVII: Best partial cross sections deduced from the optimized weighted mean of 1998 and 1999 GEANIE measurements.

Bin	$\sigma_{4_1^+ \rightarrow 2_1^+}(b)$	$\sigma_{6_1^+ \rightarrow 4_1^+}(b)$	$\sigma_{8_1^+ \rightarrow 6_1^+}(b)$	$\sigma_{10_1^+ \rightarrow 8_1^+}(b)$
1	0.001 ± 0.009	0.014 ± 0.003	0.004 ± 0.002	-0.002 ± 0.000
2	0.009 ± 0.025	0.011 ± 0.003	0.003 ± 0.002	0.000 ± 0.002
3	0.003 ± 0.013	0.014 ± 0.003	0.005 ± 0.002	0.002 ± 0.002
4	0.001 ± 0.013	0.011 ± 0.003	0.001 ± 0.002	0.000 ± 0.000
5	-0.001 ± 0.009	0.010 ± 0.003	0.006 ± 0.002	0.000 ± 0.000
6	0.023 ± 0.024	0.008 ± 0.002	0.002 ± 0.002	0.002 ± 0.002
7	0.053 ± 0.024	0.007 ± 0.002	0.002 ± 0.002	0.003 ± 0.002
8	0.036 ± 0.023	0.012 ± 0.003	-0.000 ± 0.002	0.000 ± 0.000
9	0.047 ± 0.023	0.031 ± 0.004	0.002 ± 0.002	0.000 ± 0.000
10	0.172 ± 0.030	0.080 ± 0.007	0.014 ± 0.002	-0.000 ± 0.000
11	0.238 ± 0.034	0.128 ± 0.011	0.032 ± 0.004	0.002 ± 0.002
12	0.214 ± 0.031	0.159 ± 0.014	0.044 ± 0.004	0.005 ± 0.002
13	0.238 ± 0.034	0.191 ± 0.017	0.058 ± 0.006	0.008 ± 0.002
14	0.269 ± 0.037	0.207 ± 0.018	0.069 ± 0.007	0.014 ± 0.002
15	0.299 ± 0.039	0.239 ± 0.021	0.083 ± 0.008	0.020 ± 0.002
16	0.313 ± 0.040	0.266 ± 0.023	0.106 ± 0.009	0.025 ± 0.003
17	0.342 ± 0.043	0.292 ± 0.025	0.120 ± 0.011	0.036 ± 0.004
18	0.389 ± 0.047	0.323 ± 0.028	0.139 ± 0.012	0.038 ± 0.004
19	0.374 ± 0.046	0.349 ± 0.030	0.159 ± 0.014	0.052 ± 0.005
20	0.368 ± 0.046	0.383 ± 0.033	0.181 ± 0.016	0.064 ± 0.006
21	0.425 ± 0.052	0.392 ± 0.034	0.198 ± 0.017	0.067 ± 0.006
22	0.404 ± 0.050	0.346 ± 0.030	0.185 ± 0.016	0.067 ± 0.006
23	0.233 ± 0.038	0.260 ± 0.023	0.143 ± 0.013	0.058 ± 0.005
24	0.158 ± 0.033	0.181 ± 0.016	0.096 ± 0.009	0.039 ± 0.004
25	0.115 ± 0.030	0.130 ± 0.012	0.063 ± 0.006	0.025 ± 0.003
26	0.040 ± 0.027	0.097 ± 0.009	0.053 ± 0.005	0.017 ± 0.003
27	0.026 ± 0.027	0.082 ± 0.008	0.042 ± 0.005	0.015 ± 0.003

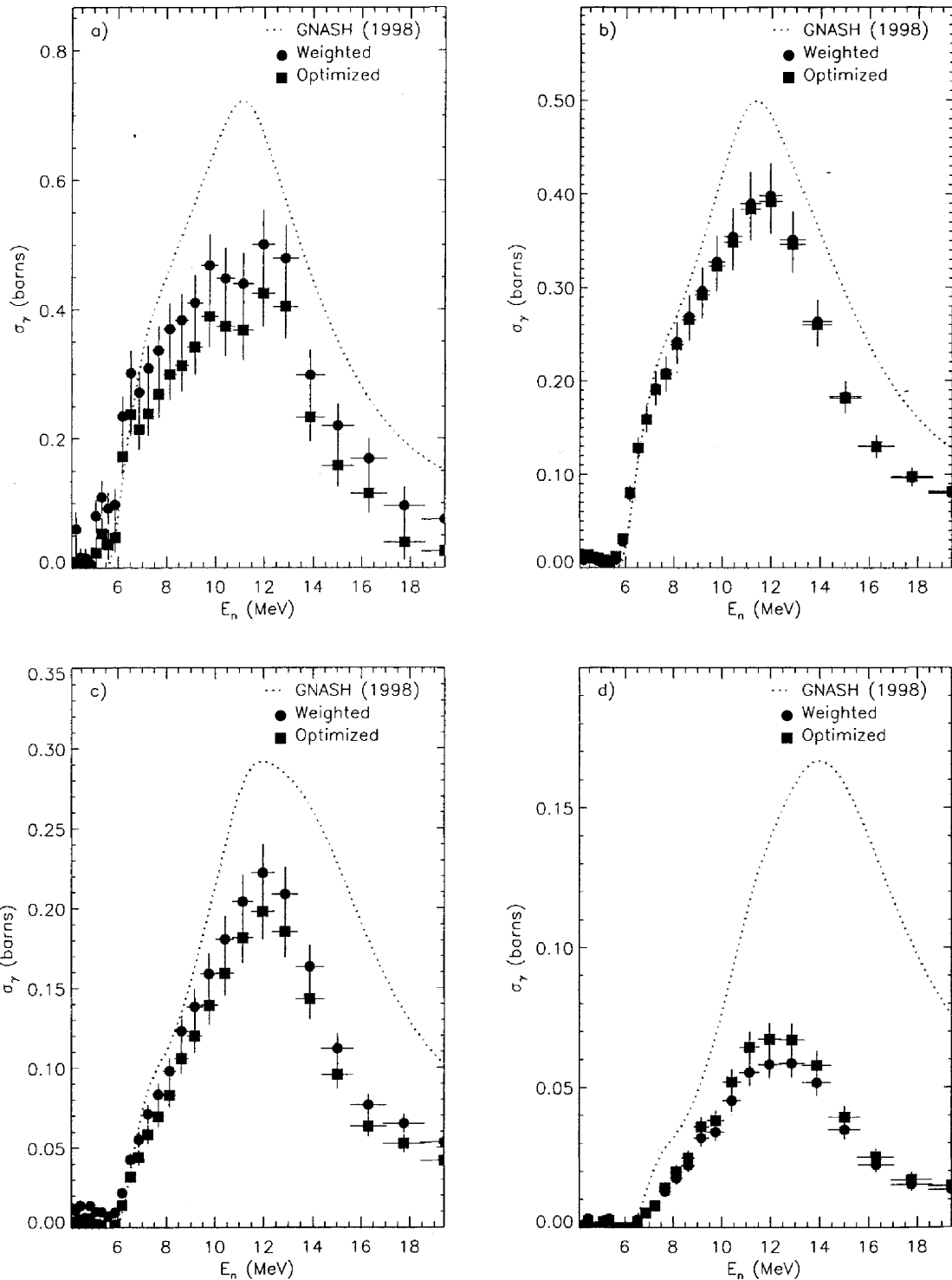


FIG. 52: Comparison of recommended partial γ -ray cross sections obtained from either the weighted **98Thin** and **99Thin**, as discussed in section XII A or from the optimized data, as discussed in section XII B. The data shown are for the a) $4 \rightarrow 2$, b) $6 \rightarrow 4$, c) $8 \rightarrow 6$, and d) $10 \rightarrow 8$ transitions.

XIII. SUMMARY OF OBSERVED LINES

In this section, the reader will find a summary of the analysis and recommended partial cross sections for all observed $^{235}\text{U}(n,n'\gamma)$ and $^{235}\text{U}(n,2n\gamma)$ transitions. The results are tabulated and plotted for easy reference while specific concerns for individual lines are briefly discussed in the text. Wherever possible, planar-detector data from both **98Thin** and **99Thin** sets have been combined using the optimization technique described in section XII B which subtracts a (small) baseline from the **99Thin** data to account for unresolved background and scales the **98Thin** data to compensate for a large uncertainty in target thickness. After these corrections, the two data sets are combined by weighted average according to equations 21 and 22. This procedure was adopted because systematic deviations were found between the **98Thin** and **99Thin** data sets which could be removed in this manner. For strong, well-resolved lines, this procedure should yield a small baseline for the **99Thin** and a consistent scale for the **98Thin**, representing to lowest order a correction to the poorly-known target thickness for the 1998 data. This is precisely what is observed for the relatively strong $E_\gamma = 152.7\text{-keV}$ and 201.0-keV transitions in ^{234}U and the $E_\gamma = 129.3\text{-keV}$ transition in ^{235}U . In fact, from the $^{234}\text{U} 4_1^+ \rightarrow 2_1^+$, $6_1^+ \rightarrow 4_1^+$, and $8_1^+ \rightarrow 6_1^+$ transitions in ^{234}U and the $5/2^+ \rightarrow 7/2^-_1$ transition in ^{235}U , we extract consistent scale factors for the **98Thin** data of 0.906 ± 0.045 , 0.948 ± 0.052 , 0.875 ± 0.051 , and 0.918 ± 0.054 respectively, which we combine by weighted average to yield a correction factor of 0.911 ± 0.025 . For other, weaker lines in the $(n,2n)$, (n,n') and $(n,3n)$ channels we expect a small positive baseline, which is indeed the case for most observed γ -rays. The scale factor however, can deviate somewhat from the average value of 0.911 ± 0.025 . This can occur, as was discussed in the case of the $10_1^+ \rightarrow 8_1^+$ transition in section VII A 2, when the peak shape is not accurately modeled, usually because of nearby contaminant peaks, whether real or generated as an artifact of the fit. By allowing for some variation in the scale factor between **98Thin** and **99Thin** data sets to provide the best match, we can at least partially compensate for the effect of contaminants before combining the data sets. In the end, by this procedure we still rely on the **98Thin** data to provide the shape of the excitation functions and on the **99Thin** to provide the overall magnitude. In cases where a transition could only be observed in the **98Thin** data, the partial cross section extracted from these data was scaled by the target-thickness correction of 0.911 ± 0.025 . For some higher-energy transitions, the statistics in planar-detector data were found to be insufficient, and the coaxial-detector data from the **98Thin** experiment were used instead to extract a partial cross section.

For most lines discussed in this section, there are several γ rays depopulating the parent level in the nucleus. For each observed γ ray, we have commented on all other transitions issued from the same level with at least 50% of the intensity of the strongest branch from that level. Because of poor statistics, branches weaker than this 50% threshold are not likely to be observed in the GEANIE data.

Where available, GNASH predictions for the lines have been included in the partial cross-section plots. These calculations were obtained on 5/13/99, and were performed based on available information at that time, which does not include the finalized values of the partial cross sections quoted in this report. Therefore, agreement or discrepancy between calculations and experimental data for individual lines should not be taken as an indicator of success or failure of the model as a whole. Deviations are expected, especially for weak lines, and occasional agreements between theory and experiment can be coincidental, especially when they do not follow a systematic pattern (e.g. agreement for all the decays out of a given band). We describe the matching between experiment and theory for individual lines for the sake of completeness, but not as a value judgment on the performance of the model as a whole.

In addition, we note that some of the GNASH partial cross sections plotted here show a discontinuity near $E_n = 9.5\text{ MeV}$ (see e.g. figures 63, 71, and 72). This discontinuity is present in the GNASH calculations themselves, and is not an artifact of the plotting process.

A Angular-Distribution Correction Factors

A detailed discussion of corrections for angular-distribution effects can be found in section XI. In this section, we present the correction factors calculated for all $(n,2n)$ and $(n,3n)$ lines of interest. We do not include angular distribution correction for (n,n') transitions because in the $E_n = 4\text{-}20\text{-MeV}$ range shown and discussed throughout this report, the alignment is negligible and no correction is necessary.

1 Angular-Distribution Correction Factor for Transitions in ^{234}U

Table XXVIII lists the properties of ^{234}U γ rays observed in the GEANIE data that are used in the calculation of angular distribution factors C_γ given by equation 19. As discussed in section XI, a “damping” factor of 0.8068 was

applied to the AVALANCHE calculation of alignments. The correction factors for each (n,2n) line of interest can be found in tables XXIX-LIV.

TABLE XXVIII: Properties used in the calculation of angular distribution correction factors for $^{235}\text{U}(n,2n)$ γ rays.
 E_γ (keV) E_x (keV) J_i J_f L_1 L_2 δ Identification of Multipolarity

E_γ (keV)	E_x (keV)	J_i	J_f	L_1	L_2	δ	Identification of Multipolarity
99.8	143.4	4	2	2	3	0	known E2
131.3	1552.6	5	6	1	2	0	known E1
152.7	296.1	6	4	2	3	0	known E2
201.0	497.0	8	6	2	3	0	known E2
244.2	741.2	10	8	2	3	0	known E2
282.6	1023.8	12	10	2	3	0	known E2
666.5	962.6	5	6	1	2	0	assume E1 ($\Delta J = 1, \pi_i\pi_f = -1$)
780.4	1277.5	7	8	1	2	0	assume E1 ($\Delta J = 1, \pi_i\pi_f = -1$)
786.3	786.3	1	0	1	2	0	known E1
805.8	849.3	3	2	1	2	0	assume E1 ($\Delta J = 1, \pi_i\pi_f = -1$)
819.2	962.6	5	4	1	2	0	assume E1 ($\Delta J = 1, \pi_i\pi_f = -1$)
829.3	1125.3	7	6	1	2	0	assume E1 ($\Delta J = 1, \pi_i\pi_f = -1$)
831.5	1127.6	5	6	1	2	0	assume E1 ($\Delta J = 1, \pi_i\pi_f = -1$)
876.0	1172.1	6	6	2	1	0	known E2
880.5	1023.7	4	4	2	1	0	assume E2 (2-phonon \rightarrow 1-phonon band)
880.5	1023.8	3	4	1	2	0	assume E1 ($\Delta J = 1, \pi_i\pi_f = -1$)
883.2	926.7	2	2	2	3	0	known E2
898.7	1194.7	6	6	1	2	0	assume E1 ($\Delta J = 0, \pi_i\pi_f = -1$)
925.0	968.6	3	2	2	1	0	assume E2 (2-phonon \rightarrow 1-phonon band)
925.9	1069.3	4	4	1	2	0	assume E1 ($\Delta J = 0, \pi_i\pi_f = -1$)
926.7	926.7	2	0	2	3	0	known E2
946.0	989.4	2	2	1	2	0	known E1
947.7	1090.9	5	4	2	3	0	assume E2 (2-phonon \rightarrow 1-phonon band)
965.8	1261.8	7	6	2	3	0	assume E2 (2-phonon \rightarrow 1-phonon band)
981.6	1277.5	7	6	1	2	0	assume E1 ($\Delta J = 1, \pi_i\pi_f = -1$)
984.2	1127.6	5	4	1	2	0	assume E1 ($\Delta J = 1, \pi_i\pi_f = -1$)

TABLE XXIX: Angular distribution correction factors calculated for the $E_\gamma = 99.8$ -keV transition using the code AVALANCHE for the sum of planar and coaxial data, and for both **98Thin** and **99Thin** data sets. Corrections marked by a “*” symbol were obtained by quadratic extrapolation from higher- E_n values in the table.

E_n (MeV)	σ_2/J	σ_2/J	98Thin planar	98Thin coaxial	99Thin planar	99Thin coaxial
5.3	0.0000	0.0000	0.9628*	N/A	0.9605*	N/A
6.0	0.7847	7.4997	0.9620	N/A	0.9596	N/A
7.0	0.7915	7.4997	0.9626	N/A	0.9602	N/A
8.0	0.7710	7.4997	0.9609	N/A	0.9584	N/A
9.0	0.7575	7.4997	0.9597	N/A	0.9572	N/A
10.0	0.7468	7.4997	0.9587	N/A	0.9561	N/A
11.0	0.7438	1.5922	0.9584	N/A	0.9558	N/A
12.0	0.7625	1.1340	0.9599	N/A	0.9575	N/A
13.0	0.7825	1.0530	0.9615	N/A	0.9592	N/A
14.0	0.8007	1.0130	0.9630	N/A	0.9608	N/A
15.0	0.8150	0.9842	0.9640	N/A	0.9619	N/A
16.0	0.8353	0.9915	0.9655	N/A	0.9635	N/A
17.0	0.8492	0.9752	0.9665	N/A	0.9645	N/A
18.0	0.8790	0.9925	0.9685	N/A	0.9666	N/A
19.0	0.9093	1.0172	0.9703	N/A	0.9685	N/A
20.0	0.9357	1.0393	0.9718	N/A	0.9701	N/A

TABLE XXX: Angular distribution correction factors calculated for the $E_\gamma = 131.3$ -keV transition using the code AVALANCHE for the sum of planar and coaxial data, and for both **98Thin** and **99Thin** data sets. Corrections marked by a “*” symbol were obtained by quadratic extrapolation from higher- E_n values in the table.

E_n (MeV)	σ_2/J	σ_2/J	98Thin planar	98Thin coaxial	99Thin planar	99Thin coaxial
5.3	0.0000	0.0000	1.0283*	N/A	1.0302*	N/A
6.0	0.0000	0.0000	1.0276*	N/A	1.0295*	N/A
7.0	0.5200	5.9998	1.0291	N/A	1.0310	N/A
8.0	0.5866	5.9998	1.0242	N/A	1.0258	N/A
9.0	0.6140	5.9998	1.0224	N/A	1.0239	N/A
10.0	0.5956	5.9998	1.0236	N/A	1.0252	N/A
11.0	0.5942	1.0898	1.0237	N/A	1.0253	N/A
12.0	0.6148	0.8890	1.0224	N/A	1.0239	N/A
13.0	0.6342	0.8394	1.0213	N/A	1.0227	N/A
14.0	0.6512	0.8126	1.0204	N/A	1.0217	N/A
15.0	0.6644	0.7932	1.0197	N/A	1.0210	N/A
16.0	0.6822	0.8010	1.0188	N/A	1.0200	N/A
17.0	0.6956	0.7914	1.0182	N/A	1.0194	N/A
18.0	0.7210	0.8080	1.0171	N/A	1.0182	N/A
19.0	0.7468	0.8294	1.0160	N/A	1.0171	N/A
20.0	0.7692	0.8486	1.0152	N/A	1.0162	N/A

TABLE XXXI: Angular distribution correction factors calculated for the $E_\gamma = 152.7$ -keV transition using the code AVALANCHE for the sum of planar and coaxial data, and for both **98Thin** and **99Thin** data sets. Corrections marked by a “*” symbol were obtained by quadratic extrapolation from higher- E_n values in the table.

E_n (MeV)	σ_2/J	σ_2/J	98Thin planar	98Thin coaxial	99Thin planar	99Thin coaxial
5.3	0.0000	0.0000	0.9282*	N/A	0.9236*	N/A
6.0	0.4333	4.9998	0.9231	N/A	0.9184	N/A
7.0	0.5010	4.9998	0.9353	N/A	0.9312	N/A
8.0	0.5028	4.9998	0.9356	N/A	0.9316	N/A
9.0	0.5020	0.8683	0.9351	N/A	0.9311	N/A
10.0	0.5037	0.7338	0.9351	N/A	0.9312	N/A
11.0	0.5065	0.6817	0.9353	N/A	0.9315	N/A
12.0	0.5225	0.6567	0.9378	N/A	0.9341	N/A
13.0	0.5387	0.6490	0.9402	N/A	0.9368	N/A
14.0	0.5523	0.6442	0.9422	N/A	0.9389	N/A
15.0	0.5625	0.6382	0.9436	N/A	0.9404	N/A
16.0	0.5767	0.6485	0.9457	N/A	0.9425	N/A
17.0	0.5870	0.6477	0.9470	N/A	0.9440	N/A
18.0	0.6073	0.6645	0.9497	N/A	0.9468	N/A
19.0	0.6275	0.6832	0.9522	N/A	0.9494	N/A
20.0	0.6448	0.6990	0.9542	N/A	0.9515	N/A

TABLE XXXII: Angular distribution correction factors calculated for the $E_\gamma = 201.0$ -keV transition using the code AVALANCHE for the sum of planar and coaxial data, and for both **98Thin** and **99Thin** data sets. Corrections marked by a “**” symbol were obtained by quadratic extrapolation from higher- E_n values in the table.

E_n (MeV)	σ_2/J	σ_2/J	98Thin planar	98Thin coaxial	99Thin planar	99Thin coaxial
5.3	0.0000	0.0000	0.9046*	N/A	0.8998*	N/A
6.0	0.2961	0.4293	0.9004	N/A	0.8956	N/A
7.0	0.3563	0.4961	0.9126	N/A	0.9081	N/A
8.0	0.3749	0.4823	0.9159	N/A	0.9117	N/A
9.0	0.3807	0.4703	0.9169	N/A	0.9127	N/A
10.0	0.3851	0.4562	0.9175	N/A	0.9134	N/A
11.0	0.3900	0.4506	0.9183	N/A	0.9143	N/A
12.0	0.4051	0.4586	0.9213	N/A	0.9174	N/A
13.0	0.4195	0.4657	0.9241	N/A	0.9203	N/A
14.0	0.4306	0.4699	0.9262	N/A	0.9225	N/A
15.0	0.4389	0.4711	0.9277	N/A	0.9241	N/A
16.0	0.4499	0.4818	0.9298	N/A	0.9262	N/A
17.0	0.4586	0.4866	0.9314	N/A	0.9279	N/A
18.0	0.4745	0.5024	0.9342	N/A	0.9309	N/A
19.0	0.4894	0.5184	0.9369	N/A	0.9336	N/A
20.0	0.5025	0.5314	0.9391	N/A	0.9359	N/A

TABLE XXXIII: Angular distribution correction factors calculated for the $E_\gamma = 244.2$ -keV transition using the code AVALANCHE for the sum of planar and coaxial data, and for both **98Thin** and **99Thin** data sets. Corrections marked by a “*” symbol were obtained by quadratic extrapolation from higher- E_n values in the table.

E_n (MeV)	σ_2/J	σ_2/J	98Thin planar	98Thin coaxial	99Thin planar	99Thin coaxial
5.3	0.0000	0.0000	0.8931*	N/A	0.8891*	N/A
6.0	0.2509	0.2441	0.8912	N/A	0.8872	N/A
7.0	0.2864	0.3040	0.8991	N/A	0.8949	N/A
8.0	0.3105	0.3328	0.9042	N/A	0.9001	N/A
9.0	0.3200	0.3398	0.9061	N/A	0.9020	N/A
10.0	0.3254	0.3397	0.9071	N/A	0.9030	N/A
11.0	0.3308	0.3434	0.9082	N/A	0.9042	N/A
12.0	0.3437	0.3579	0.9110	N/A	0.9070	N/A
13.0	0.3563	0.3690	0.9136	N/A	0.9097	N/A
14.0	0.3653	0.3754	0.9155	N/A	0.9116	N/A
15.0	0.3720	0.3791	0.9168	N/A	0.9130	N/A
16.0	0.3810	0.3892	0.9188	N/A	0.9150	N/A
17.0	0.3887	0.3962	0.9203	N/A	0.9166	N/A
18.0	0.4017	0.4106	0.9231	N/A	0.9194	N/A
19.0	0.4137	0.4247	0.9255	N/A	0.9219	N/A
20.0	0.4242	0.4359	0.9276	N/A	0.9241	N/A

TABLE XXXIV: Angular distribution correction factors calculated for the $E_\gamma = 282.6$ -keV transition using the code AVALANCHE for the sum of planar and coaxial data, and for both **98Thin** and **99Thin** data sets. Corrections marked by a “*” symbol were obtained by quadratic extrapolation from higher- E_n values in the table.

E_n (MeV)	σ_2/J	σ_2/J	98Thin planar	98Thin coaxial	99Thin planar	99Thin coaxial
5.3	0.0000	0.0000	0.8919*	N/A	0.8880*	N/A
6.0	0.0000	0.0000	0.8934*	N/A	0.8895*	N/A
7.0	0.2513	0.2173	0.8934	N/A	0.8895	N/A
8.0	0.2759	0.2569	0.8987	N/A	0.8947	N/A
9.0	0.2872	0.2721	0.9011	N/A	0.8970	N/A
10.0	0.2923	0.2756	0.9020	N/A	0.8981	N/A
11.0	0.2969	0.2817	0.9030	N/A	0.8990	N/A
12.0	0.3076	0.2970	0.9054	N/A	0.9014	N/A
13.0	0.3184	0.3092	0.9077	N/A	0.9037	N/A
14.0	0.3255	0.3162	0.9092	N/A	0.9053	N/A
15.0	0.3306	0.3203	0.9103	N/A	0.9063	N/A
16.0	0.3382	0.3297	0.9119	N/A	0.9080	N/A
17.0	0.3450	0.3373	0.9134	N/A	0.9095	N/A
18.0	0.3558	0.3503	0.9158	N/A	0.9119	N/A
19.0	0.3658	0.3627	0.9179	N/A	0.9141	N/A
20.0	0.3742	0.3725	0.9197	N/A	0.9159	N/A

TABLE XXXV: Angular distribution correction factors calculated for the $E_\gamma = 666.5$ -keV transition using the code AVALANCHE for the sum of planar and coaxial data, and for both **98Thin** and **99Thin** data sets. Corrections marked by a “*” symbol were obtained by quadratic extrapolation from higher- E_n values in the table.

E_n (MeV)	σ_2/J	σ_2/J	98Thin planar	98Thin coaxial	99Thin planar	99Thin coaxial
5.3	0.0000	0.0000	1.0268*	0.9808*	1.0286*	0.9812*
6.0	0.0000	0.0000	1.0264*	0.9811*	1.0282*	0.9815*
7.0	0.5546	5.9998	1.0270	0.9806	1.0289	0.9810
8.0	0.5978	5.9998	1.0240	0.9827	1.0257	0.9831
9.0	0.6028	5.9998	1.0237	0.9829	1.0253	0.9833
10.0	0.5984	1.2002	1.0240	0.9827	1.0256	0.9831
11.0	0.6002	0.9282	1.0239	0.9828	1.0255	0.9832
12.0	0.6176	0.8244	1.0228	0.9835	1.0243	0.9839
13.0	0.6344	0.7976	1.0218	0.9842	1.0233	0.9846
14.0	0.6496	0.7844	1.0209	0.9848	1.0224	0.9852
15.0	0.6614	0.7722	1.0203	0.9853	1.0217	0.9856
16.0	0.6782	0.7828	1.0195	0.9859	1.0208	0.9862
17.0	0.6900	0.7764	1.0189	0.9863	1.0202	0.9866
18.0	0.7142	0.7936	1.0178	0.9870	1.0190	0.9873
19.0	0.7382	0.8148	1.0168	0.9878	1.0179	0.9880
20.0	0.7592	0.8332	1.0160	0.9883	1.0170	0.9886

TABLE XXXVI: Angular distribution correction factors calculated for the $E_\gamma = 780.4$ -keV transition using the code AVALANCHE for the sum of planar and coaxial data, and for both **98Thin** and **99Thin** data sets. Corrections marked by a “**” symbol were obtained by quadratic extrapolation from higher- E_n values in the table.

E_n (MeV)	σ_2/J	σ_2/J	98Thin planar	98Thin coaxial	99Thin planar	99Thin coaxial
5.3	0.0000	0.0000	1.0491*	0.9660*	1.0526*	0.9666*
6.0	0.0000	0.0000	1.0477*	0.9669*	1.0511*	0.9675*
7.0	0.3516	0.6496	1.0489	0.9661	1.0524	0.9668
8.0	0.4106	0.6100	1.0418	0.9707	1.0448	0.9712
9.0	0.4277	0.5854	1.0399	0.9720	1.0427	0.9725
10.0	0.4293	0.5546	1.0397	0.9721	1.0425	0.9726
11.0	0.4346	0.5363	1.0391	0.9725	1.0418	0.9730
12.0	0.4506	0.5327	1.0373	0.9736	1.0400	0.9741
13.0	0.4657	0.5354	1.0358	0.9747	1.0383	0.9752
14.0	0.4779	0.5379	1.0345	0.9755	1.0370	0.9760
15.0	0.4873	0.5376	1.0336	0.9761	1.0360	0.9766
16.0	0.4999	0.5489	1.0324	0.9769	1.0347	0.9774
17.0	0.5097	0.5519	1.0315	0.9775	1.0337	0.9780
18.0	0.5276	0.5683	1.0300	0.9786	1.0321	0.9790
19.0	0.5449	0.5857	1.0285	0.9796	1.0305	0.9800
20.0	0.5599	0.6000	1.0273	0.9804	1.0293	0.9807

TABLE XXXVII: Angular distribution correction factors calculated for the $E_{\gamma} = 786.3$ -keV transition using the code AVALANCHE for the sum of planar and coaxial data, and for both **98Thin** and **99Thin** data sets. Corrections marked by a “*” symbol were obtained by quadratic extrapolation from higher- E_n values in the table.

E_n (MeV)	σ_2/J	σ_2/J	98Thin planar	98Thin coaxial	99Thin planar	99Thin coaxial
5.3	0.0000	0.0000	1.0012*	0.9991*	1.0013*	0.9991*
6.0	26.1800	0.0000	1.0001	0.9999	1.0001	0.9999
7.0	3.8620	0.0000	1.0037	0.9972	1.0040	0.9973
8.0	3.2340	0.0000	1.0053	0.9960	1.0057	0.9961
9.0	3.0840	0.0000	1.0059	0.9956	1.0063	0.9957
10.0	2.9390	0.0000	1.0065	0.9952	1.0069	0.9953
11.0	2.8720	0.0000	1.0068	0.9949	1.0072	0.9950
12.0	2.8860	0.0000	1.0067	0.9950	1.0072	0.9951
13.0	2.9300	0.0000	1.0065	0.9951	1.0070	0.9952
14.0	2.9850	0.0000	1.0063	0.9953	1.0067	0.9954
15.0	3.0320	0.0000	1.0061	0.9954	1.0065	0.9955
16.0	3.1060	0.0000	1.0058	0.9957	1.0062	0.9958
17.0	3.1550	0.0000	1.0056	0.9958	1.0060	0.9959
18.0	3.2690	0.0000	1.0052	0.9961	1.0056	0.9962
19.0	3.3880	0.0000	1.0049	0.9964	1.0052	0.9964
20.0	3.4930	0.0000	1.0046	0.9966	1.0049	0.9966

TABLE XXXVIII: Angular distribution correction factors calculated for the $E_\gamma = 805.8$ -keV transition using the code AVALANCHE for the sum of planar and coaxial data, and for both **98Thin** and **99Thin** data sets. Corrections marked by a “*” symbol were obtained by quadratic extrapolation from higher- E_n values in the table.

E_n (MeV)	σ_2/J	σ_2/J	98Thin planar	98Thin coaxial	99Thin planar	99Thin coaxial
5.3	0.0000	0.0000	1.0178*	0.9873*	1.0189*	0.9876*
6.0	0.0000	0.0000	1.0186*	0.9868*	1.0198*	0.9871*
7.0	1.0927	9.9997	1.0185	0.9869	1.0196	0.9872
8.0	1.0347	9.9997	1.0205	0.9855	1.0218	0.9858
9.0	1.0127	9.9997	1.0214	0.9849	1.0227	0.9852
10.0	0.9833	9.9997	1.0226	0.9841	1.0240	0.9844
11.0	0.9743	9.9997	1.0230	0.9838	1.0245	0.9841
12.0	0.9927	1.6670	1.0222	0.9843	1.0236	0.9847
13.0	1.0143	1.4457	1.0213	0.9850	1.0226	0.9853
14.0	1.0360	1.3650	1.0205	0.9855	1.0217	0.9858
15.0	1.0537	1.3123	1.0198	0.9860	1.0210	0.9863
16.0	1.0800	1.3173	1.0189	0.9866	1.0201	0.9869
17.0	1.0980	1.2843	1.0183	0.9870	1.0194	0.9873
18.0	1.1370	1.3020	1.0171	0.9879	1.0181	0.9881
19.0	1.1770	1.3323	1.0160	0.9886	1.0170	0.9889
20.0	1.2123	1.3603	1.0151	0.9892	1.0160	0.9895

TABLE XXXIX: Angular distribution correction factors calculated for the $E_\gamma = 819.2$ -keV transition using the code AVALANCHE for the sum of planar and coaxial data, and for both **98Thin** and **99Thin** data sets. Corrections marked by a “*” symbol were obtained by quadratic extrapolation from higher- E_n values in the table.

E_n (MeV)	σ_2/J	σ_2/J	98Thin planar	98Thin coaxial	99Thin planar	99Thin coaxial
5.3	0.0000	0.0000	1.0471*	0.9673*	1.0503*	0.9680*
6.0	0.0000	0.0000	1.0464*	0.9678*	1.0496*	0.9684*
7.0	0.5546	5.9998	1.0476	0.9670	1.0508	0.9677
8.0	0.5978	5.9998	1.0422	0.9705	1.0450	0.9711
9.0	0.6028	5.9998	1.0416	0.9709	1.0444	0.9714
10.0	0.5984	1.2002	1.0421	0.9705	1.0449	0.9711
11.0	0.6002	0.9282	1.0419	0.9707	1.0447	0.9713
12.0	0.6176	0.8244	1.0400	0.9719	1.0426	0.9725
13.0	0.6344	0.7976	1.0382	0.9731	1.0408	0.9736
14.0	0.6496	0.7844	1.0367	0.9741	1.0391	0.9746
15.0	0.6614	0.7722	1.0356	0.9748	1.0379	0.9754
16.0	0.6782	0.7828	1.0340	0.9759	1.0363	0.9763
17.0	0.6900	0.7764	1.0330	0.9765	1.0352	0.9770
18.0	0.7142	0.7936	1.0311	0.9778	1.0332	0.9783
19.0	0.7382	0.8148	1.0293	0.9791	1.0313	0.9795
20.0	0.7592	0.8332	1.0279	0.9800	1.0297	0.9804

TABLE XL: Angular distribution correction factors calculated for the $E_\gamma = 829.3$ -keV transition using the code AVALANCHE for the sum of planar and coaxial data, and for both **98Thin** and **99Thin** data sets. Corrections marked by a “**” symbol were obtained by quadratic extrapolation from higher- E_n values in the table.

E_n (MeV)	σ_2/J	σ_2/J	98Thin planar	98Thin coaxial	99Thin planar	99Thin coaxial
5.3	0.0000	0.0000	1.0765*	0.9497*	1.0819*	0.9507*
6.0	0.0000	0.0000	1.0742*	0.9510*	1.0794*	0.9521*
7.0	0.3513	0.6274	1.0755	0.9502	1.0808	0.9513
8.0	0.4041	0.5907	1.0655	0.9562	1.0700	0.9571
9.0	0.4246	0.5734	1.0618	0.9584	1.0660	0.9593
10.0	0.4280	0.5464	1.0612	0.9588	1.0654	0.9597
11.0	0.4334	0.5301	1.0602	0.9594	1.0644	0.9603
12.0	0.4497	0.5284	1.0574	0.9611	1.0614	0.9619
13.0	0.4649	0.5317	1.0549	0.9626	1.0587	0.9634
14.0	0.4769	0.5346	1.0531	0.9638	1.0567	0.9646
15.0	0.4861	0.5343	1.0516	0.9647	1.0552	0.9655
16.0	0.4984	0.5456	1.0498	0.9658	1.0532	0.9666
17.0	0.5080	0.5487	1.0484	0.9667	1.0517	0.9674
18.0	0.5256	0.5651	1.0460	0.9682	1.0492	0.9689
19.0	0.5426	0.5821	1.0438	0.9696	1.0468	0.9703
20.0	0.5574	0.5963	1.0420	0.9708	1.0449	0.9715

TABLE XLI: Angular distribution correction factors calculated for the $E_{\gamma} = 831.5$ -keV transition using the code AVALANCHE for the sum of planar and coaxial data, and for both **98Thin** and **99Thin** data sets. Corrections marked by a “*” symbol were obtained by quadratic extrapolation from higher- E_n values in the table.

E_n (MeV)	σ_2/J	σ_2/J	98Thin planar	98Thin coaxial	99Thin planar	99Thin coaxial
5.3	0.0000	0.0000	1.0278*	0.9803*	1.0296*	0.9807*
6.0	0.0000	0.0000	1.0272*	0.9807*	1.0291*	0.9811*
7.0	0.5404	5.9998	1.0280	0.9801	1.0299	0.9805
8.0	0.5910	5.9998	1.0244	0.9826	1.0260	0.9830
9.0	0.6034	5.9998	1.0236	0.9831	1.0252	0.9835
10.0	0.5980	1.3238	1.0239	0.9829	1.0255	0.9833
11.0	0.6002	0.9536	1.0238	0.9830	1.0254	0.9834
12.0	0.6184	0.8342	1.0227	0.9838	1.0242	0.9841
13.0	0.6358	0.8046	1.0216	0.9845	1.0231	0.9848
14.0	0.6510	0.7902	1.0208	0.9851	1.0222	0.9854
15.0	0.6632	0.7774	1.0202	0.9855	1.0215	0.9858
16.0	0.6802	0.7878	1.0193	0.9861	1.0206	0.9864
17.0	0.6924	0.7808	1.0187	0.9865	1.0200	0.9868
18.0	0.7168	0.7980	1.0176	0.9873	1.0188	0.9876
19.0	0.7412	0.8192	1.0166	0.9880	1.0177	0.9883
20.0	0.7626	0.8378	1.0158	0.9886	1.0168	0.9888

TABLE XLII: Angular distribution correction factors calculated for the $E_\gamma = 876.0$ -keV transition using the code AVALANCHE for the sum of planar and coaxial data, and for both **98Thin** and **99Thin** data sets. Corrections marked by a “*” symbol were obtained by quadratic extrapolation from higher- E_n values in the table.

E_n (MeV)	σ_2/J	σ_2/J	98Thin planar	98Thin coaxial	99Thin planar	99Thin coaxial
5.3	0.0000	0.0000	1.0699*	0.9540*	1.0746*	0.9551*
6.0	0.0000	0.0000	1.0673*	0.9554*	1.0720*	0.9565*
7.0	0.4193	4.9998	1.0688	0.9543	1.0740	0.9552
8.0	0.4888	4.9998	1.0562	0.9619	1.0605	0.9626
9.0	0.5020	1.0168	1.0535	0.9634	1.0577	0.9641
10.0	0.4960	0.7793	1.0534	0.9632	1.0580	0.9638
11.0	0.4998	0.7060	1.0521	0.9639	1.0568	0.9644
12.0	0.5195	0.6727	1.0487	0.9660	1.0532	0.9664
13.0	0.5375	0.6615	1.0459	0.9677	1.0503	0.9681
14.0	0.5522	0.6540	1.0438	0.9690	1.0480	0.9694
15.0	0.5633	0.6465	1.0422	0.9700	1.0464	0.9703
16.0	0.5780	0.6563	1.0405	0.9711	1.0445	0.9714
17.0	0.5893	0.6547	1.0392	0.9720	1.0430	0.9723
18.0	0.6105	0.6717	1.0371	0.9734	1.0407	0.9737
19.0	0.6313	0.6908	1.0351	0.9748	1.0385	0.9750
20.0	0.6495	0.7072	1.0336	0.9758	1.0368	0.9761

TABLE XLIII: Angular distribution correction factors calculated for the $E_\gamma = 880.5\text{-keV}$ ($E_x = 1023.7\text{-keV}$, $J^\pi = 4^+$) transition using the code AVALANCHE for the sum of planar and coaxial data, and for both **98Thin** and **99Thin** data sets. Corrections marked by a “*” symbol were obtained by quadratic extrapolation from higher- E_n values in the table.

E_n (MeV)	σ_2/J	σ_2/J	98Thin planar	98Thin coaxial	99Thin planar	99Thin coaxial
5.3	0.0000	0.0000	1.0270*	0.9809*	1.0289*	0.9814*
6.0	0.0000	0.0000	1.0270*	0.9809*	1.0289*	0.9813*
7.0	0.7290	7.4997	1.0281	0.9801	1.0301	0.9805
8.0	0.7788	7.4997	1.0249	0.9823	1.0267	0.9826
9.0	0.7685	7.4997	1.0255	0.9818	1.0274	0.9822
10.0	0.7445	7.4997	1.0270	0.9808	1.0290	0.9812
11.0	0.7400	7.4997	1.0273	0.9806	1.0293	0.9810
12.0	0.7608	1.2070	1.0257	0.9816	1.0277	0.9820
13.0	0.7820	1.0885	1.0243	0.9826	1.0262	0.9829
14.0	0.8013	1.0350	1.0232	0.9833	1.0250	0.9836
15.0	0.8163	0.9995	1.0223	0.9839	1.0241	0.9842
16.0	0.8375	1.0050	1.0212	0.9846	1.0230	0.9849
17.0	0.8525	0.9852	1.0205	0.9852	1.0222	0.9854
18.0	0.8832	1.0017	1.0192	0.9861	1.0208	0.9863
19.0	0.9145	1.0265	1.0180	0.9869	1.0195	0.9871
20.0	0.9420	1.0490	1.0170	0.9876	1.0184	0.9878

TABLE XLIV: Angular distribution correction factors calculated for the $E_\gamma = 880.5\text{-keV}$ ($E_x = 1023.8\text{-keV}$, $J^\pi = 3^-$) transition using the code AVALANCHE for the sum of planar and coaxial data, and for both **98Thin** and **99Thin** data sets. Corrections marked by a “*” symbol were obtained by quadratic extrapolation from higher- E_n values in the table.

E_n (MeV)	σ_2/J	σ_2/J	98Thin planar	98Thin coaxial	99Thin planar	99Thin coaxial
5.3	0.0000	0.0000	1.0070*	0.9949*	1.0075*	0.9950*
6.0	0.0000	0.0000	1.0074*	0.9946*	1.0079*	0.9947*
7.0	1.1027	9.9997	1.0074	0.9946	1.0080	0.9947
8.0	1.0550	9.9997	1.0081	0.9941	1.0087	0.9942
9.0	1.0273	9.9997	1.0085	0.9938	1.0091	0.9939
10.0	0.9930	9.9997	1.0091	0.9934	1.0097	0.9935
11.0	0.9820	9.9997	1.0093	0.9932	1.0099	0.9934
12.0	0.9983	1.7253	1.0090	0.9934	1.0096	0.9936
13.0	1.0193	1.4703	1.0086	0.9937	1.0092	0.9938
14.0	1.0410	1.3813	1.0083	0.9939	1.0089	0.9941
15.0	1.0590	1.3250	1.0080	0.9941	1.0086	0.9942
16.0	1.0853	1.3290	1.0077	0.9944	1.0082	0.9945
17.0	1.1040	1.2937	1.0074	0.9946	1.0079	0.9947
18.0	1.1437	1.3113	1.0069	0.9949	1.0074	0.9950
19.0	1.1840	1.3413	1.0065	0.9952	1.0069	0.9953
20.0	1.2197	1.3697	1.0061	0.9955	1.0065	0.9956

TABLE XLV: Angular distribution correction factors calculated for the $E_{\gamma} = 883.2$ -keV transition using the code AVALANCHE for the sum of planar and coaxial data, and for both **98Thin** and **99Thin** data sets. Corrections marked by a “*” symbol were obtained by quadratic extrapolation from higher- E_n values in the table.

E_n (MeV)	σ_2/J	σ_2/J	98Thin planar	98Thin coaxial	99Thin planar	99Thin coaxial
5.3	0.0000	0.0000	1.0027*	0.9980*	1.0029*	0.9980*
6.0	0.0000	0.0000	1.0029*	0.9978*	1.0031*	0.9979*
7.0	1.6970	14.9995	1.0031	0.9977	1.0033	0.9978
8.0	1.6345	14.9995	1.0033	0.9975	1.0036	0.9976
9.0	1.5770	14.9995	1.0036	0.9974	1.0038	0.9974
10.0	1.4810	14.9995	1.0041	0.9970	1.0043	0.9971
11.0	1.4485	14.9995	1.0042	0.9969	1.0045	0.9969
12.0	1.4720	14.9995	1.0041	0.9970	1.0044	0.9970
13.0	1.5050	2.5260	1.0039	0.9971	1.0042	0.9972
14.0	1.5385	2.1960	1.0037	0.9972	1.0040	0.9973
15.0	1.5655	2.0435	1.0036	0.9973	1.0039	0.9974
16.0	1.6050	2.0285	1.0034	0.9975	1.0037	0.9975
17.0	1.6320	1.9490	1.0033	0.9975	1.0036	0.9976
18.0	1.6920	1.9645	1.0031	0.9977	1.0033	0.9978
19.0	1.7545	2.0070	1.0029	0.9979	1.0031	0.9979
20.0	1.8090	2.0485	1.0027	0.9980	1.0029	0.9980

TABLE XLVI: Angular distribution correction factors calculated for the $E_\gamma = 898.7$ -keV transition using the code AVALANCHE for the sum of planar and coaxial data, and for both **98Thin** and **99Thin** data sets. Corrections marked by a “*” symbol were obtained by quadratic extrapolation from higher- E_n values in the table.

E_n (MeV)	σ_2/J	σ_2/J	98Thin planar	98Thin coaxial	99Thin planar	99Thin coaxial
5.3	0.0000	0.0000	0.9124*	1.0765*	0.9069*	1.0750*
6.0	0.0000	0.0000	0.9145*	1.0743*	0.9092*	1.0729*
7.0	0.4247	4.9998	0.9121	1.0768	0.9066	1.0752
8.0	0.4842	2.0377	0.9243	1.0645	0.9195	1.0633
9.0	0.5005	0.8625	0.9274	1.0615	0.9228	1.0603
10.0	0.4997	0.7442	0.9272	1.0617	0.9226	1.0605
11.0	0.5038	0.6843	0.9280	1.0609	0.9234	1.0597
12.0	0.5212	0.6533	0.9311	1.0579	0.9267	1.0568
13.0	0.5370	0.6458	0.9338	1.0553	0.9296	1.0542
14.0	0.5507	0.6427	0.9361	1.0532	0.9320	1.0522
15.0	0.5612	0.6378	0.9378	1.0516	0.9338	1.0506
16.0	0.5758	0.6488	0.9400	1.0495	0.9362	1.0486
17.0	0.5865	0.6482	0.9416	1.0480	0.9379	1.0471
18.0	0.6070	0.6650	0.9446	1.0454	0.9410	1.0445
19.0	0.6275	0.6840	0.9473	1.0429	0.9439	1.0421
20.0	0.6450	0.7000	0.9495	1.0409	0.9462	1.0402

TABLE XLVII: Angular distribution correction factors calculated for the $E_\gamma = 925.0$ -keV transition using the code AVALANCHE for the sum of planar and coaxial data, and for both **98Thin** and **99Thin** data sets. Corrections marked by a “*” symbol were obtained by quadratic extrapolation from higher- E_n values in the table.

E_n (MeV)	σ_2/J	σ_2/J	98Thin planar	98Thin coaxial	99Thin planar	99Thin coaxial
5.3	0.0000	0.0000	0.9935*	1.0049*	0.9930*	1.0048*
6.0	0.0000	0.0000	0.9932*	1.0051*	0.9928*	1.0050*
7.0	1.0447	9.9997	0.9930	1.0053	0.9926	1.0052
8.0	1.0573	9.9997	0.9932	1.0051	0.9927	1.0050
9.0	1.0310	9.9997	0.9929	1.0054	0.9924	1.0053
10.0	0.9840	9.9997	0.9922	1.0059	0.9917	1.0058
11.0	0.9710	9.9997	0.9920	1.0060	0.9915	1.0059
12.0	0.9927	1.9643	0.9924	1.0058	0.9919	1.0057
13.0	1.0180	1.5377	0.9928	1.0055	0.9923	1.0054
14.0	1.0420	1.4110	0.9932	1.0052	0.9927	1.0051
15.0	1.0610	1.3400	0.9935	1.0050	0.9929	1.0049
16.0	1.0880	1.3393	0.9938	1.0047	0.9933	1.0047
17.0	1.1067	1.3000	0.9940	1.0046	0.9935	1.0045
18.0	1.1473	1.3160	0.9944	1.0043	0.9940	1.0042
19.0	1.1883	1.3463	0.9948	1.0040	0.9943	1.0039
20.0	1.2250	1.3750	0.9951	1.0038	0.9947	1.0037

TABLE XLVIII: Angular distribution correction factors calculated for the $E_\gamma = 925.9$ -keV transition using the code AVALANCHE for the sum of planar and coaxial data, and for both **98Thin** and **99Thin** data sets. Corrections marked by a “*” symbol were obtained by quadratic extrapolation from higher- E_n values in the table.

E_n (MeV)	σ_2/J	σ_2/J	98Thin planar	98Thin coaxial	99Thin planar	99Thin coaxial
5.3	0.0000	0.0000	0.9597*	1.0324*	0.9571*	1.0317*
6.0	0.0000	0.0000	0.9594*	1.0326*	0.9567*	1.0320*
7.0	0.7462	7.4997	0.9582	1.0336	0.9555	1.0329
8.0	0.7742	7.4997	0.9608	1.0314	0.9582	1.0308
9.0	0.7648	7.4997	0.9599	1.0321	0.9573	1.0315
10.0	0.7492	7.4997	0.9585	1.0333	0.9558	1.0327
11.0	0.7465	1.8747	0.9583	1.0336	0.9555	1.0329
12.0	0.7632	1.1338	0.9598	1.0322	0.9572	1.0316
13.0	0.7817	1.0495	0.9614	1.0309	0.9589	1.0303
14.0	0.7993	1.0123	0.9628	1.0296	0.9604	1.0290
15.0	0.8135	0.9845	0.9640	1.0287	0.9616	1.0281
16.0	0.8343	0.9930	0.9655	1.0274	0.9632	1.0268
17.0	0.8485	0.9758	0.9665	1.0265	0.9643	1.0260
18.0	0.8788	0.9932	0.9685	1.0248	0.9664	1.0244
19.0	0.9093	1.0177	0.9704	1.0233	0.9684	1.0228
20.0	0.9360	1.0397	0.9719	1.0221	0.9700	1.0216

TABLE XLIX: Angular distribution correction factors calculated for the $E_\gamma = 926.7$ -keV transition using the code AVALANCHE for the sum of planar and coaxial data, and for both **98Thin** and **99Thin** data sets. Corrections marked by a “*” symbol were obtained by quadratic extrapolation from higher- E_n values in the table.

E_n (MeV)	σ_2/J	σ_2/J	98Thin planar	98Thin coaxial	99Thin planar	99Thin coaxial
5.3	0.0000	0.0000	0.9876*	1.0095*	0.9867*	1.0093*
6.0	0.0000	0.0000	0.9865*	1.0103*	0.9856*	1.0101*
7.0	1.6970	14.9995	0.9857	1.0109	0.9848	1.0107
8.0	1.6345	14.9995	0.9846	1.0118	0.9836	1.0115
9.0	1.5770	14.9995	0.9835	1.0126	0.9824	1.0124
10.0	1.4810	14.9995	0.9814	1.0143	0.9802	1.0140
11.0	1.4485	14.9995	0.9806	1.0150	0.9793	1.0147
12.0	1.4720	14.9995	0.9812	1.0145	0.9799	1.0142
13.0	1.5050	2.5260	0.9820	1.0139	0.9808	1.0136
14.0	1.5385	2.1960	0.9827	1.0133	0.9815	1.0130
15.0	1.5655	2.0435	0.9833	1.0128	0.9821	1.0126
16.0	1.6050	2.0285	0.9840	1.0122	0.9830	1.0120
17.0	1.6320	1.9490	0.9845	1.0118	0.9835	1.0116
18.0	1.6920	1.9645	0.9856	1.0110	0.9846	1.0108
19.0	1.7545	2.0070	0.9866	1.0102	0.9857	1.0100
20.0	1.8090	2.0485	0.9873	1.0096	0.9865	1.0094

TABLE L: Angular distribution correction factors calculated for the $E_\gamma = 946.0$ -keV transition using the code AVALANCHE for the sum of planar and coaxial data, and for both **98Thin** and **99Thin** data sets. Corrections marked by a “*” symbol were obtained by quadratic extrapolation from higher- E_n values in the table.

E_n (MeV)	σ_2/J	σ_2/J	98Thin planar	98Thin coaxial	99Thin planar	99Thin coaxial
5.3	0.0000	0.0000	0.9927*	1.0054*	0.9923*	1.0053*
6.0	0.0000	0.0000	0.9918*	1.0061*	0.9912*	1.0060*
7.0	1.8995	14.9995	0.9920	1.0060	0.9914	1.0059
8.0	1.6270	14.9995	0.9891	1.0082	0.9884	1.0080
9.0	1.5610	14.9995	0.9882	1.0089	0.9874	1.0087
10.0	1.4840	14.9995	0.9870	1.0098	0.9861	1.0096
11.0	1.4550	14.9995	0.9865	1.0102	0.9855	1.0100
12.0	1.4695	3.5475	0.9867	1.0100	0.9858	1.0098
13.0	1.4955	2.3340	0.9872	1.0097	0.9863	1.0095
14.0	1.5255	2.1135	0.9876	1.0093	0.9868	1.0091
15.0	1.5505	1.9940	0.9880	1.0090	0.9872	1.0088
16.0	1.5890	1.9885	0.9886	1.0086	0.9878	1.0084
17.0	1.6150	1.9170	0.9889	1.0083	0.9882	1.0081
18.0	1.6735	1.9350	0.9897	1.0078	0.9890	1.0076
19.0	1.7335	1.9770	0.9904	1.0072	0.9897	1.0071
20.0	1.7875	2.0175	0.9909	1.0068	0.9903	1.0066

TABLE LI: Angular distribution correction factors calculated for the $E_\gamma = 947.7$ -keV transition using the code AVALANCHE for the sum of planar and coaxial data, and for both **98Thin** and **99Thin** data sets. Corrections marked by a “*” symbol were obtained by quadratic extrapolation from higher- E_n values in the table.

E_n (MeV)	σ_2/J	σ_2/J	98Thin planar	98Thin coaxial	99Thin planar	99Thin coaxial
5.3	0.0000	0.0000	0.9990*	1.0005*	0.9993*	1.0004*
6.0	0.0000	0.0000	0.9993*	1.0004*	0.9995*	1.0003*
7.0	0.5314	5.9998	1.0000	1.0000	1.0000	1.0000
8.0	0.5948	5.9998	1.0000	1.0000	1.0000	1.0000
9.0	0.6040	5.9998	1.0000	1.0000	1.0000	1.0000
10.0	0.5922	2.0714	1.0000	1.0000	1.0000	1.0000
11.0	0.5940	1.0120	1.0006	0.9997	1.0004	0.9998
12.0	0.6158	0.8656	1.0010	0.9995	1.0008	0.9996
13.0	0.6354	0.8258	1.0012	0.9994	1.0009	0.9996
14.0	0.6520	0.8038	1.0014	0.9993	1.0010	0.9995
15.0	0.6646	0.7866	1.0015	0.9993	1.0011	0.9995
16.0	0.6820	0.7950	1.0014	0.9993	1.0011	0.9995
17.0	0.6946	0.7868	1.0015	0.9993	1.0011	0.9995
18.0	0.7196	0.8036	1.0014	0.9993	1.0010	0.9995
19.0	0.7446	0.8250	1.0012	0.9994	1.0009	0.9996
20.0	0.7666	0.8438	1.0011	0.9995	1.0008	0.9996

TABLE LII: Angular distribution correction factors calculated for the $E_\gamma = 965.8$ -keV transition using the code AVALANCHE for the sum of planar and coaxial data, and for both **98Thin** and **99Thin** data sets. Corrections marked by a “*” symbol were obtained by quadratic extrapolation from higher- E_n values in the table.

E_n (MeV)	σ_2/J	σ_2/J	98Thin planar	98Thin coaxial	99Thin planar	99Thin coaxial
5.3	0.0000	0.0000	1.0115*	0.9914*	1.0128*	0.9914*
6.0	0.0000	0.0000	1.0121*	0.9912*	1.0131*	0.9913*
7.0	0.3480	4.2856	1.0129	0.9907	1.0138	0.9908
8.0	0.4163	0.7143	1.0127	0.9913	1.0130	0.9916
9.0	0.4316	0.6239	1.0135	0.9910	1.0134	0.9915
10.0	0.4284	0.5711	1.0146	0.9905	1.0143	0.9910
11.0	0.4330	0.5500	1.0151	0.9903	1.0146	0.9909
12.0	0.4511	0.5473	1.0146	0.9906	1.0141	0.9913
13.0	0.4677	0.5486	1.0142	0.9910	1.0136	0.9916
14.0	0.4807	0.5484	1.0138	0.9912	1.0132	0.9918
15.0	0.4907	0.5464	1.0136	0.9914	1.0130	0.9920
16.0	0.5036	0.5569	1.0130	0.9917	1.0124	0.9923
17.0	0.5137	0.5593	1.0127	0.9919	1.0121	0.9925
18.0	0.5321	0.5759	1.0119	0.9924	1.0114	0.9929
19.0	0.5501	0.5936	1.0111	0.9929	1.0107	0.9933
20.0	0.5656	0.6081	1.0105	0.9932	1.0101	0.9937

TABLE LIII: Angular distribution correction factors calculated for the $E_{\gamma} = 981.6$ -keV transition using the code AVALANCHE for the sum of planar and coaxial data, and for both **98Thin** and **99Thin** data sets. Corrections marked by a “*” symbol were obtained by quadratic extrapolation from higher- E_n values in the table.

E_n (MeV)	σ_2/J	σ_2/J	98Thin planar	98Thin coaxial	99Thin planar	99Thin coaxial
5.3	0.0000	0.0000	1.0767*	0.9500*	1.0824*	0.9511*
6.0	0.0000	0.0000	1.0744*	0.9513*	1.0800*	0.9524*
7.0	0.3516	0.6496	1.0764	0.9501	1.0820	0.9512
8.0	0.4106	0.6100	1.0650	0.9568	1.0698	0.9577
9.0	0.4277	0.5854	1.0619	0.9587	1.0665	0.9596
10.0	0.4293	0.5546	1.0617	0.9588	1.0662	0.9597
11.0	0.4346	0.5363	1.0607	0.9594	1.0652	0.9603
12.0	0.4506	0.5327	1.0580	0.9611	1.0622	0.9619
13.0	0.4657	0.5354	1.0555	0.9626	1.0595	0.9634
14.0	0.4779	0.5379	1.0535	0.9638	1.0574	0.9646
15.0	0.4873	0.5376	1.0521	0.9647	1.0558	0.9655
16.0	0.4999	0.5489	1.0502	0.9659	1.0538	0.9666
17.0	0.5097	0.5519	1.0488	0.9668	1.0523	0.9675
18.0	0.5276	0.5683	1.0463	0.9683	1.0496	0.9690
19.0	0.5449	0.5857	1.0441	0.9697	1.0472	0.9704
20.0	0.5599	0.6000	1.0422	0.9709	1.0452	0.9716

TABLE LIV: Angular distribution correction factors calculated for the $E_\gamma = 984.2\text{-keV}$ transition using the code AVALANCHE for the sum of planar and coaxial data, and for both **98Thin** and **99Thin** data sets. Corrections marked by a “*” symbol were obtained by quadratic extrapolation from higher- E_n values in the table.

E_n (MeV)	σ_2/J	σ_2/J	98Thin planar	98Thin coaxial	99Thin planar	99Thin coaxial
5.3	0.0000	0.0000	1.0497*	0.9663*	1.0533*	0.9670*
6.0	0.0000	0.0000	1.0487*	0.9669*	1.0522*	0.9676*
7.0	0.5404	5.9998	1.0502	0.9659	1.0538	0.9666
8.0	0.5910	5.9998	1.0435	0.9701	1.0467	0.9708
9.0	0.6034	5.9998	1.0421	0.9711	1.0451	0.9717
10.0	0.5980	1.3238	1.0427	0.9706	1.0458	0.9713
11.0	0.6002	0.9536	1.0425	0.9708	1.0455	0.9714
12.0	0.6184	0.8342	1.0404	0.9721	1.0433	0.9727
13.0	0.6358	0.8046	1.0386	0.9733	1.0413	0.9739
14.0	0.6510	0.7902	1.0370	0.9743	1.0397	0.9749
15.0	0.6632	0.7774	1.0359	0.9751	1.0384	0.9756
16.0	0.6802	0.7878	1.0343	0.9761	1.0368	0.9766
17.0	0.6924	0.7808	1.0333	0.9768	1.0356	0.9773
18.0	0.7168	0.7980	1.0313	0.9781	1.0335	0.9786
19.0	0.7412	0.8192	1.0295	0.9793	1.0316	0.9797
20.0	0.7626	0.8378	1.0280	0.9803	1.0300	0.9807

2 Angular-Distribution Correction Factor for Transitions in ^{233}U

Table LV lists the properties of $^{233}U \gamma$ rays observed in the GEANIE data that are used in the calculation of angular distribution factors C_γ given by equation 19. No "damping" factor was applied to the AVALANCHE calculation of alignments in this case. The correction factors for each (n,3n) line of interest can be found in tables LVI-LXII.

TABLE LV: Properties used in the calculation of angular distribution correction factors for $^{235}U(n,3n) \gamma$ rays.

E_γ (keV)	E_x (keV)	J_i	J_f	L_1	L_2	δ	Identification of Multipolarity
137.2	229.4	13/2	9/2	2	3	0	known E2
159.4	314.7	15/2	11/2	2	3	0	known E2
298.9	298.8	5/2	5/2	1	2	0	assume E1 ($\Delta J = 0, \pi_i \pi_f = -1$)
300.3	340.7	5/2	7/2	1	2	-0.08	known M1/E2
305.4	397.6	11/2	9/2	1	2	0	E1 ($\Delta J = 1, \pi_i \pi_f = -1$)
312.2	312.2	3/2	5/2	1	2	-0.10	known M1/E2
340.8	340.7	2.5	5/2	1	2	-0.23	known M1/E2

TABLE LVI: Angular distribution correction factors calculated for the $E_\gamma = 137.6$ -keV transition using the code AVALANCHE for the sum of planar and coaxial data, and for both **98Thin** and **99Thin** data sets. Corrections marked by a “*” symbol were obtained by quadratic extrapolation from higher- E_n values in the table.

E_n (MeV)	σ_2/J	σ_2/J	98Thin planar	98Thin coaxial	99Thin planar	99Thin coaxial
12.2	0.0000	0.0000	0.9173*	N/A	0.9128*	N/A
13.0	0.5106	0.6002	0.9226	N/A	0.9183	N/A
14.0	0.4718	0.5962	0.9147	N/A	0.9100	N/A
15.0	0.5297	0.5923	0.9261	N/A	0.9221	N/A
16.0	0.5406	0.6012	0.9282	N/A	0.9242	N/A
17.0	0.5480	0.5991	0.9295	N/A	0.9256	N/A
18.0	0.5662	0.6143	0.9327	N/A	0.9290	N/A
19.0	0.5849	0.6320	0.9359	N/A	0.9323	N/A
20.0	0.6005	0.6458	0.9383	N/A	0.9349	N/A

TABLE LVII: Angular distribution correction factors calculated for the $E_{\gamma} = 159.4$ -keV transition using the code AVALANCHE for the sum of planar and coaxial data, and for both **98Thin** and **99Thin** data sets. Corrections marked by a “*” symbol were obtained by quadratic extrapolation from higher- E_n values in the table.

E_n (MeV)	σ_2/J	σ_2/J	98Thin planar	98Thin coaxial	99Thin planar	99Thin coaxial
12.2	0.0000	0.0000	0.9079*	N/A	0.9030*	N/A
13.0	0.4515	0.5097	0.9125	N/A	0.9079	N/A
14.0	0.4221	0.5027	0.9060	N/A	0.9010	N/A
15.0	0.4679	0.5088	0.9160	N/A	0.9115	N/A
16.0	0.4777	0.5176	0.9181	N/A	0.9137	N/A
17.0	0.4847	0.5189	0.9195	N/A	0.9152	N/A
18.0	0.5005	0.5339	0.9229	N/A	0.9187	N/A
19.0	0.5167	0.5501	0.9261	N/A	0.9221	N/A
20.0	0.5301	0.5628	0.9287	N/A	0.9247	N/A

TABLE LVIII: Angular distribution correction factors calculated for the $E_\gamma = 298.9$ -keV transition using the code AVALANCHE for the sum of planar and coaxial data, and for both **98Thin** and **99Thin** data sets. Corrections marked by a “*” symbol were obtained by quadratic extrapolation from higher- E_n values in the table.

E_n (MeV)	σ_2/J	σ_2/J	98Thin planar	98Thin coaxial	99Thin planar	99Thin coaxial
12.2	0.0000	0.0000	0.9679*	N/A	0.9659*	N/A
13.0	1.2524	1.0740	0.9789	N/A	0.9776	N/A
14.0	0.8712	0.6552	0.9590	N/A	0.9564	N/A
15.0	1.3756	1.4520	0.9824	N/A	0.9813	N/A
16.0	1.4132	1.5864	0.9833	N/A	0.9822	N/A
17.0	1.4324	1.5920	0.9837	N/A	0.9827	N/A
18.0	1.4832	1.6204	0.9847	N/A	0.9838	N/A
19.0	1.5364	1.6504	0.9857	N/A	0.9848	N/A
20.0	1.5804	1.6660	0.9865	N/A	0.9857	N/A

TABLE LIX: Angular distribution correction factors calculated for the $E_{\gamma} = 300.3$ -keV transition using the code AVALANCHE for the sum of planar and coaxial data, and for both **98Thin** and **99Thin** data sets. Corrections marked by a “*” symbol were obtained by quadratic extrapolation from higher- E_n values in the table.

E_n (MeV)	σ_2/J	σ_2/J	98Thin planar	98Thin coaxial	99Thin planar	99Thin coaxial
12.2	0.0000	0.0000	1.0012*	0.9991*	1.0012*	0.9991*
13.0	1.3116	2.0772	1.0011	0.9991	1.0012	0.9991
14.0	1.2828	11.9996	1.0012	0.9991	1.0013	0.9991
15.0	1.3444	1.7332	1.0011	0.9991	1.0011	0.9992
16.0	1.3688	1.7212	1.0010	0.9992	1.0011	0.9992
17.0	1.3836	1.6464	1.0010	0.9992	1.0011	0.9992
18.0	1.4324	1.6512	1.0009	0.9992	1.0010	0.9993
19.0	1.4848	1.6844	1.0009	0.9993	1.0009	0.9993
20.0	1.5296	1.7148	1.0008	0.9993	1.0009	0.9993

TABLE LX: Angular distribution correction factors calculated for the $E_\gamma = 305.4$ -keV transition using the code AVALANCHE for the sum of planar and coaxial data, and for both **98Thin** and **99Thin** data sets. Corrections marked by a “*” symbol were obtained by quadratic extrapolation from higher- E_n values in the table.

E_n (MeV)	σ_2/J	σ_2/J	98Thin planar	98Thin coaxial	99Thin planar	99Thin coaxial
12.2	0.0000	0.0000	1.0552*	0.9593*	1.0591*	0.9602*
13.0	0.5822	0.7024	1.0520	0.9614	1.0556	0.9623
14.0	0.5540	0.7593	1.0564	0.9585	1.0603	0.9595
15.0	0.6005	0.6840	1.0494	0.9632	1.0528	0.9641
16.0	0.6124	0.6924	1.0479	0.9643	1.0511	0.9651
17.0	0.6198	0.6864	1.0469	0.9649	1.0501	0.9658
18.0	0.6402	0.7016	1.0444	0.9667	1.0474	0.9675
19.0	0.6613	0.7202	1.0420	0.9684	1.0448	0.9691
20.0	0.6787	0.7351	1.0401	0.9697	1.0428	0.9704

TABLE LXI: Angular distribution correction factors calculated for the $E_\gamma = 312.2$ -keV transition using the code AVALANCHE for the sum of planar and coaxial data, and for both **98Thin** and **99Thin** data sets. Corrections marked by a “*” symbol were obtained by quadratic extrapolation from higher- E_n values in the table.

E_n (MeV)	σ_2/J	σ_2/J	98Thin planar	98Thin coaxial	99Thin planar	99Thin coaxial
12.2	0.0000	0.0000	0.9997*	1.0002*	0.9997*	1.0002*
13.0	2.2273	0.0000	0.9997	1.0002	0.9997	1.0002
14.0	2.2260	0.0000	0.9997	1.0002	0.9997	1.0002
15.0	2.2807	0.0000	0.9997	1.0002	0.9997	1.0002
16.0	2.3227	0.0000	0.9998	1.0002	0.9997	1.0002
17.0	2.3480	0.0000	0.9998	1.0002	0.9997	1.0002
18.0	2.4327	0.0000	0.9998	1.0002	0.9998	1.0002
19.0	2.5247	0.0000	0.9998	1.0002	0.9998	1.0002
20.0	2.6020	0.0000	0.9998	1.0002	0.9998	1.0002

TABLE LXII: Angular distribution correction factors calculated for the $E_\gamma = 340.8$ -keV transition using the code AVALANCHE for the sum of planar and coaxial data, and for both **98Thin** and **99Thin** data sets. Corrections marked by a “*” symbol were obtained by quadratic extrapolation from higher- E_n values in the table.

E_n (MeV)	σ_2/J	σ_2/J	98Thin planar	98Thin coaxial	99Thin planar	99Thin coaxial
12.2	0.0000	0.0000	0.9916*	1.0067*	0.9911*	1.0065*
13.0	1.3116	2.0772	0.9919	1.0064	0.9914	1.0063
14.0	1.2828	11.9996	0.9916	1.0067	0.9911	1.0066
15.0	1.3444	1.7332	0.9923	1.0061	0.9918	1.0060
16.0	1.3688	1.7212	0.9926	1.0059	0.9921	1.0058
17.0	1.3836	1.6464	0.9927	1.0058	0.9923	1.0057
18.0	1.4324	1.6512	0.9932	1.0054	0.9928	1.0053
19.0	1.4848	1.6844	0.9937	1.0051	0.9933	1.0049
20.0	1.5296	1.7148	0.9940	1.0048	0.9936	1.0047

B Observed Lines in ^{234}U

In all, 26 lines in the (n,2n) channel have been accounted for and are presented here. Figure 53 shows these lines and their placement in the ^{234}U level scheme. The transitions are also listed in table LXIII, along with the method by which the data were analyzed. Note that in the case of the $E_\gamma = 880.6$ keV, 925.3 keV, and 946.1 keV lines observed in the GEANIE data, there are several known corresponding transitions in the (n,2n) channel which cannot be resolved in our data. Therefore the partial cross sections quoted here for these three lines likely represent the sum of the unresolved yields. It should also be mentioned that although the measured γ -ray energies quoted in the table in general agree well with the accepted values, there are a few deviations, typically at the higher γ -ray energies where the planar-detector energy calibration is less reliable. The coaxial-detector energy calibration is also prone to deviations on the order of 0.5 keV, based on individual calibration lines. Nevertheless, large deviations in γ -ray energies are rare and will be discussed on a case-by-case basis for individual transitions.

In what follows we present a short discussion of the analysis for each transition. We do not repeat here the discussion for the yrast $4_1^+ \rightarrow 2_1^+$, $6_1^+ \rightarrow 4_1^+$, $8_1^+ \rightarrow 6_1^+$ transitions, and $10_1^+ \rightarrow 8_1^+$, which can be found in section II A 3. The results of the analysis for these four lines can be found in tables LXIV, LXVI, LXVII and LXVIII and figures 54, 56, 57 and 58, respectively.

All (n,2n) lines observed in the GEANIE data peak at above 10 mb of cross section. Therefore, we do expect to be able to extract yields for transitions below a 10 mb threshold. Using the GNASH predictions as a guide, 19 transitions are expected to reach or exceed 10 mb at maximum cross section. Of these 19 transitions, the following 4 could not be extracted from the GEANIE data:

$E_\gamma = 187.4$ keV, $E_x = 1150$ keV, GNASH $\sigma_\gamma^{(max)} = 15$ mb: This transition does not exist in the current ENSDF evaluation [10]. Its parent level has been placed in the evaluated level scheme, but no transitions depopulating it have been assigned. Furthermore

$E_\gamma = 255.4$ keV, $E_x = 1218$ keV, GNASH $\sigma_\gamma^{(max)} = 12$ mb: As with the 187.4-keV line, this transition also does not exist in the current ENSDF evaluation. Its parent level has been placed in the evaluated level scheme, but no transitions depopulating it have been assigned.

$E_\gamma = 705.9$ keV, $E_x = 849.3$ keV, GNASH $\sigma_\gamma^{(max)} = 13$ mb: This line connects a 3^- level to the 4^+ member of the ground-state band. Another, slightly stronger branch out of the same level has been observed with $E_\gamma = 805.8$ keV, and is discussed below. The $E_\gamma = 705.9$ -keV transition should be only slightly weaker, according to known branching ratios, however, it could not be observed in the GEANIE data because its proximity to the energy of the $2_1^+ \rightarrow 0_1^+$ transition ($E_\gamma = 707.0$) in the high-yield fission fragment ^{90}Kr .

$E_\gamma = 795.7$ keV, $E_x = 1292.6$ keV, GNASH $\sigma_\gamma^{(max)} = 18$ mb: A hint of this line was observed in the ^{98}Th in data at $E_\gamma = 795.585 \pm 0.215$ keV, reaching a maximum cross section of 13.8 ± 3.6 mb at $E_n = 13.9$ MeV. However, the statistics are so poor that the observed yields are relatively significant only in the $E_n = 9.8\text{--}13.9$ MeV range, where they are essentially constant (within error). Furthermore, this $8^+ \rightarrow 8_1^+$ transition is known to proceed by both E0 and E2 mode, but the mixing ratio between the two is unknown. To lowest order E0 transitions proceed entirely by internal electron conversion, and therefore cannot be observed using GEANIE. Because of low statistics and an unknown E0/E2 mixing ratio, we do not include this line in the discussion of observed ^{234}U lines below.

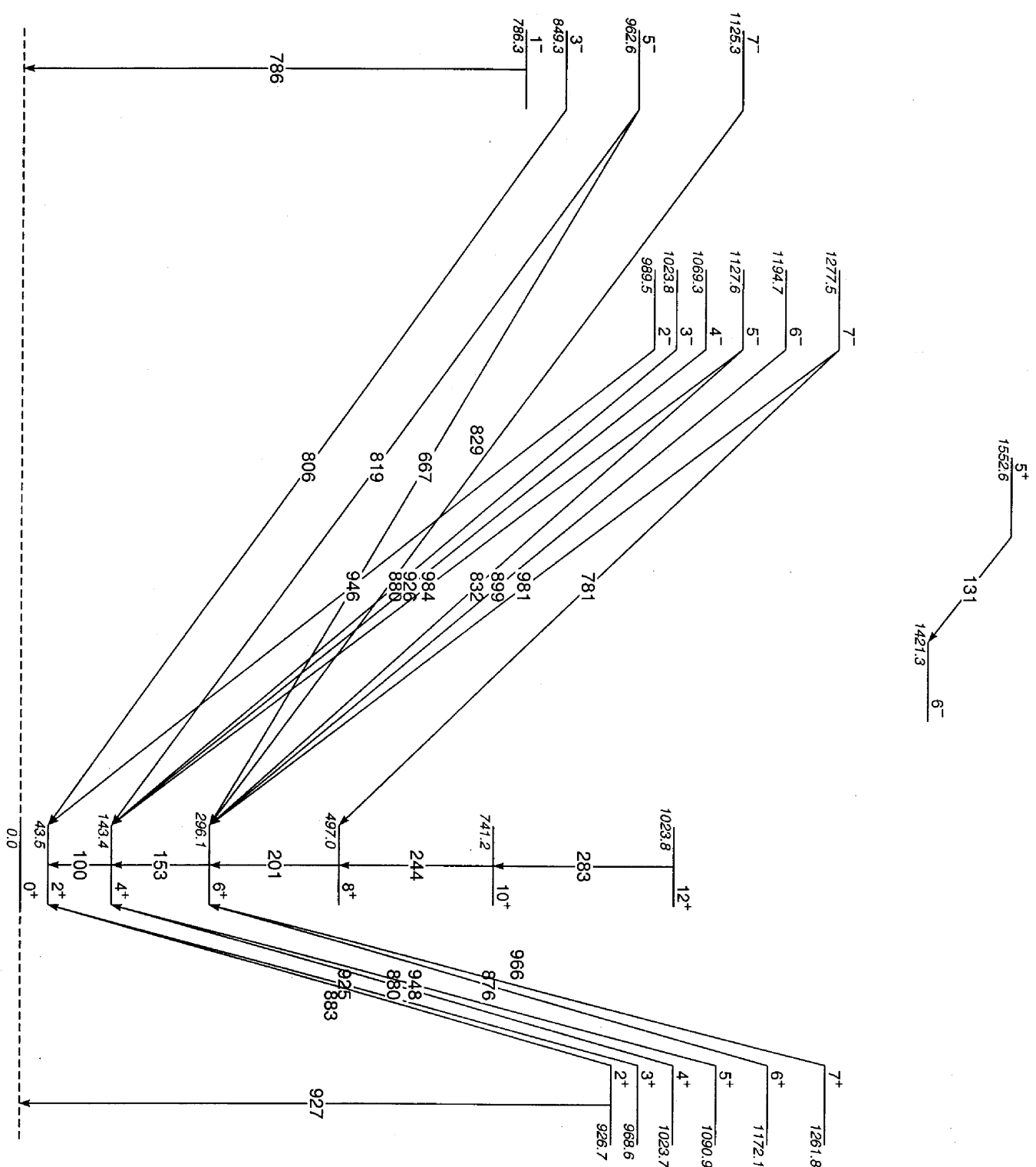


FIG. 53: Gamma rays in ^{234}U observed in the GEANIE data.

TABLE LXIII: Transitions identified in the $^{235}\text{U}(n,2n\gamma)$ channel and the method by which the data were analyzed.

$E_\gamma^{(\text{meas})}$ (keV)	Analysis method	$E_\gamma^{(\text{acc})}$ (keV)	E_x (keV)	transition
99.993 ± 2.418	unsubtracted planars, 98Thin and 99Thin optimized	99.853 ± 0.003	143.4	$4_1^+ \rightarrow 2_1^+$
131.609 ± 0.115	unsubtracted planars, 98Thin and 99Thin averaged	131.30 ± 0.01	1552.6	$5^- \rightarrow 6^-$
152.660 ± 0.111	unsubtracted planars, 98Thin and 99Thin optimized	152.720 ± 0.002	296.1	$6_1^+ \rightarrow 4_1^+$
200.961 ± 0.111	unsubtracted planars, 98Thin and 99Thin optimized	200.97 ± 0.03	497.0	$8_1^+ \rightarrow 6_1^+$
244.405 ± 2.626	unsubtracted planars, 98Thin and 99Thin optimized	244.2 ± 0.5	741.2	$10_1^+ \rightarrow 8_1^+$
282.166 ± 0.120	unsubtracted planars, 98Thin and 99Thin optimized	282.6 ± 0.5	1023.8	$12_1^+ \rightarrow 10_1^+$
666.745 ± 0.171	unsubtracted planars, 98Thin only	666.5 ± 0.1	962.6	$5^- \rightarrow 6_1^+$
780.820 ± 0.131	unsubtracted planars, 98Thin only	780.4 ± 0.2	1277.5	$7^- \rightarrow 8_1^+$
786.784 ± 0.261	unsubtracted coaxials, 98Thin only	786.27 ± 0.03	786.3	$1^- \rightarrow 0_1^+$
806.088 ± 0.143	unsubtracted planars, 98Thin only	805.80 ± 0.05	849.3	$3^- \rightarrow 2_1^+$
819.212 ± 0.261	unsubtracted coaxials, 98Thin only	819.2 ± 0.2	962.6	$5^- \rightarrow 4_1^+$
829.505 ± 0.254	unsubtracted planars, 98Thin only	829.3 ± 0.2	1125.3	$7^- \rightarrow 6_1^+$
831.613 ± 0.158	unsubtracted planars, 98Thin only	831.5 ± 0.1	1127.6	$5^- \rightarrow 6_1^+$
875.518 ± 0.128	unsubtracted planars, 98Thin only	876.0 ± 0.1	1172.1	$6_1^+ \rightarrow 6_1^+$
880.604 ± 0.122	subtracted planars, 98Thin and 99Thin optimized	880.5 ± 0.1	1023.7	$4_1^+ \rightarrow 4_1^+$
		880.5 ± 0.1	1023.8	$3^- \rightarrow 4_1^+$
883.405 ± 0.164	unsubtracted planars, 98Thin and 99Thin optimized	883.24 ± 0.04	926.7	$2_1^+ \rightarrow 2_1^+$
		883.24 ± 0.04	1809.0	$(1^-) \rightarrow 2_1^+$
898.276 ± 0.144	subtracted planars, 98Thin only	898.67 ± 0.05	1194.7	$6^- \rightarrow 6^+$
925.338 ± 0.135	unsubtracted planars, 98Thin and 99Thin optimized	925.0 ± 0.1	968.6	$3_1^+ \rightarrow 2_1^+$
		925.9 ± 0.2	1069.3	$4^- \rightarrow 4_1^+$
		926.72 ± 0.10	926.7	$2_1^+ \rightarrow 0_1^+$
946.129 ± 0.144	unsubtracted planars, 98Thin and 99Thin optimized	946.00 ± 0.03	989.4	$2^- \rightarrow 2_1^+$
		947.7 ± 0.2	1090.9	$5_1^+ \rightarrow 4_1^+$
966.266 ± 0.261	unsubtracted coaxials, 98Thin only	965.8 ± 0.1	1261.8	$7_1^+ \rightarrow 6_1^+$
981.410 ± 0.261	unsubtracted coaxials, 98Thin only	981.6 ± 0.3	1277.5	$7^- \rightarrow 6_1^+$
		980.3 ± 0.1	1023.8	$3^- \rightarrow 2_1^+$
		980.3 ± 0.1	1023.7	$4^+ \rightarrow 2_1^+$
984.814 ± 0.261	unsubtracted coaxials, 98Thin only	984.2 ± 0.1	1127.6	$5^- \rightarrow 4_1^+$

The $E_\gamma = 131.6$ keV transition (table LXV/figure 55): This γ -ray corresponds to the transition between band-head levels at $E_x = 1552.6$ keV ($J^\pi = 5^+$) and $E_x = 1421.3$ keV ($J^\pi = 6^-$). For this line, the optimization correction described above was found to produce unreliable results because of low statistics. Instead the **98Thin** and **99Thin** were directly combined by weighted average. The deduced γ -ray energy also differs from the accepted value by a sizeable amount ($\approx 2.7\sigma$). This deviation might be due in part to the proximity of this line to the strong (n,n') peak at $E_\gamma = 129.3$ keV. Furthermore, the shape of excitation function is clearly indicative of an ($n,2n$) line and an analysis of coincident data reveals no significant contamination. The level populated by the 131.6-keV transition decays primarily by a 226.5-keV transition, however because this level is long-lived ($T_{1/2} = 33.5 \mu\text{s}$), its decay is not observed in the prompt- γ -ray analysis presented here.

The $E_\gamma = 282.2$ keV transition (table LXIX/figure 59): This line is the highest observed transition in the ground-state band. The measured γ -ray energy differs somewhat from the accepted value which, however, carries a large uncertainty. As with the $10_1^+ \rightarrow 8_1^+$ transition discussed in particular in section VII A 2, the measured partial cross section for the $12_1^+ \rightarrow 10_1^+$ deviates from the GNASH prediction in both shape and magnitude. However since this is such a weak transition (less than 20 mb at maximum yield), it is neither surprising nor significant that the model does reproduce this transition well.

The $E_\gamma = 666.7$ keV transition (table LXX/figure 60): This is one of two transitions observed depopulating the 5^- member at $E_x = 962.6$ keV of the lowest-lying octupole band. Because it is very weak, this line could not be observed in the **99Thin** data. The measured partial cross section matches the GNASH prediction, within (albeit large) errors, however it should be noted that the other transition depopulating the same level ($E_\gamma = 819.2$ keV) does not. This contradicts the experimentally measured branching ratio for these two γ -rays and suggests that this 666.7-keV transition, which is expected to be the weaker member of the branch, is probably contaminated by another, unresolved transition. This conclusion is further supported by the behavior of the measured 666.7-keV excitation function, which does not appear to decrease significantly above peak cross section near $E_n = 12$ MeV.

The $E_\gamma = 780.8$ keV transition (table LXXI/figure 61): The γ -ray energy measured for this line is slightly higher than the accepted value, however both numbers carry sizeable uncertainties. Both this transition and an $E_\gamma = 981.4$ keV line depopulate a 7^- level at $E_x = 1277.5$ keV and have been observed in our data. Unlike the 666.7-keV/819.2-keV γ -ray pair, however, the measured partial cross sections for these transitions are consistent with the known branching ratio of the γ rays.

The $E_\gamma = 786.8$ keV transition (table LXXII/figure 62): This transition could barely be seen in the planar-detector data, therefore we have analyzed it using the **98Thin** coaxial-detector data. As a result, the γ -ray energy calibration is somewhat less reliable, although the measured energy for this line is still within two sigma of its accepted value. This transition connects the band head of the lowest-lying octupole band in ^{234}U to the ground state. An $E_\gamma = 742.8$ -keV transition from the same level should be observed more strongly, according to measured branching ratios, however it cannot be resolved from a nearby fission-fragment line at $E_\gamma \approx 744$ keV. Despite large uncertainties and an apparent residual baseline background of ≈ 4 mb, the measured partial cross section for this transition is significantly under-predicted by GNASH.

The $E_\gamma = 806.1$ keV transition (table LXXIII/figure 63): This γ -ray connects the 3^- member of the lowest-lying octupole band to the 2^+ member of the ground-state band. The 806.1-keV line was too weak to be seen in the **99Thin** data, therefore the partial cross section has been calculated using the **98Thin** data only, scaled by the target-thickness correction factor. Despite large uncertainties, the measured yields are only moderately higher than the GNASH prediction.

The $E_\gamma = 819.2$ keV transition (table LXXIV/figure 64): Because it is inherently weak, this high-energy γ -ray was more easily extracted from the **98Thin** coaxial-detector data. Though hampered by poor statistics, the partial cross section deduced from planar-detector data agrees with the coaxial-detector data presented here. Along with the 666.7-keV line, this transition is one of two depopulating the 5^- member of the lowest-lying octupole band and its measured partial cross-section is largely over-predicted by GNASH.

The $E_\gamma = 829.5$ keV transition (table LXXV/figure 65): Both the 829.5-keV and 831.6-keV lines are difficult to extract from our data because of their proximity to the “neutron bump” registered by the germanium detectors near $E_\gamma = 834$ keV. The 829.5-keV transition depopulates the 7^- member of the low-lying octupole band. Another transition from the same level with $E_\gamma = 628.1 \pm 0.1$ keV and 66% of the intensity of the 829.5-keV transition (according to known branching ratios) could not be observed, in part due to its proximity to an $E_\gamma = 628.6$ -keV transition in ^{127}I . The mono-isotopic nucleus ^{127}I is a component of the NaI nose-cone placed on each detector, used to suppress back-scattered γ rays.

The $E_\gamma = 831.6$ keV transition (table LXXVI/figure 66): The 831.6-keV and 984.8-keV γ rays de-excite the 5^- member of the second octupole band. The measured partial cross sections for these two lines are consistent with their experimentally-known branching ratio, and both lines are under-predicted by GNASH.

The $E_\gamma = 875.5$ keV transition (table LXXVII/figure 67): The measured γ -ray energy for this line differs from the accepted value by about three standard deviations. Furthermore, the measured excitation function suggests an unresolved baseline background. It is likely, therefore that this transition is contaminated in the GEANIE data. If we were to subtract a flat baseline of 10 mb from the measured partial cross section plotted in figure 67, a satisfactory match with the GNASH prediction would result.

The $E_\gamma = 880.6$ keV transition (table LXXVIII/figure 68): Two transitions in the known ^{234}U level scheme have been assigned a γ -ray energy of 880.5 keV, within an uncertainty of 100 eV; one from the de-excitation of the 4^+ member of the γ -phonon band, and the other from the decay of the 3^- member of the second octupole band. Since we cannot resolve these two energies, the measured partial cross section for the 880.6-keV line represents the sum of both. Because the two unresolved lines are predicted by GNASH to have comparable yields, we use the average of the angular distribution factors calculated for each one. In the unsubtracted planar-detector (and coaxial-detector) data, the partial cross section extracted for this line suffers from a sizeable baseline background (about 20 mb in the **98Thin** data and 40 mb in the **99Thin** data). This problem is greatly alleviated when we use the random-TOF-subtracted data. Despite this subtraction, a ≈ 10 -mb baseline remains for this otherwise well-behaved partial cross section. The GNASH curve plotted in figure 68, which represents the sum of yields for the two degenerate γ rays, significantly under-predicts the GEANIE values, even if an additional 10-mb baseline were to be subtracted from the data.

The $E_\gamma = 883.4$ keV transition (table LXXIX/figure 69): This γ -ray represents the decay of the γ -phonon-band head the the ground-state-band 2^+ level. At this γ -ray energy, the planar-detector-sum resolution is \approx

2.0 keV. Because of this, the 883.4-keV and 880.6-keV lines, though clearly resolvable in the planar-data fits, largely overlap. This may in part explain why the measured partial cross section for the 883.4-keV transition does not fall rapidly above ≈ 12 MeV, unlike many other observed ($n,2n$) lines. There is another 883.24-keV transition in the known ^{234}U level scheme. However this line is a weak branch from a much higher-lying level and should not therefore contribute significantly to the observed yields. As seen in figure 69, GNASH significantly under-predicts the magnitude of this excitation function.

The $E_\gamma = 898.3$ keV transition (table LXXX/figure 70): As in the case of the 880.6-keV transition, a strong baseline background was observed for this line which could be greatly reduced by using random-TOF-subtracted data. This is nevertheless a very weak line and the deduced partial cross section plotted in figure 70 still shows a residual baseline. Furthermore the measured γ -ray energy deviates from the accepted value by nearly three standard deviations. Therefore the measured yields may be contaminated and should be taken as an upper bound on the true partial cross section.

The $E_\gamma = 925.3$ keV transition (table LXXXI/figure 71): This transition is three-fold degenerate (within GEANIE detector resolution) in the known ^{234}U level scheme. It represents transitions from the 2^+ and 3^+ members of the γ -phonon band as well as a decay from the 3^- member of the second octupole band. The GNASH calculations predict that the $E_\gamma = 925.9$ -keV $4^- \rightarrow 4_1^+$ member of this multiplet should have the largest cross section, therefore we use the angular distribution factor calculated for the $E_\gamma = 925.9$ -keV line in this case. In figure 71, the partial cross section extracted for this line from the GEANIE data is compared to the sum of GNASH predictions for the three degenerate lines. The agreement between our measured partial cross section and the GNASH calculation is excellent.

The $E_\gamma = 946.1$ keV transition (table LXXXII/figure 72): This line is two-fold degenerate (within GEANIE detector resolution) in the known ^{234}U level scheme. It corresponds to decays from both the 5^+ member of the γ -phonon band and the 2^- band head of the second octupole band. As with the $E_\gamma = 880.6$ keV line, GNASH predicts comparable yields for the two members of the multiplet, therefore we use the average of the angular-distribution correction factor calculated for each, in this case. The deduced partial cross section is under-predicted by the sum of GNASH yields for the two degenerate lines by almost a factor of two.

The $E_\gamma = 966.3$ keV transition (table LXXXIII/figure 73): This transition represents the decay from the highest-observed member of the γ -phonon band ($J^\pi = 7^+$) to the ground-state-band 6^+ level. It was necessary to use the coaxial-detector data to analyze this line. As can be seen in figure 73, the GNASH calculation slightly under-predicts the measured partial cross section for this line.

The $E_\gamma = 981.4$ keV transition (table LXXXIV/figure 74): Both this transition and the 780.8-keV γ ray depopulate the 7^- member of the second octupole band and have been observed in GEANIE data. However, though the 780.8-keV transition was included in the GNASH calculation, this line was not. This line may be contaminated by two other transitions in the known ^{234}U level scheme. The first is an $E_\gamma = 980.3$ -keV transition from the $E_x = 1023.8$ keV level, which is depopulated primarily by the 880.5-keV transition discussed above. The partial cross section for this transition is predicted by GNASH to reach only ≈ 3 mb, at maximum cross section. The second contaminant is from another transition in ^{234}U also assigned an $E_\gamma = 980.3$ -keV energy. The GNASH prediction for this line does not exceed ≈ 4 mb, at maximum cross section. For comparison, the maximum partial cross section predicted by GNASH, deduced from the calculated yields for the $E_\gamma = 780.8$ -keV transition, is ≈ 10 mb.

The $E_\gamma = 984.8$ keV transition (table LXXXV/figure 75): The 984.8-keV transition depopulates the 5^- member of the second octupole band, along with the 831.6-keV γ -ray. As, was mentioned in the discussion of the 831.6-keV line, the branching ratio between these two γ -ray is consistent with the accepted value. The GNASH calculations under-predict this partial cross section by approximately a factor of two.

TABLE LXIV: Adopted partial γ -ray cross section for the $E_\gamma = 100.0$ -keV transition. The measured peak areas and deduced partial cross sections (before correction for angular distribution effects) for the **98Thin** and **99Thin** data sets are shown in columns 2–5. The partial cross section, listed in column 6, is obtained from both data sets using the optimization procedure described in section XII B. The recommended partial cross section in the last column includes a correction for angular-distribution effects.

E_n (MeV)	$A^{(1998)}$	$\sigma^{(1998)}$	$A^{(1999)}$	$\sigma^{(1999)}$	$\sigma^{(\text{opt})}$	$\sigma^{(\text{opt,corr})}$
4.090 ± 0.093	0 ± 0	0.0002 ± 0.0101	583 ± 143	0.1568 ± 0.0438	0.0011 ± 0.0091	0.0011 ± 0.0089
4.264 ± 0.099	56 ± 198	0.0092 ± 0.0340	540 ± 147	0.1435 ± 0.0436	0.0088 ± 0.0256	0.0088 ± 0.0252
4.453 ± 0.105	3 ± 70	0.0005 ± 0.0144	632 ± 151	0.1597 ± 0.0436	0.0025 ± 0.0128	0.0025 ± 0.0125
4.647 ± 0.113	4 ± 75	0.0006 ± 0.0147	557 ± 152	0.1372 ± 0.0417	0.0008 ± 0.0129	0.0008 ± 0.0127
4.861 ± 0.122	0 ± 22	0.0002 ± 0.0098	469 ± 152	0.1135 ± 0.0399	-0.0009 ± 0.0089	-0.0008 ± 0.0087
5.090 ± 0.129	469 ± 210	0.0703 ± 0.0338	394 ± 152	0.0932 ± 0.0383	0.0229 ± 0.0244	0.0233 ± 0.0241
5.333 ± 0.140	590 ± 212	0.0870 ± 0.0341	645 ± 151	0.1525 ± 0.0410	0.0574 ± 0.0252	0.0530 ± 0.0240
5.597 ± 0.149	572 ± 211	0.0817 ± 0.0328	492 ± 150	0.1152 ± 0.0385	0.0394 ± 0.0240	0.0360 ± 0.0229
5.875 ± 0.160	377 ± 213	0.0529 ± 0.0317	832 ± 153	0.1905 ± 0.0428	0.0513 ± 0.0243	0.0470 ± 0.0231
6.181 ± 0.175	1495 ± 219	0.2105 ± 0.0407	1319 ± 154	0.2966 ± 0.0511	0.1831 ± 0.0310	0.1719 ± 0.0296
6.517 ± 0.187	2035 ± 226	0.2689 ± 0.0445	1841 ± 158	0.3947 ± 0.0601	0.2529 ± 0.0350	0.2378 ± 0.0336
6.862 ± 0.201	1838 ± 227	0.2307 ± 0.0402	1892 ± 160	0.3965 ± 0.0600	0.2278 ± 0.0325	0.2141 ± 0.0312
7.237 ± 0.218	2327 ± 230	0.3037 ± 0.0476	1552 ± 158	0.3453 ± 0.0560	0.2531 ± 0.0356	0.2384 ± 0.0343
7.661 ± 0.242	2233 ± 227	0.3121 ± 0.0496	1741 ± 157	0.4138 ± 0.0642	0.2857 ± 0.0385	0.2688 ± 0.0370
8.126 ± 0.263	2502 ± 231	0.3482 ± 0.0531	1890 ± 159	0.4446 ± 0.0674	0.3181 ± 0.0410	0.2991 ± 0.0394
8.618 ± 0.284	2619 ± 234	0.3554 ± 0.0535	2067 ± 160	0.4754 ± 0.0703	0.3334 ± 0.0418	0.3133 ± 0.0402
9.160 ± 0.313	2686 ± 233	0.3708 ± 0.0553	2314 ± 161	0.5418 ± 0.0779	0.3641 ± 0.0443	0.3418 ± 0.0425
9.757 ± 0.346	3211 ± 233	0.4595 ± 0.0648	2175 ± 159	0.5312 ± 0.0775	0.4142 ± 0.0491	0.3893 ± 0.0472
10.414 ± 0.377	2835 ± 233	0.4201 ± 0.0616	2163 ± 159	0.5501 ± 0.0805	0.3987 ± 0.0482	0.3742 ± 0.0462
11.143 ± 0.425	2557 ± 230	0.4029 ± 0.0612	2097 ± 157	0.5640 ± 0.0832	0.3923 ± 0.0484	0.3681 ± 0.0464
11.960 ± 0.467	2836 ± 231	0.4607 ± 0.0677	2278 ± 159	0.6365 ± 0.0924	0.4522 ± 0.0537	0.4252 ± 0.0516
12.860 ± 0.525	2625 ± 226	0.4393 ± 0.0659	2133 ± 158	0.6077 ± 0.0896	0.4294 ± 0.0522	0.4044 ± 0.0501
13.876 ± 0.589	1589 ± 222	0.2711 ± 0.0511	1285 ± 152	0.3751 ± 0.0655	0.2475 ± 0.0392	0.2330 ± 0.0376
15.016 ± 0.660	1161 ± 217	0.1979 ± 0.0452	940 ± 149	0.2754 ± 0.0565	0.1680 ± 0.0342	0.1581 ± 0.0327
16.297 ± 0.750	693 ± 216	0.1179 ± 0.0407	992 ± 148	0.2877 ± 0.0569	0.1228 ± 0.0317	0.1151 ± 0.0303
17.759 ± 0.857	373 ± 215	0.0631 ± 0.0385	529 ± 144	0.1513 ± 0.0460	0.0430 ± 0.0283	0.0397 ± 0.0271
19.416 ± 0.971	8 ± 210	0.0013 ± 0.0362	812 ± 147	0.2264 ± 0.0506	0.0288 ± 0.0280	0.0258 ± 0.0268

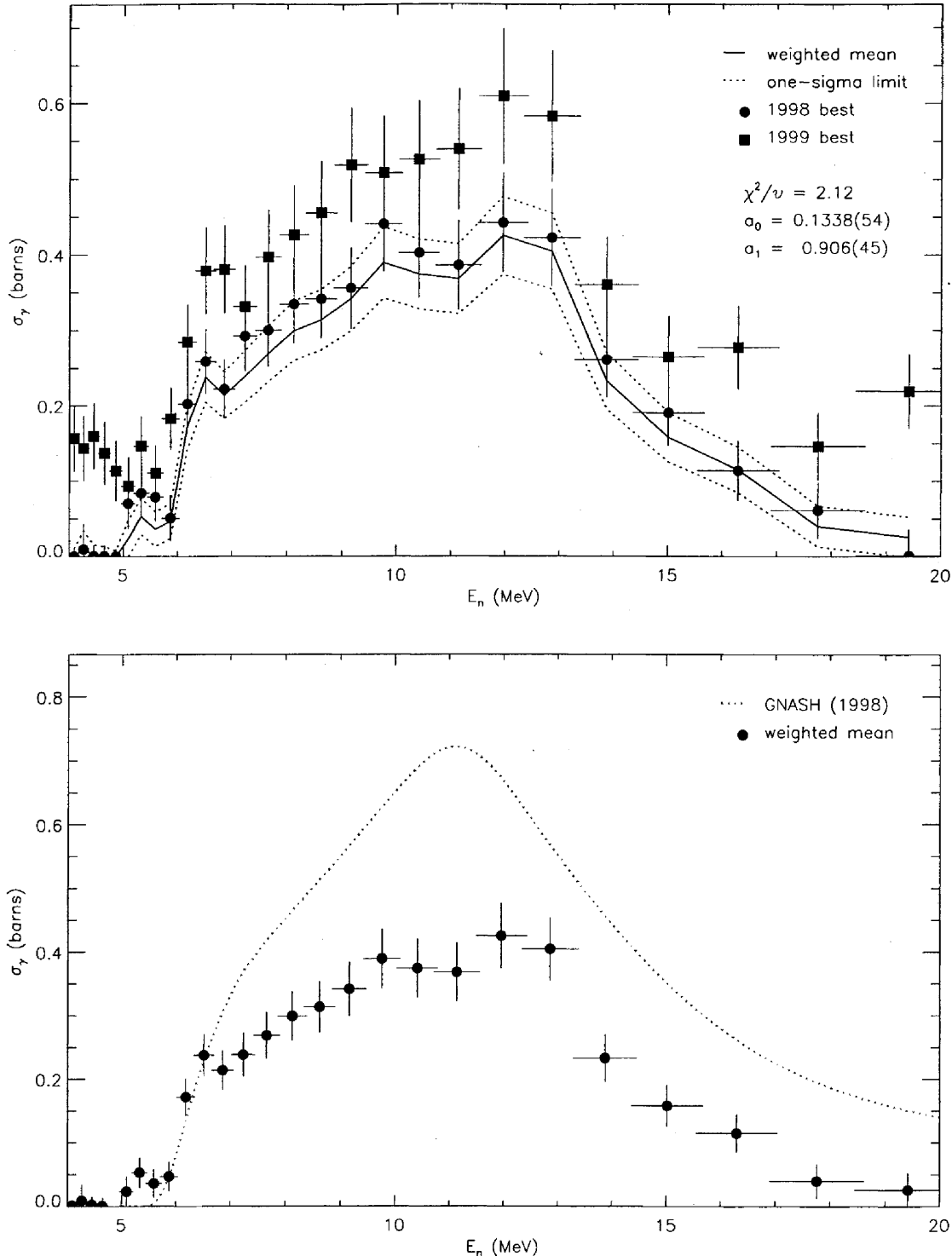


FIG. 54: Adopted $E_\gamma = 100.0$ -keV partial cross section corresponding to the data in table LXIV. The top panel shows the 1998 and 1999 partial cross sections (corrected for angular-distribution effects) and the recommended value, plotted as a solid line with a one-sigma confidence band (dotted lines). The bottom panel shows this recommended partial cross section (solid circles) compared to GNASH.

TABLE LXV: Adopted partial γ -ray cross section for the $E_\gamma = 131.6$ -keV transition. The measured peak areas and deduced partial cross sections (before correction for angular distribution effects) for the **98Thin** and **99Thin** data sets are shown in columns 2–5. The partial cross section, listed in column 6, is obtained from both data sets using a weighted average. The recommended partial cross section in the last column includes a correction for angular-distribution effects.

E_n (MeV)	$A^{(1998)}$	$\sigma^{(1998)}$	$A^{(1999)}$	$\sigma^{(1999)}$	$\sigma^{(\text{wei})}$	$\sigma^{(\text{wei,corr})}$
4.090 ± 0.093	68 ± 66	0.0017 ± 0.0027	179 ± 78	0.0053 ± 0.0024	0.0037 ± 0.0018	0.0037 ± 0.0018
4.264 ± 0.099	60 ± 67	0.0014 ± 0.0027	240 ± 79	0.0070 ± 0.0025	0.0044 ± 0.0018	0.0044 ± 0.0018
4.453 ± 0.105	216 ± 68	0.0049 ± 0.0026	186 ± 79	0.0052 ± 0.0023	0.0051 ± 0.0017	0.0051 ± 0.0017
4.647 ± 0.113	65 ± 67	0.0014 ± 0.0025	70 ± 80	0.0019 ± 0.0022	0.0017 ± 0.0017	0.0017 ± 0.0017
4.861 ± 0.122	250 ± 71	0.0056 ± 0.0026	11 ± 79	0.0003 ± 0.0021	0.0024 ± 0.0017	0.0024 ± 0.0017
5.090 ± 0.129	0 ± 0	0.0000 ± 0.0019	12 ± 84	0.0003 ± 0.0022	0.0001 ± 0.0015	0.0001 ± 0.0015
5.333 ± 0.140	55 ± 71	0.0012 ± 0.0025	82 ± 87	0.0021 ± 0.0023	0.0017 ± 0.0017	0.0017 ± 0.0017
5.597 ± 0.149	292 ± 73	0.0061 ± 0.0025	20 ± 89	0.0005 ± 0.0023	0.0031 ± 0.0017	0.0032 ± 0.0018
5.875 ± 0.160	1 ± 72	0.0000 ± 0.0023	99 ± 90	0.0025 ± 0.0023	0.0013 ± 0.0016	0.0013 ± 0.0017
6.181 ± 0.175	59 ± 72	0.0012 ± 0.0024	173 ± 90	0.0043 ± 0.0023	0.0028 ± 0.0016	0.0028 ± 0.0017
6.517 ± 0.187	116 ± 73	0.0022 ± 0.0022	28 ± 89	0.0007 ± 0.0021	0.0014 ± 0.0015	0.0014 ± 0.0016
6.862 ± 0.201	289 ± 76	0.0053 ± 0.0022	119 ± 90	0.0027 ± 0.0021	0.0040 ± 0.0015	0.0041 ± 0.0016
7.237 ± 0.218	237 ± 75	0.0045 ± 0.0023	39 ± 88	0.0010 ± 0.0022	0.0027 ± 0.0016	0.0027 ± 0.0016
7.661 ± 0.242	249 ± 75	0.0051 ± 0.0024	286 ± 90	0.0075 ± 0.0025	0.0062 ± 0.0018	0.0064 ± 0.0018
8.126 ± 0.263	423 ± 77	0.0086 ± 0.0026	280 ± 90	0.0072 ± 0.0025	0.0079 ± 0.0018	0.0081 ± 0.0018
8.618 ± 0.284	528 ± 78	0.0104 ± 0.0026	168 ± 90	0.0042 ± 0.0024	0.0070 ± 0.0018	0.0072 ± 0.0018
9.160 ± 0.313	611 ± 78	0.0123 ± 0.0028	267 ± 90	0.0069 ± 0.0025	0.0093 ± 0.0018	0.0095 ± 0.0019
9.757 ± 0.346	596 ± 78	0.0124 ± 0.0028	306 ± 90	0.0082 ± 0.0026	0.0101 ± 0.0019	0.0104 ± 0.0020
10.414 ± 0.377	638 ± 78	0.0138 ± 0.0030	464 ± 91	0.0130 ± 0.0030	0.0134 ± 0.0021	0.0137 ± 0.0022
11.143 ± 0.425	612 ± 78	0.0140 ± 0.0032	428 ± 91	0.0126 ± 0.0031	0.0133 ± 0.0022	0.0136 ± 0.0023
11.960 ± 0.467	466 ± 77	0.0110 ± 0.0031	449 ± 93	0.0138 ± 0.0033	0.0123 ± 0.0022	0.0126 ± 0.0023
12.860 ± 0.525	674 ± 80	0.0164 ± 0.0035	358 ± 93	0.0112 ± 0.0032	0.0136 ± 0.0024	0.0139 ± 0.0024
13.876 ± 0.589	435 ± 78	0.0108 ± 0.0032	231 ± 92	0.0074 ± 0.0031	0.0091 ± 0.0022	0.0092 ± 0.0023
15.016 ± 0.660	335 ± 78	0.0083 ± 0.0031	201 ± 89	0.0065 ± 0.0030	0.0074 ± 0.0022	0.0075 ± 0.0022
16.297 ± 0.750	0 ± 0	0.0000 ± 0.0022	222 ± 89	0.0071 ± 0.0030	0.0025 ± 0.0018	0.0026 ± 0.0018
17.759 ± 0.857	386 ± 78	0.0095 ± 0.0031	193 ± 88	0.0061 ± 0.0029	0.0077 ± 0.0021	0.0078 ± 0.0022
19.416 ± 0.971	0 ± 0	0.0000 ± 0.0022	280 ± 88	0.0086 ± 0.0029	0.0031 ± 0.0017	0.0031 ± 0.0018

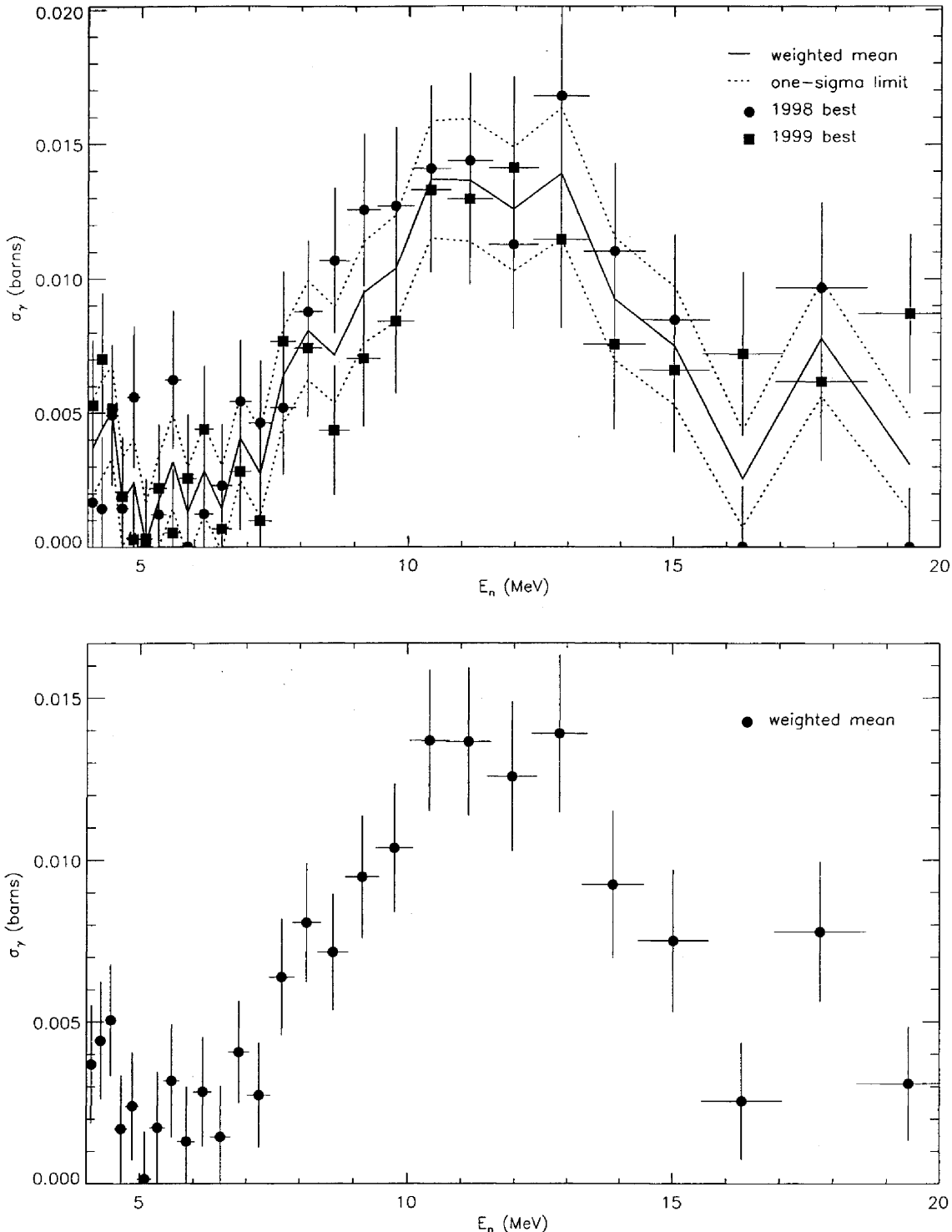


FIG. 55: Adopted $E_\gamma = 131.6$ -keV partial cross section corresponding to the data in table LXV. The top panel shows the 1998 and 1999 partial cross sections (corrected for angular-distribution effects) and the recommended value, plotted as a solid line with a one-sigma confidence band (dotted lines). The bottom panel shows this recommended partial cross section (solid circles) compared to GNASH.

TABLE LXVI: Adopted partial γ -ray cross section for the $E_\gamma = 152.7$ -keV transition. The measured peak areas and deduced partial cross sections (before correction for angular distribution effects) for the **98Thin** and **99Thin** data sets are shown in columns 2–5. The partial cross section, listed in column 6, is obtained from both data sets using the optimization procedure described in section XII B. The recommended partial cross section in the last column includes a correction for angular-distribution effects.

E_n (MeV)	$A^{(1998)}$	$\sigma^{(1998)}$	$A^{(1999)}$	$\sigma^{(1999)}$	$\sigma^{(\text{opt})}$	$\sigma^{(\text{opt,corr})}$
4.090 ± 0.093	223 ± 73	0.0126 ± 0.0044	166 ± 78	0.0105 ± 0.0051	0.0139 ± 0.0033	0.0139 ± 0.0033
4.264 ± 0.099	212 ± 73	0.0116 ± 0.0042	62 ± 78	0.0039 ± 0.0050	0.0109 ± 0.0032	0.0108 ± 0.0032
4.453 ± 0.105	237 ± 74	0.0124 ± 0.0042	172 ± 79	0.0102 ± 0.0049	0.0137 ± 0.0031	0.0137 ± 0.0031
4.647 ± 0.113	146 ± 73	0.0075 ± 0.0039	213 ± 81	0.0123 ± 0.0050	0.0111 ± 0.0030	0.0110 ± 0.0030
4.861 ± 0.122	214 ± 74	0.0110 ± 0.0040	36 ± 74	0.0020 ± 0.0043	0.0098 ± 0.0029	0.0097 ± 0.0029
5.090 ± 0.129	318 ± 76	0.0159 ± 0.0043	0 ± 9	0.0001 ± 0.0008	0.0081 ± 0.0016	0.0080 ± 0.0016
5.333 ± 0.140	231 ± 75	0.0114 ± 0.0039	0 ± 1	0.0001 ± 0.0007	0.0075 ± 0.0015	0.0073 ± 0.0015
5.597 ± 0.149	343 ± 78	0.0163 ± 0.0042	23 ± 83	0.0013 ± 0.0046	0.0125 ± 0.0031	0.0117 ± 0.0029
5.875 ± 0.160	820 ± 83	0.0384 ± 0.0059	439 ± 89	0.0236 ± 0.0056	0.0334 ± 0.0041	0.0310 ± 0.0038
6.181 ± 0.175	2015 ± 93	0.0947 ± 0.0119	1467 ± 98	0.0776 ± 0.0105	0.0869 ± 0.0079	0.0802 ± 0.0074
6.517 ± 0.187	3350 ± 104	0.1477 ± 0.0177	2572 ± 106	0.1297 ± 0.0161	0.1382 ± 0.0119	0.1281 ± 0.0112
6.862 ± 0.201	4162 ± 110	0.1743 ± 0.0207	3414 ± 112	0.1683 ± 0.0205	0.1702 ± 0.0145	0.1587 ± 0.0137
7.237 ± 0.218	4970 ± 114	0.2165 ± 0.0256	3735 ± 113	0.1955 ± 0.0237	0.2038 ± 0.0173	0.1906 ± 0.0165
7.661 ± 0.242	5076 ± 115	0.2368 ± 0.0281	3779 ± 112	0.2113 ± 0.0257	0.2212 ± 0.0188	0.2068 ± 0.0180
8.126 ± 0.263	5653 ± 118	0.2625 ± 0.0310	4633 ± 118	0.2564 ± 0.0309	0.2561 ± 0.0217	0.2391 ± 0.0207
8.618 ± 0.284	6751 ± 124	0.3057 ± 0.0359	5057 ± 121	0.2736 ± 0.0328	0.2849 ± 0.0241	0.2658 ± 0.0229
9.160 ± 0.313	7114 ± 126	0.3278 ± 0.0385	5597 ± 122	0.3083 ± 0.0369	0.3132 ± 0.0265	0.2923 ± 0.0252
9.757 ± 0.346	7726 ± 129	0.3690 ± 0.0434	5845 ± 123	0.3358 ± 0.0402	0.3462 ± 0.0293	0.3231 ± 0.0279
10.414 ± 0.377	7833 ± 129	0.3874 ± 0.0457	6227 ± 124	0.3726 ± 0.0447	0.3736 ± 0.0317	0.3486 ± 0.0302
11.143 ± 0.425	8267 ± 131	0.4348 ± 0.0515	6353 ± 125	0.4020 ± 0.0484	0.4107 ± 0.0350	0.3834 ± 0.0334
11.960 ± 0.467	8238 ± 131	0.4466 ± 0.0530	6191 ± 125	0.4070 ± 0.0491	0.4186 ± 0.0358	0.3916 ± 0.0342
12.860 ± 0.525	7022 ± 125	0.3921 ± 0.0468	5350 ± 122	0.3586 ± 0.0435	0.3686 ± 0.0316	0.3458 ± 0.0303
13.876 ± 0.589	4929 ± 115	0.2806 ± 0.0338	4080 ± 116	0.2802 ± 0.0344	0.2763 ± 0.0239	0.2599 ± 0.0230
15.016 ± 0.660	3414 ± 106	0.1942 ± 0.0237	2824 ± 109	0.1946 ± 0.0244	0.1925 ± 0.0169	0.1814 ± 0.0162
16.297 ± 0.750	2361 ± 99	0.1341 ± 0.0168	2087 ± 104	0.1424 ± 0.0184	0.1370 ± 0.0123	0.1295 ± 0.0118
17.759 ± 0.857	1905 ± 96	0.1075 ± 0.0138	1431 ± 100	0.0963 ± 0.0133	0.1026 ± 0.0095	0.0973 ± 0.0092
19.416 ± 0.971	1708 ± 95	0.0946 ± 0.0124	1150 ± 99	0.0754 ± 0.0111	0.0857 ± 0.0082	0.0817 ± 0.0080

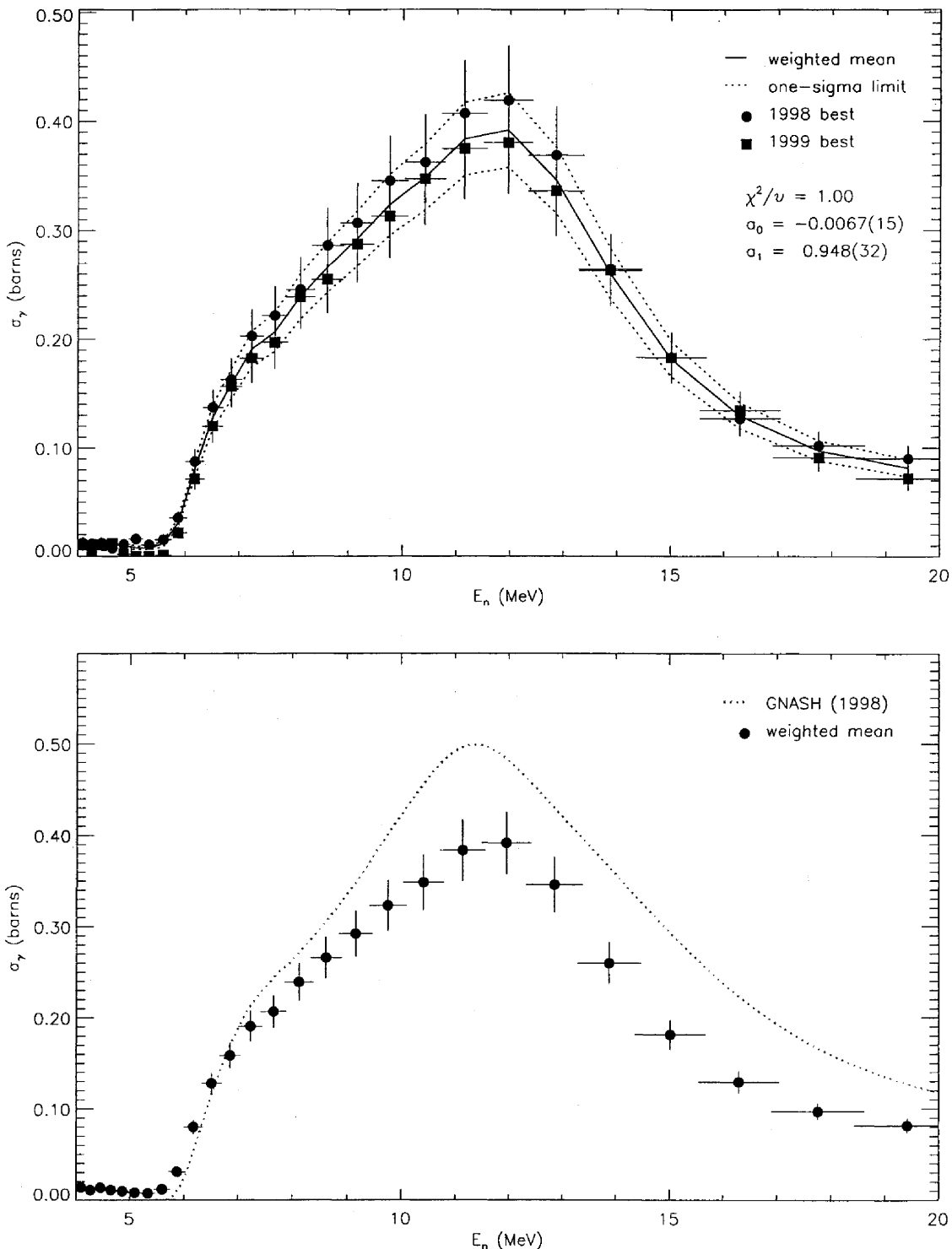


FIG. 56: Adopted $E_\gamma = 152.7$ -keV partial cross section corresponding to the data in table LXVI. The top panel shows the 1998 and 1999 partial cross sections (corrected for angular-distribution effects) and the recommended value, plotted as a solid line with a one-sigma confidence band (dotted lines). The bottom panel shows this recommended partial cross section (solid circles) compared to GNASH.

TABLE LXVII: Adopted partial γ -ray cross section for the $E_\gamma = 201.0$ -keV transition. The measured peak areas and deduced partial cross sections (before correction for angular distribution effects) for the **98Thin** and **99Thin** data sets are shown in columns 2–5. The partial cross section, listed in column 6, is obtained from both data sets using the optimization procedure described in section XII B. The recommended partial cross section in the last column includes a correction for angular-distribution effects.

E_n (MeV)	$A^{(1998)}$	$\sigma^{(1998)}$	$A^{(1999)}$	$\sigma^{(1999)}$	$\sigma^{(\text{opt})}$	$\sigma^{(\text{opt,corr})}$
4.090 ± 0.093	177 ± 71	0.0056 ± 0.0034	639 ± 87	0.0213 ± 0.0038	0.0034 ± 0.0024	0.0038 ± 0.0024
4.264 ± 0.099	58 ± 70	0.0018 ± 0.0032	813 ± 89	0.0267 ± 0.0042	0.0030 ± 0.0024	0.0033 ± 0.0024
4.453 ± 0.105	266 ± 73	0.0078 ± 0.0032	712 ± 89	0.0222 ± 0.0038	0.0051 ± 0.0023	0.0054 ± 0.0023
4.647 ± 0.113	1 ± 20	0.0000 ± 0.0023	787 ± 90	0.0240 ± 0.0039	0.0008 ± 0.0018	0.0010 ± 0.0018
4.861 ± 0.122	207 ± 73	0.0059 ± 0.0031	913 ± 92	0.0273 ± 0.0041	0.0058 ± 0.0023	0.0060 ± 0.0023
5.090 ± 0.129	40 ± 74	0.0011 ± 0.0030	856 ± 92	0.0250 ± 0.0039	0.0021 ± 0.0022	0.0024 ± 0.0022
5.333 ± 0.140	144 ± 74	0.0040 ± 0.0030	708 ± 92	0.0207 ± 0.0036	0.0024 ± 0.0022	0.0018 ± 0.0019
5.597 ± 0.149	27 ± 69	0.0007 ± 0.0028	654 ± 92	0.0189 ± 0.0034	-0.0000 ± 0.0020	-0.0004 ± 0.0018
5.875 ± 0.160	117 ± 75	0.0031 ± 0.0028	804 ± 94	0.0227 ± 0.0037	0.0026 ± 0.0021	0.0020 ± 0.0019
6.181 ± 0.175	677 ± 80	0.0177 ± 0.0035	1308 ± 97	0.0364 ± 0.0049	0.0158 ± 0.0027	0.0138 ± 0.0024
6.517 ± 0.187	1775 ± 90	0.0437 ± 0.0055	1941 ± 103	0.0515 ± 0.0064	0.0358 ± 0.0040	0.0317 ± 0.0036
6.862 ± 0.201	2342 ± 96	0.0547 ± 0.0064	2711 ± 109	0.0702 ± 0.0083	0.0490 ± 0.0048	0.0438 ± 0.0045
7.237 ± 0.218	3043 ± 100	0.0740 ± 0.0084	3023 ± 111	0.0832 ± 0.0098	0.0645 ± 0.0061	0.0581 ± 0.0056
7.661 ± 0.242	3292 ± 101	0.0857 ± 0.0096	3367 ± 112	0.0989 ± 0.0116	0.0769 ± 0.0071	0.0694 ± 0.0066
8.126 ± 0.263	3949 ± 106	0.1023 ± 0.0113	3906 ± 116	0.1136 ± 0.0132	0.0917 ± 0.0082	0.0828 ± 0.0076
8.618 ± 0.284	5316 ± 114	0.1343 ± 0.0146	4735 ± 121	0.1346 ± 0.0154	0.1170 ± 0.0102	0.1058 ± 0.0095
9.160 ± 0.313	5765 ± 116	0.1482 ± 0.0161	5336 ± 124	0.1545 ± 0.0176	0.1325 ± 0.0114	0.1200 ± 0.0106
9.757 ± 0.346	6491 ± 120	0.1729 ± 0.0187	5784 ± 126	0.1746 ± 0.0199	0.1537 ± 0.0131	0.1393 ± 0.0122
10.414 ± 0.377	7088 ± 122	0.1955 ± 0.0212	6337 ± 127	0.1992 ± 0.0228	0.1757 ± 0.0149	0.1593 ± 0.0139
11.143 ± 0.425	7661 ± 124	0.2248 ± 0.0244	6645 ± 128	0.2209 ± 0.0253	0.1999 ± 0.0169	0.1815 ± 0.0158
11.960 ± 0.467	7940 ± 125	0.2401 ± 0.0261	7059 ± 129	0.2438 ± 0.0280	0.2174 ± 0.0183	0.1980 ± 0.0172
12.860 ± 0.525	7136 ± 122	0.2223 ± 0.0243	6566 ± 127	0.2313 ± 0.0266	0.2029 ± 0.0172	0.1853 ± 0.0162
13.876 ± 0.589	5404 ± 113	0.1716 ± 0.0190	5073 ± 120	0.1831 ± 0.0213	0.1565 ± 0.0136	0.1432 ± 0.0127
15.016 ± 0.660	3626 ± 104	0.1151 ± 0.0131	3560 ± 113	0.1289 ± 0.0152	0.1046 ± 0.0095	0.0958 ± 0.0089
16.297 ± 0.750	2467 ± 97	0.0782 ± 0.0093	2471 ± 107	0.0886 ± 0.0108	0.0689 ± 0.0067	0.0632 ± 0.0063
17.759 ± 0.857	2076 ± 94	0.0654 ± 0.0080	2153 ± 105	0.0761 ± 0.0094	0.0571 ± 0.0058	0.0526 ± 0.0055
19.416 ± 0.971	1694 ± 92	0.0523 ± 0.0068	1834 ± 104	0.0632 ± 0.0080	0.0451 ± 0.0049	0.0418 ± 0.0047

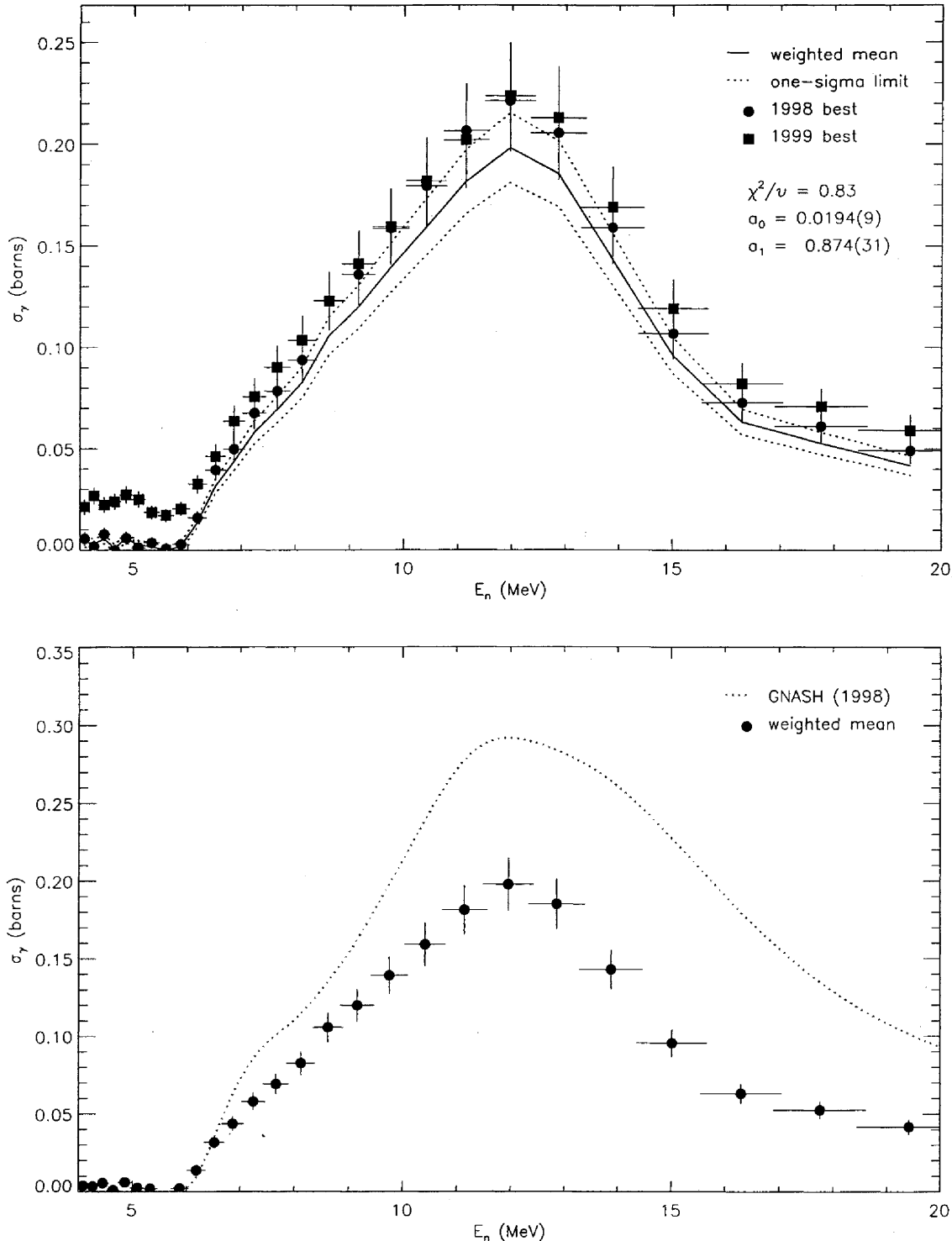


FIG. 57: Adopted $E_\gamma = 201.0$ -keV partial cross section corresponding to the data in table LXVII. The top panel shows the 1998 and 1999 partial cross sections (corrected for angular-distribution effects) and the recommended value, plotted as a solid line with a one-sigma confidence band (dotted lines). The bottom panel shows this recommended partial cross section (solid circles) compared to GNASH.

TABLE LXVIII: Adopted partial γ -ray cross section for the $E_\gamma = 244.4$ -keV transition. The measured peak areas and deduced partial cross sections (before correction for angular distribution effects) for the **98Thin** and **99Thin** data sets are shown in columns 2–5. The partial cross section, listed in column 6, is obtained from both data sets using the optimization procedure described in section XII B. The recommended partial cross section in the last column includes a correction for angular-distribution effects.

E_n (MeV)	$A^{(1998)}$	$\sigma^{(1998)}$	$A^{(1999)}$	$\sigma^{(1999)}$	$\sigma^{(\text{opt})}$	$\sigma^{(\text{opt,corr})}$
4.090 ± 0.093	121 ± 78	0.0034 ± 0.0023	0 ± 0	0.0000 ± 0.0001	-0.0017 ± 0.0001	-0.0015 ± 0.0001
4.264 ± 0.099	43 ± 77	0.0012 ± 0.0021	29 ± 87	0.0008 ± 0.0025	0.0002 ± 0.0019	0.0003 ± 0.0019
4.453 ± 0.105	200 ± 79	0.0053 ± 0.0022	21 ± 86	0.0006 ± 0.0024	0.0022 ± 0.0018	0.0023 ± 0.0018
4.647 ± 0.113	0 ± 0	0.0000 ± 0.0002	156 ± 90	0.0042 ± 0.0025	0.0001 ± 0.0003	0.0001 ± 0.0003
4.861 ± 0.122	0 ± 0	0.0000 ± 0.0002	172 ± 90	0.0046 ± 0.0024	0.0001 ± 0.0003	0.0001 ± 0.0003
5.090 ± 0.129	26 ± 80	0.0007 ± 0.0020	192 ± 93	0.0050 ± 0.0025	0.0021 ± 0.0018	0.0022 ± 0.0018
5.333 ± 0.140	135 ± 82	0.0034 ± 0.0021	138 ± 93	0.0036 ± 0.0024	0.0029 ± 0.0018	0.0026 ± 0.0016
5.597 ± 0.149	0 ± 1	0.0000 ± 0.0002	13 ± 92	0.0003 ± 0.0024	0.0000 ± 0.0003	0.0000 ± 0.0002
5.875 ± 0.160	0 ± 0	0.0000 ± 0.0002	27 ± 93	0.0007 ± 0.0023	0.0000 ± 0.0002	0.0000 ± 0.0002
6.181 ± 0.175	0 ± 0	0.0000 ± 0.0002	3 ± 53	0.0001 ± 0.0013	-0.0000 ± 0.0002	-0.0000 ± 0.0002
6.517 ± 0.187	106 ± 87	0.0024 ± 0.0020	155 ± 97	0.0036 ± 0.0023	0.0024 ± 0.0017	0.0022 ± 0.0015
6.862 ± 0.201	213 ± 91	0.0045 ± 0.0020	331 ± 100	0.0076 ± 0.0024	0.0058 ± 0.0018	0.0052 ± 0.0016
7.237 ± 0.218	456 ± 94	0.0100 ± 0.0023	298 ± 99	0.0073 ± 0.0025	0.0086 ± 0.0019	0.0077 ± 0.0017
7.661 ± 0.242	504 ± 95	0.0118 ± 0.0025	704 ± 102	0.0184 ± 0.0033	0.0158 ± 0.0023	0.0142 ± 0.0021
8.126 ± 0.263	700 ± 100	0.0164 ± 0.0029	971 ± 105	0.0250 ± 0.0039	0.0219 ± 0.0027	0.0198 ± 0.0024
8.618 ± 0.284	929 ± 102	0.0212 ± 0.0032	1198 ± 108	0.0302 ± 0.0043	0.0276 ± 0.0030	0.0249 ± 0.0027
9.160 ± 0.313	1380 ± 108	0.0321 ± 0.0041	1597 ± 111	0.0410 ± 0.0053	0.0399 ± 0.0038	0.0360 ± 0.0035
9.757 ± 0.346	1434 ± 109	0.0345 ± 0.0044	1594 ± 112	0.0427 ± 0.0056	0.0423 ± 0.0040	0.0382 ± 0.0037
10.414 ± 0.377	1788 ± 112	0.0446 ± 0.0054	2160 ± 114	0.0602 ± 0.0074	0.0574 ± 0.0051	0.0519 ± 0.0047
11.143 ± 0.425	2011 ± 114	0.0533 ± 0.0063	2621 ± 117	0.0773 ± 0.0093	0.0710 ± 0.0061	0.0643 ± 0.0057
11.960 ± 0.467	2065 ± 114	0.0565 ± 0.0066	2575 ± 117	0.0789 ± 0.0095	0.0740 ± 0.0064	0.0672 ± 0.0059
12.860 ± 0.525	2054 ± 114	0.0578 ± 0.0068	2421 ± 115	0.0756 ± 0.0092	0.0735 ± 0.0064	0.0669 ± 0.0059
13.876 ± 0.589	1833 ± 112	0.0526 ± 0.0064	1943 ± 111	0.0622 ± 0.0078	0.0633 ± 0.0057	0.0578 ± 0.0053
15.016 ± 0.660	1185 ± 105	0.0340 ± 0.0047	1395 ± 107	0.0448 ± 0.0061	0.0430 ± 0.0043	0.0393 ± 0.0040
16.297 ± 0.750	732 ± 101	0.0210 ± 0.0036	943 ± 104	0.0300 ± 0.0047	0.0274 ± 0.0033	0.0251 ± 0.0031
17.759 ± 0.857	472 ± 98	0.0134 ± 0.0031	695 ± 102	0.0218 ± 0.0040	0.0185 ± 0.0028	0.0170 ± 0.0026
19.416 ± 0.971	429 ± 99	0.0120 ± 0.0030	610 ± 103	0.0186 ± 0.0038	0.0160 ± 0.0027	0.0149 ± 0.0025

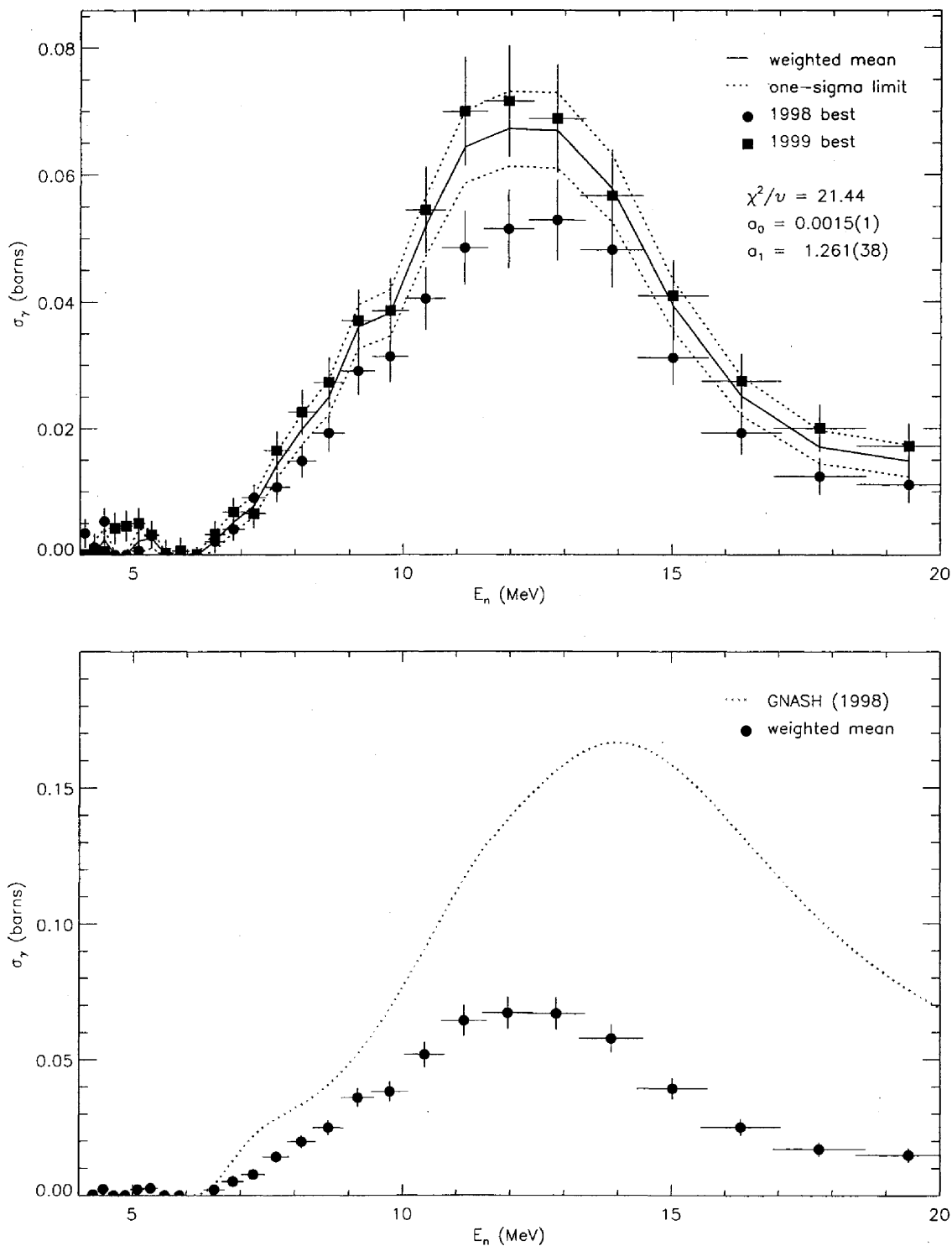


FIG. 58: Adopted $E_\gamma = 244.4$ -keV partial cross section corresponding to the data in table LXVIII. The top panel shows the 1998 and 1999 partial cross sections (corrected for angular-distribution effects) and the recommended value, plotted as a solid line with a one-sigma confidence band (dotted lines). The bottom panel shows this recommended partial cross section (solid circles) compared to GNASH.

TABLE LXIX: Adopted partial γ -ray cross section for the $E_\gamma = 282.2$ -keV transition. The measured peak areas and deduced partial cross sections (before correction for angular distribution effects) for the **98Thin** and **99Thin** data sets are shown in columns 2–5. The partial cross section, listed in column 6, is obtained from both data sets using the optimization procedure described in section XII B. The recommended partial cross section in the last column includes a correction for angular-distribution effects.

E_n (MeV)	$A^{(1998)}$	$\sigma^{(1998)}$	$A^{(1999)}$	$\sigma^{(1999)}$	$\sigma^{(\text{opt})}$	$\sigma^{(\text{opt,corr})}$
4.090 ± 0.093	325 ± 59	0.0095 ± 0.0020	215 ± 77	0.0065 ± 0.0025	0.0080 ± 0.0018	0.0079 ± 0.0018
4.264 ± 0.099	332 ± 60	0.0095 ± 0.0020	351 ± 79	0.0105 ± 0.0026	0.0100 ± 0.0018	0.0098 ± 0.0018
4.453 ± 0.105	201 ± 59	0.0055 ± 0.0017	376 ± 81	0.0107 ± 0.0026	0.0072 ± 0.0016	0.0071 ± 0.0016
4.647 ± 0.113	279 ± 60	0.0074 ± 0.0018	222 ± 80	0.0061 ± 0.0023	0.0067 ± 0.0016	0.0066 ± 0.0016
4.861 ± 0.122	254 ± 60	0.0068 ± 0.0017	324 ± 82	0.0088 ± 0.0024	0.0075 ± 0.0017	0.0074 ± 0.0016
5.090 ± 0.129	254 ± 61	0.0066 ± 0.0017	435 ± 84	0.0115 ± 0.0026	0.0084 ± 0.0017	0.0083 ± 0.0016
5.333 ± 0.140	210 ± 60	0.0054 ± 0.0016	459 ± 83	0.0122 ± 0.0026	0.0076 ± 0.0016	0.0066 ± 0.0014
5.597 ± 0.149	125 ± 60	0.0031 ± 0.0015	286 ± 84	0.0075 ± 0.0024	0.0043 ± 0.0015	0.0037 ± 0.0013
5.875 ± 0.160	215 ± 61	0.0052 ± 0.0016	134 ± 83	0.0034 ± 0.0022	0.0043 ± 0.0015	0.0037 ± 0.0013
6.181 ± 0.175	140 ± 62	0.0034 ± 0.0016	258 ± 85	0.0065 ± 0.0023	0.0042 ± 0.0015	0.0036 ± 0.0013
6.517 ± 0.187	283 ± 65	0.0065 ± 0.0016	290 ± 86	0.0070 ± 0.0022	0.0065 ± 0.0015	0.0057 ± 0.0014
6.862 ± 0.201	361 ± 67	0.0079 ± 0.0016	326 ± 88	0.0077 ± 0.0022	0.0077 ± 0.0016	0.0067 ± 0.0014
7.237 ± 0.218	306 ± 67	0.0069 ± 0.0017	579 ± 91	0.0145 ± 0.0028	0.0096 ± 0.0017	0.0083 ± 0.0015
7.661 ± 0.242	402 ± 67	0.0098 ± 0.0019	566 ± 89	0.0151 ± 0.0029	0.0121 ± 0.0019	0.0106 ± 0.0017
8.126 ± 0.263	347 ± 68	0.0084 ± 0.0018	504 ± 89	0.0133 ± 0.0028	0.0104 ± 0.0018	0.0091 ± 0.0016
8.618 ± 0.284	430 ± 70	0.0101 ± 0.0019	556 ± 91	0.0143 ± 0.0028	0.0121 ± 0.0019	0.0106 ± 0.0017
9.160 ± 0.313	608 ± 70	0.0146 ± 0.0022	465 ± 89	0.0122 ± 0.0027	0.0136 ± 0.0020	0.0120 ± 0.0018
9.757 ± 0.346	586 ± 71	0.0146 ± 0.0023	656 ± 90	0.0180 ± 0.0032	0.0166 ± 0.0022	0.0147 ± 0.0020
10.414 ± 0.377	522 ± 69	0.0135 ± 0.0022	735 ± 90	0.0210 ± 0.0035	0.0170 ± 0.0022	0.0150 ± 0.0020
11.143 ± 0.425	602 ± 70	0.0165 ± 0.0025	738 ± 89	0.0223 ± 0.0037	0.0198 ± 0.0025	0.0175 ± 0.0022
11.960 ± 0.467	627 ± 70	0.0177 ± 0.0026	975 ± 91	0.0306 ± 0.0044	0.0237 ± 0.0028	0.0210 ± 0.0025
12.860 ± 0.525	637 ± 70	0.0185 ± 0.0027	791 ± 90	0.0253 ± 0.0040	0.0224 ± 0.0027	0.0200 ± 0.0025
13.876 ± 0.589	652 ± 71	0.0193 ± 0.0028	765 ± 90	0.0251 ± 0.0041	0.0229 ± 0.0028	0.0204 ± 0.0025
15.016 ± 0.660	510 ± 70	0.0151 ± 0.0026	617 ± 88	0.0203 ± 0.0037	0.0180 ± 0.0025	0.0160 ± 0.0023
16.297 ± 0.750	326 ± 68	0.0096 ± 0.0022	560 ± 88	0.0182 ± 0.0035	0.0131 ± 0.0022	0.0117 ± 0.0020
17.759 ± 0.857	360 ± 68	0.0106 ± 0.0023	378 ± 87	0.0121 ± 0.0031	0.0114 ± 0.0021	0.0102 ± 0.0019
19.416 ± 0.971	255 ± 68	0.0074 ± 0.0021	516 ± 87	0.0162 ± 0.0033	0.0106 ± 0.0020	0.0095 ± 0.0019

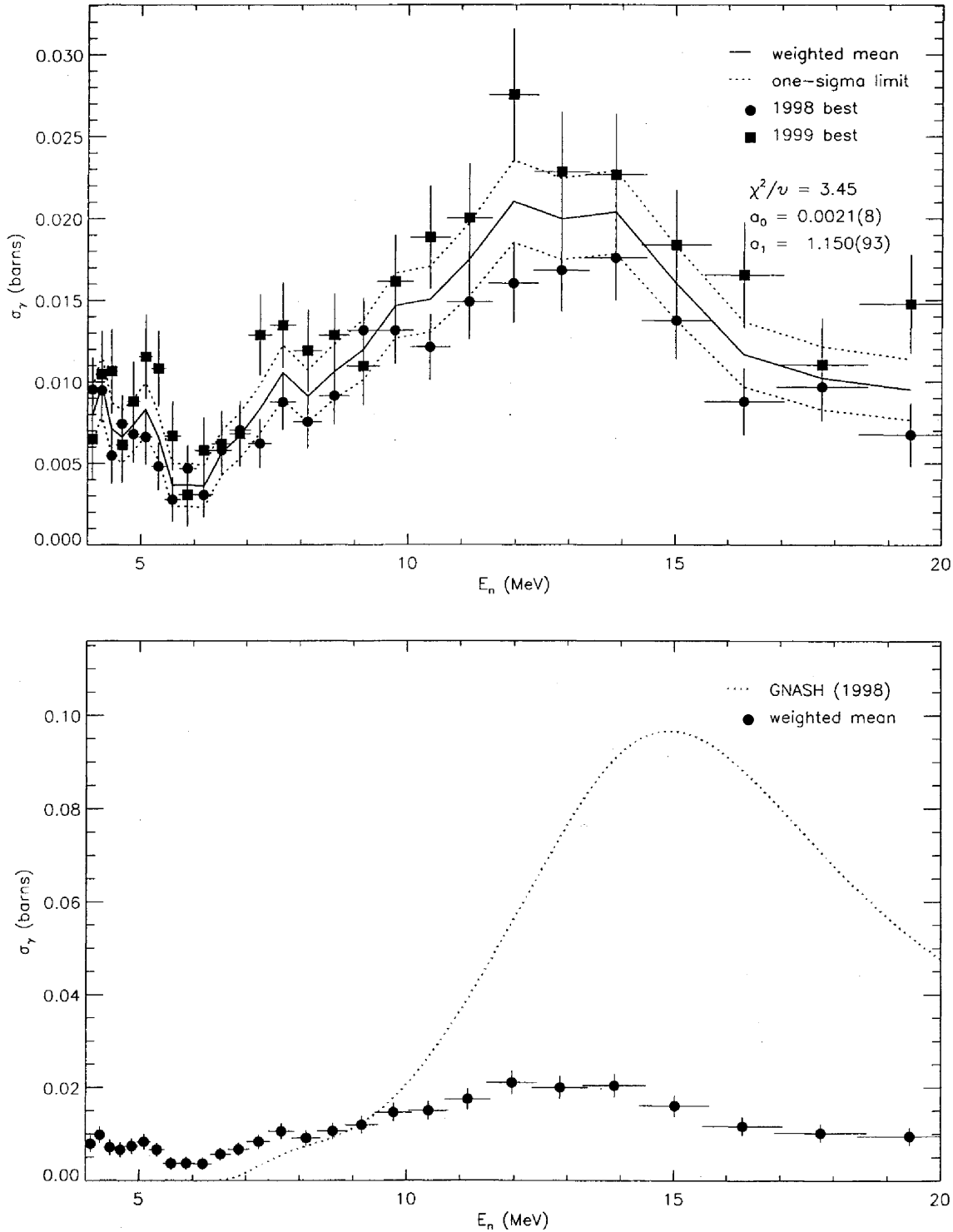


FIG. 59: Adopted $E_\gamma = 282.2$ -keV partial cross section corresponding to the data in table LXIX. The top panel shows the 1998 and 1999 partial cross sections (corrected for angular-distribution effects) and the recommended value, plotted as a solid line with a one-sigma confidence band (dotted lines). The bottom panel shows this recommended partial cross section (solid circles) compared to GNASH.

TABLE LXX: Adopted partial γ -ray cross section for the $E_\gamma = 666.7$ -keV transition. The measured peak areas and deduced partial cross section (before correction for angular distribution effects) for the **98Thin** data set are shown in columns 2 and 3, respectively. The partial cross section, listed in column 4, is obtained by scaling the **98Thin** data by a target-thickness correction factor. The recommended partial cross section in the last column includes a correction for angular-distribution effects.

E_n (MeV)	$A^{(1998)}$	$\sigma^{(1998)}$	$\sigma^{(\text{sca})}$	$\sigma^{(\text{sca,corr})}$
4.090 ± 0.093	0 ± 0	0.0001 ± 0.0007	0.0001 ± 0.0007	0.0001 ± 0.0007
4.264 ± 0.099	25 ± 57	0.0016 ± 0.0038	0.0015 ± 0.0034	0.0015 ± 0.0034
4.453 ± 0.105	130 ± 60	0.0080 ± 0.0039	0.0073 ± 0.0035	0.0073 ± 0.0035
4.647 ± 0.113	128 ± 60	0.0077 ± 0.0038	0.0071 ± 0.0034	0.0071 ± 0.0034
4.861 ± 0.122	161 ± 47	0.0098 ± 0.0031	0.0089 ± 0.0028	0.0089 ± 0.0028
5.090 ± 0.129	32 ± 59	0.0019 ± 0.0036	0.0017 ± 0.0032	0.0017 ± 0.0032
5.333 ± 0.140	113 ± 61	0.0066 ± 0.0037	0.0060 ± 0.0034	0.0062 ± 0.0034
5.597 ± 0.149	65 ± 62	0.0037 ± 0.0036	0.0033 ± 0.0033	0.0034 ± 0.0033
5.875 ± 0.160	75 ± 46	0.0042 ± 0.0027	0.0038 ± 0.0024	0.0039 ± 0.0025
6.181 ± 0.175	34 ± 60	0.0019 ± 0.0034	0.0017 ± 0.0031	0.0018 ± 0.0032
6.517 ± 0.187	127 ± 63	0.0066 ± 0.0034	0.0060 ± 0.0031	0.0062 ± 0.0032
6.862 ± 0.201	308 ± 66	0.0153 ± 0.0036	0.0139 ± 0.0033	0.0143 ± 0.0034
7.237 ± 0.218	176 ± 64	0.0091 ± 0.0035	0.0083 ± 0.0032	0.0085 ± 0.0033
7.661 ± 0.242	224 ± 64	0.0124 ± 0.0038	0.0113 ± 0.0035	0.0116 ± 0.0036
8.126 ± 0.263	278 ± 66	0.0153 ± 0.0040	0.0139 ± 0.0036	0.0143 ± 0.0037
8.618 ± 0.284	278 ± 68	0.0149 ± 0.0040	0.0136 ± 0.0036	0.0139 ± 0.0037
9.160 ± 0.313	215 ± 66	0.0117 ± 0.0038	0.0107 ± 0.0035	0.0109 ± 0.0036
9.757 ± 0.346	334 ± 67	0.0189 ± 0.0043	0.0172 ± 0.0039	0.0176 ± 0.0040
10.414 ± 0.377	368 ± 67	0.0216 ± 0.0045	0.0196 ± 0.0041	0.0201 ± 0.0043
11.143 ± 0.425	257 ± 65	0.0160 ± 0.0044	0.0146 ± 0.0040	0.0149 ± 0.0041
11.960 ± 0.467	317 ± 64	0.0204 ± 0.0046	0.0185 ± 0.0042	0.0190 ± 0.0044
12.860 ± 0.525	242 ± 64	0.0160 ± 0.0046	0.0146 ± 0.0042	0.0149 ± 0.0043
13.876 ± 0.589	287 ± 65	0.0194 ± 0.0048	0.0176 ± 0.0044	0.0180 ± 0.0046
15.016 ± 0.660	237 ± 64	0.0160 ± 0.0047	0.0145 ± 0.0043	0.0148 ± 0.0044
16.297 ± 0.750	237 ± 64	0.0159 ± 0.0046	0.0145 ± 0.0043	0.0148 ± 0.0044
17.759 ± 0.857	152 ± 65	0.0102 ± 0.0045	0.0093 ± 0.0041	0.0094 ± 0.0042
19.416 ± 0.971	171 ± 65	0.0112 ± 0.0045	0.0102 ± 0.0041	0.0104 ± 0.0042

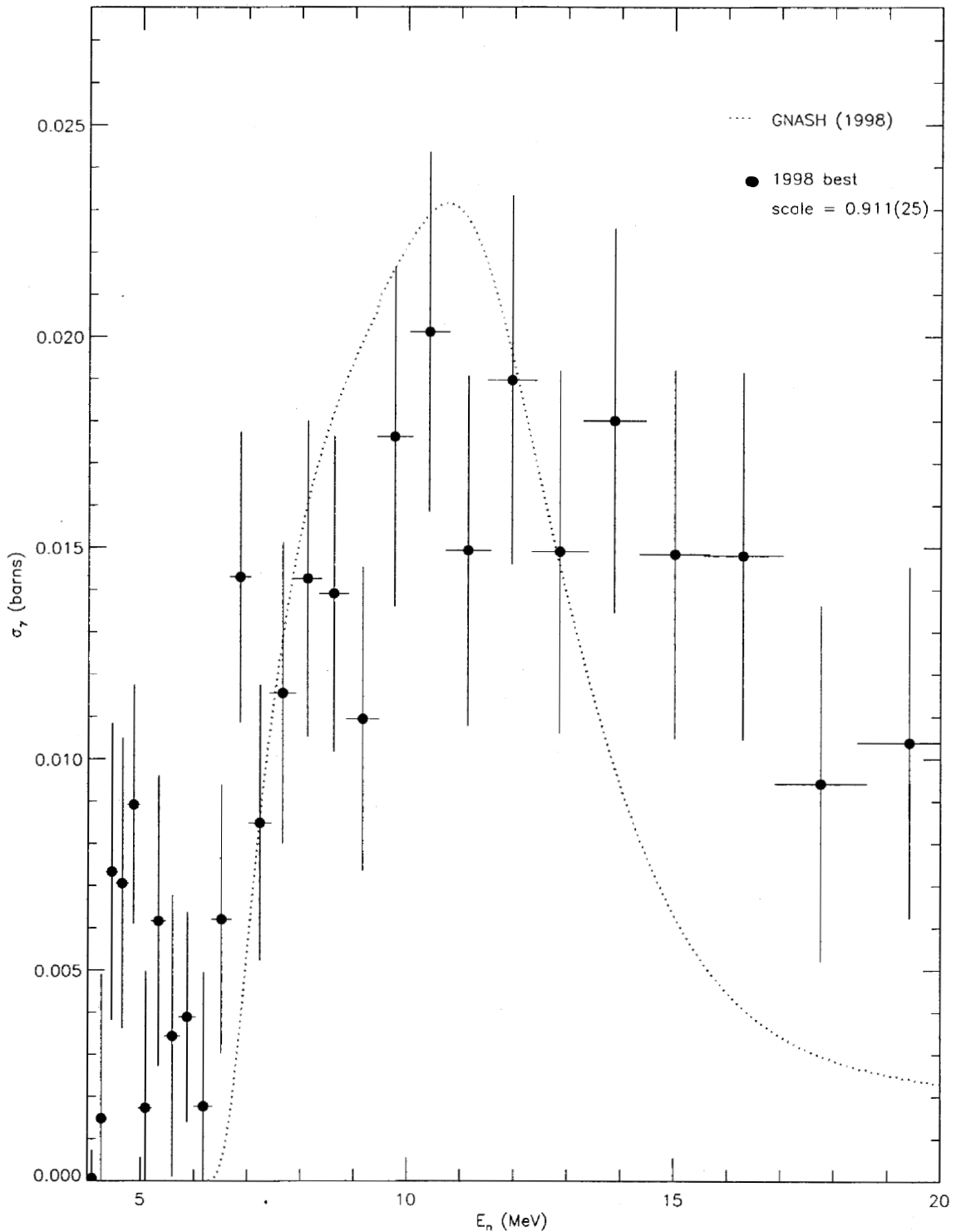


FIG. 60: Adopted $E_\gamma = 666.7$ -keV partial cross section corresponding to the data in table LXX, and corrected for angular-distribution effects. The target-thickness correction factor is shown, and the recommended partial cross section (solid circles) is compared to GNASH.

TABLE LXXI: Adopted partial γ -ray cross section for the $E_\gamma = 780.8$ -keV transition. The measured peak areas and deduced partial cross section (before correction for angular distribution effects) for the **98Thin** data set are shown in columns 2 and 3, respectively. The partial cross section, listed in column 4, is obtained by scaling the **98Thin** data by a target-thickness correction factor. The recommended partial cross section in the last column includes a correction for angular-distribution effects.

E_n (MeV)	$A^{(1998)}$	$\sigma^{(1998)}$	$\sigma^{(\text{sca})}$	$\sigma^{(\text{sca,corr})}$
4.090 \pm 0.093	111 \pm 42	0.0088 \pm 0.0040	0.0080 \pm 0.0036	0.0080 \pm 0.0036
4.264 \pm 0.099	21 \pm 43	0.0016 \pm 0.0038	0.0015 \pm 0.0035	0.0015 \pm 0.0035
4.453 \pm 0.105	19 \pm 42	0.0014 \pm 0.0036	0.0013 \pm 0.0033	0.0013 \pm 0.0033
4.647 \pm 0.113	121 \pm 44	0.0087 \pm 0.0037	0.0080 \pm 0.0034	0.0080 \pm 0.0034
4.861 \pm 0.122	49 \pm 43	0.0036 \pm 0.0036	0.0032 \pm 0.0033	0.0032 \pm 0.0033
5.090 \pm 0.129	65 \pm 44	0.0046 \pm 0.0036	0.0042 \pm 0.0033	0.0042 \pm 0.0033
5.333 \pm 0.140	37 \pm 45	0.0026 \pm 0.0036	0.0023 \pm 0.0032	0.0025 \pm 0.0034
5.597 \pm 0.149	142 \pm 44	0.0096 \pm 0.0035	0.0087 \pm 0.0032	0.0091 \pm 0.0034
5.875 \pm 0.160	96 \pm 45	0.0064 \pm 0.0034	0.0058 \pm 0.0031	0.0061 \pm 0.0033
6.181 \pm 0.175	84 \pm 45	0.0056 \pm 0.0034	0.0051 \pm 0.0031	0.0053 \pm 0.0033
6.517 \pm 0.187	94 \pm 47	0.0059 \pm 0.0033	0.0053 \pm 0.0030	0.0056 \pm 0.0032
6.862 \pm 0.201	45 \pm 47	0.0027 \pm 0.0031	0.0024 \pm 0.0029	0.0025 \pm 0.0030
7.237 \pm 0.218	59 \pm 47	0.0036 \pm 0.0033	0.0033 \pm 0.0030	0.0035 \pm 0.0031
7.661 \pm 0.242	110 \pm 46	0.0073 \pm 0.0035	0.0066 \pm 0.0032	0.0069 \pm 0.0033
8.126 \pm 0.263	103 \pm 47	0.0068 \pm 0.0035	0.0062 \pm 0.0032	0.0064 \pm 0.0034
8.618 \pm 0.284	247 \pm 50	0.0158 \pm 0.0039	0.0144 \pm 0.0036	0.0150 \pm 0.0037
9.160 \pm 0.313	257 \pm 49	0.0168 \pm 0.0039	0.0153 \pm 0.0036	0.0159 \pm 0.0038
9.757 \pm 0.346	319 \pm 49	0.0216 \pm 0.0043	0.0196 \pm 0.0039	0.0204 \pm 0.0041
10.414 \pm 0.377	234 \pm 48	0.0164 \pm 0.0041	0.0149 \pm 0.0038	0.0155 \pm 0.0039
11.143 \pm 0.425	228 \pm 47	0.0170 \pm 0.0043	0.0155 \pm 0.0039	0.0161 \pm 0.0041
11.960 \pm 0.467	226 \pm 47	0.0173 \pm 0.0044	0.0158 \pm 0.0040	0.0164 \pm 0.0042
12.860 \pm 0.525	220 \pm 47	0.0174 \pm 0.0045	0.0158 \pm 0.0041	0.0164 \pm 0.0043
13.876 \pm 0.589	154 \pm 46	0.0124 \pm 0.0044	0.0113 \pm 0.0040	0.0117 \pm 0.0041
15.016 \pm 0.660	217 \pm 47	0.0175 \pm 0.0046	0.0159 \pm 0.0042	0.0164 \pm 0.0044
16.297 \pm 0.750	167 \pm 45	0.0134 \pm 0.0043	0.0122 \pm 0.0039	0.0126 \pm 0.0041
17.759 \pm 0.857	151 \pm 46	0.0121 \pm 0.0043	0.0110 \pm 0.0039	0.0113 \pm 0.0041
19.416 \pm 0.971	65 \pm 46	0.0051 \pm 0.0041	0.0046 \pm 0.0037	0.0048 \pm 0.0038

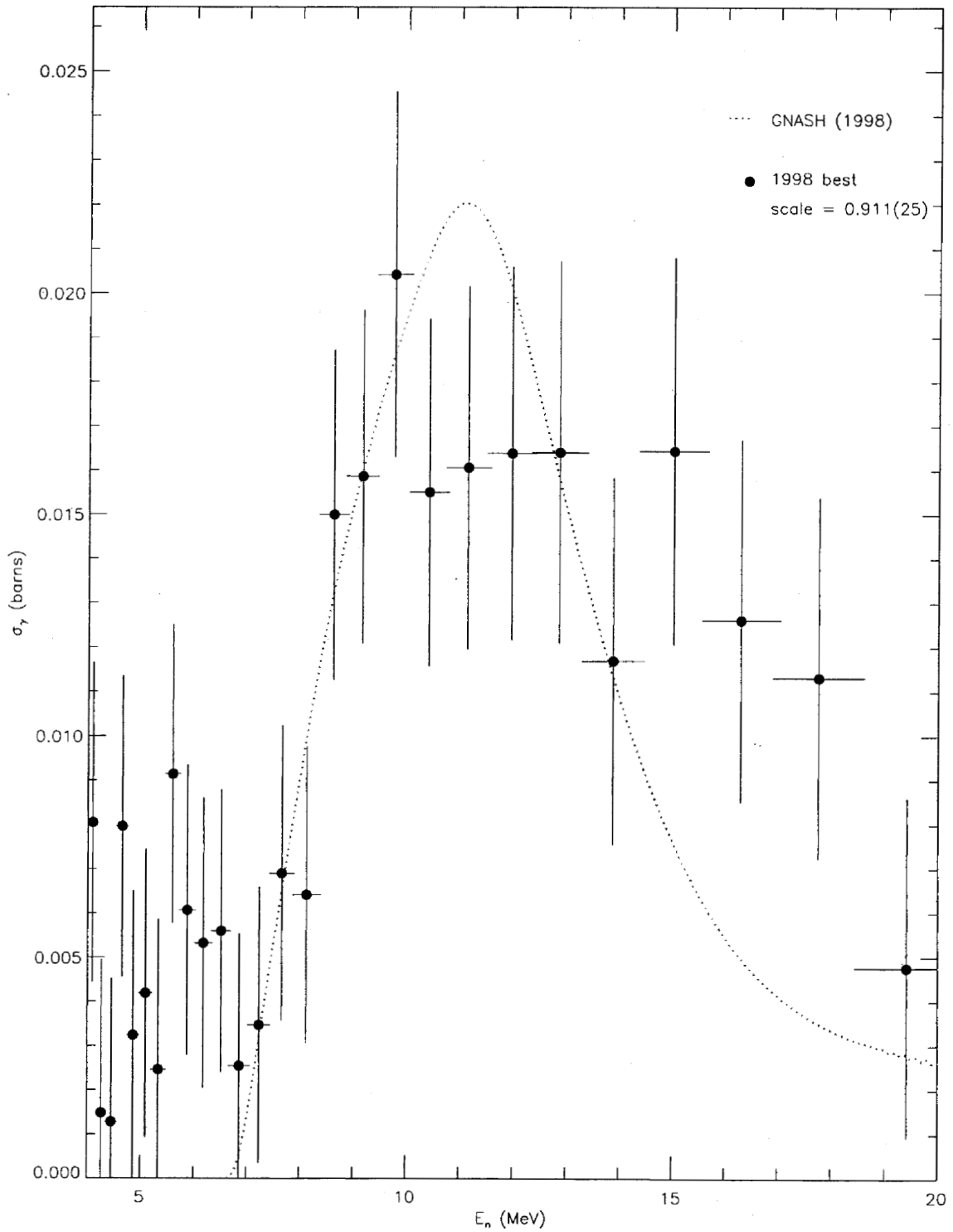


FIG. 61: Adopted $E_\gamma = 780.8$ -keV partial cross section corresponding to the data in table LXXI, and corrected for angular-distribution effects. The target-thickness correction factor is shown, and the recommended partial cross section (solid circles) is compared to GNASH.

TABLE LXXII: Adopted partial γ -ray cross section for the $E_\gamma = 786.8$ -keV transition. The measured peak areas and deduced partial cross section (before correction for angular distribution effects) for the **98Thin** data set are shown in columns 2 and 3, respectively. The partial cross section, listed in column 4, is obtained by scaling the **98Thin** data by a target-thickness correction factor. The recommended partial cross section in the last column includes a correction for angular-distribution effects.

E_n (MeV)	$A^{(1998)}$	$\sigma^{(1998)}$	$\sigma^{(\text{sca})}$	$\sigma^{(\text{sca,corr})}$
4.090 ± 0.093	54 ± 45	0.0024 ± 0.0020	0.0021 ± 0.0018	0.0021 ± 0.0018
4.264 ± 0.099	180 ± 46	0.0077 ± 0.0022	0.0070 ± 0.0020	0.0070 ± 0.0020
4.453 ± 0.105	124 ± 46	0.0050 ± 0.0020	0.0046 ± 0.0018	0.0046 ± 0.0018
4.647 ± 0.113	119 ± 47	0.0047 ± 0.0019	0.0043 ± 0.0018	0.0043 ± 0.0018
4.861 ± 0.122	33 ± 46	0.0013 ± 0.0018	0.0012 ± 0.0017	0.0012 ± 0.0017
5.090 ± 0.129	122 ± 48	0.0047 ± 0.0019	0.0043 ± 0.0018	0.0043 ± 0.0018
5.333 ± 0.140	132 ± 49	0.0050 ± 0.0020	0.0046 ± 0.0018	0.0046 ± 0.0018
5.597 ± 0.149	167 ± 50	0.0062 ± 0.0020	0.0056 ± 0.0018	0.0056 ± 0.0018
5.875 ± 0.160	34 ± 49	0.0012 ± 0.0018	0.0011 ± 0.0016	0.0011 ± 0.0016
6.181 ± 0.175	105 ± 49	0.0038 ± 0.0018	0.0035 ± 0.0017	0.0035 ± 0.0017
6.517 ± 0.187	156 ± 50	0.0053 ± 0.0018	0.0049 ± 0.0017	0.0049 ± 0.0017
6.862 ± 0.201	195 ± 52	0.0063 ± 0.0018	0.0058 ± 0.0017	0.0058 ± 0.0017
7.237 ± 0.218	258 ± 53	0.0087 ± 0.0021	0.0079 ± 0.0019	0.0079 ± 0.0019
7.661 ± 0.242	186 ± 51	0.0067 ± 0.0020	0.0061 ± 0.0018	0.0061 ± 0.0018
8.126 ± 0.263	220 ± 52	0.0079 ± 0.0021	0.0072 ± 0.0019	0.0072 ± 0.0019
8.618 ± 0.284	293 ± 54	0.0103 ± 0.0022	0.0094 ± 0.0021	0.0093 ± 0.0021
9.160 ± 0.313	153 ± 53	0.0055 ± 0.0020	0.0050 ± 0.0018	0.0050 ± 0.0018
9.757 ± 0.346	296 ± 54	0.0110 ± 0.0024	0.0100 ± 0.0022	0.0100 ± 0.0022
10.414 ± 0.377	356 ± 54	0.0137 ± 0.0026	0.0125 ± 0.0024	0.0124 ± 0.0024
11.143 ± 0.425	402 ± 54	0.0164 ± 0.0029	0.0150 ± 0.0027	0.0149 ± 0.0027
11.960 ± 0.467	209 ± 51	0.0088 ± 0.0024	0.0080 ± 0.0022	0.0080 ± 0.0022
12.860 ± 0.525	248 ± 52	0.0108 ± 0.0026	0.0098 ± 0.0024	0.0098 ± 0.0024
13.876 ± 0.589	209 ± 52	0.0092 ± 0.0025	0.0084 ± 0.0023	0.0084 ± 0.0023
15.016 ± 0.660	178 ± 52	0.0079 ± 0.0025	0.0072 ± 0.0023	0.0071 ± 0.0023
16.297 ± 0.750	150 ± 52	0.0066 ± 0.0024	0.0060 ± 0.0022	0.0060 ± 0.0022
17.759 ± 0.857	124 ± 52	0.0054 ± 0.0024	0.0050 ± 0.0022	0.0049 ± 0.0022
19.416 ± 0.971	107 ± 52	0.0046 ± 0.0023	0.0042 ± 0.0021	0.0042 ± 0.0021

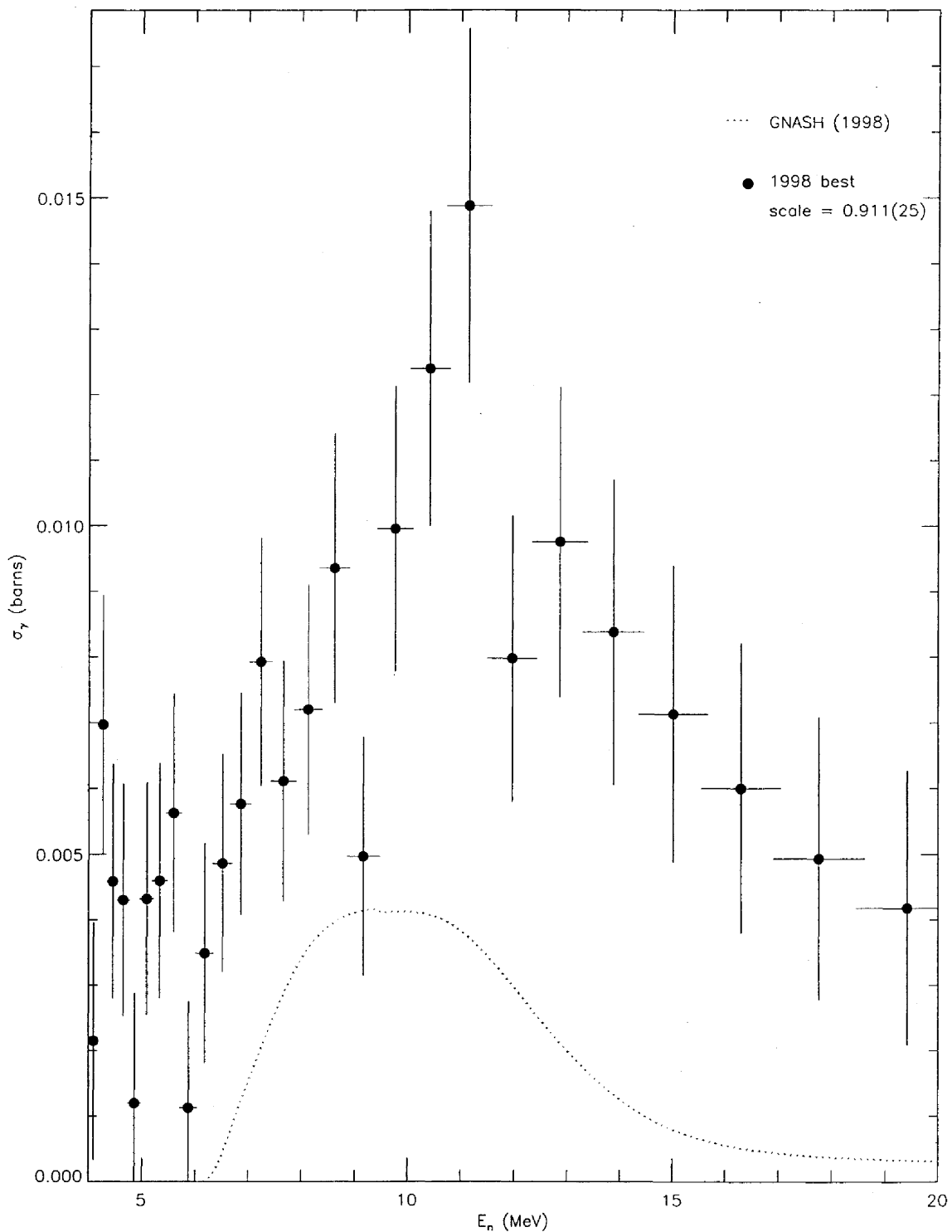


FIG. 62: Adopted $E_\gamma = 786.8$ -keV partial cross section corresponding to the data in table LXXII, and corrected for angular-distribution effects. The target-thickness correction factor is shown, and the recommended partial cross section (solid circles) is compared to GNASH.

TABLE LXXIII: Adopted partial γ -ray cross section for the $E_\gamma = 806.1$ -keV transition. The measured peak areas and deduced partial cross section (before correction for angular distribution effects) for the **98Thin** data set are shown in columns 2 and 3, respectively. The partial cross section, listed in column 4, is obtained by scaling the **98Thin** data by a target-thickness correction factor. The recommended partial cross section in the last column includes a correction for angular-distribution effects.

E_n (MeV)	$A^{(1998)}$	$\sigma^{(1998)}$	$\sigma^{(\text{sca})}$	$\sigma^{(\text{sca,corr})}$
4.090 ± 0.093	104 ± 42	0.0086 ± 0.0037	0.0078 ± 0.0034	0.0078 ± 0.0034
4.264 ± 0.099	96 ± 44	0.0077 ± 0.0037	0.0070 ± 0.0034	0.0070 ± 0.0034
4.453 ± 0.105	93 ± 45	0.0071 ± 0.0036	0.0065 ± 0.0033	0.0065 ± 0.0033
4.647 ± 0.113	141 ± 47	0.0106 ± 0.0038	0.0096 ± 0.0035	0.0096 ± 0.0035
4.861 ± 0.122	55 ± 44	0.0041 ± 0.0035	0.0038 ± 0.0031	0.0038 ± 0.0031
5.090 ± 0.129	109 ± 45	0.0080 ± 0.0035	0.0073 ± 0.0032	0.0073 ± 0.0032
5.333 ± 0.140	45 ± 47	0.0032 ± 0.0035	0.0030 ± 0.0032	0.0030 ± 0.0033
5.597 ± 0.149	70 ± 46	0.0049 ± 0.0034	0.0045 ± 0.0031	0.0045 ± 0.0031
5.875 ± 0.160	98 ± 45	0.0067 ± 0.0033	0.0061 ± 0.0030	0.0062 ± 0.0030
6.181 ± 0.175	162 ± 46	0.0112 ± 0.0035	0.0102 ± 0.0032	0.0104 ± 0.0032
6.517 ± 0.187	131 ± 47	0.0085 ± 0.0032	0.0077 ± 0.0030	0.0079 ± 0.0030
6.862 ± 0.201	150 ± 50	0.0092 ± 0.0033	0.0084 ± 0.0030	0.0085 ± 0.0031
7.237 ± 0.218	219 ± 50	0.0140 ± 0.0036	0.0127 ± 0.0033	0.0130 ± 0.0033
7.661 ± 0.242	222 ± 50	0.0152 ± 0.0038	0.0138 ± 0.0035	0.0141 ± 0.0036
8.126 ± 0.263	202 ± 49	0.0138 ± 0.0037	0.0125 ± 0.0034	0.0128 ± 0.0035
8.618 ± 0.284	292 ± 52	0.0194 ± 0.0040	0.0176 ± 0.0037	0.0180 ± 0.0038
9.160 ± 0.313	253 ± 51	0.0171 ± 0.0039	0.0156 ± 0.0036	0.0159 ± 0.0037
9.757 ± 0.346	351 ± 51	0.0246 ± 0.0044	0.0224 ± 0.0041	0.0229 ± 0.0042
10.414 ± 0.377	289 ± 51	0.0209 ± 0.0043	0.0191 ± 0.0040	0.0195 ± 0.0041
11.143 ± 0.425	313 ± 51	0.0241 ± 0.0047	0.0220 ± 0.0043	0.0225 ± 0.0045
11.960 ± 0.467	293 ± 47	0.0233 ± 0.0045	0.0212 ± 0.0042	0.0217 ± 0.0043
12.860 ± 0.525	166 ± 45	0.0136 ± 0.0041	0.0124 ± 0.0037	0.0126 ± 0.0038
13.876 ± 0.589	286 ± 47	0.0239 ± 0.0047	0.0217 ± 0.0044	0.0222 ± 0.0045
15.016 ± 0.660	195 ± 49	0.0163 ± 0.0045	0.0148 ± 0.0041	0.0151 ± 0.0042
16.297 ± 0.750	88 ± 45	0.0073 ± 0.0039	0.0067 ± 0.0036	0.0068 ± 0.0037
17.759 ± 0.857	190 ± 49	0.0157 ± 0.0045	0.0143 ± 0.0041	0.0146 ± 0.0042
19.416 ± 0.971	68 ± 46	0.0055 ± 0.0039	0.0050 ± 0.0036	0.0051 ± 0.0036

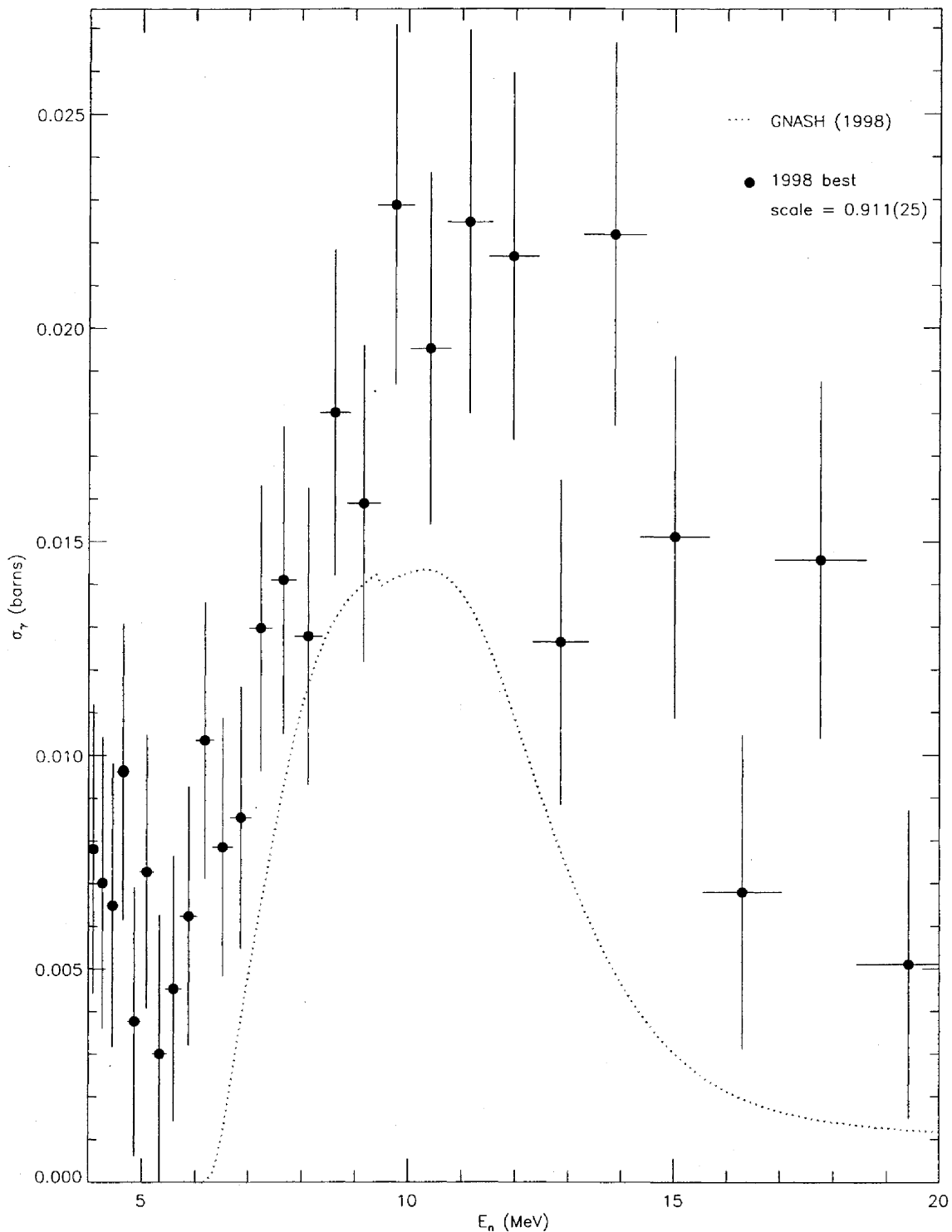


FIG. 63: Adopted $E_\gamma = 806.1$ -keV partial cross section corresponding to the data in table LXXIII, and corrected for angular-distribution effects. The target-thickness correction factor is shown, and the recommended partial cross section (solid circles) is compared to GNASH.

TABLE LXXIV: Adopted partial γ -ray cross section for the $E_\gamma = 819.2$ -keV transition. The measured peak areas and deduced partial cross section (before correction for angular distribution effects) for the **98Thin** data set are shown in columns 2 and 3, respectively. The partial cross section, listed in column 4, is obtained by scaling the **98Thin** data by a target-thickness correction factor. The recommended partial cross section in the last column includes a correction for angular-distribution effects.

E_n (MeV)	$A^{(1998)}$	$\sigma^{(1998)}$	$\sigma^{(\text{sca})}$	$\sigma^{(\text{sca,corr})}$
4.090 \pm 0.093	60 \pm 43	0.0027 \pm 0.0019	0.0024 \pm 0.0018	0.0024 \pm 0.0018
4.264 \pm 0.099	84 \pm 44	0.0036 \pm 0.0019	0.0033 \pm 0.0018	0.0033 \pm 0.0018
4.453 \pm 0.105	204 \pm 46	0.0084 \pm 0.0021	0.0077 \pm 0.0020	0.0077 \pm 0.0020
4.647 \pm 0.113	126 \pm 46	0.0051 \pm 0.0019	0.0046 \pm 0.0018	0.0046 \pm 0.0018
4.861 \pm 0.122	74 \pm 46	0.0030 \pm 0.0019	0.0027 \pm 0.0017	0.0027 \pm 0.0017
5.090 \pm 0.129	133 \pm 47	0.0053 \pm 0.0020	0.0048 \pm 0.0018	0.0048 \pm 0.0018
5.333 \pm 0.140	130 \pm 47	0.0051 \pm 0.0019	0.0046 \pm 0.0018	0.0045 \pm 0.0017
5.597 \pm 0.149	122 \pm 48	0.0046 \pm 0.0019	0.0042 \pm 0.0017	0.0040 \pm 0.0017
5.875 \pm 0.160	149 \pm 49	0.0055 \pm 0.0019	0.0050 \pm 0.0018	0.0049 \pm 0.0017
6.181 \pm 0.175	95 \pm 48	0.0035 \pm 0.0018	0.0032 \pm 0.0017	0.0031 \pm 0.0016
6.517 \pm 0.187	119 \pm 49	0.0041 \pm 0.0018	0.0038 \pm 0.0016	0.0037 \pm 0.0016
6.862 \pm 0.201	227 \pm 51	0.0075 \pm 0.0019	0.0068 \pm 0.0017	0.0066 \pm 0.0017
7.237 \pm 0.218	286 \pm 52	0.0098 \pm 0.0021	0.0090 \pm 0.0019	0.0087 \pm 0.0019
7.661 \pm 0.242	297 \pm 52	0.0109 \pm 0.0023	0.0100 \pm 0.0021	0.0097 \pm 0.0020
8.126 \pm 0.263	391 \pm 53	0.0143 \pm 0.0025	0.0131 \pm 0.0023	0.0127 \pm 0.0023
8.618 \pm 0.284	357 \pm 54	0.0128 \pm 0.0024	0.0116 \pm 0.0022	0.0113 \pm 0.0022
9.160 \pm 0.313	330 \pm 53	0.0120 \pm 0.0024	0.0109 \pm 0.0022	0.0106 \pm 0.0021
9.757 \pm 0.346	337 \pm 53	0.0127 \pm 0.0025	0.0116 \pm 0.0023	0.0112 \pm 0.0022
10.414 \pm 0.377	449 \pm 54	0.0175 \pm 0.0029	0.0160 \pm 0.0027	0.0155 \pm 0.0026
11.143 \pm 0.425	358 \pm 52	0.0149 \pm 0.0028	0.0135 \pm 0.0025	0.0131 \pm 0.0025
11.960 \pm 0.467	315 \pm 52	0.0135 \pm 0.0027	0.0123 \pm 0.0025	0.0119 \pm 0.0024
12.860 \pm 0.525	348 \pm 52	0.0154 \pm 0.0029	0.0140 \pm 0.0027	0.0136 \pm 0.0026
13.876 \pm 0.589	237 \pm 51	0.0107 \pm 0.0026	0.0097 \pm 0.0024	0.0095 \pm 0.0023
15.016 \pm 0.660	187 \pm 51	0.0084 \pm 0.0025	0.0077 \pm 0.0023	0.0075 \pm 0.0022
16.297 \pm 0.750	81 \pm 50	0.0036 \pm 0.0023	0.0033 \pm 0.0021	0.0032 \pm 0.0020
17.759 \pm 0.857	4 \pm 44	0.0002 \pm 0.0020	0.0002 \pm 0.0018	0.0002 \pm 0.0017
19.416 \pm 0.971	1 \pm 43	0.0000 \pm 0.0019	0.0000 \pm 0.0017	0.0000 \pm 0.0017

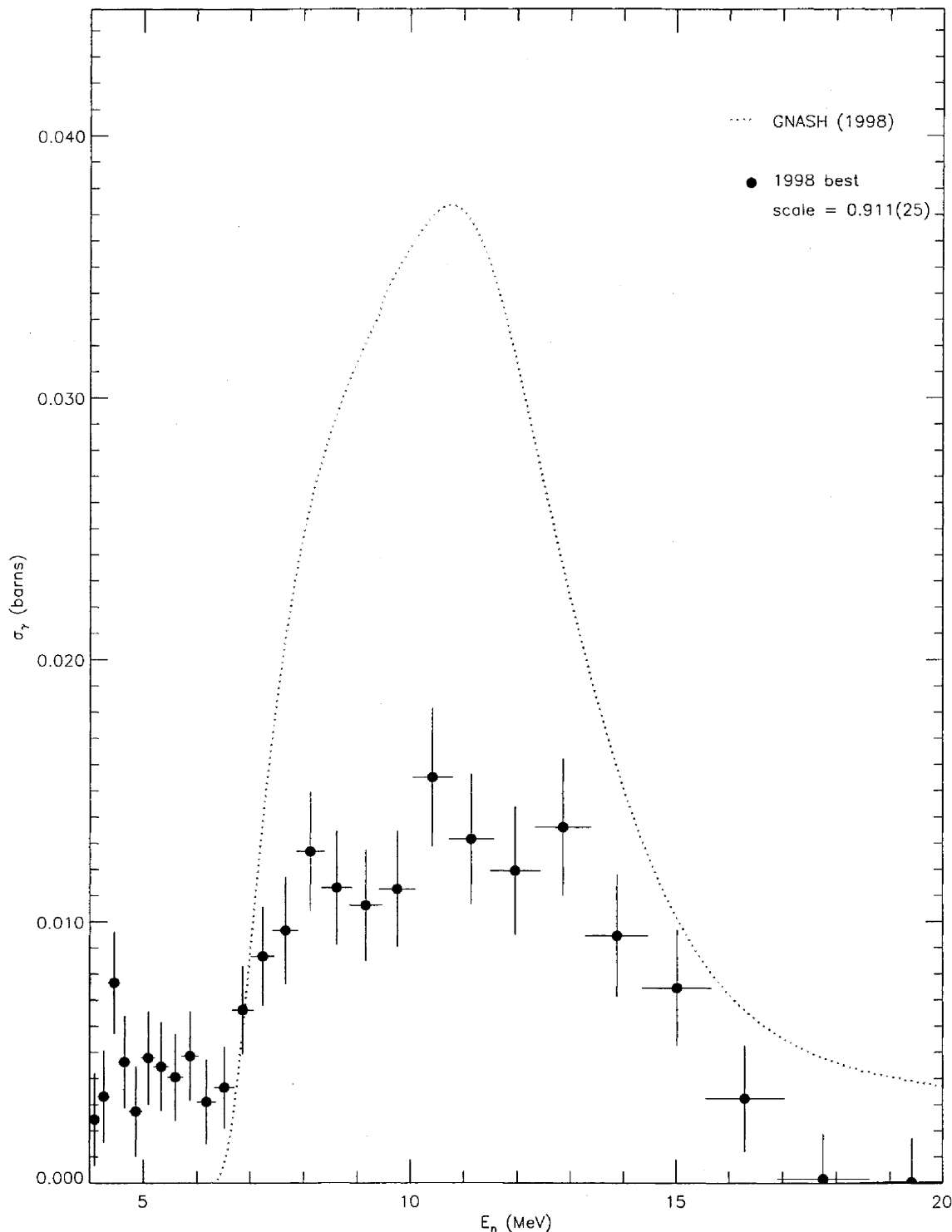


FIG. 64: Adopted $E_\gamma = 819.2$ -keV partial cross section corresponding to the data in table LXXIV, and corrected for angular-distribution effects. The target-thickness correction factor is shown, and the recommended partial cross section (solid circles) is compared to GNASH.

TABLE LXXV: Adopted partial γ -ray cross section for the $E_\gamma = 829.5$ -keV transition. The measured peak areas and deduced partial cross section (before correction for angular distribution effects) for the **98Thin** data set are shown in columns 2 and 3, respectively. The partial cross section, listed in column 4, is obtained by scaling the **98Thin** data by a target-thickness correction factor. The recommended partial cross section in the last column includes a correction for angular-distribution effects.

E_n (MeV)	$A^{(1998)}$	$\sigma^{(1998)}$	$\sigma^{(\text{sca})}$	$\sigma^{(\text{sca,corr})}$
4.090 \pm 0.093	24 \pm 42	0.0020 \pm 0.0036	0.0018 \pm 0.0033	0.0018 \pm 0.0033
4.264 \pm 0.099	0 \pm 0	0.0001 \pm 0.0007	0.0001 \pm 0.0006	0.0001 \pm 0.0006
4.453 \pm 0.105	26 \pm 44	0.0020 \pm 0.0035	0.0018 \pm 0.0032	0.0018 \pm 0.0032
4.647 \pm 0.113	79 \pm 46	0.0060 \pm 0.0036	0.0055 \pm 0.0033	0.0055 \pm 0.0033
4.861 \pm 0.122	0 \pm 0	0.0001 \pm 0.0006	0.0001 \pm 0.0006	0.0001 \pm 0.0006
5.090 \pm 0.129	0 \pm 0	0.0001 \pm 0.0006	0.0001 \pm 0.0006	0.0001 \pm 0.0006
5.333 \pm 0.140	24 \pm 48	0.0018 \pm 0.0036	0.0016 \pm 0.0032	0.0017 \pm 0.0035
5.597 \pm 0.149	10 \pm 47	0.0007 \pm 0.0034	0.0006 \pm 0.0031	0.0007 \pm 0.0033
5.875 \pm 0.160	4 \pm 46	0.0003 \pm 0.0032	0.0003 \pm 0.0030	0.0003 \pm 0.0032
6.181 \pm 0.175	35 \pm 46	0.0024 \pm 0.0033	0.0022 \pm 0.0030	0.0024 \pm 0.0032
6.517 \pm 0.187	66 \pm 47	0.0043 \pm 0.0032	0.0039 \pm 0.0029	0.0042 \pm 0.0031
6.862 \pm 0.201	119 \pm 50	0.0074 \pm 0.0032	0.0067 \pm 0.0030	0.0072 \pm 0.0032
7.237 \pm 0.218	203 \pm 51	0.0131 \pm 0.0036	0.0119 \pm 0.0033	0.0128 \pm 0.0035
7.661 \pm 0.242	159 \pm 51	0.0110 \pm 0.0037	0.0100 \pm 0.0034	0.0107 \pm 0.0037
8.126 \pm 0.263	177 \pm 51	0.0122 \pm 0.0038	0.0111 \pm 0.0034	0.0118 \pm 0.0037
8.618 \pm 0.284	179 \pm 52	0.0120 \pm 0.0037	0.0110 \pm 0.0034	0.0116 \pm 0.0036
9.160 \pm 0.313	114 \pm 51	0.0078 \pm 0.0036	0.0071 \pm 0.0033	0.0075 \pm 0.0035
9.757 \pm 0.346	137 \pm 51	0.0097 \pm 0.0038	0.0088 \pm 0.0035	0.0094 \pm 0.0037
10.414 \pm 0.377	317 \pm 53	0.0233 \pm 0.0046	0.0212 \pm 0.0042	0.0225 \pm 0.0045
11.143 \pm 0.425	232 \pm 52	0.0181 \pm 0.0045	0.0165 \pm 0.0041	0.0175 \pm 0.0044
11.960 \pm 0.467	202 \pm 49	0.0163 \pm 0.0043	0.0148 \pm 0.0040	0.0156 \pm 0.0042
12.860 \pm 0.525	185 \pm 49	0.0153 \pm 0.0044	0.0140 \pm 0.0040	0.0147 \pm 0.0043
13.876 \pm 0.589	244 \pm 50	0.0206 \pm 0.0048	0.0188 \pm 0.0044	0.0198 \pm 0.0046
15.016 \pm 0.660	226 \pm 51	0.0191 \pm 0.0048	0.0174 \pm 0.0044	0.0183 \pm 0.0046
16.297 \pm 0.750	142 \pm 48	0.0120 \pm 0.0043	0.0109 \pm 0.0039	0.0114 \pm 0.0041
17.759 \pm 0.857	116 \pm 49	0.0097 \pm 0.0043	0.0088 \pm 0.0039	0.0093 \pm 0.0041
19.416 \pm 0.971	222 \pm 49	0.0182 \pm 0.0045	0.0166 \pm 0.0041	0.0173 \pm 0.0043

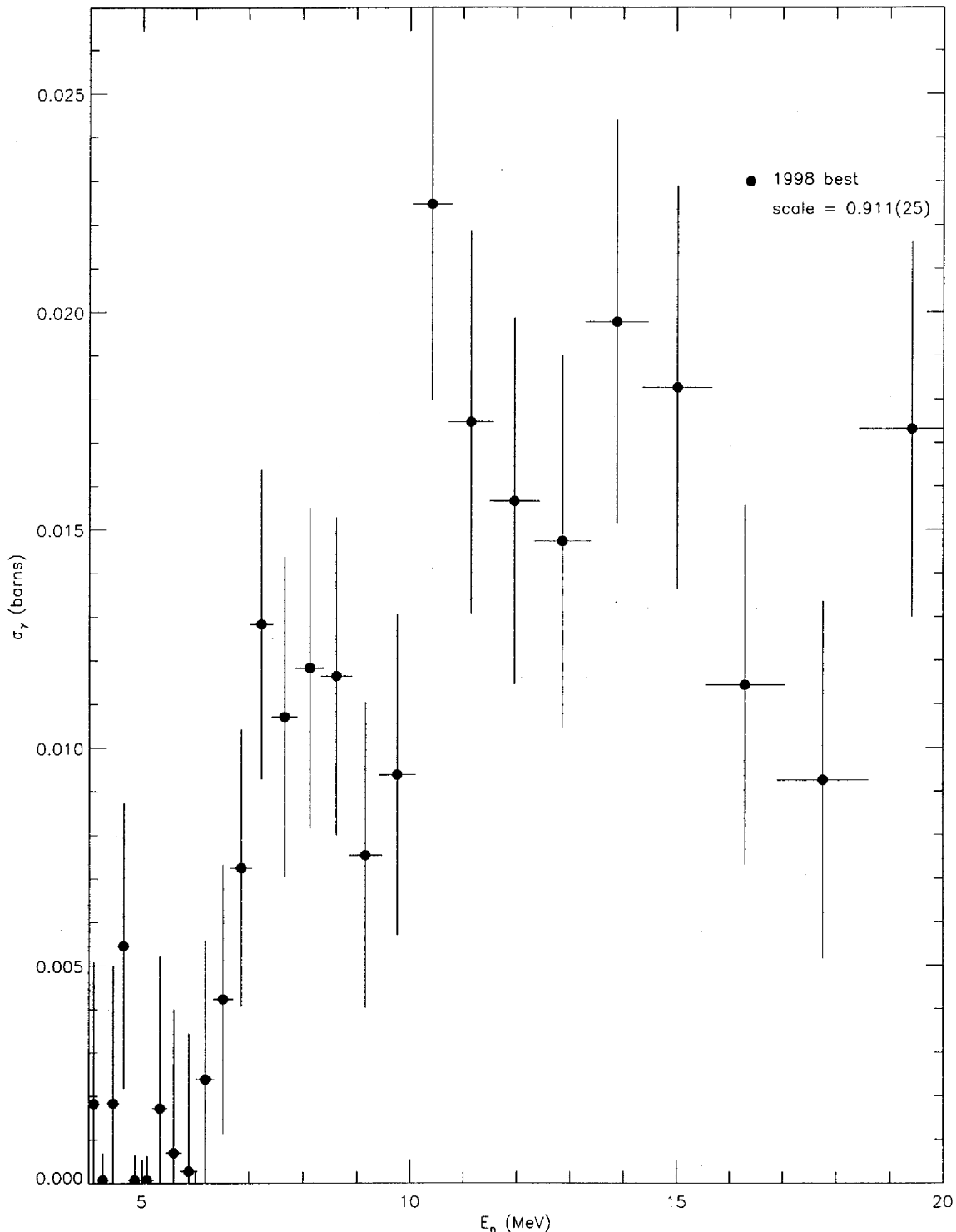


FIG. 65: Adopted $E_\gamma = 829.5$ -keV partial cross section corresponding to the data in table LXXV, and corrected for angular-distribution effects. No GNASH calculations are available for this line. The target-thickness correction factor is shown.

TABLE LXXVI: Adopted partial γ -ray cross section for the $E_\gamma = 831.6$ -keV transition. The measured peak areas and deduced partial cross section (before correction for angular distribution effects) for the **98Thin** data set are shown in columns 2 and 3, respectively. The partial cross section, listed in column 4, is obtained by scaling the **98Thin** data by a target-thickness correction factor. The recommended partial cross section in the last column includes a correction for angular-distribution effects.

E_n (MeV)	$A^{(1998)}$	$\sigma^{(1998)}$	$\sigma^{(\text{sca})}$	$\sigma^{(\text{sca,corr})}$
4.090 ± 0.093	143 ± 47	0.0120 ± 0.0042	0.0109 ± 0.0038	0.0109 ± 0.0038
4.264 ± 0.099	93 ± 47	0.0076 ± 0.0040	0.0069 ± 0.0036	0.0069 ± 0.0036
4.453 ± 0.105	136 ± 48	0.0106 ± 0.0039	0.0096 ± 0.0036	0.0096 ± 0.0036
4.647 ± 0.113	126 ± 48	0.0096 ± 0.0038	0.0087 ± 0.0035	0.0087 ± 0.0035
4.861 ± 0.122	138 ± 49	0.0105 ± 0.0039	0.0096 ± 0.0036	0.0096 ± 0.0036
5.090 ± 0.129	83 ± 47	0.0062 ± 0.0036	0.0056 ± 0.0033	0.0056 ± 0.0033
5.333 ± 0.140	90 ± 50	0.0066 ± 0.0038	0.0060 ± 0.0034	0.0062 ± 0.0035
5.597 ± 0.149	144 ± 50	0.0102 ± 0.0037	0.0093 ± 0.0034	0.0096 ± 0.0035
5.875 ± 0.160	82 ± 48	0.0057 ± 0.0034	0.0052 ± 0.0031	0.0053 ± 0.0032
6.181 ± 0.175	108 ± 49	0.0075 ± 0.0036	0.0069 ± 0.0032	0.0071 ± 0.0033
6.517 ± 0.187	118 ± 50	0.0077 ± 0.0034	0.0071 ± 0.0031	0.0072 ± 0.0032
6.862 ± 0.201	149 ± 52	0.0093 ± 0.0034	0.0085 ± 0.0031	0.0087 ± 0.0032
7.237 ± 0.218	289 ± 54	0.0187 ± 0.0040	0.0171 ± 0.0037	0.0175 ± 0.0038
7.661 ± 0.242	268 ± 53	0.0186 ± 0.0042	0.0169 ± 0.0038	0.0174 ± 0.0039
8.126 ± 0.263	327 ± 54	0.0226 ± 0.0044	0.0206 ± 0.0040	0.0211 ± 0.0042
8.618 ± 0.284	432 ± 56	0.0291 ± 0.0048	0.0265 ± 0.0044	0.0271 ± 0.0046
9.160 ± 0.313	420 ± 56	0.0288 ± 0.0048	0.0262 ± 0.0045	0.0268 ± 0.0046
9.757 ± 0.346	496 ± 56	0.0352 ± 0.0054	0.0321 ± 0.0050	0.0329 ± 0.0051
10.414 ± 0.377	378 ± 55	0.0278 ± 0.0050	0.0253 ± 0.0046	0.0259 ± 0.0047
11.143 ± 0.425	470 ± 55	0.0368 ± 0.0057	0.0335 ± 0.0053	0.0343 ± 0.0055
11.960 ± 0.467	365 ± 52	0.0294 ± 0.0052	0.0268 ± 0.0048	0.0274 ± 0.0049
12.860 ± 0.525	457 ± 54	0.0380 ± 0.0060	0.0346 ± 0.0055	0.0353 ± 0.0057
13.876 ± 0.589	413 ± 53	0.0350 ± 0.0058	0.0319 ± 0.0053	0.0325 ± 0.0055
15.016 ± 0.660	216 ± 52	0.0183 ± 0.0048	0.0166 ± 0.0044	0.0170 ± 0.0045
16.297 ± 0.750	225 ± 51	0.0190 ± 0.0048	0.0173 ± 0.0044	0.0176 ± 0.0045
17.759 ± 0.857	304 ± 53	0.0255 ± 0.0052	0.0232 ± 0.0048	0.0237 ± 0.0049
19.416 ± 0.971	215 ± 51	0.0177 ± 0.0046	0.0161 ± 0.0042	0.0164 ± 0.0043

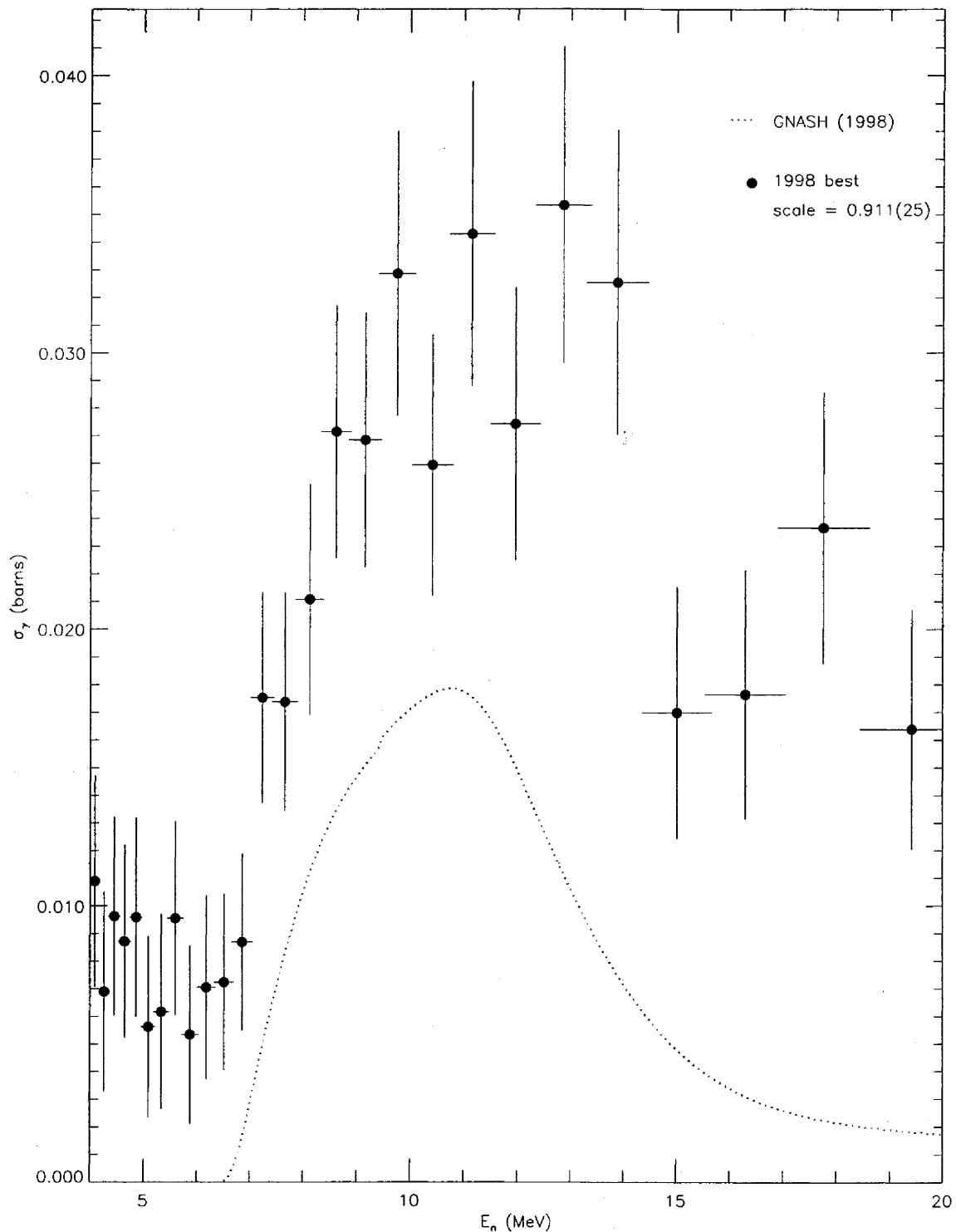


FIG. 66: Adopted $E_\gamma = 831.6$ -keV partial cross section corresponding to the data in table LXXVI, and corrected for angular-distribution effects. The target-thickness correction factor is shown, and the recommended partial cross section (solid circles) is compared to GNASH.

TABLE LXXVII: Adopted partial γ -ray cross section for the $E_\gamma = 875.5$ -keV transition. The measured peak areas and deduced partial cross section (before correction for angular distribution effects) for the **98Thin** data set are shown in columns 2 and 3, respectively. The partial cross section, listed in column 4, is obtained by scaling the **98Thin** data by a target-thickness correction factor. The recommended partial cross section in the last column includes a correction for angular-distribution effects.

E_n (MeV)	$A^{(1998)}$	$\sigma^{(1998)}$	$\sigma^{(\text{sca})}$	$\sigma^{(\text{sca,corr})}$
4.090 ± 0.093	214 ± 45	0.0195 ± 0.0046	0.0178 ± 0.0042	0.0178 ± 0.0042
4.264 ± 0.099	153 ± 45	0.0136 ± 0.0042	0.0124 ± 0.0039	0.0124 ± 0.0039
4.453 ± 0.105	119 ± 45	0.0101 ± 0.0040	0.0092 ± 0.0036	0.0092 ± 0.0036
4.647 ± 0.113	165 ± 45	0.0137 ± 0.0040	0.0124 ± 0.0036	0.0124 ± 0.0036
4.861 ± 0.122	108 ± 45	0.0090 ± 0.0039	0.0082 ± 0.0035	0.0082 ± 0.0035
5.090 ± 0.129	97 ± 45	0.0079 ± 0.0037	0.0072 ± 0.0034	0.0072 ± 0.0034
5.333 ± 0.140	164 ± 46	0.0131 ± 0.0039	0.0119 ± 0.0036	0.0127 ± 0.0038
5.597 ± 0.149	209 ± 47	0.0161 ± 0.0040	0.0147 ± 0.0036	0.0157 ± 0.0039
5.875 ± 0.160	211 ± 47	0.0160 ± 0.0039	0.0146 ± 0.0036	0.0155 ± 0.0038
6.181 ± 0.175	171 ± 46	0.0130 ± 0.0037	0.0118 ± 0.0034	0.0126 ± 0.0037
6.517 ± 0.187	155 ± 47	0.0111 ± 0.0035	0.0101 ± 0.0032	0.0108 ± 0.0035
6.862 ± 0.201	195 ± 47	0.0132 ± 0.0035	0.0120 ± 0.0032	0.0129 ± 0.0034
7.237 ± 0.218	145 ± 46	0.0102 ± 0.0034	0.0093 ± 0.0031	0.0099 ± 0.0033
7.661 ± 0.242	324 ± 48	0.0245 ± 0.0044	0.0223 ± 0.0040	0.0236 ± 0.0043
8.126 ± 0.263	352 ± 48	0.0265 ± 0.0045	0.0241 ± 0.0041	0.0254 ± 0.0044
8.618 ± 0.284	446 ± 50	0.0327 ± 0.0049	0.0298 ± 0.0045	0.0314 ± 0.0049
9.160 ± 0.313	317 ± 48	0.0237 ± 0.0043	0.0215 ± 0.0040	0.0227 ± 0.0042
9.757 ± 0.346	341 ± 48	0.0264 ± 0.0046	0.0240 ± 0.0042	0.0253 ± 0.0045
10.414 ± 0.377	424 ± 49	0.0340 ± 0.0052	0.0309 ± 0.0048	0.0326 ± 0.0051
11.143 ± 0.425	310 ± 47	0.0264 ± 0.0048	0.0240 ± 0.0044	0.0253 ± 0.0047
11.960 ± 0.467	312 ± 47	0.0274 ± 0.0050	0.0250 ± 0.0046	0.0262 ± 0.0049
12.860 ± 0.525	337 ± 48	0.0305 ± 0.0053	0.0278 ± 0.0049	0.0290 ± 0.0052
13.876 ± 0.589	272 ± 46	0.0251 ± 0.0050	0.0228 ± 0.0046	0.0239 ± 0.0048
15.016 ± 0.660	274 ± 46	0.0252 ± 0.0050	0.0230 ± 0.0046	0.0240 ± 0.0048
16.297 ± 0.750	203 ± 44	0.0187 ± 0.0045	0.0170 ± 0.0041	0.0177 ± 0.0043
17.759 ± 0.857	273 ± 46	0.0250 ± 0.0049	0.0227 ± 0.0045	0.0236 ± 0.0047
19.416 ± 0.971	149 ± 45	0.0134 ± 0.0043	0.0122 ± 0.0039	0.0126 ± 0.0040

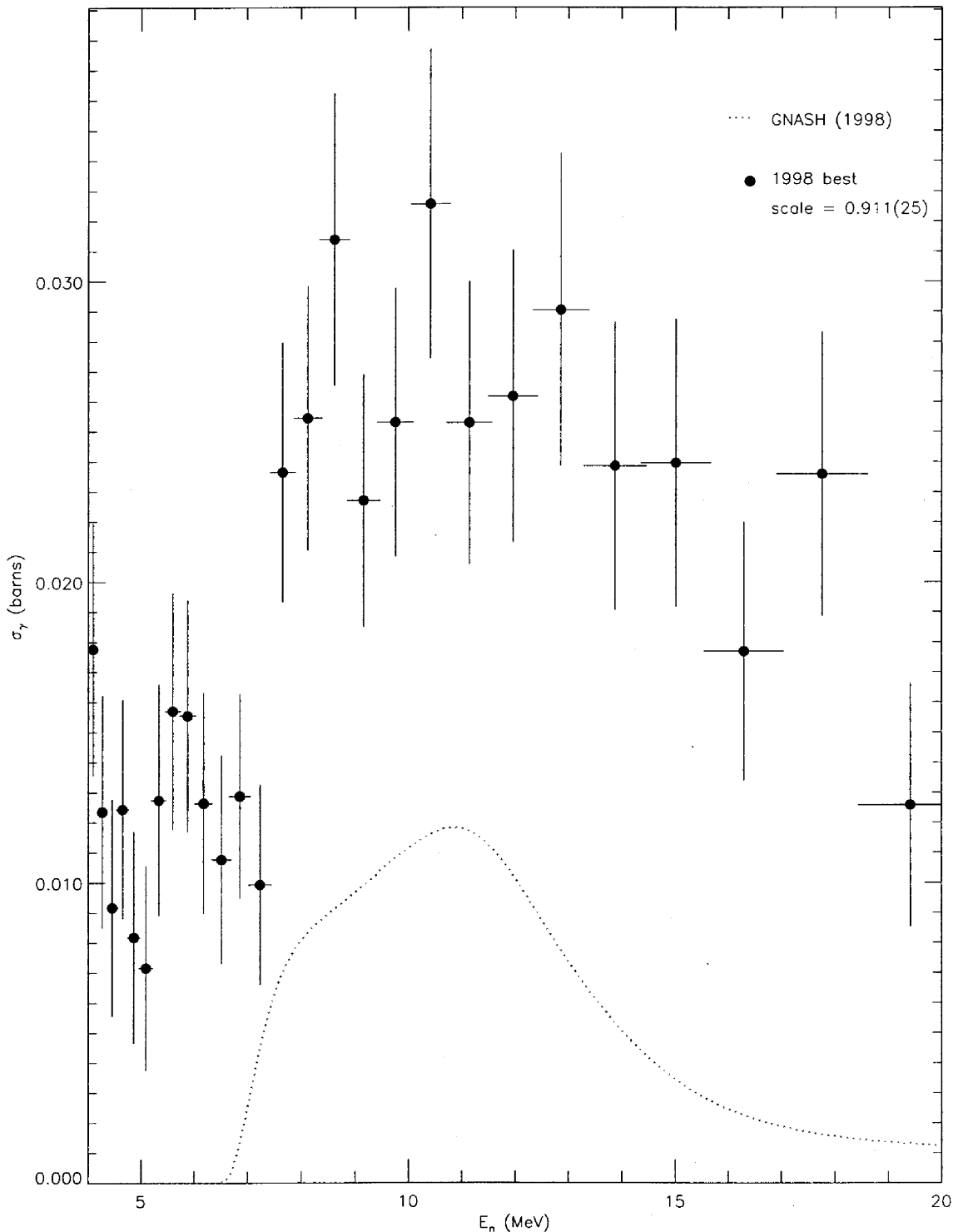


FIG. 67: Adopted $E_\gamma = 875.5$ -keV partial cross section corresponding to the data in table LXXVII, and corrected for angular-distribution effects. The target-thickness correction factor is shown, and the recommended partial cross section (solid circles) is compared to GNASH.

TABLE LXXVIII: Adopted partial γ -ray cross section for the $E_\gamma = 880.6$ -keV transition. The measured peak areas and deduced partial cross sections (before correction for angular distribution effects) for the **98Thin** and **99Thin** data sets are shown in columns 2–5. The partial cross section, listed in column 6, is obtained from both data sets using the optimization procedure described in section XII B. The recommended partial cross section in the last column includes a correction for angular-distribution effects.

E_n (MeV)	$A^{(1998)}$	$\sigma^{(1998)}$	$A^{(1999)}$	$\sigma^{(1999)}$	$\sigma^{(\text{opt})}$	$\sigma^{(\text{opt,corr})}$
4.090 ± 0.093	99 ± 45	0.0091 ± 0.0042	293 ± 67	0.0269 ± 0.0069	0.0092 ± 0.0037	0.0092 ± 0.0037
4.264 ± 0.099	112 ± 45	0.0100 ± 0.0041	287 ± 68	0.0260 ± 0.0068	0.0096 ± 0.0036	0.0097 ± 0.0036
4.453 ± 0.105	126 ± 45	0.0107 ± 0.0040	493 ± 71	0.0425 ± 0.0078	0.0138 ± 0.0036	0.0138 ± 0.0037
4.647 ± 0.113	114 ± 45	0.0095 ± 0.0039	367 ± 69	0.0308 ± 0.0068	0.0105 ± 0.0034	0.0105 ± 0.0035
4.861 ± 0.122	149 ± 46	0.0124 ± 0.0040	321 ± 70	0.0265 ± 0.0065	0.0116 ± 0.0035	0.0116 ± 0.0036
5.090 ± 0.129	149 ± 47	0.0121 ± 0.0040	314 ± 70	0.0253 ± 0.0063	0.0110 ± 0.0035	0.0110 ± 0.0035
5.333 ± 0.140	180 ± 47	0.0144 ± 0.0040	478 ± 73	0.0385 ± 0.0073	0.0161 ± 0.0037	0.0165 ± 0.0038
5.597 ± 0.149	203 ± 48	0.0157 ± 0.0040	276 ± 71	0.0220 ± 0.0062	0.0124 ± 0.0035	0.0128 ± 0.0036
5.875 ± 0.160	190 ± 47	0.0145 ± 0.0039	354 ± 73	0.0276 ± 0.0065	0.0134 ± 0.0035	0.0138 ± 0.0035
6.181 ± 0.175	120 ± 46	0.0092 ± 0.0036	475 ± 74	0.0364 ± 0.0070	0.0113 ± 0.0033	0.0116 ± 0.0034
6.517 ± 0.187	151 ± 48	0.0108 ± 0.0036	416 ± 72	0.0304 ± 0.0063	0.0114 ± 0.0032	0.0117 ± 0.0033
6.862 ± 0.201	360 ± 50	0.0245 ± 0.0042	479 ± 73	0.0342 ± 0.0065	0.0222 ± 0.0038	0.0228 ± 0.0039
7.237 ± 0.218	349 ± 50	0.0247 ± 0.0043	467 ± 73	0.0354 ± 0.0068	0.0228 ± 0.0039	0.0234 ± 0.0040
7.661 ± 0.242	571 ± 51	0.0433 ± 0.0058	676 ± 72	0.0548 ± 0.0085	0.0414 ± 0.0052	0.0424 ± 0.0054
8.126 ± 0.263	539 ± 51	0.0407 ± 0.0056	843 ± 76	0.0676 ± 0.0097	0.0438 ± 0.0053	0.0447 ± 0.0055
8.618 ± 0.284	665 ± 53	0.0490 ± 0.0062	839 ± 74	0.0658 ± 0.0094	0.0491 ± 0.0057	0.0502 ± 0.0059
9.160 ± 0.313	625 ± 52	0.0468 ± 0.0061	901 ± 76	0.0719 ± 0.0101	0.0496 ± 0.0057	0.0507 ± 0.0059
9.757 ± 0.346	595 ± 51	0.0462 ± 0.0061	919 ± 73	0.0765 ± 0.0105	0.0504 ± 0.0058	0.0516 ± 0.0060
10.414 ± 0.377	526 ± 51	0.0423 ± 0.0059	692 ± 72	0.0600 ± 0.0092	0.0427 ± 0.0054	0.0437 ± 0.0056
11.143 ± 0.425	551 ± 51	0.0471 ± 0.0065	754 ± 69	0.0691 ± 0.0101	0.0490 ± 0.0059	0.0502 ± 0.0061
11.960 ± 0.467	511 ± 50	0.0450 ± 0.0063	688 ± 70	0.0655 ± 0.0100	0.0464 ± 0.0058	0.0475 ± 0.0060
12.860 ± 0.525	469 ± 49	0.0426 ± 0.0062	702 ± 70	0.0682 ± 0.0103	0.0454 ± 0.0058	0.0464 ± 0.0059
13.876 ± 0.589	398 ± 49	0.0369 ± 0.0059	457 ± 66	0.0455 ± 0.0084	0.0339 ± 0.0052	0.0346 ± 0.0053
15.016 ± 0.660	382 ± 48	0.0353 ± 0.0057	563 ± 66	0.0562 ± 0.0092	0.0367 ± 0.0052	0.0374 ± 0.0053
16.297 ± 0.750	282 ± 45	0.0261 ± 0.0049	393 ± 66	0.0389 ± 0.0079	0.0248 ± 0.0044	0.0253 ± 0.0045
17.759 ± 0.857	229 ± 46	0.0210 ± 0.0047	362 ± 65	0.0353 ± 0.0075	0.0202 ± 0.0042	0.0206 ± 0.0043
19.416 ± 0.971	243 ± 46	0.0219 ± 0.0047	368 ± 65	0.0350 ± 0.0074	0.0207 ± 0.0042	0.0211 ± 0.0042

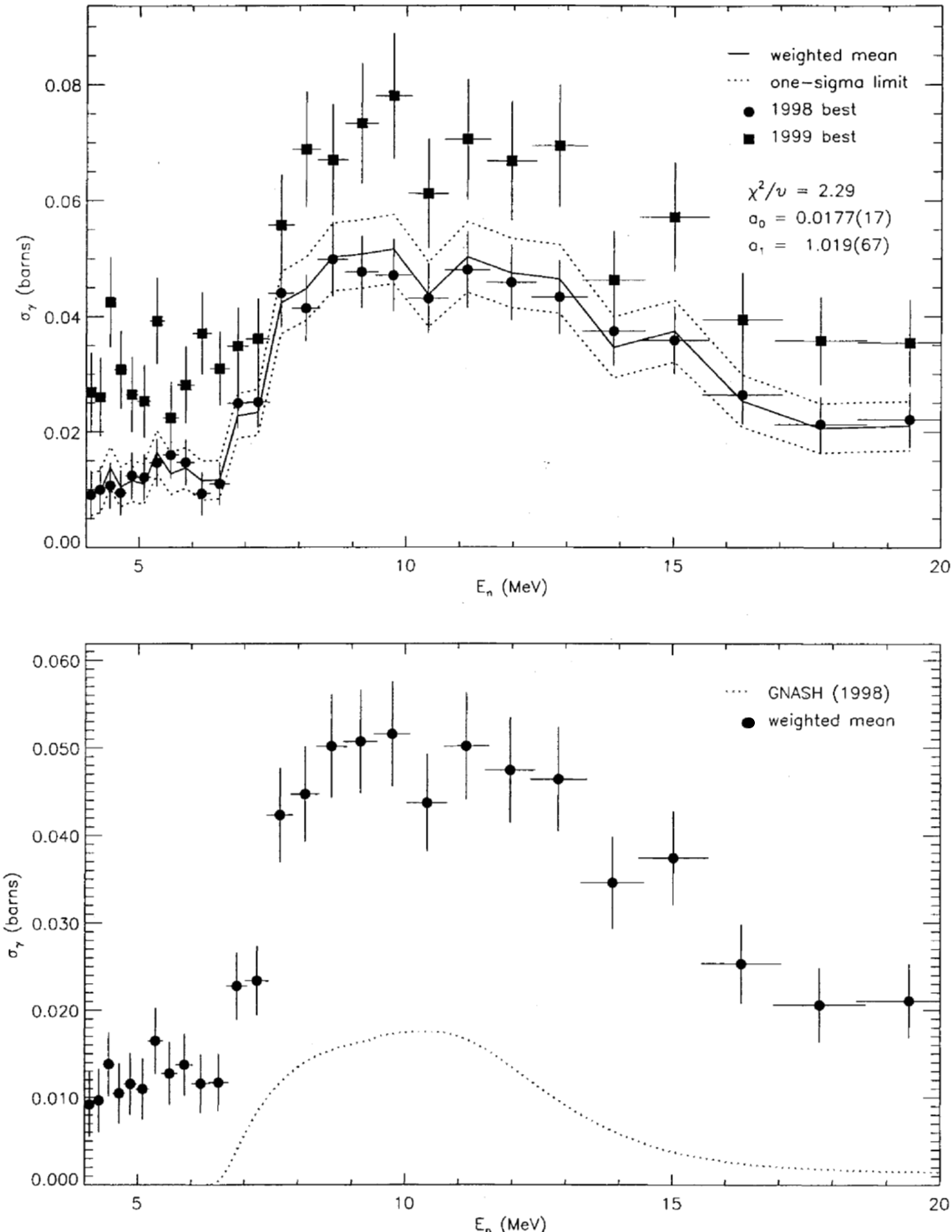


FIG. 68: Adopted $E_\gamma = 880.6$ -keV partial cross section corresponding to the data in table LXXVIII. The top panel shows the 1998 and 1999 partial cross sections (corrected for angular-distribution effects) and the recommended value, plotted as a solid line with a one-sigma confidence band (dotted lines). The bottom panel shows this recommended partial cross section (solid circles) compared to GNASH.

TABLE LXXIX: Adopted partial γ -ray cross section for the $E_\gamma = 883.4$ -keV transition. The measured peak areas and deduced partial cross sections (before correction for angular distribution effects) for the **98Thin** and **99Thin** data sets are shown in columns 2–5. The partial cross section, listed in column 6, is obtained from both data sets using the optimization procedure described in section XII B. The recommended partial cross section in the last column includes a correction for angular-distribution effects.

E_n (MeV)	$A^{(1998)}$	$\sigma^{(1998)}$	$A^{(1999)}$	$\sigma^{(1999)}$	$\sigma^{(\text{opt})}$	$\sigma^{(\text{opt,corr})}$
4.090 ± 0.093	78 ± 44	0.0073 ± 0.0044	79 ± 53	0.0074 ± 0.0053	0.0064 ± 0.0036	0.0064 ± 0.0036
4.264 ± 0.099	0 ± 0	0.0001 ± 0.0015	4 ± 51	0.0004 ± 0.0050	-0.0001 ± 0.0015	-0.0001 ± 0.0015
4.453 ± 0.105	0 ± 0	0.0001 ± 0.0014	60 ± 55	0.0053 ± 0.0051	0.0003 ± 0.0014	0.0003 ± 0.0014
4.647 ± 0.113	0 ± 0	0.0001 ± 0.0014	0 ± 0	0.0001 ± 0.0015	-0.0011 ± 0.0011	-0.0011 ± 0.0011
4.861 ± 0.122	21 ± 44	0.0018 ± 0.0040	92 ± 57	0.0077 ± 0.0051	0.0032 ± 0.0033	0.0032 ± 0.0033
5.090 ± 0.129	150 ± 46	0.0124 ± 0.0042	116 ± 57	0.0095 ± 0.0050	0.0104 ± 0.0034	0.0104 ± 0.0035
5.333 ± 0.140	49 ± 45	0.0040 ± 0.0039	145 ± 58	0.0119 ± 0.0051	0.0063 ± 0.0033	0.0063 ± 0.0033
5.597 ± 0.149	42 ± 45	0.0033 ± 0.0038	134 ± 58	0.0109 ± 0.0051	0.0054 ± 0.0032	0.0054 ± 0.0032
5.875 ± 0.160	12 ± 44	0.0009 ± 0.0036	99 ± 58	0.0079 ± 0.0049	0.0026 ± 0.0031	0.0026 ± 0.0031
6.181 ± 0.175	156 ± 46	0.0121 ± 0.0040	32 ± 57	0.0025 ± 0.0047	0.0069 ± 0.0032	0.0069 ± 0.0033
6.517 ± 0.187	119 ± 47	0.0087 ± 0.0037	121 ± 58	0.0090 ± 0.0046	0.0081 ± 0.0031	0.0081 ± 0.0031
6.862 ± 0.201	175 ± 47	0.0121 ± 0.0037	286 ± 60	0.0208 ± 0.0051	0.0151 ± 0.0032	0.0152 ± 0.0032
7.237 ± 0.218	174 ± 48	0.0126 ± 0.0039	204 ± 59	0.0158 ± 0.0051	0.0134 ± 0.0033	0.0135 ± 0.0033
7.661 ± 0.242	125 ± 46	0.0097 ± 0.0039	334 ± 59	0.0276 ± 0.0059	0.0154 ± 0.0035	0.0154 ± 0.0035
8.126 ± 0.263	221 ± 47	0.0170 ± 0.0042	237 ± 59	0.0194 ± 0.0055	0.0177 ± 0.0036	0.0178 ± 0.0036
8.618 ± 0.284	262 ± 49	0.0197 ± 0.0043	240 ± 59	0.0192 ± 0.0054	0.0191 ± 0.0037	0.0192 ± 0.0037
9.160 ± 0.313	273 ± 49	0.0209 ± 0.0045	230 ± 58	0.0187 ± 0.0053	0.0195 ± 0.0037	0.0196 ± 0.0038
9.757 ± 0.346	137 ± 45	0.0109 ± 0.0039	177 ± 56	0.0150 ± 0.0052	0.0120 ± 0.0034	0.0121 ± 0.0034
10.414 ± 0.377	175 ± 47	0.0143 ± 0.0043	246 ± 56	0.0217 ± 0.0057	0.0170 ± 0.0037	0.0171 ± 0.0037
11.143 ± 0.425	243 ± 48	0.0212 ± 0.0049	231 ± 55	0.0216 ± 0.0059	0.0211 ± 0.0041	0.0212 ± 0.0041
11.960 ± 0.467	196 ± 46	0.0176 ± 0.0047	271 ± 54	0.0263 ± 0.0063	0.0210 ± 0.0041	0.0211 ± 0.0041
12.860 ± 0.525	226 ± 47	0.0209 ± 0.0051	225 ± 54	0.0223 ± 0.0062	0.0213 ± 0.0042	0.0214 ± 0.0043
13.876 ± 0.589	188 ± 46	0.0177 ± 0.0049	261 ± 53	0.0265 ± 0.0064	0.0212 ± 0.0042	0.0213 ± 0.0043
15.016 ± 0.660	122 ± 43	0.0115 ± 0.0045	207 ± 52	0.0211 ± 0.0061	0.0148 ± 0.0039	0.0149 ± 0.0039
16.297 ± 0.750	168 ± 43	0.0158 ± 0.0046	290 ± 53	0.0292 ± 0.0065	0.0208 ± 0.0041	0.0208 ± 0.0041
17.759 ± 0.857	148 ± 45	0.0138 ± 0.0047	186 ± 52	0.0185 ± 0.0058	0.0154 ± 0.0039	0.0154 ± 0.0039
19.416 ± 0.971	118 ± 44	0.0108 ± 0.0044	172 ± 52	0.0167 ± 0.0056	0.0127 ± 0.0037	0.0127 ± 0.0037

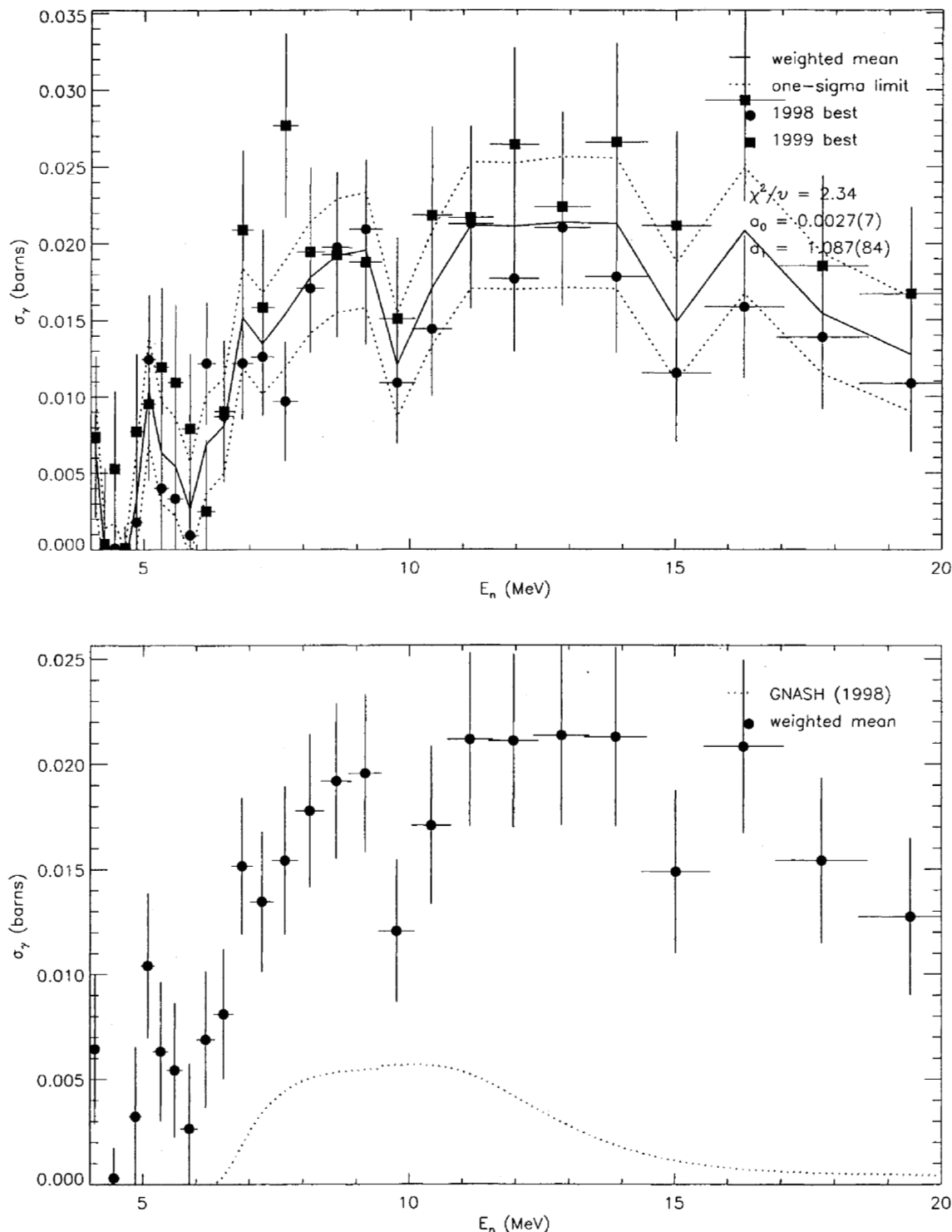


FIG. 69: Adopted $E_\gamma = 883.4$ -keV partial cross section corresponding to the data in table LXXIX. The top panel shows the 1998 and 1999 partial cross sections (corrected for angular-distribution effects) and the recommended value, plotted as a solid line with a one-sigma confidence band (dotted lines). The bottom panel shows this recommended partial cross section (solid circles) compared to GNASH.

TABLE LXXX: Adopted partial γ -ray cross section for the $E_\gamma = 898.3$ -keV transition. The measured peak areas and deduced partial cross section (before correction for angular distribution effects) for the **98Thin** data set are shown in columns 2 and 3, respectively. The partial cross section, listed in column 4, is obtained by scaling the **98Thin** data by a target-thickness correction factor. The recommended partial cross section in the last column includes a correction for angular-distribution effects.

E_n (MeV)	$A^{(1998)}$	$\sigma^{(1998)}$	$\sigma^{(\text{sca})}$	$\sigma^{(\text{sca,corr})}$
4.090 \pm 0.093	258 \pm 48	0.0244 \pm 0.0052	0.0222 \pm 0.0047	0.0222 \pm 0.0047
4.264 \pm 0.099	215 \pm 48	0.0198 \pm 0.0048	0.0180 \pm 0.0044	0.0180 \pm 0.0044
4.453 \pm 0.105	139 \pm 47	0.0122 \pm 0.0043	0.0111 \pm 0.0039	0.0111 \pm 0.0039
4.647 \pm 0.113	115 \pm 46	0.0099 \pm 0.0041	0.0090 \pm 0.0037	0.0090 \pm 0.0037
4.861 \pm 0.122	41 \pm 45	0.0035 \pm 0.0039	0.0032 \pm 0.0036	0.0032 \pm 0.0036
5.090 \pm 0.129	189 \pm 49	0.0159 \pm 0.0044	0.0145 \pm 0.0040	0.0145 \pm 0.0040
5.333 \pm 0.140	79 \pm 47	0.0065 \pm 0.0039	0.0060 \pm 0.0036	0.0054 \pm 0.0033
5.597 \pm 0.149	176 \pm 49	0.0141 \pm 0.0042	0.0128 \pm 0.0038	0.0117 \pm 0.0035
5.875 \pm 0.160	114 \pm 47	0.0090 \pm 0.0038	0.0082 \pm 0.0035	0.0075 \pm 0.0032
6.181 \pm 0.175	108 \pm 47	0.0085 \pm 0.0038	0.0078 \pm 0.0035	0.0071 \pm 0.0032
6.517 \pm 0.187	124 \pm 48	0.0092 \pm 0.0037	0.0084 \pm 0.0034	0.0076 \pm 0.0031
6.862 \pm 0.201	100 \pm 48	0.0070 \pm 0.0035	0.0064 \pm 0.0031	0.0059 \pm 0.0029
7.237 \pm 0.218	182 \pm 48	0.0133 \pm 0.0038	0.0121 \pm 0.0034	0.0111 \pm 0.0031
7.661 \pm 0.242	138 \pm 47	0.0108 \pm 0.0038	0.0099 \pm 0.0035	0.0091 \pm 0.0032
8.126 \pm 0.263	240 \pm 49	0.0188 \pm 0.0042	0.0171 \pm 0.0039	0.0158 \pm 0.0036
8.618 \pm 0.284	223 \pm 48	0.0170 \pm 0.0040	0.0155 \pm 0.0037	0.0144 \pm 0.0034
9.160 \pm 0.313	306 \pm 49	0.0237 \pm 0.0044	0.0216 \pm 0.0041	0.0200 \pm 0.0038
9.757 \pm 0.346	323 \pm 49	0.0260 \pm 0.0047	0.0236 \pm 0.0043	0.0219 \pm 0.0040
10.414 \pm 0.377	345 \pm 50	0.0287 \pm 0.0050	0.0261 \pm 0.0046	0.0242 \pm 0.0043
11.143 \pm 0.425	245 \pm 48	0.0217 \pm 0.0048	0.0198 \pm 0.0044	0.0183 \pm 0.0041
11.960 \pm 0.467	240 \pm 47	0.0219 \pm 0.0048	0.0199 \pm 0.0044	0.0186 \pm 0.0041
12.860 \pm 0.525	246 \pm 47	0.0231 \pm 0.0050	0.0211 \pm 0.0046	0.0197 \pm 0.0043
13.876 \pm 0.589	308 \pm 47	0.0295 \pm 0.0054	0.0269 \pm 0.0050	0.0251 \pm 0.0047
15.016 \pm 0.660	247 \pm 46	0.0237 \pm 0.0050	0.0215 \pm 0.0046	0.0202 \pm 0.0043
16.297 \pm 0.750	198 \pm 47	0.0189 \pm 0.0049	0.0172 \pm 0.0045	0.0162 \pm 0.0042
17.759 \pm 0.857	205 \pm 47	0.0195 \pm 0.0049	0.0177 \pm 0.0045	0.0167 \pm 0.0042
19.416 \pm 0.971	221 \pm 47	0.0206 \pm 0.0048	0.0188 \pm 0.0044	0.0178 \pm 0.0042

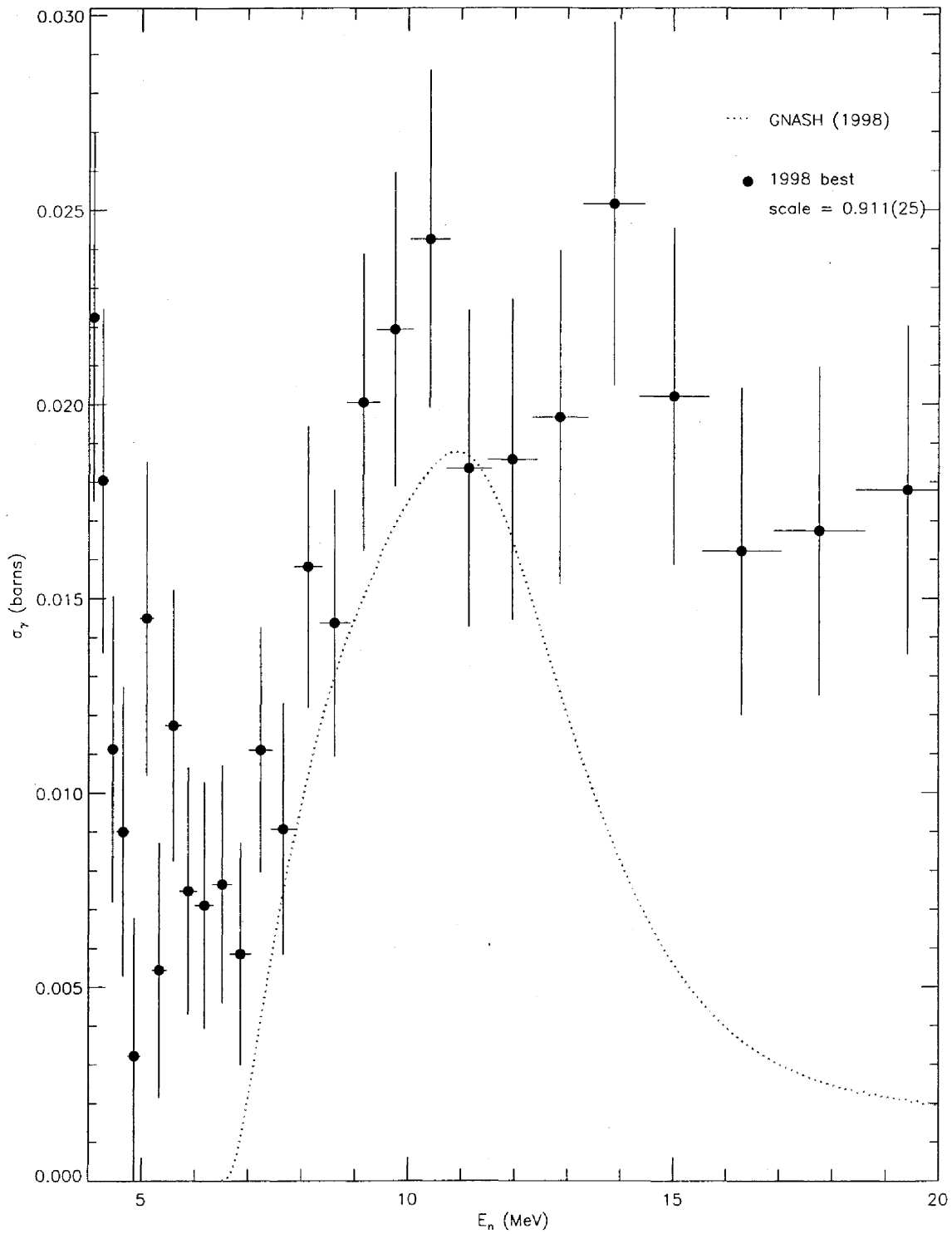


FIG. 70: Adopted $E_\gamma = 898.3$ -keV partial cross section corresponding to the data in table LXXX, and corrected for angular-distribution effects. The target-thickness correction factor is shown, and the recommended partial cross section (solid circles) is compared to GNASH.

TABLE LXXXI: Adopted partial γ -ray cross section for the $E_\gamma = 925.3$ -keV transition. The measured peak areas and deduced partial cross sections (before correction for angular distribution effects) for the **98Thin** and **99Thin** data sets are shown in columns 2–5. The partial cross section, listed in column 6, is obtained from both data sets using the optimization procedure described in section XII B. The recommended partial cross section in the last column includes a correction for angular-distribution effects.

E_n (MeV)	$A^{(1998)}$	$\sigma^{(1998)}$	$A^{(1999)}$	$\sigma^{(1999)}$	$\sigma^{(\text{opt})}$	$\sigma^{(\text{opt,corr})}$
4.090 ± 0.093	5 ± 38	0.0005 ± 0.0039	70 ± 46	0.0069 ± 0.0046	0.0013 ± 0.0024	0.0013 ± 0.0023
4.264 ± 0.099	122 ± 42	0.0116 ± 0.0043	166 ± 48	0.0161 ± 0.0050	0.0095 ± 0.0027	0.0095 ± 0.0026
4.453 ± 0.105	133 ± 41	0.0121 ± 0.0041	1 ± 19	0.0001 ± 0.0018	0.0013 ± 0.0018	0.0013 ± 0.0017
4.647 ± 0.113	95 ± 42	0.0085 ± 0.0040	85 ± 49	0.0076 ± 0.0045	0.0056 ± 0.0024	0.0056 ± 0.0024
4.861 ± 0.122	118 ± 44	0.0106 ± 0.0042	22 ± 49	0.0019 ± 0.0043	0.0049 ± 0.0025	0.0048 ± 0.0025
5.090 ± 0.129	65 ± 43	0.0057 ± 0.0039	120 ± 50	0.0103 ± 0.0045	0.0049 ± 0.0024	0.0049 ± 0.0024
5.333 ± 0.140	72 ± 42	0.0062 ± 0.0038	17 ± 51	0.0015 ± 0.0044	0.0029 ± 0.0023	0.0027 ± 0.0022
5.597 ± 0.149	87 ± 44	0.0072 ± 0.0038	24 ± 50	0.0020 ± 0.0043	0.0035 ± 0.0023	0.0033 ± 0.0022
5.875 ± 0.160	22 ± 42	0.0018 ± 0.0035	86 ± 51	0.0072 ± 0.0043	0.0020 ± 0.0022	0.0019 ± 0.0021
6.181 ± 0.175	55 ± 43	0.0045 ± 0.0037	88 ± 52	0.0072 ± 0.0043	0.0035 ± 0.0022	0.0033 ± 0.0021
6.517 ± 0.187	83 ± 44	0.0064 ± 0.0035	34 ± 52	0.0027 ± 0.0041	0.0033 ± 0.0022	0.0031 ± 0.0021
6.862 ± 0.201	100 ± 46	0.0073 ± 0.0035	135 ± 53	0.0103 ± 0.0042	0.0057 ± 0.0022	0.0054 ± 0.0021
7.237 ± 0.218	170 ± 46	0.0129 ± 0.0038	209 ± 54	0.0169 ± 0.0048	0.0103 ± 0.0024	0.0098 ± 0.0023
7.661 ± 0.242	399 ± 49	0.0324 ± 0.0052	271 ± 53	0.0235 ± 0.0053	0.0219 ± 0.0033	0.0209 ± 0.0032
8.126 ± 0.263	448 ± 50	0.0363 ± 0.0055	273 ± 53	0.0234 ± 0.0052	0.0234 ± 0.0035	0.0223 ± 0.0033
8.618 ± 0.284	451 ± 48	0.0356 ± 0.0052	332 ± 54	0.0278 ± 0.0055	0.0249 ± 0.0034	0.0238 ± 0.0033
9.160 ± 0.313	476 ± 51	0.0382 ± 0.0056	292 ± 53	0.0249 ± 0.0053	0.0247 ± 0.0035	0.0236 ± 0.0034
9.757 ± 0.346	474 ± 50	0.0394 ± 0.0058	289 ± 52	0.0257 ± 0.0054	0.0256 ± 0.0036	0.0244 ± 0.0035
10.414 ± 0.377	504 ± 50	0.0434 ± 0.0061	491 ± 54	0.0455 ± 0.0071	0.0345 ± 0.0042	0.0329 ± 0.0041
11.143 ± 0.425	451 ± 48	0.0413 ± 0.0061	440 ± 52	0.0431 ± 0.0070	0.0327 ± 0.0041	0.0312 ± 0.0040
11.960 ± 0.467	526 ± 49	0.0497 ± 0.0068	211 ± 49	0.0215 ± 0.0055	0.0265 ± 0.0041	0.0252 ± 0.0039
12.860 ± 0.525	245 ± 46	0.0238 ± 0.0052	322 ± 50	0.0334 ± 0.0064	0.0204 ± 0.0034	0.0195 ± 0.0033
13.876 ± 0.589	298 ± 44	0.0296 ± 0.0054	260 ± 50	0.0276 ± 0.0062	0.0220 ± 0.0035	0.0210 ± 0.0034
15.016 ± 0.660	191 ± 43	0.0189 ± 0.0048	174 ± 49	0.0186 ± 0.0056	0.0139 ± 0.0030	0.0133 ± 0.0029
16.297 ± 0.750	93 ± 43	0.0092 ± 0.0045	202 ± 48	0.0213 ± 0.0056	0.0093 ± 0.0028	0.0089 ± 0.0027
17.759 ± 0.857	149 ± 45	0.0146 ± 0.0048	61 ± 47	0.0064 ± 0.0050	0.0081 ± 0.0029	0.0078 ± 0.0028
19.416 ± 0.971	116 ± 44	0.0112 ± 0.0045	59 ± 47	0.0060 ± 0.0048	0.0065 ± 0.0027	0.0062 ± 0.0026

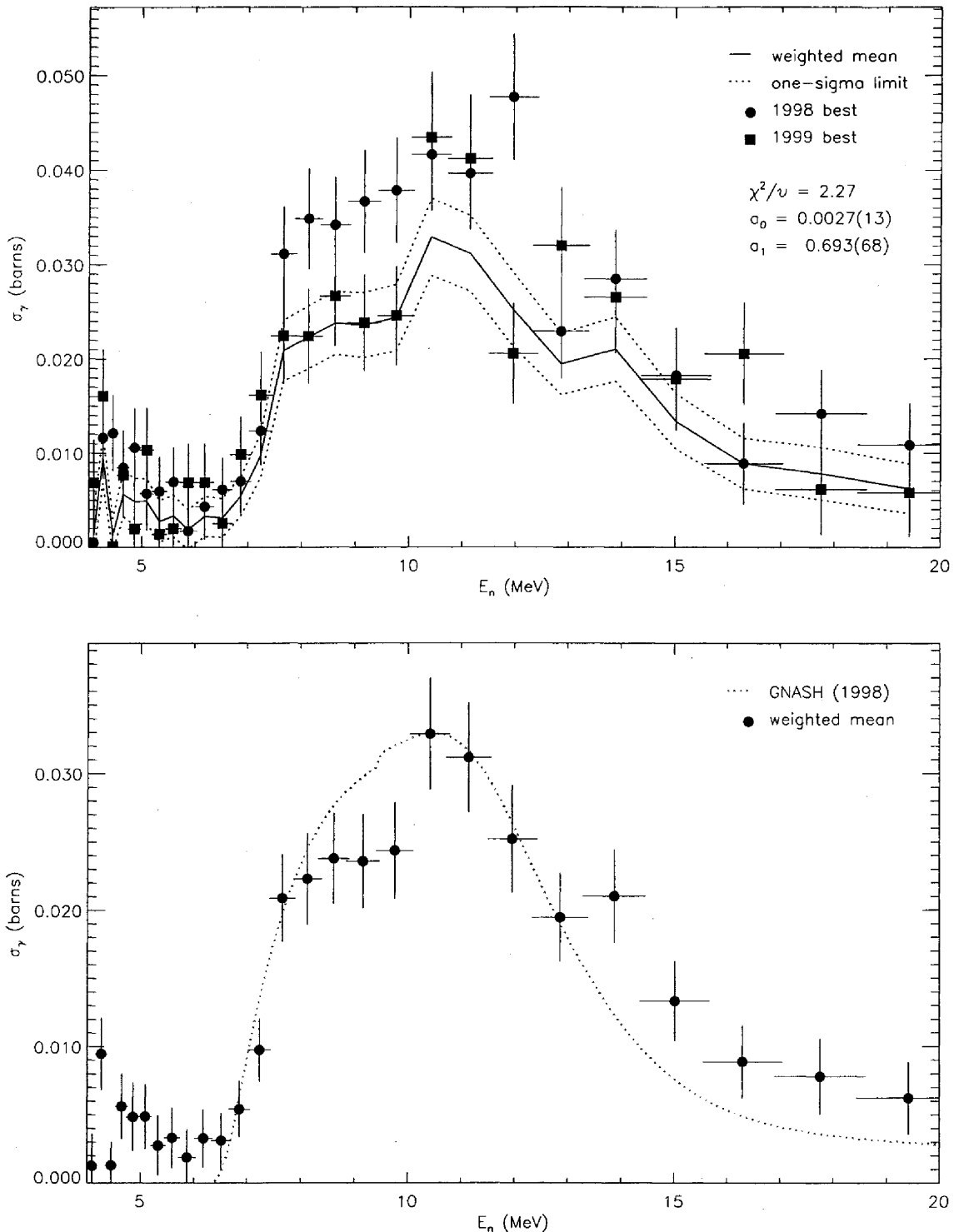


FIG. 71: Adopted $E_\gamma = 925.3$ -keV partial cross section corresponding to the data in table LXXXI. The top panel shows the 1998 and 1999 partial cross sections (corrected for angular-distribution effects) and the recommended value, plotted as a solid line with a one-sigma confidence band (dotted lines). The bottom panel shows this recommended partial cross section (solid circles) compared to GNASH.

TABLE LXXXII: Adopted partial γ -ray cross section for the $E_\gamma = 946.1$ -keV transition. The measured peak areas and deduced partial cross sections (before correction for angular distribution effects) for the **98Thin** and **99Thin** data sets are shown in columns 2–5. The partial cross section, listed in column 6, is obtained from both data sets using the optimization procedure described in section XII B. The recommended partial cross section in the last column includes a correction for angular-distribution effects.

E_n (MeV)	$A^{(1998)}$	$\sigma^{(1998)}$	$A^{(1999)}$	$\sigma^{(1999)}$	$\sigma^{(\text{opt})}$	$\sigma^{(\text{opt,corr})}$
4.090 ± 0.093	0 ± 0	0.0001 ± 0.0009	0 ± 0	0.0001 ± 0.0007	-0.0026 ± 0.0005	-0.0026 ± 0.0005
4.264 ± 0.099	0 ± 0	0.0001 ± 0.0009	73 ± 46	0.0073 ± 0.0047	0.0001 ± 0.0006	0.0001 ± 0.0006
4.453 ± 0.105	0 ± 0	0.0001 ± 0.0009	72 ± 49	0.0068 ± 0.0047	0.0001 ± 0.0006	0.0001 ± 0.0006
4.647 ± 0.113	0 ± 1	0.0001 ± 0.0008	60 ± 50	0.0055 ± 0.0047	0.0001 ± 0.0006	0.0001 ± 0.0006
4.861 ± 0.122	29 ± 41	0.0027 ± 0.0039	71 ± 51	0.0064 ± 0.0047	0.0014 ± 0.0023	0.0014 ± 0.0023
5.090 ± 0.129	0 ± 0	0.0001 ± 0.0008	80 ± 52	0.0071 ± 0.0047	0.0001 ± 0.0006	0.0001 ± 0.0006
5.333 ± 0.140	0 ± 0	0.0001 ± 0.0008	93 ± 53	0.0082 ± 0.0048	0.0001 ± 0.0005	0.0001 ± 0.0005
5.597 ± 0.149	0 ± 2	0.0001 ± 0.0008	115 ± 53	0.0101 ± 0.0048	0.0001 ± 0.0005	0.0001 ± 0.0005
5.875 ± 0.160	0 ± 0	0.0001 ± 0.0008	58 ± 54	0.0050 ± 0.0047	0.0000 ± 0.0005	0.0000 ± 0.0005
6.181 ± 0.175	0 ± 0	0.0001 ± 0.0008	58 ± 53	0.0049 ± 0.0045	0.0000 ± 0.0005	0.0000 ± 0.0005
6.517 ± 0.187	0 ± 3	0.0001 ± 0.0008	56 ± 54	0.0045 ± 0.0044	0.0000 ± 0.0005	0.0000 ± 0.0005
6.862 ± 0.201	64 ± 45	0.0048 ± 0.0035	162 ± 55	0.0127 ± 0.0046	0.0040 ± 0.0021	0.0040 ± 0.0021
7.237 ± 0.218	149 ± 46	0.0117 ± 0.0038	109 ± 54	0.0091 ± 0.0046	0.0067 ± 0.0023	0.0067 ± 0.0023
7.661 ± 0.242	159 ± 45	0.0133 ± 0.0041	252 ± 53	0.0225 ± 0.0054	0.0108 ± 0.0025	0.0107 ± 0.0025
8.126 ± 0.263	343 ± 47	0.0286 ± 0.0049	289 ± 56	0.0255 ± 0.0057	0.0196 ± 0.0031	0.0194 ± 0.0031
8.618 ± 0.284	357 ± 48	0.0290 ± 0.0049	261 ± 55	0.0225 ± 0.0054	0.0188 ± 0.0030	0.0187 ± 0.0030
9.160 ± 0.313	415 ± 49	0.0344 ± 0.0053	520 ± 58	0.0457 ± 0.0072	0.0275 ± 0.0035	0.0273 ± 0.0035
9.757 ± 0.346	518 ± 50	0.0445 ± 0.0062	471 ± 57	0.0431 ± 0.0071	0.0326 ± 0.0040	0.0324 ± 0.0040
10.414 ± 0.377	522 ± 48	0.0464 ± 0.0063	366 ± 54	0.0349 ± 0.0065	0.0307 ± 0.0039	0.0305 ± 0.0039
11.143 ± 0.425	381 ± 46	0.0360 ± 0.0057	285 ± 52	0.0287 ± 0.0062	0.0240 ± 0.0036	0.0238 ± 0.0035
11.960 ± 0.467	450 ± 47	0.0439 ± 0.0064	311 ± 53	0.0326 ± 0.0067	0.0288 ± 0.0040	0.0286 ± 0.0040
12.860 ± 0.525	306 ± 45	0.0307 ± 0.0055	269 ± 50	0.0287 ± 0.0063	0.0216 ± 0.0035	0.0214 ± 0.0034
13.876 ± 0.589	220 ± 43	0.0225 ± 0.0050	230 ± 49	0.0252 ± 0.0061	0.0164 ± 0.0031	0.0163 ± 0.0031
15.016 ± 0.660	165 ± 42	0.0169 ± 0.0047	28 ± 47	0.0031 ± 0.0052	0.0073 ± 0.0028	0.0072 ± 0.0028
16.297 ± 0.750	43 ± 40	0.0044 ± 0.0042	17 ± 47	0.0018 ± 0.0052	0.0012 ± 0.0025	0.0012 ± 0.0025
17.759 ± 0.857	57 ± 42	0.0058 ± 0.0044	0 ± 5	0.0001 ± 0.0009	-0.0053 ± 0.0009	-0.0053 ± 0.0009
19.416 ± 0.971	0 ± 0	0.0001 ± 0.0009	111 ± 48	0.0116 ± 0.0052	0.0001 ± 0.0006	0.0001 ± 0.0006

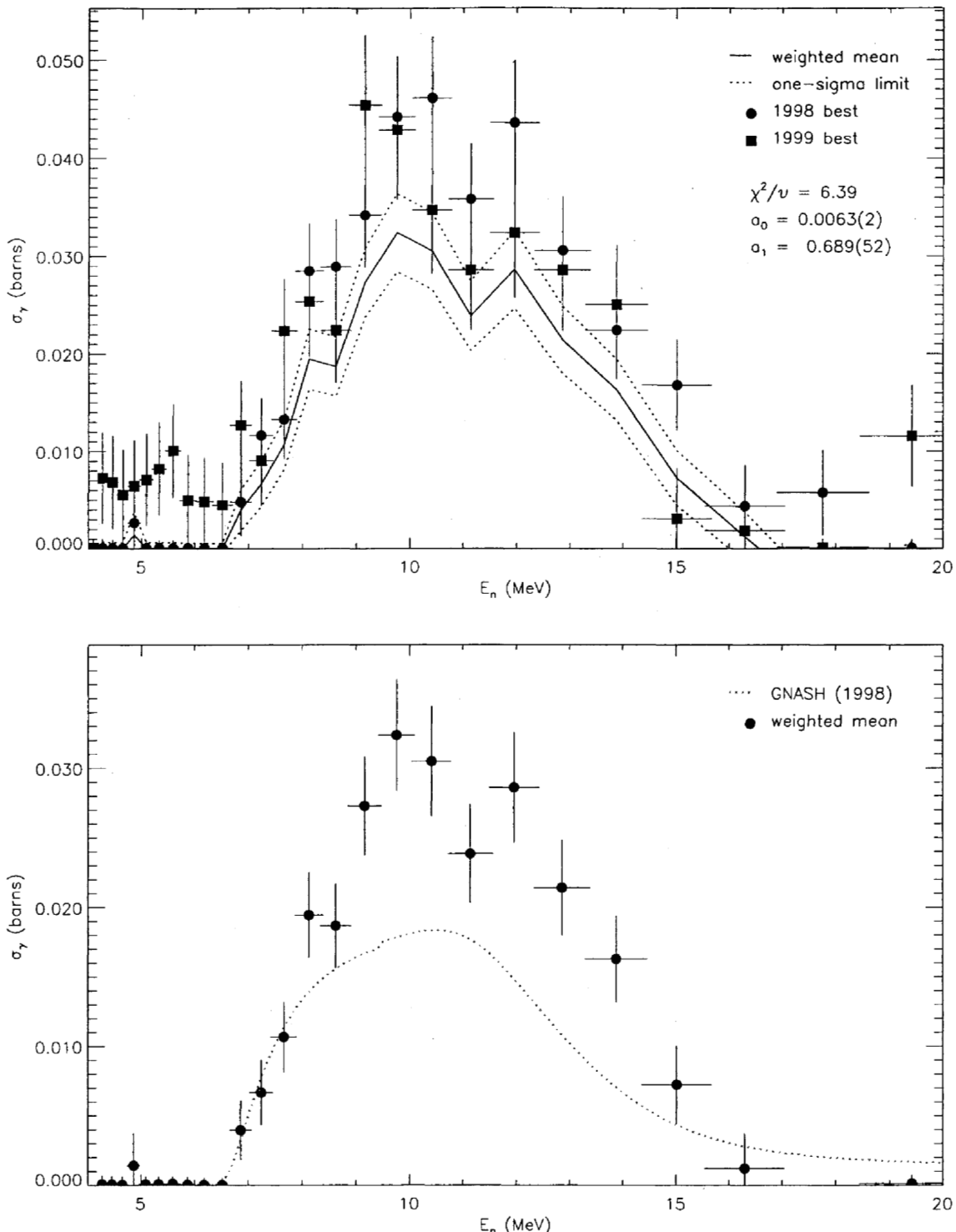


FIG. 72: Adopted $E_\gamma = 946.1$ -keV partial cross section corresponding to the data in table LXXXII. The top panel shows the 1998 and 1999 partial cross sections (corrected for angular-distribution effects) and the recommended value, plotted as a solid line with a one-sigma confidence band (dotted lines). The bottom panel shows this recommended partial cross section (solid circles) compared to GNASH.

TABLE LXXXIII: Adopted partial γ -ray cross section for the $E_\gamma = 966.3$ -keV transition. The measured peak areas and deduced partial cross section (before correction for angular distribution effects) for the **98Thin** data set are shown in columns 2 and 3, respectively. The partial cross section, listed in column 4, is obtained by scaling the **98Thin** data by a target-thickness correction factor. The recommended partial cross section in the last column includes a correction for angular-distribution effects.

E_n (MeV)	$A^{(1998)}$	$\sigma^{(1998)}$	$\sigma^{(\text{sca})}$	$\sigma^{(\text{sca,corr})}$
4.090 \pm 0.093	6 \pm 40	0.0003 \pm 0.0020	0.0003 \pm 0.0019	0.0003 \pm 0.0019
4.264 \pm 0.099	121 \pm 42	0.0060 \pm 0.0022	0.0055 \pm 0.0020	0.0055 \pm 0.0020
4.453 \pm 0.105	42 \pm 41	0.0020 \pm 0.0019	0.0018 \pm 0.0018	0.0018 \pm 0.0018
4.647 \pm 0.113	69 \pm 43	0.0032 \pm 0.0020	0.0029 \pm 0.0018	0.0029 \pm 0.0018
4.861 \pm 0.122	50 \pm 43	0.0023 \pm 0.0020	0.0021 \pm 0.0018	0.0021 \pm 0.0018
5.090 \pm 0.129	0 \pm 0	0.0000 \pm 0.0000	0.0000 \pm 0.0000	0.0000 \pm 0.0000
5.333 \pm 0.140	118 \pm 45	0.0052 \pm 0.0021	0.0048 \pm 0.0019	0.0047 \pm 0.0019
5.597 \pm 0.149	24 \pm 44	0.0010 \pm 0.0019	0.0009 \pm 0.0017	0.0009 \pm 0.0017
5.875 \pm 0.160	55 \pm 45	0.0023 \pm 0.0019	0.0021 \pm 0.0017	0.0021 \pm 0.0017
6.181 \pm 0.175	110 \pm 45	0.0047 \pm 0.0020	0.0043 \pm 0.0018	0.0042 \pm 0.0018
6.517 \pm 0.187	82 \pm 46	0.0033 \pm 0.0019	0.0030 \pm 0.0017	0.0029 \pm 0.0017
6.862 \pm 0.201	150 \pm 48	0.0057 \pm 0.0019	0.0052 \pm 0.0018	0.0051 \pm 0.0017
7.237 \pm 0.218	193 \pm 48	0.0076 \pm 0.0021	0.0069 \pm 0.0019	0.0069 \pm 0.0019
7.661 \pm 0.242	285 \pm 48	0.0120 \pm 0.0024	0.0109 \pm 0.0022	0.0108 \pm 0.0022
8.126 \pm 0.263	280 \pm 48	0.0117 \pm 0.0024	0.0107 \pm 0.0022	0.0106 \pm 0.0022
8.618 \pm 0.284	269 \pm 49	0.0110 \pm 0.0023	0.0100 \pm 0.0022	0.0099 \pm 0.0021
9.160 \pm 0.313	319 \pm 49	0.0133 \pm 0.0025	0.0121 \pm 0.0023	0.0120 \pm 0.0023
9.757 \pm 0.346	364 \pm 50	0.0157 \pm 0.0028	0.0143 \pm 0.0026	0.0142 \pm 0.0026
10.414 \pm 0.377	319 \pm 48	0.0143 \pm 0.0027	0.0130 \pm 0.0025	0.0129 \pm 0.0025
11.143 \pm 0.425	427 \pm 50	0.0203 \pm 0.0033	0.0185 \pm 0.0030	0.0183 \pm 0.0030
11.960 \pm 0.467	336 \pm 48	0.0164 \pm 0.0030	0.0150 \pm 0.0028	0.0148 \pm 0.0028
12.860 \pm 0.525	237 \pm 47	0.0120 \pm 0.0027	0.0109 \pm 0.0025	0.0108 \pm 0.0025
13.876 \pm 0.589	182 \pm 47	0.0094 \pm 0.0026	0.0085 \pm 0.0024	0.0084 \pm 0.0024
15.016 \pm 0.660	182 \pm 47	0.0094 \pm 0.0026	0.0085 \pm 0.0024	0.0084 \pm 0.0024
16.297 \pm 0.750	151 \pm 46	0.0077 \pm 0.0025	0.0071 \pm 0.0023	0.0070 \pm 0.0023
17.759 \pm 0.857	81 \pm 46	0.0041 \pm 0.0024	0.0038 \pm 0.0022	0.0037 \pm 0.0022
19.416 \pm 0.971	66 \pm 46	0.0033 \pm 0.0023	0.0030 \pm 0.0021	0.0030 \pm 0.0021

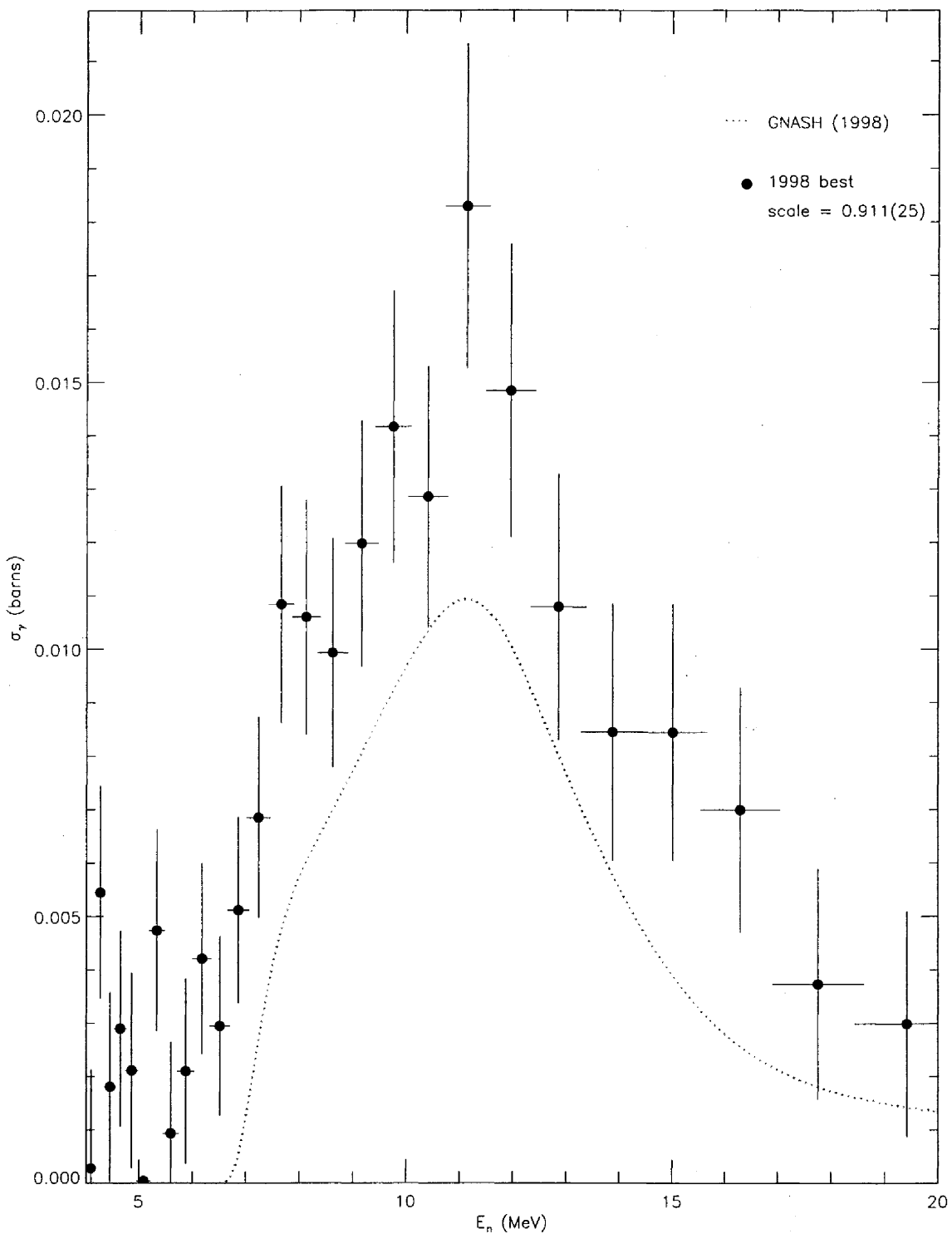


FIG. 73: Adopted $E_\gamma = 966.3$ -keV partial cross section corresponding to the data in table LXXXIII, and corrected for angular-distribution effects. The target-thickness correction factor is shown, and the recommended partial cross section (solid circles) is compared to GNASH.

TABLE LXXXIV: Adopted partial γ -ray cross section for the $E_\gamma = 981.4\text{-keV}$ transition. The measured peak areas and deduced partial cross section (before correction for angular distribution effects) for the **98Thin** data set are shown in columns 2 and 3, respectively. The partial cross section, listed in column 4, is obtained by scaling the **98Thin** data by a target-thickness correction factor. The recommended partial cross section in the last column includes a correction for angular-distribution effects.

E_n (MeV)	$A^{(1998)}$	$\sigma^{(1998)}$	$\sigma^{(\text{sca})}$	$\sigma^{(\text{sca,corr})}$
4.090 \pm 0.093	8 \pm 39	0.0004 \pm 0.0020	0.0004 \pm 0.0018	0.0004 \pm 0.0018
4.264 \pm 0.099	0 \pm 14	0.0000 \pm 0.0007	0.0000 \pm 0.0006	0.0000 \pm 0.0006
4.453 \pm 0.105	107 \pm 42	0.0051 \pm 0.0021	0.0046 \pm 0.0019	0.0046 \pm 0.0019
4.647 \pm 0.113	62 \pm 42	0.0029 \pm 0.0020	0.0026 \pm 0.0018	0.0026 \pm 0.0018
4.861 \pm 0.122	181 \pm 44	0.0085 \pm 0.0023	0.0077 \pm 0.0021	0.0077 \pm 0.0021
5.090 \pm 0.129	79 \pm 44	0.0036 \pm 0.0020	0.0033 \pm 0.0019	0.0033 \pm 0.0019
5.333 \pm 0.140	104 \pm 45	0.0047 \pm 0.0021	0.0043 \pm 0.0019	0.0040 \pm 0.0018
5.597 \pm 0.149	51 \pm 45	0.0022 \pm 0.0020	0.0020 \pm 0.0018	0.0019 \pm 0.0017
5.875 \pm 0.160	101 \pm 46	0.0043 \pm 0.0020	0.0039 \pm 0.0018	0.0037 \pm 0.0018
6.181 \pm 0.175	57 \pm 45	0.0024 \pm 0.0019	0.0022 \pm 0.0018	0.0021 \pm 0.0017
6.517 \pm 0.187	86 \pm 46	0.0035 \pm 0.0019	0.0031 \pm 0.0017	0.0030 \pm 0.0016
6.862 \pm 0.201	135 \pm 48	0.0052 \pm 0.0019	0.0047 \pm 0.0018	0.0045 \pm 0.0017
7.237 \pm 0.218	158 \pm 48	0.0063 \pm 0.0020	0.0057 \pm 0.0019	0.0054 \pm 0.0018
7.661 \pm 0.242	215 \pm 48	0.0091 \pm 0.0023	0.0083 \pm 0.0021	0.0079 \pm 0.0020
8.126 \pm 0.263	217 \pm 47	0.0092 \pm 0.0022	0.0084 \pm 0.0020	0.0080 \pm 0.0020
8.618 \pm 0.284	280 \pm 49	0.0116 \pm 0.0024	0.0105 \pm 0.0022	0.0101 \pm 0.0021
9.160 \pm 0.313	211 \pm 49	0.0089 \pm 0.0023	0.0081 \pm 0.0021	0.0077 \pm 0.0020
9.757 \pm 0.346	317 \pm 50	0.0138 \pm 0.0027	0.0126 \pm 0.0024	0.0121 \pm 0.0024
10.414 \pm 0.377	278 \pm 48	0.0125 \pm 0.0026	0.0114 \pm 0.0024	0.0110 \pm 0.0023
11.143 \pm 0.425	257 \pm 48	0.0123 \pm 0.0027	0.0112 \pm 0.0025	0.0108 \pm 0.0024
11.960 \pm 0.467	236 \pm 47	0.0117 \pm 0.0027	0.0106 \pm 0.0024	0.0102 \pm 0.0024
12.860 \pm 0.525	265 \pm 48	0.0135 \pm 0.0029	0.0123 \pm 0.0026	0.0118 \pm 0.0026
13.876 \pm 0.589	137 \pm 46	0.0071 \bullet 0.0025	0.0065 \pm 0.0023	0.0062 \pm 0.0022
15.016 \pm 0.660	89 \pm 45	0.0046 \pm 0.0024	0.0042 \pm 0.0022	0.0041 \pm 0.0021
16.297 \pm 0.750	15 \pm 44	0.0008 \pm 0.0023	0.0007 \pm 0.0021	0.0007 \pm 0.0020
17.759 \pm 0.857	59 \pm 45	0.0030 \pm 0.0023	0.0028 \pm 0.0021	0.0027 \pm 0.0021
19.416 \pm 0.971	25 \pm 45	0.0013 \pm 0.0023	0.0011 \pm 0.0021	0.0011 \pm 0.0020

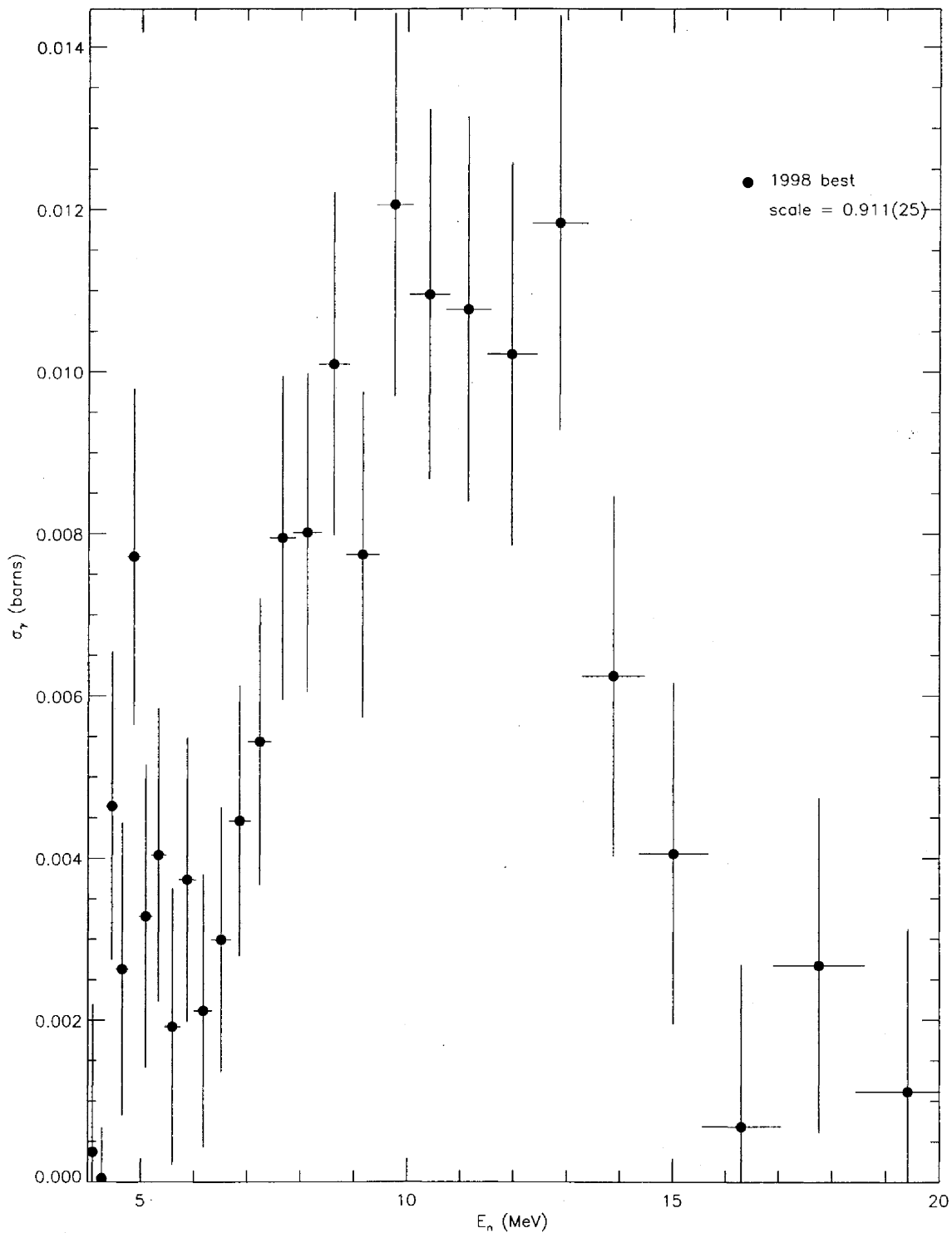


FIG. 74: Adopted $E_\gamma = 981.4$ -keV partial cross section corresponding to the data in table LXXXIV, and corrected for angular-distribution effects. No GNASH calculations are available for this line. The target-thickness correction factor is shown.

TABLE LXXXV: Adopted partial γ -ray cross section for the $E_\gamma = 984.8$ -keV transition. The measured peak areas and deduced partial cross section (before correction for angular distribution effects) for the **98Thin** data set are shown in columns 2 and 3, respectively. The partial cross section, listed in column 4, is obtained by scaling the **98Thin** data by a target-thickness correction factor. The recommended partial cross section in the last column includes a correction for angular-distribution effects.

E_n (MeV)	$A^{(1998)}$	$\sigma^{(1998)}$	$\sigma^{(\text{sca})}$	$\sigma^{(\text{sca,corr})}$
4.090 \pm 0.093	0 \pm 0	0.0001 \pm 0.0000	0.0000 \pm 0.0000	0.0000 \pm 0.0000
4.264 \pm 0.099	0 \pm 0	0.0000 \pm 0.0000	0.0000 \pm 0.0000	0.0000 \pm 0.0000
4.453 \pm 0.105	0 \pm 0	0.0000 \pm 0.0000	0.0000 \pm 0.0000	0.0000 \pm 0.0000
4.647 \pm 0.113	0 \pm 0	0.0000 \pm 0.0000	0.0000 \pm 0.0000	0.0000 \pm 0.0000
4.861 \pm 0.122	0 \pm 0	0.0000 \pm 0.0000	0.0000 \pm 0.0000	0.0000 \pm 0.0000
5.090 \pm 0.129	81 \pm 51	0.0037 \pm 0.0024	0.0034 \pm 0.0021	0.0034 \pm 0.0021
5.333 \pm 0.140	63 \pm 52	0.0028 \pm 0.0024	0.0026 \pm 0.0021	0.0025 \pm 0.0021
5.597 \pm 0.149	129 \pm 53	0.0056 \pm 0.0024	0.0051 \pm 0.0022	0.0049 \pm 0.0021
5.875 \pm 0.160	50 \pm 52	0.0021 \pm 0.0022	0.0019 \pm 0.0020	0.0019 \pm 0.0020
6.181 \pm 0.175	112 \pm 52	0.0048 \pm 0.0023	0.0044 \pm 0.0021	0.0042 \pm 0.0020
6.517 \pm 0.187	149 \pm 54	0.0060 \pm 0.0023	0.0054 \pm 0.0021	0.0053 \pm 0.0020
6.862 \pm 0.201	94 \pm 55	0.0036 \pm 0.0021	0.0033 \pm 0.0019	0.0032 \pm 0.0019
7.237 \pm 0.218	167 \pm 55	0.0066 \pm 0.0023	0.0060 \pm 0.0021	0.0058 \pm 0.0020
7.661 \pm 0.242	245 \pm 56	0.0104 \pm 0.0026	0.0095 \pm 0.0024	0.0092 \pm 0.0024
8.126 \pm 0.263	248 \pm 56	0.0105 \pm 0.0026	0.0095 \pm 0.0024	0.0093 \pm 0.0024
8.618 \pm 0.284	236 \pm 57	0.0097 \pm 0.0026	0.0089 \pm 0.0024	0.0086 \pm 0.0023
9.160 \pm 0.313	383 \pm 59	0.0160 \pm 0.0030	0.0146 \pm 0.0028	0.0142 \pm 0.0027
9.757 \pm 0.346	405 \pm 58	0.0176 \pm 0.0032	0.0160 \pm 0.0029	0.0156 \pm 0.0029
10.414 \pm 0.377	412 \pm 58	0.0185 \pm 0.0033	0.0169 \pm 0.0031	0.0164 \pm 0.0030
11.143 \pm 0.425	289 \pm 56	0.0138 \pm 0.0031	0.0126 \pm 0.0028	0.0122 \pm 0.0028
11.960 \pm 0.467	356 \pm 56	0.0176 \pm 0.0034	0.0160 \pm 0.0031	0.0155 \pm 0.0031
12.860 \pm 0.525	157 \pm 54	0.0080 \pm 0.0029	0.0073 \pm 0.0026	0.0071 \pm 0.0026
13.876 \pm 0.589	199 \pm 55	0.0103 \pm 0.0031	0.0094 \pm 0.0028	0.0091 \pm 0.0027
15.016 \pm 0.660	115 \pm 53	0.0060 \pm 0.0028	0.0054 \pm 0.0026	0.0053 \pm 0.0025
16.297 \pm 0.750	98 \pm 53	0.0051 \pm 0.0028	0.0046 \pm 0.0025	0.0045 \pm 0.0025
17.759 \pm 0.857	117 \pm 54	0.0060 \pm 0.0029	0.0055 \pm 0.0026	0.0053 \pm 0.0025
19.416 \pm 0.971	104 \pm 55	0.0052 \pm 0.0028	0.0048 \pm 0.0026	0.0047 \pm 0.0025

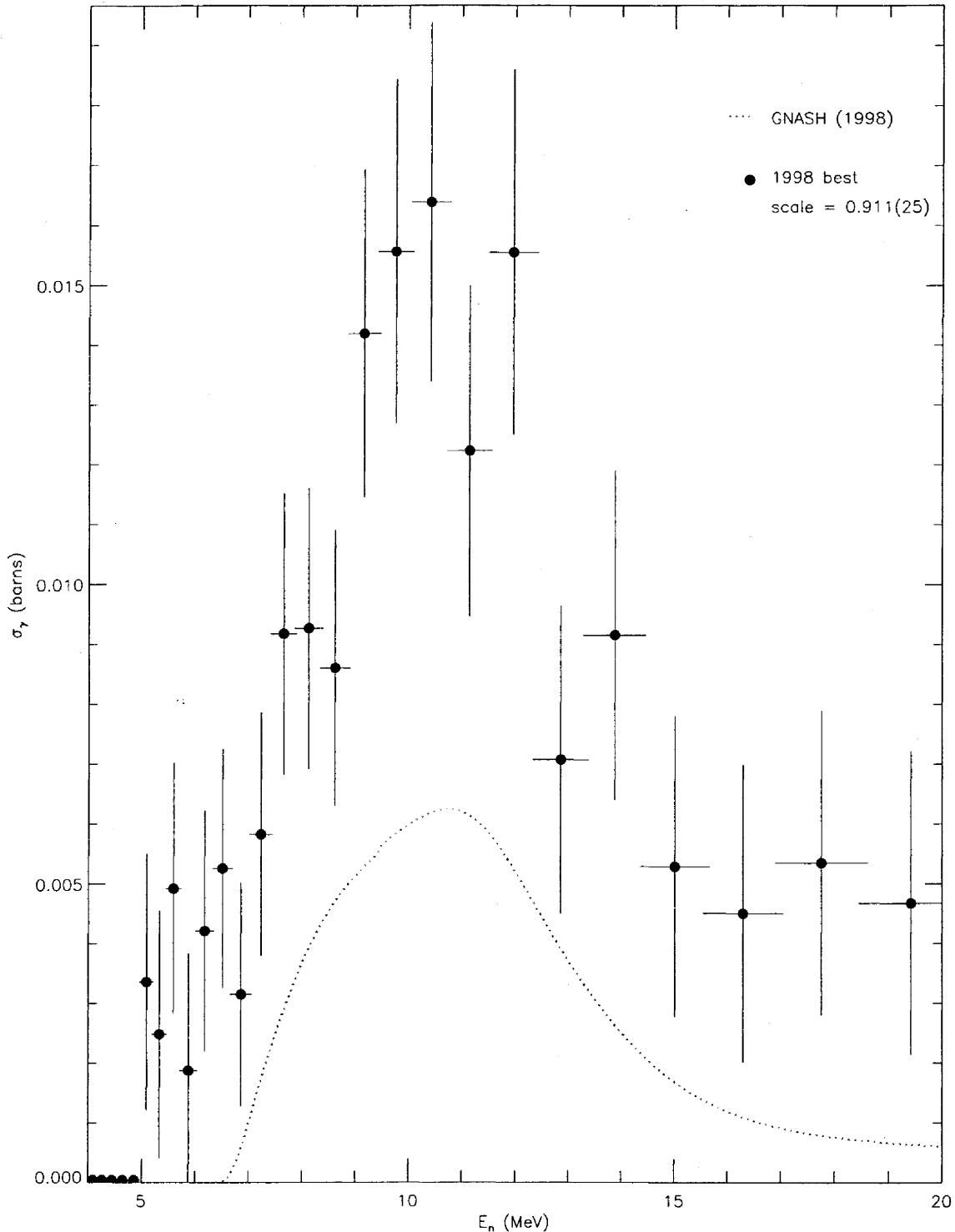


FIG. 75: Adopted $E_\gamma = 984.8$ -keV partial cross section corresponding to the data in table LXXXV, and corrected for angular-distribution effects. The target-thickness correction factor is shown, and the recommended partial cross section (solid circles) is compared to GNASH.

The partial γ -ray cross section extracted for the $4_1^+ \rightarrow 2_1^+$ transition carries large uncertainties because of the difficulties involved in resolving the γ -ray peak (see e.g. the discussion in section II A 3). Quantitative information was obtained from this line in spite of considerable spectroscopic difficulties and that the transition could be observed at all should be taken as a testament to the advantages of the γ -ray technique over neutron-counting experiments for measuring reaction cross sections. Because this low-lying transition represents a large fraction of the de-excitation of ^{234}U (up to 85% of the $(n,2n)$ cross section at e.g. $E_n = 12$ MeV according to GNASH), it is useful to assess the reliability of the yields measured for this transition using the GEANIE data. To this end, and given the plethora of transitions analyzed in ^{234}U and discussed in this section, it is instructive to compare the measured $4_1^+ \rightarrow 2_1^+$ partial cross section to the sum of all measured yields for transitions feeding the 4_1^+ state, namely the 152.7, 819.2, 880.6, 925.3, 946.1, and 984.8-keV γ rays. A difficulty arises for those transitions feeding the 4_1^+ level which are known to be degenerate within the GEANIE data resolution. This is the case for the 925.3-keV and 946.1-keV lines discussed in this section. The 880.6-keV γ -ray is also twofold degenerate, however both transitions decay into the 4_1^+ state. Since the specific contribution to the 4_1^+ level from those degenerate lines cannot be extracted, we compare the measured $4_1^+ \rightarrow 2_1^+$ partial cross section to the sum with (“high sum”) and without (“low sum”) the 925.3-keV and 946.1-keV γ -ray contributions. There are of course other, unobserved transitions which populate the 4_1^+ level, but the ones used in the sums account for at least 93% of the population of the 4_1^+ state by discrete γ rays in the GNASH calculations. The measured $4_1^+ \rightarrow 2_1^+$ yields and both summed partial cross sections are plotted in figure 76a. Panels b) and c) of that same figure show the difference between the “low sum” and “high sum” yields respectively, normalized to the uncertainty in the measured $4_1^+ \rightarrow 2_1^+$ partial cross section. In general, the agreement between the measured $4_1^+ \rightarrow 2_1^+$ yields and either sum seems to deteriorate gradually with increasing neutron energy. For those points above threshold, the majority of $4_1^+ \rightarrow 2_1^+$ yields are within one standard deviation of the “low sum” and all but the last two points are within two standard deviations. The $E_n = 17.8$ MeV and $E_n = 19.4$ MeV $4_1^+ \rightarrow 2_1^+$ yields fall below the “low sum” yields by 2.7 and 2.5 standard deviations respectively. Compared to the “high sum”-yields, most measured $4_1^+ \rightarrow 2_1^+$ yields are within two standard deviations and all yields are within three. In light of this comparison, the quoted $4_1^+ \rightarrow 2_1^+$ partial γ -ray yields appear reliable, within error, below the peak cross section at $E_n = 12$ MeV. Above $E_n = 12$ MeV the $4_1^+ \rightarrow 2_1^+$ partial cross section may be under-estimated by up to three standard deviations.

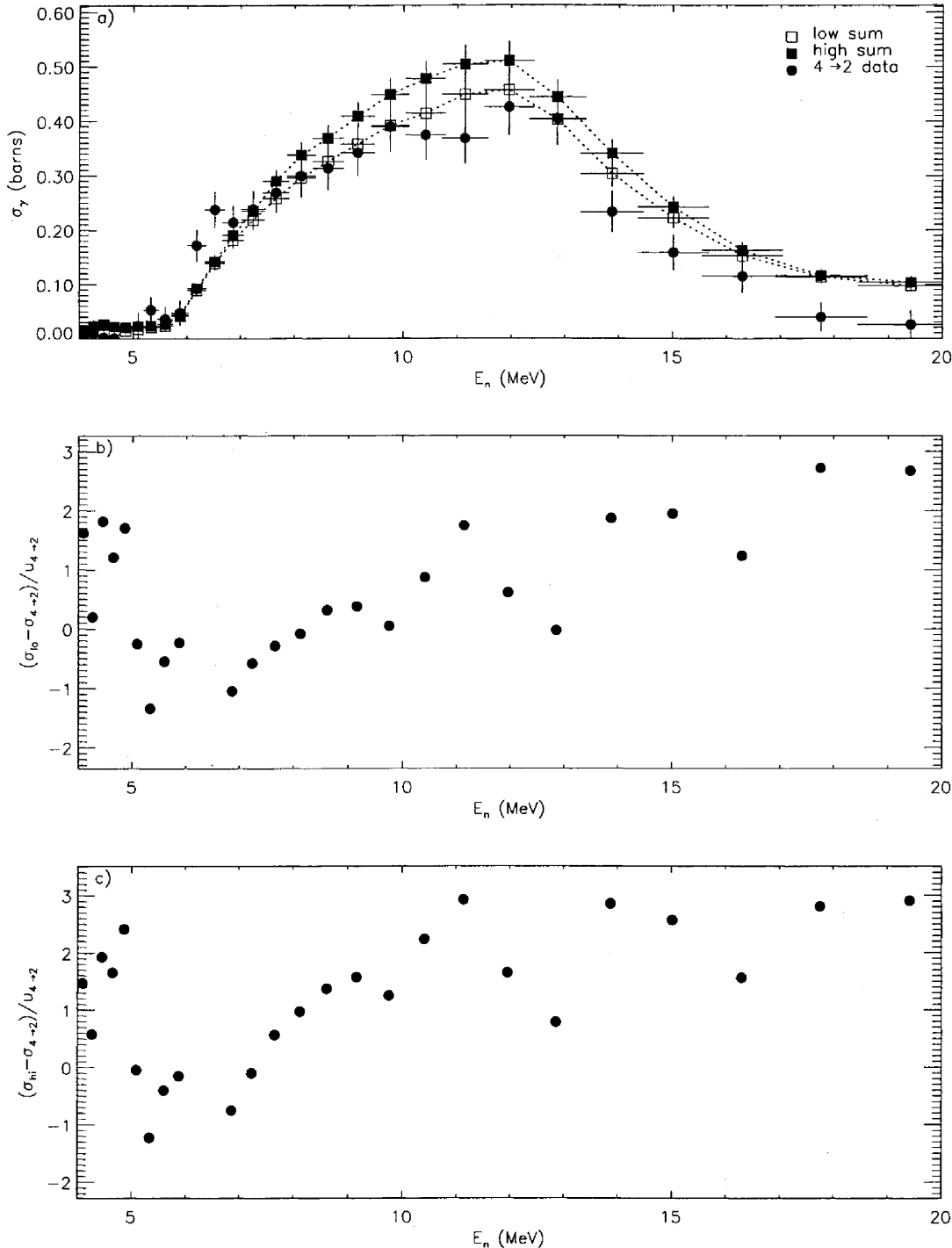


FIG. 76: Consistency check for the $4_1^+ \rightarrow 2_1^+$ partial cross section. Panel a) shows the measured $4_1^+ \rightarrow 2_1^+$ excitation function (solid circles, and the sum of measured yields feeding the 4^+ level with (solid squares) and without (empty squares) the 925.3-keV and 946.1-keV γ -ray contributions. The difference between the sums and the $4_1^+ \rightarrow 2_1^+$ yields, normalized to the uncertainty (u_{4-2}) in the $4_1^+ \rightarrow 2_1^+$ yields is shown in b) for the sum without the 925.3-keV and 946.1-keV γ -ray contributions, and in c) for the sum with those contributions.

C Observed Lines in ^{235}U

Partial γ -ray cross sections have also been extracted for a total of 13 lines in the $^{235}\text{U}(\text{n},\text{n}'\gamma)$ channel. These lines are placed in the ^{235}U level scheme in figure 77. Each line is also listed in table LXXXVI along with the method by which it was analyzed. Two complications arise when extracting partial cross section from (n,n') lines. The first difficulty is due to the odd neutron number which results in a larger number of low-lying levels than the ^{234}U case due to the coupling of the additional neutron. As a consequence, the (n,n') reaction cross section strength is fragmented among many decay paths and it is more difficult to find a small set of “representative” γ rays, as in the case of the $4_1^+ \rightarrow 2_1^+$ or $6_1^+ \rightarrow 4_1^+$ transitions in ^{234}U . In fact, a single γ -ray, with $E_\gamma = 129.3$ keV, was found to have the largest cross section, exceeding all other observed $(\text{n},\text{n}'\gamma)$ partial cross sections by at least a factor of five. Yet even this line represents less than 10% of the full (n,n') reaction cross section [11]. The second complication encountered in the analysis of $(\text{n},\text{n}'\gamma)$ partial cross sections is of an experimental nature. Because neutrons at WNR are produced by spallation from a pulsed proton beam, it is possible for neutrons associated with a given pulse to reach the ^{235}U sample at the same time as slower neutrons from a previous pulse. In that case, the measured yield is the sum of yields from all micropulses which contribute to the neutron flux. This effect is referred to as beam “wrap-around”. The “wrapped” neutron energy $E_{n,i}^{(\text{wrap})}$ from the previous i^{th} micropulse ($i = 1$ refers to the last micropulse, $i = 2$ to the one before last, etc...) can be related to the neutron energy E_n for the current micropulse using relativistic kinematics. In the report on the 1997 $^{235}\text{U}(\text{n},2\text{n})$ cross section measurement [5], we presented the formulas to convert from time-of-flight to neutron energy:

$$\xi \equiv \frac{c}{d} \Delta t \quad (27)$$

$$E_n = E_0 \left[\frac{\xi + 1}{\sqrt{\xi(\xi + 2)}} - 1 \right] \quad (28)$$

where c is the speed of light (0.2998 m/ns), d is the flight path length (20.34 m), E_0 is the rest-mass energy of the neutron (939.56 MeV), Δt is the time of flight measured relative to the detection time of the γ flash, and ξ is a dimensionless time-of-flight defined in terms of Δt . We invert this formula to calculate the dimensionless time-of-flight corresponding to a measured neutron energy E_n associated with the current micropulse:

$$\xi = \frac{E_n + E_0}{\sqrt{E_n(E_n + 2E_0)}} - 1 \quad (29)$$

A neutron from the previous i^{th} micropulse will travel for an additional time of $i \times \delta t$, where δt is the micropulse spacing. In both 1998 and 1999 GEANIE experiments, successive proton micropulses (within a single macropulse) were separated by $\delta t = 1.8 \mu\text{s}$. The corresponding increase in dimensionless time is:

$$i \times \delta \xi \equiv i \times \frac{c}{d} \delta t \quad (30)$$

Using equation 28 we can then calculate the energy of this slower neutron (i.e. the “wrapped” neutron energy):

$$E_{n,i}^{(\text{wrap})}(\xi) = E_0 \left[\frac{\xi + i\delta\xi + 1}{\sqrt{(\xi + i\delta\xi)(\xi + i\delta\xi + 2)}} - 1 \right] \quad (31)$$

where ξ in this equation is calculated using equation 29 for the energy E_n of the neutron in the current micropulse (i.e. the “unwrapped” neutron energy). The relationship between “wrapped” and “unwrapped” neutron energies given by equation 31 is plotted in figure 78 for wrap-around from the first- and second-wrapped micropulses (i.e. $i = 1$ and 2, respectively). The lowest-lying ^{235}U level from which a partial γ -ray cross section could be extracted is at $E_x = 129.3$ keV. At this excitation energy, “wrap-around” neutrons from the $i \geq 2$ previous micropulse do not present a concern for $E_n \leq 20$ MeV, as can be seen in figure 78. However, neutron energies in the 4.1–19.4-MeV range in the current micropulse correspond to wrapped energies in the 294–402-keV range, well above the threshold for population of the $E_x = 129.3$ keV level. Several other lines presented here fall into this category. In cases where “wrap-around” is a concern, we have used the random-TOF-subtracted data in our analysis. In those data, a constant number

of background counts is subtracted in each neutron-energy bin. Therefore, this approach will properly account for “wrap-around” effects only if the “wrapped” neutron flux and population cross section for the level of interest at the corresponding “wrapped” energies combine to produce a constant background (as a function of neutron energy). Upcoming GEANIE measurements with a longer ($3.6\ \mu s$) micropulse spacing will test this assumption. However, in the interest of the present discussion, we can provide a rough test based on the available data for the high-yield 129.3-keV line.

In theory, the neutron-flux normalization N_ϕ calculated using equation 5 should take on the same values as a function of neutron energy regardless of which fission-foil data, the ^{235}U - or ^{238}U -foil data, is used. If we attribute the observed difference in N_ϕ values—which we attempt to compensate for with a flat baseline subtraction of ^{235}U -foil counts—to “wrap around” neutrons, then this difference is a measure of the “wrap-around” neutron flux. This difference (labeled ΔN_ϕ) is plotted in figure 79a) for the **98Thin** data. The “wrapped” energies for this difference were calculated using equation 31 taking care to use the appropriate path length for the fission foils (18.48 m). The “wrap-around” neutron flux in this energy range is almost constant, except for the last point which drops by a large amount, but carries a sizeable uncertainty. Next we calculate the γ -ray partial cross section for the 129.3-keV line using the Hauser-Feshbach code CINDY [24] [25]. This partial cross section is plotted in panel b) of the same figure over the “wrapped” energy range. The 129.3-keV partial cross section appears relatively constant over this energy range, because i) the $E_n = 294\text{--}402\text{-keV}$ range is well beyond the population threshold for the line and ii) this energy range is relatively narrow. Finally, we solve equation 8 for the peak areas due to “wrap-around” neutron background, using the neutron flux normalization plotted in figure 79a) and the calculated yields in figure 79b). The predicted background counts are plotted in panel c) as a one-sigma band, and compared to the actual background counts subtracted from the **98Thin** γ -ray data. the predicted and actual background are in excellent agreement. We conclude that, at least in the case of the 129.3-keV transition, the constant-background assumption is reasonable.

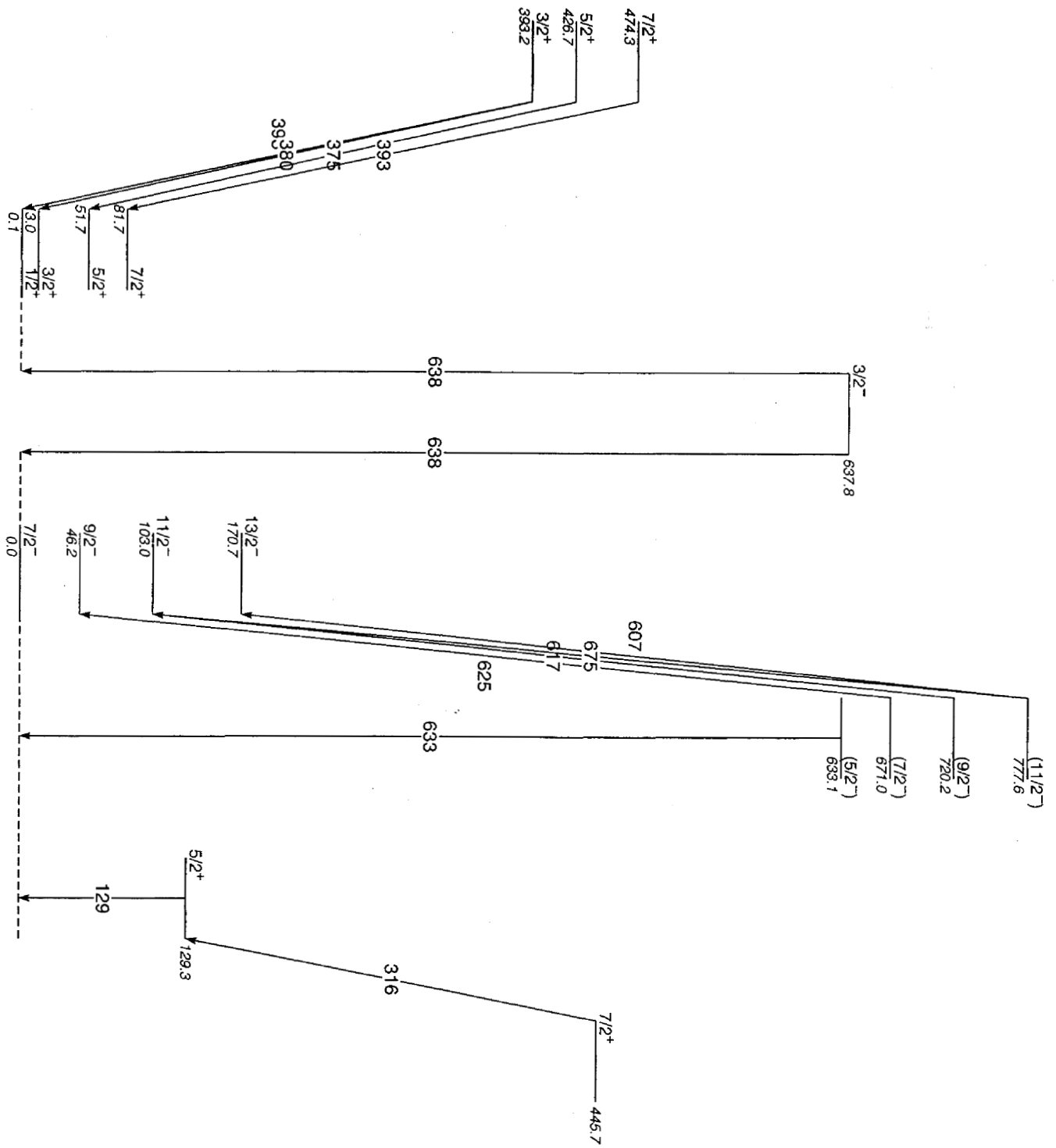
FIG. 77: Gamma rays in ^{235}U observed in the GEANIE data.

TABLE LXXXVI: Transitions identified in the $^{235}\text{U}(\text{n},\text{n}'\gamma)$ channel and the method by which the data were analyzed.

$E_{\gamma}^{(\text{meas})}$ (keV)	Analysis method	$E_{\gamma}^{(\text{acc})}$ (keV)	E_x (keV)	transition
129.335 \pm 0.111	subtracted planars, 98Thin and 99Thin optimized	129.297 \pm 0.002	129.3	$5/2^+ \rightarrow 7/2^-_1$
316.519 \pm 0.116	subtracted planars, 98Thin and 99Thin optimized	316.440 \pm 0.006	445.7	$7/2^+ \rightarrow 5/2^+$
375.074 \pm 0.171	unsubtracted planars, 98Thin only	375.045 \pm 0.006	426.7	$5/2^+ \rightarrow 5/2^+$
380.118 \pm 0.189	unsubtracted planars, 98Thin and 99Thin optimized	380.173 \pm 0.002	393.2	$3/2^+ \rightarrow 3/2^+$
392.509 \pm 0.140	subtracted planars, 98Thin and 99Thin optimized	392.560 \pm 0.005	474.3	$7/2^+ \rightarrow 7/2^+$
		393.136 \pm 0.002	393.2	$3/2^+ \rightarrow 1/2^+$
606.847 \pm 0.125	unsubtracted planars, 98Thin and 99Thin optimized	606.9 \pm 0.2	777.6	$(11/2)^- \rightarrow 13/2^-_1$
617.582 \pm 0.267	subtracted planars, 98Thin and 99Thin optimized	617.10 \pm 0.10	720.2	$(9/2)^- \rightarrow 11/2^-_1$
624.937 \pm 0.300	unsubtracted planars, 98Thin and 99Thin optimized	624.78 \pm 0.02	671.0	$(7/2)^- \rightarrow 9/2^-_1$
		624.754 \pm 0.005	637.8	$3/2^- \rightarrow 3/2^+$
633.098 \pm 0.159	unsubtracted planars, 98Thin and 99Thin optimized	633.090 \pm 0.006	633.1	$(5/2)^- \rightarrow 7/2^-_1$
637.712 \pm 0.161	unsubtracted planars, 98Thin and 99Thin optimized	637.795 \pm 0.005	637.8	$3/2^- \rightarrow 7/2^-_1$
		637.717 \pm 0.005	637.8	$3/2^- \rightarrow 1/2^+$
674.218 \pm 0.138	unsubtracted planars, 98Thin and 99Thin optimized	674.5 \pm 0.3	777.6	$(11/2)^- \rightarrow 11/2^-_1$

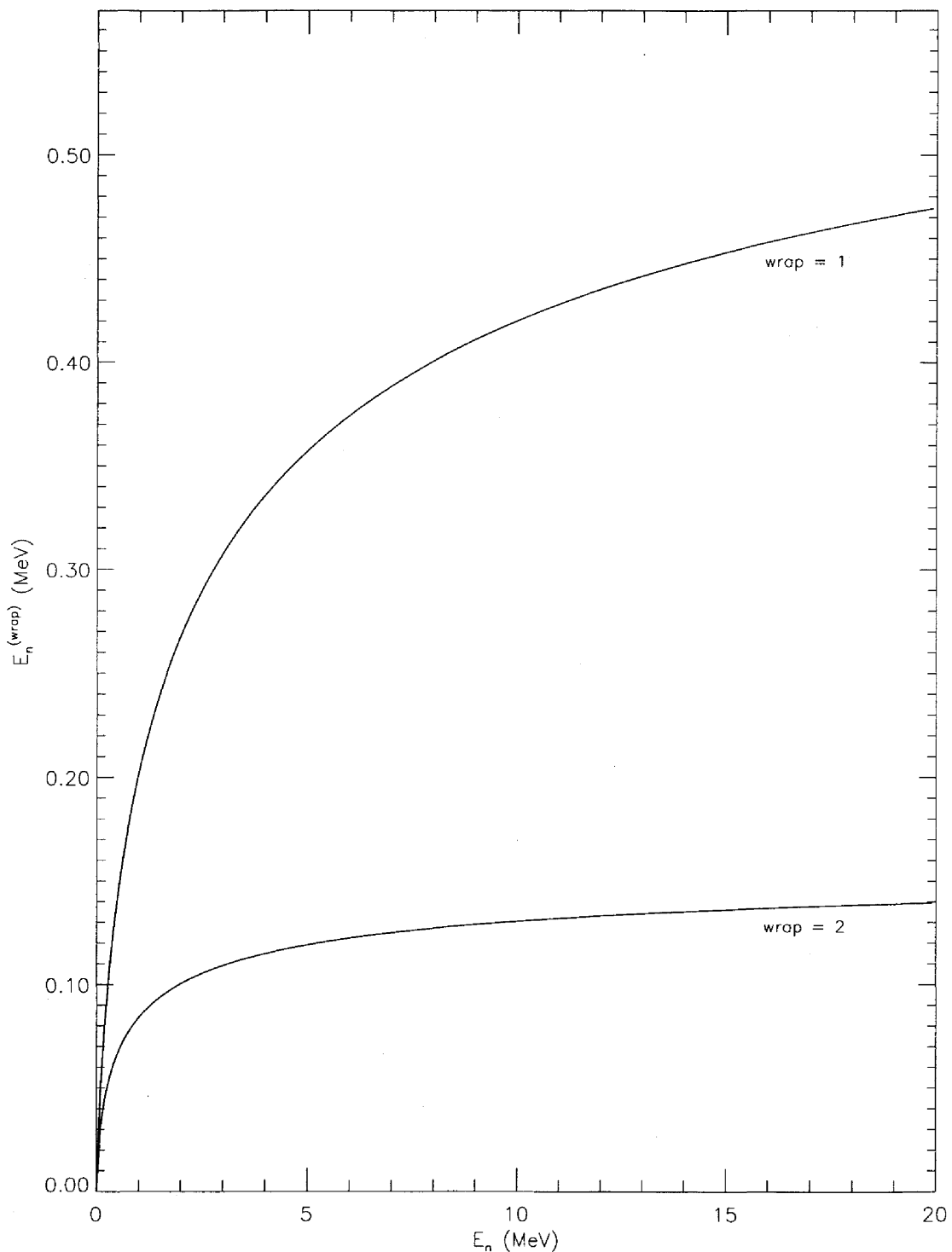


FIG. 78: Wrap-around curves relating the energy of neutrons in the current micropulse to those from prior micropulses. The curves are calculated using equation 31, and wrap-around curves from the last ("wrap = 1") and before-last ("wrap = 2") micropulses are plotted.

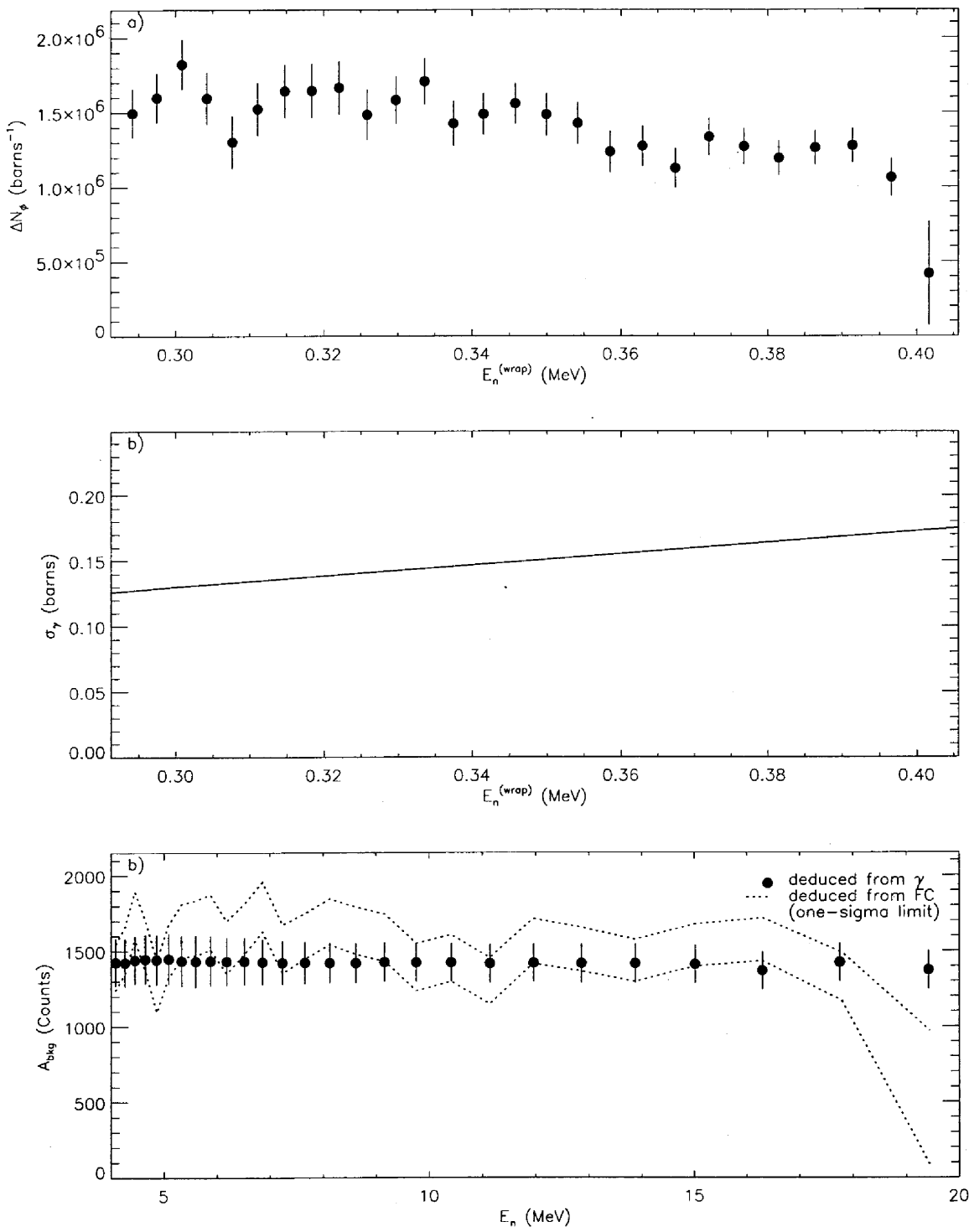


FIG. 79: Estimation of the “wrap-around” background. The difference in flux normalization N_ϕ between ^{235}U and ^{238}U fission-foil data is plotted as a function of “wrapped” neutron energy in a), the calculated 129.3-keV partial cross section is shown in b), and the estimated background counts (dotted lines) are compared to the actual counts (solid circles) deduced from the random-TOF spectrum in c).

The $E_\gamma = 129.3$ keV transition (table LXXXVII/figure 80): This high-yield γ ray depopulates the band head of the $K^\pi = 5/2^+$ band at $E_x = 129.3$ keV. Of all the (n,n') transitions discussed in this section, the 129.3-keV line is the strongest and also the most susceptible to “wrap-around” background. Therefore, we have used the random-TOF-subtracted data in the analysis of this γ ray. The validity of this approach is discussed above. The extracted partial cross section for this line is in excellent agreement with the GNASH prediction.

The $E_\gamma = 316.5$ keV transition (table LXXXVIII/figure 81): This transition connects the band head of a $K^\pi = 7/2^+$ band to the $K^\pi = 5/2^+$ band head from which the 129.3-keV γ -ray is produced. In principle, the excitation energy of the parent level for the 316.5-keV γ -ray is sufficiently high to ignore “wrap-around” effects, however a strong 316.6-keV line can be seen in the “beam-off” spectrum (i.e. the spectrum from γ rays measured between beam macropulses, when there are no incident neutrons). Therefore, we expect a baseline background for this line from a slowly (i.e. $\gg 1.8 \mu s$) decaying contaminant and adopt the partial cross section extracted from random-TOF-subtracted data. By comparison, no such contaminant line was observed in the “beam-off” spectrum for the 129.3-keV transition. As can be seen in figure 81, the agreement with the GNASH calculation is very good. A 445.740 ± 0.006 keV transition, known to depopulate the same level with 67% of the intensity of the 316.5-keV line could not be observed in the GEANIE data. The nearest peak in the spectrum, located at $E_\gamma = 444.944 \pm 0.120$ keV is very weak and displays an essentially flat excitation function about ≈ 7 mb.

The $E_\gamma = 375.1$ keV transition (table LXXXIX/figure 82): Because this transition de-excites a level at $E_x = 426.7$ keV, there is no need to correct for “wrap-around” effects. An inspection of the “beam-off” spectrum reveals the nearest possible contaminant is at $E_\gamma = 373.9$ keV, which is easily resolved within planar-detector resolution. Therefore, we adopt the unsubtracted data in extracting γ -ray yields. Because it is weak, this line could not be observed in the **99Thin** data, and only the **98Thin** data, scaled by the target-thickness correction have been used. Within relatively large error bars, this line also shows a “bump” in the excitation function starting near $E_n \approx 9$ MeV. In general, the measured yields for this transition exceed the GNASH prediction by slightly more than a factor of two. However, because of manifest contamination, the measured partial cross section for this line should be interpreted with caution. Furthermore, a 413.7-keV transition issued from the same level should be observed with 94% of the intensity of the 375.1-keV γ ray. No such line could be found in the GEANIE data. Peaks were found on either side of this transition in the spectra at $E_\gamma = 412.092 \pm 0.124$ keV and 415.080 ± 0.113 keV respectively. Both satellite peaks display excitation functions that appear essentially constant as a function of incident neutron energy.

The $E_\gamma = 380.1$ keV transition (table XC/figure 83): This is one of two γ rays depopulating the $J^\pi = 3/2^+$ level at $E_x = 393.2$ keV. The “beam-off” spectrum shows the nearest possible contaminant at $E_\gamma = 381.3$ keV, and the excitation energy of the parent level for the 380.1-keV transition is sufficiently high to ignore “wrap-around” effects. Not surprisingly, it was found that a random-TOF subtraction had little effect on the measured partial cross section for this line. Therefore we use the unsubtracted data for this transition. The yields extracted in this manner are in good agreement with GNASH. The branching ratio for the 380.1-keV/393.1-keV pair of γ rays cannot be checked using the GEANIE data because the 393.1-keV member of the pair is two-fold degenerate (within detector resolution) in the (n,n') channel. Nevertheless, the measured partial cross section for the 380.1-keV line is lower than the one measured for the 392.5-keV line, as expected from the known branching ratio, whether contamination is a concern or not.

The $E_\gamma = 392.5$ keV transition (table XCI/figure 84): This line represents two degenerate transitions, both from the $K^\pi = 3/2^+$ band with band head at $E_x = 393.2$ keV. Though “wrap-around” effects are not a concern for this line, a line at $E_\gamma = 393.0$ keV can be seen in the “beam-off” spectrum. The random-TOF subtraction was found to have a sizeable effect on the measured partial cross section, reducing it overall by ≈ 7 mb. It is not clear whether a background subtraction should be applied to this line. However, because i) there is evidence from the “beam-off” spectrum for a long-lived contaminant and ii) the subtraction improves the overall agreement with the GNASH prediction for the combination of the two degenerate γ rays, we adopt the random-TOF subtraction in our analysis. Another line issued from the same level and with $E_\gamma = 422.598 \pm 0.002$ keV should be observed with 58% of the intensity of the 392.5-keV transition. However, this line is contaminated by an $E_\gamma = 422.494 \pm 0.123$ keV peak in the GEANIE data with an apparent threshold near ≈ 9 MeV. A likely assignment for that contaminant is the $E_\gamma = 312.90 \pm 0.10$ keV transition, originating from the $E_x = 479.0$ -keV level in ^{126}I and produced via the $(n,2n)$ reaction on ^{127}I . The mono-isotopic nucleus ^{127}I is a component of the NaI nose-cone placed on each detector, used to suppress back-scattered γ rays, and the threshold for the $^{127}\text{I}(n,2n)$ reaction is $E_n = 9.2$ MeV.

The $E_\gamma = 606.8$ keV transition (table XCII/figure 85): This transition originates from a level at $E_x = 777.6$ keV, well above the “wrap-around” threshold. There is no evidence for any long-lived contamination from the

beam-off spectrum, therefore we adopt the unsubtracted GEANIE data in the analysis. A second transition weaker branch from the same level with $E_\gamma = 674.5$ keV has also been observed. There is no GNASH prediction for this partial cross section.

The $E_\gamma = 617.6$ keV transition (table XCIII/figure 86): A sizeable contaminant is observed for this line at $E_\gamma = 617.8$ keV in the “beam-off” spectrum. Therefore we use the subtracted GEANIE data in the analysis. This results in only a ≈ 2 mb reduction in overall yield. The measured partial cross section is slightly under-predicted by GNASH.

The $E_\gamma = 624.9$ keV transition (table XCIV/figure 87): There is no evidence for contamination of this line based on the “beam-off” spectrum, and the parent level at $E_x = 671.0$ keV is well above “wrap-around” threshold. This transition is degenerate with a decay from the $3/2^+$ level at $E_x = 637.8$ keV, however this potential contaminant is a weak branch from the parent level and is predicted by GNASH to be less than 2.2 mb at maximum cross section. The unsubtracted GEANIE data have been used in the analysis, and the resulting partial cross section is roughly a factor of two larger than the GNASH prediction.

The $E_\gamma = 633.1$ keV transition (table XCV/figure 88): There is no evidence from the “beam-off” spectrum that this line is contaminated by a long-lived component. The unsubtracted GEANIE data have been used to extract the partial cross section. This line is close in energy to the $E_\gamma = 631.1$ $6_1^+ \rightarrow 4_1^+$ transition in the high-yield fission fragment ^{142}Ba . Though the two lines can be resolved for the most part in the γ -ray spectrum, there may be a small amount of contamination which could account for the apparent “flattening” of the 633.1-keV partial cross section observed in figure 88 in the $E_n = 6\text{--}10$ -MeV range.

The $E_\gamma = 637.7$ keV transition (table XCVI/figure 89): The parent level for this transition decays to both the ground state and $T_{1/2} \approx 25$ -min isomer level in ^{235}U . Because the difference in energy between the two final levels is small ($\Delta E_\gamma = 76.8$ eV), the two γ rays cannot be resolved in the GEANIE data and the measured partial cross section represent the sum of both. The sum of GNASH predictions for the yields of the two degenerate lines slightly under-predicts our measured cross section.

The $E_\gamma = 674.5$ keV transition (table XCVII/figure 90): This transition originates from a level at $E_x = 777.6$ keV, as with the 606.8-keV line—the other observed transition from this level—we adopt the unsubtracted GEANIE data in the analysis. There is no GNASH prediction for this partial cross section.

TABLE LXXXVII: Adopted partial γ -ray cross section for the $E_\gamma = 129.3$ -keV transition. The measured peak areas and deduced partial cross sections for the **98Thin** and **99Thin** data sets are shown in columns 2–5. The recommended partial cross section, listed in column 6, is obtained from both data sets using the optimization procedure described in section XII B.

E_n (MeV)	$A^{(1998)}$	$\sigma^{(1998)}$	$A^{(1999)}$	$\sigma^{(1999)}$	$\sigma^{(\text{opt})}$
4.090 ± 0.093	4684 ± 112	0.1217 ± 0.0144	3808 ± 118	0.1194 ± 0.0141	0.1143 ± 0.0099
4.264 ± 0.099	4853 ± 113	0.1227 ± 0.0144	3910 ± 119	0.1211 ± 0.0143	0.1156 ± 0.0100
4.453 ± 0.105	4988 ± 114	0.1203 ± 0.0141	3998 ± 121	0.1177 ± 0.0139	0.1128 ± 0.0097
4.647 ± 0.113	5456 ± 117	0.1287 ± 0.0150	4142 ± 122	0.1190 ± 0.0140	0.1174 ± 0.0100
4.861 ± 0.122	5663 ± 118	0.1342 ± 0.0156	4420 ± 125	0.1247 ± 0.0146	0.1227 ± 0.0105
5.090 ± 0.129	5654 ± 119	0.1306 ± 0.0152	4130 ± 126	0.1139 ± 0.0134	0.1153 ± 0.0099
5.333 ± 0.140	5644 ± 120	0.1283 ± 0.0149	4330 ± 128	0.1193 ± 0.0140	0.1173 ± 0.0100
5.597 ± 0.149	5933 ± 122	0.1305 ± 0.0151	4460 ± 129	0.1217 ± 0.0142	0.1195 ± 0.0102
5.875 ± 0.160	5109 ± 118	0.1104 ± 0.0128	4119 ± 128	0.1099 ± 0.0129	0.1043 ± 0.0089
6.181 ± 0.175	4096 ± 113	0.0888 ± 0.0104	3135 ± 123	0.0822 ± 0.0098	0.0806 ± 0.0070
6.517 ± 0.187	3581 ± 111	0.0729 ± 0.0085	2305 ± 119	0.0576 ± 0.0071	0.0603 ± 0.0054
6.862 ± 0.201	2661 ± 106	0.0515 ± 0.0061	2080 ± 118	0.0508 ± 0.0064	0.0478 ± 0.0044
7.237 ± 0.218	1979 ± 102	0.0398 ± 0.0049	1567 ± 115	0.0406 ± 0.0055	0.0373 ± 0.0036
7.661 ± 0.242	1426 ± 99	0.0307 ± 0.0041	1081 ± 111	0.0300 ± 0.0046	0.0279 ± 0.0030
8.126 ± 0.263	937 ± 96	0.0201 ± 0.0031	813 ± 110	0.0223 ± 0.0039	0.0189 ± 0.0023
8.618 ± 0.284	704 ± 94	0.0147 ± 0.0026	677 ± 110	0.0181 ± 0.0036	0.0142 ± 0.0020
9.160 ± 0.313	681 ± 94	0.0145 ± 0.0026	601 ± 108	0.0164 ± 0.0035	0.0135 ± 0.0020
9.757 ± 0.346	544 ± 93	0.0120 ± 0.0025	395 ± 108	0.0112 ± 0.0033	0.0103 ± 0.0019
10.414 ± 0.377	314 ± 91	0.0072 ± 0.0022	434 ± 107	0.0129 ± 0.0035	0.0075 ± 0.0018
11.143 ± 0.425	286 ± 91	0.0069 ± 0.0023	189 ± 106	0.0059 ± 0.0034	0.0056 ± 0.0018
11.960 ± 0.467	34 ± 90	0.0009 ± 0.0023	120 ± 108	0.0039 ± 0.0035	0.0010 ± 0.0018
12.860 ± 0.525	162 ± 91	0.0042 ± 0.0024	94 ± 108	0.0031 ± 0.0036	0.0030 ± 0.0019
13.876 ± 0.589	288 ± 92	0.0076 ± 0.0026	214 ± 108	0.0073 ± 0.0038	0.0064 ± 0.0020
15.016 ± 0.660	19 ± 91	0.0005 ± 0.0024	44 ± 104	0.0015 ± 0.0036	0.0001 ± 0.0019
16.297 ± 0.750	44 ± 90	0.0012 ± 0.0024	139 ± 106	0.0047 ± 0.0036	0.0014 ± 0.0019
17.759 ± 0.857	80 ± 91	0.0021 ± 0.0024	123 ± 105	0.0041 ± 0.0035	0.0018 ± 0.0019
19.416 ± 0.971	130 ± 91	0.0033 ± 0.0024	234 ± 105	0.0076 ± 0.0035	0.0036 ± 0.0019

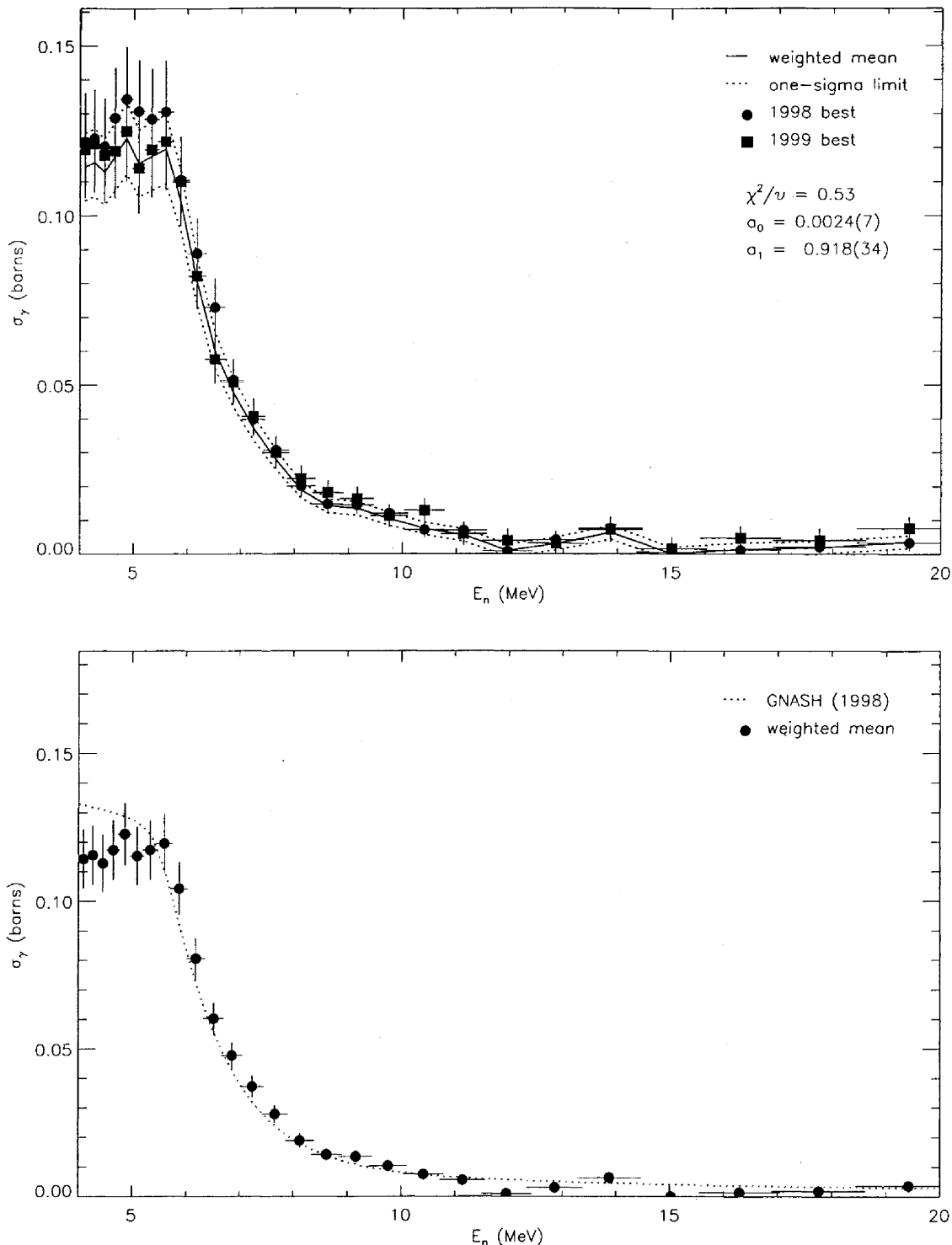


FIG. 80: Adopted $E_\gamma = 129.3$ -keV partial cross section corresponding to the data in table LXXXVII. The top panel shows the 1998 and 1999 partial cross sections and the recommended value, plotted as a solid line with a one-sigma confidence band (dotted lines). The bottom panel shows this recommended partial cross section (solid circles) compared to GNASH.

TABLE LXXXVIII: Adopted partial γ -ray cross section for the $E_\gamma = 316.5$ -keV transition. The measured peak areas and deduced partial cross sections for the **98Thin** and **99Thin** data sets are shown in columns 2–5. The recommended partial cross section, listed in column 6, is obtained from both data sets using the optimization procedure described in section XII B.

E_n (MeV)	$A^{(1998)}$	$\sigma^{(1998)}$	$A^{(1999)}$	$\sigma^{(1999)}$	$\sigma^{(\text{opt})}$
4.090 ± 0.093	370 ± 54	0.0191 ± 0.0034	356 ± 71	0.0189 ± 0.0043	0.0138 ± 0.0025
4.264 ± 0.099	318 ± 54	0.0160 ± 0.0032	343 ± 71	0.0180 ± 0.0042	0.0119 ± 0.0023
4.453 ± 0.105	253 ± 54	0.0121 ± 0.0029	359 ± 73	0.0179 ± 0.0042	0.0097 ± 0.0021
4.647 ± 0.113	331 ± 55	0.0155 ± 0.0030	325 ± 73	0.0158 ± 0.0040	0.0111 ± 0.0022
4.861 ± 0.122	381 ± 57	0.0180 ± 0.0033	410 ± 75	0.0195 ± 0.0042	0.0135 ± 0.0024
5.090 ± 0.129	342 ± 56	0.0157 ± 0.0030	332 ± 75	0.0155 ± 0.0039	0.0111 ± 0.0022
5.333 ± 0.140	230 ± 55	0.0104 ± 0.0027	372 ± 76	0.0173 ± 0.0040	0.0085 ± 0.0019
5.597 ± 0.149	263 ± 57	0.0115 ± 0.0028	310 ± 76	0.0143 ± 0.0039	0.0086 ± 0.0020
5.875 ± 0.160	257 ± 57	0.0111 ± 0.0027	187 ± 75	0.0084 ± 0.0035	0.0068 ± 0.0019
6.181 ± 0.175	282 ± 57	0.0122 ± 0.0027	265 ± 77	0.0117 ± 0.0037	0.0082 ± 0.0020
6.517 ± 0.187	266 ± 59	0.0108 ± 0.0026	274 ± 77	0.0116 ± 0.0035	0.0075 ± 0.0019
6.862 ± 0.201	172 ± 58	0.0066 ± 0.0023	352 ± 79	0.0145 ± 0.0036	0.0057 ± 0.0016
7.237 ± 0.218	272 ± 59	0.0109 ± 0.0026	82 ± 77	0.0036 ± 0.0034	0.0054 ± 0.0018
7.661 ± 0.242	167 ± 58	0.0072 ± 0.0026	16 ± 75	0.0007 ± 0.0035	0.0031 ± 0.0017
8.126 ± 0.263	73 ± 58	0.0031 ± 0.0025	200 ± 77	0.0093 ± 0.0037	0.0027 ± 0.0016
8.618 ± 0.284	77 ± 58	0.0032 ± 0.0024	121 ± 77	0.0055 ± 0.0035	0.0020 ± 0.0016
9.160 ± 0.313	31 ± 58	0.0013 ± 0.0025	112 ± 77	0.0052 ± 0.0036	0.0009 ± 0.0018
9.757 ± 0.346	141 ± 60	0.0062 ± 0.0027	121 ± 76	0.0058 ± 0.0037	0.0037 ± 0.0018
10.414 ± 0.377	82 ± 57	0.0037 ± 0.0026	165 ± 76	0.0083 ± 0.0039	0.0028 ± 0.0017
11.143 ± 0.425	77 ± 57	0.0037 ± 0.0028	266 ± 75	0.0141 ± 0.0043	0.0038 ± 0.0018
11.960 ± 0.467	48 ± 57	0.0024 ± 0.0029	186 ± 75	0.0102 ± 0.0043	0.0024 ± 0.0018
12.860 ± 0.525	41 ± 57	0.0021 ± 0.0029	188 ± 75	0.0106 ± 0.0044	0.0023 ± 0.0019
13.876 ± 0.589	88 ± 57	0.0046 ± 0.0030	0 ± 0	0.0001 ± 0.0000	-0.0032 ± 0.0009
15.016 ± 0.660	53 ± 58	0.0028 ± 0.0030	110 ± 75	0.0063 ± 0.0044	0.0019 ± 0.0020
16.297 ± 0.750	6 ± 58	0.0003 ± 0.0030	54 ± 75	0.0031 ± 0.0043	-0.0001 ± 0.0019
17.759 ± 0.857	21 ± 59	0.0011 ± 0.0031	101 ± 75	0.0057 ± 0.0043	0.0009 ± 0.0019
19.416 ± 0.971	57 ± 60	0.0029 ± 0.0031	14 ± 75	0.0008 ± 0.0041	0.0008 ± 0.0019

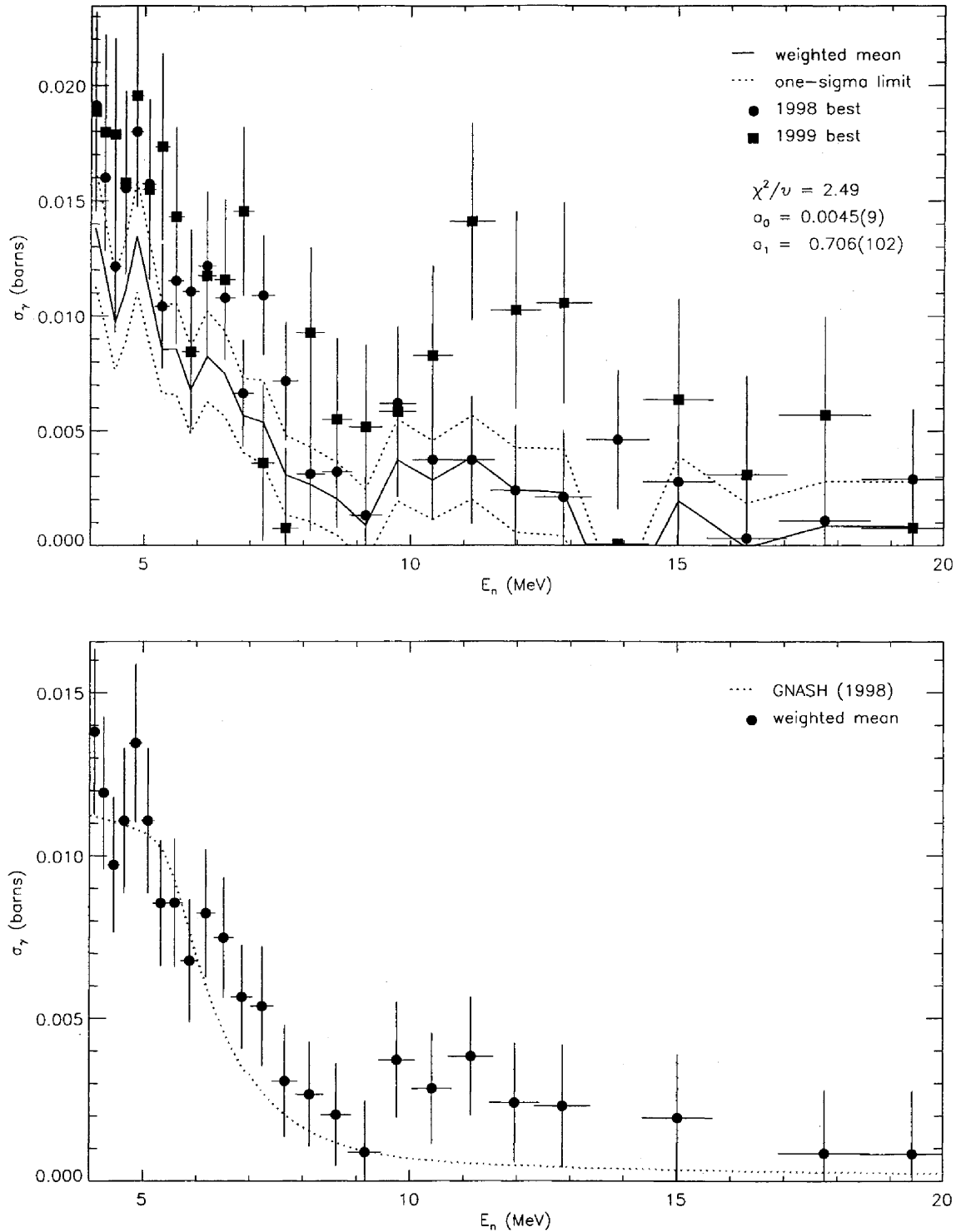


FIG. 81: Adopted $E_\gamma = 316.5$ -keV partial cross section corresponding to the data in table LXXXVIII. The top panel shows the 1998 and 1999 partial cross sections and the recommended value, plotted as a solid line with a one-sigma confidence band (dotted lines). The bottom panel shows this recommended partial cross section (solid circles) compared to GNASH.

TABLE LXXXIX: Adopted partial γ -ray cross section for the $E_\gamma = 375.1$ -keV transition. The measured peak areas and deduced partial cross section for the **98Thin** data set are shown in columns 2 and 3, respectively. The recommended partial cross section, listed in column 4, is obtained by scaling the **98Thin** data by a target-thickness correction factor.

E_n (MeV)	$A^{(1998)}$	$\sigma^{(1998)}$	$\sigma^{(\text{sca})}$
4.090 \pm 0.093	450 \pm 69	0.0233 \pm 0.0043	0.0212 \pm 0.0039
4.264 \pm 0.099	426 \pm 69	0.0215 \pm 0.0041	0.0196 \pm 0.0038
4.453 \pm 0.105	507 \pm 70	0.0244 \pm 0.0042	0.0222 \pm 0.0038
4.647 \pm 0.113	520 \pm 71	0.0244 \pm 0.0041	0.0223 \pm 0.0038
4.861 \pm 0.122	516 \pm 71	0.0244 \pm 0.0042	0.0222 \pm 0.0038
5.090 \pm 0.129	453 \pm 71	0.0209 \pm 0.0039	0.0190 \pm 0.0036
5.333 \pm 0.140	546 \pm 73	0.0247 \pm 0.0041	0.0225 \pm 0.0038
5.597 \pm 0.149	481 \pm 71	0.0211 \pm 0.0038	0.0192 \pm 0.0035
5.875 \pm 0.160	393 \pm 72	0.0169 \pm 0.0035	0.0154 \pm 0.0032
6.181 \pm 0.175	383 \pm 71	0.0166 \pm 0.0035	0.0151 \pm 0.0032
6.517 \pm 0.187	367 \pm 74	0.0149 \pm 0.0033	0.0136 \pm 0.0031
6.862 \pm 0.201	382 \pm 75	0.0147 \pm 0.0032	0.0134 \pm 0.0030
7.237 \pm 0.218	262 \pm 74	0.0105 \pm 0.0031	0.0096 \pm 0.0029
7.661 \pm 0.242	176 \pm 72	0.0076 \pm 0.0032	0.0069 \pm 0.0029
8.126 \pm 0.263	247 \pm 74	0.0106 \pm 0.0033	0.0096 \pm 0.0030
8.618 \pm 0.284	112 \pm 73	0.0047 \pm 0.0031	0.0043 \pm 0.0028
9.160 \pm 0.313	208 \pm 73	0.0088 \pm 0.0032	0.0080 \pm 0.0029
9.757 \pm 0.346	354 \pm 73	0.0156 \pm 0.0036	0.0142 \pm 0.0033
10.414 \pm 0.377	318 \pm 72	0.0145 \pm 0.0036	0.0132 \pm 0.0033
11.143 \pm 0.425	260 \pm 70	0.0126 \pm 0.0036	0.0115 \pm 0.0033
11.960 \pm 0.467	231 \pm 71	0.0115 \pm 0.0037	0.0105 \pm 0.0034
12.860 \pm 0.525	319 \pm 71	0.0164 \pm 0.0040	0.0149 \pm 0.0037
13.876 \pm 0.589	241 \pm 71	0.0126 \pm 0.0039	0.0115 \pm 0.0036
15.016 \pm 0.660	178 \pm 71	0.0093 \pm 0.0038	0.0085 \pm 0.0035
16.297 \pm 0.750	154 \pm 71	0.0080 \pm 0.0038	0.0073 \pm 0.0035
17.759 \pm 0.857	73 \pm 72	0.0038 \pm 0.0038	0.0035 \pm 0.0034
19.416 \pm 0.971	373 \pm 76	0.0190 \pm 0.0043	0.0173 \pm 0.0040

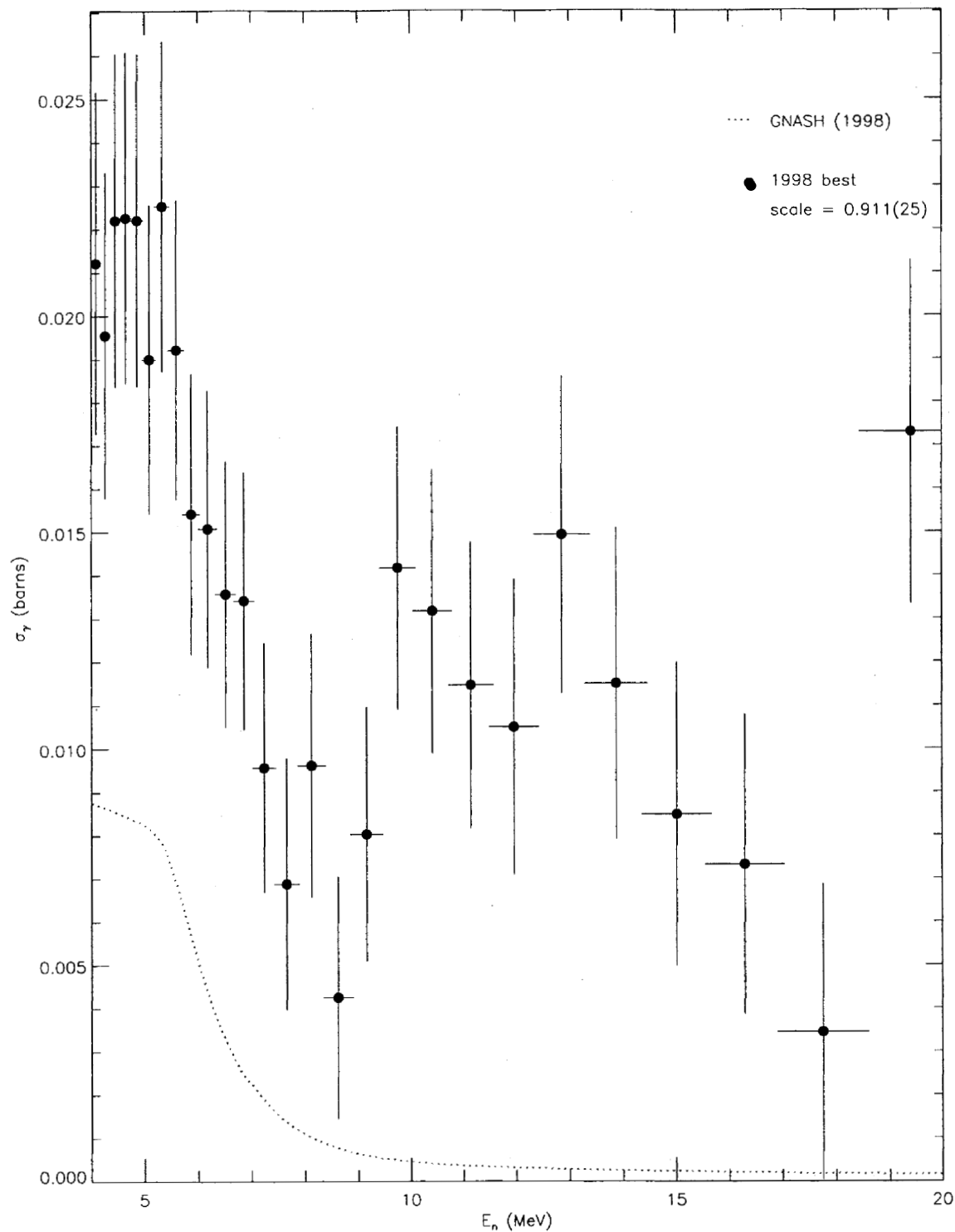


FIG. 82: Adopted $E_\gamma = 375.1$ -keV partial cross section corresponding to the data in table LXXXIX. The target-thickness correction factor is shown, and the recommended partial cross section (solid circles) is compared to GNASH.

TABLE XC: Adopted partial γ -ray cross section for the $E_\gamma = 380.1$ -keV transition. The measured peak areas and deduced partial cross sections for the **98Thin** and **99Thin** data sets are shown in columns 2–5. The recommended partial cross section, listed in column 6, is obtained from both data sets using the optimization procedure described in section XII B.

E_n (MeV)	$A^{(1998)}$	$\sigma^{(1998)}$	$A^{(1999)}$	$\sigma^{(1999)}$	$\sigma^{(\text{opt})}$
4.090 ± 0.093	175 ± 57	0.0091 ± 0.0031	331 ± 74	0.0174 ± 0.0044	0.0057 ± 0.0016
4.264 ± 0.099	178 ± 57	0.0090 ± 0.0030	140 ± 72	0.0073 ± 0.0039	0.0043 ± 0.0015
4.453 ± 0.105	214 ± 57	0.0103 ± 0.0029	191 ± 75	0.0095 ± 0.0039	0.0052 ± 0.0015
4.647 ± 0.113	242 ± 58	0.0114 ± 0.0030	216 ± 76	0.0104 ± 0.0039	0.0058 ± 0.0015
4.861 ± 0.122	225 ± 59	0.0106 ± 0.0030	241 ± 77	0.0114 ± 0.0039	0.0056 ± 0.0015
5.090 ± 0.129	264 ± 60	0.0121 ± 0.0030	258 ± 78	0.0120 ± 0.0039	0.0064 ± 0.0016
5.333 ± 0.140	287 ± 60	0.0130 ± 0.0030	316 ± 79	0.0146 ± 0.0040	0.0072 ± 0.0016
5.597 ± 0.149	241 ± 61	0.0106 ± 0.0029	234 ± 79	0.0107 ± 0.0038	0.0055 ± 0.0015
5.875 ± 0.160	262 ± 60	0.0113 ± 0.0028	137 ± 78	0.0061 ± 0.0036	0.0050 ± 0.0015
6.181 ± 0.175	322 ± 62	0.0139 ± 0.0030	253 ± 79	0.0111 ± 0.0037	0.0070 ± 0.0016
6.517 ± 0.187	119 ± 62	0.0048 ± 0.0026	137 ± 80	0.0058 ± 0.0034	0.0023 ± 0.0012
6.862 ± 0.201	219 ± 63	0.0084 ± 0.0026	138 ± 81	0.0057 ± 0.0034	0.0039 ± 0.0013
7.237 ± 0.218	80 ± 62	0.0032 ± 0.0025	151 ± 81	0.0066 ± 0.0036	0.0017 ± 0.0012
7.661 ± 0.242	142 ± 62	0.0061 ± 0.0027	0 ± 3	0.0000 ± 0.0004	-0.0032 ± 0.0004
8.126 ± 0.263	86 ± 61	0.0037 ± 0.0026	164 ± 80	0.0076 ± 0.0038	0.0020 ± 0.0013
8.618 ± 0.284	103 ± 63	0.0043 ± 0.0027	268 ± 81	0.0121 ± 0.0039	0.0028 ± 0.0013
9.160 ± 0.313	90 ± 62	0.0038 ± 0.0027	88 ± 79	0.0040 ± 0.0037	0.0017 ± 0.0013
9.757 ± 0.346	0 ± 0	0.0000 ± 0.0001	79 ± 78	0.0038 ± 0.0038	0.0000 ± 0.0001
10.414 ± 0.377	181 ± 62	0.0082 ± 0.0029	122 ± 77	0.0061 ± 0.0039	0.0038 ± 0.0015
11.143 ± 0.425	60 ± 61	0.0029 ± 0.0030	21 ± 74	0.0011 ± 0.0039	0.0009 ± 0.0014
11.960 ± 0.467	117 ± 61	0.0058 ± 0.0031	10 ± 71	0.0005 ± 0.0039	0.0020 ± 0.0015
12.860 ± 0.525	45 ± 60	0.0023 ± 0.0031	149 ± 76	0.0083 ± 0.0044	0.0015 ± 0.0015
13.876 ± 0.589	119 ± 61	0.0062 ± 0.0033	30 ± 75	0.0017 ± 0.0043	0.0024 ± 0.0016
15.016 ± 0.660	100 ± 62	0.0052 ± 0.0033	25 ± 75	0.0014 ± 0.0043	0.0020 ± 0.0016
16.297 ± 0.750	67 ± 63	0.0035 ± 0.0033	154 ± 77	0.0088 ± 0.0045	0.0021 ± 0.0016
17.759 ± 0.857	195 ± 64	0.0101 ± 0.0035	15 ± 76	0.0008 ± 0.0043	0.0037 ± 0.0017
19.416 ± 0.971	65 ± 63	0.0033 ± 0.0032	135 ± 78	0.0074 ± 0.0044	0.0019 ± 0.0015

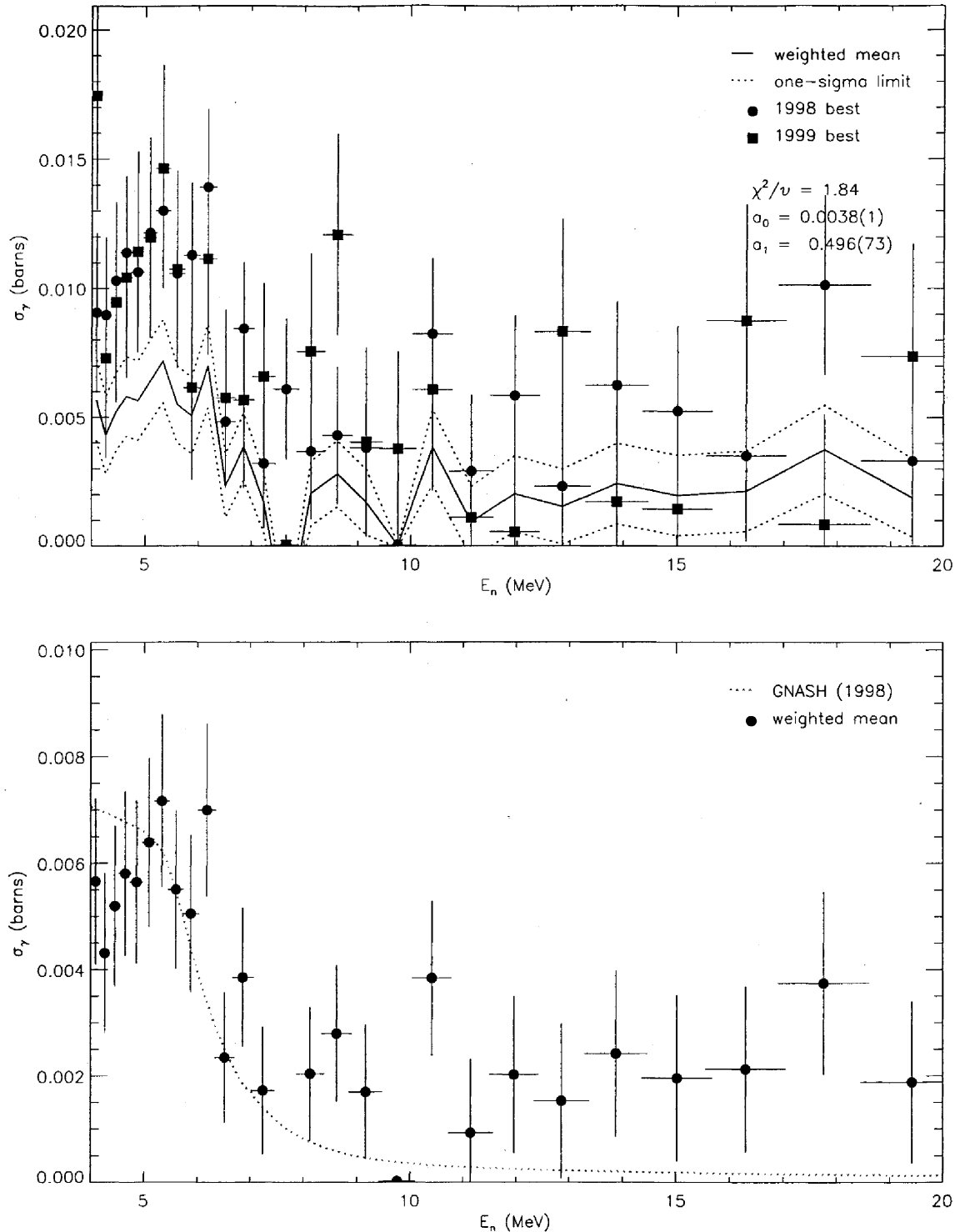


FIG. 83: Adopted $E_\gamma = 380.1$ -keV partial cross section corresponding to the data in table XC. The top panel shows the 1998 and 1999 partial cross sections and the recommended value, plotted as a solid line with a one-sigma confidence band (dotted lines). The bottom panel shows this recommended partial cross section (solid circles) compared to GNASH.

TABLE XCI: Adopted partial γ -ray cross section for the $E_\gamma = 392.5$ -keV transition. The measured peak areas and deduced partial cross sections for the **98Thin** and **99Thin** data sets are shown in columns 2–5. The recommended partial cross section, listed in column 6, is obtained from both data sets using the optimization procedure described in section XII B.

E_n (MeV)	$A^{(1998)}$	$\sigma^{(1998)}$	$A^{(1999)}$	$\sigma^{(1999)}$	$\sigma^{(\text{opt})}$
4.090 ± 0.093	346 ± 57	0.0184 ± 0.0036	343 ± 73	0.0186 ± 0.0045	0.0145 ± 0.0024
4.264 ± 0.099	261 ± 57	0.0135 ± 0.0032	470 ± 75	0.0251 ± 0.0049	0.0127 ± 0.0022
4.453 ± 0.105	270 ± 57	0.0133 ± 0.0031	247 ± 73	0.0125 ± 0.0040	0.0101 ± 0.0021
4.647 ± 0.113	329 ± 59	0.0159 ± 0.0033	133 ± 75	0.0066 ± 0.0038	0.0095 ± 0.0022
4.861 ± 0.122	255 ± 58	0.0124 ± 0.0031	369 ± 75	0.0180 ± 0.0042	0.0109 ± 0.0021
5.090 ± 0.129	223 ± 58	0.0105 ± 0.0029	265 ± 77	0.0126 ± 0.0039	0.0086 ± 0.0019
5.333 ± 0.140	260 ± 59	0.0121 ± 0.0030	362 ± 78	0.0172 ± 0.0042	0.0105 ± 0.0020
5.597 ± 0.149	235 ± 59	0.0106 ± 0.0029	292 ± 78	0.0137 ± 0.0040	0.0088 ± 0.0019
5.875 ± 0.160	183 ± 59	0.0081 ± 0.0027	246 ± 78	0.0113 ± 0.0038	0.0068 ± 0.0018
6.181 ± 0.175	277 ± 60	0.0123 ± 0.0029	31 ± 76	0.0014 ± 0.0034	0.0063 ± 0.0019
6.517 ± 0.187	147 ± 61	0.0061 ± 0.0026	2 ± 78	0.0001 ± 0.0034	0.0031 ± 0.0017
6.862 ± 0.201	102 ± 60	0.0040 ± 0.0024	225 ± 80	0.0095 ± 0.0035	0.0040 ± 0.0016
7.237 ± 0.218	35 ± 60	0.0014 ± 0.0025	41 ± 78	0.0018 ± 0.0035	0.0010 ± 0.0016
7.661 ± 0.242	9 ± 52	0.0004 ± 0.0023	20 ± 76	0.0010 ± 0.0036	0.0002 ± 0.0015
8.126 ± 0.263	80 ± 60	0.0035 ± 0.0027	161 ± 78	0.0076 ± 0.0038	0.0034 ± 0.0017
8.618 ± 0.284	91 ± 61	0.0039 ± 0.0026	0 ± 0	0.0000 ± 0.0000	-0.0009 ± 0.0000
9.160 ± 0.313	41 ± 60	0.0018 ± 0.0026	24 ± 76	0.0011 ± 0.0036	0.0010 ± 0.0017
9.757 ± 0.346	74 ± 60	0.0033 ± 0.0027	67 ± 76	0.0033 ± 0.0037	0.0024 ± 0.0017
10.414 ± 0.377	53 ± 59	0.0025 ± 0.0028	0 ± 0	0.0001 ± 0.0000	-0.0009 ± 0.0000
11.143 ± 0.425	17 ± 56	0.0008 ± 0.0028	0 ± 0	0.0001 ± 0.0000	-0.0009 ± 0.0000
11.960 ± 0.467	81 ± 58	0.0041 ± 0.0030	0 ± 4	0.0001 ± 0.0002	-0.0009 ± 0.0002
12.860 ± 0.525	0 ± 0	0.0001 ± 0.0000	62 ± 73	0.0036 ± 0.0042	0.0000 ± 0.0000
13.876 ± 0.589	0 ± 0	0.0001 ± 0.0000	0 ± 0	0.0001 ± 0.0000	-0.0003 ± 0.0000
15.016 ± 0.660	18 ± 59	0.0010 ± 0.0032	0 ± 0	0.0001 ± 0.0000	-0.0009 ± 0.0000
16.297 ± 0.750	0 ± 0	0.0001 ± 0.0000	4 ± 74	0.0002 ± 0.0043	0.0000 ± 0.0000
17.759 ± 0.857	12 ± 60	0.0006 ± 0.0032	75 ± 75	0.0043 ± 0.0043	0.0011 ± 0.0020
19.416 ± 0.971	0 ± 0	0.0001 ± 0.0000	0 ± 0	0.0001 ± 0.0000	-0.0003 ± 0.0000

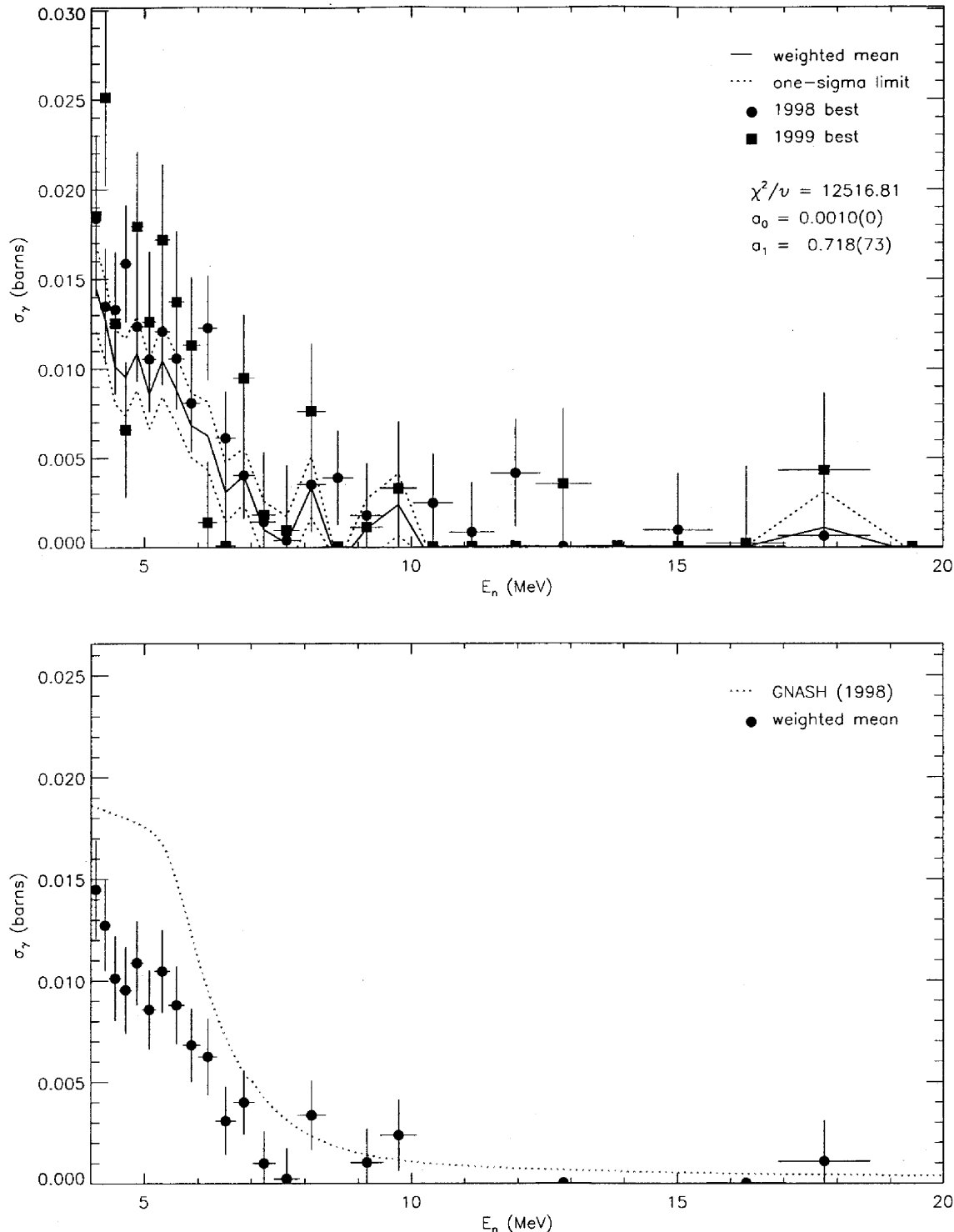


FIG. 84: Adopted $E_\gamma = 392.5$ -keV partial cross section corresponding to the data in table XCI. The top panel shows the 1998 and 1999 partial cross sections and the recommended value, plotted as a solid line with a one-sigma confidence band (dotted lines). The bottom panel shows this recommended partial cross section (solid circles) compared to GNASH.

TABLE XCII: Adopted partial γ -ray cross section for the $E_\gamma = 606.8$ -keV transition. The measured peak areas and deduced partial cross sections for the **98Thin** and **99Thin** data sets are shown in columns 2–5. The recommended partial cross section, listed in column 6, is obtained from both data sets using the optimization procedure described in section XII B.

E_n (MeV)	$A^{(1998)}$	$\sigma^{(1998)}$	$A^{(1999)}$	$\sigma^{(1999)}$	$\sigma^{(\text{opt})}$
4.090 ± 0.093	325 ± 70	0.0214 ± 0.0056	461 ± 90	0.0306 ± 0.0069	0.0153 ± 0.0035
4.264 ± 0.099	296 ± 70	0.0190 ± 0.0053	437 ± 91	0.0286 ± 0.0068	0.0135 ± 0.0033
4.453 ± 0.105	432 ± 70	0.0264 ± 0.0054	310 ± 91	0.0193 ± 0.0061	0.0147 ± 0.0036
4.647 ± 0.113	357 ± 79	0.0213 ± 0.0056	315 ± 92	0.0191 ± 0.0060	0.0126 ± 0.0034
4.861 ± 0.122	315 ± 70	0.0189 ± 0.0050	208 ± 88	0.0124 ± 0.0054	0.0098 ± 0.0031
5.090 ± 0.129	330 ± 80	0.0193 ± 0.0054	349 ± 91	0.0204 ± 0.0058	0.0122 ± 0.0032
5.333 ± 0.140	339 ± 69	0.0195 ± 0.0048	362 ± 92	0.0211 ± 0.0059	0.0123 ± 0.0031
5.597 ± 0.149	357 ± 80	0.0199 ± 0.0052	215 ± 91	0.0124 ± 0.0054	0.0101 ± 0.0031
5.875 ± 0.160	271 ± 69	0.0148 ± 0.0045	160 ± 89	0.0090 ± 0.0051	0.0073 ± 0.0027
6.181 ± 0.175	249 ± 69	0.0137 ± 0.0044	246 ± 90	0.0136 ± 0.0052	0.0079 ± 0.0026
6.517 ± 0.187	388 ± 81	0.0200 ± 0.0049	100 ± 90	0.0053 ± 0.0048	0.0077 ± 0.0030
6.862 ± 0.201	428 ± 83	0.0210 ± 0.0048	383 ± 92	0.0198 ± 0.0052	0.0128 ± 0.0031
7.237 ± 0.218	327 ± 84	0.0167 ± 0.0049	127 ± 89	0.0070 ± 0.0050	0.0073 ± 0.0028
7.661 ± 0.242	291 ± 81	0.0159 ± 0.0050	109 ± 87	0.0064 ± 0.0052	0.0069 ± 0.0029
8.126 ± 0.263	284 ± 79	0.0154 ± 0.0049	114 ± 88	0.0066 ± 0.0052	0.0069 ± 0.0028
8.618 ± 0.284	362 ± 83	0.0192 ± 0.0051	190 ± 88	0.0108 ± 0.0051	0.0093 ± 0.0030
9.160 ± 0.313	223 ± 81	0.0120 ± 0.0049	127 ± 86	0.0073 ± 0.0050	0.0057 ± 0.0027
9.757 ± 0.346	187 ± 80	0.0104 ± 0.0050	129 ± 84	0.0078 ± 0.0051	0.0052 ± 0.0026
10.414 ± 0.377	282 ± 78	0.0163 ± 0.0052	180 ± 84	0.0113 ± 0.0054	0.0084 ± 0.0030
11.143 ± 0.425	191 ± 77	0.0118 ± 0.0053	36 ± 80	0.0024 ± 0.0053	0.0044 ± 0.0028
11.960 ± 0.467	182 ± 78	0.0115 ± 0.0055	237 ± 80	0.0163 ± 0.0058	0.0077 ± 0.0029
12.860 ± 0.525	146 ± 78	0.0095 ± 0.0056	164 ± 79	0.0115 ± 0.0057	0.0057 ± 0.0027
13.876 ± 0.589	21 ± 77	0.0014 ± 0.0056	139 ± 78	0.0100 ± 0.0057	0.0018 ± 0.0027
15.016 ± 0.660	164 ± 77	0.0109 ± 0.0057	63 ± 78	0.0046 ± 0.0057	0.0046 ± 0.0030
16.297 ± 0.750	0 ± 4	0.0001 ± 0.0023	68 ± 78	0.0049 ± 0.0056	0.0001 ± 0.0012
17.759 ± 0.857	150 ± 80	0.0099 ± 0.0058	121 ± 78	0.0085 ± 0.0056	0.0051 ± 0.0030
19.416 ± 0.971	64 ± 70	0.0041 ± 0.0051	173 ± 80	0.0119 ± 0.0057	0.0033 ± 0.0026

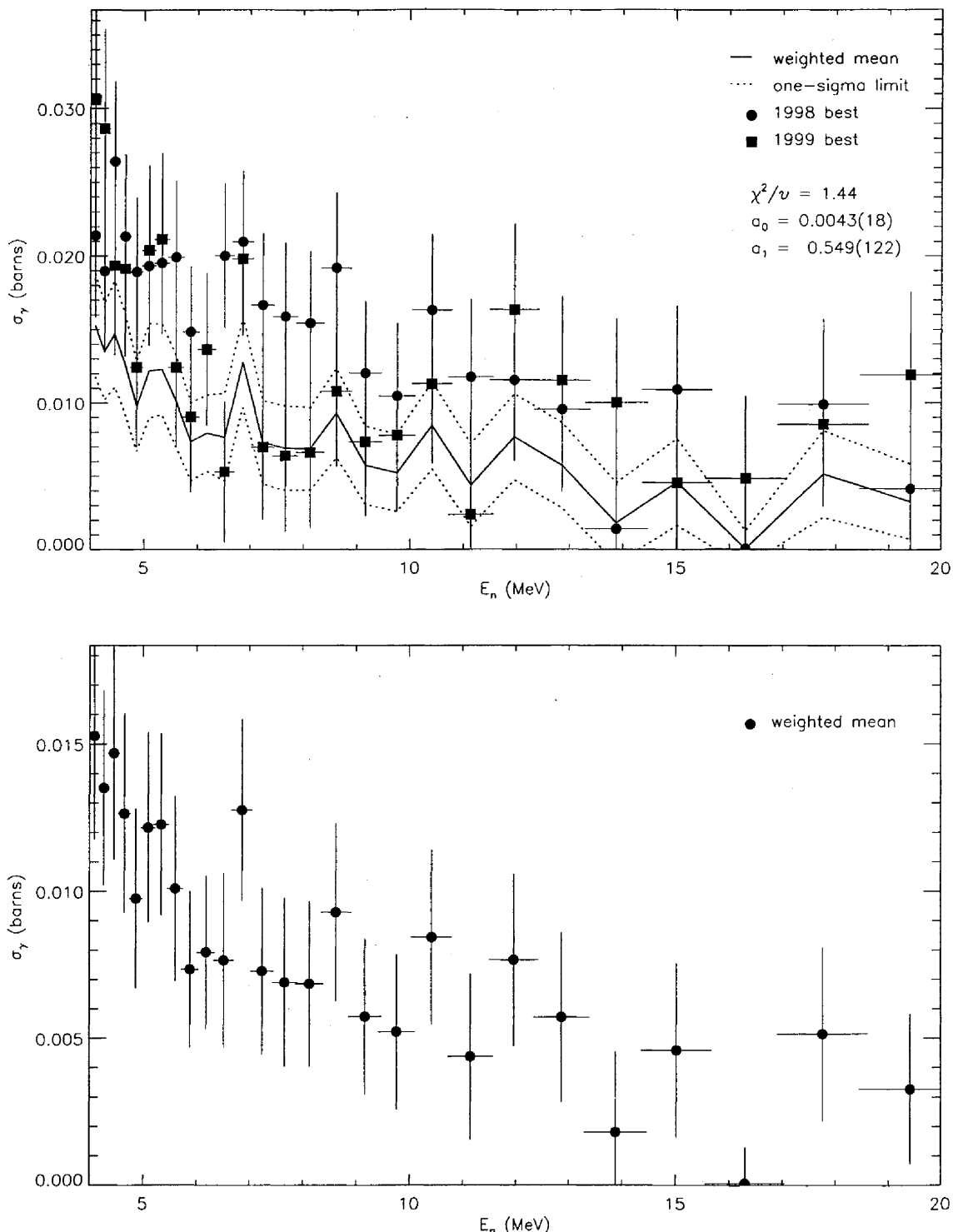


FIG. 85: Adopted $E_\gamma = 606.8$ -keV partial cross section corresponding to the data in table XCII. The top panel shows the 1998 and 1999 partial cross sections and the recommended value, plotted as a solid line with a one-sigma confidence band (dotted lines). The bottom panel shows this recommended partial cross section (solid circles) by itself.

TABLE XCIII: Adopted partial γ -ray cross section for the $E_\gamma = 617.6$ -keV transition. The measured peak areas and deduced partial cross sections for the **98Thin** and **99Thin** data sets are shown in columns 2–5. The recommended partial cross section, listed in column 6, is obtained from both data sets using the optimization procedure described in section XII B.

E_n (MeV)	$A^{(1998)}$	$\sigma^{(1998)}$	$A^{(1999)}$	$\sigma^{(1999)}$	$\sigma^{(\text{opt})}$
4.090 ± 0.093	399 ± 75	0.0279 ± 0.0059	602 ± 93	0.0424 ± 0.0081	0.0237 ± 0.0047
4.264 ± 0.099	475 ± 76	0.0323 ± 0.0061	578 ± 93	0.0402 ± 0.0079	0.0253 ± 0.0049
4.453 ± 0.105	394 ± 75	0.0256 ± 0.0055	491 ± 93	0.0325 ± 0.0071	0.0192 ± 0.0043
4.647 ± 0.113	319 ± 73	0.0202 ± 0.0050	488 ± 93	0.0315 ± 0.0069	0.0161 ± 0.0039
4.861 ± 0.122	350 ± 74	0.0223 ± 0.0052	525 ± 94	0.0332 ± 0.0070	0.0178 ± 0.0041
5.090 ± 0.129	373 ± 74	0.0232 ± 0.0051	567 ± 95	0.0351 ± 0.0070	0.0188 ± 0.0041
5.333 ± 0.140	307 ± 73	0.0188 ± 0.0048	533 ± 94	0.0330 ± 0.0069	0.0157 ± 0.0038
5.597 ± 0.149	224 ± 74	0.0133 ± 0.0046	598 ± 96	0.0366 ± 0.0071	0.0129 ± 0.0035
5.875 ± 0.160	285 ± 75	0.0166 ± 0.0046	583 ± 96	0.0349 ± 0.0069	0.0148 ± 0.0036
6.181 ± 0.175	134 ± 72	0.0078 ± 0.0043	583 ± 94	0.0343 ± 0.0067	0.0088 ± 0.0031
6.517 ± 0.187	188 ± 74	0.0103 ± 0.0042	529 ± 96	0.0297 ± 0.0063	0.0096 ± 0.0031
6.862 ± 0.201	134 ± 75	0.0070 ± 0.0040	534 ± 94	0.0293 ± 0.0061	0.0073 ± 0.0029
7.237 ± 0.218	248 ± 75	0.0134 ± 0.0043	268 ± 91	0.0156 ± 0.0056	0.0077 ± 0.0031
7.661 ± 0.242	141 ± 74	0.0082 ± 0.0044	304 ± 89	0.0189 ± 0.0059	0.0058 ± 0.0031
8.126 ± 0.263	131 ± 74	0.0076 ± 0.0043	195 ± 89	0.0120 ± 0.0056	0.0036 ± 0.0030
8.618 ± 0.284	61 ± 73	0.0034 ± 0.0041	332 ± 90	0.0200 ± 0.0058	0.0032 ± 0.0029
9.160 ± 0.313	205 ± 75	0.0117 ± 0.0044	328 ± 87	0.0201 ± 0.0058	0.0081 ± 0.0032
9.757 ± 0.346	101 ± 72	0.0060 ± 0.0043	236 ± 86	0.0151 ± 0.0057	0.0036 ± 0.0030
10.414 ± 0.377	54 ± 71	0.0033 ± 0.0044	322 ± 85	0.0214 ± 0.0061	0.0035 ± 0.0030
11.143 ± 0.425	59 ± 71	0.0039 ± 0.0047	243 ± 83	0.0171 ± 0.0061	0.0028 ± 0.0032
11.960 ± 0.467	207 ± 72	0.0139 ± 0.0050	119 ± 81	0.0087 ± 0.0060	0.0054 ± 0.0035
12.860 ± 0.525	113 ± 71	0.0078 ± 0.0050	64 ± 79	0.0048 ± 0.0059	0.0013 ± 0.0034
13.876 ± 0.589	57 ± 71	0.0040 ± 0.0050	220 ± 79	0.0168 ± 0.0063	0.0028 ± 0.0034
15.016 ± 0.660	102 ± 73	0.0072 ± 0.0052	387 ± 79	0.0297 ± 0.0069	0.0080 ± 0.0036
16.297 ± 0.750	49 ± 71	0.0035 ± 0.0050	224 ± 78	0.0170 ± 0.0062	0.0026 ± 0.0034
17.759 ± 0.857	177 ± 75	0.0124 ± 0.0054	216 ± 79	0.0162 ± 0.0062	0.0070 ± 0.0037
19.416 ± 0.971	187 ± 75	0.0129 ± 0.0053	183 ± 80	0.0134 ± 0.0060	0.0062 ± 0.0036

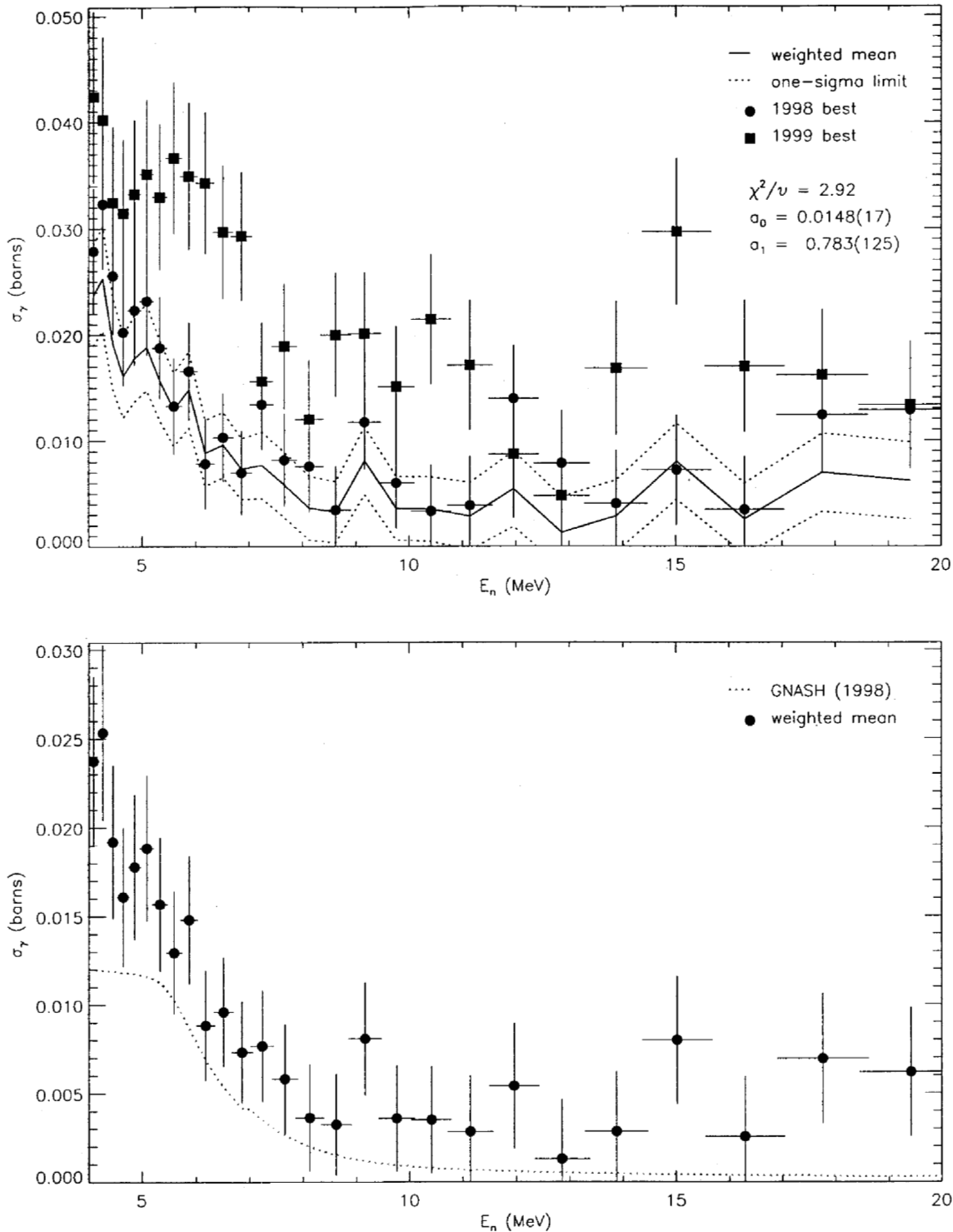


FIG. 86: Adopted $E_\gamma = 617.6$ -keV partial cross section corresponding to the data in table XCIII. The top panel shows the 1998 and 1999 partial cross sections and the recommended value, plotted as a solid line with a one-sigma confidence band (dotted lines). The bottom panel shows this recommended partial cross section (solid circles) compared to GNASH.

TABLE XCIV: Adopted partial γ -ray cross section for the $E_\gamma = 624.9$ -keV transition. The measured peak areas and deduced partial cross sections for the **98Thin** and **99Thin** data sets are shown in columns 2–5. The recommended partial cross section, listed in column 6, is obtained from both data sets using the optimization procedure described in section XII B.

E_n (MeV)	$A^{(1998)}$	$\sigma^{(1998)}$	$A^{(1999)}$	$\sigma^{(1999)}$	$\sigma^{(\text{opt})}$
4.090 ± 0.093	379 ± 72	0.0266 ± 0.0061	507 ± 87	0.0358 ± 0.0073	0.0244 ± 0.0045
4.264 ± 0.099	357 ± 71	0.0244 ± 0.0058	502 ± 88	0.0350 ± 0.0073	0.0227 ± 0.0043
4.453 ± 0.105	268 ± 69	0.0175 ± 0.0052	473 ± 88	0.0314 ± 0.0068	0.0174 ± 0.0038
4.647 ± 0.113	388 ± 70	0.0247 ± 0.0055	473 ± 89	0.0306 ± 0.0067	0.0214 ± 0.0041
4.861 ± 0.122	341 ± 71	0.0218 ± 0.0054	448 ± 89	0.0284 ± 0.0065	0.0191 ± 0.0039
5.090 ± 0.129	407 ± 73	0.0254 ± 0.0055	497 ± 90	0.0309 ± 0.0066	0.0219 ± 0.0041
5.333 ± 0.140	270 ± 71	0.0166 ± 0.0050	419 ± 89	0.0260 ± 0.0062	0.0153 ± 0.0036
5.597 ± 0.149	379 ± 71	0.0225 ± 0.0051	334 ± 90	0.0205 ± 0.0060	0.0166 ± 0.0037
5.875 ± 0.160	371 ± 71	0.0216 ± 0.0050	326 ± 89	0.0196 ± 0.0058	0.0157 ± 0.0036
6.181 ± 0.175	210 ± 71	0.0123 ± 0.0047	420 ± 89	0.0248 ± 0.0059	0.0124 ± 0.0034
6.517 ± 0.187	272 ± 70	0.0149 ± 0.0045	254 ± 89	0.0143 ± 0.0053	0.0105 ± 0.0032
6.862 ± 0.201	270 ± 72	0.0141 ± 0.0043	331 ± 90	0.0182 ± 0.0053	0.0114 ± 0.0031
7.237 ± 0.218	217 ± 73	0.0118 ± 0.0045	229 ± 87	0.0134 ± 0.0053	0.0085 ± 0.0031
7.661 ± 0.242	149 ± 71	0.0087 ± 0.0046	65 ± 85	0.0041 ± 0.0053	0.0037 ± 0.0032
8.126 ± 0.263	154 ± 70	0.0089 ± 0.0045	329 ± 87	0.0203 ± 0.0058	0.0090 ± 0.0032
8.618 ± 0.284	137 ± 72	0.0077 ± 0.0045	299 ± 87	0.0181 ± 0.0056	0.0077 ± 0.0032
9.160 ± 0.313	16 ± 68	0.0009 ± 0.0043	252 ± 84	0.0155 ± 0.0054	0.0029 ± 0.0030
9.757 ± 0.346	14 ± 69	0.0008 ± 0.0045	148 ± 82	0.0095 ± 0.0054	0.0011 ± 0.0031
10.414 ± 0.377	178 ± 70	0.0110 ± 0.0048	40 ± 79	0.0027 ± 0.0053	0.0040 ± 0.0033
11.143 ± 0.425	47 ± 67	0.0031 ± 0.0049	97 ± 79	0.0068 ± 0.0056	0.0015 ± 0.0033
11.960 ± 0.467	117 ± 67	0.0079 ± 0.0051	132 ± 78	0.0097 ± 0.0058	0.0051 ± 0.0035
12.860 ± 0.525	11 ± 59	0.0008 ± 0.0046	115 ± 76	0.0086 ± 0.0058	0.0008 ± 0.0032
13.876 ± 0.589	17 ± 68	0.0012 ± 0.0053	164 ± 76	0.0126 ± 0.0060	0.0024 ± 0.0036
15.016 ± 0.660	93 ± 68	0.0066 ± 0.0053	0 ± 3	0.0001 ± 0.0006	-0.0063 ± 0.0012
16.297 ± 0.750	108 ± 68	0.0076 ± 0.0053	35 ± 73	0.0027 ± 0.0056	0.0021 ± 0.0035
17.759 ± 0.857	0 ± 2	0.0001 ± 0.0022	201 ± 74	0.0151 ± 0.0058	0.0007 ± 0.0017
19.416 ± 0.971	0 ± 0	0.0001 ± 0.0021	30 ± 73	0.0022 ± 0.0054	-0.0004 ± 0.0017

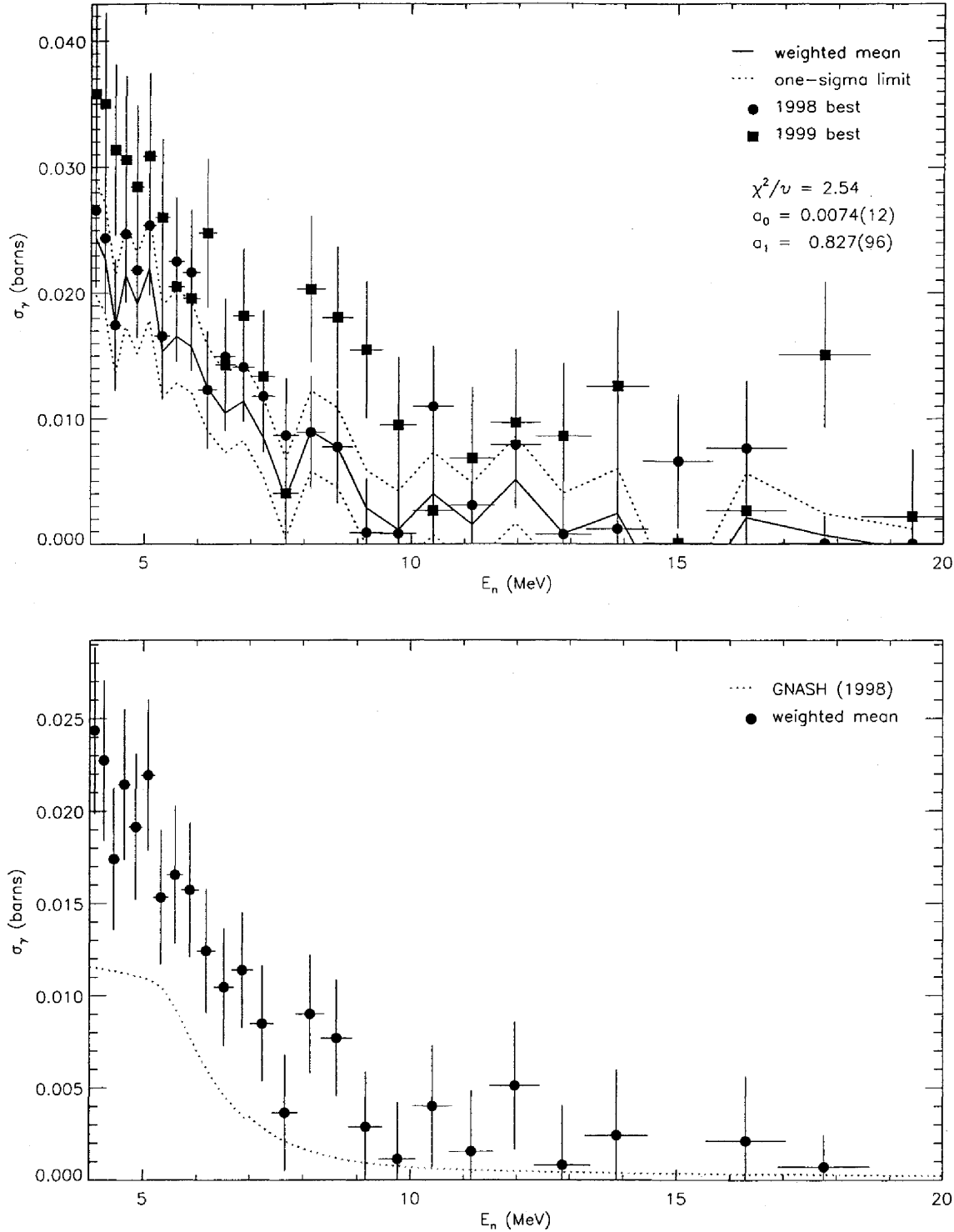


FIG. 87: Adopted $E_\gamma = 624.9$ -keV partial cross section corresponding to the data in table XCIV. The top panel shows the 1998 and 1999 partial cross sections and the recommended value, plotted as a solid line with a one-sigma confidence band (dotted lines). The bottom panel shows this recommended partial cross section (solid circles) compared to GNASH.

TABLE XCV: Adopted partial γ -ray cross section for the $E_\gamma = 633.1$ -keV transition. The measured peak areas and deduced partial cross sections for the **98Thin** and **99Thin** data sets are shown in columns 2–5. The recommended partial cross section, listed in column 6, is obtained from both data sets using the optimization procedure described in section XII B.

E_n (MeV)	$A^{(1998)}$	$\sigma^{(1998)}$	$A^{(1999)}$	$\sigma^{(1999)}$	$\sigma^{(\text{opt})}$
4.090 ± 0.093	283 ± 57	0.0196 ± 0.0048	520 ± 79	0.0362 ± 0.0068	0.0262 ± 0.0042
4.264 ± 0.099	314 ± 57	0.0211 ± 0.0047	396 ± 79	0.0272 ± 0.0062	0.0241 ± 0.0041
4.453 ± 0.105	376 ± 58	0.0241 ± 0.0048	403 ± 80	0.0264 ± 0.0060	0.0257 ± 0.0041
4.647 ± 0.113	511 ± 60	0.0321 ± 0.0052	427 ± 81	0.0272 ± 0.0060	0.0303 ± 0.0044
4.861 ± 0.122	381 ± 58	0.0240 ± 0.0047	413 ± 82	0.0259 ± 0.0059	0.0254 ± 0.0040
5.090 ± 0.129	375 ± 59	0.0231 ± 0.0046	397 ± 82	0.0243 ± 0.0057	0.0241 ± 0.0039
5.333 ± 0.140	424 ± 60	0.0257 ± 0.0047	373 ± 82	0.0228 ± 0.0056	0.0249 ± 0.0040
5.597 ± 0.149	363 ± 58	0.0213 ± 0.0043	336 ± 82	0.0204 ± 0.0055	0.0214 ± 0.0037
5.875 ± 0.160	195 ± 58	0.0112 ± 0.0038	287 ± 81	0.0170 ± 0.0052	0.0137 ± 0.0033
6.181 ± 0.175	263 ± 58	0.0152 ± 0.0040	272 ± 80	0.0158 ± 0.0050	0.0158 ± 0.0033
6.517 ± 0.187	280 ± 58	0.0152 ± 0.0038	328 ± 82	0.0182 ± 0.0050	0.0168 ± 0.0032
6.862 ± 0.201	272 ± 60	0.0140 ± 0.0037	339 ± 82	0.0184 ± 0.0049	0.0160 ± 0.0031
7.237 ± 0.218	217 ± 59	0.0116 ± 0.0037	199 ± 80	0.0115 ± 0.0048	0.0119 ± 0.0031
7.661 ± 0.242	206 ± 59	0.0118 ± 0.0039	234 ± 78	0.0144 ± 0.0051	0.0131 ± 0.0033
8.126 ± 0.263	215 ± 59	0.0123 ± 0.0039	241 ± 79	0.0147 ± 0.0051	0.0135 ± 0.0033
8.618 ± 0.284	203 ± 59	0.0113 ± 0.0038	187 ± 79	0.0111 ± 0.0049	0.0115 ± 0.0032
9.160 ± 0.313	197 ± 59	0.0112 ± 0.0038	61 ± 76	0.0037 ± 0.0046	0.0083 ± 0.0031
9.757 ± 0.346	257 ± 58	0.0151 ± 0.0040	146 ± 75	0.0092 ± 0.0049	0.0129 ± 0.0033
10.414 ± 0.377	192 ± 57	0.0117 ± 0.0040	180 ± 74	0.0118 ± 0.0051	0.0120 ± 0.0033
11.143 ± 0.425	119 ± 55	0.0077 ± 0.0040	150 ± 72	0.0104 ± 0.0052	0.0090 ± 0.0033
11.960 ± 0.467	38 ± 55	0.0025 ± 0.0041	26 ± 70	0.0019 ± 0.0051	0.0023 ± 0.0033
12.860 ± 0.525	114 ± 55	0.0078 ± 0.0043	103 ± 69	0.0076 ± 0.0052	0.0079 ± 0.0034
13.876 ± 0.589	9 ± 54	0.0006 ± 0.0042	111 ± 68	0.0084 ± 0.0052	0.0038 ± 0.0014
15.016 ± 0.660	103 ± 56	0.0072 ± 0.0044	0 ± 5	0.0001 ± 0.0006	0.0008 ± 0.0014
16.297 ± 0.750	167 ± 57	0.0117 ± 0.0046	0 ± 0	0.0001 ± 0.0005	0.0010 ± 0.0013
17.759 ± 0.857	65 ± 56	0.0045 ± 0.0043	0 ± 0	0.0001 ± 0.0005	0.0005 ± 0.0013
19.416 ± 0.971	0 ± 0	0.0001 ± 0.0019	0 ± 0	0.0001 ± 0.0005	0.0001 ± 0.0011

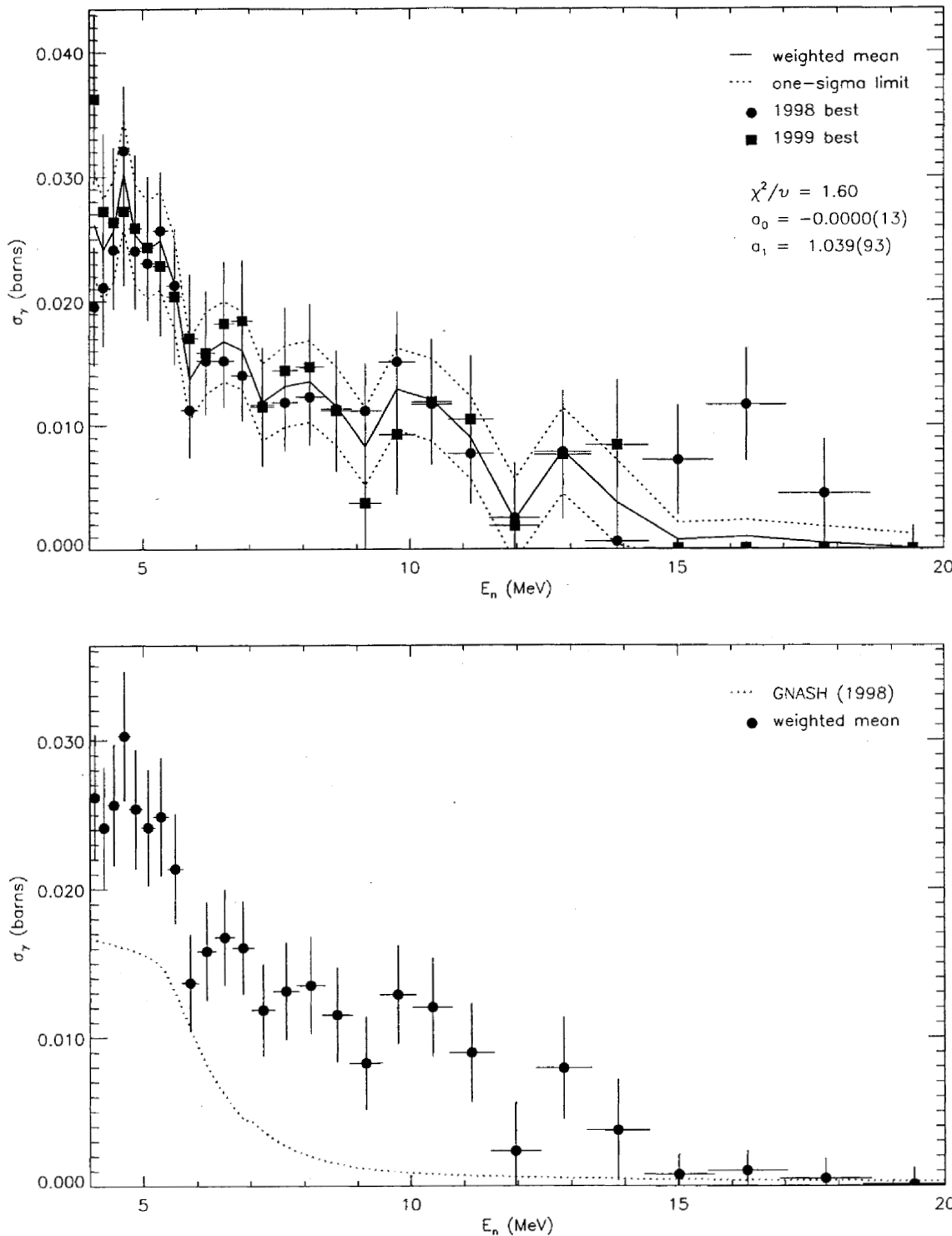


FIG. 88: Adopted $E_\gamma = 633.1$ -keV partial cross section corresponding to the data in table XCV. The top panel shows the 1998 and 1999 partial cross sections and the recommended value, plotted as a solid line with a one-sigma confidence band (dotted lines). The bottom panel shows this recommended partial cross section (solid circles) compared to GNASH.

TABLE XCVI: Adopted partial γ -ray cross section for the $E_\gamma = 637.7$ -keV transition. The measured peak areas and deduced partial cross sections for the **98Thin** and **99Thin** data sets are shown in columns 2–5. The recommended partial cross section, listed in column 6, is obtained from both data sets using the optimization procedure described in section XII B.

E_n (MeV)	$A^{(1998)}$	$\sigma^{(1998)}$	$A^{(1999)}$	$\sigma^{(1999)}$	$\sigma^{(\text{opt})}$
4.090 ± 0.093	265 ± 51	0.0164 ± 0.0037	400 ± 70	0.0249 ± 0.0052	0.0191 ± 0.0034
4.264 ± 0.099	289 ± 51	0.0174 ± 0.0036	289 ± 70	0.0178 ± 0.0048	0.0165 ± 0.0033
4.453 ± 0.105	175 ± 50	0.0100 ± 0.0032	468 ± 72	0.0274 ± 0.0052	0.0149 ± 0.0030
4.647 ± 0.113	231 ± 50	0.0130 ± 0.0032	317 ± 72	0.0181 ± 0.0046	0.0141 ± 0.0030
4.861 ± 0.122	239 ± 51	0.0135 ± 0.0033	484 ± 74	0.0271 ± 0.0051	0.0177 ± 0.0032
5.090 ± 0.129	304 ± 52	0.0167 ± 0.0034	331 ± 73	0.0181 ± 0.0045	0.0163 ± 0.0031
5.333 ± 0.140	177 ± 51	0.0096 ± 0.0030	345 ± 74	0.0189 ± 0.0046	0.0120 ± 0.0028
5.597 ± 0.149	254 ± 52	0.0133 ± 0.0031	237 ± 74	0.0129 ± 0.0043	0.0121 ± 0.0029
5.875 ± 0.160	168 ± 51	0.0086 ± 0.0029	313 ± 74	0.0166 ± 0.0044	0.0105 ± 0.0027
6.181 ± 0.175	180 ± 50	0.0093 ± 0.0028	403 ± 74	0.0210 ± 0.0045	0.0124 ± 0.0027
6.517 ± 0.187	241 ± 52	0.0117 ± 0.0029	217 ± 73	0.0108 ± 0.0038	0.0101 ± 0.0026
6.862 ± 0.201	206 ± 52	0.0095 ± 0.0026	385 ± 75	0.0187 ± 0.0042	0.0118 ± 0.0025
7.237 ± 0.218	48 ± 50	0.0023 ± 0.0025	213 ± 73	0.0110 ± 0.0040	0.0038 ± 0.0023
7.661 ± 0.242	135 ± 51	0.0069 ± 0.0028	221 ± 71	0.0122 ± 0.0042	0.0077 ± 0.0026
8.126 ± 0.263	47 ± 49	0.0024 ± 0.0026	177 ± 71	0.0096 ± 0.0040	0.0035 ± 0.0024
8.618 ± 0.284	45 ± 51	0.0022 ± 0.0026	92 ± 70	0.0049 ± 0.0038	0.0018 ± 0.0023
9.160 ± 0.313	55 ± 50	0.0028 ± 0.0027	276 ± 71	0.0150 ± 0.0042	0.0055 ± 0.0024
9.757 ± 0.346	92 ± 49	0.0048 ± 0.0027	123 ± 68	0.0070 ± 0.0040	0.0044 ± 0.0024
10.414 ± 0.377	120 ± 50	0.0065 ± 0.0029	52 ± 66	0.0031 ± 0.0039	0.0039 ± 0.0026
11.143 ± 0.425	98 ± 49	0.0057 ± 0.0030	132 ± 65	0.0082 ± 0.0042	0.0054 ± 0.0027
11.960 ± 0.467	54 ± 48	0.0032 ± 0.0030	120 ± 64	0.0078 ± 0.0043	0.0035 ± 0.0026
12.860 ± 0.525	27 ± 49	0.0017 ± 0.0031	66 ± 62	0.0044 ± 0.0042	0.0012 ± 0.0027
13.876 ± 0.589	80 ± 49	0.0050 ± 0.0032	0 ± 0	0.0001 ± 0.0006	-0.0031 ± 0.0012
15.016 ± 0.660	46 ± 49	0.0029 ± 0.0032	0 ± 4	0.0001 ± 0.0007	-0.0033 ± 0.0012
16.297 ± 0.750	106 ± 48	0.0066 ± 0.0032	112 ± 61	0.0075 ± 0.0042	0.0057 ± 0.0028
17.759 ± 0.857	2 ± 49	0.0001 ± 0.0032	97 ± 60	0.0064 ± 0.0041	0.0010 ± 0.0027
19.416 ± 0.971	57 ± 49	0.0035 ± 0.0031	18 ± 60	0.0012 ± 0.0039	0.0009 ± 0.0026

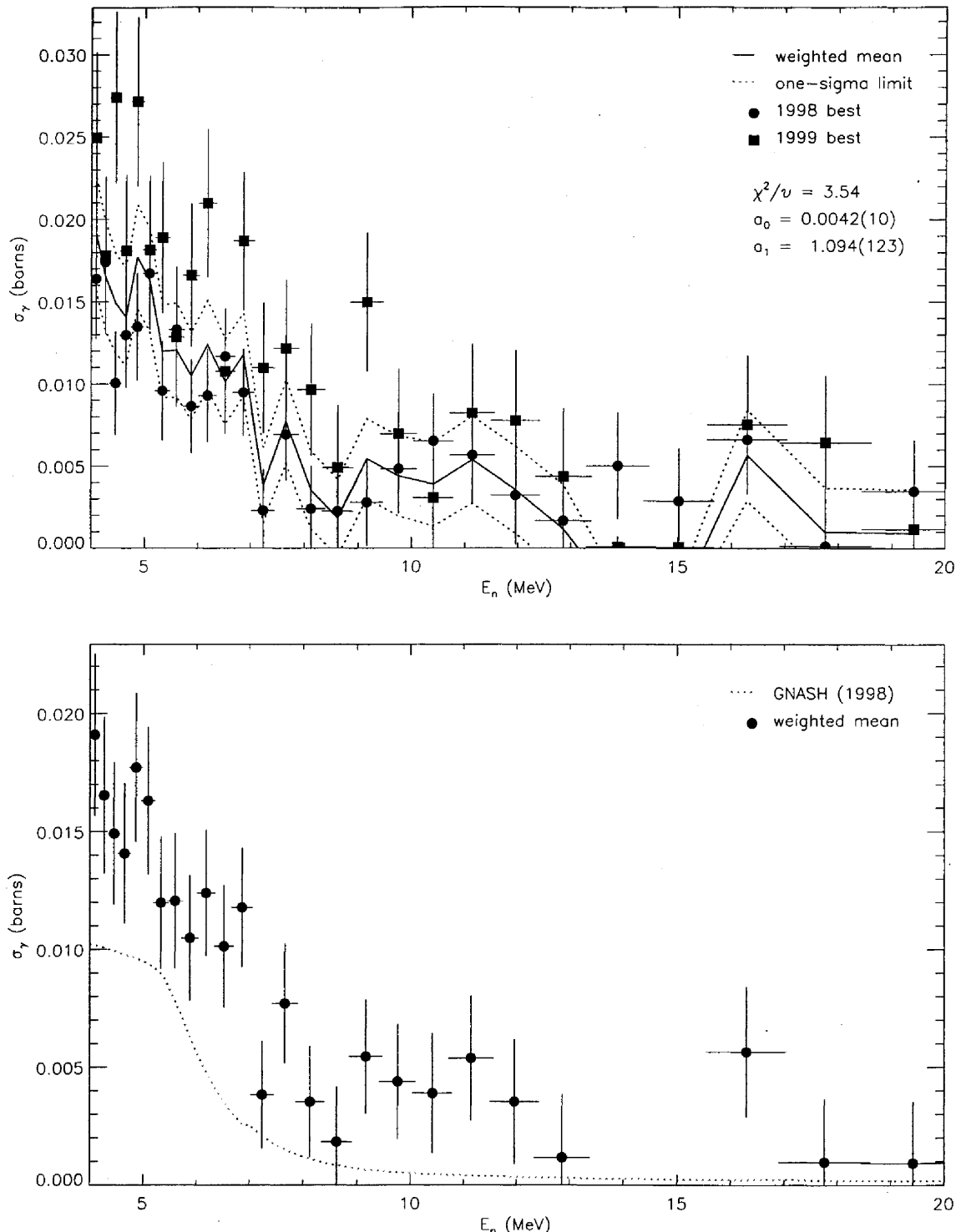


FIG. 89: Adopted $E_\gamma = 637.7$ -keV partial cross section corresponding to the data in table XCVI. The top panel shows the 1998 and 1999 partial cross sections and the recommended value, plotted as a solid line with a one-sigma confidence band (dotted lines). The bottom panel shows this recommended partial cross section (solid circles) compared to GNASH.

TABLE XCVII: Adopted partial γ -ray cross section for the $E_\gamma = 674.2$ -keV transition. The measured peak areas and deduced partial cross sections for the **98Thin** and **99Thin** data sets are shown in columns 2–5. The recommended partial cross section, listed in column 6, is obtained from both data sets using the optimization procedure described in section XII B.

E_n (MeV)	$A^{(1998)}$	$\sigma^{(1998)}$	$A^{(1999)}$	$\sigma^{(1999)}$	$\sigma^{(\text{opt})}$
4.090 ± 0.093	231 ± 47	0.0178 ± 0.0045	89 ± 61	0.0069 ± 0.0049	0.0072 ± 0.0024
4.264 ± 0.099	238 ± 47	0.0178 ± 0.0044	162 ± 62	0.0124 ± 0.0050	0.0084 ± 0.0024
4.453 ± 0.105	304 ± 48	0.0217 ± 0.0044	213 ± 63	0.0155 ± 0.0050	0.0106 ± 0.0026
4.647 ± 0.113	276 ± 48	0.0193 ± 0.0043	87 ± 63	0.0062 ± 0.0046	0.0074 ± 0.0024
4.861 ± 0.122	268 ± 49	0.0188 ± 0.0043	198 ± 65	0.0138 ± 0.0048	0.0091 ± 0.0024
5.090 ± 0.129	363 ± 50	0.0248 ± 0.0046	178 ± 65	0.0121 ± 0.0047	0.0107 ± 0.0028
5.333 ± 0.140	290 ± 51	0.0195 ± 0.0043	108 ± 65	0.0073 ± 0.0046	0.0077 ± 0.0024
5.597 ± 0.149	244 ± 50	0.0159 ± 0.0040	110 ± 66	0.0074 ± 0.0046	0.0067 ± 0.0022
5.875 ± 0.160	242 ± 49	0.0155 ± 0.0038	156 ± 65	0.0103 ± 0.0045	0.0071 ± 0.0021
6.181 ± 0.175	187 ± 49	0.0120 ± 0.0037	243 ± 66	0.0157 ± 0.0047	0.0066 ± 0.0019
6.517 ± 0.187	273 ± 50	0.0164 ± 0.0037	62 ± 65	0.0038 ± 0.0041	0.0059 ± 0.0021
6.862 ± 0.201	297 ± 51	0.0170 ± 0.0037	299 ± 68	0.0180 ± 0.0046	0.0093 ± 0.0022
7.237 ± 0.218	147 ± 49	0.0087 ± 0.0034	115 ± 66	0.0074 ± 0.0044	0.0041 ± 0.0017
7.661 ± 0.242	160 ± 49	0.0102 ± 0.0037	187 ± 65	0.0128 ± 0.0047	0.0054 ± 0.0018
8.126 ± 0.263	180 ± 49	0.0114 ± 0.0037	46 ± 64	0.0031 ± 0.0044	0.0044 ± 0.0019
8.618 ± 0.284	166 ± 51	0.0103 ± 0.0037	10 ± 64	0.0007 ± 0.0043	0.0036 ± 0.0018
9.160 ± 0.313	152 ± 50	0.0096 ± 0.0037	89 ± 64	0.0060 ± 0.0044	0.0042 ± 0.0018
9.757 ± 0.346	132 ± 49	0.0086 ± 0.0037	73 ± 63	0.0051 ± 0.0045	0.0037 ± 0.0018
10.414 ± 0.377	158 ± 49	0.0107 ± 0.0039	55 ± 62	0.0040 ± 0.0046	0.0043 ± 0.0019
11.143 ± 0.425	83 ± 48	0.0060 ± 0.0040	40 ± 60	0.0031 ± 0.0047	0.0024 ± 0.0018
11.960 ± 0.467	114 ± 47	0.0084 ± 0.0041	138 ± 60	0.0111 ± 0.0051	0.0044 ± 0.0019
12.860 ± 0.525	66 ● 47	0.0050 ± 0.0041	143 ± 59	0.0117 ± 0.0051	0.0031 ± 0.0018
13.876 ± 0.589	26 ± 47	0.0020 ± 0.0042	32 ± 57	0.0027 ± 0.0049	0.0008 ± 0.0018
15.016 ± 0.660	8 ± 46	0.0006 ± 0.0041	111 ± 58	0.0093 ± 0.0051	0.0010 ± 0.0017
16.297 ± 0.750	110 ± 48	0.0085 ± 0.0043	11 ± 57	0.0009 ± 0.0049	0.0030 ± 0.0020
17.759 ± 0.857	84 ± 48	0.0065 ± 0.0043	73 ± 58	0.0060 ± 0.0049	0.0030 ± 0.0019
19.416 ± 0.971	0 ± 0	0.0001 ± 0.0020	0 ± 0	0.0001 ± 0.0010	-0.0005 ± 0.0008

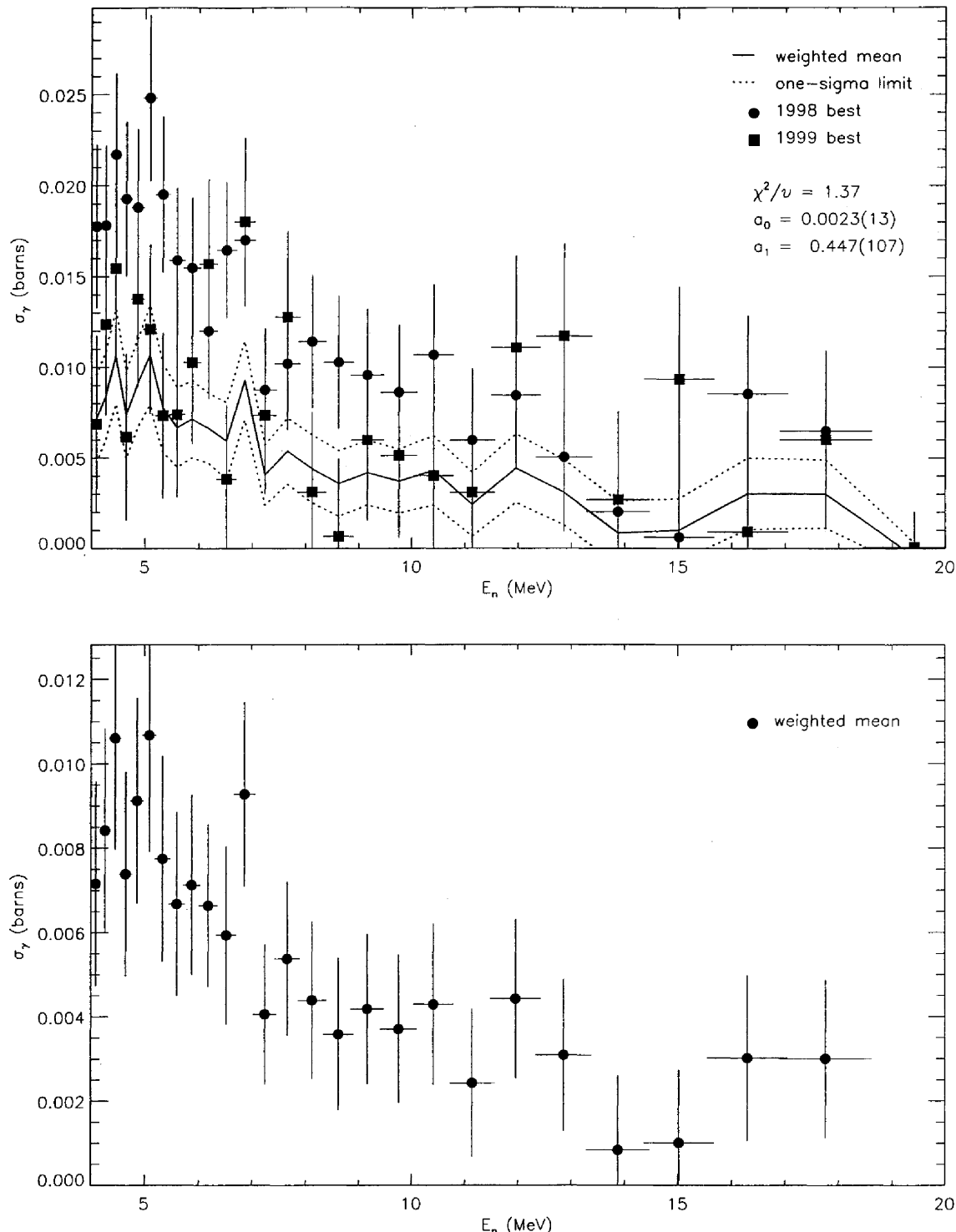


FIG. 90: Adopted $E_\gamma = 674.2$ -keV partial cross section corresponding to the data in table XCVII. The top panel shows the 1998 and 1999 partial cross sections and the recommended value, plotted as a solid line with a one-sigma confidence band (dotted lines). The bottom panel shows this recommended partial cross section (solid circles) compared to GNASH.

D Observed Lines in ^{233}U

Transitions in the $^{235}\text{U}(\text{n},3\text{n})$ are particularly difficult to observe, because like the (n,n') γ rays, they are produced by the de-excitation of the product nucleus through highly fragmented decay paths. The overall reaction cross section for the $(\text{n},3\text{n})$ channel is, however, considerably weaker than the (n,n') reaction cross section. As a result, only 7 transitions in ^{233}U have been identified from GEANIE data, and almost all suffer from some degree of manifest contamination. These γ rays and their placement in the ^{233}U level scheme are shown in figure 91, and listed in table XCVIII. As can be seen from this figure, many expected transitions within and between bands could not be observed. In particular, the $11/2_1^+ \rightarrow 7/2_1^+$ and $9/2_1^+ \rightarrow 5/2_1^+$ transitions in the ground-state band are obfuscated by strong x-ray lines. The strongest-branch transition from the $9/2^-$ member of the $K^\pi = 5/2^-$ band, an $E_\gamma = 313.34(20)$ -keV transition, could not be resolved from the $6_1^+ \rightarrow 4_1^+$ ground-state transition in the high-yield fission fragment ^{128}Te . The next-strongest branch out of that level, an $E_\gamma = 261.66(20)$ -keV transition to the yrast $9/2_1^+$ state, was not observed; a nearby line with energy $E_\gamma = 262.695(281)$ displays an excitation function characteristic of the $^{235}\text{U}(\text{n},3\text{n})$ channel, but the disparity in γ -ray energy where the calibration should be more reliable makes this a tenuous candidate for the $9/2^- \rightarrow 9/2_1^+$ transition. For completeness, we note that the measured yield for this $E_\gamma = 262.695(281)$ line rises to a maximum of 4.2 mb at $E_n = 19.4$ MeV, assuming it is a pure E1 transition. The expected strong-branch $E_\gamma = 280.40(20)$ -keV decay from the $7/2^-$ member of the $K^\pi = 5/2^-$ band was also not observed. The closest observed line at $E_\gamma = 279.068(164)$ would peak at a yield of 6.1 mb, assuming a pure E1 assignment for the corresponding $7/2^- \rightarrow 7/2_1^+$ transition.

For many of the $(\text{n},3\text{n}\gamma)$ transitions discussed here, a non-vanishing yield was measured below the population threshold for the parent level. This problem is a consequence of the weakness of the lines analyzed. This residual baseline was somewhat reduced in some cases by using the random-TOF-subtracted data.

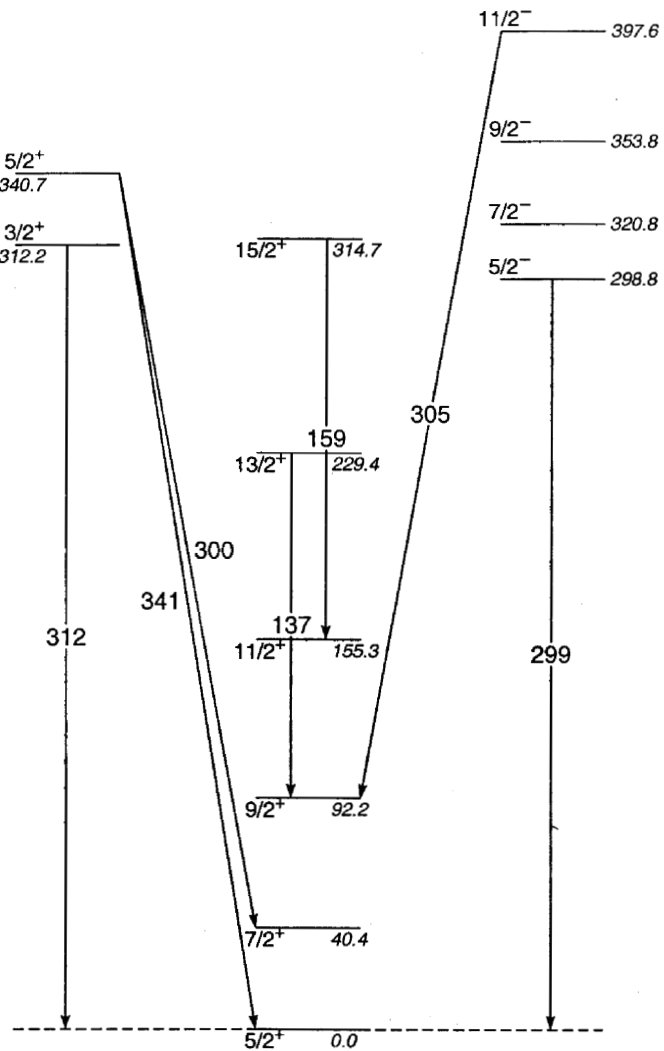


FIG. 91: Gamma rays in ^{233}U observed in the GEANIE data.

TABLE XCVIII: Transitions identified in the $^{235}\text{U}(n,3n\gamma)$ channel and the method by which the data were analyzed.

$E_\gamma^{(\text{meas})}$ (keV)	Analysis method	$E_\gamma^{(\text{acc})}$ (keV)	E_x (keV)	transition
137.607 ± 0.131	subtracted planars, 98Thin and 99Thin optimized	137.2 ± 0.2	229.4	$13/2_1^+ \rightarrow 9/2_1^+$
159.952 ± 0.114	subtracted planars, 98Thin and 99Thin optimized	159.4 ± 0.1	314.7	$15/2_1^+ \rightarrow 11/2_1^+$
298.545 ± 0.113	unsubtracted planars, 98Thin and 99Thin averaged	298.89 ± 0.20	298.8	$5/2^- \rightarrow 5/2_1^+$
300.537 ± 0.118	subtracted planars, 98Thin and 99Thin optimized	300.34 ± 0.02	340.7	$5/2^+ \rightarrow 7/2_1^+$
305.242 ± 0.130	subtracted planars, 98Thin and 99Thin optimized	305.4 ± 0.2	397.6	$11/2^- \rightarrow 9/2_1^+$
311.974 ± 0.115	unsubtracted planars, 98Thin and 99Thin optimized	312.17 ± 0.02	312.2	$3/2^+ \rightarrow 5/2_1^+$
340.628 ± 0.155	subtracted planars, 98Thin and 99Thin optimized	340.81 ± 0.03	340.7	$5/2^+ \rightarrow 5/2_1^+$

The $E_\gamma = 137.6$ keV transition (table XCIX/figure 92): This ground-state-band transition shows residual counts below threshold, and its measured energy deviates from the accepted value by ≈ 0.4 keV, both telltale signs of either contamination or an improper fit. Nevertheless, the yields appear significantly over-estimated by the GNASH calculation.

The $E_\gamma = 160.0$ keV transition (table C/figure 93): Another ground-state-band transition, this line is clearly contaminated by the $E_\gamma = 160.19(5)$ -keV transition from the level at $E_x = 357.3$ keV in ^{235}U . Fortunately, the (n,n') line's yield has nearly vanished when the $(n,3n)$ threshold is reached.

The $E_\gamma = 298.5$ keV transition (table CI/figure 94): This transition, from the band head of a $K^\pi = 5/2^-$ band is strongly contaminated, most likely by the $E_\gamma = 297.0(1)$ -keV $4_1^+ \rightarrow 2_1^+$ transition in the very-high-yield fission fragment ^{134}Te . Extreme caution should be used in interpreting measured yield for this $(n,3n)$ line.

The $E_\gamma = 300.5$ keV transition (table CII/figure 95): This γ ray, one of two depopulating the $5/2^+$ level at $E_x = 340.7$ keV also displays non-vanishing yields below threshold. The observed yields for this line and the other member of the pair at $E_\gamma = 340.6$ keV are consistent with the known branching ratios for these lines, provided no additional baselines are subtracted from either excitation function. The partial cross section for this γ ray is greatly under-predicted by GNASH.

The $E_\gamma = 305.2$ keV transition (table CIII/figure 96): This $13/2^- \rightarrow 9/2_1^+$ transition also suffers from non-vanishing yield below threshold. It is greatly over-predicted by the GNASH calculation.

The $E_\gamma = 312.0$ keV transition (table CIV/figure 97): Residual counts below threshold are seen for this line as well. Some caution is warranted in interpreting yields for this γ -ray as it may be contaminated by an $E_\gamma = 312.90 \pm 0.10$ keV originating from the $E_x = 479.0$ -keV level in ^{126}I produced via the $(n,2n)$ reaction on ^{127}I . The mono-isotopic nucleus ^{127}I is a component of the NaI nose-cone placed on each detector, used to suppress back-scattered γ rays. The strongest branch from the $E_x = 479.0$ -keV level in ^{126}I is a 422.4-keV transition, for which there is evidence in the GEANIE data.

The $E_\gamma = 340.6$ keV transition (table CV/figure 98): This is the second member of the pair of γ rays seen de-exciting the $E_x = 340.7$ -keV level in ^{233}U . The measured partial cross section for this line is much greater than the corresponding GNASH prediction.

TABLE XCIX: Adopted partial γ -ray cross section for the $E_\gamma = 137.6$ -keV transition. The measured peak areas and deduced partial cross sections (before correction for angular distribution effects) for the **98Thin** and **99Thin** data sets are shown in columns 2–5. The partial cross section, listed in column 6, is obtained from both data sets using the optimization procedure described in section XII B. The recommended partial cross section in the last column includes a correction for angular-distribution effects.

E_n (MeV)	$A^{(1998)}$	$\sigma^{(1998)}$	$A^{(1999)}$	$\sigma^{(1999)}$	$\sigma^{(\text{opt})}$	$\sigma^{(\text{opt,corr})}$
4.090 ± 0.093	108 ± 75	0.0089 ± 0.0063	13 ± 96	0.0013 ± 0.0093	0.0041 ± 0.0037	0.0041 ± 0.0037
4.264 ± 0.099	219 ± 77	0.0176 ± 0.0066	260 ± 99	0.0250 ± 0.0100	0.0123 ± 0.0041	0.0121 ± 0.0040
4.453 ± 0.105	149 ± 76	0.0114 ± 0.0060	194 ± 100	0.0177 ± 0.0094	0.0079 ± 0.0036	0.0077 ± 0.0036
4.647 ± 0.113	210 ± 78	0.0158 ± 0.0062	192 ± 101	0.0171 ± 0.0092	0.0101 ± 0.0038	0.0099 ± 0.0038
4.861 ± 0.122	218 ± 79	0.0164 ± 0.0063	157 ± 102	0.0137 ± 0.0091	0.0099 ± 0.0039	0.0097 ± 0.0038
5.090 ± 0.129	131 ± 79	0.0096 ± 0.0059	63 ± 103	0.0054 ± 0.0088	0.0051 ± 0.0035	0.0050 ± 0.0035
5.333 ± 0.140	151 ± 80	0.0109 ± 0.0059	13 ± 99	0.0011 ± 0.0085	0.0050 ± 0.0035	0.0049 ± 0.0035
5.597 ± 0.149	186 ± 81	0.0130 ± 0.0059	0 ± 0	0.0001 ± 0.0000	-0.0018 ± 0.0020	-0.0018 ± 0.0020
5.875 ± 0.160	106 ± 82	0.0073 ± 0.0057	288 ± 111	0.0238 ± 0.0096	0.0062 ± 0.0034	0.0060 ± 0.0034
6.181 ± 0.175	298 ± 83	0.0206 ± 0.0062	354 ± 112	0.0288 ± 0.0097	0.0145 ± 0.0040	0.0143 ± 0.0040
6.517 ± 0.187	205 ± 85	0.0133 ± 0.0057	279 ± 113	0.0216 ± 0.0091	0.0094 ± 0.0035	0.0092 ± 0.0035
6.862 ± 0.201	374 ± 87	0.0230 ± 0.0060	280 ± 114	0.0212 ± 0.0090	0.0146 ± 0.0040	0.0144 ± 0.0039
7.237 ± 0.218	288 ± 86	0.0184 ± 0.0059	74 ± 111	0.0060 ± 0.0090	0.0097 ± 0.0038	0.0095 ± 0.0037
7.661 ± 0.242	305 ± 86	0.0209 ± 0.0064	46 ± 111	0.0040 ± 0.0096	0.0105 ± 0.0041	0.0103 ± 0.0041
8.126 ± 0.263	318 ± 86	0.0217 ± 0.0064	366 ± 112	0.0311 ± 0.0102	0.0154 ± 0.0042	0.0152 ± 0.0041
8.618 ± 0.284	386 ± 87	0.0257 ± 0.0066	230 ± 112	0.0191 ± 0.0096	0.0156 ± 0.0043	0.0153 ± 0.0043
9.160 ± 0.313	281 ± 87	0.0190 ± 0.0063	217 ± 112	0.0184 ± 0.0097	0.0120 ± 0.0040	0.0118 ± 0.0040
9.757 ± 0.346	340 ± 87	0.0238 ± 0.0067	203 ± 110	0.0179 ± 0.0100	0.0144 ± 0.0043	0.0142 ± 0.0043
10.414 ± 0.377	282 ± 85	0.0205 ± 0.0066	91 ± 111	0.0084 ± 0.0103	0.0112 ± 0.0042	0.0110 ± 0.0042
11.143 ± 0.425	386 ± 87	0.0298 ± 0.0076	216 ± 112	0.0210 ± 0.0112	0.0180 ± 0.0050	0.0177 ± 0.0050
11.960 ± 0.467	197 ± 86	0.0157 ± 0.0071	394 ± 114	0.0398 ± 0.0125	0.0127 ± 0.0044	0.0125 ± 0.0044
12.860 ± 0.525	398 ± 88	0.0326 ± 0.0082	130 ± 114	0.0134 ± 0.0119	0.0179 ± 0.0054	0.0161 ± 0.0050
13.876 ± 0.589	300 ± 87	0.0251 ± 0.0079	295 ± 115	0.0311 ± 0.0127	0.0172 ± 0.0051	0.0154 ± 0.0046
15.016 ± 0.660	566 ± 89	0.0473 ± 0.0094	349 ± 115	0.0370 ± 0.0130	0.0300 ± 0.0065	0.0272 ± 0.0060
16.297 ± 0.750	829 ± 92	0.0692 ± 0.0114	546 ± 115	0.0573 ± 0.0140	0.0459 ± 0.0080	0.0419 ± 0.0075
17.759 ± 0.857	1036 ± 94	0.0859 ± 0.0130	538 ± 115	0.0556 ± 0.0137	0.0522 ± 0.0089	0.0478 ± 0.0084
19.416 ± 0.971	1124 ± 94	0.0914 ± 0.0135	615 ± 115	0.0620 ± 0.0139	0.0568 ± 0.0092	0.0524 ± 0.0088

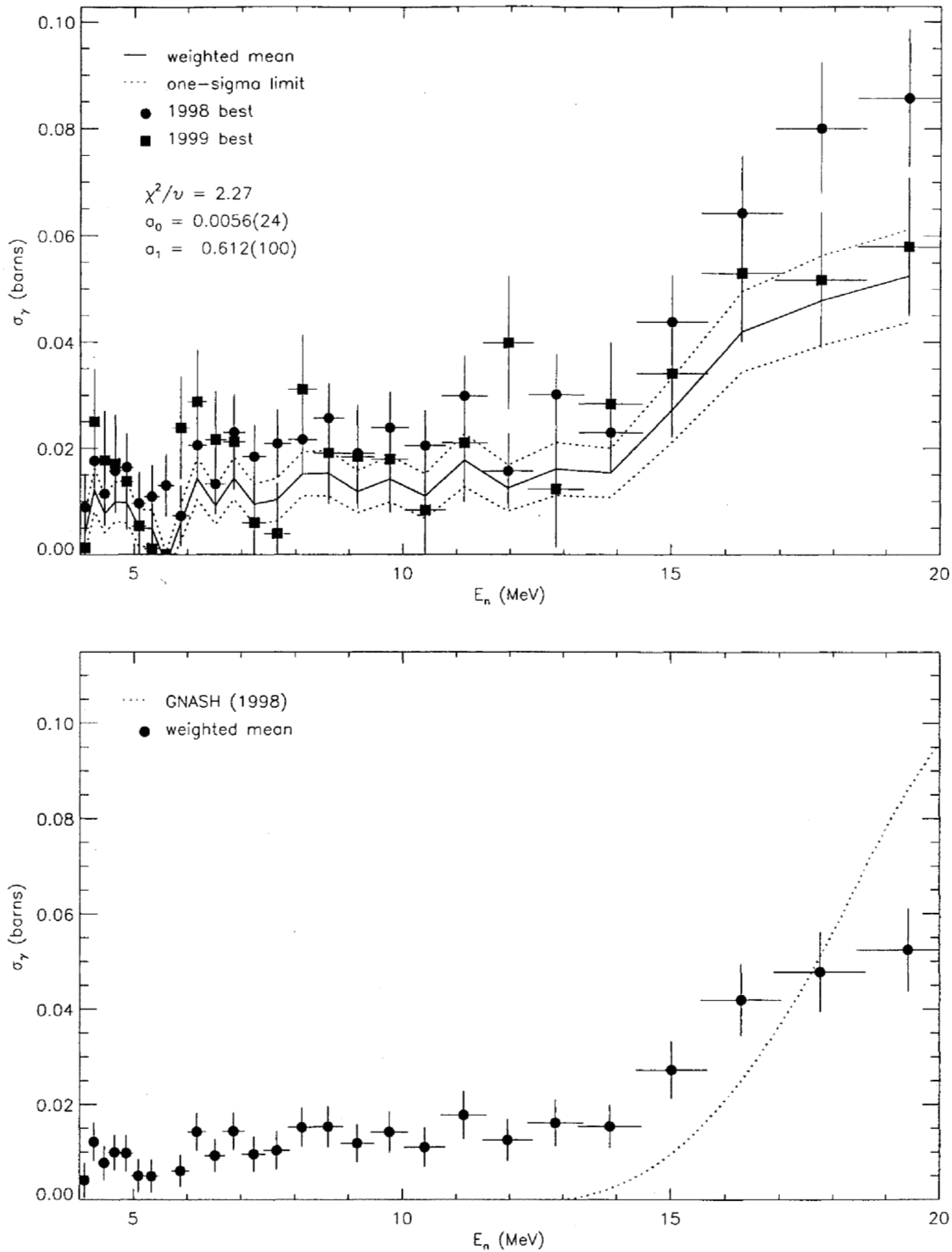


FIG. 92: Adopted $E_\gamma = 137.6$ -keV partial cross section corresponding to the data in table XCIX. The top panel shows the 1998 and 1999 partial cross sections (corrected for angular-distribution effects) and the recommended value, plotted as a solid line with a one-sigma confidence band (dotted lines). The bottom panel shows this recommended partial cross section (solid circles) compared to GNASH.

TABLE C: Adopted partial γ -ray cross section for the $E_\gamma = 160.0$ -keV transition. The measured peak areas and deduced partial cross sections (before correction for angular distribution effects) for the **98Thin** and **99Thin** data sets are shown in columns 2–5. The partial cross section, listed in column 6, is obtained from both data sets using the optimization procedure described in section XII B. The recommended partial cross section in the last column includes a correction for angular-distribution effects.

E_n (MeV)	$A^{(1998)}$	$\sigma^{(1998)}$	$A^{(1999)}$	$\sigma^{(1999)}$	$\sigma^{(\text{opt})}$	$\sigma^{(\text{opt,corr})}$
4.090 ± 0.093	935 ± 85	0.0464 ± 0.0068	764 ± 106	0.0421 ± 0.0077	0.0426 ± 0.0050	0.0428 ± 0.0050
4.264 ± 0.099	1098 ± 86	0.0531 ± 0.0073	750 ± 107	0.0408 ± 0.0075	0.0456 ± 0.0052	0.0457 ± 0.0052
4.453 ± 0.105	1126 ± 87	0.0519 ± 0.0071	989 ± 108	0.0512 ± 0.0082	0.0491 ± 0.0053	0.0492 ± 0.0053
4.647 ± 0.113	1132 ± 87	0.0511 ± 0.0070	1073 ± 109	0.0542 ± 0.0084	0.0495 ± 0.0053	0.0497 ± 0.0053
4.861 ± 0.122	1263 ± 89	0.0573 ± 0.0076	777 ± 109	0.0385 ± 0.0070	0.0462 ± 0.0052	0.0463 ± 0.0052
5.090 ± 0.129	1271 ± 90	0.0561 ± 0.0075	901 ± 110	0.0437 ± 0.0074	0.0483 ± 0.0052	0.0484 ± 0.0052
5.333 ± 0.140	1379 ± 90	0.0599 ± 0.0078	1100 ± 112	0.0533 ± 0.0082	0.0544 ± 0.0056	0.0545 ± 0.0056
5.597 ± 0.149	1359 ± 91	0.0572 ± 0.0075	904 ± 112	0.0434 ± 0.0074	0.0486 ± 0.0053	0.0487 ± 0.0053
5.875 ± 0.160	1498 ± 94	0.0619 ± 0.0079	965 ± 113	0.0453 ± 0.0075	0.0515 ± 0.0055	0.0516 ± 0.0055
6.181 ± 0.175	1222 ± 92	0.0507 ± 0.0068	864 ± 114	0.0398 ± 0.0070	0.0440 ± 0.0049	0.0441 ± 0.0049
6.517 ± 0.187	1240 ± 94	0.0483 ± 0.0065	867 ± 116	0.0381 ± 0.0067	0.0420 ± 0.0047	0.0421 ± 0.0047
6.862 ± 0.201	1074 ± 94	0.0397 ± 0.0056	436 ± 116	0.0187 ± 0.0054	0.0292 ± 0.0039	0.0292 ± 0.0039
7.237 ± 0.218	860 ± 92	0.0331 ± 0.0051	323 ± 115	0.0147 ± 0.0055	0.0248 ± 0.0037	0.0248 ± 0.0037
7.661 ± 0.242	511 ± 90	0.0210 ± 0.0044	431 ± 114	0.0210 ± 0.0061	0.0202 ± 0.0034	0.0203 ± 0.0034
8.126 ± 0.263	372 ± 89	0.0152 ± 0.0040	309 ± 113	0.0149 ± 0.0057	0.0148 ± 0.0031	0.0148 ± 0.0031
8.618 ± 0.284	380 ± 90	0.0152 ± 0.0040	118 ± 113	0.0056 ± 0.0054	0.0123 ± 0.0030	0.0123 ± 0.0030
9.160 ± 0.313	383 ± 89	0.0156 ± 0.0040	315 ± 113	0.0151 ± 0.0057	0.0151 ± 0.0031	0.0151 ± 0.0031
9.757 ± 0.346	437 ± 89	0.0184 ± 0.0043	112 ± 111	0.0056 ± 0.0056	0.0142 ± 0.0032	0.0142 ± 0.0032
10.414 ± 0.377	167 ± 86	0.0073 ± 0.0038	86 ± 110	0.0045 ± 0.0058	0.0069 ± 0.0029	0.0070 ± 0.0029
11.143 ± 0.425	234 ± 87	0.0109 ± 0.0042	0 ± 0	0.0001 ± 0.0000	0.0058 ± 0.0017	0.0058 ± 0.0017
11.960 ± 0.467	285 ± 87	0.0136 ± 0.0044	49 ± 111	0.0028 ± 0.0064	0.0106 ± 0.0034	0.0107 ± 0.0034
12.860 ± 0.525	206 ± 88	0.0102 ± 0.0045	31 ± 112	0.0018 ± 0.0065	0.0082 ± 0.0034	0.0076 ± 0.0031
13.876 ± 0.589	351 ± 89	0.0176 ± 0.0049	205 ± 114	0.0123 ± 0.0070	0.0156 ± 0.0037	0.0143 ± 0.0034
15.016 ± 0.660	561 ± 91	0.0282 ± 0.0056	276 ± 115	0.0166 ± 0.0072	0.0233 ± 0.0042	0.0215 ± 0.0039
16.297 ± 0.750	607 ± 92	0.0304 ± 0.0058	298 ± 115	0.0177 ± 0.0071	0.0249 ± 0.0043	0.0230 ± 0.0040
17.759 ± 0.857	964 ± 94	0.0480 ± 0.0072	503 ± 116	0.0295 ± 0.0076	0.0382 ± 0.0051	0.0354 ± 0.0048
19.416 ± 0.971	1064 ± 96	0.0520 ± 0.0075	576 ± 118	0.0329 ± 0.0078	0.0415 ± 0.0053	0.0387 ± 0.0050

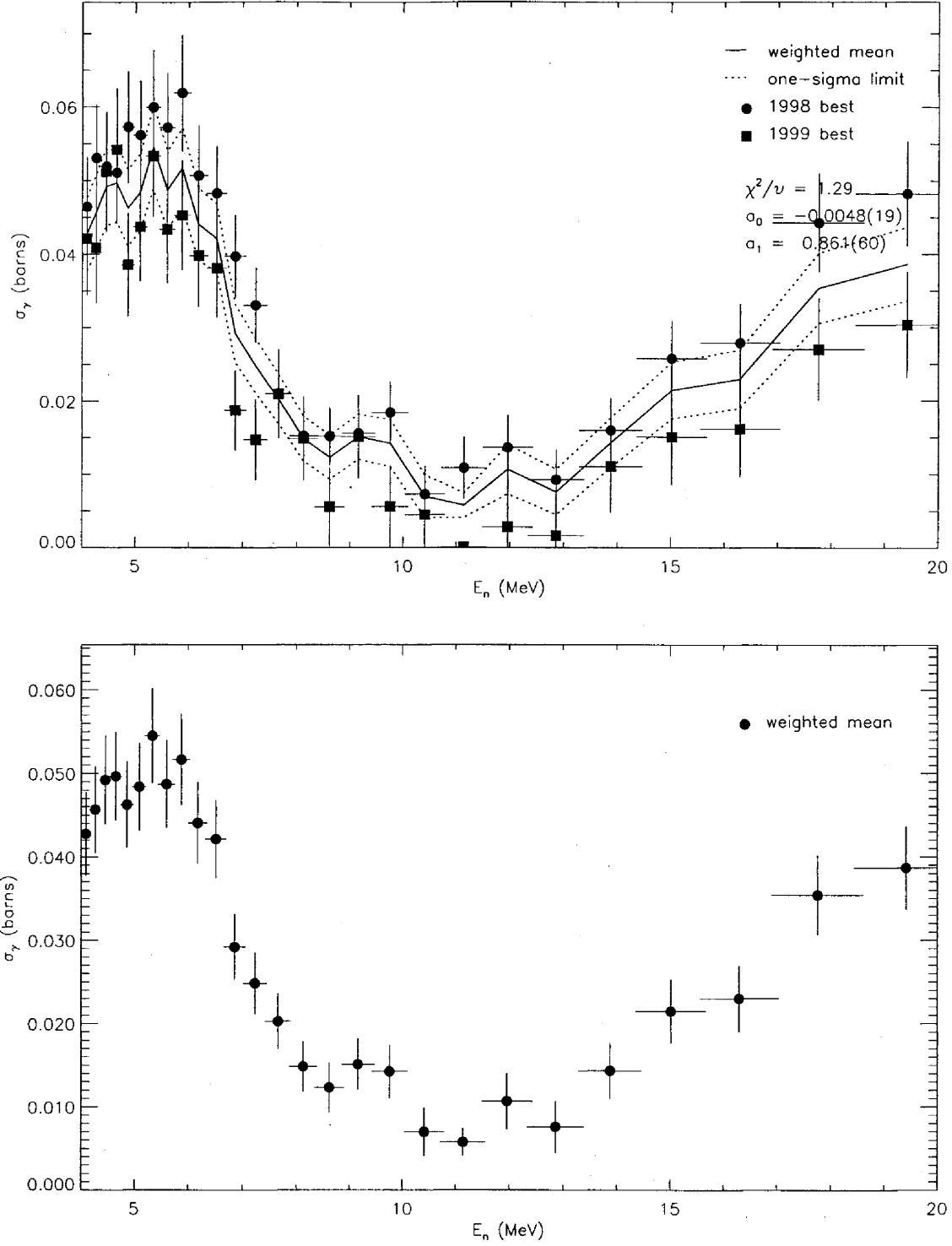


FIG. 93: Adopted $E_\gamma = 160.0$ -keV partial cross section corresponding to the data in table C. The top panel shows the 1998 and 1999 partial cross sections (corrected for angular-distribution effects) and the recommended value, plotted as a solid line with a one-sigma confidence band (dotted lines). The bottom panel shows this recommended partial cross section (solid circles) by itself.

TABLE CI: Adopted partial γ -ray cross section for the $E_\gamma = 298.5$ -keV transition. The measured peak areas and deduced partial cross sections (before correction for angular distribution effects) for the **98Thin** and **99Thin** data sets are shown in columns 2–5. The partial cross section, listed in column 6, is obtained from both data sets using a weighted average. The recommended partial cross section in the last column includes a correction for angular-distribution effects.

E_n (MeV)	$A^{(1998)}$	$\sigma^{(1998)}$	$A^{(1999)}$	$\sigma^{(1999)}$	$\sigma(\text{wei})$	$\sigma(\text{wei,corr})$
4.090 ± 0.093	188 ± 52	0.0048 ± 0.0014	293 ± 68	0.0076 ± 0.0020	0.0057 ± 0.0011	0.0057 ± 0.0011
4.264 ± 0.099	230 ± 53	0.0057 ± 0.0014	260 ± 68	0.0067 ± 0.0019	0.0060 ± 0.0011	0.0060 ± 0.0011
4.453 ± 0.105	208 ± 53	0.0049 ± 0.0013	502 ± 72	0.0123 ± 0.0022	0.0069 ± 0.0012	0.0069 ± 0.0012
4.647 ± 0.113	237 ± 54	0.0055 ± 0.0014	458 ± 72	0.0109 ± 0.0021	0.0071 ± 0.0011	0.0071 ± 0.0011
4.861 ± 0.122	316 ± 56	0.0073 ± 0.0015	498 ± 73	0.0117 ± 0.0021	0.0087 ± 0.0012	0.0087 ± 0.0012
5.090 ± 0.129	276 ± 55	0.0062 ± 0.0014	518 ± 75	0.0119 ± 0.0022	0.0079 ± 0.0012	0.0079 ± 0.0012
5.333 ± 0.140	311 ± 56	0.0069 ± 0.0014	586 ± 75	0.0134 ± 0.0023	0.0087 ± 0.0012	0.0087 ± 0.0012
5.597 ± 0.149	400 ± 58	0.0086 ± 0.0015	741 ± 77	0.0168 ± 0.0025	0.0107 ± 0.0013	0.0107 ± 0.0013
5.875 ± 0.160	427 ± 58	0.0090 ± 0.0015	853 ± 79	0.0189 ± 0.0027	0.0114 ± 0.0013	0.0114 ± 0.0013
6.181 ± 0.175	390 ± 58	0.0083 ± 0.0015	658 ± 77	0.0143 ± 0.0023	0.0100 ± 0.0012	0.0100 ± 0.0012
6.517 ± 0.187	448 ± 60	0.0089 ± 0.0015	705 ± 79	0.0146 ± 0.0023	0.0106 ± 0.0012	0.0106 ± 0.0012
6.862 ± 0.201	537 ± 62	0.0101 ± 0.0015	659 ± 80	0.0134 ± 0.0022	0.0112 ± 0.0013	0.0112 ± 0.0013
7.237 ± 0.218	585 ± 63	0.0115 ± 0.0017	964 ± 82	0.0208 ± 0.0029	0.0138 ± 0.0014	0.0138 ± 0.0014
7.661 ± 0.242	515 ± 62	0.0108 ± 0.0017	809 ± 80	0.0186 ± 0.0027	0.0129 ± 0.0014	0.0129 ± 0.0014
8.126 ± 0.263	493 ± 62	0.0103 ± 0.0016	687 ± 80	0.0157 ± 0.0025	0.0119 ± 0.0014	0.0119 ± 0.0014
8.618 ± 0.284	370 ± 61	0.0076 ± 0.0014	795 ± 81	0.0177 ± 0.0026	0.0099 ± 0.0013	0.0099 ± 0.0013
9.160 ± 0.313	477 ± 62	0.0099 ± 0.0016	695 ± 79	0.0158 ± 0.0025	0.0116 ± 0.0014	0.0116 ± 0.0014
9.757 ± 0.346	512 ± 62	0.0110 ± 0.0017	666 ± 78	0.0158 ± 0.0025	0.0125 ± 0.0014	0.0125 ± 0.0014
10.414 ± 0.377	416 ± 60	0.0093 ± 0.0016	669 ± 78	0.0165 ± 0.0026	0.0112 ± 0.0014	0.0112 ± 0.0014
11.143 ± 0.425	762 ± 63	0.0181 ± 0.0023	756 ± 77	0.0197 ± 0.0030	0.0187 ± 0.0018	0.0187 ± 0.0018
11.960 ± 0.467	1495 ± 70	0.0365 ± 0.0040	880 ± 78	0.0238 ± 0.0034	0.0292 ± 0.0026	0.0292 ± 0.0026
12.860 ± 0.525	834 ± 64	0.0210 ± 0.0026	653 ± 76	0.0180 ± 0.0029	0.0197 ± 0.0019	0.0192 ± 0.0019
13.876 ± 0.589	1027 ± 66	0.0264 ± 0.0031	665 ± 77	0.0188 ± 0.0030	0.0225 ± 0.0022	0.0215 ± 0.0021
15.016 ± 0.660	1016 ± 67	0.0261 ± 0.0031	779 ± 78	0.0221 ± 0.0033	0.0242 ± 0.0023	0.0238 ± 0.0023
16.297 ± 0.750	1083 ± 68	0.0277 ± 0.0033	877 ± 80	0.0247 ± 0.0035	0.0263 ± 0.0024	0.0258 ± 0.0024
17.759 ± 0.857	1163 ± 69	0.0296 ± 0.0034	894 ± 79	0.0248 ± 0.0035	0.0273 ± 0.0024	0.0268 ± 0.0025
19.416 ± 0.971	1051 ± 68	0.0262 ± 0.0031	974 ± 80	0.0263 ± 0.0036	0.0263 ± 0.0024	0.0259 ± 0.0024

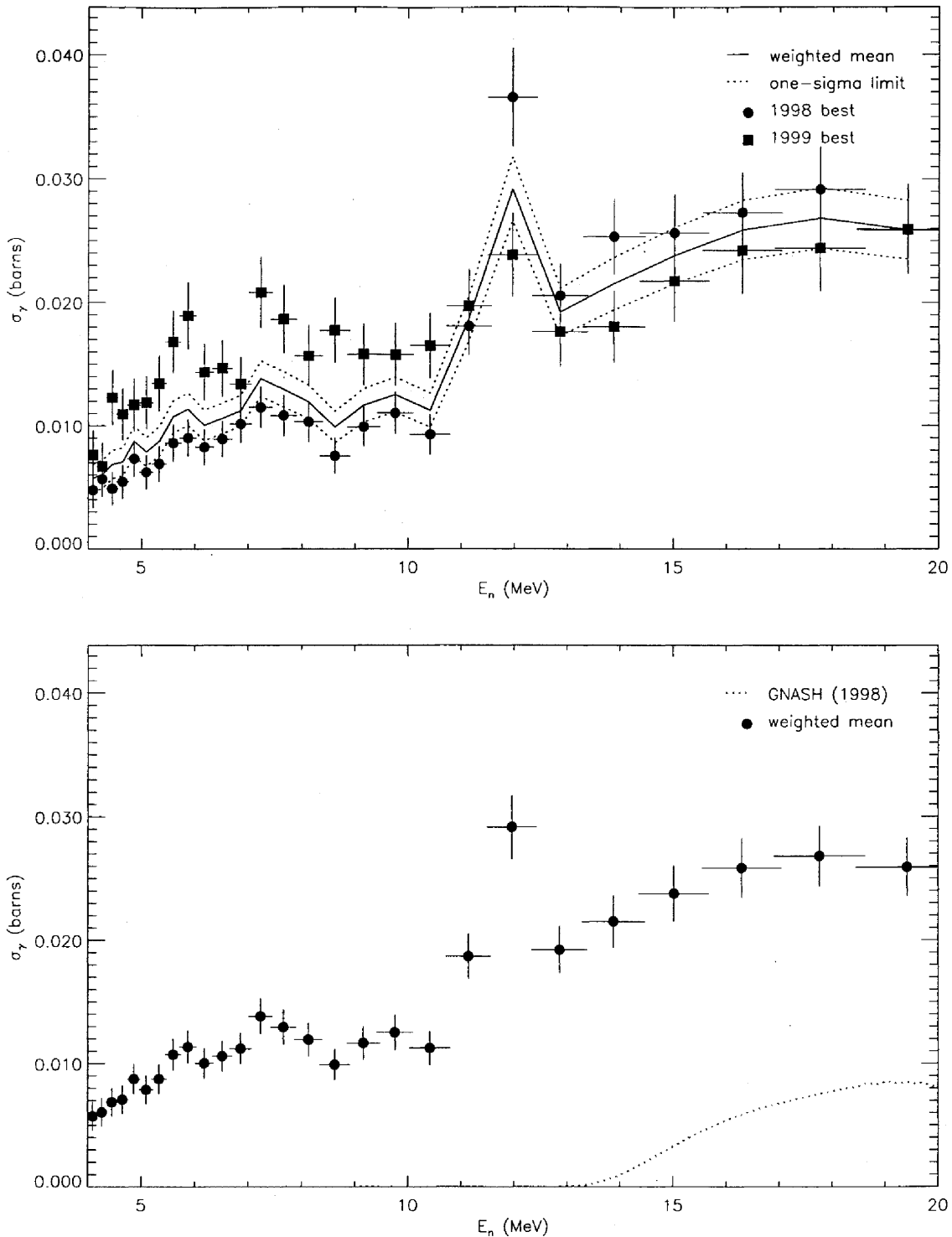


FIG. 94: Adopted $E_\gamma = 298.5$ -keV partial cross section corresponding to the data in table CI. The top panel shows the 1998 and 1999 partial cross sections (corrected for angular-distribution effects) and the recommended value, plotted as a solid line with a one-sigma confidence band (dotted lines). The bottom panel shows this recommended partial cross section (solid circles) compared to GNASH.

TABLE CII: Adopted partial γ -ray cross section for the $E_\gamma = 300.5$ -keV transition. The measured peak areas and deduced partial cross sections (before correction for angular distribution effects) for the **98Thin** and **99Thin** data sets are shown in columns 2–5. The partial cross section, listed in column 6, is obtained from both data sets using the optimization procedure described in section XII B. The recommended partial cross section in the last column includes a correction for angular-distribution effects.

E_n (MeV)	$A^{(1998)}$	$\sigma^{(1998)}$	$A^{(1999)}$	$\sigma^{(1999)}$	$\sigma^{(\text{opt})}$	$\sigma^{(\text{opt,corr})}$
4.090 ± 0.093	40 ± 51	0.0021 ± 0.0027	222 ± 73	0.0120 ± 0.0042	0.0031 ± 0.0020	0.0031 ± 0.0019
4.264 ± 0.099	149 ± 52	0.0076 ± 0.0028	80 ± 72	0.0043 ± 0.0039	0.0048 ± 0.0022	0.0048 ± 0.0022
4.453 ± 0.105	137 ± 53	0.0067 ± 0.0027	66 ± 74	0.0033 ± 0.0038	0.0041 ± 0.0021	0.0041 ± 0.0021
4.647 ± 0.113	175 ± 54	0.0083 ± 0.0027	0 ± 2	0.0000 ± 0.0001	-0.0002 ± 0.0013	-0.0003 ± 0.0013
4.861 ± 0.122	170 ± 54	0.0081 ± 0.0027	191 ± 76	0.0093 ± 0.0038	0.0065 ± 0.0022	0.0065 ± 0.0022
5.090 ± 0.129	178 ± 55	0.0083 ± 0.0027	0 ± 0	0.0000 ± 0.0000	-0.0002 ± 0.0013	-0.0003 ± 0.0013
5.333 ± 0.140	213 ± 55	0.0098 ± 0.0027	275 ± 78	0.0130 ± 0.0040	0.0085 ± 0.0023	0.0085 ± 0.0023
5.597 ± 0.149	116 ± 55	0.0051 ± 0.0025	173 ± 78	0.0081 ± 0.0038	0.0044 ± 0.0019	0.0044 ± 0.0019
5.875 ± 0.160	122 ± 56	0.0053 ± 0.0025	170 ± 78	0.0078 ± 0.0037	0.0044 ± 0.0019	0.0044 ± 0.0019
6.181 ± 0.175	206 ± 57	0.0090 ± 0.0027	181 ± 79	0.0081 ± 0.0037	0.0067 ± 0.0022	0.0067 ± 0.0022
6.517 ± 0.187	205 ± 58	0.0084 ± 0.0025	132 ± 79	0.0057 ± 0.0035	0.0056 ± 0.0021	0.0056 ± 0.0021
6.862 ± 0.201	204 ± 59	0.0080 ± 0.0024	135 ± 80	0.0057 ± 0.0034	0.0054 ± 0.0020	0.0054 ± 0.0020
7.237 ± 0.218	276 ± 60	0.0112 ± 0.0027	242 ± 81	0.0108 ± 0.0038	0.0087 ± 0.0023	0.0086 ± 0.0023
7.661 ± 0.242	210 ± 59	0.0091 ± 0.0027	186 ± 80	0.0089 ± 0.0039	0.0070 ± 0.0023	0.0070 ± 0.0022
8.126 ± 0.263	183 ± 59	0.0079 ± 0.0027	358 ± 82	0.0169 ± 0.0043	0.0082 ± 0.0022	0.0081 ± 0.0022
8.618 ± 0.284	283 ± 61	0.0119 ± 0.0028	224 ± 82	0.0103 ± 0.0040	0.0089 ± 0.0025	0.0089 ± 0.0025
9.160 ± 0.313	183 ± 60	0.0079 ± 0.0027	253 ± 81	0.0119 ± 0.0040	0.0070 ± 0.0022	0.0070 ± 0.0022
9.757 ± 0.346	234 ± 60	0.0104 ± 0.0029	248 ± 80	0.0121 ± 0.0041	0.0087 ± 0.0024	0.0086 ± 0.0024
10.414 ± 0.377	232 ± 60	0.0107 ± 0.0030	268 ± 80	0.0137 ± 0.0044	0.0093 ± 0.0025	0.0092 ± 0.0025
11.143 ± 0.425	132 ± 58	0.0065 ± 0.0029	204 ± 78	0.0110 ± 0.0044	0.0059 ± 0.0023	0.0059 ± 0.0022
11.960 ± 0.467	161 ± 59	0.0081 ± 0.0031	161 ± 78	0.0090 ± 0.0045	0.0065 ± 0.0024	0.0064 ± 0.0024
12.860 ± 0.525	141 ± 58	0.0073 ± 0.0031	199 ± 79	0.0114 ± 0.0047	0.0065 ± 0.0024	0.0065 ± 0.0024
13.876 ± 0.589	101 ± 58	0.0054 ± 0.0031	144 ± 78	0.0084 ± 0.0047	0.0046 ± 0.0023	0.0046 ± 0.0023
15.016 ± 0.660	147 ± 60	0.0078 ± 0.0033	288 ± 79	0.0169 ± 0.0050	0.0081 ± 0.0026	0.0081 ± 0.0026
16.297 ± 0.750	271 ± 61	0.0143 ± 0.0036	222 ± 80	0.0129 ± 0.0049	0.0110 ± 0.0030	0.0110 ± 0.0030
17.759 ± 0.857	360 ± 63	0.0189 ± 0.0038	423 ± 81	0.0242 ± 0.0054	0.0176 ± 0.0035	0.0176 ± 0.0035
19.416 ± 0.971	413 ± 63	0.0213 ± 0.0039	451 ± 81	0.0252 ± 0.0054	0.0193 ± 0.0036	0.0193 ± 0.0036

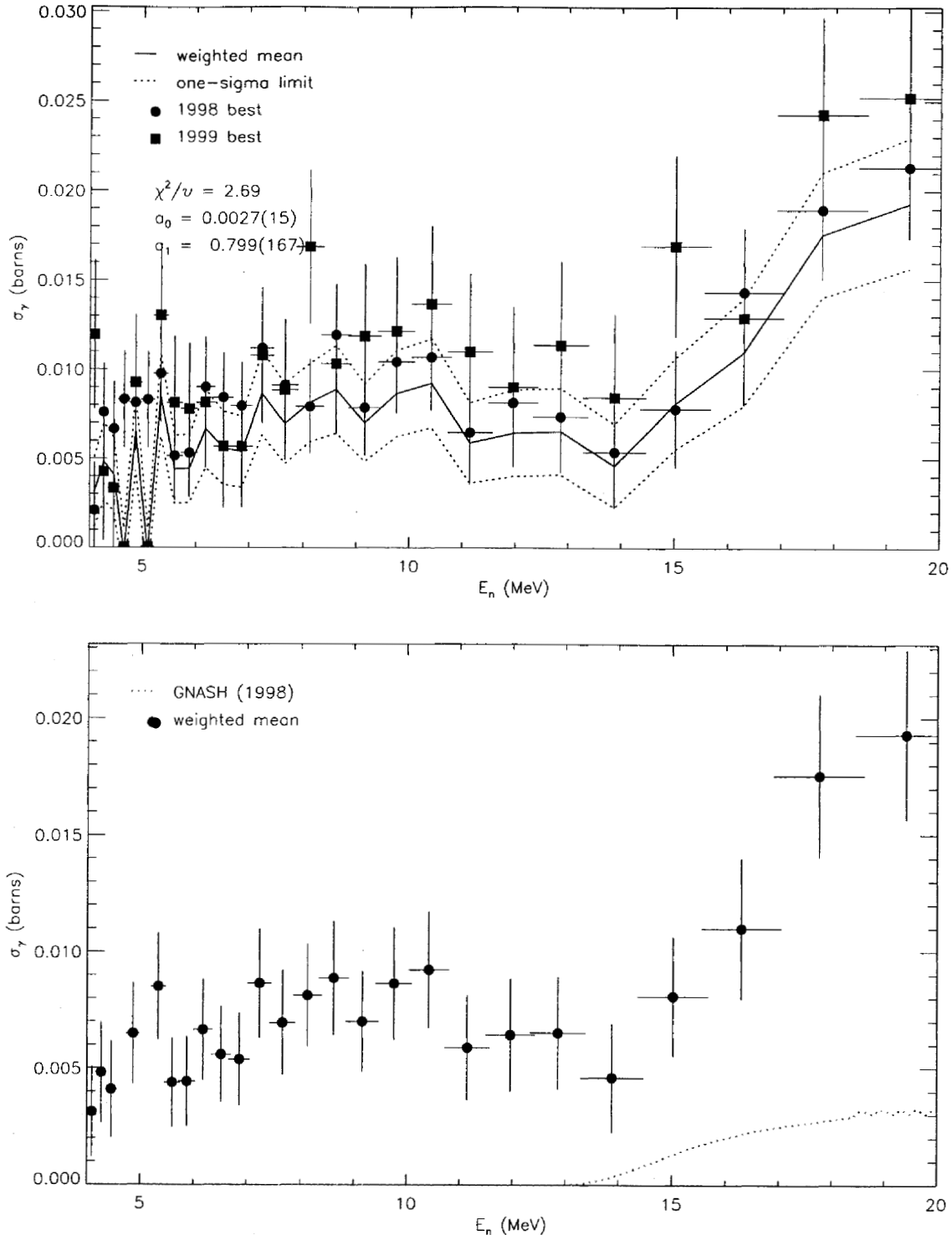


FIG. 95: Adopted $E_\gamma = 300.5$ -keV partial cross section corresponding to the data in table CII. The top panel shows the 1998 and 1999 partial cross sections (corrected for angular-distribution effects) and the recommended value, plotted as a solid line with a one-sigma confidence band (dotted lines). The bottom panel shows this recommended partial cross section (solid circles) compared to GNASH.

TABLE CIII: Adopted partial γ -ray cross section for the $E_\gamma = 305.2$ -keV transition. The measured peak areas and deduced partial cross sections (before correction for angular distribution effects) for the **98Thin** and **99Thin** data sets are shown in columns 2–5. The partial cross section, listed in column 6, is obtained from both data sets using the optimization procedure described in section XII B. The recommended partial cross section in the last column includes a correction for angular-distribution effects.

E_n (MeV)	$A^{(1998)}$	$\sigma^{(1998)}$	$A^{(1999)}$	$\sigma^{(1999)}$	$\sigma^{(\text{opt})}$	$\sigma^{(\text{opt,corr})}$
4.090 ± 0.093	30 ± 48	0.0008 ± 0.0012	145 ± 68	0.0038 ± 0.0019	0.0008 ± 0.0008	0.0008 ± 0.0008
4.264 ± 0.099	69 ± 49	0.0017 ± 0.0012	113 ± 68	0.0030 ± 0.0018	0.0012 ± 0.0008	0.0012 ± 0.0008
4.453 ± 0.105	110 ± 50	0.0026 ± 0.0012	144 ± 70	0.0036 ± 0.0018	0.0018 ± 0.0008	0.0018 ± 0.0008
4.647 ± 0.113	63 ± 50	0.0015 ± 0.0012	192 ± 70	0.0047 ± 0.0018	0.0014 ± 0.0008	0.0014 ± 0.0008
4.861 ± 0.122	106 ± 51	0.0025 ± 0.0012	104 ± 71	0.0025 ± 0.0017	0.0015 ± 0.0008	0.0015 ± 0.0008
5.090 ± 0.129	179 ± 52	0.0041 ± 0.0013	82 ± 71	0.0019 ± 0.0017	0.0022 ± 0.0008	0.0022 ± 0.0008
5.333 ± 0.140	149 ± 52	0.0034 ± 0.0012	199 ± 73	0.0046 ± 0.0018	0.0025 ± 0.0008	0.0025 ± 0.0008
5.597 ± 0.149	42 ± 52	0.0009 ± 0.0011	169 ± 73	0.0039 ± 0.0017	0.0009 ± 0.0007	0.0009 ± 0.0007
5.875 ± 0.160	0 ± 0	0.0000 ± 0.0000	90 ± 73	0.0020 ± 0.0017	0.0000 ± 0.0000	0.0000 ± 0.0000
6.181 ± 0.175	139 ± 54	0.0030 ± 0.0012	36 ± 73	0.0008 ± 0.0016	0.0014 ± 0.0008	0.0014 ± 0.0008
6.517 ± 0.187	108 ± 54	0.0022 ± 0.0011	154 ± 75	0.0033 ± 0.0016	0.0015 ± 0.0007	0.0015 ± 0.0007
6.862 ± 0.201	150 ± 56	0.0029 ± 0.0011	87 ± 75	0.0018 ± 0.0016	0.0016 ± 0.0007	0.0016 ± 0.0007
7.237 ± 0.218	204 ± 57	0.0041 ± 0.0012	242 ± 77	0.0053 ± 0.0018	0.0030 ± 0.0008	0.0030 ± 0.0008
7.661 ± 0.242	178 ± 56	0.0038 ± 0.0013	156 ± 76	0.0037 ± 0.0018	0.0025 ± 0.0008	0.0025 ± 0.0008
8.126 ± 0.263	122 ± 56	0.0026 ± 0.0012	196 ± 76	0.0045 ± 0.0018	0.0020 ± 0.0008	0.0020 ± 0.0008
8.618 ± 0.284	146 ± 57	0.0030 ± 0.0012	216 ± 76	0.0049 ± 0.0018	0.0023 ± 0.0008	0.0023 ± 0.0008
9.160 ± 0.313	148 ± 57	0.0031 ± 0.0012	230 ± 76	0.0053 ± 0.0018	0.0025 ± 0.0008	0.0025 ± 0.0008
9.757 ± 0.346	201 ± 57	0.0044 ± 0.0013	282 ± 76	0.0068 ± 0.0020	0.0035 ± 0.0009	0.0035 ± 0.0009
10.414 ± 0.377	206 ± 56	0.0047 ± 0.0014	411 ± 76	0.0103 ± 0.0022	0.0042 ± 0.0009	0.0043 ± 0.0009
11.143 ± 0.425	77 ± 55	0.0019 ± 0.0013	259 ± 74	0.0069 ± 0.0021	0.0020 ± 0.0009	0.0020 ± 0.0009
11.960 ± 0.467	232 ± 57	0.0058 ± 0.0015	133 ± 73	0.0037 ± 0.0021	0.0036 ± 0.0010	0.0036 ± 0.0010
12.860 ± 0.525	275 ± 57	0.0070 ± 0.0016	177 ± 74	0.0050 ± 0.0021	0.0045 ± 0.0011	0.0048 ± 0.0011
13.876 ± 0.589	216 ± 57	0.0056 ± 0.0016	191 ± 73	0.0055 ± 0.0022	0.0039 ± 0.0010	0.0042 ± 0.0011
15.016 ± 0.660	185 ± 58	0.0048 ± 0.0016	367 ± 76	0.0106 ± 0.0025	0.0044 ± 0.0011	0.0047 ± 0.0011
16.297 ± 0.750	435 ± 60	0.0113 ± 0.0019	480 ± 78	0.0137 ± 0.0027	0.0090 ± 0.0013	0.0096 ± 0.0014
17.759 ± 0.857	568 ± 62	0.0147 ± 0.0022	371 ± 76	0.0105 ± 0.0024	0.0098 ± 0.0014	0.0104 ± 0.0015
19.416 ± 0.971	669 ± 63	0.0170 ± 0.0023	477 ± 77	0.0131 ± 0.0026	0.0118 ± 0.0015	0.0124 ± 0.0016

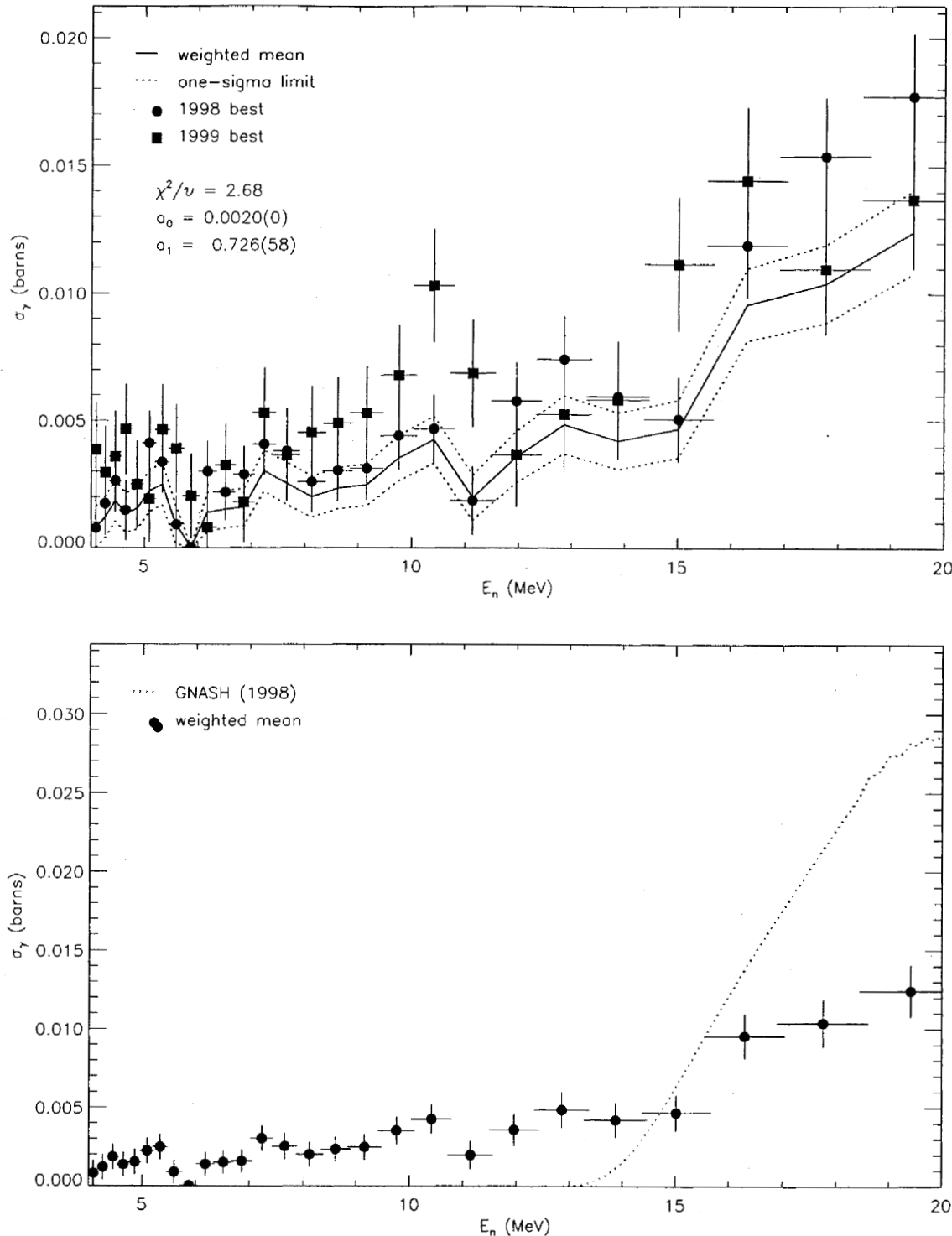


FIG. 96: Adopted $E_\gamma = 305.2$ -keV partial cross section corresponding to the data in table CIII. The top panel shows the 1998 and 1999 partial cross sections (corrected for angular-distribution effects) and the recommended value, plotted as a solid line with a one-sigma confidence band (dotted lines). The bottom panel shows this recommended partial cross section (solid circles) compared to GNASH.

TABLE CIV: Adopted partial γ -ray cross section for the $E_\gamma = 312.0$ -keV transition. The measured peak areas and deduced partial cross sections (before correction for angular distribution effects) for the **98Thin** and **99Thin** data sets are shown in columns 2–5. The partial cross section, listed in column 6, is obtained from both data sets using the optimization procedure described in section XII B. The recommended partial cross section in the last column includes a correction for angular-distribution effects.

E_n (MeV)	$A^{(1998)}$	$\sigma^{(1998)}$	$A^{(1999)}$	$\sigma^{(1999)}$	$\sigma^{(\text{opt})}$	$\sigma^{(\text{opt,corr})}$
4.090 ± 0.093	128 ± 49	0.0066 ± 0.0026	47 ± 66	0.0025 ± 0.0035	0.0035 ± 0.0019	0.0035 ± 0.0019
4.264 ± 0.099	110 ± 50	0.0055 ± 0.0026	141 ± 68	0.0073 ± 0.0037	0.0041 ± 0.0018	0.0041 ± 0.0018
4.453 ± 0.105	187 ± 50	0.0089 ± 0.0026	157 ± 69	0.0078 ± 0.0035	0.0062 ± 0.0019	0.0062 ± 0.0019
4.647 ± 0.113	214 ± 51	0.0100 ± 0.0026	83 ± 68	0.0040 ± 0.0033	0.0056 ± 0.0019	0.0056 ± 0.0019
4.861 ± 0.122	144 ± 51	0.0068 ± 0.0025	130 ± 71	0.0062 ± 0.0035	0.0046 ± 0.0018	0.0046 ± 0.0018
5.090 ± 0.129	212 ± 53	0.0097 ± 0.0026	224 ± 73	0.0104 ± 0.0036	0.0073 ± 0.0019	0.0073 ± 0.0019
5.333 ± 0.140	210 ± 53	0.0094 ± 0.0026	346 ± 73	0.0160 ± 0.0038	0.0086 ± 0.0019	0.0085 ± 0.0019
5.597 ± 0.149	118 ± 52	0.0051 ± 0.0023	202 ± 73	0.0093 ± 0.0035	0.0043 ± 0.0017	0.0043 ± 0.0017
5.875 ± 0.160	175 ± 53	0.0075 ± 0.0024	209 ± 74	0.0094 ± 0.0035	0.0058 ± 0.0018	0.0058 ± 0.0018
6.181 ± 0.175	147 ± 53	0.0063 ± 0.0024	334 ± 75	0.0147 ± 0.0037	0.0062 ± 0.0017	0.0062 ± 0.0017
6.517 ± 0.187	259 ± 56	0.0104 ± 0.0025	288 ± 76	0.0121 ± 0.0035	0.0082 ± 0.0019	0.0082 ± 0.0019
6.862 ± 0.201	235 ± 57	0.0090 ± 0.0024	207 ± 76	0.0085 ± 0.0033	0.0065 ± 0.0017	0.0064 ± 0.0017
7.237 ± 0.218	420 ± 59	0.0167 ± 0.0029	217 ± 77	0.0095 ± 0.0035	0.0106 ± 0.0022	0.0105 ± 0.0022
7.661 ± 0.242	223 ± 56	0.0095 ± 0.0026	81 ± 74	0.0038 ± 0.0035	0.0055 ± 0.0019	0.0055 ± 0.0019
8.126 ± 0.263	350 ± 58	0.0149 ± 0.0029	398 ± 77	0.0184 ± 0.0041	0.0125 ± 0.0022	0.0125 ± 0.0022
8.618 ± 0.284	280 ± 59	0.0116 ± 0.0027	285 ± 77	0.0129 ± 0.0038	0.0091 ± 0.0020	0.0091 ± 0.0020
9.160 ± 0.313	150 ± 57	0.0063 ± 0.0025	325 ± 77	0.0149 ± 0.0039	0.0062 ± 0.0018	0.0062 ± 0.0018
9.757 ± 0.346	271 ± 57	0.0118 ± 0.0028	428 ± 77	0.0205 ± 0.0044	0.0110 ± 0.0021	0.0110 ± 0.0021
10.414 ± 0.377	266 ± 57	0.0120 ± 0.0029	293 ± 75	0.0146 ± 0.0041	0.0098 ± 0.0021	0.0098 ± 0.0021
11.143 ± 0.425	146 ± 55	0.0070 ± 0.0028	311 ± 74	0.0164 ± 0.0043	0.0070 ± 0.0020	0.0069 ± 0.0020
11.960 ± 0.467	177 ± 56	0.0088 ± 0.0029	341 ± 74	0.0187 ± 0.0046	0.0086 ± 0.0022	0.0086 ± 0.0022
12.860 ± 0.525	334 ± 58	0.0170 ± 0.0035	211 ± 74	0.0118 ± 0.0044	0.0117 ± 0.0025	0.0116 ± 0.0026
13.876 ± 0.589	325 ± 58	0.0169 ± 0.0035	272 ± 74	0.0156 ± 0.0046	0.0129 ± 0.0026	0.0128 ± 0.0026
15.016 ± 0.660	539 ± 61	0.0280 ± 0.0043	589 ± 77	0.0338 ± 0.0059	0.0247 ± 0.0034	0.0246 ± 0.0034
16.297 ± 0.750	594 ± 62	0.0308 ± 0.0045	510 ± 78	0.0290 ± 0.0055	0.0246 ± 0.0035	0.0246 ± 0.0035
17.759 ± 0.857	762 ± 64	0.0393 ± 0.0052	780 ± 79	0.0437 ± 0.0067	0.0344 ± 0.0042	0.0343 ± 0.0042
19.416 ± 0.971	949 ± 66	0.0480 ± 0.0060	680 ± 79	0.0372 ± 0.0061	0.0356 ± 0.0044	0.0355 ± 0.0044

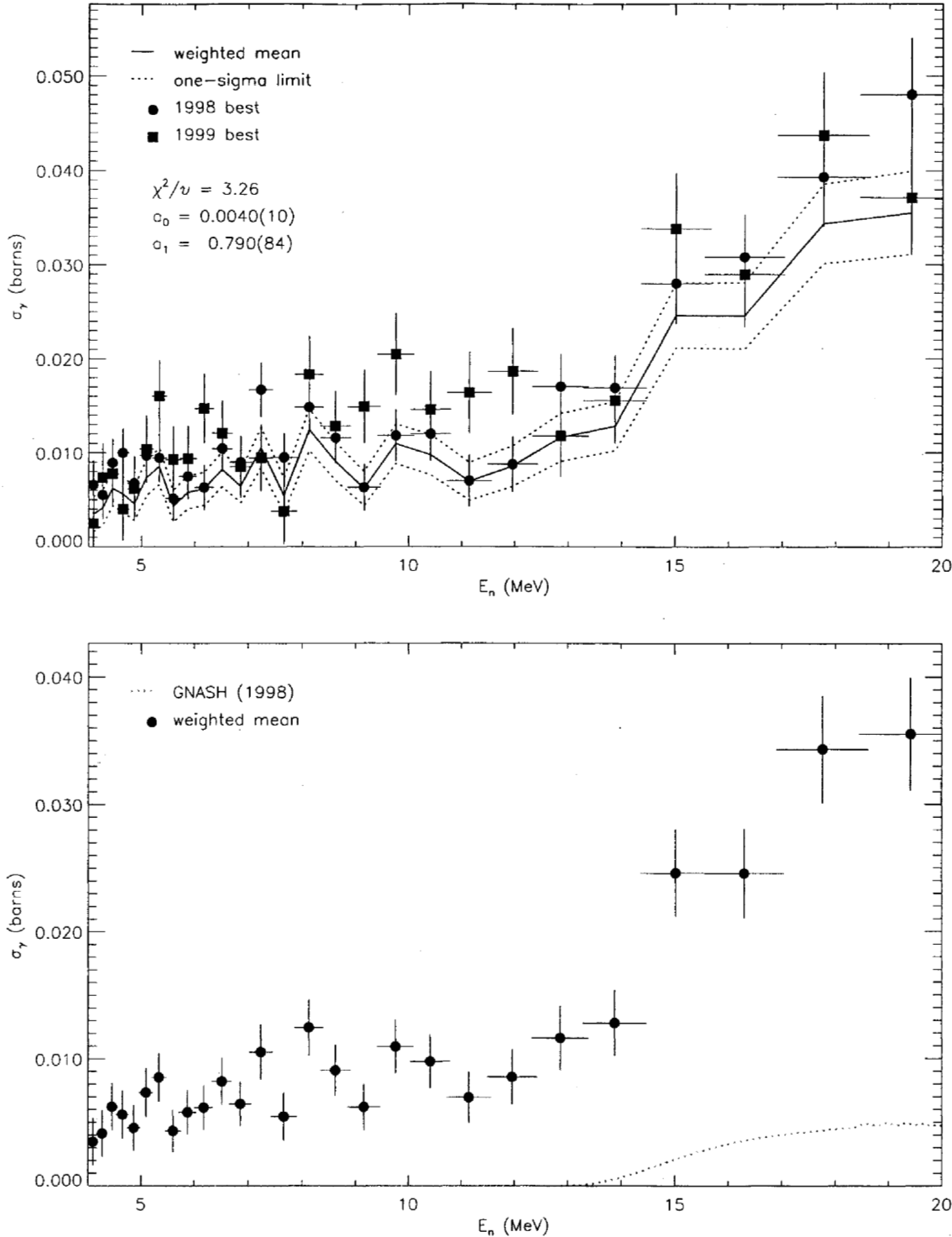


FIG. 97: Adopted $E_\gamma = 312.0$ -keV partial cross section corresponding to the data in table CIV. The top panel shows the 1998 and 1999 partial cross sections (corrected for angular-distribution effects) and the recommended value, plotted as a solid line with a one-sigma confidence band (dotted lines). The bottom panel shows this recommended partial cross section (solid circles) compared to GNASH.

TABLE CV: Adopted partial γ -ray cross section for the $E_\gamma = 340.6$ -keV transition. The measured peak areas and deduced partial cross sections (before correction for angular distribution effects) for the **98Thin** and **99Thin** data sets are shown in columns 2–5. The partial cross section, listed in column 6, is obtained from both data sets using the optimization procedure described in section XII B. The recommended partial cross section in the last column includes a correction for angular-distribution effects.

E_n (MeV)	$A^{(1998)}$	$\sigma^{(1998)}$	$A^{(1999)}$	$\sigma^{(1999)}$	$\sigma^{(\text{opt})}$	$\sigma^{(\text{opt,corr})}$
4.090 ± 0.093	87 ± 56	0.0043 ± 0.0028	97 ± 84	0.0050 ± 0.0043	0.0031 ± 0.0020	0.0031 ± 0.0020
4.264 ± 0.099	2 ± 52	0.0001 ± 0.0025	0 ± 0	0.0001 ± 0.0000	-0.0009 ± 0.0015	-0.0009 ± 0.0015
4.453 ± 0.105	73 ± 57	0.0034 ± 0.0027	145 ± 88	0.0070 ± 0.0043	0.0027 ± 0.0019	0.0027 ± 0.0019
4.647 ± 0.113	105 ± 58	0.0048 ± 0.0027	55 ± 68	0.0026 ± 0.0032	0.0028 ± 0.0019	0.0028 ± 0.0019
4.861 ± 0.122	27 ± 58	0.0012 ± 0.0026	69 ± 89	0.0032 ± 0.0041	0.0008 ± 0.0018	0.0008 ± 0.0018
5.090 ± 0.129	135 ± 60	0.0060 ± 0.0027	13 ± 89	0.0006 ± 0.0040	0.0033 ± 0.0020	0.0033 ± 0.0020
5.333 ± 0.140	53 ± 58	0.0023 ± 0.0025	152 ± 91	0.0068 ± 0.0042	0.0020 ± 0.0018	0.0020 ± 0.0018
5.597 ± 0.149	11 ± 60	0.0005 ± 0.0025	2 ± 70	0.0001 ± 0.0031	-0.0002 ± 0.0017	-0.0002 ± 0.0017
5.875 ± 0.160	202 ± 62	0.0084 ± 0.0027	0 ± 0	0.0000 ± 0.0000	0.0022 ± 0.0018	0.0023 ± 0.0018
6.181 ± 0.175	128 ± 61	0.0053 ± 0.0026	79 ± 91	0.0034 ± 0.0039	0.0034 ± 0.0019	0.0034 ± 0.0019
6.517 ± 0.187	136 ± 63	0.0053 ± 0.0025	58 ± 93	0.0024 ± 0.0038	0.0032 ± 0.0019	0.0032 ± 0.0019
6.862 ± 0.201	101 ± 64	0.0038 ± 0.0024	165 ± 95	0.0066 ± 0.0039	0.0029 ± 0.0017	0.0029 ± 0.0017
7.237 ± 0.218	0 ± 0	0.0000 ± 0.0000	114 ± 96	0.0048 ± 0.0041	0.0000 ± 0.0000	0.0000 ± 0.0000
7.661 ± 0.242	112 ± 63	0.0046 ± 0.0027	58 ± 92	0.0026 ± 0.0042	0.0029 ± 0.0019	0.0029 ± 0.0019
8.126 ± 0.263	6 ± 57	0.0002 ± 0.0024	0 ± 0	0.0000 ± 0.0000	-0.0007 ± 0.0015	-0.0007 ± 0.0015
8.618 ± 0.284	235 ± 67	0.0095 ± 0.0029	152 ± 95	0.0066 ± 0.0042	0.0064 ± 0.0023	0.0064 ± 0.0023
9.160 ± 0.313	203 ± 66	0.0083 ± 0.0028	32 ± 93	0.0014 ± 0.0041	0.0047 ± 0.0022	0.0047 ± 0.0022
9.757 ± 0.346	152 ± 66	0.0064 ± 0.0029	278 ± 94	0.0129 ± 0.0046	0.0056 ± 0.0021	0.0056 ± 0.0021
10.414 ± 0.377	138 ± 65	0.0061 ± 0.0029	96 ± 91	0.0046 ± 0.0044	0.0040 ± 0.0021	0.0040 ± 0.0021
11.143 ± 0.425	191 ± 64	0.0089 ± 0.0031	197 ± 91	0.0101 ± 0.0048	0.0067 ± 0.0024	0.0067 ± 0.0024
11.960 ± 0.467	251 ± 65	0.0121 ± 0.0034	307 ± 92	0.0163 ± 0.0052	0.0099 ± 0.0027	0.0099 ± 0.0027
12.860 ± 0.525	322 ± 66	0.0160 ± 0.0037	348 ± 92	0.0188 ± 0.0054	0.0129 ± 0.0031	0.0128 ± 0.0031
13.876 ± 0.589	297 ± 66	0.0150 ± 0.0037	141 ± 91	0.0078 ± 0.0051	0.0095 ± 0.0030	0.0094 ± 0.0030
15.016 ± 0.660	421 ± 68	0.0213 ± 0.0041	403 ± 94	0.0224 ± 0.0058	0.0170 ± 0.0036	0.0169 ± 0.0036
16.297 ± 0.750	490 ± 70	0.0247 ± 0.0043	303 ± 94	0.0167 ± 0.0055	0.0166 ± 0.0038	0.0164 ± 0.0038
17.759 ± 0.857	661 ± 72	0.0331 ± 0.0049	445 ± 95	0.0242 ± 0.0058	0.0230 ± 0.0044	0.0229 ± 0.0045
19.416 ± 0.971	612 ± 73	0.0301 ± 0.0047	521 ± 96	0.0276 ± 0.0060	0.0234 ± 0.0043	0.0232 ± 0.0043

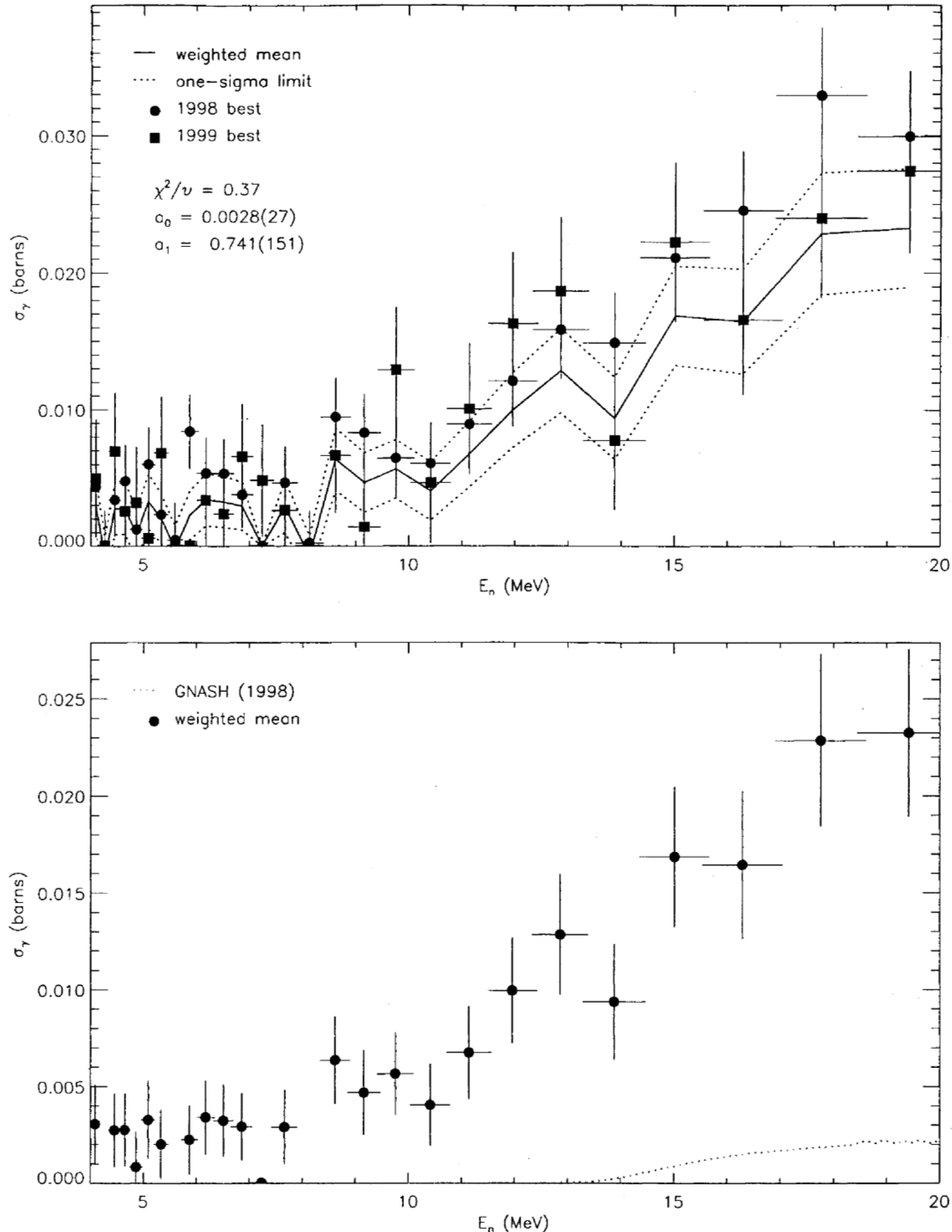


FIG. 98: Adopted $E_\gamma = 340.6$ -keV partial cross section corresponding to the data in table CV. The top panel shows the 1998 and 1999 partial cross sections (corrected for angular-distribution effects), plotted as a solid line with a one-sigma confidence band (dotted lines). The bottom panel shows this recommended partial cross section (solid circles) compared to GNASH.

XIV. CONCLUSION

We have presented the analysis of $n+^{235}\text{U}$ data acquired using the GEANIE spectrometer at LANSCE/WNR. Absolute partial γ -ray cross sections for observed transitions in the $^{235}\text{U}(n,2n)$, $^{235}(n,n')$ and $^{235}(n,3n)$ channels, and in the 5-20 MeV neutron energy range have been extracted. Thin- and thick-sample data acquired in 1998 and the data acquired in 1999 were analyzed as three separate sets. For the 1998 and 1999 data, recommended partial cross sections were deduced, along with an uncertainty reflecting three sources of error: i) random fluctuations, ii) systematic variability in neutron-energy-dependent factors, and iii) systematic variability in global factors which only affect the overall magnitude of the cross sections. These recommended values and associated uncertainties were tested in each case against variations in the analysis technique. For the 1999 data in particular, the $^{56}\text{Fe} \ 2_1^+ \rightarrow 0_1^+$ yield measured in-beam with the ^{235}U sample was found to be in excellent agreement with the accepted standard at $E_n = 14.5$ MeV, thereby providing an independent verification of the entire procedure used to convert measured γ -ray counts into partial cross sections. The 1998- and 1999-deduced results were combined, wherever possible, to produce final, recommended values and uncertainties. A summary of all lines analyzed in the GEANIE data can be found in section XIII.

At present, the measured partial cross sections are over-estimated in calculations using the Hauser-Feshbach reaction code GNASH. However, work is currently in progress at both Lawrence Livermore [26] and Los Alamos [27] National Laboratories to improve the reaction models used to predict both the $^{235}\text{U}(n,2n\gamma)$ and $^{239}\text{Pu}(n,2n\gamma)$ cross sections. In addition we are using transitions from off-yrast states in the $(n,2n)$ channel from the 1998 and 1999 data sets to provide a correction to model calculations where the present lack of knowledge of the complete low-lying structure of the $(n,2n)$ channel nucleus causes a large part of the discrepancy between observed and calculated cross sections. The resulting improvements to the model calculations will be applied to the measurements described in this report to deduce a reliable $(n,2n)$ reaction cross section.

This work is supported by the U.S. Department of Energy under contract numbers W-7405-ENG-48 (LLNL) and W-7405-ENG-36 (LANL).

REFERENCES

- [1] L.A. Bernstein, *et al.*, manuscript in preparation.
- [2] J. Frehaut, A. Bertin, R. Bois, E. Gryntakis, and C.A. Philis, *Radiation Effects* **96**, 219 (1986).
- [3] J. Frehaut, A. Bertin, and R. Bois, *Nucl. Sci. and Eng.* **74**, 29 (1980).
- [4] J.A. Becker, and R.O. Nelson, *Nucl. Phys. News Intl.* **7**, 11 (1997).
- [5] W. Younes, J.A. Becker, L.A. Bernstein, D.E. Archer, M.A. Stoyer, D.P. McNabb, K. Hauschild, D.M. Drake, G.D. Johns, R.O. Nelson, W.S. Wilburn, LLNL Rep. UCRL-ID-132627 (1998).
- [6] W. Younes, manuscript in preparation.
- [7] P.G. Young, E.D. Arthur, and M.B. Chadwick, LANL Rep. No. LA-12343-MS (1992). The GNASH calculations presented in this report were obtained on 5/13/99.
- [8] W. Younes, manuscript in preparation.
- [9] D.P. McNabb, manuscript in preparation.
- [10] Data extracted using the NNDC On-Line Data Service from the ENSDF database, file revised as of 8/25/99. M.R. Bhat, *Evaluated Nuclear Structure Data File (ENSDF)*, **Nuclear Data for Science and Technology**, page 817, edited by S.M. Qaim (Springer-Verlag, Berlin, Germany, 1992).
- [11] P. Rose, "ENDF/B summary Documentation", Fourth Ed. (ENDF/B-VI), Brookhaven Natl. Lab. Rep., BNL-NCS-17541, (1992).
- [12] J.F. Briesmeister, LANL Rep. LA-7396-M-Rev.2 (1986).
- [13] S.A. Wender, S. Balestrini, A. Brown, R.C. Haight, C.M. Laymon, T.M. Lee, P.W. Lisowski, W. McCorkle, R.O. Nelson, W. Parker, N.W. Hill, *Nucl. Instr. and Meth. A* **336**, 226 (1993).
- [14] J.M. Blatt and V.F. Weisskopf, *Theoretical Nuclear Physics*, Dover Publications Inc., New York, 1991, p. 394.
- [15] P.R. Bevington and D.K. Robinson, *Data Reduction and Error Analysis for the Physical Sciences*, 2nd ed., McGraw-Hill, San Francisco, 1992., p. 157.
- [16] ibid. p. 59.
- [17] ibid. p. 41.
- [18] S.P. Simakov, *et al.*, IAEA Report INDC (CCP)-413 (1998).
- [19] H. Morinaga and V.F. T. Yamazaki, *In-Beam Gamma-Ray Spectroscopy*, North Holland Publishing Company, Amsterdam, 1976, p. 50.
- [20] D.C. Camp and A.L. Van Lehn, *Nucl. Instr. and Meth.* **76**, 192 (1969).

- [21] S. Tabor, private communication (June 2000).
- [22] P. Cejnar, S. Drissi, and J. Kern, Nucl. Phys. A **602**, 225 (1996).
- [23] AVALANCHE calculations performed by P.E. Garrett (June 2000).
- [24] E. Sheldon and U.C. Rodgers, Comp. Phys. Comm. **6**, 99 (1973).
- [25] CINDY Calculation performed by P.E. Garrett (May 2000).
- [26] H. Chen, M.A. Ross, G. Reffo, R.M. White, W. Younes, LLNL Rep. UCRL-ID-137718 (2000).
- [27] M.B. Chadwick and P.G. Young, LANL Rep. No. LA-UR-99-2885 (1999).
- [28] G. Audi and A.H. Wapstra, Nucl. Phys. A **595**, 409 (1995).

APPENDIX A: LINES USED FOR γ -RAY ENERGY CALIBRATION IN 1998 DATA

Gamma-ray-energy calibration lines.

$E_{\gamma}^{(true)}$ (keV)	$E_{\gamma}^{(cal)}$ (keV)	$E_{\gamma}^{(true)} - E_{\gamma}^{(cal)}$ (keV)	Identification
87.300(5)	87.158(17)	0.142	Pb Kb2 x ray
89.957(5)	89.957(1)	-0.000	Th Ka2 x ray
92.282(5)	92.266(7)	0.016	Pa Ka2 x ray
93.350(5)	93.352(1)	-0.002	Th Ka1 x ray
94.654(1)	94.655(1)	-0.001	U Ka2 x ray
95.863(5)	95.880(4)	-0.017	Pa Ka1 x ray
98.434(10)	98.433(1)	0.001	U Ka1 x ray
102.270(3)	102.351(4)	-0.081	^{231}Pa Ex = 102.3 keV
104.819(5)	104.743(8)	0.076	Th Kb3 x ray
105.604(5)	105.605(6)	-0.001	Th Kb1 x ray
111.298(5)	111.290(2)	0.008	U Kb1 or Pa Kb2 x ray
114.445(5)	114.465(2)	-0.020	U Kb2 x ray
115.377(5)	115.309(3)	0.068	U K02,3 x ray
117.320(50)	117.408(15)	-0.088	$^{235}\text{U}(n,f)143\text{Ba}$
120.900(20)	120.906(3)	-0.006	^{230}Th Ex = 174.1 keV from 1.1% ^{234}U or ^{98}Y Ex = 495.8 keV
125.118(29)	125.075(7)	0.043	$^{235}\text{U}(n,f)99\text{Y}$
129.297(2)	129.335(5)	-0.038	$^{235}\text{U}(n,n)235\text{U}$ Ex = 129.3 keV
140.760(40)	140.771(11)	-0.011	^{231}Th Ex = 236.9 keV
143.764(2)	143.751(1)	0.013	^{231}Th Ex = 185.7 KeV
151.750(120)	151.661(20)	0.089	$^{235}\text{U}(n,f)102\text{Zr}$
152.720(2)	152.660(7)	0.060	$^{235}\text{U}(n,2n)234\text{U}$ Ex = 296.1 keV
163.358(2)	163.344(1)	0.014	^{231}Th Ex = 205.3 KeV
182.520(20)	182.423(6)	0.097	^{231}Th Ex = 387.8 keV
185.712(1)	185.714(1)	-0.002	^{231}Th Ex = 185.7 keV
192.200(100)	192.280(12)	-0.081	$^{235}\text{U}(n,f)104\text{Mo}$
194.940(10)	194.943(3)	-0.003	^{231}Th Ex = 236.9 keV
197.142(4)	197.162(1)	-0.020	^{19}F Ex = 197.1 keV
200.970(30)	200.961(5)	0.009	$^{235}\text{U}(n,2n)234\text{U}$ Ex = 497.0 keV
202.111(3)	202.119(5)	-0.008	^{231}Th Ex = 387.8 keV
205.309(2)	205.318(1)	-0.009	^{231}Th Ex = 205.3 keV
212.531(9)	212.505(11)	0.026	$^{235}\text{U}(n,f)100\text{Zr}$
221.399(1)	221.329(12)	0.070	^{231}Th Ex = 221.4 keV
223.900(100)	223.838(14)	0.062	$^{235}\text{U}(n,f)99\text{Y}$
233.469(3)	233.645(81)	-0.176	^{231}Th Ex = 275.4 keV
238.632(2)	238.643(19)	-0.011	^{212}Bi Ex = 238.6 keV
258.420(50)	258.452(50)	-0.032	$^{235}\text{U}(n,f)146\text{Ce}$
269.600(100)	269.727(39)	-0.127	$^{235}\text{U}(n,f)99\text{Y}$
295.070(90)	295.053(33)	0.017	$^{235}\text{U}(n,f)148\text{Ce}$
297.000(100)	297.023(18)	-0.023	$^{235}\text{U}(n,f)134\text{Te}$
314.120(20)	313.996(10)	0.124	$^{235}\text{U}(n,f)128\text{Te}$

Gamma-ray-energy calibration lines.

316.440(6)	316.519(32)	-0.079	235U(n,n)235U Ex = 445.7 keV
326.480(120)	326.361(31)	0.119	235U(n,f)102Zr
332.380(50)	332.653(35)	-0.273	235U(n,f)146Ba
340.810(30)	340.628(108)	0.182	235U(n,3n)233U Ex = 340.7 keV
345.900(30)	345.870(39)	0.030	231Th Ex = 387.8 keV
352.200(100)	351.922(8)	0.278	235U(n,f)136Te
359.598(14)	359.544(17)	0.054	235U(n,f)142Ba
368.400(100)	368.536(76)	-0.136	235U(n,f)104Mo
376.657(15)	376.607(17)	0.050	235U(n,f)140Xe
380.173(2)	380.118(152)	0.055	235U(n,n)235U Ex = 393.2 keV
381.359(7)	381.232(26)	0.127	235U(n,f)136Xe
382.300(100)	382.517(60)	-0.216	235U(n,f)132Te
409.780(50)	409.884(73)	-0.104	235U(n,f)146Ce
411.020(40)	411.041(123)	-0.022	235U(n,n)235U Ex = 608.1 keV
417.950(100)	417.925(13)	0.025	127I Ex = 418.0 keV (from NaI)
460.020(50)	460.015(49)	0.005	235U(n,f)88Kr
490.360(100)	490.524(147)	-0.164	127I Ex = 1235.1 keV (from NaI)
493.100(200)	493.030(26)	0.070	235U(n,f)143Ba
519.200(100)	519.598(28)	-0.398	235U(n,f)104Mo
528.250(50)	528.311(34)	-0.061	235U(n,f)140Ba
620.505(19)	620.427(37)	0.078	235U(n,f)98Zr
624.780(20)	624.937(278)	-0.157	235U(n,n)235U Ex = 671.0 keV or 235U(n,f)100Zr
637.795(5)	637.712(117)	0.083	235U(n,n)235U Ex = 637.795 keV
647.580(30)	647.552(38)	0.028	235U(n,f)98Zr
707.130(50)	707.196(24)	-0.066	235U(n,f)90Kr
744.700(90)	744.768(206)	-0.068	127I Ex = 744.7 keV (from NaI)
775.280(60)	775.474(59)	-0.194	235U(n,f)88Kr
793.530(20)	793.635(53)	-0.105	235U(n,f)130Te
798.920(30)	799.007(59)	-0.087	235U(n,n)235U Ex = 812.0 keV
803.100(50)	803.057(27)	0.043	206Pb(n,n) Ex = 803.1 keV
815.000(100)	814.889(27)	0.111	235U(n,f)96Sr
836.910(100)	836.922(31)	-0.012	235U(n,f)94Sr
843.740(30)	843.747(42)	-0.007	27Al Ex = 843.8 keV
973.900(100)	973.528(132)	0.372	235U(n,f)132Te

APPENDIX B: VALUES OF (N,F) CROSS SECTIONS USED IN CALCULATING THE NEUTRON FLUX

Cross Sections for $^{235}\text{U}(n,f)$ from ENDF/B-VI.5

E_n (MeV)	$\sigma_{^{235}\text{U}(n,f)}$
0.10	1.5724 ± 0.0236
0.10	1.5580 ± 0.0234
0.11	1.5320 ± 0.0230
0.12	1.4961 ± 0.0224
0.13	1.4688 ± 0.0220
0.14	1.4433 ± 0.0216
0.15	1.4203 ± 0.0213
0.15	1.4188 ± 0.0213
0.16	1.4081 ± 0.0211
0.17	1.3967 ± 0.0210
0.17	1.3942 ± 0.0209
0.17	1.3930 ± 0.0209
0.18	1.3800 ± 0.0207
0.19	1.3647 ± 0.0205
0.20	1.3537 ± 0.0203
0.20	1.3510 ± 0.0203
0.21	1.3370 ± 0.0201
0.22	1.3265 ± 0.0199
0.23	1.3197 ± 0.0198
0.23	1.3178 ± 0.0198
0.23	1.3130 ± 0.0197
0.23	1.3100 ± 0.0197
0.24	1.3070 ± 0.0196
0.24	1.3030 ± 0.0195
0.25	1.2930 ± 0.0194
0.25	1.2926 ± 0.0194
0.26	1.2690 ± 0.0190
0.27	1.2500 ± 0.0187
0.28	1.2424 ± 0.0186
0.28	1.2350 ± 0.0185
0.29	1.2318 ± 0.0185
0.30	1.2310 ± 0.0185
0.30	1.2300 ± 0.0185
0.33	1.2300 ± 0.0185
0.33	1.2273 ± 0.0184
0.34	1.2257 ± 0.0184
0.35	1.2230 ± 0.0183
0.36	1.2194 ± 0.0183
0.37	1.2155 ± 0.0182
0.38	1.2130 ± 0.0182
0.39	1.2042 ± 0.0181
0.40	1.2020 ± 0.0180
0.42	1.1940 ± 0.0179
0.42	1.1900 ± 0.0179
0.43	1.1865 ± 0.0178
0.43	1.1833 ± 0.0177
0.44	1.1751 ± 0.0176
0.45	1.1684 ± 0.0175
0.45	1.1662 ± 0.0175
0.47	1.1510 ± 0.0173
0.48	1.1504 ± 0.0173

Cross Sections for $^{235}\text{U}(\text{n},\text{f})$ from ENDF/B-VI.5

0.50	1.1410 \pm 0.0171
0.52	1.1365 \pm 0.0170
0.54	1.1300 \pm 0.0169
0.55	1.1273 \pm 0.0169
0.55	1.1266 \pm 0.0169
0.57	1.1220 \pm 0.0168
0.60	1.1185 \pm 0.0179
0.65	1.1182 \pm 0.0179
0.65	1.1179 \pm 0.0179
0.70	1.1135 \pm 0.0178
0.75	1.1120 \pm 0.0178
0.77	1.1111 \pm 0.0178
0.80	1.1100 \pm 0.0178
0.85	1.1135 \pm 0.0178
0.90	1.1372 \pm 0.0182
0.90	1.1403 \pm 0.0182
0.94	1.1691 \pm 0.0187
0.96	1.1876 \pm 0.0190
0.98	1.1992 \pm 0.0192
1.00	1.1969 \pm 0.0215
1.04	1.1955 \pm 0.0215
1.09	1.1941 \pm 0.0215
1.10	1.1938 \pm 0.0215
1.20	1.1994 \pm 0.0216
1.25	1.2020 \pm 0.0216
1.30	1.2082 \pm 0.0217
1.34	1.2125 \pm 0.0218
1.40	1.2200 \pm 0.0220
1.44	1.2245 \pm 0.0220
1.50	1.2321 \pm 0.0222
1.60	1.2435 \pm 0.0224
1.70	1.2529 \pm 0.0226
1.75	1.2575 \pm 0.0226
1.80	1.2619 \pm 0.0227
2.00	1.2714 \pm 0.0229
2.20	1.2699 \pm 0.0229
2.40	1.2561 \pm 0.0226
2.50	1.2500 \pm 0.0225
2.60	1.2442 \pm 0.0224
2.80	1.2220 \pm 0.0220
3.00	1.2010 \pm 0.0276
3.50	1.1554 \pm 0.0266
3.60	1.1473 \pm 0.0264
4.00	1.1295 \pm 0.0260
4.50	1.1011 \pm 0.0253
4.70	1.0923 \pm 0.0251
5.00	1.0617 \pm 0.0244
5.25	1.0521 \pm 0.0242
5.30	1.0502 \pm 0.0242
5.32	1.0490 \pm 0.0241
5.50	1.0388 \pm 0.0239
5.75	1.0405 \pm 0.0239
5.80	1.0408 \pm 0.0239
6.00	1.0985 \pm 0.0242
6.20	1.1817 \pm 0.0260
6.25	1.2085 \pm 0.0266

Cross Sections for $^{235}\text{U}(\text{n},\text{f})$ from ENDF/B-VI.5

6.50	1.3481 \pm 0.0297
6.75	1.4458 \pm 0.0318
7.00	1.5467 \pm 0.0340
7.25	1.6211 \pm 0.0357
7.50	1.6964 \pm 0.0373
7.75	1.7300 \pm 0.0381
8.00	1.7606 \pm 0.0387
8.25	1.7704 \pm 0.0389
8.50	1.7800 \pm 0.0392
8.75	1.7749 \pm 0.0390
9.00	1.7700 \pm 0.0389
9.25	1.7628 \pm 0.0388
9.50	1.7557 \pm 0.0386
9.75	1.7485 \pm 0.0385
10.00	1.7415 \pm 0.0313
10.25	1.7365 \pm 0.0313
10.50	1.7317 \pm 0.0312
10.75	1.7267 \pm 0.0311
11.00	1.7219 \pm 0.0310
11.25	1.7194 \pm 0.0309
11.50	1.7170 \pm 0.0309
11.75	1.7259 \pm 0.0311
12.00	1.7347 \pm 0.0208
12.19	1.7668 \pm 0.0212
12.25	1.7760 \pm 0.0213
12.50	1.8175 \pm 0.0218
12.75	1.8588 \pm 0.0223
13.00	1.9002 \pm 0.0228
13.25	1.9401 \pm 0.0233
13.50	1.9801 \pm 0.0238
13.75	2.0200 \pm 0.0242
14.00	2.0600 \pm 0.0165
14.25	2.0701 \pm 0.0166
14.50	2.0800 \pm 0.0312
14.75	2.0845 \pm 0.0313
15.00	2.0890 \pm 0.0418
15.25	2.0890 \pm 0.0418
15.50	2.0890 \pm 0.0418
15.75	2.0890 \pm 0.0418
16.00	2.0890 \pm 0.0522
16.50	2.0652 \pm 0.0516
17.00	2.0413 \pm 0.0612
17.50	2.0080 \pm 0.0602
17.96	1.9772 \pm 0.0593
18.00	1.9748 \pm 0.0592
18.50	1.9537 \pm 0.0586
19.00	1.9325 \pm 0.0773
19.50	1.9334 \pm 0.0773
20.00	1.9343 \pm 0.0774

Cross Sections for $^{235}\text{U}(\text{n},\text{f})$ from ENDF/B-VI.5

E_n (MeV)	$\sigma_{235\text{U}(n,f)}$
0.10	0.0000 ± 0.0000
0.11	0.0000 ± 0.0000
0.11	0.0004 ± 0.0000
0.11	0.0000 ± 0.0000
0.12	0.0000 ± 0.0000
0.12	0.0010 ± 0.0000
0.12	0.0000 ± 0.0000
0.12	0.0000 ± 0.0000
0.12	0.0000 ± 0.0000
0.12	0.0000 ± 0.0000
0.12	0.0000 ± 0.0000
0.12	0.0003 ± 0.0000
0.12	0.0000 ± 0.0000
0.12	0.0000 ± 0.0000
0.12	0.0007 ± 0.0000
0.12	0.0000 ± 0.0000
0.12	0.0000 ± 0.0000
0.12	0.0003 ± 0.0000
0.13	0.0000 ± 0.0000
0.13	0.0000 ± 0.0000
0.13	0.0011 ± 0.0000
0.13	0.0000 ± 0.0000
0.13	0.0000 ± 0.0000
0.13	0.0000 ± 0.0000
0.13	0.0008 ± 0.0000
0.13	0.0000 ± 0.0000
0.14	0.0000 ± 0.0000
0.14	0.0004 ± 0.0000
0.14	0.0000 ± 0.0000
0.14	0.0000 ± 0.0000
0.14	0.0012 ± 0.0000
0.14	0.0000 ± 0.0000
0.14	0.0000 ± 0.0000
0.14	0.0003 ± 0.0000
0.14	0.0000 ± 0.0000
0.15	0.0000 ± 0.0000
0.15	0.0010 ± 0.0000
0.15	0.0001 ± 0.0000
0.16	0.0001 ± 0.0000
0.17	0.0001 ± 0.0000
0.18	0.0001 ± 0.0000
0.19	0.0001 ± 0.0000
0.20	0.0001 ± 0.0000
0.21	0.0001 ± 0.0000
0.22	0.0001 ± 0.0000
0.23	0.0001 ± 0.0000
0.23	0.0001 ± 0.0000
0.24	0.0001 ± 0.0000
0.24	0.0001 ± 0.0000
0.25	0.0001 ± 0.0000
0.26	0.0001 ± 0.0000
0.27	0.0001 ± 0.0000

Cross Sections for $^{235}\text{U}(\text{n},\text{f})$ from ENDF/B-VI.5

0.28	0.0001 \pm 0.0000
0.30	0.0001 \pm 0.0000
0.38	0.0002 \pm 0.0000
0.40	0.0003 \pm 0.0000
0.42	0.0003 \pm 0.0000
0.43	0.0003 \pm 0.0000
0.44	0.0003 \pm 0.0000
0.45	0.0003 \pm 0.0000
0.46	0.0003 \pm 0.0000
0.47	0.0003 \pm 0.0000
0.50	0.0004 \pm 0.0000
0.55	0.0006 \pm 0.0000
0.58	0.0007 \pm 0.0000
0.59	0.0008 \pm 0.0000
0.60	0.0008 \pm 0.0000
0.62	0.0009 \pm 0.0000
0.64	0.0011 \pm 0.0000
0.65	0.0012 \pm 0.0000
0.66	0.0013 \pm 0.0000
0.68	0.0016 \pm 0.0000
0.70	0.0017 \pm 0.0000
0.75	0.0026 \pm 0.0000
0.78	0.0036 \pm 0.0001
0.80	0.0045 \pm 0.0001
0.85	0.0072 \pm 0.0001
0.88	0.0108 \pm 0.0002
0.90	0.0136 \pm 0.0002
0.93	0.0155 \pm 0.0002
0.95	0.0165 \pm 0.0003
0.97	0.0158 \pm 0.0003
1.00	0.0140 \pm 0.0003
1.02	0.0157 \pm 0.0003
1.03	0.0169 \pm 0.0003
1.05	0.0200 \pm 0.0004
1.08	0.0270 \pm 0.0005
1.10	0.0300 \pm 0.0005
1.13	0.0360 \pm 0.0006
1.14	0.0381 \pm 0.0007
1.15	0.0392 \pm 0.0007
1.17	0.0402 \pm 0.0007
1.20	0.0421 \pm 0.0008
1.23	0.0403 \pm 0.0007
1.24	0.0400 \pm 0.0007
1.25	0.0391 \pm 0.0007
1.28	0.0502 \pm 0.0009
1.30	0.0650 \pm 0.0012
1.35	0.1119 \pm 0.0020
1.40	0.1855 \pm 0.0033
1.45	0.2822 \pm 0.0051
1.48	0.3310 \pm 0.0060
1.50	0.3560 \pm 0.0064
1.52	0.3805 \pm 0.0068
1.55	0.3990 \pm 0.0072
1.57	0.4125 \pm 0.0074
1.60	0.4226 \pm 0.0076
1.70	0.4550 \pm 0.0082

Cross Sections for $^{235}\text{U}(\text{n},\text{f})$ from ENDF/B-VI.5

1.80	0.4820 ± 0.0087
1.90	0.5070 ± 0.0091
2.00	0.5250 ± 0.0095
2.10	0.5355 ± 0.0096
2.20	0.5391 ± 0.0097
2.40	0.5373 ± 0.0097
2.60	0.5328 ± 0.0096
2.80	0.5270 ± 0.0095
3.00	0.5160 ± 0.0119
3.20	0.5210 ± 0.0120
3.60	0.5354 ± 0.0123
4.00	0.5483 ± 0.0126
4.50	0.5496 ± 0.0126
4.70	0.5470 ± 0.0126
5.00	0.5405 ± 0.0124
5.30	0.5430 ± 0.0125
5.50	0.5500 ± 0.0126
5.80	0.5731 ± 0.0132
6.00	0.6153 ± 0.0135
6.20	0.6859 ± 0.0151
6.50	0.8257 ± 0.0182
6.70	0.8870 ± 0.0195
7.00	0.9403 ± 0.0207
7.30	0.9680 ± 0.0213
7.50	0.9807 ± 0.0216
7.75	0.9910 ± 0.0218
8.00	0.9935 ± 0.0219
8.50	1.0000 ± 0.0220
9.00	0.9979 ± 0.0220
10.00	0.9868 ± 0.0178
11.00	0.9830 ± 0.0177
11.50	0.9830 ± 0.0177
12.00	0.9850 ± 0.0118
13.00	1.0130 ± 0.0122
14.00	1.1300 ± 0.0090
14.50	1.1550 ± 0.0173
15.00	1.1980 ± 0.0240
16.00	1.2593 ± 0.0315
17.00	1.2561 ± 0.0377
18.00	1.2493 ± 0.0375
19.00	1.2954 ± 0.0518
20.00	1.3521 ± 0.0541

APPENDIX C: ENERGY-INDEPENDENT SYSTEMATIC UNCERTAINTIES

TABLE CIX: Contribution of systematic uncertainties from neutron-energy-independent factors. The last two rows show the internal conversion and efficiency correction factors for the $2 \rightarrow 0$ transition in ^{56}Fe . Definitions for the symbols used can be found in section II A 2

Factor	98Thin (%)	98Thick (%)	99Thin (%)
ϵ_d	0.4	0.4	0.4
f_{fc}	3.0	3.0	3.0
a_{FC1}	0.7	0.7	0.7
a_{FC2}	4.8	4.8	4.8
f_{ge}	3.0	3.0	3.0
a_{sample}	7.1	5.0	0.6
$1 + \alpha_{4 \rightarrow 2}$	5.6	5.6	5.6
$\epsilon_{4 \rightarrow 2}$	5.7	6.3	5.3
$1 + \alpha_{6 \rightarrow 4}$	4.1	4.1	4.1
$\epsilon_{6 \rightarrow 4}$	6.4	6.9	4.9
$1 + \alpha_{8 \rightarrow 6}$	2.5	2.5	2.5
$\epsilon_{8 \rightarrow 6}$	5.2	5.8	4.6
$1 + \alpha_{10 \rightarrow 8}$	1.6	1.6	1.6
$\epsilon_{10 \rightarrow 8}$	4.8	5.2	4.5
$1 + \alpha_{Fe}$	N/A	N/A	0.0
ϵ_{Fe}	N/A	N/A	5.5

APPENDIX D: PARTITION OF RELATIVE UNCERTAINTIES

1 Notation and Formalism

The γ -ray cross-section uncertainties discussed throughout this report include contributions from all the terms used in their calculation. In many practical applications, these partial γ -ray cross sections are combined by various algebraic operations, thereby introducing correlations between their uncertainties. If those correlations are ignored, the resulting uncertainty is likely overestimated. In this appendix, we partition the uncertainty for each partial cross section calculated in the ($n, 2n$) channel into (approximately independent) components which can be combined to yield a more appropriate measure of uncertainty.

In order to avoid confusion with the symbol σ , already used to denote cross sections, we introduce the following nomenclature for any random variable x :

$$u_x \equiv \text{uncertainty in } x \quad (\text{D1})$$

$$v_x \equiv \text{variance of } x = u_x^2 \quad (\text{D2})$$

$$\rho_x \equiv \text{relative uncertainty in } x = \frac{u_x}{x} \quad (\text{D3})$$

These quantities are subject to the error-propagation rules discussed in reference [17].

a The case of a single data set

It is convenient to rewrite the expression used to calculate the partial γ -ray cross sections (see equ. 3-5 and 8) as a product of four terms, determined by their dependency on γ -ray and neutron energies:

$$\sigma_\gamma \equiv C \times f_1(E_\gamma) \times f_2(E_n) \times f_3(E_\gamma, E_n) \quad (\text{D4})$$

where C is a constant independent of either γ -ray or neutron energy. These terms can be written explicitly as:

$$C \equiv \frac{\epsilon_d}{a_{sample}} \times \frac{1 - f_{fc}}{1 - f_{ge}} \quad (D5)$$

$$f_1(E_\gamma) \equiv \frac{1 + \alpha_\gamma}{\epsilon_\gamma} \quad (D6)$$

$$f_2(E_n) \equiv \frac{1}{\sum_\tau \omega_\tau(E_n) \sum_i N_{fc}(\tau) \sigma_{(n,f)}(\tau) \times a_{fout}^i} \quad (D7)$$

$$f_3(E_\gamma, E_n) \equiv A_\gamma(E_n) \times C_\gamma(E_n) \quad (D8)$$

The parameters in these equations are discussed in sections II A 2 and XI (in the case of C_γ). The symbol $\omega_\tau(E_n)$ refers to the integral weighting factor in equation 5. The corresponding total relative variance is obtained as the sum of relative variances for each of the four terms:

$$\rho_{tot}^2 \equiv \rho_c^2 + \rho_\gamma^2 + \rho_n^2 + \rho_{\gamma n}^2 \quad (D9)$$

where ρ_c , ρ_γ , ρ_n , and $\rho_{\gamma n}$ are the relative uncertainties for the terms C , $f_1(E_\gamma)$, $f_2(E_n)$, and $f_3(E_\gamma, E_n)$, respectively.

b The case of combined data sets

For those cases where the partial γ -ray cross section is obtained as the weighted average of the 1998 and 1999 GEANIE data sets, equation D4 is no longer strictly applicable. However, to the extent that the individual terms in the equation are approximately the same between the two data sets (after appropriate scaling of the 1998 and baseline subtraction for the 1999 data), the relative uncertainties can be approximately partitioned using equation D9. In order to derive the appropriate expressions for combined data sets, we consider the general case of two variables, x and y , each obtained as the product of two terms:

$$x \equiv x_1 \times x_2 \quad (D10)$$

$$y \equiv y_1 \times y_2 \quad (D11)$$

These terms carry uncertainties (u_{x_1} for x_1 , u_{x_2} for x_2 , u_{y_1} for y_1 , and u_{y_2} for y_2), which we assume to be uncorrelated. The variables x and y can be thought of as separate measurements of the same quantity. Similarly, x_1 and y_1 on the one hand, and x_2 and y_2 on the other can be considered as separate instances of the same quantity.

If z is the weighted mean of x and y , calculated according to the prescription in [16], then we can write:

$$z \equiv w_x x + w_y y \quad (D12)$$

$$v_z = w_x^2 v_x + w_y^2 v_y \quad (D13)$$

$$w_x \equiv \frac{\frac{1}{v_x}}{\frac{1}{v_x} + \frac{1}{v_y}} \quad (D14)$$

$$w_y \equiv \frac{\frac{1}{v_y}}{\frac{1}{v_x} + \frac{1}{v_y}} \quad (D15)$$

Now we wish to partition the uncertainty in the weighted mean z in a manner that reflects the partitions of x and y into products of similar terms. Mathematically, this is akin to writing z as a product of two terms as well, the first, (x') dependent only on the related variables x_1 and y_1 , and the second, (y') dependent only on x_2 and y_2 :

$$z \equiv x' y' \quad (D16)$$

$$\rho_z^2 = \rho_{x'}^2 + \rho_{y'}^2 \quad (D17)$$

In the case where $x = y$ (but not necessarily $u_x = u_y$), equations D12-D15 reduce to:

$$z = x = y \quad (\text{D18})$$

$$\rho_z^2 = \frac{\rho_x^2 \rho_y^2}{\rho_x^2 + \rho_y^2} \quad (\text{D19})$$

$$w_x = \frac{\rho_y^2}{\rho_x^2 + \rho_y^2} \quad (\text{D20})$$

$$w_y = \frac{\rho_x^2}{\rho_x^2 + \rho_y^2} \quad (\text{D21})$$

This represents the hoped for situation where the separate measurements x and y yield the same value, albeit with different uncertainties. In that special case, it is a matter of algebra to show that the relative variance ρ_z^2 can be written in the suggestive form:

$$\rho_z^2 = \underbrace{\frac{\rho_{x_1}^2 \rho_{x_2}^2}{\rho_{x_1}^2 + \rho_{x_2}^2}}_{\rho_{x'}^2} + \underbrace{\frac{\rho_{y_1}^2 \rho_{y_2}^2}{\rho_{y_1}^2 + \rho_{y_2}^2}}_{\rho_{y'}^2} + \underbrace{\frac{(\rho_{x_2}^2 \rho_{y_1}^2 - \rho_{x_1}^2 \rho_{y_2}^2)^2}{(\rho_{x_1}^2 + \rho_{y_1}^2)(\rho_{x_2}^2 + \rho_{y_2}^2)(\rho_{x_1}^2 + \rho_{x_2}^2 + \rho_{y_1}^2 + \rho_{y_2}^2)}}_{\Delta \rho^2} \quad (\text{D22})$$

where we have identified the first two terms on the right-hand side with the partitioned relative variances $\rho_{x'}^2$ and $\rho_{y'}^2$. Strictly speaking, equation D22 can only be thought of as a partition of the relative variance of the weighted mean to the extent that the residual term $\Delta \rho^2$ can be neglected. This condition is easily verified, and for most practical applications, $\Delta \rho^2$ is indeed small.

2 Specific Applications

In this section we illustrate the benefits of the partitioning dictated by equations D4 and D9, by citing three applications where the uncertainty components may be recombined to yield a more appropriate (and typically smaller) overall uncertainty.

a Ratio of distinct γ -ray cross sections evaluated at the same neutron energy

$$\frac{\sigma_{\gamma_i}(E_n)}{\sigma_{\gamma_j}(E_n)} = \frac{f_1(E_{\gamma_i}) \times f_3(E_{\gamma_i}, E_n)}{f_1(E_{\gamma_j}) \times f_3(E_{\gamma_j}, E_n)} \quad (\text{D23})$$

$$\Rightarrow \rho^2 \left[\frac{\sigma_{\gamma_i}(E_n)}{\sigma_{\gamma_j}(E_n)} \right] = \rho_{\gamma_i}^2 + \rho_{\gamma_i n}^2 + \rho_{\gamma_j}^2 + \rho_{\gamma_j n}^2 \quad (\text{D24})$$

b Ratio of a γ -ray cross section evaluated at distinct neutron energies

$$\frac{\sigma_\gamma(E_n^{(1)})}{\sigma_\gamma(E_n^{(2)})} = \frac{f_2(E_n^{(1)}) \times f_3(E_\gamma, E_n^{(1)})}{f_2(E_n^{(2)}) \times f_3(E_\gamma, E_n^{(2)})} \quad (\text{D25})$$

$$\Rightarrow \rho^2 \left[\frac{\sigma_\gamma(E_n^{(1)})}{\sigma_\gamma(E_n^{(2)})} \right] = \rho_{n_1}^2 + \rho_{\gamma n_1}^2 + \rho_{n_2}^2 + \rho_{\gamma n_2}^2 \quad (\text{D26})$$

c *Sum of individual γ -ray cross sections evaluated at the same neutron energy*

$$\sum_i \sigma_{\gamma_i}(E_n) = C \times f_2(E_n) \times \sum_i f_1(E_{\gamma_i}) \times f_3(E_{\gamma_i}, E_n) \quad (\text{D27})$$

$$\begin{aligned} \Rightarrow \rho^2 \left[\sum_i \sigma_{\gamma_i}(E_n) \right] &= \rho_c^2 + \rho_n^2 + \rho^2 \left[\sum_i f_1(E_{\gamma_i}) \times f_3(E_{\gamma_i}, E_n) \right] \\ &= \rho_c^2 + \rho_n^2 + \frac{\sum_i v \{ f_1(E_{\gamma_i}) \times f_3(E_{\gamma_i}, E_n) \}}{\left[\sum_i f_1(E_{\gamma_i}) \times f_3(E_{\gamma_i}, E_n) \right]^2} \\ &= \rho_c^2 + \rho_n^2 + \frac{\sum_i \sigma_{\gamma_i}^2(E_n) \times (\rho_{\gamma_i}^2 + \rho_{\gamma_i n}^2)}{\left[\sum_i \sigma_{\gamma_i}(E_n) \right]^2} \end{aligned} \quad (\text{D28})$$

3 Tabulated Results for the $^{235}\text{U}(\text{n},2\text{n})$ Channel

Finally, we list here the partitioned relative uncertainties extracted for the $(\text{n},2\text{n}\gamma)$ lines discussed in the text. First, we cite a few caveats which apply to the tables below:

1. The partition formulas (equ. D9 and D22) are used to calculate ρ_c , ρ_γ , and ρ_n explicitly. The remaining contribution is then attributed entirely to $\rho_{\gamma n}$. This ensures that the calculated value of ρ_{tot} is consistent with the total uncertainty calculated by exact error propagation.
2. In theory, the constant-term relative error partition ρ_c should be identical for all γ rays and at all neutron energies. In practice however, its value depends on which data are used. Thus three distinct values of ρ_c can be identified in the tables below depending on whether the accepted cross sections were obtained:
 - (a) by weighted mean of the 1998 and 1999 planar-detector data ($\rho_c = 0.0599$),
 - (b) from the 1998 planar-detector data alone ($\rho_c = 0.0823$), or
 - (c) from the 1998 coaxial-detector data alone ($\rho_c = 0.0824$).

The value of the constant term in equation D4 (or its weighted-mean equivalent) is also different in each of these three cases. These considerations complicate the examples quoted in section D 2 somewhat.

3. The value of ρ_n should also be the same for all γ rays, however, for the same reasons discussed for ρ_c , this is not necessarily the case.

TABLE CX: Partition of the relative uncertainties for the $E_\gamma = 99.8$ -keV transition from the level at $E_x = 143.4$ keV in the ^{234}U nucleus.

E_n (MeV)	σ_γ (b)	ρ_c	ρ_γ	ρ_n	$\rho_{\gamma n}$	ρ_{tot}
4.0900 ± 0.0930	0.0011 ± 0.0090	0.0599	0.0554	0.0255	8.1515	8.1519
4.2640 ± 0.0990	0.0088 ± 0.0252	0.0599	0.0554	0.0250	2.8581	2.8594
4.4530 ± 0.1050	0.0025 ± 0.0125	0.0599	0.0554	0.0240	5.0025	5.0032
4.6470 ± 0.1130	0.0008 ± 0.0127	0.0599	0.0554	0.0234	15.4204	15.4206
4.8610 ± 0.1220	-0.0008 ± 0.0087	0.0599	0.0554	0.0233	10.7494	10.7497
5.0900 ± 0.1290	0.0233 ± 0.0241	0.0599	0.0554	0.0228	1.0270	1.0305
5.3330 ± 0.1400	0.0530 ± 0.0240	0.0599	0.0554	0.0227	0.4434	0.4514
5.5970 ± 0.1490	0.0360 ± 0.0228	0.0599	0.0554	0.0223	0.6268	0.6325
5.8750 ± 0.1600	0.0470 ± 0.0231	0.0599	0.0554	0.0218	0.4831	0.4905
6.1810 ± 0.1750	0.1719 ± 0.0295	0.0599	0.0554	0.0215	0.1487	0.1710
6.5170 ± 0.1870	0.2378 ± 0.0332	0.0599	0.0554	0.0202	0.1114	0.1396
6.8620 ± 0.2010	0.2141 ± 0.0309	0.0599	0.0554	0.0194	0.1173	0.1442
7.2370 ± 0.2180	0.2384 ± 0.0340	0.0599	0.0554	0.0202	0.1144	0.1420
7.6610 ± 0.2420	0.2688 ± 0.0366	0.0599	0.0554	0.0215	0.1066	0.1359
8.1260 ± 0.2630	0.2991 ± 0.0390	0.0599	0.0554	0.0213	0.0991	0.1301
8.6180 ± 0.2840	0.3133 ± 0.0397	0.0599	0.0554	0.0208	0.0946	0.1266
9.1600 ± 0.3130	0.3418 ± 0.0420	0.0599	0.0554	0.0212	0.0893	0.1228
9.7570 ± 0.3460	0.3893 ± 0.0466	0.0599	0.0554	0.0220	0.0845	0.1195
10.4140 ± 0.3770	0.3742 ± 0.0457	0.0599	0.0554	0.0228	0.0877	0.1219
11.1430 ± 0.4250	0.3681 ± 0.0459	0.0599	0.0554	0.0241	0.0909	0.1245
11.9600 ± 0.4670	0.4252 ± 0.0510	0.0599	0.0554	0.0248	0.0842	0.1198
12.8600 ± 0.5250	0.4044 ± 0.0496	0.0599	0.0554	0.0253	0.0878	0.1225
13.8760 ± 0.5890	0.2330 ± 0.0373	0.0599	0.0554	0.0258	0.1351	0.1599
15.0160 ± 0.6600	0.1581 ± 0.0325	0.0599	0.0554	0.0258	0.1867	0.2054
16.2970 ± 0.7500	0.1151 ± 0.0302	0.0599	0.0554	0.0257	0.2476	0.2620
17.7590 ± 0.8570	0.0397 ± 0.0271	0.0599	0.0554	0.0256	0.6746	0.6800
19.4160 ± 0.9710	0.0258 ± 0.0269	0.0599	0.0554	0.0261	1.0313	1.0349

TABLE CXI: Partition of the relative uncertainties for the $E_\gamma = 131.3$ -keV transition from the level at $E_x = 1552.6$ keV in the ^{234}U nucleus.

E_n (MeV)	σ_γ (b)	ρ_c	ρ_γ	ρ_n	$\rho_{\gamma n}$	ρ_{tot}
4.0900 ± 0.0930	0.0037 ± 0.0018	0.0599	0.0448	0.0255	0.4849	0.4913
4.2640 ± 0.0990	0.0044 ± 0.0018	0.0599	0.0448	0.0250	0.4036	0.4112
4.4530 ± 0.1050	0.0051 ± 0.0017	0.0599	0.0448	0.0240	0.3334	0.3425
4.6470 ± 0.1130	0.0017 ± 0.0017	0.0599	0.0448	0.0234	0.9722	0.9753
4.8610 ± 0.1220	0.0024 ± 0.0017	0.0599	0.0448	0.0233	0.6862	0.6907
5.0900 ± 0.1290	0.0001 ± 0.0015	0.0599	0.0448	0.0228	9.8984	9.8987
5.3330 ± 0.1400	0.0017 ± 0.0017	0.0599	0.0448	0.0227	0.9953	0.9984
5.5970 ± 0.1490	0.0032 ± 0.0018	0.0599	0.0448	0.0223	0.5441	0.5497
5.8750 ± 0.1600	0.0013 ± 0.0017	0.0599	0.0448	0.0218	1.2964	1.2988
6.1810 ± 0.1750	0.0028 ± 0.0017	0.0599	0.0448	0.0215	0.5903	0.5954
6.5170 ± 0.1870	0.0014 ± 0.0016	0.0599	0.0448	0.0202	1.0906	1.0934
6.8620 ± 0.2010	0.0041 ± 0.0016	0.0599	0.0448	0.0194	0.3811	0.3889
7.2370 ± 0.2180	0.0027 ± 0.0016	0.0599	0.0448	0.0202	0.5875	0.5926
7.6610 ± 0.2420	0.0064 ± 0.0018	0.0599	0.0448	0.0215	0.2720	0.2829
8.1260 ± 0.2630	0.0081 ± 0.0018	0.0599	0.0448	0.0213	0.2145	0.2282
8.6180 ± 0.2840	0.0072 ± 0.0018	0.0599	0.0448	0.0208	0.2386	0.2509
9.1600 ± 0.3130	0.0095 ± 0.0019	0.0599	0.0448	0.0212	0.1835	0.1993
9.7570 ± 0.3460	0.0104 ± 0.0020	0.0599	0.0448	0.0220	0.1742	0.1908
10.4140 ± 0.3770	0.0137 ± 0.0022	0.0599	0.0448	0.0228	0.1383	0.1589
11.1430 ± 0.4250	0.0136 ± 0.0023	0.0599	0.0448	0.0241	0.1468	0.1665
11.9600 ± 0.4670	0.0126 ± 0.0023	0.0599	0.0448	0.0248	0.1654	0.1832
12.8600 ± 0.5250	0.0139 ± 0.0024	0.0599	0.0448	0.0253	0.1555	0.1744
13.8760 ± 0.5890	0.0092 ± 0.0023	0.0599	0.0448	0.0258	0.2336	0.2466
15.0160 ± 0.6600	0.0075 ± 0.0022	0.0599	0.0448	0.0258	0.2821	0.2930
16.2970 ± 0.7500	0.0026 ± 0.0018	0.0599	0.0448	0.0257	0.7051	0.7096
17.7590 ± 0.8570	0.0078 ± 0.0022	0.0599	0.0448	0.0256	0.2660	0.2775
19.4160 ± 0.9710	0.0031 ± 0.0018	0.0599	0.0448	0.0261	0.5644	0.5699

TABLE CXII: Partition of the relative uncertainties for the $E_\gamma = 152.7$ -keV transition from the level at $E_x = 296.1$ keV in the ^{234}U nucleus.

E_n (MeV)	σ_γ (b)	ρ_c	ρ_γ	ρ_n	$\rho_{\gamma n}$	ρ_{tot}
4.0900 ± 0.0930	0.0139 ± 0.0033	0.0599	0.0490	0.0255	0.2223	0.2367
4.2640 ± 0.0990	0.0108 ± 0.0032	0.0599	0.0490	0.0250	0.2817	0.2932
4.4530 ± 0.1050	0.0137 ± 0.0031	0.0599	0.0490	0.0240	0.2137	0.2286
4.6470 ± 0.1130	0.0110 ± 0.0030	0.0599	0.0490	0.0234	0.2580	0.2703
4.8610 ± 0.1220	0.0097 ± 0.0029	0.0599	0.0490	0.0233	0.2894	0.3005
5.0900 ± 0.1290	0.0080 ± 0.0016	0.0599	0.0490	0.0228	0.1796	0.1969
5.3330 ± 0.1400	0.0073 ± 0.0015	0.0599	0.0490	0.0227	0.1841	0.2009
5.5970 ± 0.1490	0.0117 ± 0.0029	0.0599	0.0490	0.0223	0.2304	0.2441
5.8750 ± 0.1600	0.0310 ± 0.0038	0.0599	0.0490	0.0218	0.0911	0.1215
6.1810 ± 0.1750	0.0802 ± 0.0073	0.0599	0.0490	0.0215	0.0422	0.0907
6.5170 ± 0.1870	0.1281 ± 0.0111	0.0599	0.0490	0.0202	0.0329	0.0864
6.8620 ± 0.2010	0.1587 ± 0.0136	0.0599	0.0490	0.0194	0.0308	0.0855
7.2370 ± 0.2180	0.1906 ± 0.0163	0.0599	0.0490	0.0202	0.0300	0.0854
7.6610 ± 0.2420	0.2068 ± 0.0177	0.0599	0.0490	0.0215	0.0300	0.0857
8.1260 ± 0.2630	0.2391 ± 0.0204	0.0599	0.0490	0.0213	0.0295	0.0855
8.6180 ± 0.2840	0.2658 ± 0.0227	0.0599	0.0490	0.0208	0.0289	0.0852
9.1600 ± 0.3130	0.2923 ± 0.0249	0.0599	0.0490	0.0212	0.0287	0.0852
9.7570 ± 0.3460	0.3231 ± 0.0276	0.0599	0.0490	0.0220	0.0286	0.0854
10.4140 ± 0.3770	0.3486 ± 0.0298	0.0599	0.0490	0.0228	0.0286	0.0856
11.1430 ± 0.4250	0.3834 ± 0.0330	0.0599	0.0490	0.0241	0.0286	0.0859
11.9600 ± 0.4670	0.3916 ± 0.0338	0.0599	0.0490	0.0248	0.0288	0.0862
12.8600 ± 0.5250	0.3458 ± 0.0299	0.0599	0.0490	0.0253	0.0292	0.0865
13.8760 ± 0.5890	0.2599 ± 0.0227	0.0599	0.0490	0.0258	0.0309	0.0872
15.0160 ± 0.6600	0.1814 ± 0.0160	0.0599	0.0490	0.0258	0.0339	0.0883
16.2970 ± 0.7500	0.1295 ± 0.0117	0.0599	0.0490	0.0257	0.0391	0.0904
17.7590 ± 0.8570	0.0973 ± 0.0091	0.0599	0.0490	0.0256	0.0455	0.0933
19.4160 ± 0.9710	0.0817 ± 0.0079	0.0599	0.0490	0.0261	0.0513	0.0964

TABLE CXIII: Partition of the relative uncertainties for the $E_\gamma = 201.0\text{-keV}$ transition from the level at $E_x = 497.0\text{ keV}$ in the ^{234}U nucleus.

E_n (MeV)	σ_γ (b)	ρ_c	ρ_γ	ρ_n	$\rho_{\gamma n}$	ρ_{tot}
4.0900 ± 0.0930	0.0038 ± 0.0024	0.0599	0.0390	0.0255	0.6188	0.6234
4.2640 ± 0.0990	0.0033 ± 0.0024	0.0599	0.0390	0.0250	0.7152	0.7192
4.4530 ± 0.1050	0.0054 ± 0.0023	0.0599	0.0390	0.0240	0.4144	0.4212
4.6470 ± 0.1130	0.0010 ± 0.0018	0.0599	0.0390	0.0234	1.8632	1.8647
4.8610 ± 0.1220	0.0060 ± 0.0023	0.0599	0.0390	0.0233	0.3760	0.3834
5.0900 ± 0.1290	0.0024 ± 0.0022	0.0599	0.0390	0.0228	0.9173	0.9203
5.3330 ± 0.1400	0.0018 ± 0.0019	0.0599	0.0390	0.0227	1.0462	1.0489
5.5970 ± 0.1490	-0.0004 ± 0.0018	0.0599	0.0390	0.0223	5.0526	5.0532
5.8750 ± 0.1600	0.0020 ± 0.0019	0.0599	0.0390	0.0218	0.9418	0.9447
6.1810 ± 0.1750	0.0138 ± 0.0024	0.0599	0.0390	0.0215	0.1552	0.1722
6.5170 ± 0.1870	0.0317 ± 0.0036	0.0599	0.0390	0.0202	0.0835	0.1118
6.8620 ± 0.2010	0.0438 ± 0.0044	0.0599	0.0390	0.0194	0.0670	0.0998
7.2370 ± 0.2180	0.0581 ± 0.0055	0.0599	0.0390	0.0202	0.0594	0.0951
7.6610 ± 0.2420	0.0694 ± 0.0064	0.0599	0.0390	0.0215	0.0551	0.0928
8.1260 ± 0.2630	0.0828 ± 0.0075	0.0599	0.0390	0.0213	0.0511	0.0904
8.6180 ± 0.2840	0.1058 ± 0.0093	0.0599	0.0390	0.0208	0.0466	0.0878
9.1600 ± 0.3130	0.1200 ± 0.0104	0.0599	0.0390	0.0212	0.0443	0.0867
9.7570 ± 0.3460	0.1393 ± 0.0120	0.0599	0.0390	0.0220	0.0425	0.0860
10.4140 ± 0.3770	0.1593 ± 0.0136	0.0599	0.0390	0.0228	0.0408	0.0854
11.1430 ± 0.4250	0.1815 ± 0.0155	0.0599	0.0390	0.0241	0.0396	0.0852
11.9600 ± 0.4670	0.1980 ± 0.0168	0.0599	0.0390	0.0248	0.0387	0.0850
12.8600 ± 0.5250	0.1853 ± 0.0158	0.0599	0.0390	0.0253	0.0396	0.0855
13.8760 ± 0.5890	0.1432 ± 0.0125	0.0599	0.0390	0.0258	0.0431	0.0874
15.0160 ± 0.6600	0.0958 ± 0.0087	0.0599	0.0390	0.0258	0.0506	0.0913
16.2970 ± 0.7500	0.0632 ± 0.0062	0.0599	0.0390	0.0257	0.0622	0.0982
17.7590 ± 0.8570	0.0526 ± 0.0054	0.0599	0.0390	0.0256	0.0689	0.1025
19.4160 ± 0.9710	0.0418 ± 0.0046	0.0599	0.0390	0.0261	0.0792	0.1098

TABLE CXIV: Partition of the relative uncertainties for the $E_\gamma = 244.2$ -keV transition from the level at $E_x = 741.2$ keV in the ^{234}U nucleus.

E_n (MeV)	σ_γ (b)	ρ_c	ρ_γ	ρ_n	$\rho_{\gamma n}$	ρ_{tot}
4.0900 ± 0.0930	-0.0015 ± 0.0001	0.0599	0.0348	0.0255	0.0362	0.0822
4.2640 ± 0.0990	0.0003 ± 0.0019	0.0599	0.0348	0.0250	5.4827	5.4832
4.4530 ± 0.1050	0.0023 ± 0.0018	0.0599	0.0348	0.0240	0.7634	0.7669
4.6470 ± 0.1130	0.0001 ± 0.0003	0.0599	0.0348	0.0234	4.2213	4.2219
4.8610 ± 0.1220	0.0001 ± 0.0003	0.0599	0.0348	0.0233	3.8953	3.8960
5.0900 ± 0.1290	0.0022 ± 0.0018	0.0599	0.0348	0.0228	0.8128	0.8160
5.3330 ± 0.1400	0.0026 ± 0.0016	0.0599	0.0348	0.0227	0.6003	0.6047
5.5970 ± 0.1490	0.0000 ± 0.0002	0.0599	0.0348	0.0223	18.1326	18.1328
5.8750 ± 0.1600	0.0000 ± 0.0002	0.0599	0.0348	0.0218	13.9459	13.9461
6.1810 ± 0.1750	-0.0000 ± 0.0002	0.0599	0.0348	0.0215	8.4648	8.4651
6.5170 ± 0.1870	0.0022 ± 0.0015	0.0599	0.0348	0.0202	0.6972	0.7009
6.8620 ± 0.2010	0.0052 ± 0.0016	0.0599	0.0348	0.0194	0.2943	0.3030
7.2370 ± 0.2180	0.0077 ± 0.0017	0.0599	0.0348	0.0202	0.2117	0.2237
7.6610 ± 0.2420	0.0142 ± 0.0021	0.0599	0.0348	0.0215	0.1290	0.1480
8.1260 ± 0.2630	0.0198 ± 0.0024	0.0599	0.0348	0.0213	0.0982	0.1221
8.6180 ± 0.2840	0.0249 ± 0.0027	0.0599	0.0348	0.0208	0.0799	0.1078
9.1600 ± 0.3130	0.0360 ± 0.0034	0.0599	0.0348	0.0212	0.0615	0.0950
9.7570 ± 0.3460	0.0382 ± 0.0036	0.0599	0.0348	0.0220	0.0609	0.0948
10.4140 ± 0.3770	0.0519 ± 0.0046	0.0599	0.0348	0.0228	0.0507	0.0888
11.1430 ± 0.4250	0.0643 ± 0.0056	0.0599	0.0348	0.0241	0.0464	0.0868
11.9600 ± 0.4670	0.0672 ± 0.0058	0.0599	0.0348	0.0248	0.0460	0.0868
12.8600 ± 0.5250	0.0669 ± 0.0058	0.0599	0.0348	0.0253	0.0465	0.0872
13.8760 ± 0.5890	0.0578 ± 0.0052	0.0599	0.0348	0.0258	0.0514	0.0900
15.0160 ± 0.6600	0.0393 ± 0.0039	0.0599	0.0348	0.0258	0.0670	0.0997
16.2970 ± 0.7500	0.0251 ± 0.0030	0.0599	0.0348	0.0257	0.0962	0.1213
17.7590 ± 0.8570	0.0170 ± 0.0026	0.0599	0.0348	0.0256	0.1343	0.1532
19.4160 ± 0.9710	0.0149 ± 0.0025	0.0599	0.0348	0.0261	0.1515	0.1686

TABLE CXV: Partition of the relative uncertainties for the $E_\gamma = 282.6$ -keV transition from the level at $E_x = 1023.8$ keV in the ^{234}U nucleus.

E_n (MeV)	σ_γ (b)	ρ_c	ρ_γ	ρ_n	$\rho_{\gamma n}$	ρ_{tot}
4.0900 \pm 0.0930	0.0079 \pm 0.0018	0.0599	0.0331	0.0255	0.2124	0.2246
4.2640 \pm 0.0990	0.0098 \pm 0.0018	0.0599	0.0331	0.0250	0.1702	0.1851
4.4530 \pm 0.1050	0.0071 \pm 0.0016	0.0599	0.0331	0.0240	0.2160	0.2279
4.6470 \pm 0.1130	0.0066 \pm 0.0016	0.0599	0.0331	0.0234	0.2325	0.2435
4.8610 \pm 0.1220	0.0074 \pm 0.0016	0.0599	0.0331	0.0233	0.2081	0.2203
5.0900 \pm 0.1290	0.0083 \pm 0.0016	0.0599	0.0331	0.0228	0.1843	0.1979
5.3330 \pm 0.1400	0.0066 \pm 0.0014	0.0599	0.0331	0.0227	0.2021	0.2146
5.5970 \pm 0.1490	0.0037 \pm 0.0013	0.0599	0.0331	0.0223	0.3479	0.3553
5.8750 \pm 0.1600	0.0037 \pm 0.0013	0.0599	0.0331	0.0218	0.3495	0.3568
6.1810 \pm 0.1750	0.0036 \pm 0.0013	0.0599	0.0331	0.0215	0.3557	0.3628
6.5170 \pm 0.1870	0.0057 \pm 0.0014	0.0599	0.0331	0.0202	0.2292	0.2400
6.8620 \pm 0.2010	0.0067 \pm 0.0014	0.0599	0.0331	0.0194	0.1953	0.2078
7.2370 \pm 0.2180	0.0083 \pm 0.0015	0.0599	0.0331	0.0202	0.1641	0.1789
7.6610 \pm 0.2420	0.0106 \pm 0.0017	0.0599	0.0331	0.0215	0.1412	0.1584
8.1260 \pm 0.2630	0.0091 \pm 0.0016	0.0599	0.0331	0.0213	0.1613	0.1765
8.6180 \pm 0.2840	0.0106 \pm 0.0017	0.0599	0.0331	0.0208	0.1422	0.1591
9.1600 \pm 0.3130	0.0120 \pm 0.0018	0.0599	0.0331	0.0212	0.1350	0.1528
9.7570 \pm 0.3460	0.0147 \pm 0.0020	0.0599	0.0331	0.0220	0.1151	0.1357
10.4140 \pm 0.3770	0.0150 \pm 0.0020	0.0599	0.0331	0.0228	0.1130	0.1340
11.1430 \pm 0.4250	0.0175 \pm 0.0022	0.0599	0.0331	0.0241	0.1058	0.1283
11.9600 \pm 0.4670	0.0210 \pm 0.0025	0.0599	0.0331	0.0248	0.0943	0.1191
12.8600 \pm 0.5250	0.0200 \pm 0.0025	0.0599	0.0331	0.0253	0.1004	0.1241
13.8760 \pm 0.5890	0.0204 \pm 0.0025	0.0599	0.0331	0.0258	0.1012	0.1249
15.0160 \pm 0.6600	0.0160 \pm 0.0023	0.0599	0.0331	0.0258	0.1207	0.1411
16.2970 \pm 0.7500	0.0117 \pm 0.0020	0.0599	0.0331	0.0257	0.1540	0.1705
17.7590 \pm 0.8570	0.0102 \pm 0.0019	0.0599	0.0331	0.0256	0.1747	0.1893
19.4160 \pm 0.9710	0.0095 \pm 0.0019	0.0599	0.0331	0.0261	0.1810	0.1952

TABLE CXVI: Partition of the relative uncertainties for the $E_\gamma = 666.5$ -keV transition from the level at $E_x = 962.6$ keV in the ^{234}U nucleus.

E_n (MeV)	σ_γ (b)	ρ_c	ρ_γ	ρ_n	$\rho_{\gamma n}$	ρ_{tot}
4.0900 \pm 0.0930	0.0001 \pm 0.0007	0.0823	0.0490	0.0385	11.0819	11.0824
4.2640 \pm 0.0990	0.0015 \pm 0.0034	0.0823	0.0490	0.0375	2.3227	2.3250
4.4530 \pm 0.1050	0.0073 \pm 0.0035	0.0823	0.0490	0.0359	0.4693	0.4804
4.6470 \pm 0.1130	0.0071 \pm 0.0034	0.0823	0.0490	0.0352	0.4767	0.4875
4.8610 \pm 0.1220	0.0089 \pm 0.0028	0.0823	0.0490	0.0354	0.2999	0.3168
5.0900 \pm 0.1290	0.0017 \pm 0.0032	0.0823	0.0490	0.0347	1.8760	1.8788
5.3330 \pm 0.1400	0.0062 \pm 0.0034	0.0823	0.0490	0.0342	0.5492	0.5586
5.5970 \pm 0.1490	0.0034 \pm 0.0033	0.0823	0.0490	0.0332	0.9693	0.9746
5.8750 \pm 0.1600	0.0039 \pm 0.0025	0.0823	0.0490	0.0326	0.6314	0.6394
6.1810 \pm 0.1750	0.0018 \pm 0.0032	0.0823	0.0490	0.0324	1.7947	1.7976
6.5170 \pm 0.1870	0.0062 \pm 0.0032	0.0823	0.0490	0.0302	0.5043	0.5142
6.8620 \pm 0.2010	0.0143 \pm 0.0034	0.0823	0.0490	0.0286	0.2187	0.2405
7.2370 \pm 0.2180	0.0085 \pm 0.0033	0.0823	0.0490	0.0295	0.3699	0.3832
7.6610 \pm 0.2420	0.0116 \pm 0.0036	0.0823	0.0490	0.0313	0.2910	0.3080
8.1260 \pm 0.2630	0.0143 \pm 0.0037	0.0823	0.0490	0.0312	0.2420	0.2622
8.6180 \pm 0.2840	0.0139 \pm 0.0037	0.0823	0.0490	0.0304	0.2491	0.2686
9.1600 \pm 0.3130	0.0109 \pm 0.0036	0.0823	0.0490	0.0310	0.3123	0.3281
9.7570 \pm 0.3460	0.0176 \pm 0.0040	0.0823	0.0490	0.0320	0.2049	0.2284
10.4140 \pm 0.3770	0.0201 \pm 0.0043	0.0823	0.0490	0.0331	0.1862	0.2120
11.1430 \pm 0.4250	0.0149 \pm 0.0041	0.0823	0.0490	0.0351	0.2578	0.2772
11.9600 \pm 0.4670	0.0190 \pm 0.0044	0.0823	0.0490	0.0361	0.2064	0.2304
12.8600 \pm 0.5250	0.0149 \pm 0.0043	0.0823	0.0490	0.0370	0.2696	0.2885
13.8760 \pm 0.5890	0.0180 \pm 0.0046	0.0823	0.0490	0.0375	0.2311	0.2530
15.0160 \pm 0.6600	0.0148 \pm 0.0044	0.0823	0.0490	0.0375	0.2752	0.2938
16.2970 \pm 0.7500	0.0148 \pm 0.0043	0.0823	0.0490	0.0375	0.2752	0.2938
17.7590 \pm 0.8570	0.0094 \pm 0.0042	0.0823	0.0490	0.0374	0.4345	0.4465
19.4160 \pm 0.9710	0.0104 \pm 0.0042	0.0823	0.0490	0.0381	0.3864	0.3999

TABLE CXVII: Partition of the relative uncertainties for the $E_\gamma = 780.4$ -keV transition from the level at $E_x = 1277.5$ keV in the ^{234}U nucleus.

E_n (MeV)	σ_γ (b)	ρ_c	ρ_γ	ρ_n	$\rho_{\gamma n}$	ρ_{tot}
4.0900 ± 0.0930	0.0080 ± 0.0036	0.0823	0.0560	0.0385	0.4351	0.4480
4.2640 ± 0.0990	0.0015 ± 0.0035	0.0823	0.0560	0.0375	2.3414	2.3438
4.4530 ± 0.1050	0.0013 ± 0.0033	0.0823	0.0560	0.0359	2.5419	2.5441
4.6470 ± 0.1130	0.0080 ± 0.0034	0.0823	0.0560	0.0352	0.4136	0.4269
4.8610 ± 0.1220	0.0032 ± 0.0033	0.0823	0.0560	0.0354	1.0034	1.0090
5.0900 ± 0.1290	0.0042 ± 0.0033	0.0823	0.0560	0.0347	0.7699	0.7771
5.3330 ± 0.1400	0.0025 ± 0.0034	0.0823	0.0560	0.0342	1.3766	1.3806
5.5970 ± 0.1490	0.0091 ± 0.0034	0.0823	0.0560	0.0332	0.3533	0.3686
5.8750 ± 0.1600	0.0061 ± 0.0033	0.0823	0.0560	0.0326	0.5311	0.5413
6.1810 ± 0.1750	0.0053 ± 0.0033	0.0823	0.0560	0.0324	0.6068	0.6158
6.5170 ± 0.1870	0.0056 ± 0.0032	0.0823	0.0560	0.0302	0.5612	0.5708
6.8620 ± 0.2010	0.0025 ± 0.0030	0.0823	0.0560	0.0286	1.1714	1.1760
7.2370 ± 0.2180	0.0035 ± 0.0031	0.0823	0.0560	0.0295	0.8936	0.8996
7.6610 ± 0.2420	0.0069 ± 0.0033	0.0823	0.0560	0.0313	0.4717	0.4831
8.1260 ± 0.2630	0.0064 ± 0.0034	0.0823	0.0560	0.0312	0.5123	0.5228
8.6180 ± 0.2840	0.0150 ± 0.0037	0.0823	0.0560	0.0304	0.2257	0.2485
9.1600 ± 0.3130	0.0159 ± 0.0038	0.0823	0.0560	0.0310	0.2135	0.2376
9.7570 ± 0.3460	0.0204 ± 0.0041	0.0823	0.0560	0.0320	0.1726	0.2019
10.4140 ± 0.3770	0.0155 ± 0.0039	0.0823	0.0560	0.0331	0.2304	0.2532
11.1430 ± 0.4250	0.0161 ± 0.0041	0.0823	0.0560	0.0351	0.2325	0.2553
11.9600 ± 0.4670	0.0164 ± 0.0042	0.0823	0.0560	0.0361	0.2345	0.2573
12.8600 ± 0.5250	0.0164 ± 0.0043	0.0823	0.0560	0.0370	0.2409	0.2632
13.8760 ± 0.5890	0.0117 ± 0.0041	0.0823	0.0560	0.0375	0.3374	0.3538
15.0160 ± 0.6600	0.0164 ± 0.0044	0.0823	0.0560	0.0375	0.2442	0.2663
16.2970 ± 0.7500	0.0126 ± 0.0041	0.0823	0.0560	0.0375	0.3060	0.3239
17.7590 ± 0.8570	0.0113 ± 0.0041	0.0823	0.0560	0.0374	0.3440	0.3601
19.4160 ± 0.9710	0.0048 ± 0.0038	0.0823	0.0560	0.0381	0.7975	0.8046

TABLE CXVIII: Partition of the relative uncertainties for the $E_\gamma = 786.3$ -keV transition from the level at $E_x = 786.3$ keV in the ^{234}U nucleus.

E_n (MeV)	σ_γ (b)	ρ_c	ρ_γ	ρ_n	$\rho_{\gamma n}$	ρ_{tot}
4.0900 ± 0.0930	0.0021 ± 0.0018	0.0824	0.0780	0.0385	0.8333	0.8419
4.2640 ± 0.0990	0.0070 ± 0.0020	0.0824	0.0780	0.0375	0.2556	0.2821
4.4530 ± 0.1050	0.0046 ± 0.0018	0.0824	0.0780	0.0359	0.3710	0.3896
4.6470 ± 0.1130	0.0043 ± 0.0018	0.0824	0.0780	0.0352	0.3950	0.4124
4.8610 ± 0.1220	0.0012 ± 0.0017	0.0824	0.0780	0.0354	1.3939	1.3990
5.0900 ± 0.1290	0.0043 ± 0.0018	0.0824	0.0780	0.0347	0.3934	0.4109
5.3330 ± 0.1400	0.0046 ± 0.0018	0.0824	0.0780	0.0342	0.3721	0.3905
5.5970 ± 0.1490	0.0056 ± 0.0018	0.0824	0.0780	0.0332	0.3004	0.3229
5.8750 ± 0.1600	0.0011 ± 0.0016	0.0824	0.0780	0.0326	1.4414	1.4462
6.1810 ± 0.1750	0.0035 ± 0.0017	0.0824	0.0780	0.0324	0.4673	0.4820
6.5170 ± 0.1870	0.0049 ± 0.0017	0.0824	0.0780	0.0302	0.3215	0.3423
6.8620 ± 0.2010	0.0058 ± 0.0017	0.0824	0.0780	0.0286	0.2678	0.2923
7.2370 ± 0.2180	0.0079 ± 0.0019	0.0824	0.0780	0.0295	0.2069	0.2379
7.6610 ± 0.2420	0.0061 ± 0.0018	0.0824	0.0780	0.0313	0.2753	0.2994
8.1260 ± 0.2630	0.0072 ± 0.0019	0.0824	0.0780	0.0312	0.2377	0.2652
8.6180 ± 0.2840	0.0093 ± 0.0021	0.0824	0.0780	0.0304	0.1860	0.2200
9.1600 ± 0.3130	0.0050 ± 0.0018	0.0824	0.0780	0.0310	0.3473	0.3667
9.7570 ± 0.3460	0.0100 ± 0.0022	0.0824	0.0780	0.0320	0.1841	0.2187
10.4140 ± 0.3770	0.0124 ± 0.0024	0.0824	0.0780	0.0331	0.1537	0.1939
11.1430 ± 0.4250	0.0149 ± 0.0027	0.0824	0.0780	0.0351	0.1366	0.1810
11.9600 ± 0.4670	0.0080 ± 0.0022	0.0824	0.0780	0.0361	0.2453	0.2727
12.8600 ± 0.5250	0.0098 ± 0.0024	0.0824	0.0780	0.0370	0.2112	0.2426
13.8760 ± 0.5890	0.0084 ± 0.0023	0.0824	0.0780	0.0375	0.2501	0.2772
15.0160 ± 0.6600	0.0071 ± 0.0023	0.0824	0.0780	0.0375	0.2932	0.3166
16.2970 ± 0.7500	0.0060 ± 0.0022	0.0824	0.0780	0.0375	0.3476	0.3675
17.7590 ± 0.8570	0.0049 ± 0.0022	0.0824	0.0780	0.0374	0.4201	0.4368
19.4160 ± 0.9710	0.0042 ± 0.0021	0.0824	0.0780	0.0381	0.4866	0.5011

TABLE CXIX: Partition of the relative uncertainties for the $E_\gamma = 805.8$ -keV transition from the level at $E_x = 849.3$ keV in the ^{234}U nucleus.

E_n (MeV)	σ_γ (b)	ρ_c	ρ_γ	ρ_n	$\rho_{\gamma n}$	ρ_{tot}
4.0900 ± 0.0930	0.0078 ± 0.0034	0.0823	0.0560	0.0385	0.4196	0.4329
4.2640 ± 0.0990	0.0070 ± 0.0034	0.0823	0.0560	0.0375	0.4746	0.4864
4.4530 ± 0.1050	0.0065 ± 0.0033	0.0823	0.0560	0.0359	0.5003	0.5114
4.6470 ± 0.1130	0.0096 ± 0.0035	0.0823	0.0560	0.0352	0.3437	0.3596
4.8610 ± 0.1220	0.0038 ± 0.0031	0.0823	0.0560	0.0354	0.8284	0.8351
5.0900 ± 0.1290	0.0073 ± 0.0032	0.0823	0.0560	0.0347	0.4269	0.4397
5.3330 ± 0.1400	0.0030 ± 0.0033	0.0823	0.0560	0.0342	1.0773	1.0824
5.5970 ± 0.1490	0.0045 ± 0.0031	0.0823	0.0560	0.0332	0.6790	0.6870
5.8750 ± 0.1600	0.0062 ± 0.0030	0.0823	0.0560	0.0326	0.4754	0.4868
6.1810 ± 0.1750	0.0104 ± 0.0032	0.0823	0.0560	0.0324	0.2942	0.3123
6.5170 ± 0.1870	0.0079 ± 0.0030	0.0823	0.0560	0.0302	0.3708	0.3851
6.8620 ± 0.2010	0.0085 ± 0.0031	0.0823	0.0560	0.0286	0.3434	0.3587
7.2370 ± 0.2180	0.0130 ± 0.0033	0.0823	0.0560	0.0295	0.2359	0.2578
7.6610 ± 0.2420	0.0141 ± 0.0036	0.0823	0.0560	0.0313	0.2328	0.2551
8.1260 ± 0.2630	0.0128 ± 0.0035	0.0823	0.0560	0.0312	0.2508	0.2716
8.6180 ± 0.2840	0.0180 ± 0.0038	0.0823	0.0560	0.0304	0.1843	0.2117
9.1600 ± 0.3130	0.0159 ± 0.0037	0.0823	0.0560	0.0310	0.2084	0.2331
9.7570 ± 0.3460	0.0229 ± 0.0042	0.0823	0.0560	0.0320	0.1512	0.1839
10.4140 ± 0.3770	0.0195 ± 0.0041	0.0823	0.0560	0.0331	0.1829	0.2108
11.1430 ± 0.4250	0.0225 ± 0.0045	0.0823	0.0560	0.0351	0.1691	0.1994
11.9600 ± 0.4670	0.0217 ± 0.0043	0.0823	0.0560	0.0361	0.1673	0.1980
12.8600 ± 0.5250	0.0126 ± 0.0038	0.0823	0.0560	0.0370	0.2814	0.3008
13.8760 ± 0.5890	0.0222 ± 0.0045	0.0823	0.0560	0.0375	0.1713	0.2017
15.0160 ± 0.6600	0.0151 ± 0.0042	0.0823	0.0560	0.0375	0.2597	0.2807
16.2970 ± 0.7500	0.0068 ± 0.0037	0.0823	0.0560	0.0375	0.5293	0.5399
17.7590 ± 0.8570	0.0146 ± 0.0042	0.0823	0.0560	0.0374	0.2665	0.2869
19.4160 ± 0.9710	0.0051 ± 0.0036	0.0823	0.0560	0.0381	0.6989	0.7070

TABLE CXX: Partition of the relative uncertainties for the $E_\gamma = 819.2$ -keV transition from the level at $E_x = 962.6$ keV in the ^{234}U nucleus.

E_n (MeV)	σ_γ (b)	ρ_c	ρ_γ	ρ_n	$\rho_{\gamma n}$	ρ_{tot}
4.0900 ± 0.0930	0.0024 ± 0.0018	0.0824	0.0770	0.0385	0.7167	0.7265
4.2640 ± 0.0990	0.0033 ± 0.0018	0.0824	0.0770	0.0375	0.5238	0.5371
4.4530 ± 0.1050	0.0077 ± 0.0020	0.0824	0.0770	0.0359	0.2255	0.2547
4.6470 ± 0.1130	0.0046 ± 0.0018	0.0824	0.0770	0.0352	0.3651	0.3837
4.8610 ± 0.1220	0.0027 ± 0.0017	0.0824	0.0770	0.0354	0.6216	0.6328
5.0900 ± 0.1290	0.0048 ± 0.0018	0.0824	0.0770	0.0347	0.3534	0.3726
5.3330 ± 0.1400	0.0045 ± 0.0017	0.0824	0.0770	0.0342	0.3624	0.3811
5.5970 ± 0.1490	0.0040 ± 0.0017	0.0824	0.0770	0.0332	0.3942	0.4114
5.8750 ± 0.1600	0.0049 ± 0.0017	0.0824	0.0770	0.0326	0.3298	0.3501
6.1810 ± 0.1750	0.0031 ± 0.0016	0.0824	0.0770	0.0324	0.5059	0.5193
6.5170 ± 0.1870	0.0037 ± 0.0016	0.0824	0.0770	0.0302	0.4125	0.4287
6.8620 ± 0.2010	0.0066 ± 0.0017	0.0824	0.0770	0.0286	0.2261	0.2542
7.2370 ± 0.2180	0.0087 ± 0.0019	0.0824	0.0770	0.0295	0.1835	0.2174
7.6610 ± 0.2420	0.0097 ± 0.0020	0.0824	0.0770	0.0313	0.1769	0.2121
8.1260 ± 0.2630	0.0127 ± 0.0023	0.0824	0.0770	0.0312	0.1378	0.1808
8.6180 ± 0.2840	0.0113 ± 0.0022	0.0824	0.0770	0.0304	0.1533	0.1928
9.1600 ± 0.3130	0.0106 ± 0.0021	0.0824	0.0770	0.0310	0.1625	0.2002
9.7570 ± 0.3460	0.0112 ± 0.0022	0.0824	0.0770	0.0320	0.1592	0.1978
10.4140 ± 0.3770	0.0155 ± 0.0026	0.0824	0.0770	0.0331	0.1228	0.1700
11.1430 ± 0.4250	0.0132 ± 0.0025	0.0824	0.0770	0.0351	0.1474	0.1889
11.9600 ± 0.4670	0.0119 ± 0.0024	0.0824	0.0770	0.0361	0.1670	0.2047
12.8600 ± 0.5250	0.0136 ± 0.0026	0.0824	0.0770	0.0370	0.1515	0.1925
13.8760 ± 0.5890	0.0095 ± 0.0023	0.0824	0.0770	0.0375	0.2166	0.2471
15.0160 ± 0.6600	0.0075 ± 0.0022	0.0824	0.0770	0.0375	0.2739	0.2986
16.2970 ± 0.7500	0.0032 ± 0.0020	0.0824	0.0770	0.0375	0.6178	0.6291
17.7590 ± 0.8570	0.0002 ± 0.0017	0.0824	0.0770	0.0374	11.0000	11.0007
19.4160 ± 0.9710	0.0000 ± 0.0017	0.0824	0.0770	0.0381	43.0000	43.0002

TABLE CXXI: Partition of the relative uncertainties for the $E_\gamma = 829.3$ -keV transition from the level at $E_x = 1125.3$ keV in the ^{234}U nucleus.

E_n (MeV)	σ_γ (b)	ρ_c	ρ_γ	ρ_n	$\rho_{\gamma n}$	ρ_{tot}
4.0900 \pm 0.0930	0.0018 \pm 0.0033	0.0823	0.0550	0.0385	1.7836	1.7868
4.2640 \pm 0.0990	0.0001 \pm 0.0006	0.0823	0.0550	0.0375	8.2733	8.2740
4.4530 \pm 0.1050	0.0018 \pm 0.0032	0.0823	0.0550	0.0359	1.7220	1.7252
4.6470 \pm 0.1130	0.0055 \pm 0.0033	0.0823	0.0550	0.0352	0.5916	0.6009
4.8610 \pm 0.1220	0.0001 \pm 0.0006	0.0823	0.0550	0.0354	8.2733	8.2739
5.0900 \pm 0.1290	0.0001 \pm 0.0006	0.0823	0.0550	0.0347	8.2733	8.2739
5.3330 \pm 0.1400	0.0017 \pm 0.0035	0.0823	0.0550	0.0342	2.0296	2.0323
5.5970 \pm 0.1490	0.0007 \pm 0.0033	0.0823	0.0550	0.0332	4.7723	4.7735
5.8750 \pm 0.1600	0.0003 \pm 0.0032	0.0823	0.0550	0.0326	11.6845	11.6850
6.1810 \pm 0.1750	0.0024 \pm 0.0032	0.0823	0.0550	0.0324	1.3356	1.3397
6.5170 \pm 0.1870	0.0042 \pm 0.0031	0.0823	0.0550	0.0302	0.7235	0.7309
6.8620 \pm 0.2010	0.0072 \pm 0.0032	0.0823	0.0550	0.0286	0.4266	0.4389
7.2370 \pm 0.2180	0.0128 \pm 0.0035	0.0823	0.0550	0.0295	0.2557	0.2758
7.6610 \pm 0.2420	0.0107 \pm 0.0037	0.0823	0.0550	0.0313	0.3259	0.3421
8.1260 \pm 0.2630	0.0118 \pm 0.0037	0.0823	0.0550	0.0312	0.2930	0.3108
8.6180 \pm 0.2840	0.0116 \pm 0.0036	0.0823	0.0550	0.0304	0.2952	0.3129
9.1600 \pm 0.3130	0.0075 \pm 0.0035	0.0823	0.0550	0.0310	0.4539	0.4656
9.7570 \pm 0.3460	0.0094 \pm 0.0037	0.0823	0.0550	0.0320	0.3780	0.3920
10.4140 \pm 0.3770	0.0225 \pm 0.0045	0.0823	0.0550	0.0331	0.1711	0.2004
11.1430 \pm 0.4250	0.0175 \pm 0.0044	0.0823	0.0550	0.0351	0.2283	0.2513
11.9600 \pm 0.4670	0.0156 \pm 0.0042	0.0823	0.0550	0.0361	0.2473	0.2688
12.8600 \pm 0.5250	0.0147 \pm 0.0043	0.0823	0.0550	0.0370	0.2698	0.2897
13.8760 \pm 0.5890	0.0198 \pm 0.0046	0.0823	0.0550	0.0375	0.2092	0.2345
15.0160 \pm 0.6600	0.0183 \pm 0.0046	0.0823	0.0550	0.0375	0.2300	0.2532
16.2970 \pm 0.7500	0.0114 \pm 0.0041	0.0823	0.0550	0.0375	0.3439	0.3599
17.7590 \pm 0.8570	0.0093 \pm 0.0041	0.0823	0.0550	0.0374	0.4291	0.4420
19.4160 \pm 0.9710	0.0173 \pm 0.0043	0.0823	0.0550	0.0381	0.2252	0.2490

TABLE CXXII: Partition of the relative uncertainties for the $E_\gamma = 831.5$ -keV transition from the level at $E_x = 1127.6$ keV in the ^{234}U nucleus.

E_n (MeV)	σ_γ (b)	ρ_c	ρ_γ	ρ_n	$\rho_{\gamma n}$	ρ_{tot}
4.0900 \pm 0.0930	0.0109 \pm 0.0038	0.0823	0.0550	0.0385	0.3336	0.3501
4.2640 \pm 0.0990	0.0069 \pm 0.0036	0.0823	0.0550	0.0375	0.5130	0.5238
4.4530 \pm 0.1050	0.0096 \pm 0.0036	0.0823	0.0550	0.0359	0.3581	0.3732
4.6470 \pm 0.1130	0.0087 \pm 0.0035	0.0823	0.0550	0.0352	0.3865	0.4005
4.8610 \pm 0.1220	0.0096 \pm 0.0036	0.0823	0.0550	0.0354	0.3600	0.3751
5.0900 \pm 0.1290	0.0056 \pm 0.0033	0.0823	0.0550	0.0347	0.5748	0.5843
5.3330 \pm 0.1400	0.0062 \pm 0.0035	0.0823	0.0550	0.0342	0.5635	0.5732
5.5970 \pm 0.1490	0.0096 \pm 0.0035	0.0823	0.0550	0.0332	0.3528	0.3679
5.8750 \pm 0.1600	0.0053 \pm 0.0032	0.0823	0.0550	0.0326	0.5944	0.6035
6.1810 \pm 0.1750	0.0071 \pm 0.0033	0.0823	0.0550	0.0324	0.4607	0.4723
6.5170 \pm 0.1870	0.0072 \pm 0.0032	0.0823	0.0550	0.0302	0.4301	0.4424
6.8620 \pm 0.2010	0.0087 \pm 0.0032	0.0823	0.0550	0.0286	0.3542	0.3689
7.2370 \pm 0.2180	0.0175 \pm 0.0038	0.0823	0.0550	0.0295	0.1906	0.2168
7.6610 \pm 0.2420	0.0174 \pm 0.0039	0.0823	0.0550	0.0313	0.2017	0.2268
8.1260 \pm 0.2630	0.0211 \pm 0.0042	0.0823	0.0550	0.0312	0.1689	0.1982
8.6180 \pm 0.2840	0.0271 \pm 0.0046	0.0823	0.0550	0.0304	0.1334	0.1689
9.1600 \pm 0.3130	0.0268 \pm 0.0046	0.0823	0.0550	0.0310	0.1371	0.1719
9.7570 \pm 0.3460	0.0329 \pm 0.0051	0.0823	0.0550	0.0320	0.1168	0.1564
10.4140 \pm 0.3770	0.0259 \pm 0.0047	0.0823	0.0550	0.0331	0.1492	0.1821
11.1430 \pm 0.4250	0.0343 \pm 0.0055	0.0823	0.0550	0.0351	0.1209	0.1602
11.9600 \pm 0.4670	0.0274 \pm 0.0049	0.0823	0.0550	0.0361	0.1464	0.1804
12.8600 \pm 0.5250	0.0353 \pm 0.0057	0.0823	0.0550	0.0370	0.1221	0.1615
13.8760 \pm 0.5890	0.0325 \pm 0.0055	0.0823	0.0550	0.0375	0.1322	0.1694
15.0160 \pm 0.6600	0.0170 \pm 0.0045	0.0823	0.0550	0.0375	0.2450	0.2669
16.2970 \pm 0.7500	0.0176 \pm 0.0045	0.0823	0.0550	0.0375	0.2309	0.2541
17.7590 \pm 0.8570	0.0237 \pm 0.0049	0.0823	0.0550	0.0374	0.1782	0.2072
19.4160 \pm 0.9710	0.0164 \pm 0.0043	0.0823	0.0550	0.0381	0.2416	0.2638

TABLE CXXIII: Partition of the relative uncertainties for the $E_\gamma = 876.0$ -keV transition from the level at $E_x = 1172.1$ keV in the ^{234}U nucleus.

E_n (MeV)	σ_γ (b)	ρ_c	ρ_γ	ρ_n	$\rho_{\gamma n}$	ρ_{tot}
4.0900 ± 0.0930	0.0178 ± 0.0042	0.0823	0.0540	0.0385	0.2109	0.2359
4.2640 ± 0.0990	0.0124 ± 0.0039	0.0823	0.0540	0.0375	0.2949	0.3132
4.4530 ± 0.1050	0.0092 ± 0.0036	0.0823	0.0540	0.0359	0.3792	0.3934
4.6470 ± 0.1130	0.0124 ± 0.0036	0.0823	0.0540	0.0352	0.2735	0.2928
4.8610 ± 0.1220	0.0082 ± 0.0035	0.0823	0.0540	0.0354	0.4178	0.4307
5.0900 ± 0.1290	0.0072 ± 0.0034	0.0823	0.0540	0.0347	0.4652	0.4768
5.3330 ± 0.1400	0.0127 ± 0.0038	0.0823	0.0540	0.0342	0.2823	0.3010
5.5970 ± 0.1490	0.0157 ± 0.0039	0.0823	0.0540	0.0332	0.2268	0.2495
5.8750 ± 0.1600	0.0155 ± 0.0038	0.0823	0.0540	0.0326	0.2247	0.2475
6.1810 ± 0.1750	0.0126 ± 0.0037	0.0823	0.0540	0.0324	0.2709	0.2900
6.5170 ± 0.1870	0.0108 ± 0.0035	0.0823	0.0540	0.0302	0.3050	0.3219
6.8620 ± 0.2010	0.0129 ± 0.0034	0.0823	0.0540	0.0286	0.2429	0.2637
7.2370 ± 0.2180	0.0099 ± 0.0033	0.0823	0.0540	0.0295	0.3191	0.3352
7.6610 ± 0.2420	0.0236 ± 0.0043	0.0823	0.0540	0.0313	0.1506	0.1826
8.1260 ± 0.2630	0.0254 ± 0.0044	0.0823	0.0540	0.0312	0.1390	0.1731
8.6180 ± 0.2840	0.0314 ± 0.0048	0.0823	0.0540	0.0304	0.1151	0.1545
9.1600 ± 0.3130	0.0227 ± 0.0042	0.0823	0.0540	0.0310	0.1538	0.1852
9.7570 ± 0.3460	0.0253 ± 0.0045	0.0823	0.0540	0.0320	0.1433	0.1768
10.4140 ± 0.3770	0.0326 ± 0.0051	0.0823	0.0540	0.0331	0.1185	0.1576
11.1430 ± 0.4250	0.0253 ± 0.0047	0.0823	0.0540	0.0351	0.1540	0.1862
11.9600 ± 0.4670	0.0262 ± 0.0049	0.0823	0.0540	0.0361	0.1531	0.1855
12.8600 ± 0.5250	0.0290 ± 0.0052	0.0823	0.0540	0.0370	0.1450	0.1791
13.8760 ± 0.5890	0.0239 ± 0.0048	0.0823	0.0540	0.0375	0.1714	0.2012
15.0160 ± 0.6600	0.0240 ± 0.0048	0.0823	0.0540	0.0375	0.1702	0.2001
16.2970 ± 0.7500	0.0177 ± 0.0043	0.0823	0.0540	0.0375	0.2188	0.2429
17.7590 ± 0.8570	0.0236 ± 0.0047	0.0823	0.0540	0.0374	0.1708	0.2007
19.4160 ± 0.9710	0.0126 ± 0.0040	0.0823	0.0540	0.0381	0.3039	0.3217

TABLE CXXIV: Partition of the relative uncertainties for the $E_\gamma = 880.5$ -keV transition from the level at $E_x = 1023.7$ keV in the ^{234}U nucleus.

E_n (MeV)	σ_γ (b)	ρ_c	ρ_γ	ρ_n	$\rho_{\gamma n}$	ρ_{tot}
4.0900 ± 0.0930	0.0092 ± 0.0037	0.0599	0.0382	0.0255	0.3949	0.4021
4.2640 ± 0.0990	0.0097 ± 0.0036	0.0599	0.0382	0.0250	0.3703	0.3779
4.4530 ± 0.1050	0.0138 ± 0.0037	0.0599	0.0382	0.0240	0.2536	0.2644
4.6470 ± 0.1130	0.0105 ± 0.0035	0.0599	0.0382	0.0234	0.3209	0.3295
4.8610 ± 0.1220	0.0116 ± 0.0036	0.0599	0.0382	0.0233	0.2987	0.3079
5.0900 ± 0.1290	0.0110 ± 0.0035	0.0599	0.0382	0.0228	0.3116	0.3204
5.3330 ± 0.1400	0.0165 ± 0.0038	0.0599	0.0382	0.0227	0.2147	0.2273
5.5970 ± 0.1490	0.0128 ± 0.0036	0.0599	0.0382	0.0223	0.2730	0.2830
5.8750 ± 0.1600	0.0138 ± 0.0035	0.0599	0.0382	0.0218	0.2458	0.2568
6.1810 ± 0.1750	0.0116 ± 0.0034	0.0599	0.0382	0.0215	0.2827	0.2923
6.5170 ± 0.1870	0.0117 ± 0.0033	0.0599	0.0382	0.0202	0.2722	0.2820
6.8620 ± 0.2010	0.0228 ± 0.0039	0.0599	0.0382	0.0194	0.1523	0.1692
7.2370 ± 0.2180	0.0234 ± 0.0040	0.0599	0.0382	0.0202	0.1537	0.1705
7.6610 ± 0.2420	0.0424 ± 0.0054	0.0599	0.0382	0.0215	0.1026	0.1266
8.1260 ± 0.2630	0.0447 ± 0.0055	0.0599	0.0382	0.0213	0.0967	0.1218
8.6180 ± 0.2840	0.0502 ± 0.0059	0.0599	0.0382	0.0208	0.0905	0.1169
9.1600 ± 0.3130	0.0507 ± 0.0059	0.0599	0.0382	0.0212	0.0894	0.1161
9.7570 ± 0.3460	0.0516 ± 0.0060	0.0599	0.0382	0.0220	0.0886	0.1156
10.4140 ± 0.3770	0.0437 ± 0.0056	0.0599	0.0382	0.0228	0.1029	0.1271
11.1430 ± 0.4250	0.0502 ± 0.0061	0.0599	0.0382	0.0241	0.0954	0.1213
11.9600 ± 0.4670	0.0475 ± 0.0060	0.0599	0.0382	0.0248	0.1010	0.1259
12.8600 ± 0.5250	0.0464 ± 0.0059	0.0599	0.0382	0.0253	0.1028	0.1275
13.8760 ± 0.5890	0.0346 ± 0.0053	0.0599	0.0382	0.0258	0.1324	0.1524
15.0160 ± 0.6600	0.0374 ± 0.0053	0.0599	0.0382	0.0258	0.1206	0.1423
16.2970 ± 0.7500	0.0253 ± 0.0045	0.0599	0.0382	0.0257	0.1617	0.1784
17.7590 ± 0.8570	0.0206 ± 0.0043	0.0599	0.0382	0.0256	0.1932	0.2074
19.4160 ± 0.9710	0.0211 ± 0.0042	0.0599	0.0382	0.0261	0.1865	0.2013

TABLE CXXV: Partition of the relative uncertainties for the $E_\gamma = 883.2$ -keV transition from the level at $E_x = 926.7$ keV in the ^{234}U nucleus.

E_n (MeV)	σ_γ (b)	ρ_c	ρ_γ	ρ_n	$\rho_{\gamma n}$	ρ_{tot}
4.0900 ± 0.0930	0.0064 ± 0.0036	0.0599	0.0382	0.0255	0.5514	0.5565
4.2640 ± 0.0990	-0.0001 ± 0.0015	0.0599	0.0382	0.0250	12.5019	12.5022
4.4530 ± 0.1050	0.0003 ± 0.0015	0.0599	0.0382	0.0240	4.9813	4.9818
4.6470 ± 0.1130	-0.0011 ± 0.0011	0.0599	0.0382	0.0234	0.9758	0.9787
4.8610 ± 0.1220	0.0032 ± 0.0033	0.0599	0.0382	0.0233	1.0219	1.0246
5.0900 ± 0.1290	0.0104 ± 0.0035	0.0599	0.0382	0.0228	0.3227	0.3312
5.3330 ± 0.1400	0.0063 ± 0.0033	0.0599	0.0382	0.0227	0.5182	0.5235
5.5970 ± 0.1490	0.0054 ± 0.0032	0.0599	0.0382	0.0223	0.5891	0.5937
5.8750 ± 0.1600	0.0026 ± 0.0031	0.0599	0.0382	0.0218	1.1686	1.1710
6.1810 ± 0.1750	0.0069 ± 0.0033	0.0599	0.0382	0.0215	0.4651	0.4710
6.5170 ± 0.1870	0.0081 ± 0.0031	0.0599	0.0382	0.0202	0.3757	0.3829
6.8620 ± 0.2010	0.0152 ± 0.0032	0.0599	0.0382	0.0194	0.2000	0.2131
7.2370 ± 0.2180	0.0135 ± 0.0033	0.0599	0.0382	0.0202	0.2358	0.2471
7.6610 ± 0.2420	0.0154 ± 0.0035	0.0599	0.0382	0.0215	0.2158	0.2282
8.1260 ± 0.2630	0.0178 ± 0.0036	0.0599	0.0382	0.0213	0.1905	0.2045
8.6180 ± 0.2840	0.0192 ± 0.0037	0.0599	0.0382	0.0208	0.1780	0.1928
9.1600 ± 0.3130	0.0196 ± 0.0038	0.0599	0.0382	0.0212	0.1771	0.1920
9.7570 ± 0.3460	0.0121 ± 0.0034	0.0599	0.0382	0.0220	0.2715	0.2815
10.4140 ± 0.3770	0.0171 ± 0.0037	0.0599	0.0382	0.0228	0.2058	0.2189
11.1430 ± 0.4250	0.0212 ± 0.0041	0.0599	0.0382	0.0241	0.1798	0.1948
11.9600 ± 0.4670	0.0211 ± 0.0041	0.0599	0.0382	0.0248	0.1798	0.1949
12.8600 ± 0.5250	0.0214 ± 0.0043	0.0599	0.0382	0.0253	0.1848	0.1996
13.8760 ± 0.5890	0.0213 ± 0.0043	0.0599	0.0382	0.0258	0.1848	0.1997
15.0160 ± 0.6600	0.0149 ± 0.0039	0.0599	0.0382	0.0258	0.2493	0.2605
16.2970 ± 0.7500	0.0208 ± 0.0041	0.0599	0.0382	0.0257	0.1818	0.1969
17.7590 ± 0.8570	0.0154 ± 0.0039	0.0599	0.0382	0.0256	0.2432	0.2547
19.4160 ± 0.9710	0.0127 ± 0.0037	0.0599	0.0382	0.0261	0.2829	0.2928

TABLE CXXVI: Partition of the relative uncertainties for the $E_\gamma = 898.7$ -keV transition from the level at $E_x = 1194.7$ keV in the ^{234}U nucleus.

E_n (MeV)	σ_γ (b)	ρ_c	ρ_γ	ρ_n	$\rho_{\gamma n}$	ρ_{tot}
4.0900 \pm 0.0930	0.0222 \pm 0.0047	0.0823	0.0500	0.0385	0.1860	0.2130
4.2640 \pm 0.0990	0.0180 \pm 0.0044	0.0823	0.0500	0.0375	0.2233	0.2460
4.4530 \pm 0.1050	0.0111 \pm 0.0039	0.0823	0.0500	0.0359	0.3381	0.3534
4.6470 \pm 0.1130	0.0090 \pm 0.0037	0.0823	0.0500	0.0352	0.4000	0.4129
4.8610 \pm 0.1220	0.0032 \pm 0.0036	0.0823	0.0500	0.0354	1.0976	1.1023
5.0900 \pm 0.1290	0.0145 \pm 0.0040	0.0823	0.0500	0.0347	0.2593	0.2787
5.3330 \pm 0.1400	0.0054 \pm 0.0033	0.0823	0.0500	0.0342	0.5955	0.6042
5.5970 \pm 0.1490	0.0117 \pm 0.0035	0.0823	0.0500	0.0332	0.2795	0.2975
5.8750 \pm 0.1600	0.0075 \pm 0.0032	0.0823	0.0500	0.0326	0.4130	0.4254
6.1810 \pm 0.1750	0.0071 \pm 0.0032	0.0823	0.0500	0.0324	0.4359	0.4476
6.5170 \pm 0.1870	0.0076 \pm 0.0031	0.0823	0.0500	0.0302	0.3879	0.4008
6.8620 \pm 0.2010	0.0059 \pm 0.0029	0.0823	0.0500	0.0286	0.4807	0.4910
7.2370 \pm 0.2180	0.0111 \pm 0.0031	0.0823	0.0500	0.0295	0.2649	0.2834
7.6610 \pm 0.2420	0.0091 \pm 0.0032	0.0823	0.0500	0.0313	0.3415	0.3562
8.1260 \pm 0.2630	0.0158 \pm 0.0036	0.0823	0.0500	0.0312	0.2057	0.2293
8.6180 \pm 0.2840	0.0144 \pm 0.0034	0.0823	0.0500	0.0304	0.2167	0.2391
9.1600 \pm 0.3130	0.0200 \pm 0.0038	0.0823	0.0500	0.0310	0.1621	0.1911
9.7570 \pm 0.3460	0.0219 \pm 0.0040	0.0823	0.0500	0.0320	0.1537	0.1842
10.4140 \pm 0.3770	0.0242 \pm 0.0043	0.0823	0.0500	0.0331	0.1471	0.1789
11.1430 \pm 0.4250	0.0183 \pm 0.0041	0.0823	0.0500	0.0351	0.1975	0.2225
11.9600 \pm 0.4670	0.0186 \pm 0.0041	0.0823	0.0500	0.0361	0.1974	0.2226
12.8600 \pm 0.5250	0.0197 \pm 0.0043	0.0823	0.0500	0.0370	0.1927	0.2186
13.8760 \pm 0.5890	0.0251 \pm 0.0047	0.0823	0.0500	0.0375	0.1546	0.1860
15.0160 \pm 0.6600	0.0202 \pm 0.0043	0.0823	0.0500	0.0375	0.1879	0.2145
16.2970 \pm 0.7500	0.0162 \pm 0.0042	0.0823	0.0500	0.0375	0.2387	0.2601
17.7590 \pm 0.8570	0.0167 \pm 0.0042	0.0823	0.0500	0.0374	0.2306	0.2527
19.4160 \pm 0.9710	0.0178 \pm 0.0042	0.0823	0.0500	0.0381	0.2141	0.2379

TABLE CXXVII: Partition of the relative uncertainties for the $E_\gamma = 925.0$ -keV transition from the level at $E_x = 968.6$ keV in the ^{234}U nucleus.

E_n (MeV)	σ_γ (b)	ρ_c	ρ_γ	ρ_n	$\rho_{\gamma n}$	ρ_{tot}
4.0900 \pm 0.0930	0.0013 \pm 0.0023	0.0599	0.0354	0.0255	1.8492	1.8507
4.2640 \pm 0.0990	0.0095 \pm 0.0026	0.0599	0.0354	0.0250	0.2697	0.2796
4.4530 \pm 0.1050	0.0013 \pm 0.0017	0.0599	0.0354	0.0240	1.3394	1.3414
4.6470 \pm 0.1130	0.0056 \pm 0.0024	0.0599	0.0354	0.0234	0.4217	0.4281
4.8610 \pm 0.1220	0.0048 \pm 0.0025	0.0599	0.0354	0.0233	0.5097	0.5149
5.0900 \pm 0.1290	0.0049 \pm 0.0024	0.0599	0.0354	0.0228	0.4774	0.4829
5.3330 \pm 0.1400	0.0027 \pm 0.0022	0.0599	0.0354	0.0227	0.7986	0.8019
5.5970 \pm 0.1490	0.0033 \pm 0.0022	0.0599	0.0354	0.0223	0.6666	0.6706
5.8750 \pm 0.1600	0.0019 \pm 0.0021	0.0599	0.0354	0.0218	1.1069	1.1093
6.1810 \pm 0.1750	0.0033 \pm 0.0021	0.0599	0.0354	0.0215	0.6469	0.6510
6.5170 \pm 0.1870	0.0031 \pm 0.0021	0.0599	0.0354	0.0202	0.6591	0.6631
6.8620 \pm 0.2010	0.0054 \pm 0.0021	0.0599	0.0354	0.0194	0.3783	0.3851
7.2370 \pm 0.2180	0.0098 \pm 0.0023	0.0599	0.0354	0.0202	0.2274	0.2386
7.6610 \pm 0.2420	0.0209 \pm 0.0032	0.0599	0.0354	0.0215	0.1356	0.1539
8.1260 \pm 0.2630	0.0223 \pm 0.0033	0.0599	0.0354	0.0213	0.1312	0.1500
8.6180 \pm 0.2840	0.0238 \pm 0.0033	0.0599	0.0354	0.0208	0.1197	0.1400
9.1600 \pm 0.3130	0.0236 \pm 0.0034	0.0599	0.0354	0.0212	0.1260	0.1455
9.7570 \pm 0.3460	0.0244 \pm 0.0035	0.0599	0.0354	0.0220	0.1247	0.1445
10.4140 \pm 0.3770	0.0329 \pm 0.0041	0.0599	0.0354	0.0228	0.1000	0.1239
11.1430 \pm 0.4250	0.0312 \pm 0.0040	0.0599	0.0354	0.0241	0.1051	0.1283
11.9600 \pm 0.4670	0.0252 \pm 0.0039	0.0599	0.0354	0.0248	0.1373	0.1559
12.8600 \pm 0.5250	0.0195 \pm 0.0033	0.0599	0.0354	0.0253	0.1503	0.1676
13.8760 \pm 0.5890	0.0210 \pm 0.0034	0.0599	0.0354	0.0258	0.1441	0.1621
15.0160 \pm 0.6600	0.0133 \pm 0.0029	0.0599	0.0354	0.0258	0.2070	0.2199
16.2970 \pm 0.7500	0.0089 \pm 0.0027	0.0599	0.0354	0.0257	0.2938	0.3030
17.7590 \pm 0.8570	0.0078 \pm 0.0028	0.0599	0.0354	0.0256	0.3484	0.3562
19.4160 \pm 0.9710	0.0062 \pm 0.0026	0.0599	0.0354	0.0261	0.4165	0.4231

TABLE CXXVIII: Partition of the relative uncertainties for the $E_\gamma = 946.0$ -keV transition from the level at $E_x = 989.4$ keV in the ^{234}U nucleus.

E_n (MeV)	σ_γ (b)	ρ_c	ρ_γ	ρ_n	$\rho_{\gamma n}$	ρ_{tot}
4.0900 ± 0.0930	-0.0026 ± 0.0005	0.0599	0.0354	0.0255	0.1658	0.1815
4.2640 ± 0.0990	0.0001 ± 0.0006	0.0599	0.0354	0.0250	7.3587	7.3591
4.4530 ± 0.1050	0.0001 ± 0.0006	0.0599	0.0354	0.0240	8.1522	8.1525
4.6470 ± 0.1130	0.0001 ± 0.0006	0.0599	0.0354	0.0234	11.2344	11.2346
4.8610 ± 0.1220	0.0014 ± 0.0023	0.0599	0.0354	0.0233	1.6314	1.6330
5.0900 ± 0.1290	0.0001 ± 0.0006	0.0599	0.0354	0.0228	7.7387	7.7390
5.3330 ± 0.1400	0.0001 ± 0.0005	0.0599	0.0354	0.0227	6.4739	6.4743
5.5970 ± 0.1490	0.0001 ± 0.0005	0.0599	0.0354	0.0223	5.1378	5.1384
5.8750 ± 0.1600	0.0000 ± 0.0005	0.0599	0.0354	0.0218	12.8728	12.8730
6.1810 ± 0.1750	0.0000 ± 0.0005	0.0599	0.0354	0.0215	13.7258	13.7260
6.5170 ± 0.1870	0.0000 ± 0.0005	0.0599	0.0354	0.0202	18.1430	18.1432
6.8620 ± 0.2010	0.0040 ± 0.0021	0.0599	0.0354	0.0194	0.5312	0.5361
7.2370 ± 0.2180	0.0067 ± 0.0023	0.0599	0.0354	0.0202	0.3430	0.3505
7.6610 ± 0.2420	0.0107 ± 0.0025	0.0599	0.0354	0.0215	0.2257	0.2372
8.1260 ± 0.2630	0.0194 ± 0.0031	0.0599	0.0354	0.0213	0.1408	0.1585
8.6180 ± 0.2840	0.0187 ± 0.0030	0.0599	0.0354	0.0208	0.1452	0.1623
9.1600 ± 0.3130	0.0273 ± 0.0035	0.0599	0.0354	0.0212	0.1073	0.1296
9.7570 ± 0.3460	0.0324 ± 0.0040	0.0599	0.0354	0.0220	0.0993	0.1232
10.4140 ± 0.3770	0.0305 ± 0.0039	0.0599	0.0354	0.0228	0.1060	0.1288
11.1430 ± 0.4250	0.0238 ± 0.0035	0.0599	0.0354	0.0241	0.1289	0.1484
11.9600 ± 0.4670	0.0286 ± 0.0040	0.0599	0.0354	0.0248	0.1173	0.1386
12.8600 ± 0.5250	0.0214 ± 0.0034	0.0599	0.0354	0.0253	0.1427	0.1607
13.8760 ± 0.5890	0.0163 ± 0.0031	0.0599	0.0354	0.0258	0.1770	0.1919
15.0160 ± 0.6600	0.0072 ± 0.0028	0.0599	0.0354	0.0258	0.3818	0.3889
16.2970 ± 0.7500	0.0012 ± 0.0025	0.0599	0.0354	0.0257	2.0825	2.0838
17.7590 ± 0.8570	-0.0053 ± 0.0009	0.0599	0.0354	0.0256	0.1502	0.1674
19.4160 ± 0.9710	0.0001 ± 0.0006	0.0599	0.0354	0.0261	4.3895	4.3902

TABLE CXXIX: Partition of the relative uncertainties for the $E_\gamma = 965.8$ -keV transition from the level at $E_x = 1261.8$ keV in the ^{234}U nucleus.

E_n (MeV)	σ_γ (b)	ρ_c	ρ_γ	ρ_n	$\rho_{\gamma n}$	ρ_{tot}
4.0900 ± 0.0930	0.0003 ± 0.0019	0.0824	0.0720	0.0385	6.6667	6.6677
4.2640 ± 0.0990	0.0055 ± 0.0020	0.0824	0.0720	0.0375	0.3471	0.3659
4.4530 ± 0.1050	0.0018 ± 0.0018	0.0824	0.0720	0.0359	0.9762	0.9830
4.6470 ± 0.1130	0.0029 ± 0.0018	0.0824	0.0720	0.0352	0.6232	0.6337
4.8610 ± 0.1220	0.0021 ± 0.0018	0.0824	0.0720	0.0354	0.8600	0.8677
5.0900 ± 0.1290	0.0000 ± 0.0000	0.0824	0.0720	0.0347	0.0000	0.1148
5.3330 ± 0.1400	0.0047 ± 0.0019	0.0824	0.0720	0.0342	0.3822	0.3990
5.5970 ± 0.1490	0.0009 ± 0.0017	0.0824	0.0720	0.0332	1.8335	1.8371
5.8750 ± 0.1600	0.0021 ± 0.0017	0.0824	0.0720	0.0326	0.8186	0.8265
6.1810 ± 0.1750	0.0042 ± 0.0018	0.0824	0.0720	0.0324	0.4099	0.4254
6.5170 ± 0.1870	0.0029 ± 0.0017	0.0824	0.0720	0.0302	0.5615	0.5729
6.8620 ± 0.2010	0.0051 ± 0.0017	0.0824	0.0720	0.0286	0.3210	0.3403
7.2370 ± 0.2180	0.0069 ± 0.0019	0.0824	0.0720	0.0295	0.2500	0.2745
7.6610 ± 0.2420	0.0108 ± 0.0022	0.0824	0.0720	0.0313	0.1703	0.2048
8.1260 ± 0.2630	0.0106 ± 0.0022	0.0824	0.0720	0.0312	0.1732	0.2073
8.6180 ± 0.2840	0.0099 ± 0.0021	0.0824	0.0720	0.0304	0.1839	0.2161
9.1600 ± 0.3130	0.0120 ± 0.0023	0.0824	0.0720	0.0310	0.1556	0.1928
9.7570 ± 0.3460	0.0142 ± 0.0026	0.0824	0.0720	0.0320	0.1396	0.1803
10.4140 ± 0.3770	0.0129 ± 0.0025	0.0824	0.0720	0.0331	0.1525	0.1906
11.1430 ± 0.4250	0.0183 ± 0.0030	0.0824	0.0720	0.0351	0.1197	0.1660
11.9600 ± 0.4670	0.0148 ± 0.0028	0.0824	0.0720	0.0361	0.1450	0.1852
12.8600 ± 0.5250	0.0108 ± 0.0025	0.0824	0.0720	0.0370	0.1999	0.2309
13.8760 ± 0.5890	0.0084 ± 0.0024	0.0824	0.0720	0.0375	0.2594	0.2841
15.0160 ± 0.6600	0.0084 ± 0.0024	0.0824	0.0720	0.0375	0.2594	0.2841
16.2970 ± 0.7500	0.0070 ± 0.0023	0.0824	0.0720	0.0375	0.3057	0.3268
17.7590 ± 0.8570	0.0037 ± 0.0022	0.0824	0.0720	0.0374	0.5685	0.5801
19.4160 ± 0.9710	0.0030 ± 0.0021	0.0824	0.0720	0.0381	0.6974	0.7070

TABLE CXXX: Partition of the relative uncertainties for the $E_\gamma = 981.6$ -keV transition from the level at $E_x = 1277.5$ keV in the ^{234}U nucleus.

E_n (MeV)	σ_γ (b)	ρ_c	ρ_γ	ρ_n	$\rho_{\gamma n}$	ρ_{tot}
4.0900 ± 0.0930	0.0004 ± 0.0018	0.0824	0.0710	0.0385	4.8750	4.8764
4.2640 ± 0.0990	0.0000 ± 0.0000	0.0824	0.0710	0.0375	0.0000	0.1151
4.4530 ± 0.1050	0.0046 ± 0.0019	0.0824	0.0710	0.0359	0.3925	0.4089
4.6470 ± 0.1130	0.0026 ± 0.0018	0.0824	0.0710	0.0352	0.6774	0.6870
4.8610 ± 0.1220	0.0077 ± 0.0021	0.0824	0.0710	0.0354	0.2431	0.2687
5.0900 ± 0.1290	0.0033 ± 0.0019	0.0824	0.0710	0.0347	0.5570	0.5685
5.3330 ± 0.1400	0.0040 ± 0.0018	0.0824	0.0710	0.0342	0.4334	0.4482
5.5970 ± 0.1490	0.0019 ± 0.0017	0.0824	0.0710	0.0332	0.8827	0.8900
5.8750 ± 0.1600	0.0037 ± 0.0018	0.0824	0.0710	0.0326	0.4561	0.4701
6.1810 ± 0.1750	0.0021 ± 0.0017	0.0824	0.0710	0.0324	0.7899	0.7980
6.5170 ± 0.1870	0.0030 ± 0.0016	0.0824	0.0710	0.0302	0.5355	0.5472
6.8620 ± 0.2010	0.0045 ± 0.0017	0.0824	0.0710	0.0286	0.3564	0.3738
7.2370 ± 0.2180	0.0054 ± 0.0018	0.0824	0.0710	0.0295	0.3048	0.3250
7.6610 ± 0.2420	0.0079 ± 0.0020	0.0824	0.0710	0.0313	0.2247	0.2516
8.1260 ± 0.2630	0.0080 ± 0.0020	0.0824	0.0710	0.0312	0.2180	0.2456
8.6180 ± 0.2840	0.0101 ± 0.0021	0.0824	0.0710	0.0304	0.1768	0.2098
9.1600 ± 0.3130	0.0077 ± 0.0020	0.0824	0.0710	0.0310	0.2336	0.2595
9.7570 ± 0.3460	0.0121 ± 0.0024	0.0824	0.0710	0.0320	0.1597	0.1959
10.4140 ± 0.3770	0.0110 ± 0.0023	0.0824	0.0710	0.0331	0.1745	0.2082
11.1430 ± 0.4250	0.0108 ± 0.0024	0.0824	0.0710	0.0351	0.1884	0.2204
11.9600 ± 0.4670	0.0102 ± 0.0024	0.0824	0.0710	0.0361	0.2007	0.2311
12.8600 ± 0.5250	0.0118 ± 0.0026	0.0824	0.0710	0.0370	0.1828	0.2159
13.8760 ± 0.5890	0.0062 ± 0.0022	0.0824	0.0710	0.0375	0.3367	0.3558
15.0160 ± 0.6600	0.0041 ± 0.0021	0.0824	0.0710	0.0375	0.5062	0.5191
16.2970 ± 0.7500	0.0007 ± 0.0020	0.0824	0.0710	0.0375	2.9334	2.9357
17.7590 ± 0.8570	0.0027 ± 0.0021	0.0824	0.0710	0.0374	0.7631	0.7717
19.4160 ± 0.9710	0.0011 ± 0.0020	0.0824	0.0710	0.0381	1.8002	1.8039

TABLE CXXXI: Partition of the relative uncertainties for the $E_\gamma = 984.2$ -keV transition from the level at $E_x = 1127.6$ keV in the ^{234}U nucleus.

E_n (MeV)	σ_γ (b)	ρ_c	ρ_γ	ρ_n	$\rho_{\gamma n}$	ρ_{tot}
4.0900 ± 0.0930	0.0000 ± 0.0000	0.0824	0.0710	0.0385	0.0000	0.1154
4.2640 ± 0.0990	0.0000 ± 0.0000	0.0824	0.0710	0.0375	0.0000	0.1151
4.4530 ± 0.1050	0.0000 ± 0.0000	0.0824	0.0710	0.0359	0.0000	0.1146
4.6470 ± 0.1130	0.0000 ± 0.0000	0.0824	0.0710	0.0352	0.0000	0.1143
4.8610 ± 0.1220	0.0000 ± 0.0000	0.0824	0.0710	0.0354	0.0000	0.1144
5.0900 ± 0.1290	0.0034 ± 0.0021	0.0824	0.0710	0.0347	0.6296	0.6399
5.3330 ± 0.1400	0.0025 ± 0.0021	0.0824	0.0710	0.0342	0.8258	0.8336
5.5970 ± 0.1490	0.0049 ± 0.0021	0.0824	0.0710	0.0332	0.4116	0.4270
5.8750 ± 0.1600	0.0019 ± 0.0020	0.0824	0.0710	0.0326	1.0403	1.0465
6.1810 ± 0.1750	0.0042 ± 0.0020	0.0824	0.0710	0.0324	0.4650	0.4786
6.5170 ± 0.1870	0.0053 ± 0.0020	0.0824	0.0710	0.0302	0.3633	0.3804
6.8620 ± 0.2010	0.0032 ± 0.0019	0.0824	0.0710	0.0286	0.5856	0.5963
7.2370 ± 0.2180	0.0058 ± 0.0020	0.0824	0.0710	0.0295	0.3303	0.3490
7.6610 ± 0.2420	0.0092 ± 0.0024	0.0824	0.0710	0.0313	0.2299	0.2563
8.1260 ± 0.2630	0.0093 ± 0.0024	0.0824	0.0710	0.0312	0.2272	0.2538
8.6180 ± 0.2840	0.0086 ± 0.0023	0.0824	0.0710	0.0304	0.2428	0.2678
9.1600 ± 0.3130	0.0142 ± 0.0027	0.0824	0.0710	0.0310	0.1561	0.1927
9.7570 ± 0.3460	0.0156 ± 0.0029	0.0824	0.0710	0.0320	0.1454	0.1844
10.4140 ± 0.3770	0.0164 ± 0.0030	0.0824	0.0710	0.0331	0.1430	0.1827
11.1430 ± 0.4250	0.0122 ± 0.0028	0.0824	0.0710	0.0351	0.1954	0.2264
11.9600 ± 0.4670	0.0155 ± 0.0031	0.0824	0.0710	0.0361	0.1593	0.1962
12.8600 ± 0.5250	0.0071 ± 0.0026	0.0824	0.0710	0.0370	0.3449	0.3635
13.8760 ± 0.5890	0.0091 ± 0.0027	0.0824	0.0710	0.0375	0.2775	0.3004
15.0160 ± 0.6600	0.0053 ± 0.0025	0.0824	0.0710	0.0375	0.4615	0.4757
16.2970 ± 0.7500	0.0045 ± 0.0025	0.0824	0.0710	0.0375	0.5414	0.5535
17.7590 ± 0.8570	0.0053 ± 0.0025	0.0824	0.0710	0.0374	0.4622	0.4763
19.4160 ± 0.9710	0.0047 ± 0.0025	0.0824	0.0710	0.0381	0.5294	0.5418

APPENDIX E: DETAILED CHECK OF CALCULATIONS

In this section we carry out a simplified version of the calculations used to obtain the partial γ -ray cross sections quoted in this paper to check the calculations in detail at each step. To this end, we examine the extracted yield for the $6_1^+ \rightarrow 4_1^+$ in the $E_n = 11.511\text{-}12.360\text{-MeV}$ bin (i.e. bin 21 in all yield tables found in this paper) using the ^{235}U fission-foil normalization. We assume that the process leading to the sorted data (e.g. data acquisition, detector-energy and -time alignment in the sort, etc ...) are free from substantive errors. Certainly the agreement with the ^{56}Fe partial cross section and internal consistency checks (between **98Thin**, **98Thick**, and **99Thin** data sets) seem to support this assumption. Therefore, our goal is to discount systematic mistakes in the analysis by presenting each step in detail, and with adequate approximations to make the derivation easy to follow but still preserve convincing agreement with the more sophisticated calculation. Thus, equations 3, 4, 5, and 8 are combined and simplified to yield:

$$\sigma_{(n,2n\gamma)}(E_n) = \frac{1 + \alpha}{\epsilon_\gamma(1 - f_{ge})} \times \frac{A}{\left(\frac{N_{fc} \times a_{sample}}{\epsilon_d(1 - f_{fc})\sigma_{^{235}\text{U}(n,f)} \times a_{^{235}\text{U}}}\right)} \quad (\text{E1})$$

where the symbols are explained in sections II A 2 and II A 3. We present this simplified calculation for both the **98Thin** and **99Thin**.

1 Analysis of the **98Thin** Data Set

a Kinematics

We begin by ignoring the complicated formula (equation 6) used to extract the neutron-energy-bin centroid and use instead the midpoint $\bar{E}_n = 11.936$ MeV of the $11.511\text{-}12.360\text{-MeV}$ range, which agrees very well with the value of 11.952 MeV obtained by the more sophisticated treatment. The distance traveled by both neutrons and gammas from the spallation source to the ^{235}U foil in the fission chamber is $d = 18.482$ m. Rather than using equation 29 we calculate the time-of-flight (TOF) relative to the γ flash classically. The γ -ray TOF is simply d/c , where $c \approx 0.300$ m/ns is the speed of light in a vacuum. Similarly, the TOF of a neutron with kinetic energy E_n is d/v where:

$$E_n = \frac{1}{2}mv^2 \quad (\text{E2})$$

with m , the neutron rest mass. Therefore, the TOF of the neutron relative to the γ ray is given by:

$$\Delta t = \frac{d}{v} - \frac{d}{c} = \frac{d}{c} \left(\sqrt{\frac{mc^2}{2E_n}} - 1 \right) \quad (\text{E3})$$

Using the neutron rest energy $mc^2 = 939.56$ MeV, we obtain:

$$E_n^{(min)} = 11.511 \text{ MeV} \Rightarrow \Delta t_{max} = 331.96 \text{ ns} \quad (\text{E4})$$

$$E_n^{(max)} = 12.360 \text{ MeV} \Rightarrow \Delta t_{min} = 318.20 \text{ ns} \quad (\text{E5})$$

The values obtained with the relativistic treatment of equation 29 are $\Delta t_{min} = 321.94$ ns and $\Delta t_{max} = 335.57$ ns, in good agreement with the classical values. The distance from the spallation target to the focal point of the GEANIE spectrometer is $d = 20.34$ m. In this case the corresponding TOFs are:

$$E_n^{(min)} = 11.511 \text{ MeV} \Rightarrow \Delta t_{max} = 365.33 \text{ ns} \quad (\text{E6})$$

$$E_n^{(max)} = 12.360 \text{ MeV} \Rightarrow \Delta t_{min} = 350.19 \text{ ns} \quad (\text{E7})$$

in good agreement with the relativistic values of $\Delta t_{min} = 354.31$ ns and $\Delta t_{max} = 369.31$ ns

b Analysis of the Fission-Chamber Data

The fission-chamber data corresponding to neutron-induced fission events were sorted into the TOF spectra shown in figure 3. In the ^{235}U -foil spectrum, the γ flash can be seen at channel position $x_f = 323$ (each digitization channel corresponds to 0.5 ns and the absolute position of the γ flash is arbitrary, i.e. channel position zero does not hold any special significance). the TOFs calculated in equations E4 and E5 therefore correspond to channel positions:

$$x_{min} = \lfloor 323 + 318.20/0.5 \rfloor = 959 \quad (\text{E8})$$

$$x_{max} = \lfloor 323 + 331.96/0.5 \rfloor = 986 \quad (\text{E9})$$

where the “ $\lfloor \cdot \rfloor$ ” symbols denote the mathematical “floor” function (i.e. $\lfloor x \rfloor$ is the greatest integer not larger than x). This truncation method has been chosen as a matter of convention and can, in principle produce slight discrepancies from a different approach, such as rounding the channel number to the nearest integer. However, in the actual calculation of the flux normalization N_ϕ using equation 5, each channel is included in the calculation with a weighting factor, and considerations in converting from a real-valued TOF to an integer channel number are irrelevant. The number of counts in the ^{235}U -foil TOF spectrum between these channel positions is:

$$N_{fc}^{(\text{raw})} = 5963 \pm 77 \quad (\text{E10})$$

As discussed in section II A 2, a baseline background is subtracted to remove counts due to beam wrap-around. For the present calculation, we verify visually that the baseline lies at a height of ≈ 24 counts/channel. Therefore the subtracted count is:

$$N_{fc} \approx 5963 - 24(986 - 959 + 1) = 5291 \quad (\text{E11})$$

The actual value, found in table II, is 5498 ± 74 , and differs from our estimate by only 4%. The discrepancy is due to the slight difference in TOFs produced by the classical and relativistic approaches.

Next, we estimate the number of ^{235}U atoms per unit area in the ^{235}U fission foil (i.e. the areal density). The foil is approximately $400 \mu\text{g}/\text{cm}^2$ thick, and is 98.208%-enriched in ^{235}U isotope. The atomic mass of ^{235}U is $235.043923062(2115)$ u [28], where $1 \text{ u} = 1.66053873 \times 10^{-24} \text{ g}$. Thus the areal density of ^{235}U in the fission foil is:

$$\begin{aligned} & 400 \times 10^{-6} \left(\frac{\text{g}}{\text{cm}^2} \right) \times \frac{1}{235.043923062 \times 1.66053873 \times 10^{-24}} \left(\frac{\text{atoms}}{\text{g}} \right) \times 10^{-24} \left(\frac{\text{cm}^2}{\text{b}} \right) \times 0.98208 \\ & = 1.0065 \times 10^{-6} \frac{\text{atoms}}{\text{b}} \end{aligned} \quad (\text{E12})$$

The value for this number, measured by α -decay counting [9], is $1.037(7) \times 10^{-6}$ atoms/b, which agrees to within 3% with the approximate value.

Next, we obtain the $^{235}\text{U}(\text{n},\text{f})$ cross section from the ENDF/B-VI evaluation [11] for the neutron energy closest to the midpoint value $\bar{E}_n = 11.936$ MeV: we find $\sigma_{(\text{n},\text{f})}(E_n = 12 \text{ MeV}) = 1.7347 \text{ b}$. The (n,f) cross section varies by 3.4% over the 11.511-12.360-MeV bin and therefore we expect the midpoint value to be fairly representative.

Deadtimes used throughout this report were obtained by comparing counts digitized in ADC (Analog-to-Digital Conversion) modules to those same counts incremented with little pre-processing in scaler modules. Occasional noise in the acquisition system can cause counts in the scaler modules to spike briefly. Therefore, as an additional precaution, an upper bound was placed on scaler counts for individual detectors. The occurrence of such noise should be a rare event, and in this section, we relax the upper-bound constraint on scaler counts for comparison. The pertinent counts are listed in table CXXXII.

TABLE CXXXII:

Detector	ADC counts	Scaler counts	Livetime = $\frac{\text{ADC counts}}{\text{Scaler counts}}$
sum of planars	4.67743×10^8	8.299444×10^8	0.5636
^{235}U foil	602879	1.00468×10^6	0.6001

The livetime obtained for the ^{235}U -fission-foil signal is 0.6001, in perfect agreement with the value of 1-0.3999 = 0.6001 calculated with the upper-bound constraint and used earlier in the report.

We can now calculate the neutron count N_{nc} for the bin, calculated using equation 3. To compare with the corresponding number in table II, equation 3 should be integrated over the 11.511-12.360-MeV bin as a function of TOF. To lowest order, we can take all quantities in the expression to be roughly constant. For the fission chamber, we take the value $\epsilon_d = 0.941$ determined in [9]. The energy increment δE , in the lowest-order approximation, can be taken as the average value over the bin; since there are 986-959+1 = 28 channels (which were added individually to obtain the number of counts $N_{fc} = 5291$ in the fission-foil data) in this $\Delta E = 12.360-11.511 = 0.849$ MeV bin, we deduce $\delta E \approx \Delta E/28 = 0.0303$ MeV. Thus, we calculate:

$$N_{nc} = \frac{5291}{0.941 \times 0.6001 \times 0.0303 \times 1.7347 \times 1.0065 \times 10^{-6}} \quad (\text{E13})$$

$$= 1.771 \times 10^{11} \text{ n/MeV} \quad (\text{E14})$$

which agrees within 4% with the value of 1.709×10^{11} in table II. The δE factor in the denominator is included only as a matter of convention and is canceled out in the final calculation of the flux normalization N_ϕ (see equation 4). Therefore, we can remove the ambiguity introduced by this factor by directly examining the number of neutrons (call it N_{nn}) counted in this bin for the duration of the experiment. In the simple calculation delineated here, this number is $N_{nn} = 1.771 \times 10^{11} \times 0.0303 = 5.366 \times 10^9$ neutrons. The number obtained by the more sophisticated approach (i.e. from equation 3 without the δE factor) is 5.310×10^9 neutrons, or a 1.0% discrepancy.

Again as a matter of convention, the sample areal density (a_{sample}) is incorporated into the calculation of the flux normalization factor N_ϕ , which carries units of barn^{-1} . Thus, the final step in the fission-chamber data analysis requires a_{sample} , in order to calculate N_ϕ according to equation 4. We re-derive the sample areal density from basic sample-properties measurements. The **98Thin** sample consisted of two laminated packages each containing two ^{235}U -enriched foils. The total mass of the first package was 4.56 g, with the plastic laminant accounting for 0.36 g of that mass. The average area of the two foils in the first package was determined to be 15.8 cm^2 . Similarly, the second package had a total mass of 4.96 g, with a 0.36 g plastic laminant and an average area of 15.5 cm^2 for its two constituent foils. Therefore, the total areal density of the sample is:

$$\frac{4.56 - 0.36}{15.8} + \frac{4.96 - 0.36}{15.5} = 0.562 \text{ g/cm}^2 \quad (\text{E15})$$

This areal density must be corrected for the 93.2324% isotopic enrichment in ^{235}U :

$$0.932324 \times 0.562 = 0.524 \text{ g/cm}^2 \quad (\text{E16})$$

In perfect agreement with the value quoted in [9]. In addition, because the sample was positioned at 19° with respect to the beam direction, the effective areal density of the sample is obtained by increasing the 0° -with-respect-to-beam value above by a factor of $1/\cos(19^\circ)$:

$$\frac{0.524}{\cos(19^\circ)} = 0.555 \text{ g/cm}^2 \quad (\text{E17})$$

which we convert for computational convenience into units of atoms/barn:

$$0.555 \left(\frac{\text{g}}{\text{cm}^2} \right) \times \frac{1}{235.043923062 \times 1.66053873 \times 10^{-24}} \left(\frac{\text{atoms}}{\text{g}} \right) \times 10^{-24} \left(\frac{\text{cm}^2}{\text{b}} \right) \\ = 0.00142 \left(\frac{\text{atoms}}{\text{b}} \right) \quad (\text{E18})$$

Thus, using equation 4 it follows that:

$$N_\phi = 1.771 \times 10^{11} \times 0.00142 \times 0.0303 \quad (\text{E19})$$

$$= 7.620 \times 10^6 \text{ b}^{-1} \quad (\text{E20})$$

The value quoted in table II, $6.993 \times 10^6 \text{ b}^{-1}$, agrees within 9%. This discrepancy is noticeably larger than those encountered before. About 4% of that deviation is already seen in the calculation of the neutron count N_{nc} and can be attributed to a combination of the slight difference in channel ranges between classical and relativistic formulations and to the constant-value approximation in the terms of equation 4. The remainder of the discrepancy is due to the correction for neutron-TOF distribution applied in the more sophisticated treatment used in this report and formulated in equation 5. In fact, almost all of the remaining discrepancy can be directly attributed to the smoothing-over-channels that is naturally implemented by equation 5. This can be made manifest by applying equation 5 assuming no timing uncertainty (i.e. $\sigma_\tau = 0$). The value obtained in this extreme limit is $N_\phi = 6.965 \times 10^6 \text{ b}^{-1}$, or essentially unchanged. Thus we conclude that the remaining 5% discrepancy between the approximate and sophisticated calculations of N_ϕ is due primarily to the smoothing effect of the weighting factors in equation 5, which compensates for sizeable fluctuation in the low-statistics fission-foil spectrum.

c Analysis of the γ -ray Data

The γ -ray data from the **98Thin** set were sorted into a matrix of counts with γ -ray energy along one axis, and neutron TOF along the other. As with the fission-chamber data, the TOF axis is digitized into 0.5-ns channels. For the γ -ray data, the γ flash centroid is found at channel position $x_f = 532$, so that the TOF-channel range corresponding to the 11.511–12.360-MeV bin can be obtained from the TOFs determined above:

$$x_{min} = \lfloor 532 + 350.19/0.5 \rfloor = 1232 \quad (\text{E21})$$

$$x_{max} = \lfloor 532 + 365.33/0.5 \rfloor = 1262 \quad (\text{E22})$$

A γ -ray energy spectrum for the 11.511–12.360-MeV bin is generated by placing a TOF cut from channel 1232 to channel 1262 on the E_γ -TOF matrix. A portion of that spectrum—determined using the more appropriate relativistic TOFs—which includes the $6_1^+ \rightarrow 4_1^+$ transition can be seen in figure 7d). As an independent test of the fitting code XGAM used in this report, we obtain the number of counts under the $6_1^+ \rightarrow 4_1^+$ peak in this spectrum by two additional methods. First we use an entirely different fitting code, GF2, written by D.C. Radford and commonly used in γ -ray spectroscopy analysis. This fit yields an area of 7953 ± 133 counts for the $6_1^+ \rightarrow 4_1^+$ peak, with $\chi^2/\nu = 2.33$ for the fitted region around the peak. Second, we simply sum the counts under the peak, with a linear baseline subtraction determined from the background height on either side of the peak. This procedure yields an area of 8397 ± 126 counts. The XGAM estimate for the $6_1^+ \rightarrow 4_1^+$ peak area, listed in table V, is 8238 ± 131 and agrees within 4% with either alternate method. The discrepancy between GF2 and XGAM fit is not surprising. A more sophisticated peak shape formulation was used in XGAM to account for Gaussian asymmetry as well as low- and high-energy tails in the peaks. All of these effects are observed in the data. These contributions to the peak shape were parameterized from the fit to the entire spectrum and are therefore believed to be accurate and robust. The parameters for these peak-shape components are listed in table I for the **98Thin** fits. Therefore, it is expected that some of the counts will be missed by the GF2 fits, specifically in the high-energy tail.

In the fission-chamber data analysis above, we discussed in particular the procedure by which real-valued TOFs were converted to integer channel numbers. In that case, because the formulas used to extract the flux normalization provided a natural smoothing-over-channels, concerns regarding channel-number rounding were shown to be irrelevant. In the case of the γ -ray data, the situation is seemingly different since, at first glance, no comparable smoothing is carried out (see equation 8). However, since the peak areas are obtained by fitting, the results are made more stable against the exact choice of channels. For completeness, we have extracted the $6_1^+ \rightarrow 4_1^+$ peak area using GF2 for rounded (rather than truncated) values of the channel numbers. In that case $x_{min} = 1232$ and $x_{max} = 1263$. The corresponding fit yields an area of 8011 ± 129 counts for the $6_1^+ \rightarrow 4_1^+$ peak, with $\chi^2/\nu = 2.47$ for the fitted region around the peak, which differs by 0.7% from the truncated-channel approach.

The livetime for the sum of planar detectors is shown in table CXXXII and agrees within 3% with the value used in this report. The slight discrepancy is due to occasional noise in the system, which is more likely to affect the livetime value obtained in this appendix.

Finally, we require the total internal conversion coefficient, which we obtain for the $6_1^+ \rightarrow 4_1^+$ transition from the ENSDF tabulation [10] as $\alpha = 2.19$ (in agreement with the value found in [9]). We also require the γ -ray detection efficiency. Since there is no simple way of obtaining this number, we use the value of 0.01526 calculated by McNabb [9] for a 150-keV γ ray. Combining all the quantities in this appendix, and using equation E1, we obtain:

$$\sigma_{6_1^+ \rightarrow 4_1^+} (11.511 - 12.360 \text{ MeV}) = \frac{1 + 2.19}{0.01526 \times 0.5636} \times \frac{7953}{7.620 \times 10^6}$$

$$= 0.387 b \quad (E23)$$

The partial cross section of 0.446 b, calculated by more sophisticated means for this bin, can be found in table V and agrees within 15% with the approximate value. The discrepancy can be entirely accounted for by the approximations made here for ease of presentation.

2 Analysis of the **99Thin** Data Set

a Kinematics

Because none of the pertinent quantities changed between the 1998 and 1999 GEANIE experiments, the TOFs calculated above for the **98Thin** data set remain the same.

b Analysis of the Fission-Chamber Data

The position of the γ flash in the fission-chamber TOF spectrum is differs between the **98Thin** and **99Thin** data sets. For the **99Thin**, we have $x_f = 85$ in the fission chamber. Since the value of this position is arbitrary, the difference between data sets is of no consequence, as long as we calculate the appropriate channel numbers for the fission-chamber data analysis:

$$x_{min} = \lfloor 85 + 318.20/0.5 \rfloor = 721 \quad (E24)$$

$$x_{max} = \lfloor 85 + 331.96/0.5 \rfloor = 748 \quad (E25)$$

Following the same procedure as for the **98Thin** analysis we find:

$$N_{fc}^{(\text{raw})} = 7106 \pm 84 \quad (E26)$$

for the ^{235}U fission-foil data. A visual inspection reveals a baseline of ≈ 25 counts/channel, consistent with observations for the **98Thin** data. Thus:

$$N_{fc} \approx 7106 - 25(748 - 721 + 1) = 6406 \quad (E27)$$

which is within 1.4% of the actual value 6497, found in table XI. The livetimes for this experiment are calculated using the numbers in table CXXXIII.

TABLE CXXXIII:

Detector	ADC counts	Scaler counts	Livetime = $\frac{\text{ADC counts}}{\text{Scaler counts}}$
sum of planars	4.16854×10^8	1.44655×10^8	0.2882
^{235}U foil	656310	1.91243×10^6	0.3432

We can therefore calculate N_{nc} as we did for the **98Thin** data:

$$N_{nc} = \frac{6406}{0.941 \times 0.3432 \times 0.0303 \times 1.7347 \times 1.0065 \times 10^{-6}} \quad (E28)$$

$$= 3.749 \times 10^{11} \text{ n/MeV} \quad (E29)$$

which is within 6.0% of the actual value of 3.536×10^{11} , found in table XI. Here again, a direct comparison of the energy-integrated number of neutrons N_{nn} yields 1.136×10^{10} in the simplified approach, compared to 1.098×10^{10} in the more sophisticated treatment, or less than a 3.5% discrepancy.

Next, in order to calculate the sample density, we compile the mass and average area of each of its component foils in table CXXXIV.

TABLE CXXXIV:

Foil id	Mass (g)	Area (cm ²)	Mass/Area (g/cm ²)
268	0.7607	6.56605	0.1158
269	0.7739	6.41419	0.1206
270	0.7884	6.36053	0.1240
271	0.7957	6.50501	0.1223

Adding the individual areal densities yields:

$$0.1158 + 0.1206 + 0.1240 + 0.1223 = 0.4827 \text{ g/cm}^2 \quad (\text{E30})$$

which we correct for the sample enrichment:

$$0.4827 \times 0.932324 = 0.4500 \text{ g/cm}^2 \quad (\text{E31})$$

and for the sample orientation with respect to beam:

$$\frac{0.4500}{\cos 19^\circ} = 0.4759 \text{ g/cm}^2 \quad (\text{E32})$$

and convert into units of atoms/barn:

$$\frac{0.4759 \times 10^{-24}}{235.043923062 \times 1.66053873 \times 10^{-24}} = 0.1219 \text{ atoms/b} \quad (\text{E33})$$

From this, we calculate:

$$\begin{aligned} N_\phi &= 3.479 \times 10^{11} \times 0.1219 \times 0.0303 \\ &= 1.385 \times 10^7 \text{ b}^{-1} \end{aligned} \quad (\text{E34})$$

The actual value quoted in table XI is 1.265 b^{-1} , or a 9% discrepancy. The same over-estimation of N_ϕ was observed in the **98Thin** data analysis and has been accounted for in terms of the approximations made in the present calculation.

c Analysis of the γ -ray Data

The γ -flash position in the γ -ray TOF is at $x_f = 227$. Therefore we calculate the channel limits:

$$x_{min} = \lfloor 227 + 350.19/0.5 \rfloor = 927 \quad (\text{E35})$$

$$x_{max} = \lfloor 227 + 365.33/0.5 \rfloor = 957 \quad (\text{E36})$$

The GF2 fit corresponding to that channel range yields an area of 5691 ± 123 counts for the $6_1^+ \rightarrow 4_1^+$ peak, with a $\chi^2/\nu = 1.057$ for the fitted region. The corresponding area obtained with XGAM is 6191 ± 125 , or an 8.8% discrepancy. This is a relatively sizeable disagreement between the two fitting codes. Part of the discrepancy can be attributed to the difference in TOFs between the classical and relativistic calculations. If the same GF2 fit is applied to the channel range $x_{min} = 935$ to $x_{max} = 965$, which corresponds to the relativistic TOFs, an area of 5965 ± 124 counts is obtained for the $6_1^+ \rightarrow 4_1^+$ peak, which reduces the discrepancy between GF2 and XGAM to 3.8%. Another contribution to the discrepancy is due to the high-energy tails included in the XGAM peak shapes. Repeating the XGAM fit for the $x = 927-957$ -channel bin without high-energy tails yields an area of 5699 ± 119 counts, in perfect agreement with the GF2 result. These high-energy tails are known to exist in the GEANIE data and have been observed in individual detectors. They are more prominent in **99Thin** than **98Thin** spectra and account for $\approx 6.0\%$

of the area of any given peak. Because this component of the peak shape has been set by a fit to the entire γ -ray spectrum, we expect it to be as accurate and reliable as possible, given the statistics of the **99Thin** data.

The deadtime for the planar detectors is given in table CXXXIII as 0.2882. The efficiency for a 150-keV γ ray has been calculated [9] to be 0.01313. Using these results we calculate an approximate cross section:

$$\begin{aligned}\sigma_{6_1^+ \rightarrow 4_1^+} (11.511 - 12.360 \text{ MeV}) &= \frac{1 + 2.19}{0.01313 \times 0.2882} \times \frac{5691}{1.385 \times 10^7} \\ &= 0.346 \text{ b}\end{aligned}\quad (\text{E37})$$

which differs from the tabulated value of 0.407 barns by $\approx 18\%$. This discrepancy can be accounted for by the approximations made in the present calculation.

APPENDIX F: CHECK OF XGAM BACKGROUND FITS

The background underneath each peak in the spectrum (i.e. those counts which do not contribute to the peak's area) has two components: i) a continuum background, modeled by a polynomial function in the XGAM fits, and ii) a Compton-scattering background, modeled by a smooth step function (specifically, the functional form is generated by the error function $erf(x)$). The true background, approximated by these two components in the XGAM fits, has a complicated form which results from the combination of among other effects, the detector response, unsuppressed Compton-scattering events, electronic cutoff settings, and unresolved discrete γ rays. In nearly all γ -ray spectroscopy analysis, the continuum background is modeled locally (typically, over a range encompassing a dozen or so peaks) by a low-order polynomial (usually linear or quadratic). This approach—though flexible and convenient—incorporates a significant drawback into the fitting procedure by not ensuring continuity and smoothness (i.e. higher-order differentiability) from one fitted region to the next. In XGAM these boundary conditions are automatically enforced by the use of a single polynomial over the entire spectrum to reproduce the continuum background. However, some care must be exercised to ensure that the polynomial is sufficiently constrained by the data in the fitted spectrum. If the polynomial is given too many degrees of freedom, it may display local oscillations not warranted by the data, for the sake of improving the overall fit.

In this section, we verify that the polynomials used in the fits of the **98Thin** and **99Thin** data sets are well-behaved. For the $4_1^+ \rightarrow 2_1^+$, $6_1^+ \rightarrow 4_1^+$, $8_1^+ \rightarrow 6_1^+$, and $10_1^+ \rightarrow 8_1^+$ transitions, we have repeated the XGAM fits with the same peak-shape parameters but in a region localized around the peak of interest and using a linear-polynomial for the continuum background. The results of these localized fits are compared for the four transitions in tables CXXXV–CXXXVIII. For convenience, the comparison in the tables is quantified by the statistic:

$$\frac{\Delta A}{\sigma} \equiv \frac{A^{(\text{adopted})} - A^{(\text{linear})}}{\sqrt{\sigma_{A^{(\text{adopted})}}^2 + \sigma_{A^{(\text{linear})}}^2}} \quad (\text{F1})$$

where $A^{(\text{adopted})}$ is the peak area adopted in the body of this report and obtained using a polynomial function fitted over the entire spectrum to model the continuum background, and $A^{(\text{linear})}$ is the peak area obtained using a localized fit, with a linear-polynomial background. In almost all cases, it found that F1 yields a value smaller than one. In other words, the uncertainties obtained in the fits more than adequately compensate for any deviations due to the choice of a large polynomial order used in the global fit versus a low polynomial order in local fits.

In figures 99–119 we display the background used for both **98Thin** and **99Thin** fits of each neutron energy bin above the $(n,2n)$ threshold. The backgrounds shown include the contributions from the continuum–background polynomial as well as individual Compton steps. These figures are that i) the background parameterization produces a reasonable shape underneath each spectrum and ii) the background shape is stable from one neutron–energy bin to the next, and no localized undulations are produced in a given bin as a result of decreased peak statistics. We mention in passing a few features that the attentive reader may notice in these figures:

- the background is higher in the **99Thin** than in **98Thin** data in the x-ray region. This results from two factors: i) the Compton step was less pronounced in the 1999 data and ii) the 1999 data were acquired and analyzed with higher dispersion in the ADC modules (i.e. full energy range digitized over 16384 channels versus 8192 in the 1998 experiments), this results in less-pronounced “clumping” of peaks in the dense x-ray region compared to the 1998 data.

- The apparent discontinuity in background shape observed under the strongest peaks is produced by the Compton step. The appearance of a sharp step is caused by the expanded plotting range, in actuality, the function form produces a locally smooth shape. Furthermore, the size of the step is proportional to the peak height, so that it appears more pronounced for the stronger lines.
- Some variations in background shape can be observed over the full range of the spectrum, however they follows the shape of the spectrum itself and always occur on a scale far larger than the width of a peak.
- The peak observed at 847 keV in the ⁹⁹Thin data is produced by the $2_1^+ \rightarrow$ transition in ⁵⁶Fe, because of the ^{nat}Fe foils included in the 1999 run, but not in the 1998 experiment.

TABLE CXXXV: Comparison of adopted XGAM fits for the $4_1^+ \rightarrow 2_1^+$ to XGAM fits with a linear background.

E_n (MeV)	$A^{(1998)}$ (adopted)	$A^{(1998)}$ (linear bkg)	$\Delta A/\sigma$	$A^{(1999)}$ (adopted)	$A^{(1999)}$ (linear bkg)	$\Delta A/\sigma$
4.090 ± 0.093	0 ± 60	0 ± 0	0.00	583 ± 145	644 ± 146	-0.30
4.264 ± 0.099	56 ± 207	71 ± 198	-0.05	540 ± 149	601 ± 150	-0.29
4.453 ± 0.105	3 ± 92	0 ± 39	0.03	632 ± 153	579 ± 154	0.24
4.647 ± 0.113	4 ± 96	7 ± 153	-0.02	557 ± 154	603 ± 156	-0.21
4.861 ± 0.122	0 ± 64	0 ± 20	0.00	469 ± 154	474 ± 151	-0.02
5.090 ± 0.129	469 ± 218	490 ± 210	-0.07	394 ± 154	514 ± 156	-0.55
5.333 ± 0.140	590 ± 220	613 ± 211	-0.08	645 ± 153	699 ± 155	-0.25
5.597 ± 0.149	572 ± 219	576 ± 211	-0.01	492 ± 152	556 ± 155	-0.29
5.875 ± 0.160	377 ± 221	379 ± 212	-0.01	832 ± 155	867 ± 156	-0.16
6.181 ± 0.175	1495 ± 227	1516 ± 219	-0.07	1319 ± 156	1251 ± 157	0.31
6.517 ± 0.187	2035 ± 234	2071 ± 226	-0.11	1841 ± 160	1757 ± 161	0.37
6.862 ± 0.201	1838 ± 235	1885 ± 227	-0.14	1892 ± 162	1845 ± 163	0.20
7.237 ± 0.218	2327 ± 238	2358 ± 230	-0.09	1552 ± 160	1608 ± 161	-0.25
7.661 ± 0.242	2233 ± 235	2265 ± 227	-0.10	1741 ± 159	1770 ± 160	-0.13
8.126 ± 0.263	2502 ± 239	2542 ± 230	-0.12	1890 ± 161	1945 ± 162	-0.24
8.618 ± 0.284	2619 ± 242	2653 ± 234	-0.10	2067 ± 162	2171 ± 163	-0.45
9.160 ± 0.313	2686 ± 241	2729 ± 233	-0.13	2314 ± 163	2346 ± 164	-0.14
9.757 ± 0.346	3211 ± 241	3254 ± 233	-0.13	2175 ± 161	2272 ± 162	-0.42
10.414 ± 0.377	2835 ± 241	2881 ± 232	-0.14	2163 ± 161	2214 ± 162	-0.22
11.143 ± 0.425	2557 ± 238	2597 ± 230	-0.12	2097 ± 159	2171 ± 160	-0.33
11.960 ± 0.467	2836 ± 239	2867 ± 231	-0.09	2278 ± 161	2348 ± 162	-0.31
12.860 ± 0.525	2625 ± 234	2658 ± 226	-0.10	2133 ± 160	2195 ± 161	-0.27
13.876 ± 0.589	1589 ± 230	1612 ± 222	-0.07	1285 ± 154	1279 ± 155	0.03
15.016 ± 0.660	1161 ± 225	1182 ± 217	-0.07	940 ± 151	986 ± 152	-0.21
16.297 ± 0.750	693 ± 224	711 ± 216	-0.06	992 ± 150	1099 ± 151	-0.50
17.759 ± 0.857	373 ± 223	404 ± 214	-0.10	529 ± 146	606 ± 147	-0.37
19.416 ± 0.971	8 ± 218	27 ± 214	-0.06	812 ± 149	880 ± 150	-0.32

TABLE CXXXVI: Comparison of adopted XGAM fits for the $6_1^+ \rightarrow 4_1^+$ to XGAM fits with a linear background.

E_n (MeV)	$A^{(1998)}$ (adopted)	$A^{(1998)}$ (linear bkg)	$\Delta A/\sigma$	$A^{(1999)}$ (adopted)	$A^{(1999)}$ (linear bkg)	$\Delta A/\sigma$
4.090 \pm 0.093	223 \pm 73	248 \pm 73	-0.24	166 \pm 79	152 \pm 79	0.13
4.264 \pm 0.099	212 \pm 73	213 \pm 73	-0.01	62 \pm 79	20 \pm 79	0.38
4.453 \pm 0.105	237 \pm 74	235 \pm 74	0.02	172 \pm 80	117 \pm 80	0.49
4.647 \pm 0.113	146 \pm 73	135 \pm 72	0.11	213 \pm 82	188 \pm 81	0.22
4.861 \pm 0.122	214 \pm 74	194 \pm 74	0.19	36 \pm 75	1 \pm 39	0.41
5.090 \pm 0.129	318 \pm 76	284 \pm 76	0.32	0 \pm 15	0 \pm 0	0.00
5.333 \pm 0.140	231 \pm 75	232 \pm 75	-0.01	0 \pm 12	4 \pm 56	-0.07
5.597 \pm 0.149	343 \pm 78	350 \pm 78	-0.06	23 \pm 84	34 \pm 85	-0.09
5.875 \pm 0.160	820 \pm 83	798 \pm 83	0.19	439 \pm 90	418 \pm 89	0.17
6.181 \pm 0.175	2015 \pm 93	2012 \pm 93	0.02	1467 \pm 99	1405 \pm 99	0.44
6.517 \pm 0.187	3350 \pm 104	3344 \pm 103	0.04	2572 \pm 107	2484 \pm 107	0.58
6.862 \pm 0.201	4162 \pm 110	4148 \pm 109	0.09	3414 \pm 113	3404 \pm 113	0.06
7.237 \pm 0.218	4970 \pm 114	4965 \pm 114	0.03	3735 \pm 114	3658 \pm 113	0.48
7.661 \pm 0.242	5076 \pm 115	5073 \pm 115	0.02	3779 \pm 113	3814 \pm 113	-0.22
8.126 \pm 0.263	5653 \pm 118	5638 \pm 118	0.09	4633 \pm 119	4638 \pm 119	-0.03
8.618 \pm 0.284	6751 \pm 124	6759 \pm 125	-0.05	5057 \pm 122	5092 \pm 121	-0.20
9.160 \pm 0.313	7114 \pm 126	7094 \pm 126	0.11	5597 \pm 123	5549 \pm 123	0.28
9.757 \pm 0.346	7726 \pm 129	7708 \pm 129	0.10	5845 \pm 124	5831 \pm 124	0.08
10.414 \pm 0.377	7833 \pm 129	7827 \pm 129	0.03	6227 \pm 125	6240 \pm 125	-0.07
11.143 \pm 0.425	8267 \pm 131	8257 \pm 131	0.05	6353 \pm 126	6361 \pm 126	-0.04
11.960 \pm 0.467	8238 \pm 131	8230 \pm 132	0.04	6191 \pm 126	6178 \pm 126	0.07
12.860 \pm 0.525	7022 \pm 125	7021 \pm 125	0.01	5350 \pm 123	5347 \pm 122	0.02
13.876 \pm 0.589	4929 \pm 115	4871 \pm 115	0.36	4080 \pm 117	4053 \pm 117	0.16
15.016 \pm 0.660	3414 \pm 106	3403 \pm 106	0.07	2824 \pm 110	2857 \pm 109	-0.21
16.297 \pm 0.750	2361 \pm 99	2364 \pm 100	-0.02	2087 \pm 105	2113 \pm 105	-0.18
17.759 \pm 0.857	1905 \pm 96	1874 \pm 96	0.23	1431 \pm 101	1512 \pm 100	-0.57
19.416 \pm 0.971	1708 \pm 95	1711 \pm 96	-0.02	1150 \pm 100	1217 \pm 99	-0.48

TABLE CXXXVII: Comparison of adopted XGAM fits for the $8_1^+ \rightarrow 6_1^+$ to XGAM fits with a linear background.

E_n (MeV)	$A^{(1998)}$ (adopted)	$A^{(1998)}$ (linear bkg)	$\Delta A/\sigma$	$A^{(1999)}$ (adopted)	$A^{(1999)}$ (linear bkg)	$\Delta A/\sigma$
4.090 \pm 0.093	177 \pm 106	261 \pm 79	-0.64	639 \pm 88	549 \pm 91	0.71
4.264 \pm 0.099	58 \pm 105	61 \pm 78	-0.02	813 \pm 90	700 \pm 93	0.88
4.453 \pm 0.105	266 \pm 107	282 \pm 81	-0.12	712 \pm 90	697 \pm 94	0.12
4.647 \pm 0.113	1 \pm 81	19 \pm 72	-0.17	787 \pm 91	733 \pm 95	0.41
4.861 \pm 0.122	207 \pm 107	243 \pm 81	-0.27	913 \pm 93	900 \pm 97	0.10
5.090 \pm 0.129	40 \pm 108	111 \pm 82	-0.52	856 \pm 93	834 \pm 97	0.16
5.333 \pm 0.140	144 \pm 108	169 \pm 82	-0.18	708 \pm 93	602 \pm 93	0.81
5.597 \pm 0.149	27 \pm 104	81 \pm 82	-0.41	654 \pm 93	517 \pm 96	1.03
5.875 \pm 0.160	117 \pm 108	173 \pm 83	-0.41	804 \pm 95	710 \pm 98	0.69
6.181 \pm 0.175	677 \pm 112	754 \pm 88	-0.54	1308 \pm 98	1264 \pm 101	0.31
6.517 \pm 0.187	1775 \pm 119	1853 \pm 98	-0.51	1941 \pm 103	1855 \pm 104	0.59
6.862 \pm 0.201	2342 \pm 124	2358 \pm 104	-0.10	2711 \pm 109	2667 \pm 113	0.28
7.237 \pm 0.218	3043 \pm 127	3041 \pm 108	0.01	3023 \pm 111	2991 \pm 115	0.20
7.661 \pm 0.242	3292 \pm 128	3303 \pm 108	-0.07	3367 \pm 112	3322 \pm 117	0.28
8.126 \pm 0.263	3949 \pm 132	3957 \pm 113	-0.05	3906 \pm 116	3911 \pm 120	-0.03
8.618 \pm 0.284	5316 \pm 138	5318 \pm 121	-0.01	4735 \pm 121	4576 \pm 121	0.93
9.160 \pm 0.313	5765 \pm 140	5757 \pm 123	0.04	5336 \pm 124	5380 \pm 128	-0.25
9.757 \pm 0.346	6491 \pm 143	6487 \pm 127	0.02	5784 \pm 126	5757 \pm 126	0.15
10.414 \pm 0.377	7088 \pm 145	7088 \pm 129	0.00	6337 \pm 127	6354 \pm 131	-0.09
11.143 \pm 0.425	7661 \pm 147	7701 \pm 131	-0.20	6645 \pm 128	6631 \pm 131	0.08
11.960 \pm 0.467	7940 \pm 147	7969 \pm 132	-0.15	7059 \pm 129	7105 \pm 133	-0.25
12.860 \pm 0.525	7136 \pm 145	7066 \pm 129	0.36	6566 \pm 127	6500 \pm 131	0.36
13.876 \pm 0.589	5404 \pm 137	5364 \pm 121	0.22	5073 \pm 120	4943 \pm 124	0.75
15.016 \pm 0.660	3626 \pm 130	3617 \pm 111	0.05	3560 \pm 113	3566 \pm 117	-0.04
16.297 \pm 0.750	2467 \pm 125	2394 \pm 105	0.45	2471 \pm 107	2408 \pm 111	0.41
17.759 \pm 0.857	2076 \pm 122	1932 \pm 102	0.90	2153 \pm 105	2049 \pm 109	0.69
19.416 \pm 0.971	1694 \pm 121	1608 \pm 100	0.55	1834 \pm 104	1796 \pm 104	0.26

TABLE CXXXVIII: Comparison of adopted XGAM fits for the $10_1^+ \rightarrow 8_1^+$ to XGAM fits with a linear background.

E_n (MeV)	$A^{(1998)}$ (adopted)	$A^{(1998)}$ (linear bkg)	$\Delta A/\sigma$	$A^{(1999)}$ (adopted)	$A^{(1999)}$ (linear bkg)	$\Delta A/\sigma$
4.090 \pm 0.093	121 \pm 78	84 \pm 78	0.33	0 \pm 11	0 \pm 0	0.00
4.264 \pm 0.099	43 \pm 77	16 \pm 71	0.26	29 \pm 88	0 \pm 0	0.33
4.453 \pm 0.105	200 \pm 79	170 \pm 79	0.27	21 \pm 87	0 \pm 0	0.24
4.647 \pm 0.113	0 \pm 8	0 \pm 1	0.00	156 \pm 91	109 \pm 89	0.37
4.861 \pm 0.122	0 \pm 8	1 \pm 7	-0.09	172 \pm 91	128 \pm 90	0.34
5.090 \pm 0.129	26 \pm 80	0 \pm 0	0.32	192 \pm 94	154 \pm 92	0.29
5.333 \pm 0.140	135 \pm 82	101 \pm 82	0.29	138 \pm 94	104 \pm 92	0.26
5.597 \pm 0.149	0 \pm 8	0 \pm 0	0.00	13 \pm 93	0 \pm 0	0.14
5.875 \pm 0.160	0 \pm 8	0 \pm 0	0.00	27 \pm 94	5 \pm 77	0.18
6.181 \pm 0.175	0 \pm 8	0 \pm 0	0.00	3 \pm 54	0 \pm 0	0.06
6.517 \pm 0.187	106 \pm 87	74 \pm 86	0.26	155 \pm 98	102 \pm 96	0.39
6.862 \pm 0.201	213 \pm 91	169 \pm 91	0.34	331 \pm 101	287 \pm 100	0.31
7.237 \pm 0.218	456 \pm 94	413 \pm 94	0.32	298 \pm 100	243 \pm 99	0.39
7.661 \pm 0.242	504 \pm 95	453 \pm 94	0.38	704 \pm 103	647 \pm 102	0.39
8.126 \pm 0.263	700 \pm 100	651 \pm 99	0.35	971 \pm 106	920 \pm 105	0.34
8.618 \pm 0.284	929 \pm 102	814 \pm 102	0.80	1198 \pm 109	1148 \pm 108	0.33
9.160 \pm 0.313	1380 \pm 108	1337 \pm 108	0.28	1597 \pm 112	1551 \pm 111	0.29
9.757 \pm 0.346	1434 \pm 109	1388 \pm 109	0.30	1594 \pm 113	1548 \pm 111	0.29
10.414 \pm 0.377	1788 \pm 112	1743 \pm 112	0.28	2160 \pm 115	2132 \pm 114	0.17
11.143 \pm 0.425	2011 \pm 114	1961 \pm 114	0.31	2621 \pm 118	2545 \pm 116	0.46
11.960 \pm 0.467	2065 \pm 114	2018 \pm 114	0.29	2575 \pm 118	2537 \pm 116	0.23
12.860 \pm 0.525	2054 \pm 114	2011 \pm 114	0.27	2421 \pm 116	2381 \pm 115	0.25
13.876 \pm 0.589	1833 \pm 112	1784 \pm 112	0.31	1943 \pm 112	1894 \pm 111	0.31
15.016 \pm 0.660	1185 \pm 105	1133 \pm 105	0.35	1395 \pm 108	1339 \pm 107	0.37
16.297 \pm 0.750	732 \pm 101	690 \pm 101	0.29	943 \pm 105	894 \pm 104	0.33
17.759 \pm 0.857	472 \pm 98	435 \pm 97	0.27	695 \pm 103	653 \pm 101	0.29
19.416 \pm 0.971	429 \pm 99	395 \pm 98	0.24	610 \pm 104	555 \pm 102	0.38

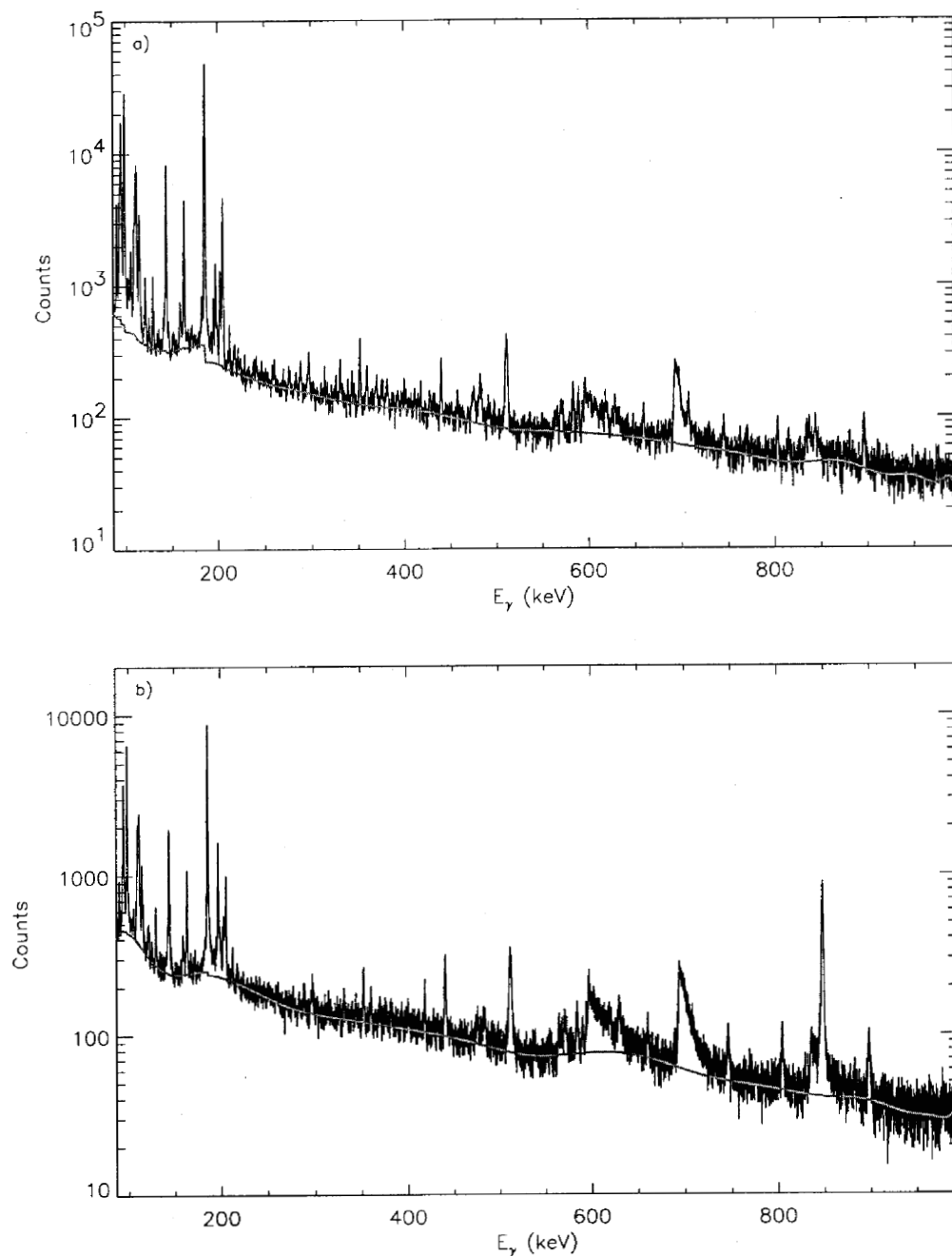


FIG. 99: Background used in the XGAM fit of bin 7 ($\bar{E}_n = 5.3$ MeV) for the a) **98Thin** and b) **99Thin** γ -ray spectra.

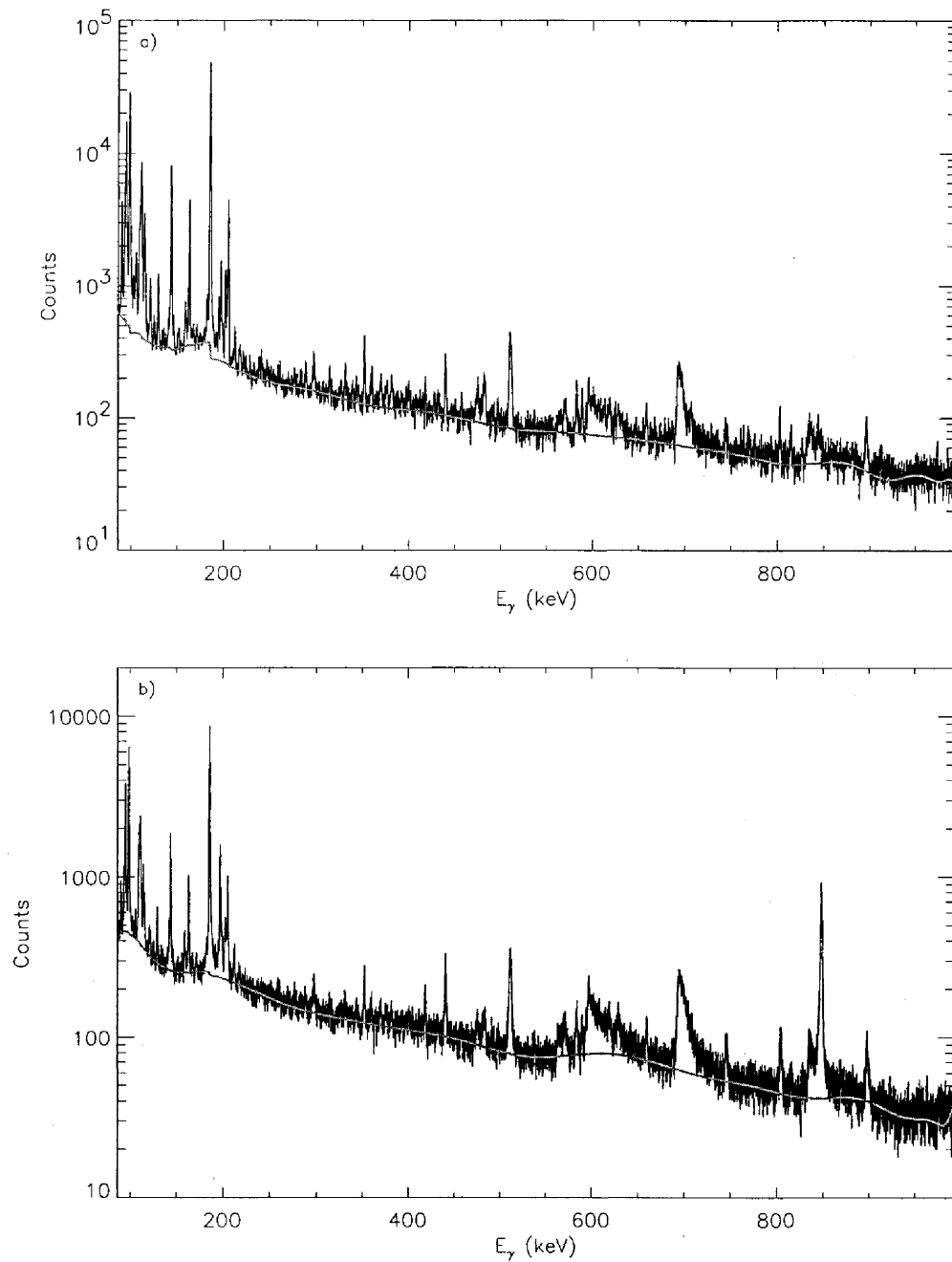


FIG. 100: Background used in the XGAM fit of bin 8 ($\bar{E}_n = 5.6$ MeV) for the a) 98Thin and b) 99Thin γ -ray spectra.

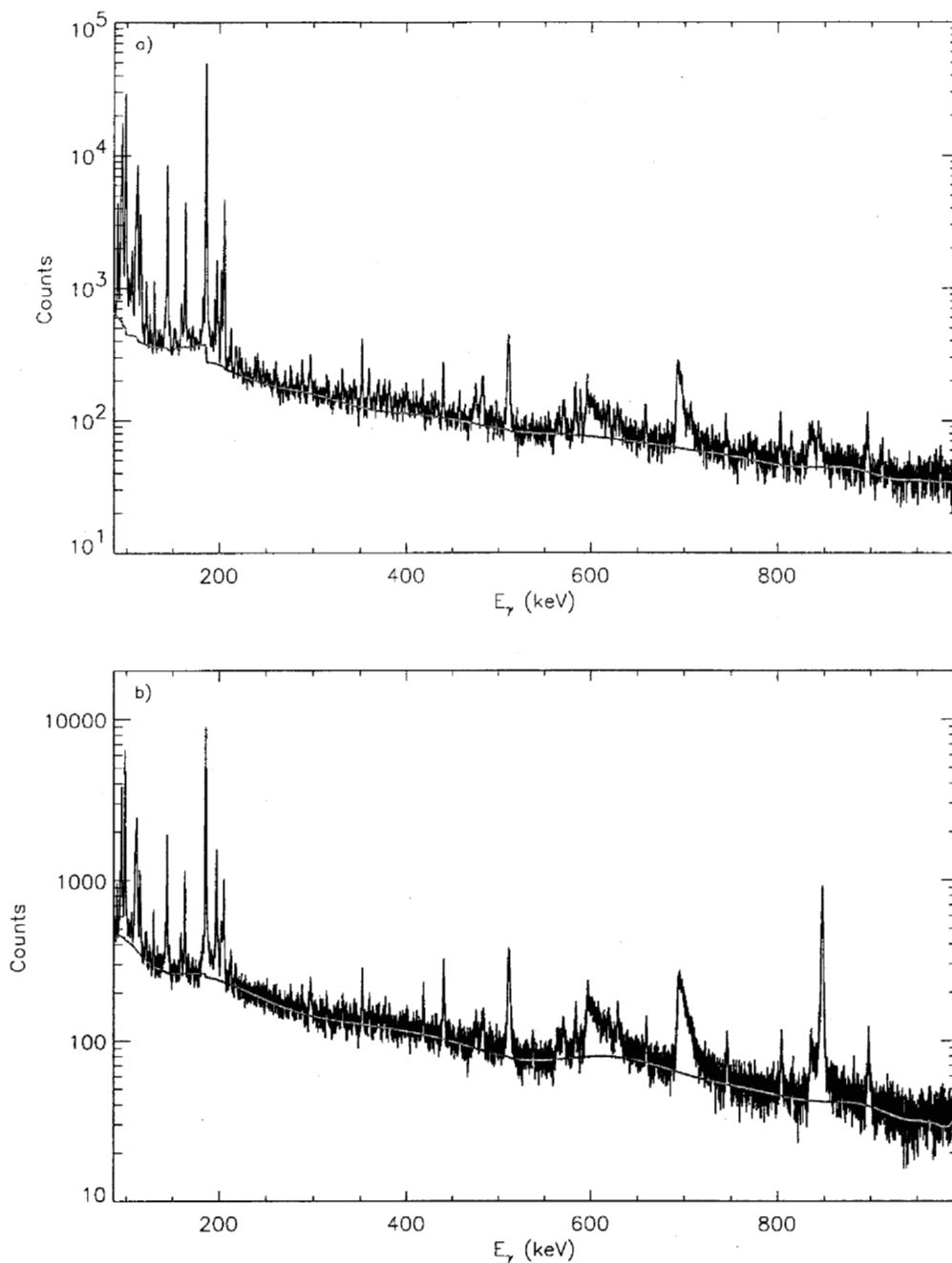


FIG. 101: Background used in the XGAM fit of bin 9 ($\bar{E}_n = 5.9$ MeV) for the a) **98Thin** and b) **99Thin** γ -ray spectra.

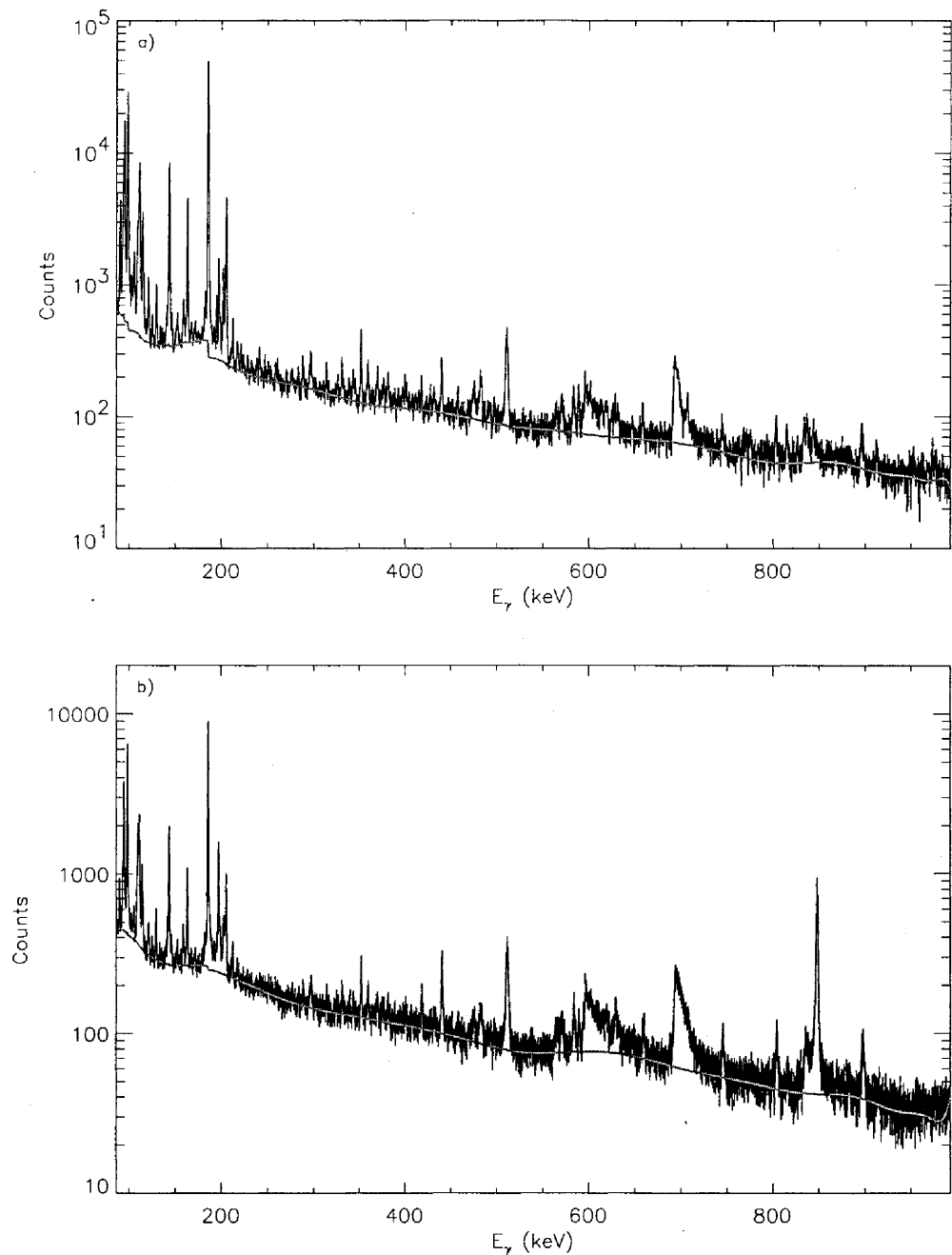


FIG. 102: Background used in the XGAM fit of bin 10 ($\bar{E}_n = 6.2$ MeV) for the a) **98Thin** and b) **99Thin** γ -ray spectra.

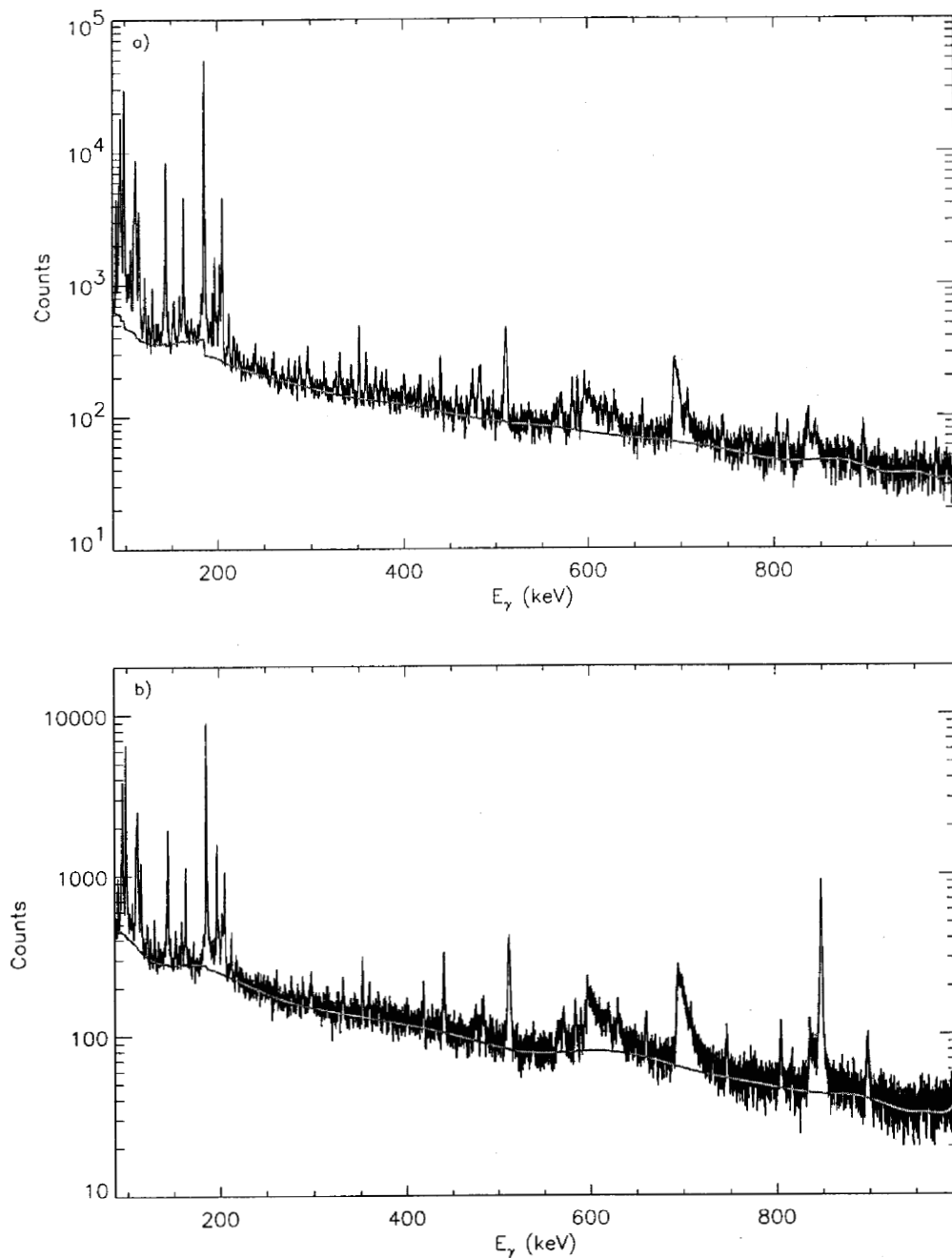


FIG. 103: Background used in the XGAM fit of bin 11 ($\bar{E}_n = 6.5$ MeV) for the a) **98Thin** and b) **99Thin** γ -ray spectra.

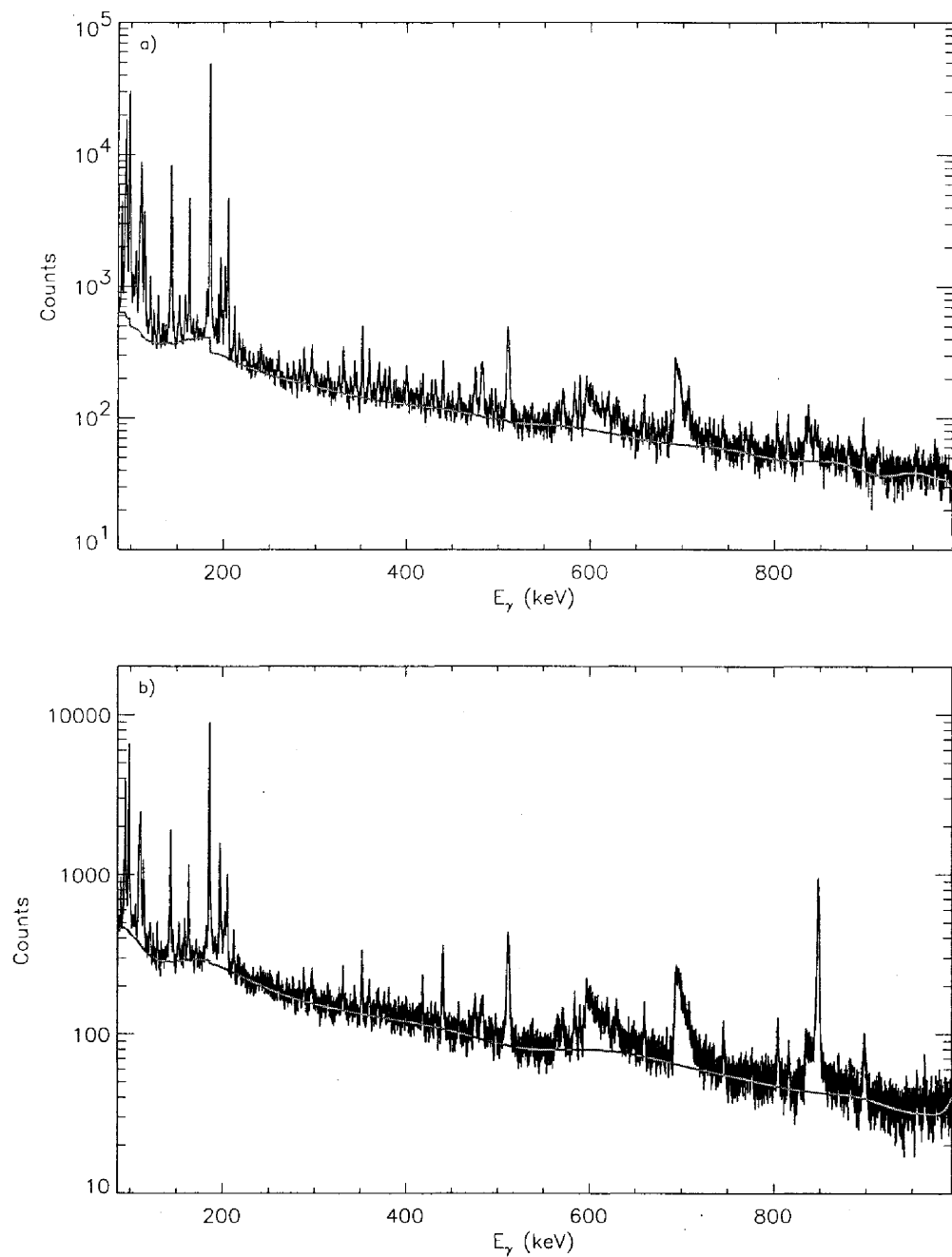


FIG. 104: Background used in the XGAM fit of bin 12 ($\bar{E}_n = 6.9$ MeV) for the a) **98Thin** and b) **99Thin** γ -ray spectra.

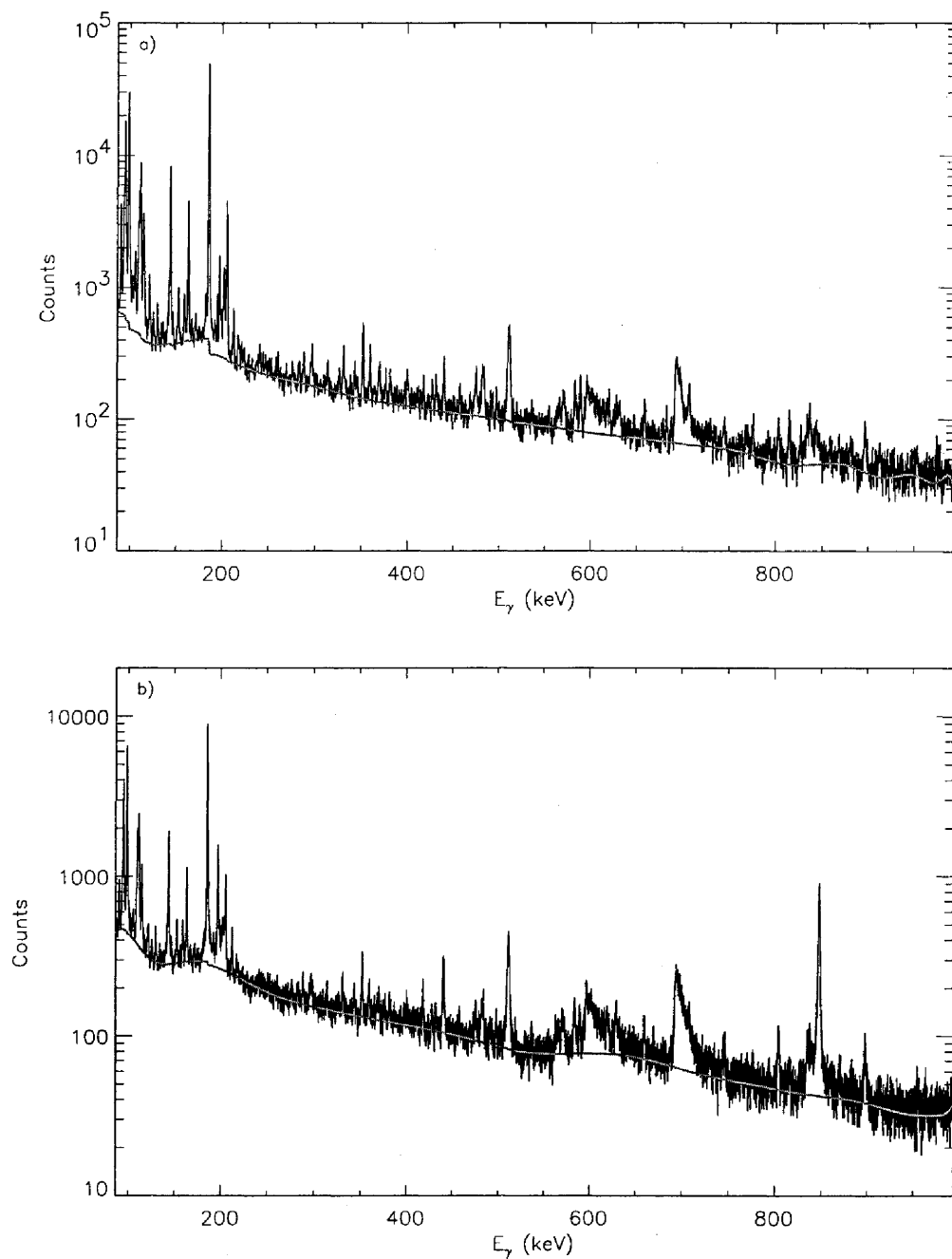


FIG. 105: Background used in the XGAM fit of bin 13 ($\bar{E}_n = 7.2$ MeV) for the a) **98Thin** and b) **99Thin** γ -ray spectra.

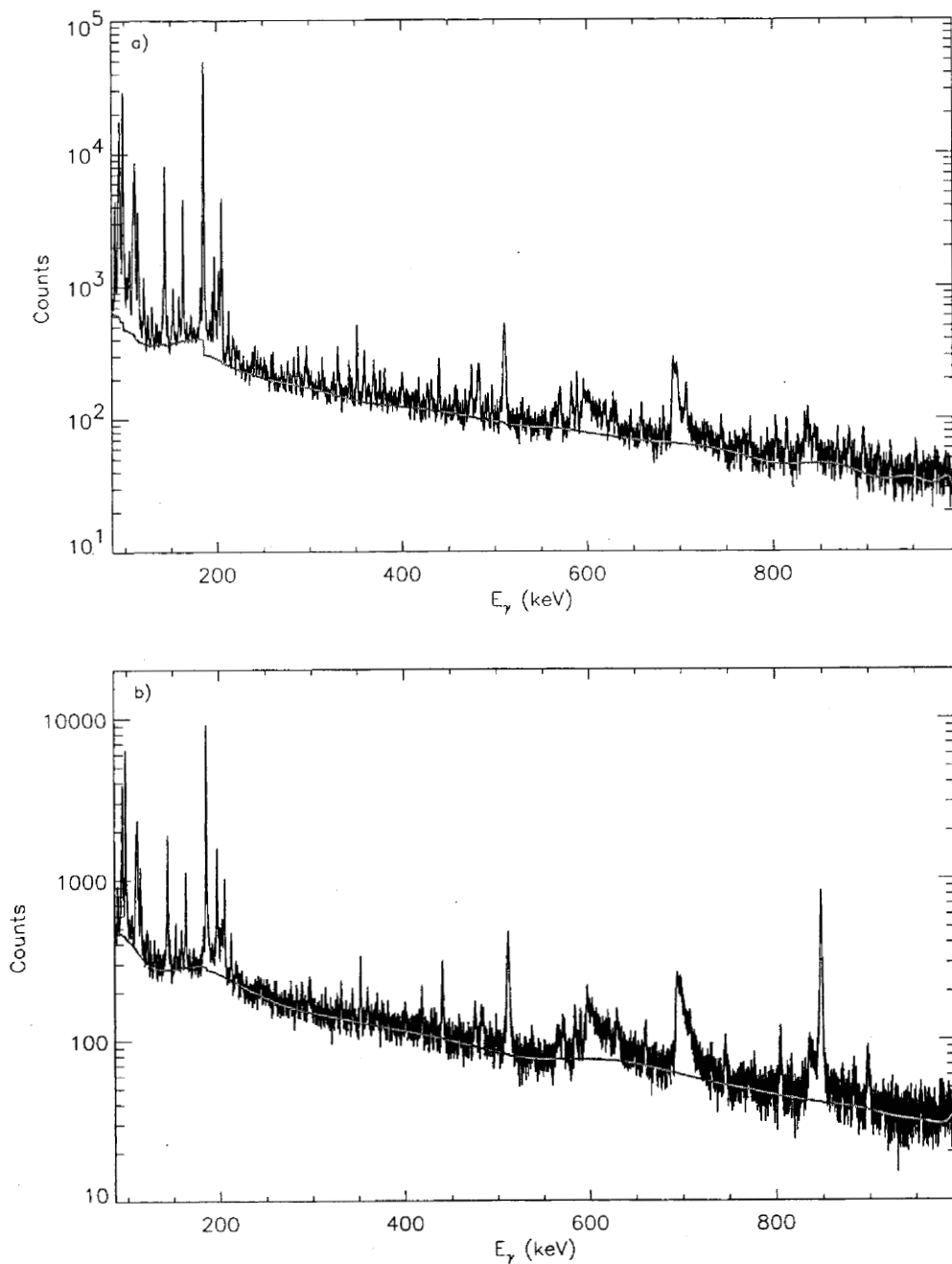


FIG. 106: Background used in the XGAM fit of bin 14 ($\bar{E}_n = 7.6$ MeV) for the a) **98Thin** and b) **99Thin** γ -ray spectra.

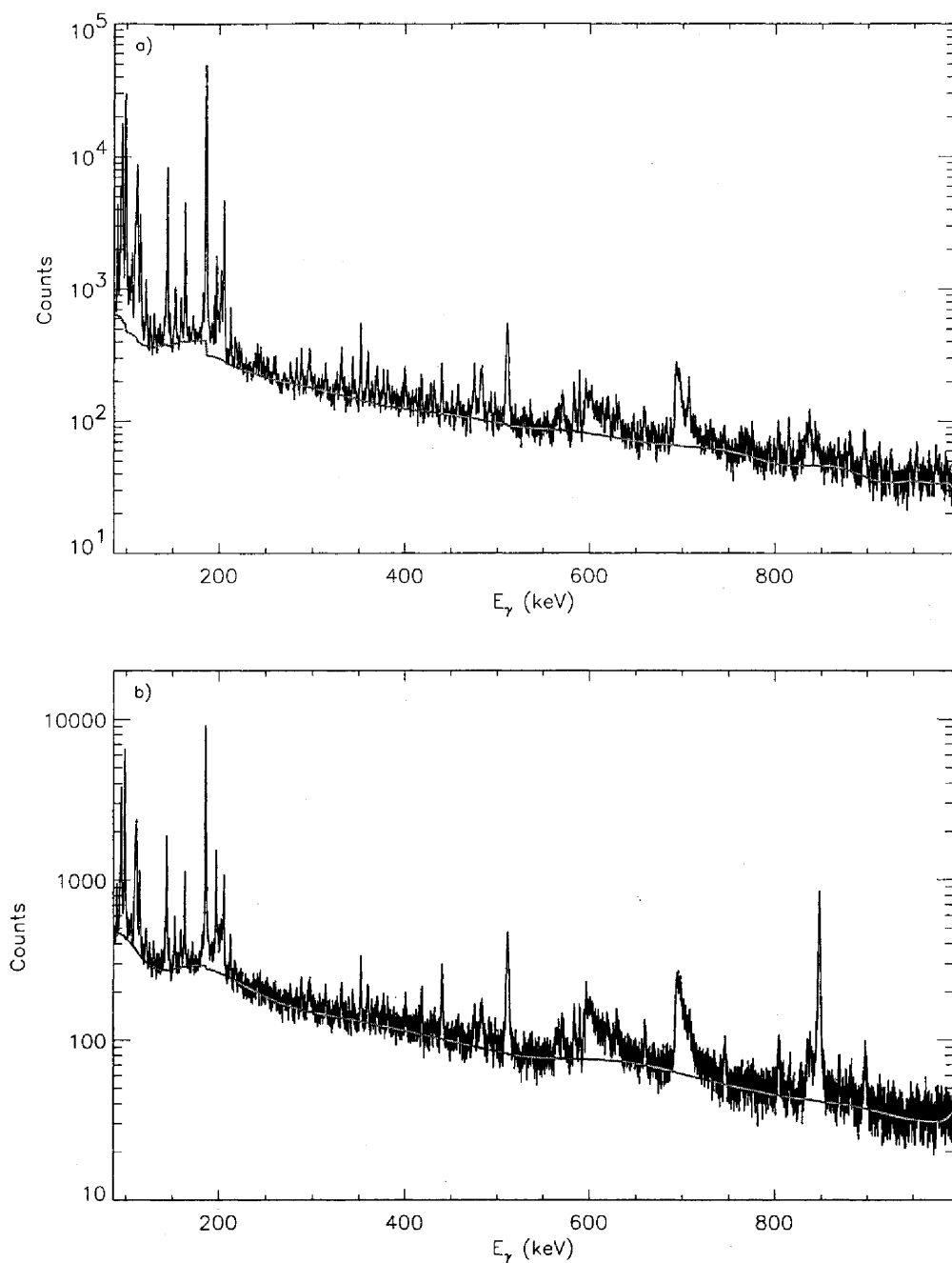


FIG. 107: Background used in the XGAM fit of bin 15 ($\bar{E}_n = 8.1$ MeV) for the a) **98Thin** and b) **99Thin** γ -ray spectra.

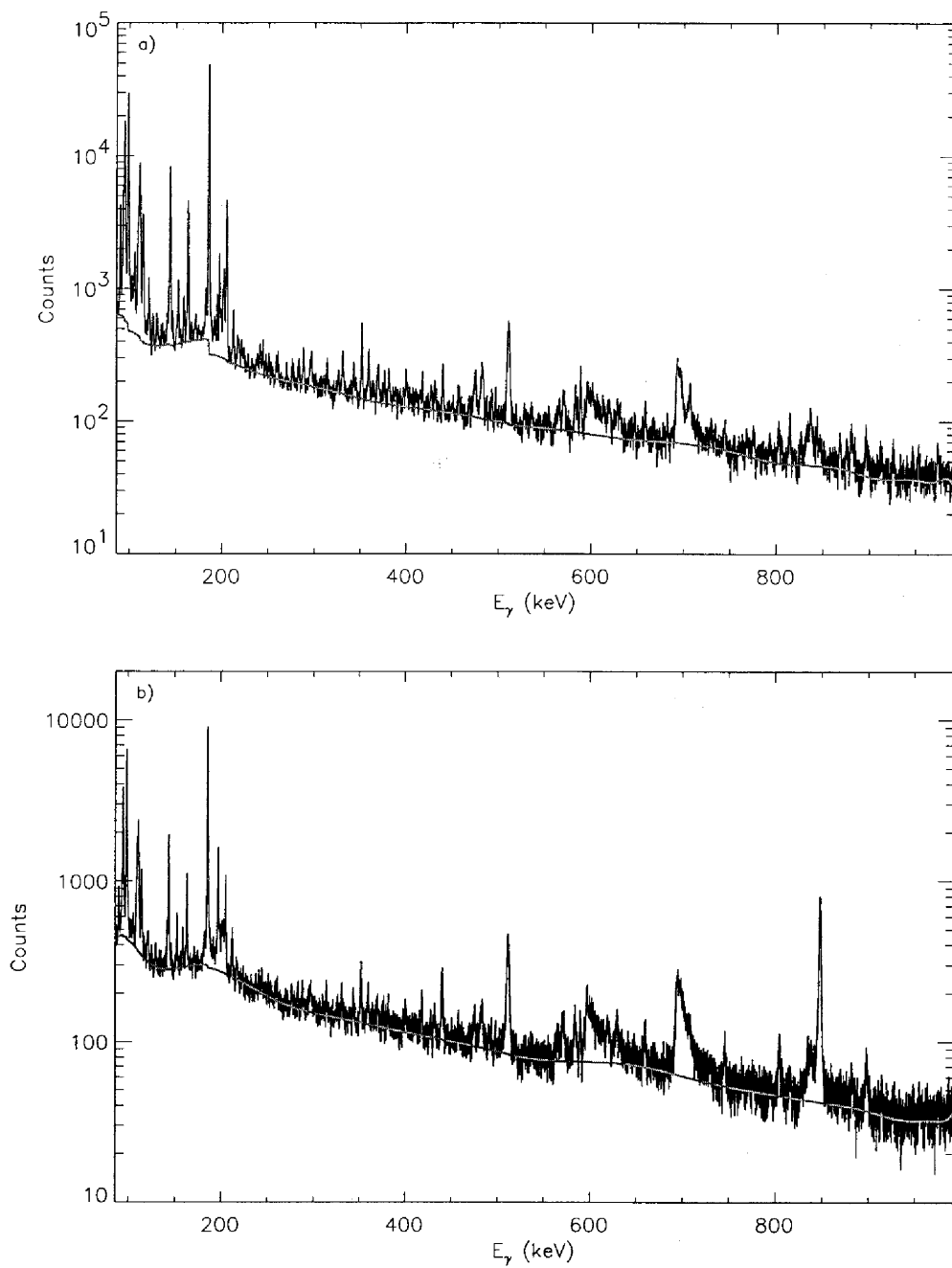


FIG. 108: Background used in the XGAM fit of bin 16 ($\bar{E}_n = 8.6$ MeV) for the a) **98Thin** and b) **99Thin** γ -ray spectra.

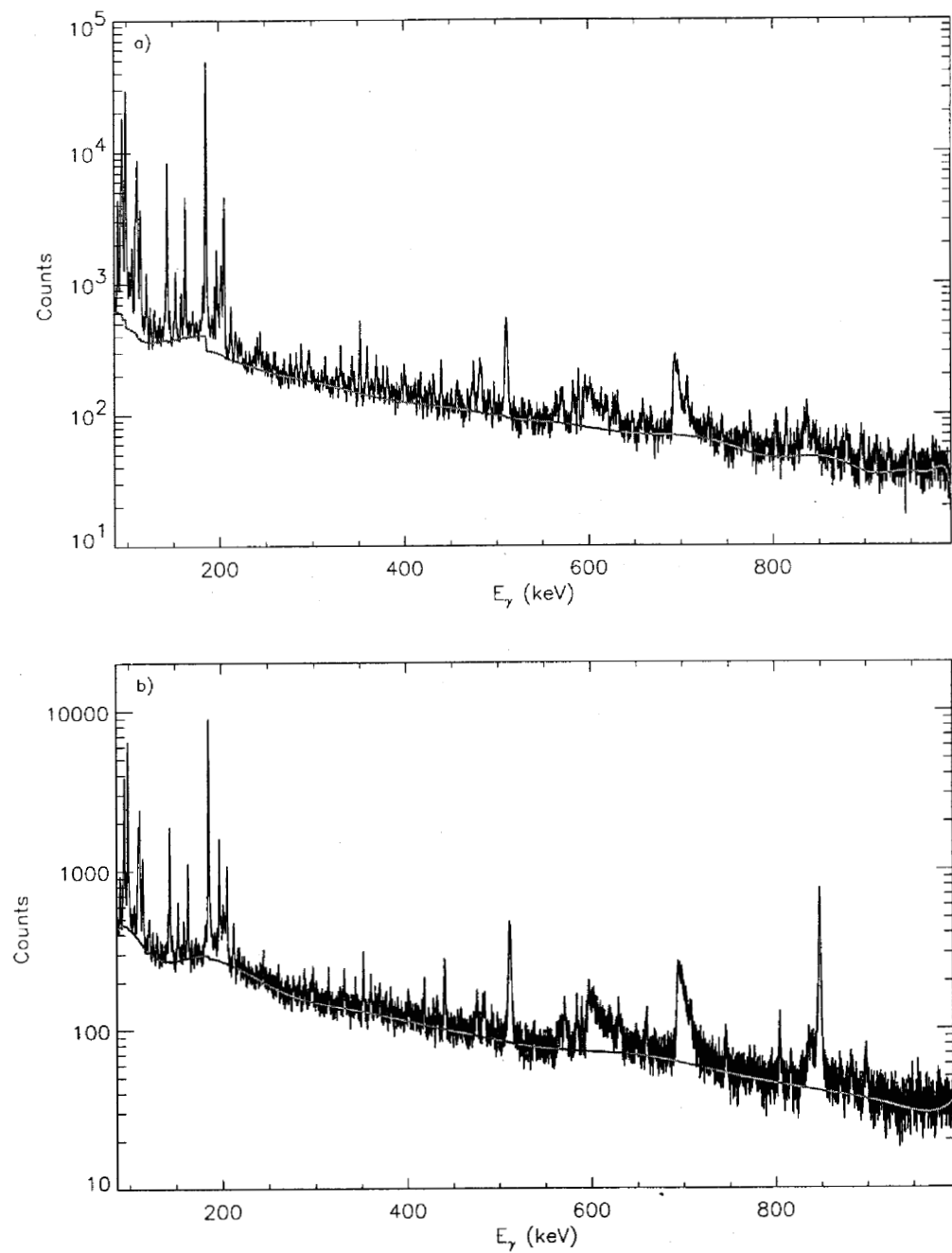


FIG. 109: Background used in the XGAM fit of bin 17 ($\bar{E}_n = 9.2$ MeV) for the a) **98Thin** and b) **99Thin** γ -ray spectra.

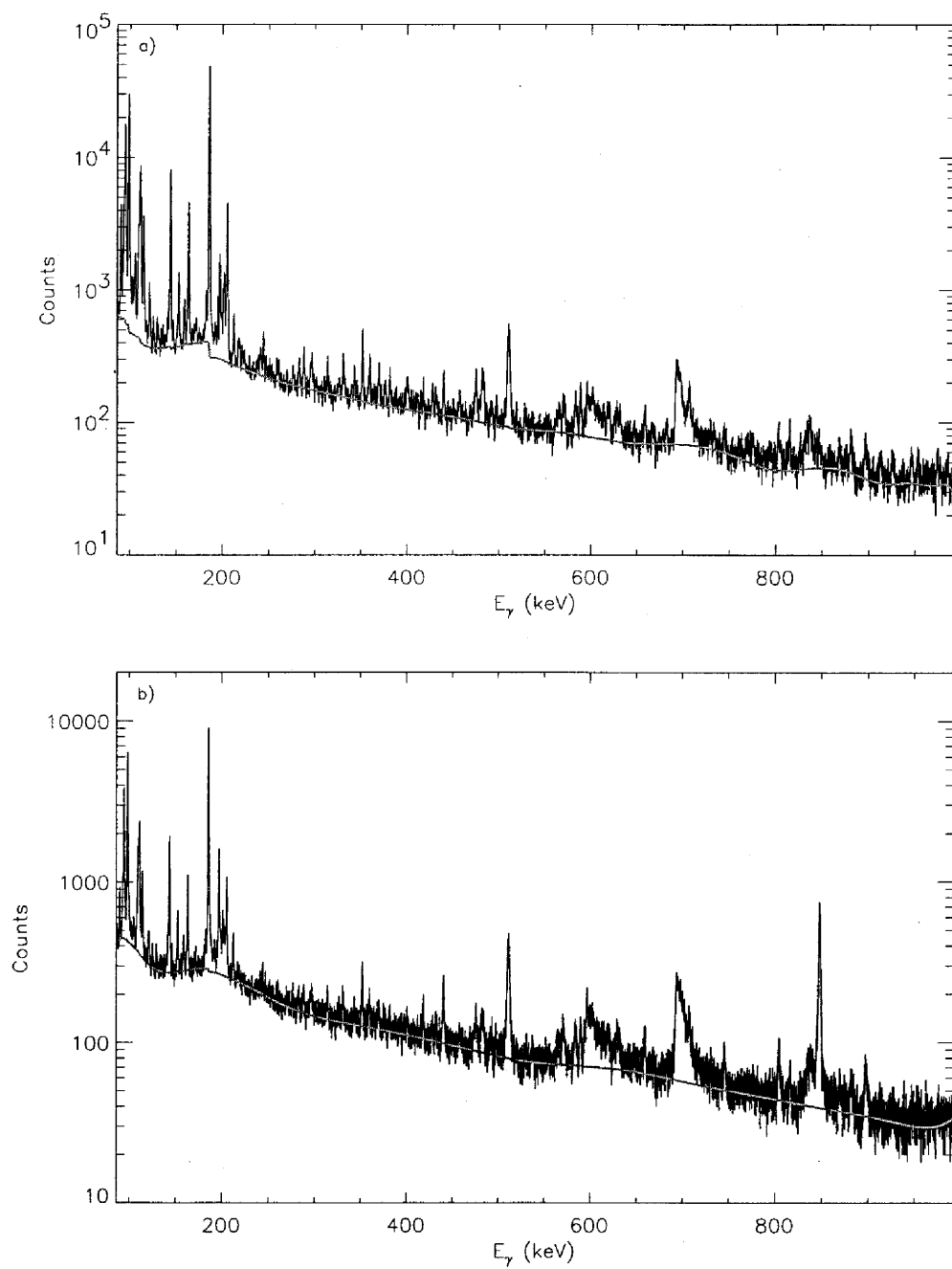


FIG. 110: Background used in the XGAM fit of bin 18 ($\bar{E}_n = 9.8$ MeV) for the a) **98Thin** and b) **99Thin** γ -ray spectra.

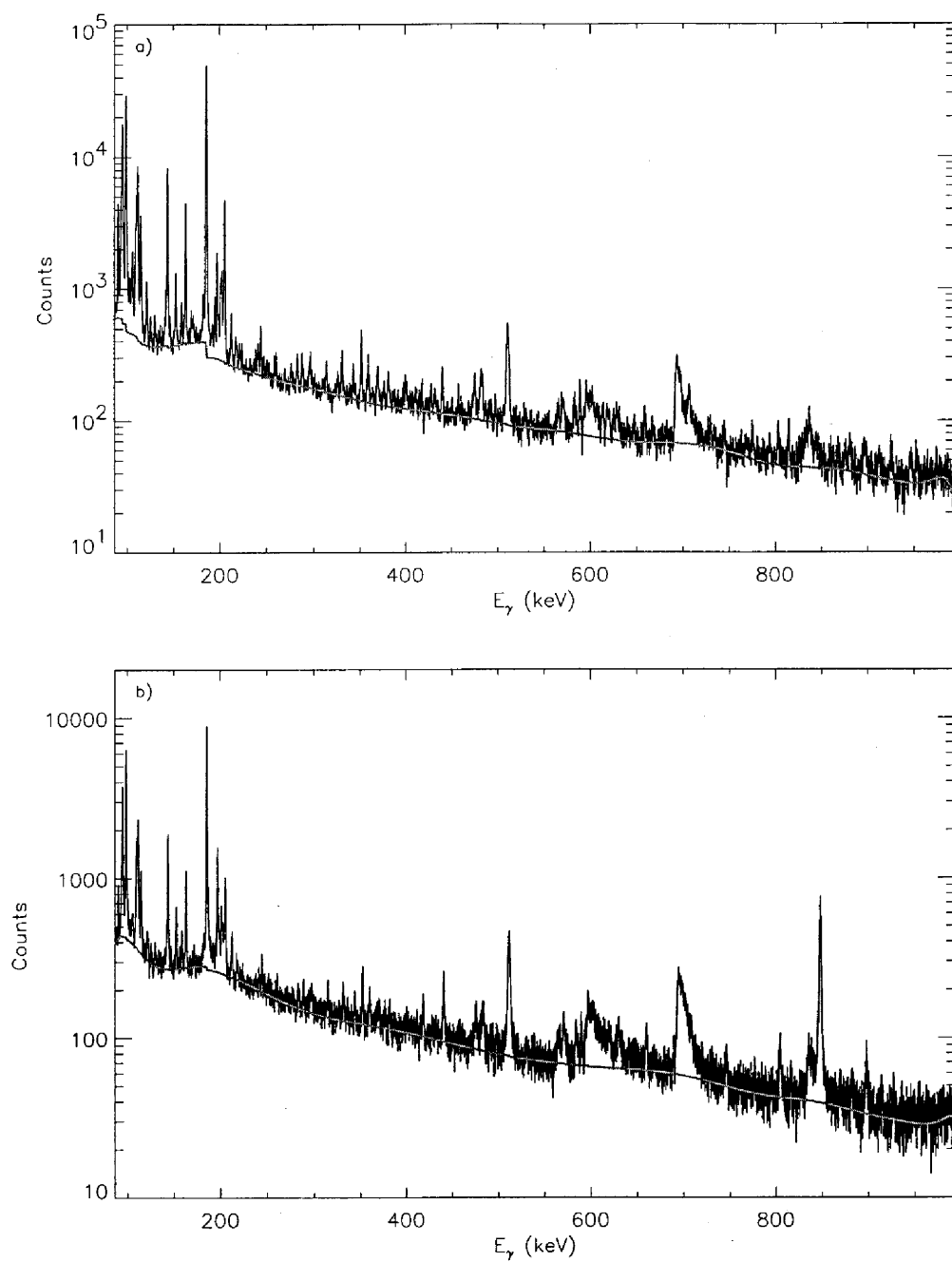


FIG. 111: Background used in the XGAM fit of bin 19 ($\bar{E}_n = 10.4$ MeV) for the a) **98Thin** and b) **99Thin** γ -ray spectra.

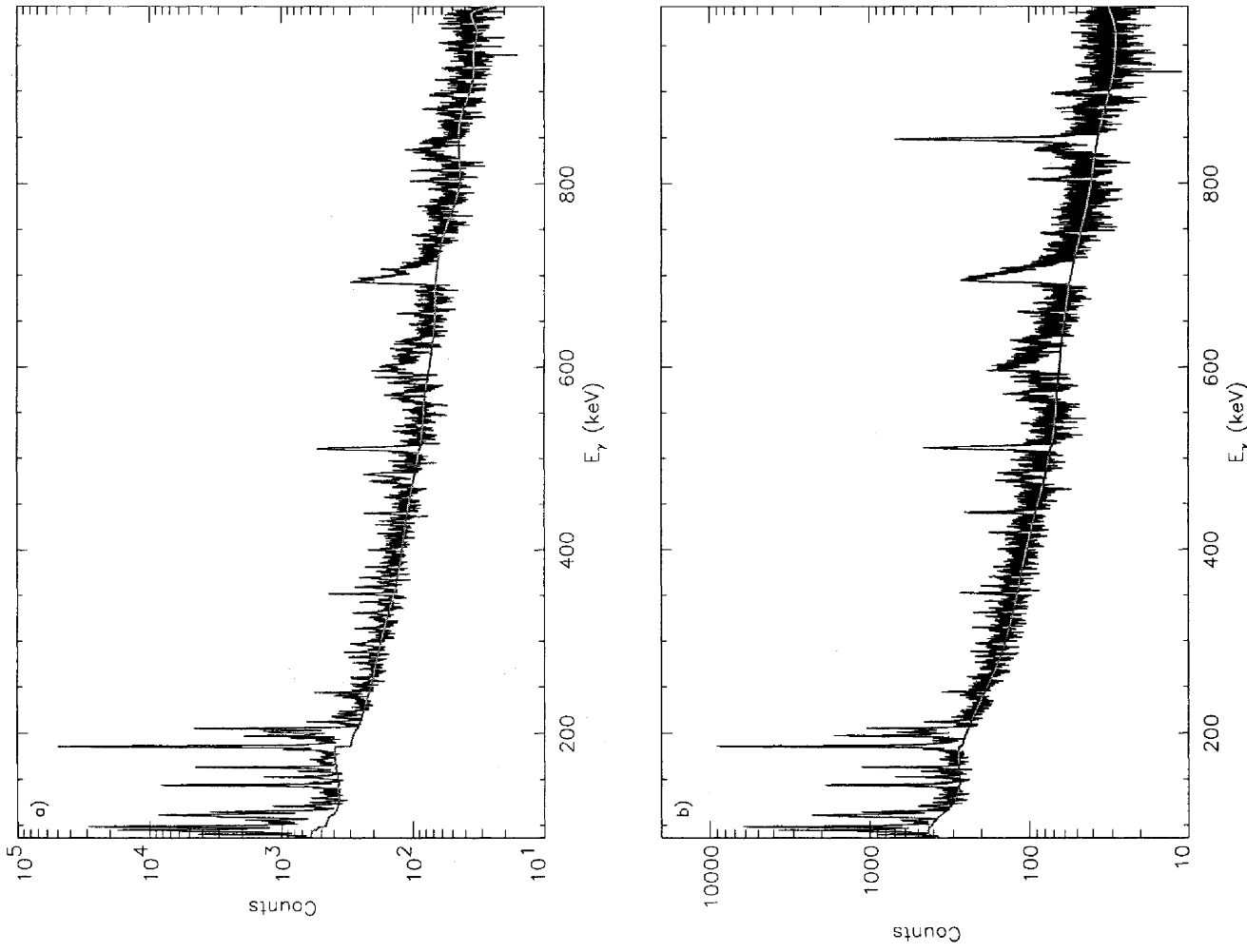


FIG. 112: Background used in the XGAM fit of bin 20 ($\bar{E}_n = 11.1$ MeV) for the a) 98Thin and b) 99Thin γ -ray spectra.

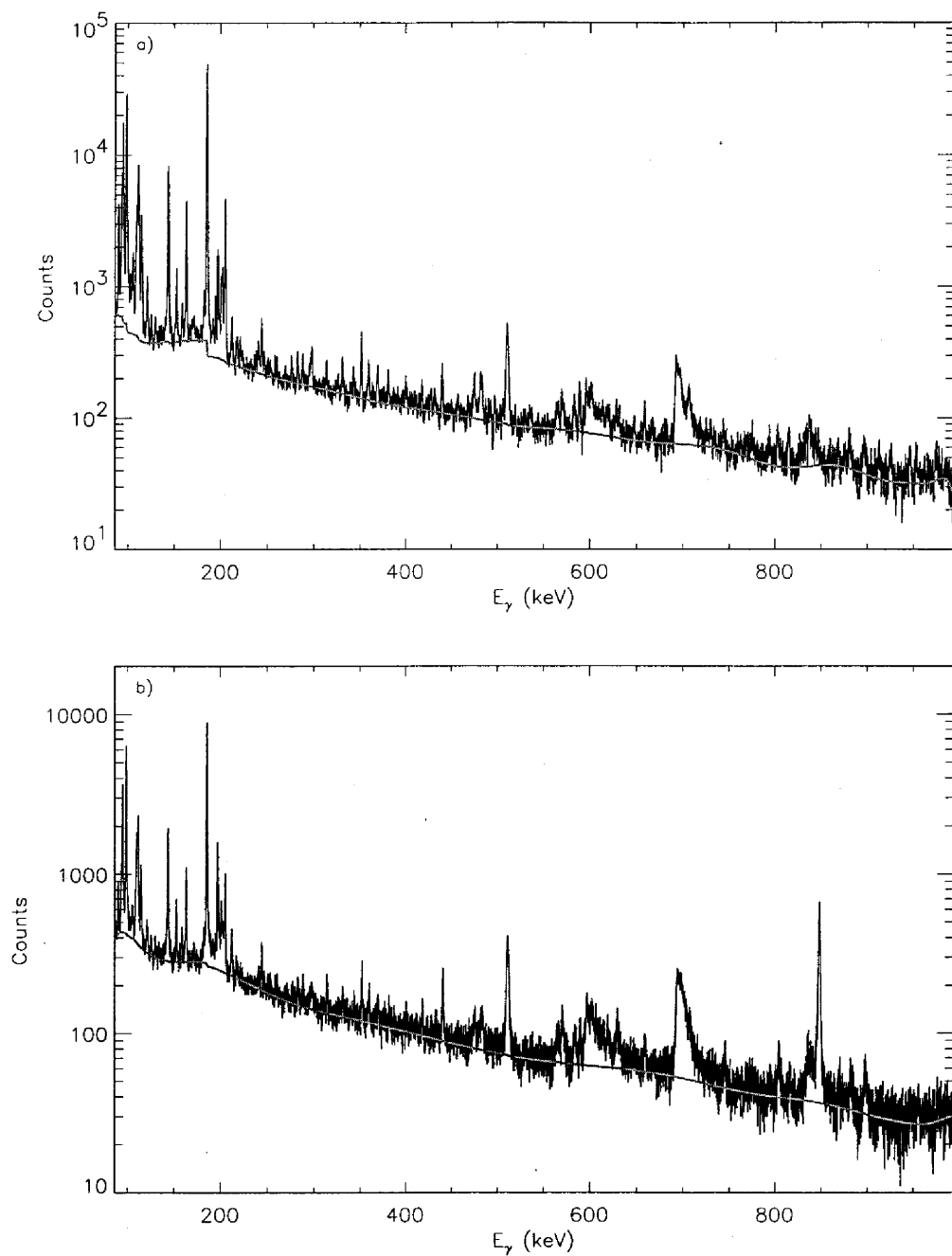


FIG. 113: Background used in the XGAM fit of bin 21 ($\bar{E}_n = 12.0$ MeV) for the a) **98Thin** and b) **99Thin** γ -ray spectra.

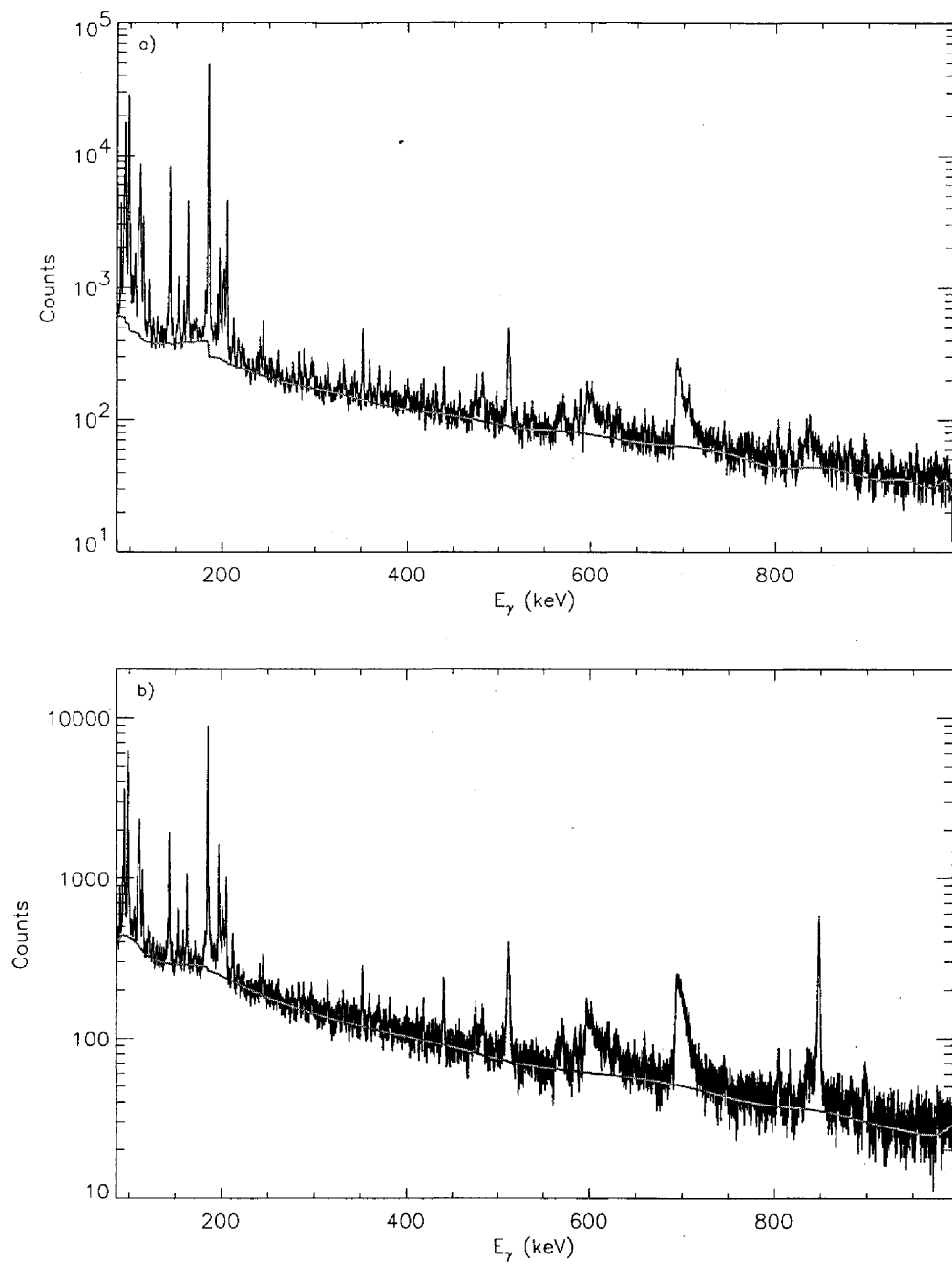


FIG. 114: Background used in the XGAM fit of bin 22 ($\bar{E}_n = 12.9$ MeV) for the a) **98Thin** and b) **99Thin** γ -ray spectra.

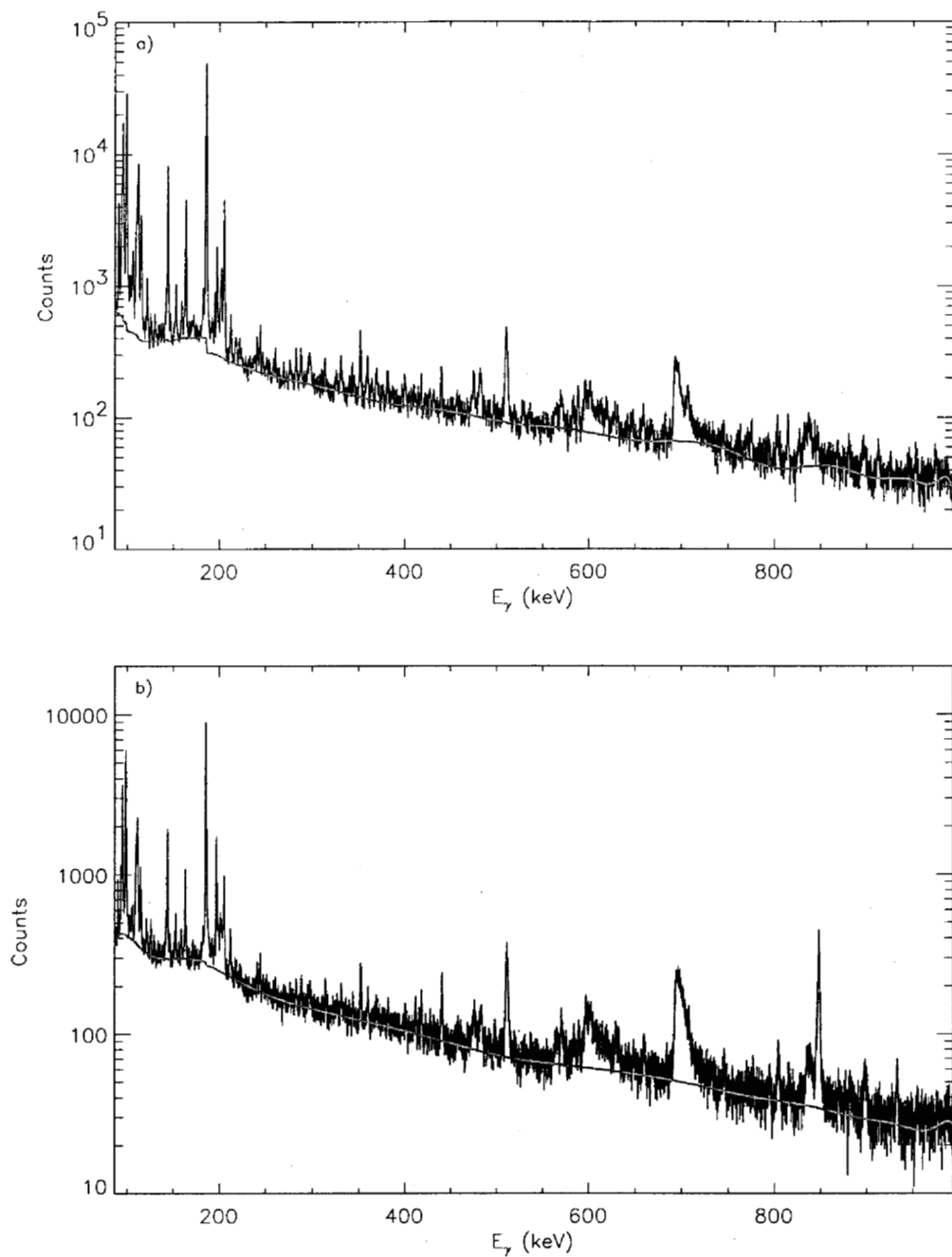
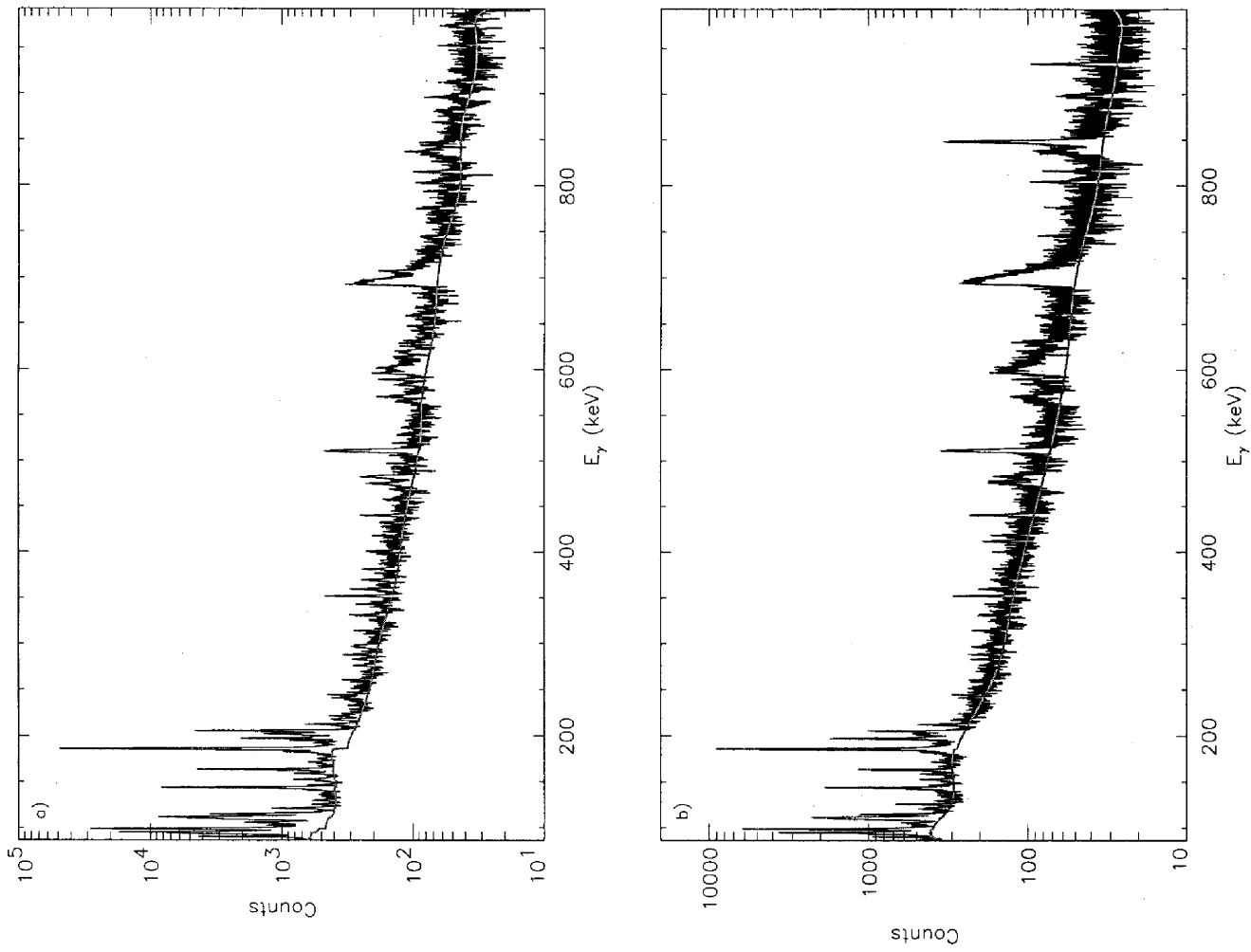


FIG. 115: Background used in the XGAM fit of bin 23 ($\bar{E}_n = 13.9$ MeV) for the a) **98Thin** and b) **99Thin** γ -ray spectra.

FIG. 116: Background used in the XGAM fit of bin 24 ($\bar{E}_n = 15.0$ MeV) for the a) 98Thin and b) 99Thin γ -ray spectra.



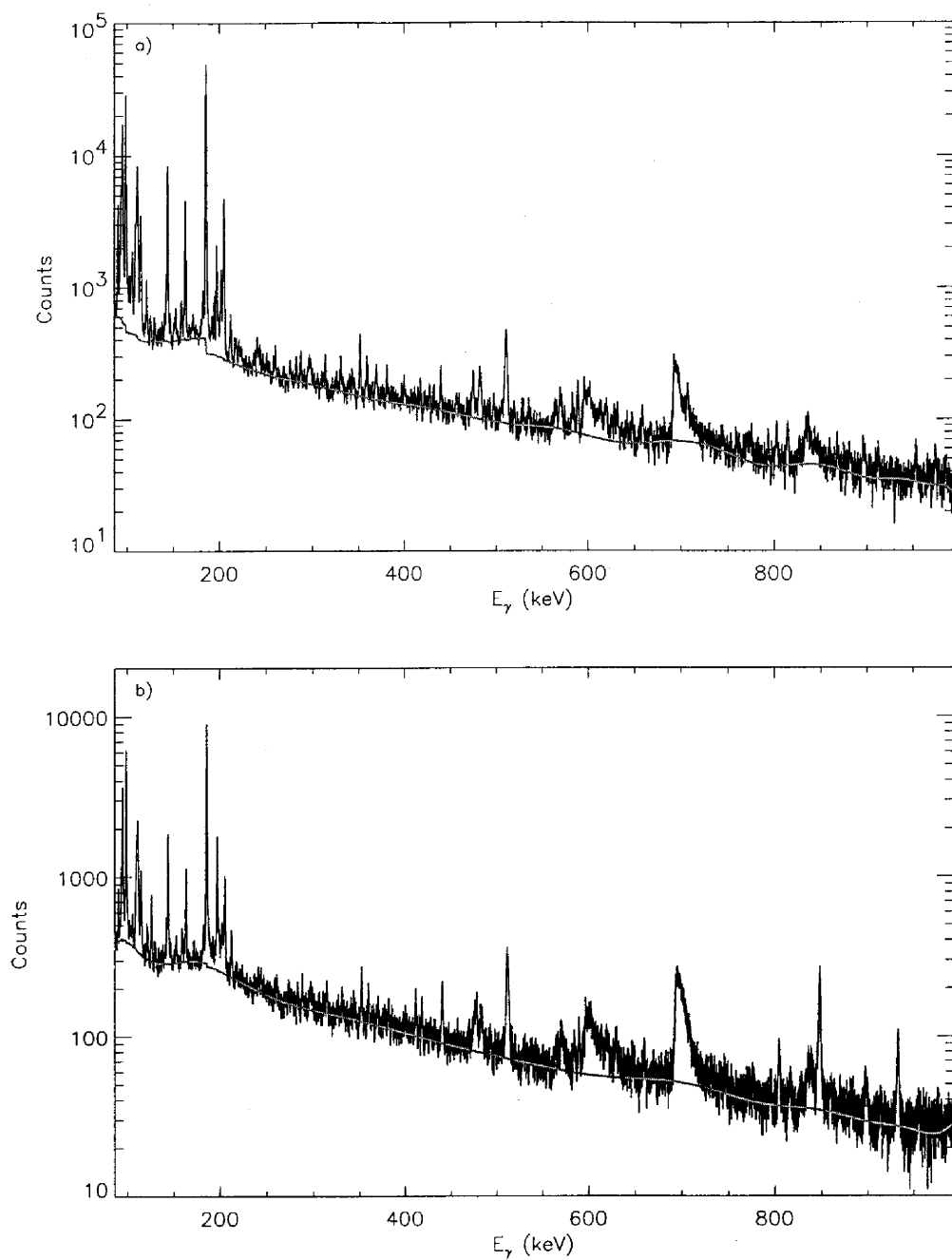


FIG. 117: Background used in the XGAM fit of bin 25 ($\bar{E}_n = 16.3$ MeV) for the a) **98Thin** and b) **99Thin** γ -ray spectra.

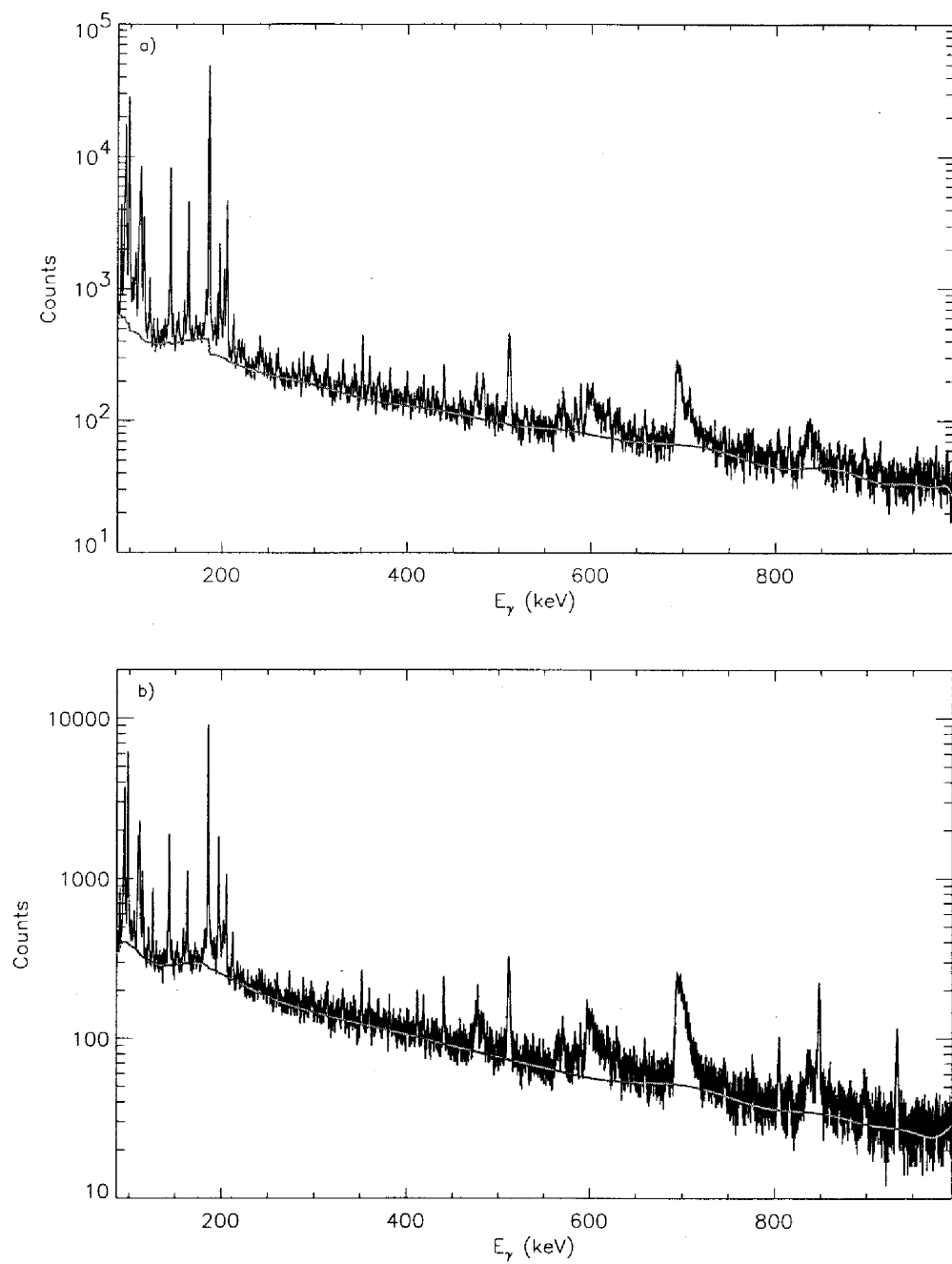


FIG. 118: Background used in the XGAM fit of bin 26 ($\bar{E}_n = 17.8$ MeV) for the a) **98Thin** and b) **99Thin** γ -ray spectra.

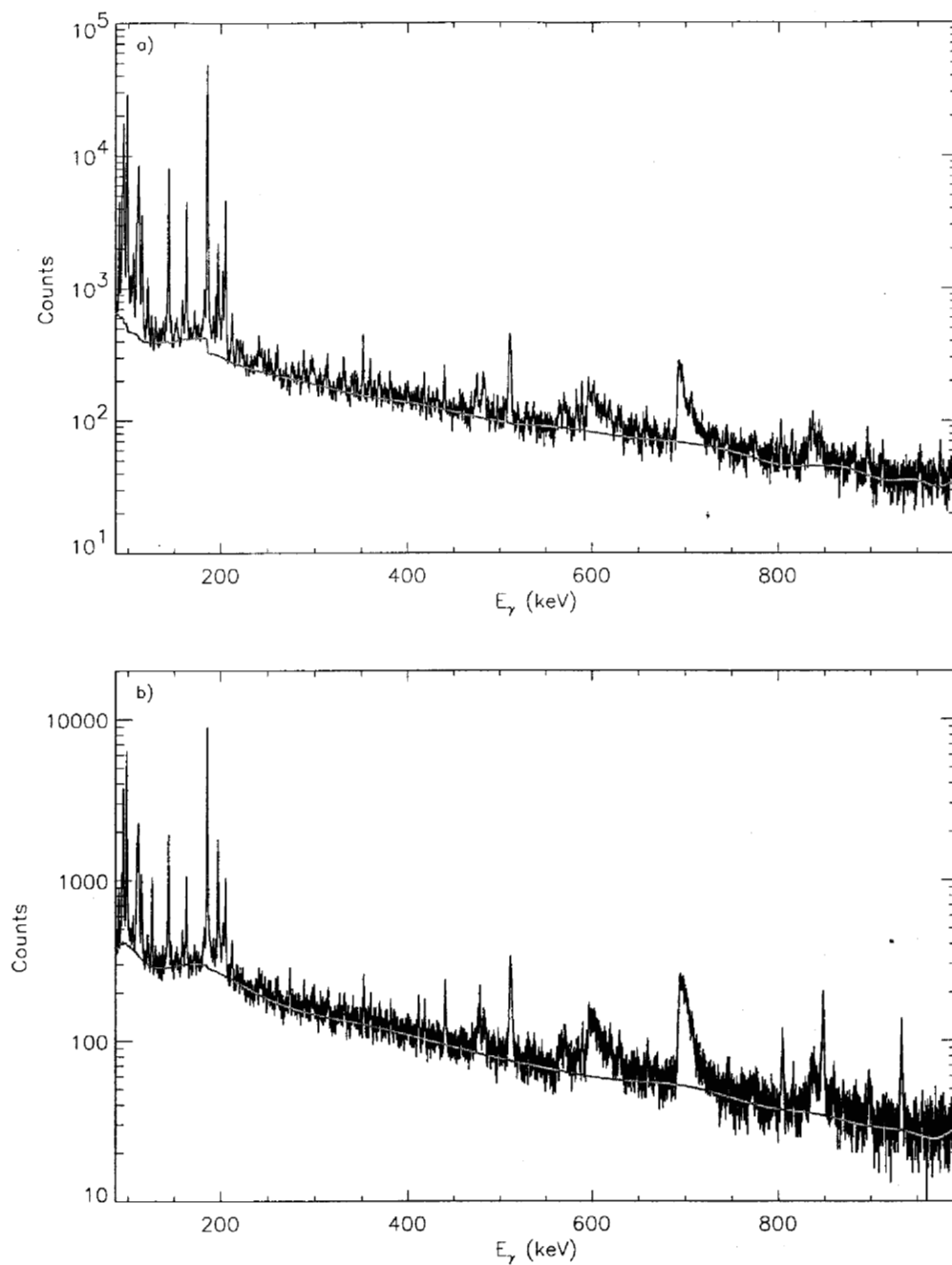


FIG. 119: Background used in the XGAM fit of bin 27 ($\bar{E}_n = 19.4$ MeV) for the a) **98Thin** and b) **99Thin** γ -ray spectra.

University of California
Lawrence Livermore National Laboratory
Technical Information Department
Livermore, CA 94551